UNIVERSITY OF STRATHCLYDE

DEPARTMENT OF MECHANICS OF MATERIALS

A STUDY ON PIPE BENDS

An Analysis of the Smooth Pipe Bend with Flanged End Constraints Under Out-of-Plane Bending and the Development of Experimental Techniques in the Creep of Pipe Bends

Thesis Presented for the

Degree of Doctor of Philosophy

by

Kenneth Rae, MSc, BSc

September 1984

A STUDY ON PIPE BENDS

An Analysis of the Smooth Pipe Bend with Flanged End Constraints Under Out-of-Plane Bending and the Development of Experimental Techniques in the Creep of Pipe Bends

ABSTRACT

In the design of piping systems the importance of the pipe bend is well established. Recent publications have been increasingly concerned with the effect of end constraints on the behaviour of smooth pipe bends. This has been aimed almost exclusively at in-plane bending, there being no serious attempts at the solution to out-of-plane bending. In PART (1) of this thesis a theoretical solution is presented for the out-of-plane bending of linear elastic curved pipes with rigid flanges. The analysis employs the theorem of minimum total potential energy with suitable kinematically admissable displacements in the form of fourier series. Integration and minimisation is performed numerically. Results are given for a wide range of practical bend geometries. A comparison with previous theoretical predictions highlights the inadequacy of these earlier solutions. The present results are shown to be in favourable agreement with results from tests conducted by the author and more recent results using a different solution procedure.

Work in the creep of pipe bends necessitates a substantial amount of experimental work and expertise. Most publications dealing with the creep of pipe bends under bending loads fail to present much information on this aspect.

In PART (2) of this thesis a general description is given of an experimental creep programme on pipe bends. The measurement of strain at elevated temperature was accomplished using the CERL-PLANER capacitance strain gauge. It is shown that the application of this gauge to pipe bends requires particular techniques if meaningful results are to be obtained. The results of development work arising from other problems encountered during the test programme are also presented. These include the measurement of displacement and distortion at elevated temperature and the provision of an efficient and novel heating system.

Kenneth Rae.

Kenneth Rae

To DOROTHY, CAROLINE, CHARLOTTE

and JONATHAN

my wife and family

A STUDY ON PIPE BENDS

An Analysis of the Smooth Pipe Bend with Flanged End Constraints Under Out-of-Plane Bending and The Development of Experimental Techniques in The Creep of Pipe Bends

CONTENTS

page

Figures are located at the end of each section.

NOTATION

A, ($\bar{A}$)	with subscripts, displacement coefficient (non-dimensionalised)
A1, ($\bar{A}1$)	with subscripts, displacement coefficient (non-dimensionalised)
A2, ($\bar{A}2$)	with subscripts, displacement coefficient (non-dimensionalised)
B, ($\bar{B}$)	with subscripts, displacement coefficient (non-dimensionalised)
C, ($\bar{C}$)	with subscripts, displacement coefficient (non-dimensionalised)
C	$\frac{Et}{(1-\nu^2)}$
c	centreline displacement subscript
D, ($\bar{D}$)	with subscripts, displacement coefficient (non-dimensionalised)
D	$\frac{Et^3}{12(1-\nu^2)}$
D	distortion displacement subscript
E	Young's Modulus
F	capacitance gauge factor
H	shear moment stress resultant
H	with subscript, rigid section centreline displacement
I	second moment of area, $I = \pi r^3 t$
JT	total number of terms in rigid displacement series
K	with subscripts, curvature
K	flexibility factor
M	applied bending moment
M	with subscript, moment stress resultant
MT	total number of terms in circumferential distortion displacement series
N	with subscript force stress resultant
$\bar{N}$	with subscript, number of integration points
NT	total number of terms in meridional distortion displacement series

R	radius of pipe bend centreline
R'	$R + r\sin\phi$
R	with subscript, principal radius of shell curvature
R	rigid section displacement subscript
S	shear force resultant
T	$\frac{t^2}{12r^2}$
T	with subscript, rigid section centreline displacement
U	strain energy
U	with subscript, rigid section centreline displacement
V, ($\bar{V}$)	total potential energy (non-dimensionalised)
W	shear strain (curvilinear co-ordinate system)
Z	$(1 + \frac{r}{R}\sin\phi)$
j	rigid section displacement coefficient subscript
m	distortion displacement coefficient subscript
n	distortion displacement coefficient subscript
p	internal pressure
q	with subscript, shell surface loading
r	mid-surface radius of pipe cross-section
t	pipe wall thickness
u	circumferential displacement
v	tangential displacement
w	radial displacement
z	through thickness co-ordinate

α subtended bend angle

β with subscript, shell surface rotation

$\gamma_{\theta\phi}$ shear strain

γ rotation between ends of bend

γ_o nominal rotation, $\frac{MR\alpha}{EI}$

δ_{jk} kronecker delta $\begin{cases} = 1, & j = k \\ = 0, & j = k \end{cases}$

$\varepsilon(\bar{\varepsilon})$ with subscript, strain (strain factor)

Θ angle along bend measured from one end, circumferential co-ordinate

θ subscript, circumferential direction

λ pipe factor, $\frac{Rt}{r^2}$

ν poissons ratio

σ with subscript, stress

$\bar{\sigma}$ with subscript, stress factor

$\hat{\sigma}$ with subscript, peak stress factor

ϕ meridional angle measured around cross-section from midway between intrados and extrados

ϕ subscript, meridional direction

Ψ_{ej} $\begin{cases} = 1, & j \text{ - even} \\ = 0, & j \text{ - odd} \end{cases}$

Ψ_{oj} $\begin{cases} = 0, & j \text{ - odd} \\ = 1, & j \text{ - even} \end{cases}$

$\$$ $\frac{pR^2}{Ert}$

GENERAL INTRODUCTION

The trend toward higher operating temperatures and pressures in the power and petro-chemical industries has increased significantly the problems associated with the design and safety assessment of pipework components. The increased complexity in design arising from these severe environments has lead in recent years to an increased activity in the experimental and theoretical study of one particular component of the pipework system - the smooth pipe bend.

In a structural sense the pipe bend is perhaps the most important pipeline component. Its behaviour has attracted the interest of many authors over the last seventy years. It is now well established that the flexibility of smooth pipe bends can be orders of magnitude higher than an equivalent length of straight pipe with the same cross-section geometry when both are subjected to the same external bending moment. Thus conventional simple beam theory can seriously over-estimate the stiffness of the pipe bend. The additional flexibility is associated with the ability of the cross-section to "ovalise" or flatten when a bending moment is applied to it. In piping analysis the fundamental problem is to design a system with sufficient flexibility to contend with thermal expansion loading on the pipeline itself and on the vessels to which it is connected. Clearly the incorporation of pipe bends in the system satisfies these needs. However, the additional flexibility introduced by the pipe bends is at the expense of high stress concentrations produced around the cross-section which can be several orders of magnitude greater than the stresses produced in adjacent straight pipes.

Theoretical analyses usually consider the smooth bend as a sector of a toroidal shell under a pure bending moment. The majority of the

work on bends has been based on "strain" or "complementary" energy concepts although several solutions exist which make use of the more traditional approach of solving the governing thin shell equations. Until recently, most of the analytical work was concerned with what, in a shell theory sense, might be termed "axi-symmetric" solutions where cross-sectional deformations and stresses were assumed to be uniform along the length and independent of the subtended angle of the bend. This type of solution treats the problem as an isolated smooth bend with no terminal connections. When the bend is part of a piping system the natural cross-sectional deformations are constrained by the connections between it and the other components, violating the axi-symmetric assumption.

In recent years, several solutions have been developed which solve the problem of smooth bends with various end terminations. However, the bulk of this work and that of earlier authors has been aimed almost exclusively at in-plane bending. The loading condition of out-of-plane bending, which in certain instances can be the predominant loading, has received little attention. In the axi-symmetric solution the derivation is based essentially on the assumptions employed in in-plane bending. The out-of-plane bending of a smooth pipe bend poses a complex problem. This is particularly so when the effect of end constraints are considered, where the axi-symmetric solution can lead to a gross over-estimate in flexibility and stress levels. There is in fact no readily available solution dealing with this particular problem.

The primary objective of this thesis is to formulate a theoretical solution for the flexibility and stress characteristics of smooth circular pipe bends with rigid flanges under out-of-plane bending. This is presented in PART (1) of the present thesis.

Whilst conducting this theoretical work the author was also employed on a research contract to investigate the inelastic (creep) behaviour of pipe bends at elevated temperature. This work, funded by the United Kingdom Atomic Energy Authority, covered an extensive experimental programme of creep testing on a range of pipe bend geometries under essentially bending loads. From this work, problems encountered in the field of strain and displacement measurement at elevated temperature led to the development of new experimental techniques. Few details are presented in the literature relating to problems encountered in the experimental field, although there abounds numerous comparisons with theory and experiment. This may be a consequence of the high cost of such tests ensuring commercial confidence. As such, problems encountered by other workers in the field do not come to light. In PART (2) of this thesis an attempt is made to remedy this situation by presenting some of the problems and their corresponding solutions.

A historical review of relevant publications is presented in CHAPTER (1). Only work which was considered important or of some interest has been included. The majority of previous investigators confined their activities to a linear-elastic examination of circular smooth bends under in-plane bending and neglected end effects. All the available publications known to the author dealing with end constraints have been included. Work on some other important features, such as non-circular cross-sections, creep, etc, are included for comparitive purposes.

PART (1) of the thesis begins at CHAPTER (2) with some preliminary theoretical formulations. Thin shell theory is discussed

and equations for a smooth bend derived. The theorem of minimum potential energy and the application of the Rayleigh-Ritz method are discussed.

CHAPTER (3) presents a theoretical solution to the problem of a smooth bend with flanged ends under out-of-plane bending. General displacements in the form of fourier series are derived which satisfy internal and external compatibility for the problem. The results are discussed and compared to other published analytical solutions. A comprehensive set of results for flexibilities and stresses for a wide range of bend geometries are then given.

CHAPTER (4) compares the theory of CHAPTER (3) with published analytical solutions and results from experiments detailed herein.

PART (2) of this thesis begins with a general description of an experimental creep programme in CHAPTER (5). Following a description of the test equipment, details are presented of the experimental techniques developed during the course of the work.

CHAPTER (6) examines in more detail the experimental techniques discussed in CHAPTER (5). Typical results from a number of tests performed on pipe bends at room temperature and elevated temperature are given.

CHAPTER (7) draws general conclusions from the work presented in PART (1) and PART (2).

CHAPTER 1

Smooth Pipe Bends: A Historical Review

ABSTRACT

This chapter deals with the historical development of the theoretical and experimental investigations associated with smooth pipe bends subjected to various forms of loading. Publications dealing with and without end constraints are reviewed separately. Finally, the existing design procedures are examined.

CHAPTER (1)

SMOOTH PIPE BENDS: A HISTORICAL REVIEW

1.1 Introduction

Piping systems usually include a number of components and may be subjected to a variety of mechanical and thermal loadings. During the last decade technological advances in the nuclear power industry have demanded a more stringent and critical appraisal of design procedures. From this has emerged an exceedingly diverse pattern of loading conditions considering not only the static, but the dynamic state also. This diversity in loading extends to aspects such as seismic loading and aircraft impact. Under hostile environments, such as elevated temperatures, inelastic behaviour such as plasticity or creep can be introduced in component parts of the system. In the more conventional piping system, however, the design criteria are not so exacting, in that the extreme or ultimate loading cases are not so complicated or severe.

The interest in this text shall be focused on one particular component of the piping system - the smooth pipe bend. In considering this component the applied loadings will be simplified to cover the following three important cases:

1. in-plane bending
2. out-of-plane bending
3. internal pressure.

An illustration of these loadings is shown in Figure (1.1).

In general, piping systems are employed to connect together vessels which may be a considerable distance apart. As the vessels are normally positionally fixed with respect to each other the general approach in design is to ensure that the pipe line is sufficiently flexible to absorb any expansions without imposing excessive loads on the anchor

points or the pipe line itself. This flexibility can be introduced for example by incorporating bellows expansion units in the line. These, however, lead to a limited fatigue life due to the high stresses produced in the convolutions at even moderate loads. An alternative and more common method of introducing additional flexibility has been to introduce pipe bends, usually smooth curved bends but occasionally mitre or lobster back bends, in the system. They are introduced because bends are inherently more flexible than straight pipes when subject to bending loads. The increase in flexibility is, however, at the expense of high stresses produced around the cross-section of the bend. This characteristic coupled with inelastic effects due to loading gives some insight into the complexity of behaviour that can occur. An illustration of these components is shown in Figure (1.2). The mitre bend, although not so common as smooth bends has particular uses when an economic or convenience factor takes priority.

In the design of a piping system it is normally assumed that the bend cross-sections are circular and that the wall thickness is the same throughout. However, manufacturing processes are such that the attainment of a prismatic, circular cross-section is rarely achieved. The most common method of manufacture involves forcing a section of straight pipe around a specially shaped die or former. This process normally results in some ovalisation or distortion of the bend cross-sections and non-uniform thinning of the pipe walls. The quality of the bends can be improved by forging or, depending on the size of the bend, a welded fabrication using folded plate with a circumferential (longitudinal) seam weld. Both these methods, however, tend to be more expensive. As a result, in most situations a certain amount of imperfection is considered acceptable and in some cases can even be helpful.

An extensive volume of work associated with the aforementioned considerations has been written. In the following sections of this chapter the more important and relevant publications will be reviewed. Although the review is aimed primarily at the smooth pipe bend, other aspects which have contributed to the development of their study, such as mitre bends, will also be given a brief mention.

Throughout the present work reference will be made to the bend "flexibility factor". It is felt appropriate at this early stage to define this term as a number of definitions exist in the literature, particularly for the case of out-of-plane bending. For both in-plane and out-of-plane bending the flexibility factor is usually defined as follows:

$$K = \frac{\text{(the end rotation of the bend under a given load)}}{\text{(the end rotation of a similar length of straight pipe under the same load)}}$$

The "end rotation of the bend" is the change (γ) in the subtended angle (α) of the bend when the load is applied. For the case of out-of-plane bending a more detailed definition and a discussion of the effects of the pure out-of-plane moment and associated torsional moment will be given in CHAPTER (3).

So far, this refers to the normal flexibility in connection with a smooth bend when it is considered alone. When the bend is connected to two straight pipes a further definition is required. In this case any change in the flexibility of the straights local to the bend will be referred to the bend. Thus only one flexibility factor will be necessary for the determination of the behaviour of a system of a bend with straight pipes. It is convenient to consider an "assembly" made up of a bend with short straight pipes attached to the ends. The "flexibility factor" for this

situation, again for the loading conditions of in-plane and out-of-plane bending will be defined as:

$$K = \frac{\text{(the overall end rotation of the assembly under a given load - the end rotation of both straight sections loaded alone)}}{\text{(the end rotation of a straight pipe of the same length as the bend, under the same load)}}$$

Here the "overall end rotation of the assembly" is the relative rotation between the loaded ends of the straight pipes. The bend length referred to is the length of the arc of the mean radius of the bend equal to ($R\alpha$) where R is the mean radius and α is the subtended angle of the bend. In the case of out-of-plane bending the numerator in this definition of flexibility factor will naturally include the torsional effects, although this will depend on the bend angle. Note that, a 180° bend will have a pure (out-of-plane) moment along the straight sections, whereas a 90° bend will have a pure (out-of-plane) moment on one straight section and a pure torsional moment on the other. The straight pipe in this straight-bend-straight configuration will be referred to in the present work as a "tangent pipe".

It is important to recognise that the denominator in both definitions of flexibility factor refers to the nominal rotation (γ_o) of a straight pipe and not that of a curved pipe as is sometimes employed.

Reference will also be made to a "stress" and "strain concentration factor" (S.C.F.) which unless otherwise stated will be defined as:

$$SCF = \frac{\text{(the elastic stress/strain in a bend under a given load)}}{\text{(the maximum elastic stress/strain in a similar straight pipe under the same load)}}$$

In describing the co-ordinate system of the pipe bend the following terminology will be adopted:

1. the "circumferential" direction defined by the angle θ is assigned along the length of the bend;
2. the "meridional" direction defined by the angle ϕ is assigned around the bend cross-section.

When quoting and discussing or presenting the work of other authors every attempt will be made to use the notation of the present thesis and not that of the original publications, although similar notation to that of the many previous authors on the subject of pipe bends is used.

1.2 Smooth Pipe Bend Without End Effects

1.2.1 Linear Elastic Analysis

In 1911, KÁRMÁN [1] developed the first theoretical solution for smooth curved pipes under in-plane bending. He demonstrated conclusively that curved tubes were inherently more flexible than a solid curved bar or equivalent length of straight pipe. A year earlier, BANTLIN [2] had arrived at a similar conclusion from experimental work conducted on thin wall bent pipes. Bantlin found that the pipes were about five times as flexible as would be expected from the common theory of beam bending. Bantlin attributed this increase in flexibility to wrinkles and irregularities at the inside (intrados) of the bend which had arisen during the manufacturing process. He suggested that the wrinkles behaved in a "spring like" fashion. Kármán on the other hand was able to associate the increase in flexibility with the initially circular cross-section tending to ovalise or distort when the bending moment was applied (Fig. (1.3)). In doing so he assumed the tangential displacement of the cross-section could be expressed by the following series:

$$v = \sum_{n=1} A_n \sin(2n\phi), \quad n = 1,2,3 \ldots\ldots \qquad \ldots \qquad (1.1)$$

He formulated the strain energy expression using equation (1.1) and by minimising the strain energy was able to determine values for the coefficients in the displacement series. In formulating the solution Kármán did not use equations derived from thin shell theory but instead obtained his own strain-displacement relationships from the geometry of the bend. Taking one term in the displacement series of equation (1.1) Kármán was able to obtain what is usually referred to as the "Kármán first approximation" for the flexibility factor.

$$K_1 = \frac{10 + 12\lambda^2}{1 + 12\lambda^2} \quad \ldots \quad (1.2)$$

By taking two terms in the displacement series he obtained a second approximation:

$$K_2 = \frac{105 + 4136\lambda^2 + 4800\lambda^4}{3 + 536\lambda^2 + 4800\lambda^4} \quad \ldots \quad (1.3)$$

Kármán also gave numerical results for a third approximation (K_3) for values of λ he thought were necessary.

The term λ is herein referred to as the pipe factor. It is also sometimes referred to as the "pipe bend parameter" or "bend characteristic", and is given by:

$$\lambda = \frac{Rt}{r^2} \quad \ldots \quad (1.4)$$

Kármán's analysis gives results which depend uniquely on this pipe factor λ. It will be shown later, however, that when end effects are introduced then more than one parameter is required to define the solution. The flexibility factors given by Kármán are shown in Figure (1.4). They confirm his assertion that the first approximation is valid for $\lambda > 0.5$, the second approximation for $\lambda > 0.1$ and below $\lambda = 0.1$ a third approximation is necessary.

The importance of Kármán's contribution to the study of pipe bends cannot be over-emphasised. It was to form the basis of virtually all subsequent work and although restricted to in-plane bending it was also later to provide the basis for extending the analysis to out-of-plane bending. In essence, Kármán analysed a differential length of pipe using the Ritz method. Because of the lack of the digital computer he could

only consider in the analysis the hoop or meridional direction of the pipe bend. It is interesting to note that even with today's advanced computer technology his theory and assumptions are still being applied. In fact solutions developed for the axisymmetric problem by contemporary authors rarely differ from that of Kármán's by more than a single figure percentage. It is therefore worth examining the assumptions he made in some detail. His major assumptions, stated or implied, were as follows:

1. All cross-sections of the bend were assumed to deform by the same amount.
2. The mid-surface meridional strain (ε_ϕ) was assumed to be zero.
3. The circumferential strain (ε_θ) was assumed to be constant through the thickness, and hence the circumferential curvature (K_θ) was neglected.
4. R>>r. This permitted the "pipe bore term" (R + r) to be approximated to R.
5. r>>t. This implies that the solution is only applicable to thin shells.
6. Stresses normal to the shell mid-surface were neglected.
7. Shear strains were neglected.

Assumptions (1) and (7) were because of axisymmetry and pure bending. Assumption (2), sometimes referred to as the "Kármán assumption", allows the deformation of the cross-section to be expressed in terms of one displacement component. Assumption (4) limits the solution to long radius bends. Assumptions (5) and (6) are simply two of the basic assumption of thin shell theory.

In the same year, 1911, MARBEC [3] attempted to solve the identical problem by assuming that the initially circular cross-section deformed into an ellipse. The expression he obtained for the flexibility factor was:

$$K_1 = 1 + \frac{4}{3}\lambda^2 \qquad \ldots \quad (1.5)$$

Although his assumptions regarding the strain-displacement relationships were identical to Kármán's, there are serious discrepancies between the K_1 values calculated from equations (1.2) and (1.5). Curiously, although this formula has been quoted by many authors over the years, it was not until nearly 60 years later that SPENCE [4] corrected Marbec's work. Marbec failed to distinguish between the meridional angle of the initially circular cross-section and the angle used to denote the equation of his ellipse. The corrected flexibility factor is given by:

$$K_1 = \frac{2 + 3\lambda^2}{1 + 3\lambda^2} \qquad \ldots \quad (1.6)$$

Flexibility values calculated from equation (1.6) are considerably lower than those of Kármán's first approximation (1.2) as shown in Figure (1.4). This arises from the additional constraints imposed upon the solution in prescribing an elliptical deformation of the cross-section. They are, however, consistent with a lower bound strain energy analysis, but even the corrected results are of little practical value.

LORENZ [5] in 1912 published a solution based on a complementary energy approach in which he specified stresses instead of displacements. His first approximation for the flexibility factor was:

$$K_1 = 1 + \frac{3}{4\lambda^2} \qquad \ldots \quad (1.7)$$

Lorenz compared his and Kármán's work with the experiments of Bantlin and concluded that his results were more accurate. However, later work disproved this. Lorenz's main limitation arose from his choice of stress distribution. He assumed with the first approximation that the circumferential stress across the section was linear whereas Kármán's analysis demonstrated that it was not.

In 1923, TIMOSHENKO [6] investigated the case of a curved tube having a rectangular cross-section and subject to in-plane bending. Using similar assumptions to those of Kármán, he was able to determine a flexibility factor in terms of the bend geometry. The formulation for a rectangular section is rather complicated but for a square section of side b, thickness t and radius of curvature R, his flexibility factor can be expressed as:

$$K_1 = \frac{3.232 + 49.18\lambda^2}{1.232 + 49.18\lambda^2} \qquad \ldots \quad (1.8)$$

$$\text{where } \lambda = \frac{Rt}{b^2}$$

The paper did not receive much attention in the subsequent literature, probably because it is of little practical value.

HOVGAARD [7] in 1926 published the first of his many contributions to the already increasing literature on pipe bends. He attempted to produce an independent solution for in-plane bending of circular smooth bends by specifying a series for the "vertical" displacement component. This displacement he defined in the paper as the movement of the cross-section towards the centre of curvature and parallel to the plane of the bend. His resulting expression was identical to that of Kármán as might be expected. He was the first to point out the

existence of a direct meridional stress factor ($\bar{\sigma}_{\phi D}$) and gave its peak value as:

$$\bar{\sigma}_{\phi D} = \frac{2r}{R}\left(\frac{1 + 6\lambda^2}{1 + 12\lambda^2}\right) \qquad \ldots \quad (1.9)$$

Two years later, HOVGAARD [8] pointed out that if strict allegiance was to be paid to Kármán's assumptions then his expression for flexibility factors should be multiplied by a factor $(1-\nu^2)$. Kármán avoided this factor by treating the pipe as a ring and thus omitting poisson's ratio in his energy expression. Although the factor $(1-\nu^2)$ is close to unity, (0.91 for $\nu = 0.3$) it should nevertheless be included for consistency with a lower bound analysis.

WAHL [9] investigated piping systems and derived expressions for end moments and reactions. He was probably the first to investigate the effect of internal pressure, and eroneously concluded that it had little effect on the flexibility.

JENKS [10] in 1929 extended the results of Kármán to the Nth approximation, i.e.: using N terms in the displacement series. His generalised flexibility factor was given by:

$$K_N = \frac{10 + 12\lambda^2 - j}{1 + 12\lambda^2 - j} \qquad \ldots \quad (1.10)$$

where j is given as a function of λ.

Jenks, like Kármán, omitted the $(1-\nu^2)$ term from his analysis. He also provided data for the determination of stresses for values of λ down to 0.05.

In the mid-thirties, HOVGAARD [11,12] continued his work on systems by extending his analysis to three dimensions. This involved

consideration of out-of-plane loading. He suggested that as far as deformation out-of-plane was concerned, a pipe bend could be treated by the normal beam theory except for secondary effects of rotation in the plane of the bend due to the out-of-plane loading. By analysing several configurations he suggested that secondary effects of this nature could usually be neglected. There is in fact a primary effect of out-of-plane loading which was analysed properly later.

At around this time a steadily expanding literature on the analysis of piping systems arose, beginning with the simpler cases and extending to complicated three dimensional multi-branch systems. MARKL [13] gives over a hundred references to such works.

At about the same time THULOUP [14,15,16] published the first successful investigation of the combined loading effects of in-plane bending and internal pressure. His method was similar to that of Kármán, except that he specified the radial rather than the tangential component of displacement. Using one term in his solution, he obtained the following flexibility factor:

$$K_1 = \frac{10 + 12\lambda^2 + 48\$}{1 + 12\lambda^2 + 48\$} \qquad \ldots \quad (1.11)$$

$$\text{where } \$ = \frac{pr}{Et}\left(\frac{R}{t}\right)^2$$

This equation reduces to Kármán's first approximation for zero internal pressure.

In 1936, TUEDA [17] attempted to present a general solution to the pipe bend problem. His analysis could accommodate arbitrary initial pipe profiles and removed the assumption of $R >> r$. The method was mathematically complex involving the use of a power series. In the

presentation, however, he restricted the analysis to circular cross-sections.

In 1943, KARL [18] published two analyses which were basically the same as those of Kármán and Lorenz using strain energy and complementary energy respectively. For the strain energy analysis, he provided the following expression for a "third approximation" flexibility factor:

$$K_3 = \frac{252 + 73912\lambda^2 + 2446176\lambda^4 + 28822400\lambda^6}{3 + 3280\lambda^2 + 329376\lambda^4 + 2822400\lambda^6} \quad \ldots \quad (1.12)$$

In the complementary analysis, Karl used up to four terms on his stress resultant series. With one term, the solution was identical to that of Lorenz. The flexibility factor with four terms was:

$$K_4 = 1 + \frac{3}{4^2} - \frac{[261 + 152304\lambda^4 + 11289600\lambda^6]}{[360\lambda^2 + 229792\lambda^4 + 2125863\lambda^6 + 180633600\lambda^8]} \quad \ldots \quad (1.13)$$

Karl was aware that the strain energy and complementary energy methods should give lower and upper bounds respectively, on the flexibility factor. However, for certain values of λ the lower bound factor (1.12) gives higher results than the upper bound (1.13). Although he seemed to appreciate that it had something to do with the $(1 - \nu^2)$ term, for some reason he included it in the upper bound analysis. The correct bound is obtained if the term is included in the strain energy solution. Karl also demonstrated that the inclusion of $(\frac{r}{R})$ in the complementary solution only marginally effected the results. His converged flexibility factors are included in Figure (1.4).

Although some attention has been given to the problem of out-of-plane bending by Hovgaard *et al.*, it was not until 1943 that VIGNESS

[19] published the first solution of this case. His analysis is exactly similar to Kármán's analysis. For the tangential displacement of the cross-section he assumed an expression of the form:

$$v = \sum_n A_n \cos(2n\phi), n=1,2,3 \ldots \quad \ldots \quad (1.14)$$

This displacement form is of the same form as for in-plane bending but simply removed by 45° (Fig. (1.5)). From the analysis, Vigness obtained a first approximation flexibility factor identical to Kármán's (1.2). The maximum meridional bending stress was also identical but its position was moved by 45°. Out-of-plane bending, however, introduces a new problem not displayed by in-plane bending. The out-of-plane moment does not remain constant along the length of the bend. Further, for a bend angle (excluding $\alpha = 180°$) the applied and reaction loads are different to maintain external equilibrium. For example, an out-of-plane moment becomes a pure torsion at a position 90° further along the bend. It will be shown that this simple type of analysis does in fact give reasonable comparison with experimental values at a particular section. The distribution, however, is not applicable along the full length of the bend.

In 1945, BESKIN [20], apparently unaware of the work of Lorenz and Karl, performed an analysis for in-plane bending starting from equilibrium considerations and an assumed series for the circumferential stress. He considered more terms in the series than Lorenz or Karl and was able to show how many terms were necessary for a converged solution for a specified accuracy. Beskin also repeated the analysis for out-of-plane bending and showed that identical formulae are obtained for flexibility factors.

BARTHELEMY [21,22] generalised Kármán's theory for in-plane bending and Thuloup's method for combined bending and pressure. The effects of initial ovality were also considered in [22]. DE LEIRIS and BARTHELEMY [23] presented experimental evidence in support of [21] and [22], and later presented further work [24] which included the influence of thickness variations in the analysis. The authors were obviously well aware of the various effects and their importance, including the radius ratio, initial ovality, variable thickness and internal pressure, but although the work was comprehensive few results were presented.

HUBER [25] presented a solution to the problem of a smooth bend having an initially elliptical cross-section under in-plane bending. He derived a first approximation flexibility factor in terms of pipe parameters and elliptical functions which were evaluated in a separate publication [26]. For a circular cross-section his result reduces to:

$$K_1 = \frac{5.404 + 12\lambda^2}{0.5798 + 12\lambda^2} \qquad \ldots \quad (1.15)$$

This result is not the same as Kármán's first approximation, although it is not significantly different.

The advent of the Second World War resulted in significant advances in all fields of engineering. In the study of pipe bends this was depicted by the work of REISSNER [27], who in 1949 generalised the equations of rotationally symmetric thin shells and reduced these to the governing differential equations of a toriodal shell, under in-plane bending. These formed the basis of CLARK and REISSNER'S [28] solution for smooth curved tubes, under in-plane bending, using shell theory as distinct from energy methods. Trigonometric and asymptotic solutions were obtained from the equations. From the latter, the following expression was obtained for the flexibility factor:

$$K = \frac{1.65}{\lambda} \qquad \ldots \quad (1.16)$$

The maximum meridional stress was given as:

$$\bar{\sigma}_{\phi} = \mp \frac{1.892}{\lambda^{\frac{2}{3}}} \qquad \ldots \quad (1.17)$$

Clark and Reissner suggested a limit of applicability as $\lambda < 0.3$, although it can be used with reasonable accuracy up to $\lambda = 1.0$. They also obtained formulae for elliptical cross-section tubes.

In 1952, GROSS [29] and FORD [30] published the results of an extensive theoretical and experimental investigation of pipe bends. They considered the loading cases of in-plane bending and internal pressure and a combination of both. The case of out-of-plane bending was not examined. Their experiments were aimed principally at confirming the applicability of the existing theories for short radius bends, with λ values as low as 0.049. This low value of λ was achieved using a "lobster back" or mitre bend. They confirmed the need for the use of sufficient terms in the series solution at low values of λ. The radius ratio $(\frac{R}{r})$ was shown to have little effect on the flexibility factor. By using strain gauges on the inside and outside of the bend, they showed the existence of a small but significant meridional direct stress ($\sigma_{\phi D}$) and derived its value from equilibrium as:

$$\sigma_{\phi D} = -\frac{r}{R}\cos\phi \int_{\phi}^{\frac{\pi}{2}} \sigma_{\theta D} d\phi \qquad \ldots \quad (1.18)$$

where $\sigma_{\theta D}$ is the direct circumferential stress. This was added to the meridional bending stress obtained from Kármán's analysis and gave the maximum stress for a bend on the inside surface. This modification has become known as the "Gross Correction Factor". From their experi-

ments conducted on bends with combined bending and internal pressure they demonstrated that pressure causes a reduction in flexibility factor. Their work attracted a considerable amount of useful discussion and although omitting the case of out-of-plane bending, the author found both papers extremely comprehensive and clear. This was particularly so in regard to the experimental work, an aspect of the published literature not commonly encountered.

During the years 1956 and 1957, three important papers appeared dealing with combined bending and pressure.

KAFKA and DUNN [31] included the effect of pressure in a strain energy analysis by adding the work done by the pressure on the cross-section. The extra term was of a second order but nevertheless proved to be significant. The results of some experiments were also given showing reasonable agreement with their theory.

CRANDALL and DAHL [32] modified the shell approach of Clark and Reissner [28] to include the effect of internal pressure. As before, they obtained asymptotic and series solutions. The series solution gave similar results to those of Thuloup and to Kafka and Dunn. The asymptotic solution predicted lower flexibilities than the series solution, especially for higher pressures, but appeared to compare better with experimental results.

RODABAUGH and GEORGE [33] generalised the method given by Kafka and Dunn in [31] using a general displacement series for in and out-of-plane bending. For the radial displacement they assumed the following expressions:

$$\text{for out-of-plane bending:} \quad w = \sum_n A_n \sin(2n\phi), \; n=1,2,3\ldots$$
$$\text{for in-plane bending:} \quad w = \sum_n A_n \cos(2n\phi), \; n=1,2,3\ldots \qquad \ldots \quad (1.19)$$

For the case of zero pressure they defined the following number of terms necessary in the series to give an accuracy of 10%:

λ	n
≥ 0.5	1
0.4 - 0.16	2
0.12 - 0.08	3
0.06 - 0.04	4

With internal pressure they found the series to converge somewhat faster than indicated by the above values. They also gave graphical results in the form of a nomograph and presented experimental work to justify their analysis. The flexibility factors for both in-plane and out-of-plane bending were shown to be the same.

TURNER and FORD [34] in 1957 attempted an analysis for in-plane bending with as few assumptions as possible. Using a "strength of materials" approach they examined the effect of each assumption by including and removing the relevant terms in $(\frac{r}{R})$ and $(\frac{t}{r})$. They concluded that although stress distributions could be seriously in error, the flexibility factors and maximum stresses were unlikely to be in error by more than 5 to 10%.

FINDLAY and SPENCE [35] reported an experimental investigation conducted on a 6 ft 6 in. diameter, 90° smooth bend with a radius ratio $(\frac{R}{r}) = 2.94$ and a λ value of 0.107, under in-plane bending. The stress distribution at the centre of the bend showed good agreement with the theories of Kármán, Clark and Reissner and Turner and Ford. Their experimental flexibility factor was given as 12.8 which compares reasonably well with the following theoretical values:

Kármán 1st Approx.	8.93
Kármán 2nd Approx.	15.64
Kármán 3rd Approx.	16.15
Clark and Reissner	15.40
Turner and Ford	15.50

One interesting comment made by the writers in this paper concerns a criticism made of the vagueness regarding how flexibilities are measured and how there is surprisingly good agreement given in the literature beween experimental and theoretical values.

In 1966, JONES and KITCHING [36] conducted experiments on a 90° single mitre bend under various loading conditions including that of out-of-plane bending. The work was aimed principally at confirming existing design procedures. Using the KELLOG [37] formula they demonstrated that the flexibility factor for out-of-plane bending was significantly over-estimated, and presented a modification to this formula.

Smooth pipe bends are considered as a special case of mitred bends, and although the latter presents a more complex problem, it is evident that the same conclusion for out-of-plane bending applies also to the smooth pipe bend. Although this fact appears to have been hitherto neglected in the literature, it was appreciated by several previous authors. The main reason for the continuing use of an identical analytical approach to in-plane and out-of-plane bending is considered by this author to be due essentially to the complex nature of the out-of-plane problem. However, it does ensure simplification and conservatism in design and by what can be none other than "good fortune" the axisymmetric solution provides a reasonable approximation to the stress distribution, be it at one section, for both loading conditions.

JONES [38] reviewed the literature on smooth and mitred bends although the part relevant to smooth bends was very brief. In [39] he presented a generalisation of Kármán's original work. The assumption of $R >> r$ was removed and the radial displacement series was taken as:

$$w = \sum_n A_n \cos(n\beta), \quad n=2,3,4 \ldots \qquad \ldots \quad (1.20)$$

where $\beta = \phi - 90°$

Up to nine terms in the series were used and the earlier conclusions regarding the unimportance of the $R >> r$ assumption confirmed. Further discussion was also given on convergence and the relative insignificance of the odd displacement series terms, particularly for larger $(\frac{R}{r})$ ratios.

In 1967, SMITH [40] repeated for out-of-plane bending what Turner and Ford [34] had done for in-plane bending, again using a "strength of materials" type analysis. The approach and the assumptions correspond throughout. Smith considered that pure out-of-plane bending could occur at only one section, so that the solution was obtained for a very short arc length. The assumptions of $R >> r$ was not used as was the assumption $\frac{t}{2} << r$. His flexibility factors together with those of Turner and Ford for in-plane bending are reproduced in Figure (1.6). In presenting his flexibility factors, Smith plotted $K\lambda$ against λ. This shows a clear dependence on the radius ratio $(\frac{R}{r})$. However, if K is plotted against λ the dependence on $(\frac{R}{r})$ is not so apparent, and the results for in-plane and out-of-plane bending become virtually identical. Using the assumptions of Kármán, Smith was able to define a simplified flexibility factor as:

$$K = 1 + \frac{3}{4}\frac{(1-\nu^2)}{\lambda^2} \qquad \ldots \quad (1.21)$$

CHENG and THAILER [41] investigated in-plane bending using Clark and Reissner's method of analysis but included the $(\frac{r}{R})$ term in their solution. They further refined their analysis in a subsequent paper [42]. Both papers concluded that the inclusion of $(\frac{r}{R})$ had little consequence.

In 1970, Spence [4] examined the bounding characteristics of flexibility factors obtained from minimum total potential (or strain energy methods) and complementary energy methods. Spence, to some extent, resolved the dilemma concerning the $(1-\nu^2)$ term, stating that a true lower bound is only achieved from a strain energy type analysis if this term is retained in the flexibility factor. This paper also included the correction to Marbec's work mentioned earlier.

In 1971, BOND and KITCHING [43] presented a theoretical analysis associated with out-of-plane bending of multi-mitre bends. Using a strain energy analysis developed earlier by KITCHING [44] for in-plane bending, they were able to obtain reasonably accurate predictions for the stresses and flexibility of a multi-mitred bend of low λ value.

FINDLAY and SPENCE [45] published theoretical solutions for elliptical pipe bends under in-plane and out-of-plane bending. The results from their strain energy based method, demonstrate that ellipticity has a greater influence on out-of-plane bending. In [46], they extended their solution to bends of elliptic cross-section with thickness variations, and concluded that normally accepted values of thinning have virtually no effect on flexibility.

In 1972, DODGE and MOORE [47] presented a generalisation of Rodabaugh and George's method [33] for in-plane bending, out-of-plane bending and internal pressure. They also included the Gross

correction factor in the meridional peak stresses. A computer program for detailed analysis of pipe bends, based on the work in [47] was given in [48]. This program "ELBOW" was used to obtain the comprehensive set of results given in [47]. Typical results, for zero internal pressure and λ values of 0.10 and 0.25 are shown in Figure (1.7) for in-plane and out-of-plane bending. This interesting type of stress distribution around the cross-section of such a common place simple looking component was in fact one of the main attractions which drew this author to the study of pipe bends.

In the same year, BLOMFIELD and TURNER [49] published a further contribution on the same topic. From the theory of thin shells they derived a solution for the in-plane and out-of-plane bending of pipe bends. Included in this solution was a correction for the coupling effect of internal pressure. Their theoretical results showed good comparison with the work of Rodabaugh and George [33], Turner and Ford [34] and Gross and Ford [30]. The results presented, however, were limited to in-plane bending and a combination of this and internal pressure.

KITCHING and BOND [50] examined the out-of-circularity effects in a pipe bend when subjected to in-plane bending and internal pressure. Under internal pressure the out-of-circularity was found to produce a non-linear elastic behaviour.

In 1973, ROBERT and DUFORET [51] presented an analysis for the smooth pipe bend subjected to in-plane and out-of-plane bending. Based on thin shell theory, their analysis considered axisymmetry for the case of in-plane bending. For out-of-plane bending they produced a mathematical model based on "beam theory" in the circumferential

direction and "shell theory" in the meridional direction. Although the authors give a clear description of their tensorial shell theory the paper lacks detailed results. The writer found this disappointing in view of the fact that the authors in their opening paragraph state that there is a lack of theoretical results for the case of out-of-plane bending. The results that are presented are shown to give reasonable comparison with the experimental work of SMITH and FORD [52].

SEAMAN and WAN [53] presented a solution, similar to that of Clark and Reissner [28], for the lateral bending and twisting of thin-walled curved tubes. Using shell theory, trigonometric and asymptotic solutions were obtained. In an asymptotic solution for lateral bending with $(\frac{r}{R})^2 << 1$, the flexibility factor was shown to be the same as that developed in [28], i.e.:

$$K = \frac{1.65}{\lambda}$$

Seaman and Wan also investigated the case of a tube with a circumferential slit. Their results showed that the overall torsional flexibility was increased by an order of magnitude whereas the flexural flexibility was not changed by more than 50%.

THOMPSON [54] attempted an "exact" solution to the problem of a smooth curved pipe under in-plane bending. His method involved a matrix solution of the thin shell equations with prescribed displacement series. The work was intended as a prelude to an investigation of the influence of end constraints.

More recently, ARAV [55] investigated the effect of local corrugations in a smooth pipe bend subjected to in-plane bending. From experiments he was able to develop a simple theoretical model which gave

reasonable comparison with the measured stresses local to the corrugations. Tests on such bends had been made as early as 1932 by COPE and WERT [56] and in fact over 20 years earlier was the basis of Bantlin's [2] explanation for the increased flexibility.

1.2.2 Considerations Other Than Linear Elasticity

1.2.2.1 Elastic plastic behaviour

In 1966, MARCAL and PILGRIM [57] developed a computer program based on a stiffness method for the analysis of elastic-plastic shells of revolution with axisymmetric loading. A year later in 1967, MARCAL [58] extended the computer program to deal with the case of a smooth pipe bend under in-plane bending. He gave the relationship between the applied bending moment and the elastic-plastic strains up to a maximum value of 6%. Collapse moments were also given which compared favourably with the experimental results given by Gross and Ford [30].

BOLT and GREENSTREET [59], in 1971, presented an experimental investigation on the plastic collapse loads of pipe bends under both in-plane and out-of-plane bending, with and without internal pressure. They made no attempt to compare their results with theoretical computations.

In 1973, VRILLON, ROCHE and BAYLAC [60] conducted experimental work on a 90° bend of elliptical cross-section subjected to internal pressure. The bend was essentially a single mitred bend. Under this loading they considered the collapse load, bursting load and shakedown. Using finite element analysis they obtained good agreement between the experimental and calculated values of collapse load.

SPENCE and FINDLAY [61] calculated theoretical limit moments for in-plane bending of smooth circular pipe bends. In their analysis they adopted two methods. In the first method they used MARCAL and TURNER's [62] approach of utilising a linear elastic analysis as a means of estimating the limit load. For the elastic analysis the asymptotic solution of Clark and Reissner [28] was used. The results obtained from

this method were compared with an approximate limit moment derived from a creep analysis [63] using a Norton power law. The ratio of the limit moment to first yield m_L is found from:

$$m_L = \frac{\text{maximum meridional stress } (n=1)}{\text{maximum meridional stress } (n=\infty)}$$

where n = index in creep law

A year later, CALLADINE [64] obtained limit moments by working directly from a Mises yield surface with the same elastic solution used by Spence and Findlay. Calladine's results are surprisingly high for a lower bound when compared with the bounds given by Spence and Findlay in [61].

MELLOW and GRIFFIN [65] presented further results for in-plane bending collapse loads using the finite element program MARC [66].

VRILLON, MONTFORT and BEFRE [67] conducted experimental work on 180° pipe bends subjected to in-plane bending. Collapse loads compared well with their finite element analysis. In the opening mode the collapse load was found to be higher than in the closing mode. They attributed this difference to the "out of roundness" of the cross-sections. The term "out of roundness" here refers to the resultant distortion of the cross-section following loading, and not an initial out-of-roundness. The distorted shape for opening and closing modes in in-plane bending is shown in Figure (1.8). When large displacements are encountered it is clear that the increased stiffness in the opening mode is the result of an increase in the depth of the cross-section.

In 1977, SPENCE and FINDLAY [68] extended their work to bends with non-circular sections. Their results showed that initial ovality

introduced by modern manufacturing processes should have little effect on the value of the limit load.

SOBEL and NEWMAN [69] conducted experiments on a 90° pipe bend subject to in-plane bending. Using the "MARC 17" element [108] they obtained good agreement with experimental values of collapse moment.

MOORE [70] examined the plastic limit moment of a smooth pipe bend under in-plane bending. Using a lower bound solution he obtained reasonable agreement with experiment. One interesting aspect of this work was the technique employed in manufacturing the pipe bends to provide acceptable geometrical tolerances.

In 1981, PROST and AMZALLAG [71] conducted a series of tests on a variety of bend angles subjected to in-plane, out-of-plane bending and internal pressure. For 90° bends the load deflection curves indicated the out-of-plane bending case to lie midway between that of in-plane bending opening and closing. Internal pressure or a decrease in bend angle was found to increase the plastic collapse moment.

BRASCHEL, RICHTER, ZEITNER and RICHTER [72] examined the load carrying capacity of pipe bends with attached straight sections of pipes. They used a simplified analysis to determine the limit moment under in-plane bending. From a non-linear analysis using their NISA computer program [73] they obtained good comparison. This was further verified by their experimental results.

PROST, TAUPIN and DELIDAIS [74] examined the plastic behaviour of pipe bends under in-plane, out-of-plane bending and pressure.

SOBEL [75] utilised the SOUTHWELL [76] method for predicting plastic buckling loads for pipe bends.

During the last ten years a number of "elements" for the plastic analysis of pipe bends have been developed and implemented in finite element computer programs. A few of these are listed in [77 to 82]. The major problem, however, is the high cost and time involved in obtaining a solution, which in turn has restricted published data to a few examples.

1.2.2.2 Fracture and fatigue

Fatigue tests on pipe bends were performed as early as 1935 by DENNISON [83]. Later, during the 1940's and 50's further experimental studies were carried out by ROSSHEIM and MARKL [84], MARKL [85,86] and LANE [87].

The work by Markl reported in [85] is worthy of mention since it contains the results from over 400 fatigue tests on piping components, including pipe bends.

In 1969, BLOMFIELD and JACKSON [88] used an elastic plastic computer program with the relevant material property data to predict the low-cycle fatigue lifes of cupro-nickle pipe bends. Blomfield presented further results in [89].

UDOGUCHI and ASADA [90] published an investigation on the low-cycle fatigue strength of piping components. They conducted tests on branch pipe connections and pipe bends under in-plane bending. Their work was aimed principally at investigating more reliable design procedures for piping components under cyclic loading with practical applications to the nuclear industry. In a supplement to this paper they also presented results from fatigue tests conducted on a 90° mitre bend. A similar series of tests was reported by ANDO, YAGAWA *et al.* [91].

The low cycle fatigue of some nuclear piping components was examined by HEALD and KISS [92]. They presented the results of fatigue tests conducted on 26 components including elbows, tees and girth butt welds.

JAMES [93] employed fracture mechanic techniques to estimate crack extension in piping elbows.

DOYEN and MARINI [94] published the results of fatigue tests conducted on pipe bends. Their investigation was primarily concerned with defects in the seam welds at the intrados and extrados of bends made in halves.

1.2.2.3 Inelastic and creep behaviour

In 1957, KACHANOV [95] investigated the effect of creep on pipe bends under in-plane bending. Using a complementary energy method with a creep power law, Kachanov derived upper bound, second approximation, flexibility factors.

SPENCE and MACKENZIE [96] considered the same problem using strain energy and developed lower bound, first approximation, flexibility factors. The secondary creep law used in their analysis was that postulated by NORTON [97] given by:

$$\dot{\varepsilon} = B\sigma^n$$

where $\dot{\varepsilon}$ is the strain rate and B and n are material constants. The index "n" is often referred to as the creep index. The flexibility factors obtained from both methods were shown to be dependent on the creep index and the pipe factor. In 1969, SPENCE [98] extended his earlier work to include up to five terms in his displacement series. A subsequent

paper [99] presented an upper bound analysis. The flexibility factors from the upper and lower bound analyses of Spence are shown in Figure (1.9). They clearly demonstrate that creep flexibilities can be considerably higher than those of an elastic analysis. In his doctoral thesis, SPENCE [100] details his previous work together with improvements to the upper and lower bound analyses. Stress distributions, maximum stress factors and reference stresses are all presented in some detail. Some of the work developed in [100] was subsequently presented in [101] and [63]. Work on the creep of pipe bends with elliptical cross-section contained in [100] was expanded in [102], [103] and [104]. Further work by Spence on creep in short radius bends was presented in [105]. These publications gave factors for stresses and flexibilities for a range of geometries suitable for design.

In 1973, WORKMAN and RODABAUGH [106] examined the effect of creep on a piping system operating at high temperature with particular interest focused on pipe bends. They reviewed the earlier work of Kachanov and Spence but failed to notice Kachanov's typographical error in stating the pipe factor as $\sqrt{Rt}/_r$ and failed to appreciate the reason for the inclusion of the $(1-\nu^2)$ term in Spence's lower bound analysis. In the discussion to [106], Spence pointed out these errors and further errors in their work. Workman and Rodabaugh published another paper [107] a year later.

Between 1973 and 1975 several attempts at a finite element solution to the creep problem were published [77,108,109]. However, results are only available for a few typical geometries which were of particular interest to the respective authors.

In 1975, BOYLE [110] presented a dissertation on rational creep mechanics with further work on pipe bends. He approached the problem using a numerical solution to the non-linear thin shell equations developed in [110]. Boyle compared the non-linear elastic solution of pressurised curved tubes with the earlier work which included only non-linear terms involving the pressure. His results suggest that the linear analysis could be in error for high ratios of bending moment to pressure [111]. Boyle also performed a redistribution analysis to examine transient creep in pipe bends. An important conclusion from his work was that the steady state results of Spence were verified.

In 1976, BOYLE and SPENCE [112] developed an analysis for out-of-plane bending of a curved pipe in creep. A solution was achieved by minimising the total potential energy rate. To account for the effect of a bending and torsional moment their results were presented in terms of an "energy factor" as opposed to a flexibility factor. Boyle and Spence published two further papers in 1977, the first [113] on the redistribution analysis contained in [110] and the second [114] on the creep analysis of piping systems.

GRIFFITH and RODABAUGH [115] published results of creep tests conducted on 4 inch, schedule 10, pipe assemblies.

IMAZU *et al.* [116] reported the results of tests conducted on 12 inch, schedule 20, type 304 stainless steel pipe assemblies. Their comparison between the experimental results and the finite element solution was disappointing. The authors attributed the difference to the choice of the material constitutive equation and the influence of the tangent pipe end constraints.

In 1979, IMAZU and NAKUMURA [117] developed two simplified creep buckling analyses of pipe bends under in-plane bending. The two methods gave comparable results and showed some correlation with experiments. The simpler of them was based on Spence's results for elliptical bends by updating the flattening of the cross-section as creep proceeded.

WATANABE and OHTSUBO [118] examined the creep behaviour of pipe bends under in-plane bending using a simplified version of their finite ring element. Their results confirmed the earlier work of Spence and Kachanov for elastic stationary creep.

In recent years, an attempt has been made to establish an international library of benchmark solutions to the creep problem to provide a standard against which computer programs could be verified [119,120].

BOYLE and SPENCE [121] presented a state-of-the-art review of inelastic analysis method for piping systems. A detailed discussion is given of the various simplified approaches to the problem [see also 122,123,124,125]. They also compared the results of inelastic computer programs against available benchmark data. More recently in an attempt to supplement the simplified methods given in [121] a series of tests has been conducted by this author on a variety of stainless steel, type 316, pipe bends. This work and the work of other foreign establishments will be discussed more fully in PART (2) of this thesis.

1.3 Smooth Pipe Bends with End Effects

This section will be concerned principally with publications which contribute information to the study of smooth curved pipes with end constraints. Although the main text of this work is aimed at out-of-plane bending the omission of in-plane bending would severely limit the number of relevant publications. More importantly, it would do little justice to the development of the problem. As such, both types of loading will be considered with the emphasis being placed later on out-of-plane bending.

Two types of end constraint are generally encountered:

(i) flanges
(ii) tangent pipes

These constraints are illustrated in Figure (1.10).

In the subsequent analysis combinations of these two types of end constraint will also be considered. Depending on their capacity to resist distortion the flanges themselves can be considered as "thick" or "thin". Although specific boundary conditions apply to each flange type the actual specification of a thick or thin flange in practice is not so clear. This is an important aspect to bear in mind when examining the work of other authors.

As early as 1945, SYMONDS and VIGNESS in the discussion to Beskin's paper [20] presented some experimental evidence which demonstrated the importance of end effects. For a pipe bend subjected to in-plane bending with a pipe factor $\lambda = 0.043$ and radius ratio $(\frac{R}{r}) = 3$, they gave the following flexibility factors:

bend angle	type of constraint	flexibility factor K
180°	long tangent pipes	37
90°	tangent pipes	32
90°	one flange and one tangent pipe	18
90°	two flanges	8

The flexibility factor from a theory without end effects, like that given in equation (1.16) would be 38.4. The most severe form of constraint was clearly flanges which substantially reduces the flexibility. Tangent pipes had some influence particularly at smaller bend angles. In the case of out-of-plane bending they found the flexibility factor to be dependent on how the loading is applied and also which deflection is measured.

In 1951, PARDUE and VIGNESS [126] published the results of an extensive investigation into the effect of end constraints on short radius bends confirming their earlier conclusions. A more comprehensive report was published two years later [127]. Unfortunately, the author has been unable to access this paper. Pardue and Vigness investigated bends with subtended angles of 180°, 90°, 45°, with two tangent pipes, one tangent pipe plus one flange and two flanges. A variety of loading conditions was examined including that of out-of-plane bending. Several of their conclusions are worth stating at this stage. They concluded that flexibility factors and stresses for bends where end constraints are important depend on the pipe factor (λ), bend angle (α), radius ratio ($\frac{R}{r}$) and the type of loading. Under out-of-plane loading, experimental flexibility factors and stress factors for a 90° bend under various end constraints were presented. The results for flexibility factor are

shown in Figure (1.11) and show clearly the stiffening effect of the flanges. The flexibility factors presented in [126] were based on average values* and were derived from a flexibility factor where the nominal rotation (γ_o) referred to a curved pipe as opposed to a straight pipe as defined earlier in this chapter. The relationship between this flexibility factor and that defined herein for a bend angle of 90° and 180° can be written as:

$$K = \tfrac{1}{2}[K_{PV} + (1+\nu)]$$

where K = flexibility factor defined herein
K_{PV} = flexibility factor defined in [126] . . . *(1.22)*

The reduced flexibility factors defined by equation (1.22), assuming poisson's ratio (ν) = 0.3 are also shown in Figure (1.11) for the case of the flanged bend. These experimental flexibility factors for a flanged bend would appear to be the only reported results for this loading case.

Gross and Ford [30] in their experimental study determined the variation of the distortion along the bends with flanged tangents. The flattening was shown to progressively decrease away from the centre section of the bend and along the tangent pipe. In the communication to [30], Pardue and Vigness published further stress and flexibility factors for flanged bends. They also pointed out that for in-plane bending the maximum meridional stress factor ($\hat{\bar{\sigma}}_\phi$) shifted from midway between the intrados and extrados, towards the intrados as the bend length decreased and the end constraints became more rigid. Thus further discrepancies were shown to exist between the axisymmetric theories and experiment.

---

*Pardue and Vigness in fact conducted a large number of tests under various loadings and in an attempt to condense the results average values based on similar loadings were presented.

In 1955, VISSAT and DEL BUONO [128] reported tests on twelve 180° short radius bends with both flanged and tangent pipe terminations. The loading was limited to in-plane bending and only a small difference was observed between the results of different end effects. In their discussion to this paper they speculate that this small difference may have been due to the relatively thicker walled specimens used. There is, however, some doubt to be expressed in the effectiveness of their flange ring producing the flanged condition on the bend.

In 1966, Findlay and Spence [35], pointed out that since the change in diameter showed a significant variation along the bend then the flexibility would probably vary in the same manner. This has implications for experimental flexibility factors since they will be an average of the flexibility along the bend and possibly along the tangent pipes. A year later in 1967, Smith and Ford [52] suggested an empirical formula for the variation of the flexibility factor for 90° bends.

KALNINS [129,130,131] developed a numerical method for the analysis of thin shells. The technique involved multi segment integration and finite difference solution of the thin shell equations. In [131] Kalnins compares his results with the experimental results of a 90° bend with tangent pipes taken from JACOBS and SUROSKY [132]. For both in-plane and out-of-plane bending the comparison is good. One main advantage in this method is that it allows end effects to be included anywhere in the system. However, the cost of running the computer program has prevented it from being run for a comprehensive set of parameters.

In 1970, THAILER and CHENG [133] published a theoretical solution for a 180° bend with flanged ends under in-plane bending.

They selected results from the experiments of Pardue and Vigness which gave rough agreement with their theory.. In their analysis Thailer and Cheng neglected the shear strain term in their expression for the total potential energy. Further, they ignored the boundary condition of zero slope at the flange. The significance of this will become apparent later; however, it can be interpreted that their solution is applicable only to "thin" flanges and not "thick" flanges. This and other anomalies were later highlighted by THOMSON [134].

NATARAJAN and BLOMFIELD [135,136,137] reported a significant contribution to the subject of pipe bends with end constraints, and was perhaps the earliest publication on the use of the finite element method dealing with this problem. They provided flexibility factors and stresses for a variety of end constraints and a relatively wide set of geometrical parameters. An unfortunate limitation of this work and of some other finite element solutions is their inability to contend with a bend with two flanges, the problem being the specification of the necessary boundary conditions for the loaded flange.

In 1973, IMAMASA and URAGAMI [138] published an experimental study of pipe bends with end effects. They examined the loading conditions of in-plane, out-of-plane loading and internal pressure. Using a finite element program [139] they obtained relatively good comparison with their experimental results. In their experiments on a 90° bend with one tangent and one flange the highest stresses under in-plane bending occurred adjacent to the flange and not at the position of maximum ovalisation nearer the centre of the bend. Interestingly, the same result was obtained by Natarajan and Blomfield mentioned earlier. However, they considered this as a singularity in their solution and placed no significance on it.

In the same year, FINDLAY [140] published a dissertation on the effect of end constraints on pipe bends. Most of his work concerned flanged bends under in-plane loading. Findlay developed a total potential energy based theory similar to that of Thailer and Cheng with specified displacements satisfying the boundary conditions of a rigid flange. He compared his results with experiments conducted by himself and others and concluded that his solution was satisfactory. Later, however, Thomson [134] was able to detect a fatal flaw in Findlay's computer solutions which together with other anomalies shed some doubt on Findlay's work. The work was also published by FINDLAY and SPENCE in [141,142,143].

In 1974, AKSEL'RAD and KVASNIKOV [144] developed a "semi-moment" theory for curvilinear bar-shells and as an example dealt with the problem of flanged bends. They give a first approximation formula for the flexibility factor but no stress results. Aksel'rad later published a similar contribution [145] but this time his name was translated as AXELRAD.

WRIGHT, RODABAUGH and THAILER [146] performed a finite element analysis on a tapered bend with one flange and one tangent pipe using the MARC program. They also used the program of Kalnins [131] but found that the total moment acting on each cross-section varied significantly along the bend. They also discovered that the stress at the centre of the bend continued to increase with increasing tangent pipe length to values well above that predicted by theories without end effects. This casts some doubt on the earlier work of Kalnins.

SOBEL [147] suggested guidelines for the use of the MARC finite element program on pipe bends with end effects. Detailed results are given for a single elbow with two short tangent pipes.

RODABAUGH, MOORE and ISKANDER [148] obtained some results for bends with connected tangent pipes using the EPACA finite element program [149].

KANO, IWATA, ASAKURA and TAKEDA [150] compared the results for the ANSYS [151], ASKA [152] and MARC [66] finite element programs for pipe bends with tangent pipes subjected to in-plane and out-of-plane bending. Overall the stress comparisons were poor. For both in-plane and out-of-plane bending they obtained stress discontinuities at the junction of the bend and the tangent pipe. They concluded that it is necessary to use higher order elements for an accurate analysis.

OHTSUBO and WATANABE [153,154] developed a finite element model in the form of a ring. The ring element used trigonometric series in the meridional direction and Hermitian polynomials in the circumferential direction. Smooth pipe bends with tangent pipes were assembled as in the multi-mitre bend by connecting several elements together. They presented some results for 90° bends with tangents and for bends with varying thickness, but without end effects.

In 1978, WHATHAM [155] published a theoretical analysis of flanged pipe bends under in-plane bending. He used NOVOZHILOV's [156] four parameter method to solve the governing differential equations of the thin shell. In 1979, WHATHAM and THOMPSON [157] extended their work to bends under in-plane bending with flanged tangents of any length.

In 1979, BROUARD, TREMBLAIS and VRILLON [158] conducted tests on 180° and 90° bends with tangent pipes and flanges. The bends were loaded into the plastic regime with large displacements. Under in-plane bending the effect of flanges was found to be most severe on the smaller 90° bends.

KANO *et al.* [159] examined three elbow-pipe assemblies under various loadings using the FINAS finite element system [160].

TAKEDA *et al.* [161] and BATHE and ALMEIDA [162] proposed two further finite elements for pipe bends with end effects.

KWEE [163] analysed a bend with varying pipe radii using the ASKA finite element program [152].

In 1980, Thomson [134] published a dissertation on the effect of end constraints on smooth pipe bends subjected to in-plane bending. He considered both the flanged and tangent pipe termination, the latter being of any length. Thomson's analysis, which is the basis of the writer's work, is based on a strain energy approach using a version of the thin shell equations of Novozhilov [156] into which suitable displacement functions are substituted for both the "rigid" and "distortion" displacement components. His solution incorporates an elegant matrix technique whereby the minimisation and integration is performed. Thomson's results for flexibility factor are lower than those of Axelrad and Whatham, around 10%, which is consistent with his lower bound energy solution. In comparing his work with that of Findlay and Thailer and Cheng, Thomson was able to show that both solutions contained assumptions which his analysis had shown to be invalid. In particular, he highlighted the dependence on the radius ratio ($\frac{R}{r}$). The work was also published by THOMSON and SPENCE [164].

In 1981, NATARAJAN and MIRZA [165] presented a finite element with specific application to out-of-plane bending. The end constraints of two tangents and one flange plus a tangent pipe were examined. They concluded that accurate values of flexibility factor were only important when the length of the tangent pipes was small.

THOMAS [166] investigated 90° bends terminated by tangent pipes. Using the STAGSC finite difference program [167] the effect of decreasing the length of one tangent pipe was examined under the loading conditions of in-plane and out-of-plane bending.

WHATHAM [168,169,170,171] presented further work dealing with flanged end constraints subjected to a variety of loading conditions including that of internal pressure and out-of-plane bending. This work together with his earlier work was incorporated in a series of computer programs [172,173,174]. Whatham appears to be the only author who has published work on the case of out-of-plane bending on flanged bends. Although Whatham considers a fairly comprehensive set of loading conditions the end constraint of tangent pipes is examined under in-plane bending only. Whatham's work will be discussed in more detail later. His results and those of other researchers are shown in Figure (1.12). Whatham's results for out-of-plane bending are presented in the form given by equation (1.22).

ÖRY and WILCZEK [175] presented a solution for in-plane bending using the semi-membrane theory in a transfer matrix method [176]. Their results are compared with the experimental results of Gross and Ford [30] and show good agreement. Further developments of the method propose the loading conditions of internal pressure and out-of-plane bending.

THOMSON and SPENCE [177] extended their work on in-plane bending of flanged pipe bends to include the effect of internal pressure. A solution to this combined loading case, using finite element methods

was also published by NATARAJAN and MIRAZ [178]. The few results presented, however, were of poor quality. Further, they failed to state the value of pressure applicable to the results.

In a paper by MILLARD and RICARD [179] the loading condition of in-plane bending is examined using the computer program TEDEL [180]. A review of the current situation of the work on end effects is also presented in this paper. This is reproduced in Table (1.1). Table (1.1c) shows that the analytical problem of out-of-plane bending on flanged bends has not been addressed. The authors, however, have failed to include the later work of Whatham.

In summary, it may be said that although the literature abounds with solutions on in-plane bending for a variety of end constraint conditions it is only in recent years that the problem of out-of-plane bending has been seriously considered. Even here, as typified by the work of Whatham, the problem still remains secondary to that of in-plane bending. The solutions based on finite element analysis, which comprise the bulk of the work, are limited in the type of end conditions considered, neglecting the problem of the flanged bend. In the author's view, there are two main reasons for the omission of this solution. Firstly, it would appear that significant difficulties are encountered in formulating the boundary conditions at the loaded end, although it is unlikely that this problem will remain unresolved for long. Secondly, and perhaps more importantly, the development of most finite element programs dealing specifically with pipe bends is associated with the nuclear industry where such end constraints do not usually occur.

TABLE (1.1A): Experimental work [179].

Authors	Ref.	Bend angle	End effects			Loads		
			flanges	straight parts	reversed elbows	in plane	out-of-plane	pressure
SYMONDS PARDUE	189	90°	✓	✓		✓		
PARDUE VIGNESS	190	45°, 90°, 180°	✓	✓		✓	✓	
IMAMASA URAGAMI	138	90°		✓		✓	✓	✓
		40°, 50°, 60°, 90°	✓	✓		✓	✓	✓
FINDLAY SPENCE	141	45°, 90°, 100°	✓			✓		
BROUARD TREMOLAIS VRILLON	158	90°	✓	✓		✓		
		180°	✓	✓		✓	✓	
BROUARD MILLARD TOMASSIAN	191	90°		✓		✓		
		180°		✓		✓		

TABLE (1.1B): Computational work [179].

Authors	Ref.	Bend angle	End effects			Loads		
			flanges	straight parts	reversed elbows	in-plane bending	out-of-plane bending	pressure
KANO *et al.*	150	90°		✓		✓	✓	
SOBEL	147	90°		✓		✓		
NATARAJAN BLOMFIELD	137	90°	✓	✓		✓		
		30°, 90°, 180°		✓		✓		
		90°			✓	✓		
WRIGHT RODABAUGH THAILER	137	50° with variable thickness		✓		✓		
RODABAUGH ISKANDER MOORE	148	45°, 90°, 180°		✓		✓	✓	
OHTSUBO WATANABE	154	90°		✓		✓	✓	
NATARAJAN MIRZA	165	from 10° to 90°		✓			✓	
		90°	✓	✓			✓	

TABLE (1.1C): Analytical work [179].

Authors	Ref.	Bend angle	End effects			Loads		
			flanges	straight parts	reversed elbows	in-plane	out-of-plane	pressure
THAILER CHENG	133	180°	✓			✓		
FINDLAY SPENCE	142	Any	✓			✓		
THOMSON SPENCE	164	Any	✓	✓		✓		
WHATHAM THOMPSON	157	90°, 180°	✓	✓		✓		✓
MILLARD ROCHE	192	Any	✓	✓		✓		

1.4 Current Design Codes

The two most commonly employed British design codes are BS.806 [181] and BS.3351 [182] for land boilers and petro-chemical plant respectively. BS.806 was re-written in 1975 and includes a relatively extensive section on the flexibility and stressing of smooth pipe bends. A graphical presentation was used for the various stress and flexibility factors, the latter including a small variation with radius ratio. The stress factors were also slightly different for in-plane and out-of-plane bending. Correction factors were given for bends with one or two flanges within (4r) of the bend-tangent junctions. Although these were given on a graph, they can be found from the following formulae:

$$\begin{aligned} &\text{One flange, correction factor} = \lambda^{\frac{1}{6}} \\ &\text{Two flanges, correction factor} = \lambda^{\frac{1}{3}} \end{aligned} \qquad \ldots \quad (1.22)$$

No other form of end constraint was considered.

BS.3351 suggests the following flexibility and stress factors for bends without end effects:

$$K = \frac{1.65}{\lambda} \qquad \text{and} \qquad \hat{\bar{\sigma}} = \frac{0.9}{\lambda^{\frac{2}{3}}} \qquad \ldots \quad (1.23)$$

This flexibility factor is the same as that given by Clark and Reissner [28] in equation (1.16). The stress factor is similar to the Clark and Reissner asymptotic formula for the peak circumferential stress factor, which is virtually half the peak meridional stress factor given in equation (1.17). The reason for the use of the circumferential rather than the meridional stress factor is due to a peculiar continuing argument as to which is most likely to cause failure. BS.806 gives graphs of both stress factors and requires that the maximum stress range for combined

loading must satisfy certain limits. Pardue and Vigness [126] suggested that the circumferential stress factors, being constant through the wall thickness, were the most important design stresses but in the discussion which followed [126], Gross and Ford suggested that an equivalent (combination of meridional and circumferential factors) stress factor should be used as indicated by Hovgaard [11], and Markl further suggested that failure was due to either meridional or circumferential factor, whichever was the greater. Markl's suggestion was based on the results of fatigue tests given in [85]. BS.3351 also uses the correction factors given by equation (1.22) for bends with flanges.

Perhaps the most detailed British design data for smooth bends is that of the "Engineering Sciences Data Unit" (E.S.D.U.) [183]. This provides graphs for flexibility, meridional stress and equivalent stress factors, for bends with connected tangent pipes under in-plane bending. The results are based on the work of Natarajan and Blomfield [136] using finite element analysis. The effect of flanged end constraints under in-plane bending is given by E.S.D.U. in [184]. The results given here for flexibility factors and stress factors are based on the work of Thomson [134]. E.S.D.U. is the only current code which considers the tangent pipe as an end constraint. However, the loading conditions are limited to in-plane bending and do not consider the case of out-of-plane bending.

Numerous American standards are available [185,186,187,188] which give the same stress and flexibility factors as BS.3351. They also incorporate the flange corrections given by equation (1.22), i.e. for a bend with two flanges:

$$K = \frac{1.65}{\lambda^{\frac{2}{3}}} \qquad \ldots \quad (1.24)$$

and $\hat{\bar{\sigma}} = \frac{0.9}{\lambda^{\frac{1}{3}}}$ . . . *(1.25)*

It is believed that these flange corrections are largely based on the work of Pardue and Vigness [126].

To summarise the current design codes, in the context of end constraints, it is noted that for in-plane bending all of the codes, excepting E.S.D.U., suggest the correction factors given by equation (1.22). In the case of out-of-plane bending there is little guidance excepting that associated with the in-plane bending conditions.

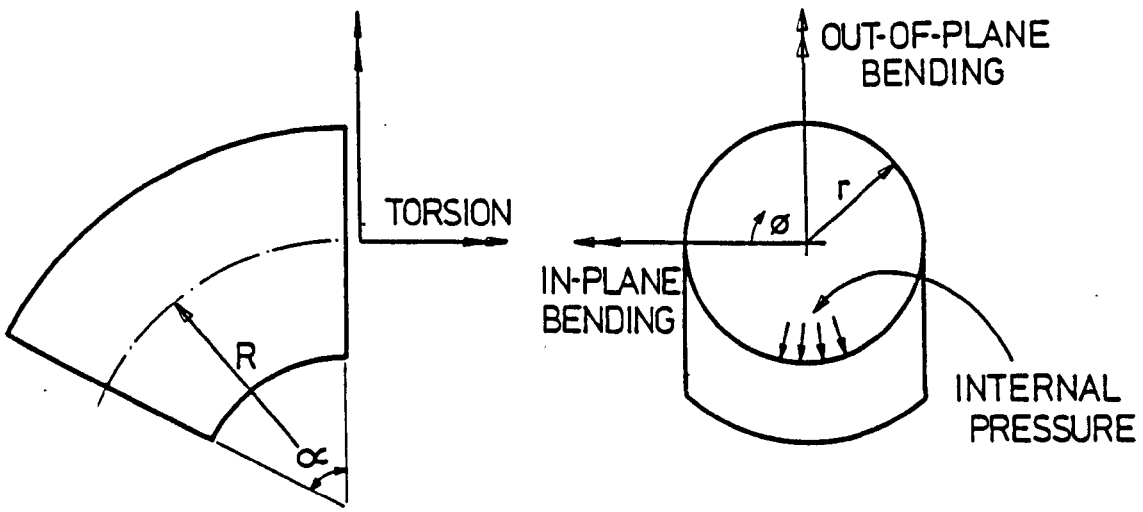

BEND LOADINGS

FIG. 1.1

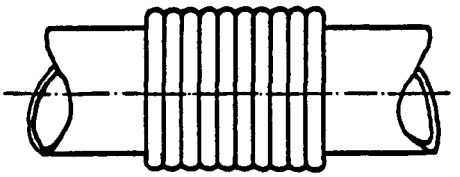

BELLOWS EXPANSION UNIT

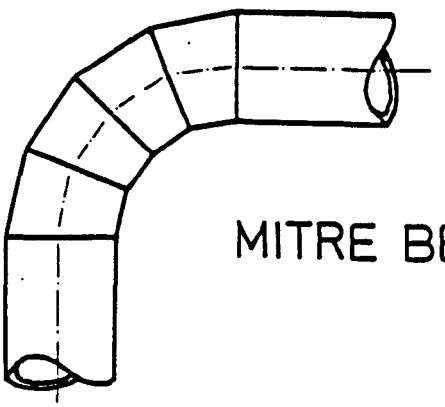

MITRE BEND

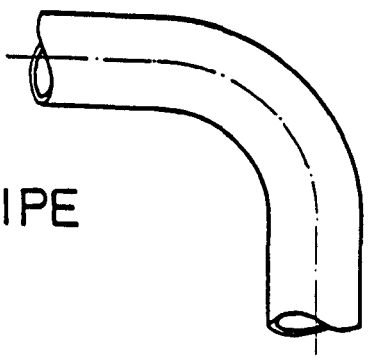

SMOOTH PIPE
BEND

PIPEWORK COMPONENTS

FIG. 1.2

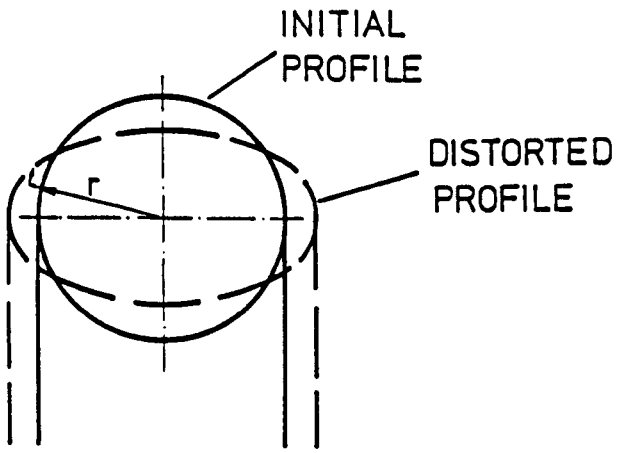

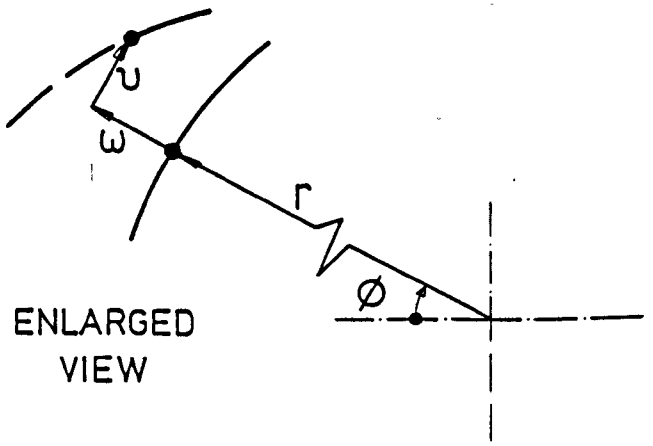

DISTORTION OF CROSS-SECTION
IN-PLANE BENDING

FIG.1.3

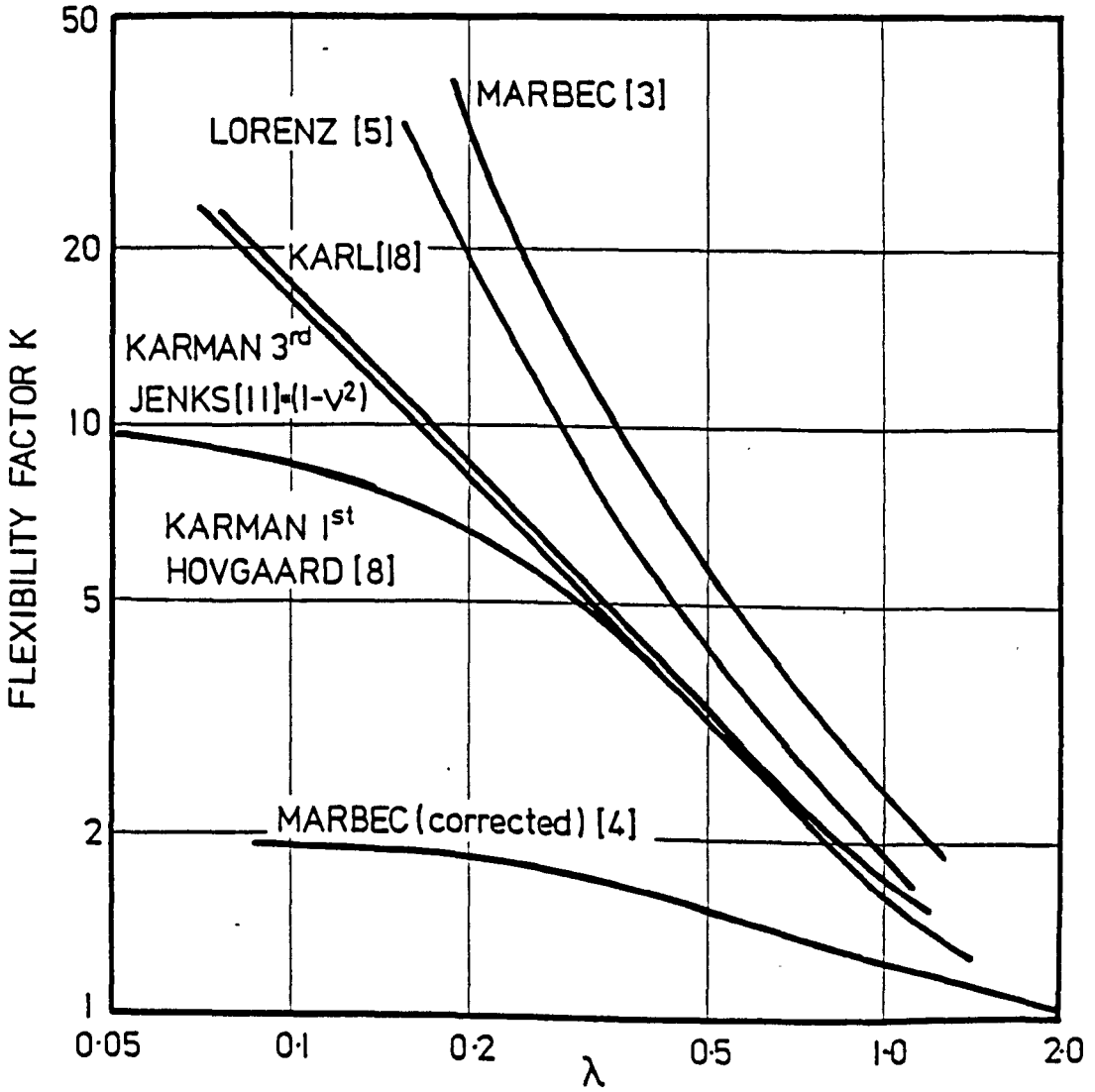

COMPARISON OF FLEXIBILITY FACTORS

FIG. 1.4

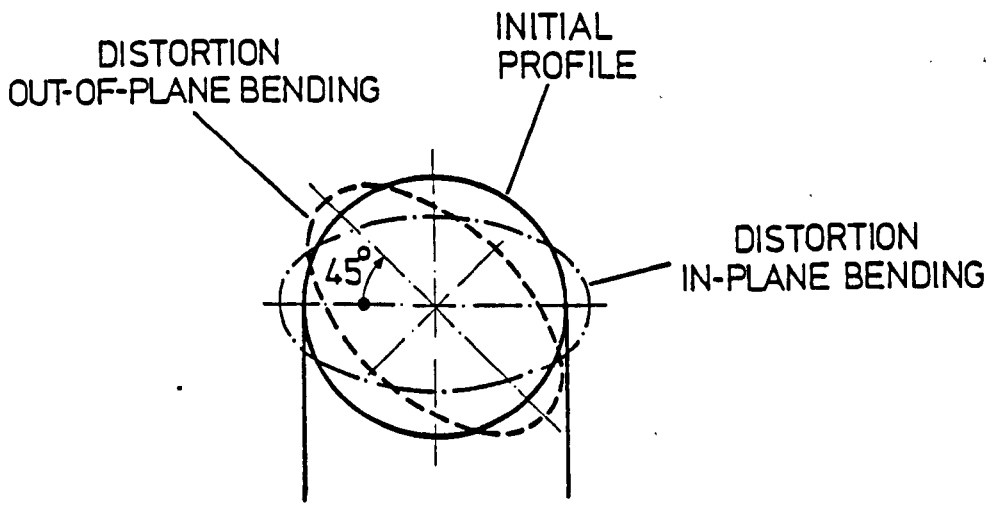

DISTORTION UNDER
IN & OUT-OF-PLANE BENDING

FIG. 1.5

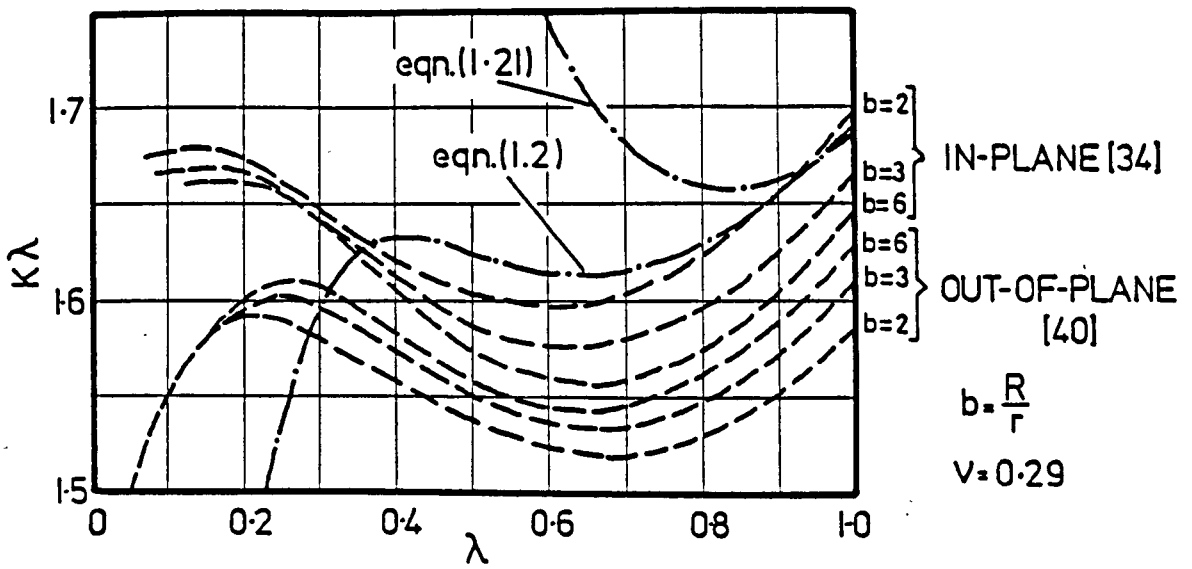

REPRODUCED FROM SMITH [40]

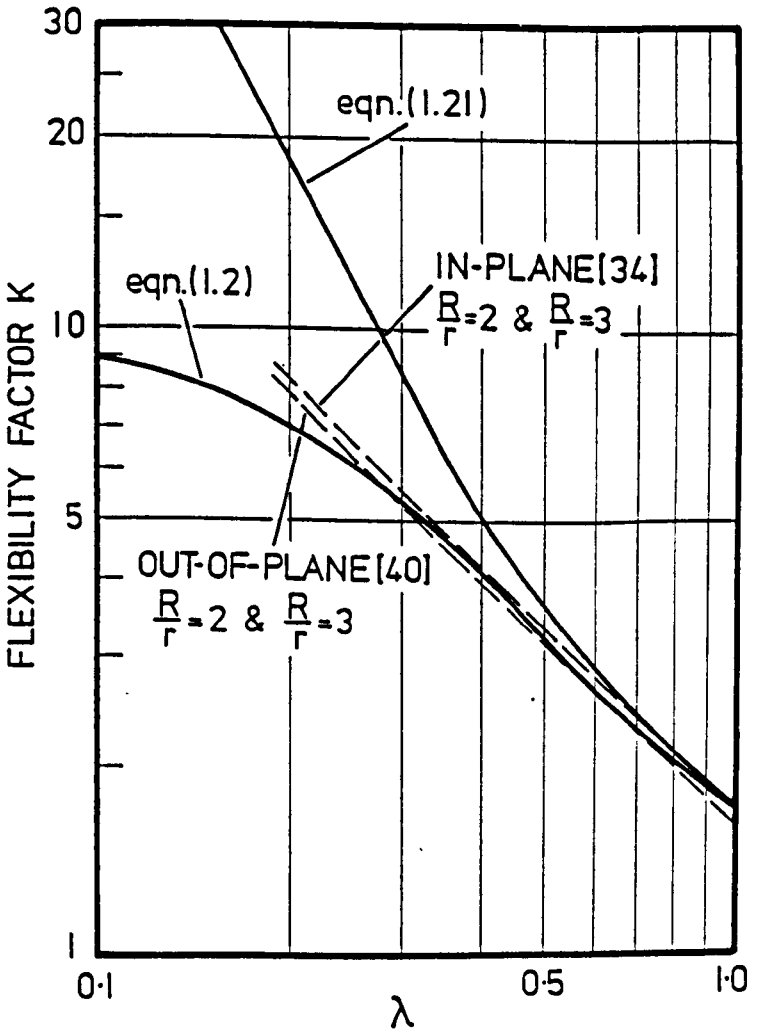

FLEXIBILITY FACTORS

TURNER & FORD [34] and SMITH [40]

FIG. 1.6

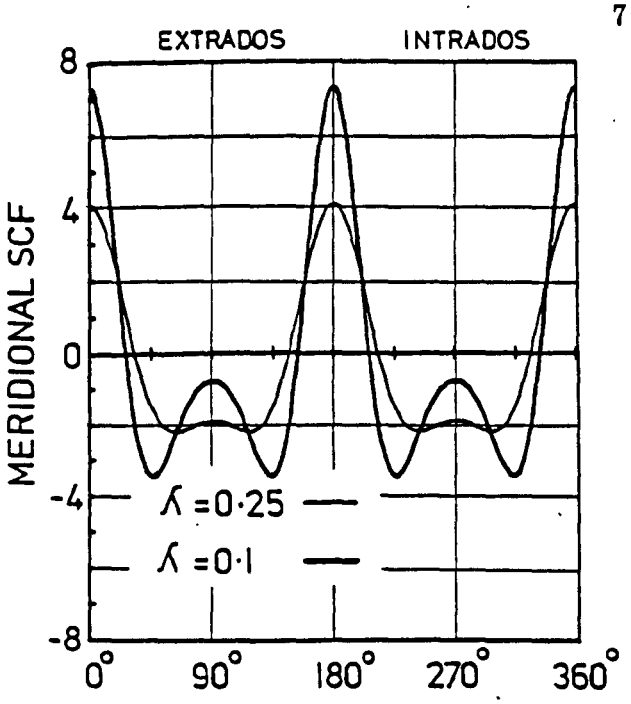

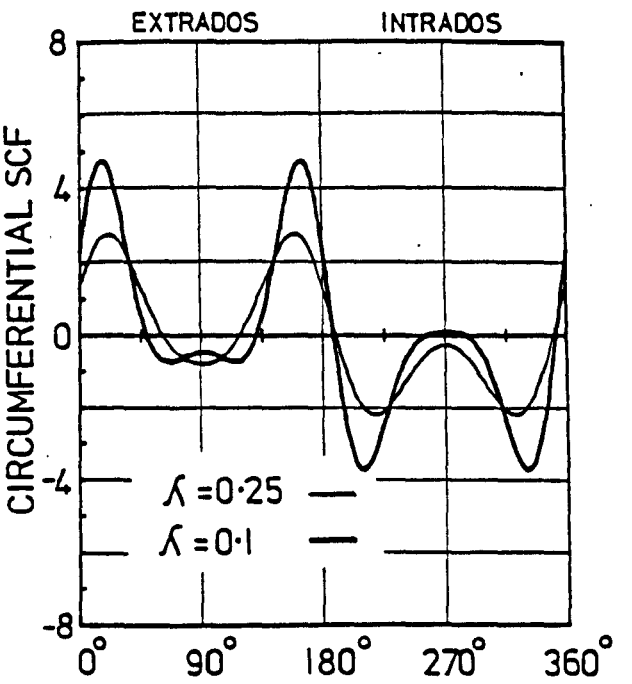

IN-PLANE BENDING

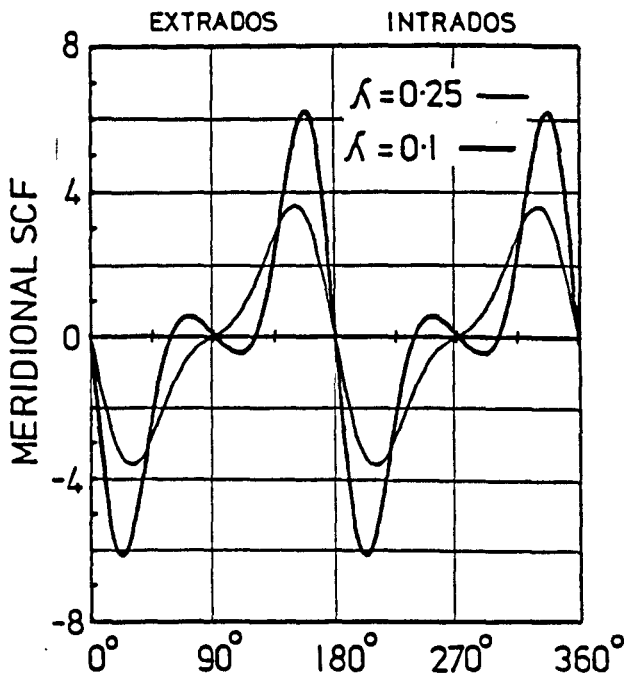

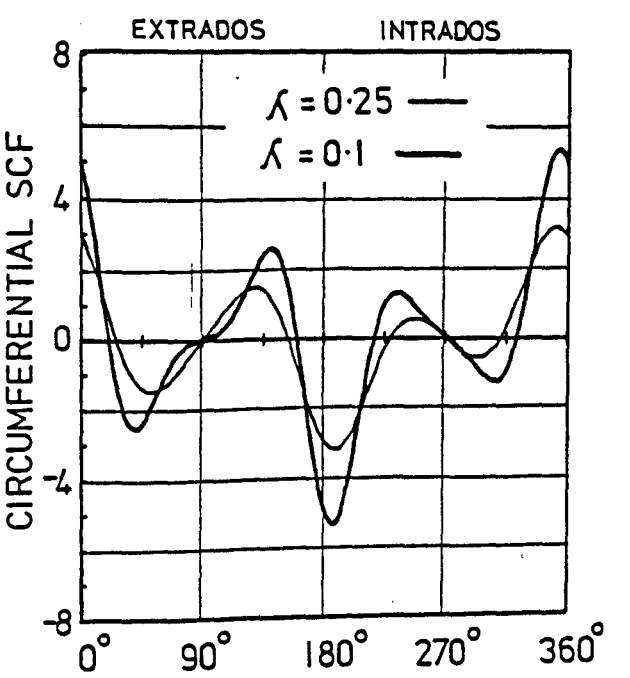

OUT-OF-PLANE BENDING

STRESS CONCENTRATION FACTORS

ELBOW [48]

FIG. 1.7

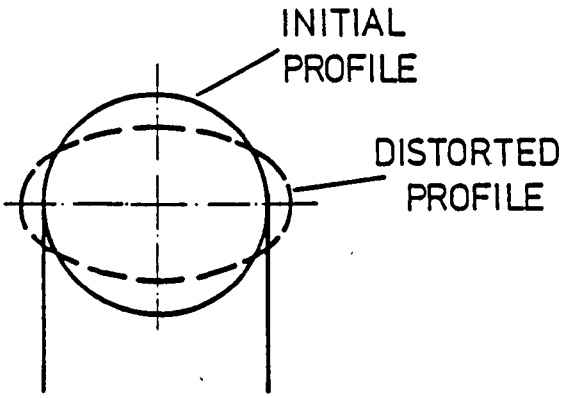

IN-PLANE LOADING CLOSING MODE

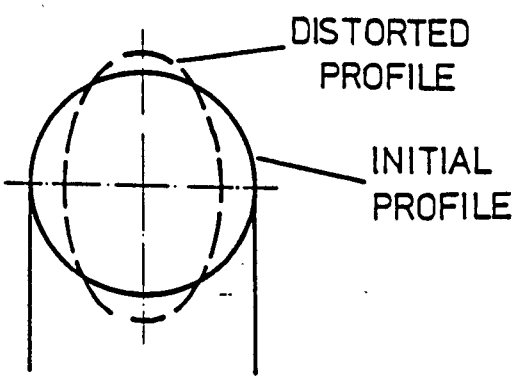

IN-PLANE LOADING OPENING MODE

DISTORTION OF CROSS-SECTION

FIG.1.8

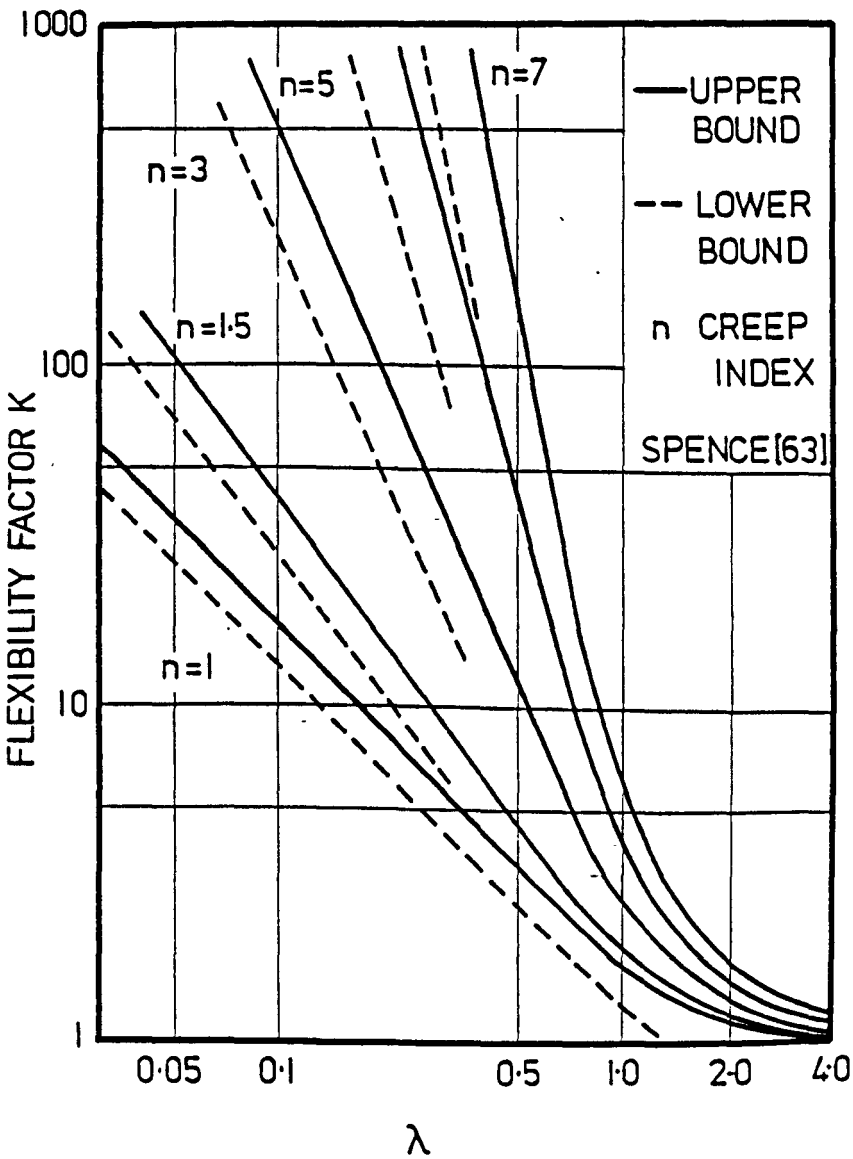

FLEXIBILITY FACTORS IN CREEP

FIG. 1.9

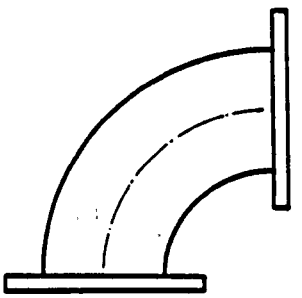

FLANGE
CONSTRAINTS

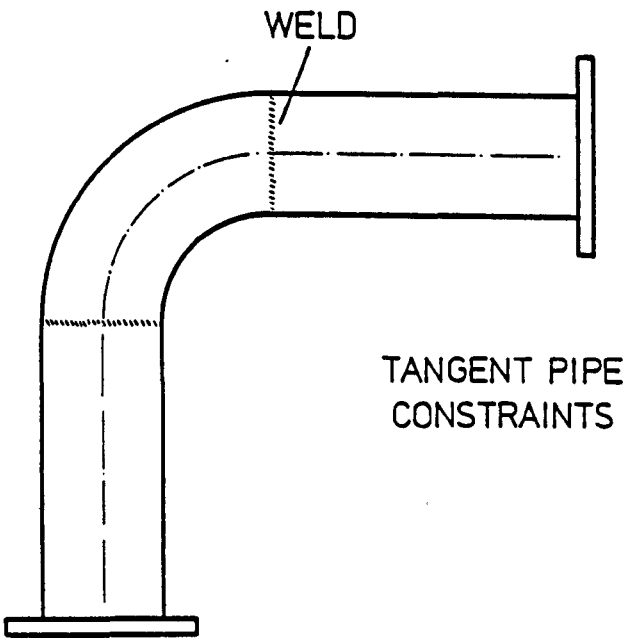

TANGENT PIPE
CONSTRAINTS

END CONSTRAINTS

FIG.1.10

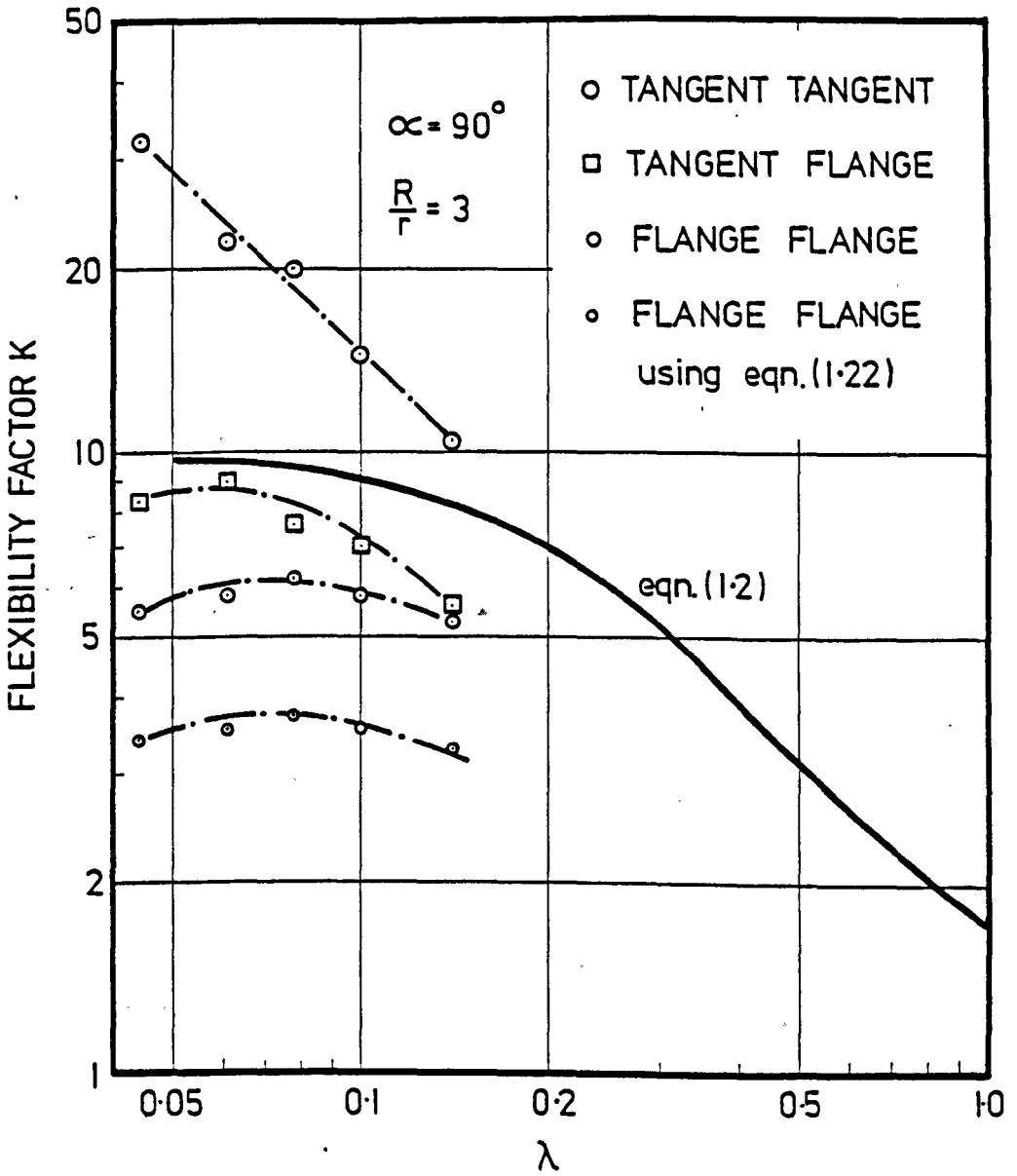

EXPERIMENTAL FLEXIBILITY FACTORS
OUT-OF-PLANE BENDING
PARDUE & VIGNESS [126]

FIG. 1.11

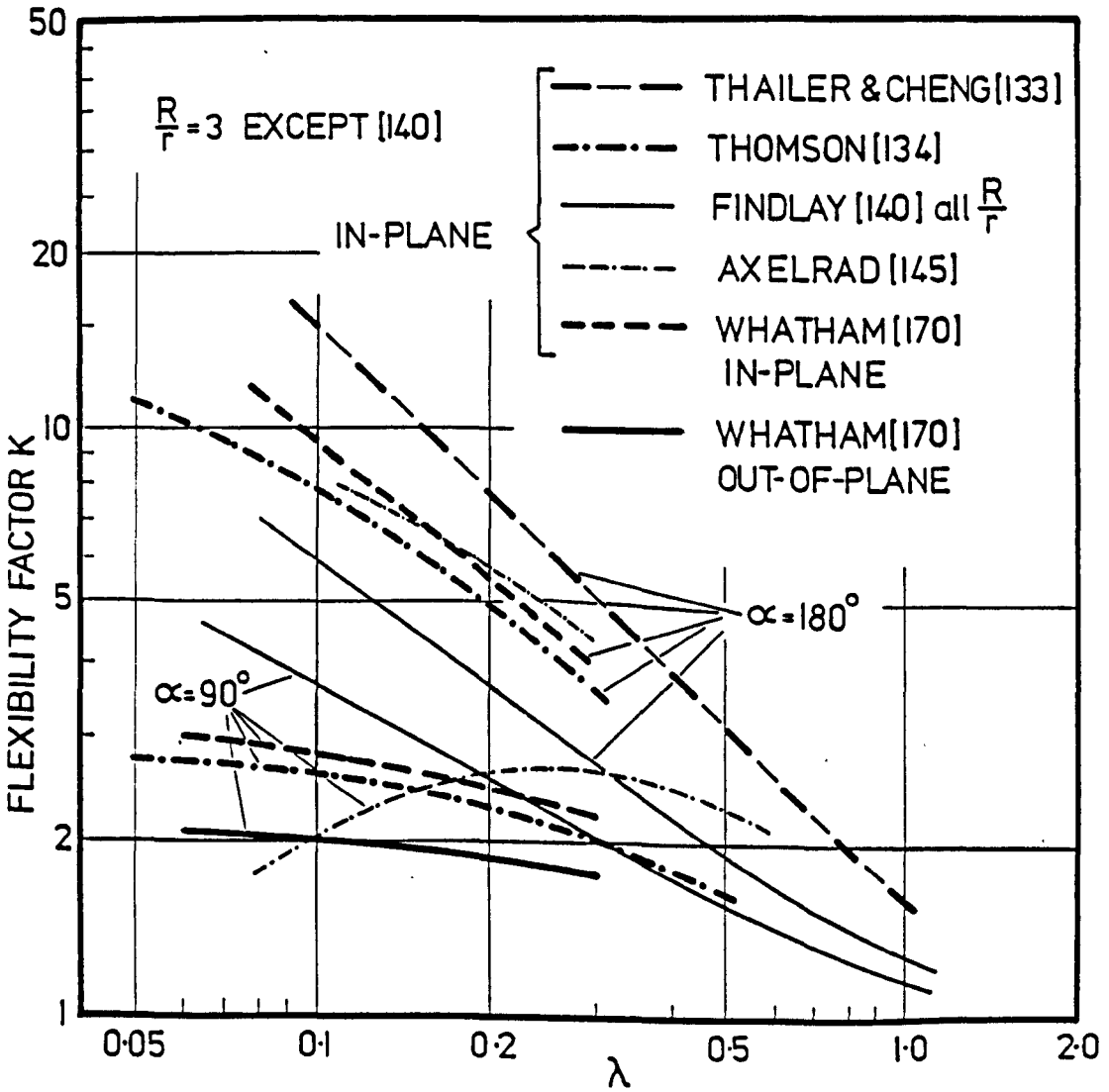

COMPARISON OF FLEXIBILITY FACTORS

FIG. 1.12

PART 1

THEORETICAL AND EXPERIMENTAL ANALYSIS OF PIPE BENDS WITH FLANGED END CONSTRAINTS UNDER OUT-OF-PLANE BENDING

CHAPTER 2

Basic Theoretical Relationships

ABSTRACT

This chapter deals with establishing the basic theoretical relationships which are required in the subsequent analysis.

Equations for a general shell in curvilinear orthogonal co-ordinates are described and an explanation is given of the choice of equations to be used herein. These are then converted to equations for a smooth pipe bend.

The theorem of minimum total potential energy is outlined and its application using the Rayleigh-Ritz method discussed.

CHAPTER (2)

BASIC THEORETICAL RELATIONSHIPS

2.1 Pipes as Thin Shells

2.1.1 Introduction

Shell theory attempts to model a thin three-dimensional structure as a two-dimensional surface. This is done to simplify the problem since solutions to three-dimensional problem in elasticity are extremely complex.

Using shell theory, the smooth pipe bend can be modelled as part of a toroidal shell. Interestingly, this approach in the study of pipe bends is only of relatively recent origin as can be seen from CHAPTER (1). In [140], however, Findlay was able to show that for the case of the smooth circular pipe bend under in-plane bending, the strain equations developed from thin shell theory eventually reduce to those originally developed by Kármán [1] from the geometry of the bend.

In the construction of thin shell theory as with the simpler theory of beam bending for example, it is worth remembering the three basic sets of equations which form the basis of all such analytical work. These are as follows:

(i) Equations of equilibrium

(ii) Kinematic relations, i.e. strain-displacement equations

(iii) Constitutive equations

Being aware of these three fundamental equations allows even the most complicated theory of shells to be more readily understood.

The method of solution to the problem of the smooth pipe bend applied herein will use the principle of minimum total potential energy. This technique, however, only requires the strain-displacement and constitutive equations together with the strain energy equation.

2.1.2 *Thin shell theory assumptions*

The basic equations governing the behaviour of thin elastic shells were derived originally by LOVE [193]. These were later modified by REISSNER [194] to form what is often referred to as the "classical" first approximation of shell theory. In formulating the compatibility and equilibrium equations, Love, and those after him, made several simplifying assumptions which can be summarised as follows:

1. The shell is considered to be thin. No rigid criterion is applied regarding the relative magnitudes of the mean radii of curvature and thickness of the cross-section but it is normally desirable to maintain the ratio of the mean radius to thickness as being more than 10.

2. Deflections are small. This assumption infers that the change in shape between the unloaded and loaded conditions is negligible, thereby allowing all derivations to be performed on the initial unloaded shape.

3. Stresses normal to the shell surface are negligible. This assumption states that the normal or radial stress is small relative to the stresses in the plane of the shell and also allows the use of the two-dimensional constitutive relations.

4. Normals to the mid-surface before deformation remain normal after deformation with no change in length. This is analogous to the Euler hypothesis of "plane sections remain plane" in beam theory, and is sometimes referred to as the "hairbrush hypothesis". It should be emphasised that the "plane sections" referred to are

through the thickness of the shell surface and not through the cross-section as in beam theory. This assumption also implies that all the strain components, including shears, normal to the surface of the shell are negligible.

The theoretical work discussed herein is based on the equations corresponding to the first order linear theory of shells. Other higher order theories have been derived which remove some of the above assumptions [195,196], but it has been established by many previous authors that the first order approximations give results which are adequate for most engineering applications.

2.1.3 General thin shell theory

Since the publication of Love's original work a number of modifications have been presented by several authors in an attempt to improve his equations. In doing so, however, many of them retained a further deficiency in the relations between the forces and the displacements. Eventually, most of the inconsistencies inherent in Love's equations were removed and a set of equations, derived independently by several authors, became "established". These equations can be found in the texts of Novozhilov [156] and KRAUSS [197].

SANDERS [198] pointed out a further inconsistency in the "established" equations. He showed that they do not give zero strains for all rigid body displacements, except for spherical shells, flat plates or symmetrically loaded shells of revolution. The inconsistency occurred in the shear curvature term which makes its significance for most problems relatively small. Sanders was able to remove this inconsistency using a method based on the principle of virtual work.

A similar set of equations was derived by KOITER [199] giving zero strain for rigid body displacements. Koiter concluded that the shear curvature inconsistency would only produce errors of the same order as those of the basic assumptions of thin shell theory.

Using a more physically intuitive approach, FLÜGGE [200] derived a set of equations for particular classes of shells. In fact, it was through this text that this author was introduced to the theory of shells. However, a more recent text by DYM [201] was found to be more useful as an introduction to the various shell theories in existence. The equations derived by Flügge are different to most other works. Further, Flügge does not separate the bending and direct strains making comparison

with other theories difficult. Dym in [201] compares Flügge's equations for a cylinder with that of Sanders and concludes that Flügge's equations will differ in regions of rapid deformation change. Thompson [54] in his work on pipe bends compared Flügge's shell theory and that of Novozhilov. For a particular range of pipe bend parameters he found the flexibility factors for in-plane bending, calculated from both theories, agreed to within 3%.

GOLDENVEIZER [202] derived a similar set of equations as Novozhilov but with a different shear curvature expression. By manipulation of the three basic equations given in section (2.1.1) he was able to obtain the three differential equations, in terms of the shell displacements, that govern shell behaviour.

DONNELL [303], MUSHTARI [204] and VLASOV [205] derived an approximate set of equations which have become internationally known as the Donnell-Mushtari-Vlasov equations. Using only the radial displacement in the curvature strain terms these equations resulted in a relatively simple set of governing differential equations. Thomson [134] used these equations with the "classical" pipe bend problem. He found the flexibility of a typical bend with a pipe factor λ of 0.5 is underestimated by 25.5%.

A set of equations particularly applicable to the pipe bend problem was derived by Axelrad [145]. These equations are suitable for a class of shells which sustain membrane or slowly varying deformation in one direction and an intensive variation in the orthogonal direction, i.e. semi-membrane theory.

In the choice of equations to be used for this particular analysis recourse was made to the methods employed by previous workers in

the field of pipe bends with end constraints. In the study of in-plane bending, Findlay [140] used the equations of Sanders. Thomson [134] and Whatham [168-171] used the equations of Novozhilov. As the analysis herein, considering out-of-plane bending, is based essentially on a development of Thomson's work, the version of the equations of Novozhilov used by Thomson were chosen. This introduces a certain degree of continuity in the work. Further, these equations are simpler than those of Sanders used by Findlay. The equations differ from the "established" equations in the shear curvature and equilibrium equations. The equations, as do those of Sanders, give zero strain for all rigid body displacements.

In orthogonal curvilinear coordinates the strain-displacement relations for a general shell are given by:

$$\varepsilon_1 = \frac{1}{A_1}\frac{\partial u_1}{\partial \alpha_1} + \frac{u_2}{A_1 A_2}\frac{\partial A_1}{\partial \alpha_2} + \frac{w}{R_1}$$

$$\varepsilon_2 = \frac{1}{A_2}\frac{\partial u_2}{\partial \alpha_2} + \frac{u_1}{A_1 A_2}\frac{\partial A_2}{\partial \alpha_1} + \frac{w}{R_2}$$

$$K_1 = \frac{1}{A_1}\frac{\partial \beta_1}{\partial \alpha_1} + \frac{\beta_2}{A_1 A_2}\frac{\partial A_1}{\partial \alpha_2}$$

$$K_2 = \frac{1}{A_2}\frac{\partial \beta_2}{\partial \alpha_2} + \frac{\beta_1}{A_1 A_2}\frac{\partial A_2}{\partial \alpha_1}$$

$$W_1 = \frac{1}{A_1}\frac{\partial u_2}{\partial \alpha_1} - \frac{u_1}{A_1 A_2}\frac{\partial A_1}{\partial \alpha_2}$$

$$W_2 = \frac{1}{A_2}\frac{\partial u_1}{\partial \alpha_2} - \frac{u_2}{A_1 A_2}\frac{\partial A_2}{\partial \alpha_1}$$

$$\tau_1 = \frac{1}{A_1}\frac{\partial \beta_2}{\partial \alpha_1} - \frac{\beta_1}{A_1 A_2}\frac{\partial A_1}{\partial \alpha_2}$$

$$\tau_2 = \frac{1}{A_2}\frac{\partial \beta_1}{\partial \alpha_2} - \frac{\beta_2}{A_1 A_2}\frac{\partial A_2}{\partial \alpha_1}$$

where $\beta_1 = \frac{u_1}{R_1} - \frac{1}{A_1}\frac{\partial w}{\partial \alpha_1}$ and $\beta_2 = \frac{u_2}{R_2} - \frac{1}{A_2}\frac{\partial w}{\partial \alpha_2}$ . . . *(2.1)*

β_1 and β_2 are the rotations of the mid-surface normal.

ϵ_1 and ϵ_2 are the mid-surface strains.

K_1 and K_2 are the curvatures. The subscripts of "1" and "2" refer to the directions of 1 and 2.

The mid-surface shear strain W is found from:

$$W = W_1 + W_2 \qquad \ldots \quad (2.2)$$

For the shear curvature τ Novozhilov gives two definitions:

$$\tau = \tau_1 + \tau_2 \qquad \ldots \quad (2.3)$$

$$\tau^* = \tau_1 + \frac{W_2}{R_1} = \tau_2 + \frac{W_1}{R_2} \qquad \ldots \quad (2.4)$$

Using the form of shear curvature given by equation (2.3) allows the shear stress resultants N_{12}, N_{21}, M_{12}, M_{21} to be found directly from:

$$N_{12} = N_{21} = \frac{Et}{2(1+\nu)} W$$

$$M_{12} = M_{21} = \frac{Et^3}{24(1+\nu)} \tau \qquad \ldots \quad (2.5)$$

This is the definition used in the "established" equations, which is variationally consistent but does not produce zero strains for a rigid body motion [201].

The form of shear curvature given by equation (2.4) results in a set of variationally consistent equations which also satisfy the conditions of zero strain for all rigid body displacements. However, in using τ^*, the shear stress resultants cannot be obtained simply by knowing W and τ^*. This will only be a problem if these resultants are required explicitly. In many situations, including the one to be considered herein, they are not. They can, however, be found approximately using the following equations:

$$N_{12} = \frac{Et}{2(1+\nu)}\left[W + \frac{t^2}{6R_2}\tau^*\right]$$

$$N_{21} = \frac{Et}{2(1+\nu)}\left[W + \frac{t^2}{6R_1}\tau^*\right]$$

$$M_{12} = M_{21} = \frac{Et^3}{12(1+\nu)}\tau^* \qquad \ldots \quad (2.6)$$

The error in these equations is of the same order as the original assumptions of thin shell theory.

Since the shear stress resultants are not required explicitly the form of the shear curvature given by equation (2.4) will be used.

The corresponding constitutive relations for a constant shell thickness and a linear isotropic material are:

$$N = C[\varepsilon_1 + \nu\varepsilon_2] \quad , \quad M_1 = D[K_1 + \nu K_2]$$

$$N_2 = C[\varepsilon_2 + \nu\varepsilon_1] \quad , \quad M_2 = D[K_2 + \nu K_1]$$

$$S = \frac{1}{2}[1-\nu]CW \quad , \quad H = [1-\nu]D\tau^*$$

$$\text{where } C = \frac{Et}{[1-\nu^2]} \quad \text{and} \quad D = \frac{Et^3}{12[1-\nu^2]} \qquad \ldots \quad (2.7)$$

The stress variables S and H in equation (2.7) are defined as follows:

$$S = N_{12} - \frac{M_{21}}{R_2} = N_{21} - \frac{M_{12}}{R_1}$$

$$H = \frac{1}{2}[M_{12} + M_{21}]$$

The equations of equilibrium are:

$$\frac{\partial(A_2 N_1)}{\partial \alpha_1} + \frac{\partial(A_1 S)}{\partial \alpha_2} + S\frac{\partial A_1}{\partial \alpha_2} - N_2 \frac{\partial A_2}{\partial \alpha_1} +$$

$$\frac{1}{R_1}\left[\frac{\partial(A_2 M_1)}{\partial \alpha_1} - M_1 \frac{\partial A_2}{\partial \alpha_1} + 2\frac{\partial(A_1 H)}{\partial \alpha_2} + 2\frac{R_1}{R_2} H \frac{\partial A_1}{\partial \alpha_2}\right] = -A_1 A_2 q_1$$

$$\frac{\partial(A_2 S)}{\partial \alpha_1} + \frac{\partial(A_1 N_2)}{\partial \alpha_2} + S\frac{\partial A_2}{\partial \alpha_1} - N_1 \frac{\partial A_1}{\partial \alpha_2} +$$

$$\frac{1}{R_2}\left[\frac{\partial(A_1 M_2)}{\partial \alpha_2} - M_1 \frac{\partial A_1}{\partial \alpha_2} + 2\frac{\partial(A_2 H)}{\partial \alpha_1} + 2\frac{R_2}{R_1} H \frac{\partial A_2}{\partial \alpha_1}\right] = -A_1 A_2 q_2$$

$$\frac{N_1}{R_1} + \frac{N_2}{R_2} - \frac{1}{A_1 A_2}\left[\frac{\partial}{\partial \alpha_1}\frac{1}{A_1}\left[\frac{\partial(A_2 M_1)}{\partial \alpha_1} + \frac{\partial(A_1 H)}{\partial \alpha_2} + H\frac{\partial A_1}{\partial \alpha_2} - M_2 \frac{\partial A_2}{\partial \alpha_1}\right] +\right.$$

$$\left.\frac{\partial}{\partial \alpha_2}\frac{1}{A_2}\left[\frac{\partial(A_2 H)}{\partial \alpha_1} + \frac{\partial(A_1 M_2)}{\partial \alpha_2} + H\frac{\partial A_2}{\partial \alpha_1} - M_1 \frac{\partial A_1}{\partial \alpha_1}\right]\right| = q_n \quad \ldots \quad (2.9)$$

The necessary boundary conditions for the solution of these equations are, at constant α_1 , specify:

$$N_1 \quad \text{or} \quad u_1$$

$$S + \frac{2H}{R_2} \quad \text{or} \quad u_2$$

$$\frac{1}{A_1 A_2}\left[2\frac{\partial (A_1 H)}{\partial \alpha_2} + \frac{\partial (A_2 M_1)}{\partial \alpha_1} - M_2 \frac{\partial A_2}{\partial \alpha_1}\right] \quad \text{or} \quad w$$

$$M_1 \quad \text{or} \quad \beta_1$$

and at constant α_2 specify:

$$N_2 \quad \text{or} \quad u_2$$

$$S + \frac{2H}{R_1} \quad \text{or} \quad u_1$$

$$\frac{1}{A_1 A_2}\left[2\frac{\partial (A_2 H)}{\partial \alpha_1} + \frac{\partial (A_1 M_2)}{\partial \alpha_2} - M_1 \frac{\partial A_1}{\partial \alpha_2}\right] \quad \text{or} \quad w$$

$$M_2 \quad \text{or} \quad \beta_2$$

. . . *(2.10)*

In the analysis of thin shells the ratio of t/R_i can be neglected with respect to unity. Employing this assumption, the strain energy equation consistent with the above equations, for a constant shell thickness, linear isotropic material is:

$$U = \frac{C}{2}\iint \left[(\varepsilon_1 + \varepsilon_2)^2 - 2(1-\nu)(\varepsilon_1\varepsilon_2 - \frac{1}{4}W^2)\right] A_1 A_2 d\alpha_1 d\alpha_2$$

$$+ \frac{D}{2}\iint \left[(K_1 + K_2)^2 - 2(1-\nu)(K_1 K_2 - \tau^{*2})\right] A_1 A_2 d\alpha_1 d\alpha_2$$

. . . *(2.11)*

2.2 The Toroidal Shell or Smooth Pipe Bend

The general thin shell equations described in section (2.1.3) require to be converted to the specific case of a toroidal shell for the analysis of the smooth pipe bend.

The geometry of the smooth pipe bend is shown in Figure (2.1).

From the theory of surfaces [206,207] the first fundamental form of the mid-surface of a shell element in curvilinear coordinate is:

$$(dS)^2 = A_1^2 (d\alpha_1)^2 + A_2^2 (d\alpha_2)^2$$

The corresponding equation for an element in the new (ϕ,θ) coordinate system shown in Figure (2.1) is:

$$(dS)^2 = r^2 (d\phi)^2 + (R')^2 (d\theta)^2 \quad , \quad R' = R + r\sin\phi$$

The principal radius of curvature in the curvilinear system are R_1 and R_2. In the new (ϕ,θ) coordinate system these become r and $R'/\sin\phi$.

The curvilinear displacements w, u_1 and u_2 become w, v and u in the (ϕ,θ) system.

Conversion of the curvilinear system to the (ϕ,θ) system therefore requires:

$$\begin{aligned} \alpha_1 &= \phi \quad , \quad A_1 = r \quad , \quad R_1 = r \\ \alpha_2 &= \theta \quad , \quad A_2 = R' \quad , \quad R_2 = R'/\sin\phi \\ w &= w \quad , \quad u_1 = v \quad , \quad u_2 = u \end{aligned} \qquad \ldots \quad (2.12)$$

The governing equations for the smooth pipe bend are thus obtained by substituting equations (2.12) into equations (2.1) and (2.6) to (2.11). From this the strain-displacement equations can be written as:

$$\varepsilon_\phi = \frac{1}{r}\left(\frac{\partial v}{\partial \phi} + w\right)$$

$$\varepsilon_\theta = \frac{1}{R'}\left(\frac{\partial u}{\partial \theta} + v\cos\phi + w\sin\phi\right)$$

$$\gamma_{\theta\phi} = \frac{1}{R'}\left(\frac{\partial v}{\partial \theta} - u\cos\phi + \frac{R'}{r}\frac{\partial u}{\partial \phi}\right)$$

$$K_\phi = \frac{1}{r^2}\left(\frac{\partial v}{\partial \phi} - \frac{\partial^2 w}{\partial \phi^2}\right)$$

$$K_\theta = \frac{1}{(R')^2}\left(\frac{\partial u}{\partial \theta}\sin\phi - \frac{\partial^2 w}{\partial \theta^2} + \frac{R'}{r}\cos\phi\left[v - \frac{\partial w}{\partial \phi}\right]\right)$$

$$K_{\theta\phi} = \frac{1}{rR'}\left(\frac{\partial u}{\partial \phi}\sin\phi + \frac{\partial v}{\partial \theta} - \frac{\partial^2 w}{\partial \theta \partial \phi} + \frac{r}{R'}\cos\phi\left[\frac{\partial w}{\partial \theta} - u\sin\phi\right]\right)$$

where $R' = R + r\sin\phi$ . . . *(2.13)*

In equation (2.13) the notation of W and τ^* has been changed to $\gamma_{\theta\phi}$ and $K_{\theta\phi}$ respectively.

The constitutive relations are:

$$N_\phi = C[\varepsilon_\phi + \nu\varepsilon_\theta] \quad , \quad N_\theta = C[\varepsilon_\theta + \nu\varepsilon_\phi]$$

$$M_\phi = D[K_\phi + \nu K_\theta] \quad , \quad M_\theta = D[K_\theta + \nu K_\phi]$$

$$S = \frac{1}{2}[1 - \nu]C\gamma_{\theta\phi} \quad , \quad H = [1 - \nu]DK_{\theta\phi}$$

where $C = \frac{Et}{(1-\nu^2)}$ and $D = \frac{Et^3}{12(1-\nu^2)}$ . . . *(2.14)*

The equilibrium equations are:

$$\frac{\partial(R' N\phi)}{\partial \phi} + r\frac{\partial S}{\partial \theta} - N_\theta r\cos\phi + \frac{1}{r}\frac{\partial(R' M_\phi)}{\partial \phi} - M_\theta \cos\phi + 2\frac{\partial H}{\partial \theta} = -rR' q_\phi$$

$$\frac{\partial(R' S)}{\partial \phi} + r\frac{\partial N_\theta}{\partial \theta} + Sr\cos\phi + \frac{r\sin\phi}{R'}\frac{\partial M_\theta}{\partial \theta} + \frac{2\sin\phi}{R'}\frac{\partial(R' H)}{\partial \phi} + 2H\cos\phi = -rR' q_\theta$$

$$-R' N\phi - r\sin\phi N_\theta + \frac{1}{r}\frac{\partial^2(R' M_\phi)}{\partial \phi^2} + 2\frac{\partial H}{\partial \theta \partial \phi} - \frac{\partial(M_\theta \cos\phi)}{\partial \phi} +$$

$$\frac{r}{R'}\frac{\partial^2 M_\theta}{\partial \theta^2} + \frac{2r\cos\phi}{R'}\frac{\partial H}{\partial \theta} = -rR' q_n \quad \ldots \quad (2.15)$$

For constant shell thickness the strain energy expression is:

$$U = \frac{C}{2}\iint \left[(\varepsilon_\phi + \varepsilon_\theta)^2 - 2(1-\nu)\left(\varepsilon_\phi \varepsilon_\theta - \frac{1}{4}\gamma^2_{\theta\phi}\right)\right] rR' d\theta d\phi$$

$$+ \frac{D}{2}\iint \left[(K_\phi + K_\theta)^2 - 2(1-\nu)(K_\phi K_\theta - K^2_{\theta\phi})\right] rR' d\theta d\phi \quad \ldots \quad (2.16)$$

The boundary conditions necessary for a solution are as follows:

at a constant ϕ, specify:

$N\phi$	or v
$S + \frac{2H}{R'}\sin\phi$	or u
$\frac{2}{r}\frac{\partial H}{\partial \theta} + \frac{1}{r}\frac{\partial M_\phi}{\partial \phi} - M_\theta r\cos\phi$	or w
M_ϕ	or β_ϕ

at constant θ, specify:

$$N_\theta \quad \text{or} \quad u$$

$$S + \frac{2H}{r} \quad \text{or} \quad v$$

$$\frac{2}{rR'}\frac{\partial(R'H)}{\partial\phi} + \frac{1}{R'}\frac{\partial M_\theta}{\partial\theta} \quad \text{or} \quad w$$

$$M_\theta \quad \text{or} \quad \beta_\theta \qquad \ldots \quad (2.17)$$

The slope of the mid-surface normals β_ϕ and β_θ given in equation (2.17) are defined as follows:

$$\beta_\phi = \frac{1}{r}\left(v - \frac{\partial w}{\partial\phi}\right)$$

$$\beta_\theta = \frac{1}{R'}\left(u\sin\phi - \frac{\partial w}{\partial\theta}\right) \qquad \ldots \quad (2.18)$$

2.3 Total Potential Energy

2.3.1 *Principle of minimum total potential energy*

The principle of minimum total potential energy can be expressed as:

$$\int_V U(\varepsilon^*)dV - \int_{S(P)} P\delta^* ds \geq \int_V U(\varepsilon)dV - \int_{S(P)} P\delta ds \quad \ldots \quad (2.19)$$

where

$\int_V U(\varepsilon^*)dV$ is the total strain energy of a compatible strain field ε^*.

$\int_{S(P)} P\delta^* ds$ is the potential energy of the applied forces where δ^* is the associated compatible displacement of the load. S(P) denotes integration over the surface where the loads are applied.

$\int_V U(\varepsilon)dV$ is the "exact" strain energy of the true strain field, ε.

$\int_{S(P)} P\delta ds$ is the potential energy of the applied forces where δ is the associated true displacement.

In the form presented, the theorem states that the total energy associated with an arbitrarily assumed compatible strain and displacement field is always greater than or equal to the energy associated with the corresponding true strain and displacement field. This is true only if the assumed strains and displacements satisfy compatibility. Thus the total energy is only a minimum at the true state.

In this "displacement prescribed" type of solution where the selected compatibility component (δ^*) is identical to the exact displacement (δ), then it follows from equation (2.19) that:

$$\int_V U(\varepsilon^*)dV \geq \int_V U(\varepsilon)dV \qquad \ldots \quad (2.20)$$

The equality sign only holds when the strain and displacement choices are exact.

If a system is subjected to a single load then, from the principle of conservation of energy, the strain energy will be equal to the work done by the external load increasing uniformly from zero. If the load is increased to a value P, where the displacement is equal to the prescribed displacement, then this can be written as:

$$\int_V U(\varepsilon^*)dV = \tfrac{1}{2}P^*\delta \qquad \ldots \quad (2.21)$$

The true state is:

$$\int_V U(\varepsilon)dV = \tfrac{1}{2}P\delta \qquad \ldots \quad (2.22)$$

Equations (2.21) and (2.22) can be combined using equation (2.20) to give:

$$P^* \geq P \qquad \ldots \quad (2.23)$$

Hence the calculated load (P^*) from an approximate solution is always greater than the exact load (P). The flexibility is inversely proportional to the applied load. Therefore, from equation (2.23), the flexibility of the system must be underestimated.

2.3.2 *Rayleigh-Ritz method*

Energy methods make use of the theorem of minimum total potential energy by prescribing displacements as a series of terms each of which is made up of a function multiplied by a coefficient. The values of the coefficients, and hence the true displacements, are obtained by finding the combination of the coefficients which give the minimum of the total potential energy function.

In the RITZ [208] method, of all the displacements that satisfy the boundary conditions, those making the total potential energy V of the system a minimum are the sought deflections pertinent to the stable equilibrium conditions. The displacements are represented in the form of a series:

$$w(x,y) = c_1 f_1(x,y) + c_2 f_2(x,y) + c_3 f_3(x,y) + \ldots . c_n f_n(x,y)$$

$$= \sum_{i=1}^{n} c_i f_i(x,y).$$

The displacements, w(x,y), comprise continuous functions that satisfy individually at least the geometrical or essential boundary conditions and are capable of representing the deflected shape. Satisfaction of the natural boundary* conditions is not required although in doing so

---

*The boundary conditions discussed here of "essential" and "natural" can be considered more as restraints imposed upon the system as opposed to boundary conditions in the true mathematical sense. The significance of these boundary conditions can best be seen by considering the following simple example of a cantilever beam of length L, loaded at its free end by a bending moment M and a shear force F.

For this problem the essential boundary conditions are:

at x=o , y=o and $\frac{dy}{dx} = o$

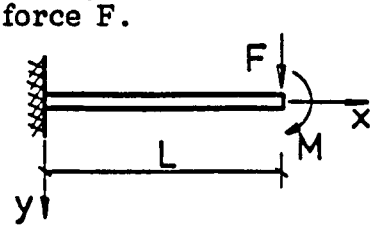

The natural boundary conditions are defined by the edge forces:
at x = L , M_z = M and the shear force v = F.

this will improve the accuracy of the displacement. In determining the c_i coefficients the total potential energy V is expressed as a function of the displacements and hence of the coefficients. The solution to the problem is then found by minimising the total potential energy expression:

$$\frac{\partial V}{\partial w} = 0$$

$$\text{therefore } \frac{\partial V}{\partial c_1} = \frac{\partial V}{\partial c_2} = \frac{\partial V}{\partial c_3} = \ldots\ldots = \frac{\partial V}{\partial c_n} = 0$$

This minimisation procedure yields n simultaneous algebraic equations in the undetermined coefficients $c_1, c_2, c_3, \ldots\ldots c_n$, from which the unknown parameters c_i can be calculated. It should be noted that during the partial differentiation all the coefficients, except the specific c_i under consideration, are taken constant.

The advantages of the Ritz method lie in the relative ease with which complex boundary conditions can be handled. It is a powerful tool yielding high accuracy in displacements, provided that suitable shape functions are employed. It is of interest to note that in the first theoretical investigation of pipe bends Kármán [1] "urges engineers to become familiar with the Ritz method, because the method is simple and ideal to develop approximate solutions to complex practical problems".

RAYLEIGH [209], in his work on vibrations, developed an energy method which involved determination of the kinetic and potential energies of the system using assumed displacement functions which satisfy the essential boundary conditions and approximates the actual modes of vibration. In the expression for displacement, Rayleigh used only one parameter. RITZ [210] extended Rayleigh's method by including more than one parameter in the displacement series. As a consequence of

this the two methods are often referred to in the literature as the Rayleigh-Ritz method.

In practise, a finite number of terms in the displacement series is usually sufficient as higher order terms rapidly become negligible. Only the "exact" displacements give the true minimum of the total potential energy, and therefore corresponds to true equilibrium. Each parameter in the displacement series contributes to the final equilibrium state and hence by truncating the series after a finite number of terms gives partial equilibrium.

A number of other variational methods such as those of GALERKIN [211] and VLASOV [212] exist in the literature. In the analysis to be presented herein the method referred to here as the Rayleigh-Ritz method will be adopted.

In the study of energy methods the author found the texts of LANGHAAR [213] and SZILARD [214] of particular use.

As a closure to this chapter, it is important to recognise that in the analysis of pipe bends, the use of the Rayleigh-Ritz method will result in an underestimation of the flexibility factor. Thus a "lower bound" is obtained on the value of flexibility. This is because the inexact shape assumed by truncating the series can be considered to be the exact shape for a case in which additional constraints have been applied to force the body to take the assumed shape, and constraints of any kind reduce deflections, that is increase apparent stiffness and thus reduce flexibility. This is not always true for more complex loadings as the deflections and stresses away from the point of application of the load are not bounded. Such lower bounds on flexibility will be useful in the study of pipe bends. Convergence of the series solution can be

examined since the addition of further terms in the series will increase the bend flexibility. Terms can be added until the change in flexibility factor is less than some arbitrary quantity.

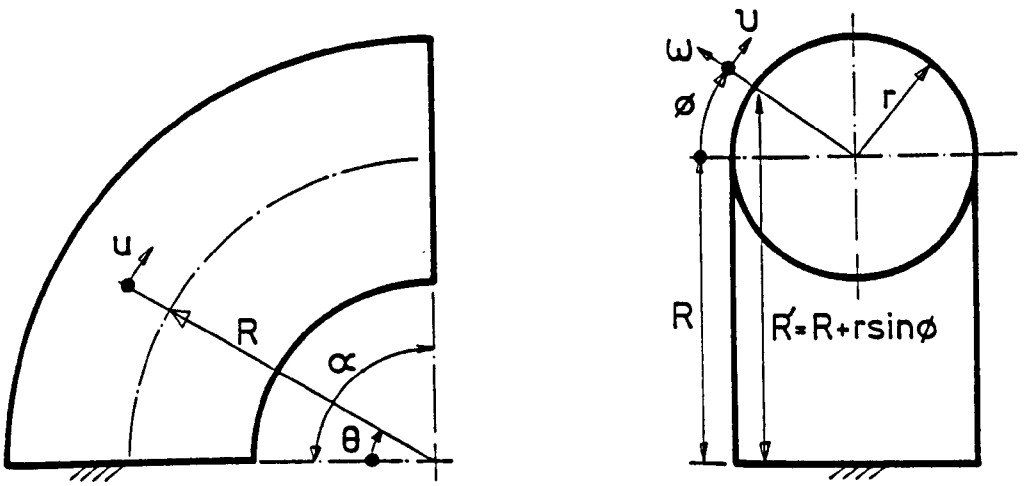

ø MERIDIONAL ANGLE

θ CIRCUMFERENTIAL ANGLE

GEOMETRY OF THE SMOOTH PIPE BEND

FIG. 2.1

CHAPTER 3

Theoretical Analysis of Flanged Bend

ABSTRACT

A theoretical solution to the problem of a smooth pipe bend with flanged end constraints under out-of-plane bending is presented.

Using the theorem of minimum total potential energy, general displacements in the form of fourier series are employed which satisfy internal and external compatibility.

A numerical solution is then presented which uses the complete strains evaluated from the strain-displacement equations.

Finally, flexibility and stress concentration factors are given for a wide range of bend geometries.

CHAPTER (3)

THEORETICAL ANALYSIS OF FLANGED BEND

3.1 Introduction

The study of out-of-plane bending of smooth pipe bends has received little attention in the literature, the emphasis in general being placed on the case of in-plane bending. This is due partly to the complexity of the problem and the fact that this type of loading, if treated generally in a fashion similar to in-plane bending, results in a conservative design. The effect of end constraints such as those defined here of thick rigid flanges, has been given even less attention. Apart from the work of Whatham, the author has been unable to discover any other theoretical work dealing specifically with these types of end constraints under out-of-plane bending. Numerous finite element packages, as discussed earlier, have at least in principle the capability of treating this problem. Usually they have been applied to the condition of tangent pipe end constraints or a combination of this and flanged end constraints.

During the early stages of the work this created something of a dilemma in that there was no basis for comparison. Some guidance, however, became available during the course of experimental work. In out-of-plane bending these experiments indicated that the flexibility factor would be less by a factor varying from $\frac{1}{3}$ to $\frac{1}{2}$ compared to in-plane bending. Later, from the results of Thomson's [134] study of in-plane bending, using the same form of end constraints, an upper bound value on the flexibility factor could be defined. This difference in flexibility factor was to some extent confirmed later by the work of Whatham.

Mid-way through the study the author was introduced to the work of Whatham [155,157]. His results had been used by Thomson in his study of in-plane bending with flanged, and later, tangent end

constraints. Later in a series of similar papers, Whatham [168-171] extended his study to cover a variety of end loading conditions including that of out-of-plane bending. Whatham appears to make no assumptions other than those of thin shell theory and appears to treat the flanges as infinitely stiff. However, in [171] he states clearly the boundary conditions of a thick flange as zero displacement and slope for the radial distortion component:

$$w_{D(\theta)} = \frac{\partial w_{D(\theta)}}{\partial \theta} = 0 \qquad \ldots (3.1)$$

The importance of these conditions will become apparent later; they can, however, be derived from the boundary conditions given by equations (2.17) and (2.18) in CHAPTER (2).

Whatham's method of solution involves the use of Novozhilov's [156] technique using three arbitary functions which have the same form as the mid-surface displacements. Fourier series are used to solve the equations for the simple case of a bend without end effects. These displacements in the present notation take the general form:

$$\begin{aligned} w &= \sum_{n=1} a_n \sin(n\beta) \\ v &= \sum_{n=0} b_n \cos(n\beta) \\ u &= \sum_{n=1} c_n \sin(n\beta) \end{aligned} \qquad \ldots (3.2)$$

where $\beta = \phi + 90°$

The flanged bend problem is then solved by superimposing on the results obtained without end effects, a set of displacements which returns the ends of the bend back from their distorted shape to the initial circular conditions. To account for the decaying flange effect these displacements include an exponential term and take the form:

$$w = \sum_{j=1} e^{-\Omega\beta} C_j \sum_{n=1} \bar{a}_{nj} \sin(n\beta)$$

$$v = \sum_{j=1} e^{-\Omega\beta} C_j \sum_{n=0} \bar{b}_{nj} \cos(n\beta)$$

$$u = \sum_{j=1} e^{-\Omega\beta} C_j \sum_{n=1} \bar{c}_{nj} \sin(n\beta) \qquad \ldots (3.3)$$

In Whatham's method the solution of the flanged pipe bend is treated as an eigenvalue problem from which the unknown function coefficients are obtained. Although the concept of a particular integral and complementary function for the no end effect and end effect solutions was relatively clear, this author found the numerical complexity of the method difficult to understand. Further, there was a distinct lack of results presented in all of Whatham's papers, again the emphasis being on in-plane bending.

From his flexibility matrix, Whatham's definition of flexibility factor is identical to Thomson's for in-plane bending:

$$\gamma = \gamma_o K \qquad \ldots (3.4)$$

where γ = actual end rotation

γ_o = nominal end rotation = $\frac{MR\alpha}{E\pi r^3 t}$

In the case of out-of-plane bending Whatham includes the effect of torsion in his definition of flexibility factor. For example, for a bend angle of 90° Whatham's definition is:

$$\gamma = \frac{MR}{4Er^3t}[K + (1+\nu)] \qquad \ldots (3.5)$$

The corresponding definition applied in this text is:

$$\gamma = \frac{MR}{2Er^3t} K \qquad \ldots (3.6)$$

The difference in equations (3.5) and (3.6) arises essentially from the definition of the nominal rotation (γ_o). In Whatham's definition (3.5) the varying torsional and out-of-plane bending moment is accounted for in the evaluation of the nominal rotation (γ_o). This is the correct form for a curved beam as would be obtained from simple energy methods. The flexibility factor K is however applied to the bending component only, the factor in torsion being taken as unity. The definition of flexibility factor K given by equation (3.6) neglects the change and variation of loading along the bend and is the same as that given by equation (3.4) for in-plane bending. It corresponds to the definition given in CHAPTER (1) where the nominal rotation is defined for a straight pipe and not a curved pipe as used by Whatham.

The actual definition adopted for flexbility factor, be it for in-plane or out-of-plane bending is in fact unimportant. All that is required is that it be clearly stated. Naturally it is of some benefit for comparison purposes if a general form is sought. In out-of-plane bending the two most common definitions found in the literature are those defined by equations (3.5) and (3.6). It will be seen later, however, that the form adopted herein (3.6), which excludes the torsion component, has two distinct advantages. Firstly, it provides a numerical value of flexibility factor which is considerably less than the in-plane bending case. This is consistent with experiment where the pipe bend is found to be stiffer under out-of-plane bending as compared with in-plane bending. Secondly, the form adopted by equation (3.6) is simpler and more direct to incorporate in the final total potential energy expression for the bend.

In out-of-plane bending, for any bend angle, Whatham's definition for flexibility factor and that used herein are related simply by:

$$K = \frac{1}{2}[K_W + (1+\nu)]\left[\frac{\alpha - \frac{1}{2}\sin(2\alpha)}{\alpha}\right] \quad . .$$

where K = flexibility factor defined by equation (3.6)

K_W = Whatham's flexibility factor . . . *(3.7)*

Whatham's results for out-of-plane bending, taken from [170] are shown in Figure (3.1) using the present definition and Whatham's definition for flexibility factor. These results were limited to radius ratios ($\frac{R}{r}$) of 2 and 3, λ values extending from 0.02 to 0.3 and bend angle (α) of 90° and 180°. Using a value of poisson's ratio (ν) = 0.3, Whatham's definition for flexibility factor gives values which are 35% higher than the present definition for these two bend angles. In Figure (3.2) a comparison is given of Whatham's results for in and out-of-plane bending for a bend angle of 180°. For in-plane bending Whatham's results appear as a straight line on the log-log graph. This is in contrast with Thomson's results, which although slightly lower, do present a well defined curve.

For the case of out-of-plane bending Whatham presents no experimental results.

Prior to a visit by Whatham early in 1983, the author received a computer tape copy of the solutions described in his later papers*. From the associated computer manuals [172-174] it became evident that his solution did not address directly the out-of-plane bending of a flanged bend. Where applicable Whatham introduces a reference bending moment which he defined by the product of the particular loading and a fictitious

---

*This program package originated from an IBM 370/195 computer. In the search for a compatible machine with direct access, an IBM 3081 at Cambridge University was found to be the most suitable. Unfortunately, after much effort the package was found to be too big to implement. This arose from the author's limited access to the system and the correspondingly small allocation of space.

moment arm. Although initially this writer found the method rather confusing, it does allow the solution to cope with direct loadings and pure bending moments. Further, it was clear that the end constraints of tangents was applicable to in-plane bending only.

3.1.1 Progress of the work

In the study of out-of-plane bending the author's work began with an investigation of the degree of approximation which could be applied successfully to the problem. In doing so, the form of the solution was to be dictated by two main criteria. Firstly, it should retain a sufficient degree of realism in the type of simplifications used, and, secondly, be capable of hand computation. This latter requirement was intended to allow hand integration of the strain energy function and remove as much as possible the dependence on computers and their associated numerical problems. These two conflicting criteria represent the age old problem in analysis whereby some form of compromise is eventually sought. It should be borne in mind, however, that by virtue of the approximations employed this naturally leads to a further set of restrictions being placed upon the solution over and above those already dictated by thin shell theory. The main simplifications employed in the analysis were as follows:

1. bend radius >> mid-surface cross-section radius, i.e. R>>r;
2. shear strain $\gamma_{\theta\phi} \simeq 0$;
3. meridional direct strain $\varepsilon_{\phi} \simeq 0$;
4. the curvatures K_{θ} and $K_{\theta\phi} \simeq 0$;
5. symmetrical distortion of the bend cross-section.

Using a variety of combinations of the above simplifications a number of analyses were carried out. The first simplification removes the cumbersome term $(1 + \frac{r}{R}\sin\phi)$. In fact the presence of this term makes hand integration virtually impossible, particularly when the term appears in the denominator. With R >> r the analysis is then limited to "long radius" bends. The remaining approximations essentially govern the size of the solution. The second assumption of zero shear strain ($\gamma_{\theta\phi}$) and also zero shear curvature ($K_{\theta\phi}$) in the fourth assumption both conflict with the first main criteria. This results from the presence of the torsional moment which is expected to dictate a dominance in the shear terms. It was found later that the neglect of the two shear terms $\gamma_{\theta\phi}$ and $K_{\theta\phi}$ had significant effects upon the solution. The last simplification (5) states that the bend cross-section distorts into a shape which is symmetrical about the planes through the bend section of $\phi = \mp 45°$. This is the normal assumption used in the no end effect theory. Initially, this was considered to be a gross simplification as such symmetry in distortion does not coincide with any of the main axes of the pipe bend. It was shown later, however, to be quite an acceptable approximation. Interestingly, the use of a full fourier series containing all the odd and even sine and cosine terms defining no particular symmetry in distortion can alter significantly the order of magnitude of the problem. As a typical example using 5 terms in each of the displacement series, the number of unknowns assuming symmetry in distortion is 95. By assuming no symmetry in distortion the number of unknowns almost doubles to 175.

From all the initial work done the author was unable to achieve much degree of success. The series convergence was exceedingly poor and equilibrium in terms of the stress and strain concentration

factors (S.C.F.) were not well satisfied. The work, however, was not lost. In being divorced from a computer, except for inversion of the coefficient matrix, the author found much of the actual computation, although in many instances exceedingly laborious, unusually effective in highlighting the problems associated with formulation of the solution. Moreover, the mere possibility of the existence of a single simplified solution was considered sufficient justification for the work.

The work was continued by a more complex solution containing only the approximations inherent in thin shell theory. This solution was implemented on an ICL 2980 main-frame computer, using complete fourier series for the distortion displacements. The method used in the program of constructing the minimisation and integration procedure was developed by the author. Unfortunately, it proved to be ineffective in running within the maximum allocation of 7200 seconds CPU time. Further modifications to the program did little to enhance the running time and the method was finally abandoned. Despite all attempts, this restriction in program running time was to prove the main stumbling block throughout the study.

A similar analysis was then performed using Thomson's method. This method uses only the values of the complete total potential energy function with the minimisation being performed using a matrix technique. This is in contrast with the previous method where the displacement coefficients of each strain component in the strain energy function were integrated separately. Here the radial distortion component of displacement was taken in two forms:

$$w(\phi) = \sum_{n=1} A_n \sin(n\phi) + B_n \cos(n\phi)$$

$$n=1,2,3, \ldots . \infty \qquad \ldots (3.8)$$

$$w(\phi) = \sum_{n=1} A_n \sin(n\phi)$$

$$n=1,2,3, \ldots . \infty \qquad \ldots (3.9)$$

For a limited number of terms the author was able to establish clearly the importance of the even sine terms and the odd cosine terms in equation (3.8) and the even sine terms in equation (3.9), the remaining terms in equations (3.8) and (3.9) being of no significance. Being able to adopt this symmetry in distortion, as mentioned earlier, resulted in a significant reduction in the size of the problem. However, it is worthwhile pointing out at this stage that this symmetry could not be employed to advantage in integration of the strain energy function. The reasons for this shall become apparent later. The main cause is the difference in symmetry displayed by the distortion displacements and rigid section displacements. This method using symmetry in the distortion displacements was then extended to examine various forms of circumferential series together with different types of non-dimensionalisation of the displacement coefficients.

The problem of excessive program running time persisted, however, with solutions using 5 terms in each displacement series taking upwards of 1500 sec. CPU time. (On this particular computer, programs running in excess of 1000 sec. CPU time were considered "big". This is not a criticism of the actual computer, the levels of use being dictated mainly by the management system.) Generally, it was found that convergence was faster for a bend angle α of 90° compared to bend angle α of 180°, for a particular λ value and $(\frac{R}{r})$ ratio. In fact, for a bend

angle $\alpha \leq 90°$ the solution appeared satisfactory. This method actually represents a general solution in that it considers any bend angle. A solution using the circumferential symmetry displayed by a bend angle α of 180° had been examined earlier without success. In order to reduce the program running time, which was greatest on a bend angle α of 180° due to the increased number of integration points, a further look was taken at this type of solution. The problem of poor convergence, however, found earlier was not resolved. The need for this solution, by reducing the integration on the flanged bend was expected to be even more important with the end condition of tangent pipes. Further, it would be useful in confirming the general solution for this particular bend angle. As shown in Figure (3.3) a bend angle α of 180° exhibits a plane of symmetry through the bend centre. This condition of symmetry arises from the equilibrium conditions peculiar to this bend geometry. It is in fact similar to two 90° bends placed back to back. In the case of in-plane bending, Thomson's results show that for a particular range of pipe bend parameters the flexibility factor for a bend angle α of 180° is approximately twice that for a 90° bend. In the case of out-of-plane bending, due to the symmetry in loading this approximation is expected to be even more valid although there will still be a limit on the applicability. The analysis of a 90° bend requires the boundary conditions on distortion displacement of a thick flange at each end. In a 180° bend this particular boundary condition cannot be applied at the centre of the bend. Here the boundary condition of a "thin flange" is required where the value of zero slope on the radial component of distortion is no longer enforced. This, together with other boundary conditions peculiar to this configuration, will still,

however, ensure that for out-of-plane bending the flexibility factor for a 180° bend, will as in the case of in-plane bending, be only approximately twice that of a 90° bend.

At around this time the service on the ICL 2980 computer began to deteriorate. Failures of the system began to appear more frequently arising from a combination of communication system failures and "crashes" on the computer itself. Added to this, the system was being over-subscribed resulting in a general slowing down and increase in turn around time. All this did little but aggravate the situation.

In a further approach to reduce the program running time, attention was focused on the methods of integration. All the work up to now had used a STANDARD SIMPSONS $\frac{1}{3}$rd RULE [215,216,217] adapted to integrate in two directions. The first modification made was storage of the integrals already evaluated. An illustration of the method is shown in Figure (3.4). In Figure (3.5) it is clearly seen that as the number of terms in the displacement series increases the amount of additional computation can reduce dramatically. A comparison made using this method is shown in Figure (3.6). Unfortunately, the approach was found to be totally dependent on the computer reliability and was eventually abandoned. A less dynamic method evaluating all the necessary integrals prior to running the program was also examined. Here, however, the filestore allocation was exceeded.

The next step was the examination of different methods of integration. For this a GAUSSIAN QUADRATURE method [218,219,220] was employed together with a combination of this and the Standard Simpson's rule. In Simpson's rule increasing the number of integration points leads theoretically to an increased accuracy. This could be accomplished simply by the changing of two variables in the input data defining the

number of points in each integration direction. Using Gaussian Quadrature the change in the number of integration points, whose position along each co-ordinate could not be defined a priori, was more awkward. Here the method required the re-definition of a group of weighting functions and coefficients which in Simpson's rule were automatically evaluated. Most standard texts on numerical integration methods define Gaussian Quadrature to require generally half the number of integration points compared with Simpson's rule, for a given accuracy. To account for the more rapidly varying displacement around the bend cross-section a combination of Gaussian Quadrature integrating in the meridional direction and Simpson's rule in the circumferential direction was then tried. For a bend angle α of 180°, however, the critical direction was found to be along the circumferential co-ordinate (θ). Further, it was discovered in all three methods that increasing the number of integration points did not as expected lead to an improved accuracy. In fact significant variations were found, with the flexibility factor reducing as the number of integration points increased. Also under particular conditions the flexibility factor diverged. Using Simpson's rule, for example, this instability occurred when the number of integration points in the circumferential direction ($\bar{N}_\theta$) equalled the number of terms in the circumferential series (m). The phenomena of requiring fewer integration points than would be normally expected is encountered in finite element analysis. This unusual characteristic termed "reduced integration", i.e. the use of fewer integration points, is discussed by ZIENKIEWICZ [221] and other writers in the field of numerical methods in finite elements. The reasons for this behaviour, however, are not entirely clear. Bathie and Almeida [162] in their

formulation of a pipe bend element on the finite element package ADINAP mention that in using low-order beam and plate elements the element can sometimes display too stiff a behaviour. The use of reduced integration can drastically improve some analysis although they do mention that spurious results may occur so that it is often difficult to assess the reliability of the solution. A typical example of reduced integration is given by TAKEDA and ISHA [222]. Using simple beam elements to model a cantilever beam they show that reduced integration can dramatically improve convergence. However, as shown in Figure (3.7) this requires the non-reduced solution as a check on convergence. Without such a check the results are meaningless. A convergence check on the pipe bend solution would require program running time in excess of the maximum permitted and although some time was spent on this approach it was eventually abandoned.

The work had now reached a stage where in terms of program running time all but a bend angle α of 180° could be analysed satisfactorily. The circumferential symmetry displayed by this bend angle was examined again. This time a solution appeared successful. The problem of previous analyses in incorrectly defining the displacement symmetries being annoyingly all too apparent. The convergence rate, however, was improved only slightly and the results did not compare well with those of the general solution. Accordingly, this solution type was abandoned and the work continued with the general form of solution applicable to any bend angle.

It was not envisaged possible to complete the work using the existing computer system, although updated to an ICL 2988. By good fortune the author was able to access another system, namely a VAX 750, giving improved running time in the sense that many of the

limiting parameters were removed. The remainder of the work was completed using this system.

In order to clarify the presentation, this chapter will deal primarily with a description of the general solution, although reference will be made to other solutions incorporating varying degrees of approximation. The method presented will use the theorem of minimum total potential energy incorporating Thomson's matrix solution. In integration the emphasis will be placed on Simpson's rule as this proved to be the most consistent and easiest to apply.

3.2 Displacements

3.2.1 Displacement formulation

In formulating the displacements the method used by Thomson [134] will be adopted. This method is similar to that used by a number of authors such as Axelrad [145] and DEN HARTOG [223] in their analysis of in-plane bending. The latter does not consider the effect of end constraints; however, the principle of combining the displacement forms of distortion in cross-section and stretching of the outer fibres in bending are the same.

In Thomson's method the displacement field, comprising a set of suitable kinematically admissable displacement functions, is considered in two parts. The first set of displacements are termed "rigid section displacements" (w_R, v_R, u_R) which are associated with the displacement of the circular tube cross-section with no change in their configuration. These displacements are akin to the simple bending mode defined by Axelrad. The second set of displacements are termed "distortion displacements" (w_D, v_D, u_D) which are associated with distortion of the cross-section. The total displacements (w, v, u) are then found by adding the two sets of displacements.

One of the main advantages in decomposing the displacements in this fashion is that the boundary conditions on the displacement functions can be applied more easily. Further, it leads to a better understanding of the complex loading condition of a bending and torsional moment both varying along the length of the bend.

The strains forming the strain energy function are then evaluated by substituting the total displacements into the strain-displacement relations given by equation (2.13).

3.2.2 Rigid section displacements

The rigid section displacements are defined as the displacements of the circular tube cross-section with the cross-section remaining circular. This requirement does not preclude the rotation of a cross-section about its own axis as will be the case due to the out-of-plane moment changing to a torsional moment. The displacements, however, must satisfy the boundary conditions and at the same time provide a variation with respect to the circumferential co-ordinate (θ).

Consider a smooth pipe bend of circular cross-section under the action of an out-of-plane bending moment M, with a circumferential mean radius of curvature R, a meridional radius of curvature r and an overall bend angle α. The bend is terminated by thick rigid flanges at both ends and under fully fixed conditions at $\theta=0°$.

The rigid section displacements of the bend will be derived from the displacements of the bend centre-line. A general illustration of these displacements is shown in Figure (3.8). $U_c(\theta)$ is the circumferential tangential displacement of the centre-line, $H_c(\theta)$ is the displacement of the centre-line in a direction normal to it and $\gamma_c(\theta)$ is the rotation of the bend centre-line associated with the out-of-plane moment M.

Another displacement remains - the rotation of the bend centre-line about its own axis due to the varying torsional moment. The applied moment M, unlike the case of in-plane bending, does not remain constant along the length of the bend. Here the applied moment M changes from a pure out-of-plane moment at $\theta=\alpha$ to a pure torsional moment at $\theta=(\alpha-90°)$. The torsional moment produces a constant value of rotation of the cross-section at a particular value of θ. This displacement as a rigid section displacement is accounted for by introducing an additional displacement $T_c(\theta)$ in the tangential displacement v_R.

The corresponding shell displacements w_R, v_R and u_R at a point on the circular cross-section are then given by:

$$w_R = -H_c(\theta)\cos\phi$$

$$v_R = H_c(\theta)\sin\phi - T_c(\theta)$$

$$u_R = \gamma_c(\theta)r\cos\phi - U_c(\theta) \qquad \ldots (3.10)$$

The above equations (3.10) represent in a most general sense the rigid section displacements of the pipe bend compatible with the applied out-of-plane bending moment. Furthermore, by virtue of their derivation the boundary conditions are automatically satisfied on all but one of the displacements, namely $T_c(\theta)$.

A further set of rigid section displacements will be considered. Here a form of coupling will be assumed between the displacements $H_c(\theta)$ and $\gamma_c(\theta)$. This coupling will take the form:

$$\gamma_c = \frac{\partial H_c(\theta)}{R\partial\theta} \qquad \ldots (3.11)$$

Equation (3.11) defines the simple mathematical relation between the displacement and slope at a point. Introducing this form of coupling reduces the number of rigid section displacement coefficients. This, however, has little effect on the overall size of the solution which is governed mainly by the product coefficients in the distortion displacements. Using this coupling the shell displacements w_R, v_R and u_R can be written as:

$$w_R = -H_c(\theta)\cos\phi$$

$$v_R = H_c(\theta)\sin\phi - T_c(\theta)$$

$$u_R = \frac{\partial H_c(\theta)}{\partial \theta}\,\frac{r}{R}\cos\phi - U_c(\theta) \qquad \ldots (3.12)$$

The form of the displacements given by equations (3.10) requires four independent series to describe the displacements, whereas in equations (3.12) only three independent series are required. A comparison of both forms of displacements showed that the latter type, incorporating coupling, gave better convergence. Further, the circumferential displacement $U_c(\theta)$ was shown in both cases to be insignificant. This displacement describes the extension of the bend centre-line. From the reduced flexibility displayed by out-of-plane bending compared with in-plane bending it is to be expected that this displacement in turn will also be small.

Accordingly, the rigid section shell displacements will be taken with the following form:

$$w_R = -H_c(\theta)\cos\phi$$

$$v_R = H_c(\theta)\sin\phi - T_c(\theta)$$

$$u_R = \frac{r}{R}\,\frac{\partial H_c(\theta)}{\partial \theta}\cos\phi \qquad \ldots (3.13)$$

If equations (3.13) are substituted into the strain displacement equations of Novozhilov as given earlier by equations (2.13) the mid-surface shear strain $\gamma_{\theta\phi}$ and shear curvature $K_{\theta\phi}$ are not zero. This is contrary to Thomson's solution for in-plane bending where both strains are zero. Equations (3.13) contain a torsional component in the displacement v_R

which gives rise to a displacement not displayed by in-plane bending. They do not constitute true rigid body motion in the manner defined by shell theory and it is important to recognise this fact. A more appropriate definition would perhaps have been that of "primary displacements" as used by Findlay [140]. Here, however, the term distortion displacements would be replaced by "secondary displacements", an alternative which was not considered suitable in describing these displacements. A more appropriate terminology has been adopted in the finite element approach. Here the equivalent terms for rigid section and distortion are replaced by beam modes and ovalisation respectively. The requirement now is to define suitable expressions for each of the displacements defined in equation (3.13), which will approximate to the true displacements. Using the Rayleigh Ritz method the displacement functions are required to satisfy the essential boundary conditions only. As described in CHAPTER (2) satisfaction of the natural boundary conditions is not deemed as a specific requirement. However, satisfaction of both sets of boundary conditions will naturally improve the accuracy of the solution.

The displacement functions will be specified as trigonometric series in the circumferential coordinate θ. The use of polynomials and a combination of polynomials and trigonometric series was examined. Both these cases, however, resulted in numerical instabilities, and as such the trigonometric series were adopted.

Using the coupled form of the rigid-section shell displacements, as given by equation (3.13), the displacement series for $H_c(\theta)$ and $T_c(\theta)$ are as follows:

(i) For the displacement $H_c(\theta)$ the boundary conditions are:

$$H_c(0) = \frac{\partial H_c(0)}{\partial \theta} = 0$$

these conditions can be satisfied using an even series:

$$H_c(\theta) = A_o + \sum_{j=1} A_j \cos\left(\frac{j\pi\theta}{2\alpha}\right) \qquad \ldots (3.14)$$

$$H_c(0) = 0 = A_o + \sum_{j=1} A_j \quad \therefore A_o = -\sum_{j=1} A_j$$

substituting in (3.14) gives:

$$H_c(\theta) = \sum_{j=1} A_j \left[\cos\left(\frac{j\pi\theta}{2\alpha}\right) - 1\right]$$

using the identity $\sin^2\beta = \frac{1}{2}(1-\cos 2\beta)$ gives:

$$H_c(\theta) = -2\sum_{j=1} A_j \sin^2\left(\frac{j\pi\theta}{4\alpha}\right) \qquad \ldots (3.15)$$

and hence $\gamma_c = \frac{1}{R}\frac{\partial H_c(\theta)}{\partial \theta} = -\frac{1}{R}\sum_{j=1} A_j \left(\frac{j\pi}{2\alpha}\right) \sin\left(\frac{j\pi\theta}{2\alpha}\right)$ $\qquad \ldots (3.16)$

(ii) For the displacement $T_c(\theta)$ the boundary conditions are:

$$T_c(0) = T_c(\alpha) = 0$$

these conditions are satisfied using an odd series of the form:

$$T_c(\theta) = \sum_{j=1} B_j \sin\left(\frac{j\pi\theta}{\alpha}\right) \qquad \ldots (3.17)$$

By substitution of equations (3.15), (3.16) and (3.17) into equation (3.13), the rigid section shell displacements can be written as:

$$w_R = \sum_{j=1} 2A_j \cos\phi \sin^2\left(\frac{j\pi\theta}{4\alpha}\right)$$

$$v_R = \sum_{j=1} -2A_j \sin\phi \sin^2\left(\frac{j\pi\theta}{4\alpha}\right) - B_j \sin\left(\frac{j\pi\theta}{\alpha}\right)$$

$$u_R = -\sum_{j=1} A_j \frac{r}{R}\left(\frac{j\pi}{2\alpha}\right) \cos\phi \sin\left(\frac{j\pi\theta}{2\alpha}\right)$$

for $j = 1,2,3 \ldots\ldots\infty$ . . . *(3.18)*

3.2.3 Distortion displacements

The distortion displacements are the displacements associated with the distortion of the circular tube cross-section. Thomson, in his description of these displacements, refrains from using the term "ovalisation", preferring instead the term distortion as the resultant shape is not always strictly oval. Much use is made in the literature of both terms. However, the terminology defined by Thomson will be adhered to here.

The flanges terminating the bend are assumed to be "thick" and rigid. As such, deformation of the cross-section and rotation of the normal to the shell mid-surface at the flange are assumed to be zero relative to the flange. However, cross-sections removed from the flange will experience varying degrees of distortion depending on their distance from the flange. Having the distortion displacement (w_D, v_D, u_D) varying in two orthogonal directions naturally leads to the displacement being split to form the components of displacement corresponding to each direction. The first component describes the distortion of the meridian ($w(\phi)$, $v(\phi)$, $u(\phi)$) giving the general distortion of the cross-section. The second component ($w(\theta)$, $v(\theta)$, $u(\theta)$) describes the variation of this distortion with respect to the circumferential co-ordinate θ.

The distortion displacements are then formed by the product of the meridional and circumferential component.

3.2.3.1 Radial distortion displacement

The expected form of the distortion is most easily sought from the radial distortion displacement w_D. It characterises the distortion shape of the cross-section and accordingly will be considered first.

The meridional component ($w(\phi)$) describing the deformation of the meridian has been defined by most authors to take the general form:

$$w(\phi) = \sum_{n=1} A_n \sin(2n\phi) \qquad n=1,2,3,4, \ldots_{\infty} \quad \ldots \quad (3.19)$$

This is the form adopted by Vigness [19] in the first study of out-of-plane bending without end effects. Later, the form of equation (3.19) was extended by Pardue and Vigness [126] to include the odd cosine terms:

$$w(\phi) = \sum_{n=3,5} A_n \cos(n\phi) + \sum_{n=2,4} A_n \sin(n\phi) \qquad n=2,3,4, \ldots_{\infty} \quad \ldots \quad (3.20)$$

Both these forms of $w(\phi)$ given by equations (3.19) and (3.20) result in a distortion shape symmetrical about the plane passing through $\phi = 45°$ and $\phi = 225°$, and are based essentially on an intuitive guess at the form of the expected distortion pattern.

For the analysis to be presented here $w(\phi)$ will be assumed to be symmetrical about the plane of the bend passing through $\phi = +45°$ and $\phi = +225°$. The complete fourier series describing the deformation and satisfying the symmetry condition is similar to that given by equation (3.20):

$$w(\phi) = \sum_{n=1,3} A_n \cos(n\phi) + \sum_{n=2,4} A_n \sin(n\phi) \qquad n=1,2,3,4 \ldots\ldots\infty \quad \ldots (3.21)$$

The n=1 term is already present in the rigid section displacement w_R and will not be included in the final form of $w(\phi)$*. Therefore, the meridional component of displacement $w(\phi)$ will be used with form given by equation (3.20):

$$w(\phi) = \sum_{n=3,5} A_n \cos(n\phi) + \sum_{n=2,4} A_n \sin(n\phi) \qquad n=2,3,4 \ldots\ldots\infty \quad \ldots (3.20)$$

The circumferential component of distortion $w(\theta)$ will be considered next. The displacement $w(\theta)$ must satisfy the boundary conditions of:

$$\text{at } \theta = 0 \text{ and } \theta = \alpha, \quad w(\theta) = \frac{\partial w(\theta)}{\partial \theta} = 0$$

These are the boundary conditions of a "thick flange" at $\theta = 0$ and $\theta = \alpha$. The condition of zero slope arises from the boundary conditions given by equation (2.18):

$$\beta_\theta = \frac{1}{R'} \left(u \sin\phi - \frac{\partial w}{\partial \theta}\right)$$

The distortion component of the slope β_θ is zero at the flange as is the distortion component of u.

In this displacement there is no requirement for symmetry with respect to the circumferential coordinate θ. Accordingly, the form of both an odd and an even fourier series will be examined.

---

* In neglecting the n=1 term the numerical stability of the solution was improved. This term was also excluded in $v(\phi)$ and $u(\phi)$.

(i) Using an odd fourier series the general form is:

$$w(\theta) = \sum_{m=1} A_m \sin(m\eta\theta)$$

$$m=1,2,3, \ldots . \infty \quad \ldots \textit{(3.22)}$$

applying a half-range expansion [224] over the interval $0 \leq \theta \leq \alpha$ gives:

$$w(\theta) = \sum_{m=1} A_m \sin(\frac{m\pi\theta}{\alpha})$$

$$m=1,2,3, \ldots . \infty \quad \ldots \textit{(3.23)}$$

this form satisfies the boundary conditions of $w(\theta)$ at $\theta = 0$ and $\theta = \alpha$; at $\theta = 0$:

$$\frac{\partial w(\theta)}{\partial \theta} = 0 = \sum_{m=1} A_m (\frac{m\pi}{\alpha}) \quad \therefore A_1 = -\sum_{m=2} mA_m,$$

$$m=2,3,4, \ldots . \infty$$

substituting in (3.23) gives:

$$w(\theta) = \sum_{m=2} A_m [\sin(\frac{m\pi\theta}{\alpha}) - m\sin(\frac{\pi\theta}{\alpha})]$$

$$m=2,3,4, \ldots . \infty \quad \ldots \textit{(3.24)}$$

at $\theta = \alpha$, $\frac{\partial w(\theta)}{\partial \theta} = 0 = \sum_{m=2} A_m (\frac{m\pi}{\alpha}) [\cos(m\pi) - \cos(\pi)]$,

$$m=2,3,4, \ldots . \infty$$

this condition is satisfied using the odd terms only: $m=3,5,7, \ldots \infty$ hence we can write (3.24) as:

$$w(\theta) = \sum_{m=3,5} A_m [\sin(\frac{m\pi\theta}{\alpha}) - m\sin(\frac{\pi\theta}{\alpha})]$$

$$m=3,5,7, \ldots . \infty \quad \ldots \textit{(3.25)}$$

this equation satisfies all the essential boundary conditions; to account for the even terms consider $\frac{\partial w(\theta)}{\partial \theta}$ evaluated from (3.24) at $\theta = \alpha$:

$$\frac{\partial w(\theta)}{\partial \theta} = 0 = \sum_{m=2,4} A_m \left(\frac{m\pi}{\alpha}\right)[+1+1] + \sum_{m=3,5} A_m \left(\frac{m\pi}{\alpha}\right)[-1+1]$$

$$\therefore A_2 = -\sum_{m=4,6} \frac{m}{2} A_m , \qquad m=4,6,8, \ldots . \infty$$

substituting in (3.24) gives:

$$w(\theta) = \sum_{m=4,6} A_m \left[\sin\left(\frac{m\pi\theta}{\alpha}\right) - \frac{m}{2}\sin\left(\frac{2\pi\theta}{\alpha}\right)\right] + \sum_{m=3,5} A_m \left[\sin\left(\frac{m\pi\theta}{\alpha}\right) - m\sin\left(\frac{\pi\theta}{\alpha}\right)\right]$$

on rearranging:

$$w(\theta) = \sum_{m=1} A1_m \left[\sin\left(\frac{2(m+1)\pi\theta}{\alpha}\right) - (m+1)\sin\left(\frac{2\pi\theta}{\alpha}\right)\right]$$

$$+A2_m \left[\sin\left(\frac{(2m+1)\pi\theta}{\alpha}\right) - (2m+1)\sin\left(\frac{\pi\theta}{\alpha}\right)\right]$$

$$m=1,2,3, \ldots . \infty \qquad \ldots \textit{(3.26)}$$

(ii) Using an even fourier series the general form is:

$$w(\theta) = A_o + \sum_{m=1} A_m \cos(m\eta\theta)$$

$$m=1,2,3, \ldots . \infty \qquad \ldots \textit{(3.27)}$$

applying a half range expansion [224] over the interval $0 \leq \theta \leq \alpha$ gives:

$$w(\theta) = A_o + \sum_{m=1} A_m \cos\left(\frac{m\pi\theta}{\alpha}\right)$$

$$m=1,2,3, \ldots . \infty \qquad \ldots \textit{(3.28)}$$

at $\theta = 0$, $w(\theta) = 0 = A_o + \sum_{m=1} A_m \quad \therefore A_o = -\sum_{m=1} A_m$, $m=1,2,3, \ldots . \infty$

substituting in (3.28) gives:

$$w(\theta) = \sum_{m=1} A_m \left[\cos\left(\frac{m\pi\theta}{\alpha}\right) - 1\right], \qquad m=1,2,3, \ldots . \infty \qquad \ldots \textit{(3.29)}$$

and using the identity $\sin^2\beta = \frac{1}{2}(1-\cos 2\beta)$ gives:

$$w(\theta) = -2 \sum_{m=1} A_m \sin^2 \left(\frac{m\pi\theta}{2\alpha}\right), \qquad m=1,2,3, \ldots\ldots\infty \qquad \ldots (3.30)$$

at $\theta = \alpha$, $w(\theta) = 0 = -2 \sum_{m=1} A_m \sin^2 \left(\frac{m\pi}{2}\right)$, $m=1,2,3, \ldots\ldots\infty$

this condition is satisfied using the even terms, $m=2,4,6, \ldots\ldots\infty$

hence we have:

$$w(\theta) = -2 \sum_{m=2,4} A_m \sin^2 \left(\frac{m\pi\theta}{2\alpha}\right), \qquad m=2,4,6, \ldots\ldots\infty \qquad \ldots (3.31)$$

the form given by (3.31) also satisfies the zero slope conditions at $\theta = 0$ and $\theta = \alpha$.

To account for the odd terms consider the form of $w(\theta)$ given by (3.29):

at $\theta = \alpha$, $w(\theta) = 0 = \sum_{m=1} A_m[\cos(m\pi) - 1]$ $\therefore A_1 = -\sum_{m=3,5} A_m$, $m=3,5,7, \ldots\ldots\infty$

substituting in (3.29) gives:

$$w(\theta) = \sum_{m=2,4} A_m\left[\cos\left(\frac{m\pi\theta}{\alpha}\right) - 1\right] + \sum_{m=3,5} A_m\left[\cos\left(\frac{m\pi\theta}{\alpha}\right) - \cos\left(\frac{\pi\theta}{\alpha}\right)\right], \qquad m=2,3,4, \ldots\ldots\infty$$

and using the following identities: $\sin^2\beta = \frac{1}{2}(1-\cos 2\beta)$ and $\cos\phi - \cos\beta = -2\sin\left(\frac{\phi+\beta}{2}\right)\sin\left(\frac{\phi-\beta}{2}\right)$

this gives:

$$w(\theta) = -2\left[\sum_{m=2,4} A_m \sin^2\left(\frac{m\pi\theta}{2\alpha}\right) + \sum_{m=3,5} A_m \sin\left(\frac{(m+1)\pi\theta}{2\alpha}\right)\sin\left(\frac{(m-1)\pi\theta}{2\alpha}\right)\right], \qquad m=2,3,4, \ldots\ldots\infty$$

and on rearranging gives:

$$w(\theta) = -2 \sum_{m=1} A1_m \sin^2\left(\frac{m\pi\theta}{\alpha}\right) + A2_m \sin\left(\frac{(m+1)\pi\theta}{\alpha}\right)\sin\left(\frac{m\pi\theta}{\alpha}\right)$$

$$m=1,2,3, \ldots\ldots\infty \quad \ldots \textit{(3.32)}$$

The choice of coefficients is purely arbitrary in the displacement functions and the use of similar coefficients in equations (3.26) and (3.32) does not infer equality, i.e.:

$$A1_m \text{ in equation (3.26)} \neq A1_m \text{ in equation (3.32)}$$

From the derivation of both the odd and even fourier series for $w(\theta)$, given by equations (3.26) and (3.32), it can be seen that not all the terms in each series are required to satisfy the essential boundary conditions. For example, in the odd fourier series (3.26) the boundary conditions are also satisfied using only the odd terms:

$$w(\theta) = \sum_{m=1} A2_m \left[\sin\left(\frac{(2m+1)\pi\theta}{\alpha}\right) - (2m+1)\sin\left(\frac{\pi\theta}{\alpha}\right)\right]$$

$$m=1,2,3, \ldots\ldots\infty \quad \ldots \textit{(3.33)}$$

Whereas in the even fourier series (3.32) the boundary conditions are also satisfied using only the even terms of the series:

$$w(\theta) = -2 \sum_{m=1} A1_m \sin^2\left(\frac{m\pi\theta}{\alpha}\right), \qquad m=1,2,3, \ldots\ldots\infty \quad \ldots \textit{(3.34)}$$

The form given by equation (3.34) represents the simplest form and in fact can be obtained by inspection. However, in the analysis of a bend angle α of 180° this form (3.34) was unable to provide the required circumferential symmetry. This was accomplished by including the odd terms of the series.

A similar result was found using the odd fourier series given by equations (3.31) and (3.32).

In choosing an appropriate series for this important displacement a comprison was made between the full odd and even fourier series. As both series gave nearly identical results, the slightly simpler form of the even fourier series (3.32) was chosen.

The radial distortion displacement w_D is found from the product of the displacement components $w(\phi)$ and $w(\theta)$. The form of w_D will be simplified using an abbreviated form on the separated odd and even terms in $w(\phi)$. This is accomplished using the following function:

$$\Psi_{ek} = \begin{cases} 1 & \text{if k is even} \\ 0 & \text{if k is odd} \end{cases} \quad \text{and} \quad \Psi_{ok} = \begin{cases} 0 & \text{if k is even} \\ 1 & \text{if k is odd} \end{cases} \qquad \ldots (3.35)$$

The distortion displacement w_D can now be written as:

$$w_D = \sum_{m=1} \sum_{n=2} [\Psi_{on}\cos(n\phi) + \Psi_{en}\sin(n\phi)]$$
$$[-2[A1_{mn}\sin^2(\tfrac{m\pi\theta}{\alpha}) + A2_{mn}\sin(\tfrac{(m+1)\pi\theta}{\alpha})\sin(\tfrac{m\pi\theta}{\alpha})]]$$
$$m=1,2,3,\ldots_{\infty}$$
$$n=2,3,4,\ldots_{\infty} \qquad \ldots (3.36)$$

3.2.3.2 Meridional tangential distortion displacement

The meridional tangential distortion displacement v_D is generally derived from, or used to derive, the radial distortion displacement w_D. This constitutes the assumption of an inextensible meridian which in shell theory is equivalent to saying that the meridional direct strain ε_ϕ is zero, i.e.:

$$\varepsilon_\phi = \frac{1}{r}\left(\frac{\partial v}{\partial \phi} + w\right) = 0$$

hence $$w = -\frac{\partial v}{\partial \phi} \qquad \ldots (3.37)$$

or $$v = -\int w d\phi + C \qquad \ldots (3.38)$$

Having already defined the form of w_D, substitution of equation (3.20) into equation (3.38) gives:

$$v(\phi) = \sum_{n=1,3} -\frac{1}{n} A_n \sin(n\phi) + \sum_{n=2,4} \frac{1}{n} A_n \cos(n\phi)$$

$$n=1,2,3, \ldots . \infty \qquad \ldots (3.39)$$

The displacement $w(\phi)$ has been defined as having symmetry through the plane $\phi = 45°$ and $\phi = 225°$. Hence the constant of integration C in (3.38) disappears.

For the main analysis the assumption of $\varepsilon_\phi = 0$ will not be used. The effect of including this assumption was, however, examined and found to be significant. Adopting the general form given by (3.39) the displacement $v(\phi)$ will be taken as:

$$v(\phi) = \sum_{n=1,3} B_n \sin(n\phi) + \sum_{n=2,4} B_n \cos(n\phi)$$

$$n=1,2,3,4, \ldots . \infty \qquad \ldots (3.40)$$

The n=1 term is already included in the rigid section displacement v_R and will not be included in the final form of $v(\phi)$. Therefore the displacement $v(\phi)$ will be taken as:

$$v(\phi) = \sum_{n=3,5} B_n \sin(n\phi) + \sum_{n=2,4} B_n \cos(n\phi)$$

$$n=2,3,4, \ldots\ldots\infty \qquad \ldots \textit{(3.41)}$$

The variation of the meridional tangential distortion displacement $v(\theta)$ in the circumferential direction will now be examined.

The boundary conditions for $v(\theta)$ are:

at $\theta = 0$ and $\theta = \alpha$, $v(\theta) = 0$

these conditions can be satisfied using an odd fourier series:

$$v(\theta) = \sum_{m=1} B_m \sin(m\eta\theta), \qquad m=1,2,3, \ldots\ldots\infty \qquad \ldots \textit{(3.42)}$$

a half-range expansion [224] taken over the interval $0 \leq \theta \leq \alpha$ satisfies the boundary conditions giving:

$$v(\theta) = \sum_{m=1} B_m \sin\left(\frac{m\pi\theta}{\alpha}\right), \qquad m=1,2,3, \ldots\ldots\infty \qquad \ldots \textit{(3.43)}$$

Using the function Ψ defined in equation (3.35) the meridional tangential distortion displacement v_D can be written as:

$$v_D = \sum_{m=1} \sum_{n=2} \left[\Psi_{on} \sin(n\phi) + \Psi_{en} \cos(n\phi)\right] B_{mn} \sin\left(\frac{m\pi\theta}{\alpha}\right)$$

$$m=1,2,3, \ldots\ldots\infty$$

$$n=2,3,4, \ldots\ldots\infty \qquad \ldots \textit{(3.44)}$$

3.2.3.3 Circumferential tangential distortion displacement

The importance of the circumferential tangential distortion displacement u_D in the study of pipe bends with end effects is not entirely clear. Furthermore, under the complex loading of out-of-plane bending it is difficult to imagine what effect it has on a purely intuitive basis. What can be said however, is that it is expected to play a less significant role under out-of-plane bending compared with in-plane bending due to the reduced flexibility in the out-of-plane mode.

For the meridional displacement component $u(\phi)$ the distortion will be assumed to be symmetrical about the plane of the bend passing through $\phi = 45°$ and $\phi = 225°$. The complete fourier series describing the deformation and satisfying the symmetry condition is given by:

$$u(\phi) = \sum_{n=1,3} C_n \cos(n\phi) + \sum_{n=2,4} C_n \sin(n\phi)$$

$$n=1,2,3,4, \ldots_{\infty} \quad \ldots \quad (3.45)$$

The n=1 term is already present in the rigid section displacement u_R and will not be included in the final form of $u(\phi)$. Therefore, the final form of the meridional component $u(\phi)$ is given by:

$$u(\phi) = \sum_{n=3,5} C_n \cos(n\phi) + \sum_{n=2,4} C_n \sin(n\phi)$$

$$n=2,3,4, \ldots_{\infty} \quad \ldots \quad (3.46)$$

The variation of the circumferential tangential distortion displacement $u(\theta)$ in the circumferential direction will now be examined.

The boundary conditions for $u(\theta)$ are:

at $\theta = 0$ and $\theta = \alpha$, $u(\theta) = 0$

these conditions are satisfied using an odd fourier series of the form:

$$u(\theta) = \sum_{m=1} C_m \sin(m\eta\theta) \ , \qquad m=1,2,3, \ldots . \infty \quad \ldots (3.47)$$

the boundary conditions are satisfied by taking a half-range expansion [224] over the interval $0 \leq \theta \leq \alpha$ to give:

$$u(\theta) = \sum_{m=1} C_m \sin(\frac{m\pi\theta}{\alpha}) \ , \qquad m=1,2,3, \ldots . \infty \quad \ldots (3.48)$$

Forming the product of the meridional $u(\phi)$ and circumferential component $u(\theta)$, the circumferential tangential distortion displacement u_D is:

$$u_D = \sum_{m=1} \sum_{n=2} [\Psi_{on}\cos(n\phi) + \Psi_{en}\sin(n\phi)] C_{mn} \sin(\frac{m\pi\theta}{\alpha})$$

$$m=1,2,3, \ldots . \infty$$
$$n=2,3,4, \ldots . \infty \quad \ldots (3.49)$$

The definition of the function Ψ is given in equation (3.35).

3.2.3.4 Distortion displacement summary

$$w_D = \sum_{m=1} \sum_{n=2} [\Psi_{on}\cos(n\phi) + \Psi_{en}\sin(n\phi)]$$
$$[A1_{mn}\sin^2(\frac{m\pi\theta}{\alpha}) + A2_{mn}\sin(\frac{(m+1)\pi\theta}{\alpha})\sin(\frac{m\pi\theta}{\alpha})]$$

$$v_D = \sum_{m=1} \sum_{n=2} [\Psi_{on}\sin(n\phi) + \Psi_{en}\cos(n\phi)] B_{mn} \sin(\frac{m\pi\theta}{\alpha})$$

$$u_D = \sum_{m=1} \sum_{n=2} [\Psi_{on}\cos(n\phi) + \Psi_{en}\sin(n\phi)] C_{mn} \sin(\frac{m\pi\theta}{\alpha})$$

$$m=1,2,3, \ldots . \infty$$
$$n=2,3,4, \ldots . \infty \quad \ldots (3.50)$$

where $A1_{mn} = -2A1_{mn}$ and $A2_{mn} = -2A2_{mn}$.

3.2.4 *Total displacements*

The total displacements are found by adding the distortion and rigid section displacements:

$$w = w_D + w_R$$
$$v = v_D + v_R$$
$$u = u_D + u_R$$

Using equations (3.18) and (3.50) the total displacements can be written as:

$$w = \sum_{m=1} \sum_{n=2} [\Psi_{on}\cos(n\phi) + \Psi_{en}\sin(n\phi)] [A1_{mn}\sin^2(\frac{m\pi\theta}{\alpha}) + A2_{mn}\sin(\frac{(m+1)\pi\theta}{\alpha})\sin(\frac{m\pi\theta}{\alpha})] + \sum_{j=1} 2A_j\cos\phi\sin^2(\frac{j\pi\theta}{4\alpha})$$

$$v = \sum_{m=1} \sum_{n=1} [\Psi_{on}\sin(n\phi) + \Psi_{en}\cos(n\phi)] B_{mn}\sin(\frac{m\pi\theta}{\alpha}) + \sum_{j=1} -2A_j\sin\phi\sin^2(\frac{j\pi\theta}{4\alpha}) - B_j\sin(\frac{j\pi\theta}{\alpha})$$

$$u = \sum_{m=1} \sum_{n=2} [\Psi_{on}\cos(n\phi) + \Psi_{en}\sin(n\phi)] C_{mn}\sin(\frac{m\pi\theta}{\alpha}) - \sum_{j=1} A_j \frac{r}{R} (\frac{j\pi}{2\alpha})\cos\phi\sin(\frac{j\pi\theta}{2\alpha})$$

$$m=1,2,3, \ldots. MT$$
$$n=2,3,4, \ldots.(NT+1)$$
$$j=1,2,3, \ldots. JT \quad \ldots \quad (3.51)$$

The previously infinite summations have been replaced here by finite sums. MT, NT and JT are the total numbers of terms in the m, n and j series, respectively.

3.3 Strains

The strains are obtained by substituting the total displacements given by equations (3.51) into the strain-displacement equations (2.13). This gives the strains as follows:

$$\varepsilon_\phi = \frac{1}{r}\Bigg[\sum_m\sum_n\Bigg[[\Psi_{on}\cos(n\phi) + \Psi_{en}\sin(n\phi)]\,[A1_{mn}\sin^2(\tfrac{m\pi\theta}{\alpha}) + A2_{mn}\sin(\tfrac{(m+1)\pi\theta}{\alpha})\sin(\tfrac{m\pi\theta}{\alpha})] + [n\Psi_{on}\cos(n\phi) - n\Psi_{en}\sin(n\phi)]\,B_{mn}\sin(\tfrac{m\pi\theta}{\alpha})\Bigg]\Bigg]$$

$$\varepsilon_\phi = \frac{1}{R'}\Bigg[\sum_j\Bigg[-\cos\phi\,[A_j(\tfrac{j\pi}{2\alpha})^2\frac{r}{R}\cos(\tfrac{j\pi\theta}{2\alpha}) + B_j\sin(\tfrac{j\pi\theta}{\alpha})]\Bigg] + \sum_m\sum_n\Bigg[[\Psi_{on}\cos(n\phi) + \Psi_{en}\sin(n\phi)]\,[\sin\phi\,[A1_{mn}\sin^2(\tfrac{m\pi\theta}{\alpha}) + A2_{mn}\sin(\tfrac{(m+1)\pi\theta}{\alpha})\sin(\tfrac{m\pi\theta}{\alpha})] + C_{mn}(\tfrac{m\pi}{\alpha})\cos(\tfrac{m\pi\theta}{\alpha})] - [\Psi_{on}\sin(n\phi) + \Psi_{en}\cos(n\phi)]B_{mn}\sin(\tfrac{m\pi\theta}{\alpha})\Bigg]\Bigg]$$

$$\gamma_{\theta\phi} = \frac{1}{R'}\Bigg[\sum_j\Bigg[A_j(\tfrac{j\pi}{2\alpha})\frac{r}{R}\sin(\tfrac{j\pi\theta}{2\alpha}) - B_j(\tfrac{j\pi}{\alpha})\cos(\tfrac{j\pi\theta}{\alpha})\Bigg] + \sum_m\sum_n\Bigg[[\Psi_{on}\sin(n\phi) + \Psi_{en}\cos(n\phi)]\,B_{mn}(\tfrac{m\pi}{\alpha})\cos(\tfrac{m\pi\theta}{\alpha}) + [-\Psi_{on}[\cos\phi\cos(n\phi) + \frac{nR'}{r}\sin(n\phi)] + \Psi_{en}[-\cos\phi\sin(n\phi) + n\frac{R'}{r}\cos(n\phi)]]\,C_{mn}\sin(\tfrac{m\pi\theta}{\alpha})\Bigg]\Bigg]$$

$$K_\phi = \frac{1}{r^2}\left[\sum_m\sum_n\left[[n^2\Psi_{on}\cos(n\phi) + n^2\Psi_{en}\sin(n\phi)][A1_{mn}\sin^2(\frac{m\pi\theta}{\alpha}) + A2_{mn}\sin(\frac{(m+1)\pi\theta}{\alpha})\sin(\frac{m\pi\theta}{\alpha})] + [n\Psi_{on}\cos(n\phi) - n\Psi_{en}\sin(n\phi)]B_{mn}\sin(\frac{m\pi\theta}{\alpha})\right]\right]$$

$$K_\theta = \frac{1}{(R')^2}\left[\sum_j - Z\cos\phi[A_j(\frac{j\pi}{2\alpha})^2\cos(\frac{j\pi\theta}{2\alpha}) + B_j\frac{R}{r}\sin(\frac{j\pi\theta}{\alpha})] + \sum_m\sum_n\left[\frac{R'}{r}\cos\phi[[-n\Psi_{on}\sin(n\phi) + n\Psi_{en}\cos(n\phi)][A1_{mn}\sin^2(\frac{m\pi\theta}{\alpha}) + A2_{mn}\sin(\frac{(m+1)\pi\theta}{\alpha})\sin(\frac{m\pi\theta}{\alpha})] + [\Psi_{on}\sin(n\phi) + \Psi_{en}\cos(n\phi)]B_{mn}\sin(\frac{m\pi\theta}{\alpha})] - [\Psi_{on}\cos(n\phi) + \Psi_{en}\sin(n\phi)][2A1_{mn}(\frac{m\pi}{\alpha})^2\cos(\frac{2m\pi\theta}{\alpha}) + A2_{mn}(\frac{\pi}{\alpha})^2[-(m^2+(m+1)^2)\sin(\frac{(m+1)\pi\theta}{\alpha})\sin(\frac{m\pi\theta}{\alpha}) + 2m(m+1)\cos(\frac{(m+1)\pi\theta}{\alpha})\cos(\frac{m\pi\theta}{\alpha})]]\right]\right]$$

$$K_{\theta\phi} = \frac{1}{(rR')}\left[\sum_j[A_j(\frac{j\pi}{2\alpha})\frac{r}{R}\sin(\frac{j\pi\theta}{2\alpha}) - B_j(\frac{j\pi}{\alpha})\cos(\frac{j\pi\theta}{\alpha})] + \sum_m\sum_n\left[[\Psi_{on}\sin(n\phi) + \Psi_{en}\cos(n\phi)]B_{mn}(\frac{m\pi}{\alpha})\cos(\frac{m\pi\theta}{\alpha}) + [\frac{r}{R'}\cos\phi[\Psi_{on}\cos(n\phi) + \Psi_{en}\sin(n\phi)] - [-n\Psi_{on}\sin(n\phi) + n\Psi_{en}\cos(n\phi)]][A1_{mn}(\frac{m\pi}{\alpha})\sin(\frac{2m\pi\theta}{\alpha}) + A2_{mn}(\frac{\pi}{\alpha})[(m+1)\cos(\frac{(m+1)\pi\theta}{\alpha})\sin(\frac{m\pi\theta}{\alpha}) + m\sin(\frac{(m+1)\pi\theta}{\alpha})\cos(\frac{m\pi\theta}{\alpha})]] + [[-n\Psi_{on}\sin(n\phi) + n\Psi_{en}\cos(n\phi)] - \frac{r}{R'}\cos\phi[\Psi_{on}\cos(n\phi) + \Psi_{en}\sin(n\phi)]]C_{mn}\sin\phi\sin(\frac{m\pi\theta}{\alpha})\right]\right] \quad \ldots (3.52)$$

where $R' = R + r\sin\phi$

$$Z = \left(1 + \frac{r}{R}\sin\phi\right)$$

$$\sum_{j} = \sum_{j=1}^{JT}, \qquad j = 1,2,3, \ldots. JT$$

$$\sum_{m} = \sum_{m=1}^{MT}, \qquad m = 1,2,3, \ldots. MT$$

$$\sum_{n} = \sum_{n=2}^{NT}, \qquad n = 2,3,4, \ldots. (NT + 1)$$

3.4 Numerical Solution

3.4.1 Introduction

In the solution to the problem of the flanged pipe bend under out-of-plane bending, using the theorem of minimum total potential energy, there are three main activities to be performed. These are as follows:

(i) Integration of the total potential energy (T.P.E.) function.

(ii) Minimisation of the T.P.E. function leading to a set of simultaneous equations involving all the unknown displacement coefficients.

(iii) Determination of the unknown displacement coefficients leading to evaluation of the total displacements, strains and stresses.

The simpler solutions, examined initially, allowed the first two functions of integration and minimisation of the T.P.E. to be performed by hand. The evaluation of the unknown coefficients was then done using a simple matrix inversion procedure.

However, the solution to be presented here given by the displacement series (3.51) and strain equations (3.52) is of a more complex form. The displacement series (3.51) developed involved the use of only the assumptions inherent in thin shell theory and included all the necessary fourier terms in their series. They also satisfy all of the essential boundary conditions for a smooth pipe bend with flanged end constraints. The strains given by equations (3.52) were derived from the displacements and satisfy the requirements of internal and external compatibility. If these strains are substituted into the expression for

the strain energy given by equation (2.16) from which the T.P.E. can be determined, then integration of the expression by hand is virtually impossible. The solution then requires the use of numerical techniques.

3.4.2 Numerical solution methods

The numerical minimum of the T.P.E. function is normally obtained in one of two basic ways.

The simplest method is to numerically integrate the whole T.P.E. function and then use a standard method of direct numerical minimisation. There are a variety of ways of performing direct minimisation. These are illustrated by the work of NELDER and MEAD [225] and HOOKE and JEEVES [226]. The majority of them use some method of searching which is based on evaluation of the complete T.P.E. function. The main advantage of this method is that it only requires the values of the T.P.E. function, for coefficient values that the minimisation routine provides, which is straightforward to program on a computer. This was the procedure used by Spence [100] in his analysis of creep in pipe bends without end effects. However, the procedure of having to numerically integrate the T.P.E. function in two dimensions and then minimise with respect to a large number of variables is time consuming. In fact in the solution to be presented here for out-of-plane bending 156 variables will be used. The time required is also indeterminate as the minimisation technique uses as many function evaluations as it needs rather than a fixed number to find the minimum. Spence only required a one dimensional integration and rarely needed to use more than 5 variables in his problem. Thomson [134] in his study of

in-plane bending of pipe bends with end constraints attempted to use this method. However, he found that the number of variables was limited to about 50 before the computer time and reliability limit of 2 hours was reached. The computer was an ICL 2980, the same machine used initially by this author. Due to the restrictions placed upon the solution this method was therefore not used here. In fact, this method is only capable of dealing with at most one third of the required unknowns. Some idea of the limit this places on the solution to out-of-plane bending can be gained by examining the maximum size of the displacement series (3.51). Here, the limit of 50 unknown variables is reached when m=n=3 for distortion displacements, and j=7 for rigid section displacements. Further, Thomson was able to adopt symmetry in integration in both the meridional and circumferential directions, thereby reducing considerably the time involved in integration. In the problem of out-of-plane bending this symmetry in integration could not be applied.

An alternative method of finding the minimum numerically involves differentiating with respect to each of the required displacement coefficients before performing the integrations. This then produces a set of simultaneous equations which can be solved. This method was used by SYMONDS [227], Jones [39] and Thailer and Cheng [133] in their analyses of the pipe bend problem. The difficulty in this method is that all of the terms in the solution matrix have to be numerically integrated separately. Although general expressions can be derived for many of the terms in the matrix there is still a large amount of hand manipulation involved in obtaining a solution. This can be avoided by evaluating the integrals prior to performing the solution. As

mentioned earlier, however, this was of little use due to user restrictions on the computer. The method has advantages over the previous method at least for a linear problem. The time required for a solution would be much smaller and determinate. This method, and variations on it, were attempted. They were abandoned, however, because of the size of the current problem and the difficulties encountered.

In the final solution to be presented here, the method developed by Thomson will be used. This method has the advantages of using only the values of the complete T.P.E. function and minimisation using a matrix technique as opposed to a direct searching method.

3.4.3 Minimisation procedure

The total potential energy expression for linear elasticity is represented by a quadratic function of the displacement coefficients. This means that when the T.P.E. function is differentiated with respect to the coefficients, the resulting equations are linear functions of the displacement coefficients. Since the displacement coefficients are not functions of the bend co-ordinates (θ,ϕ), integration can be performed without numerical values being assigned to the coefficients.

The above principles are the basis of the minimisation procedure developed by Thomson. The description of this method, in what follows, is the same as that given by Thomson. Although this description is felt to be somewhat inadequate by this author in conveying the elegance and power of the method, he has been unable to improve upon it. A better understanding is in fact gained by reading through the computer programme given in APPENDIX (1).

The method is explained by considering the following quadratic expression:

$$V = \int [a_1 x_1^2 + a_2 x_2^2 + a_3 x_1 x_2 + a_4 x_1 + a_5 x_2 + a_6] \, d\xi \qquad \ldots (3.53)$$

where a_1, a_2, a_3, a_4, a_5 and a_6 are functions of ξ and can be considered analogous to the trigonometric sine and cosine terms in the displacement series (3.51). If V is an expression for the total potential energy then the minimum of V can be found by differentiating with respect to the unknown coefficients x_1 and x_2:

$$\frac{\partial V}{\partial x_1} = 0 = \int [2a_1 x_1 + a_3 x_2 + a_4] \, d\xi$$

$$\frac{\partial V}{\partial x_2} = 0 = [2a_2 x_2 + a_3 x_1 + a_5] \, d\xi \qquad \ldots (3.54)$$

These are two simultaneous equations in two unknowns, x_1 and x_2. This can be set up as a matrix equation:

$$\begin{bmatrix} 2\int a_1 d\xi & \int a_3 d\xi \\ \int a_3 d\xi & 2\int a_2 d\xi \end{bmatrix} \begin{bmatrix} x_1 \\ x_2 \end{bmatrix} = \begin{bmatrix} -\int a_4 d\xi \\ \int a_5 d\xi \end{bmatrix}$$

or $$[A][x] = [B] \qquad \ldots (3.55)$$

where [A] is a matrix of constants, [x] is a vector of the unknowns and [B] is a vector of constants.

The terms in the matrix [A] and vector [B] can be numerically integrated and the matrix equation solved for the required coefficients x_1 and x_2. This is the basis of the second numerical method described in section (3.4.2). The difficulties arise in the setting up of equation (3.54) and the separation and programming of equation (3.55).

The new method derives the terms of the matrix [A] and vector [B] directly from the complete T.P.E. function (3.53). To explain the method, the following definitions will be used. A coefficient will be termed "active" if it is given the value of +1, "passive" if it is given the value of 0 and "negative active" if it is given the value of -1, i.e.:

$x = +1$ is active
$x = 0$ is passive
$x = -1$ is negative active.

If all the coefficients are made passive and V is evaluated then the following is obtained:

$$x_1 \text{ and } x_2 \text{ passive} \longrightarrow \int a_6 d\xi \qquad \ldots (3.56)$$

If each of the coefficients is made active in turn with the rest passive, then V becomes:

$$\begin{aligned} x_1 \text{ active} &\longrightarrow \int [a_1 + a_4 + a_6]\, d\xi \\ x_2 \text{ active} &\longrightarrow \int [a_2 + a_5 + a_6]\, d\xi \end{aligned} \qquad \ldots (3.57)$$

Similarily, if each coefficient is made negative active, with the rest passive, then:

$$\begin{aligned} x_1 \text{ negative active} &\longrightarrow \int [a_1 - a_4 + a_6]\, d\xi \\ x_2 \text{ negative active} &\longrightarrow \int [a_2 - a_5 + a_6]\, d\xi \end{aligned} \qquad \ldots (3.58)$$

Adding (3.57) and (3.58), and subtracting twice (3.56) gives:

$$\begin{aligned} &2\int a_1 d\xi \\ &2\int a_2 d\xi \end{aligned} \qquad \ldots (3.59)$$

which are the diagonal terms in the solution matrix [A].

Subtracting (3.57) from (3.58) and dividing the result by two gives:

$$-\int a_4 d\xi$$
$$-\int a_5 d\xi \qquad \ldots (3.60)$$

which are the terms of the vector [B].

The off-diagonal terms of the matrix [A] are obtained by making a term active and then the value of V is found with one of the remaining terms made active with the rest passive, i.e. two different terms are made active for each evaluation:

$$x_1 \text{ and } x_2 \text{ active} \longrightarrow \int [a_1 + a_2 + a_3 + a_4 + a_5 + a_6]\, d\xi \quad \ldots (3.61)$$

The off-diagonal term is then found by subtracting (3.56) and half of (3.59) from (3.61) and adding (3.60) to give:

$$\int a_3 d\xi \qquad \ldots (3.62)$$

Thus, the complete matrix equation can be formulated from the total potential energy function.

Generalising this to obtain a matrix of "N" equations is reasonably straightforward. The only additional comment necessary is with regard to the position of the off-diagonal terms in the matrix. If the first active coefficient is x_r and the second is x_c then the coefficient obtained should be positioned on row "r" and column "c".

The total number of function evaluations required for a solution involving "N" coefficients is $(N^2 + N + 1)$. This can be reduced by nearly half if use is made of the symmetry of the matrix obtained from the differentiation of the T.P.E. function.

The time involved in calculating the values of the T.P.E. can be reduced by just calculating the parts of the function which involve the active constants, where possible. This can represent a considerable saving in the running time of the computer program since most of the time is spent calculating the values of the function.

3.4.4 *Numerical integration*

The strain energy part of the total potential energy function has to be integrated in two dimensions, θ and ϕ. There are many different ways of numerically integrating a function of this type, examples are given in the works of Gerald [216], FOX and MAYERS [228] and TIERNAY [229] (see also section 3.1). As mentioned earlier in section (3.1) two main methods were employed. These were Simpson's Rule and Gaussian Quadrature. Simpson's $\frac{1}{3}$ rule was chosen as the most convenient method.

Consider a double integral of the form:

$$\Phi = \int_c^d \int_a^b f(\theta,\phi)\, d\theta d\phi \qquad \ldots (3.63)$$

In calculus, a double integral is evaluated as an iterated integral, i.e. the inner integral is calculated first; then the outer integral. Similarly, a double numerical integral can be found by first applying Simpson's rule to the inner integral and then the outer integral. This gives the integral as:

$$\Phi = \sum_{k=1}^{K} \sum_{j=1}^{J} W_j W_k^* f_{jk} \qquad \ldots (3.64)$$

where f_{jk} are the values of the function $f(\theta,\phi)$ at θ_j and ϕ_k. The intervals $\theta = a$ to $\theta = b$ and $\phi = c$ to $\phi = d$ are subdivided into (J-1) and (K-1) intervals, respectively. θ_j and ϕ_k therefore correspond to:

$$\theta_j = a + j\Delta\theta \qquad \text{and} \qquad \phi = c + k\Delta\phi$$

$$\text{where } \Delta\theta = \frac{(b-a)}{(J-1)} \qquad \text{and} \qquad \Delta\phi = \frac{(d-c)}{(K-1)} \qquad \ldots \textit{(3.65)}$$

W_j and W_k^* in equation (3.64) are the weighting functions applied to each value of the function, f_{jk}. For Simpson's rule in two-dimensions, these functions are given by:

$$W_1 = W_J = \frac{\Delta\theta}{3} \qquad \text{and} \qquad W_1^* = W_K^* = \frac{\Delta\phi}{3}$$

$$W_j = \frac{\Delta\theta}{3}(3 + (-1)^j) \qquad W_k = \frac{\Delta\phi}{3}(3 + (-1)^k)$$

$$\text{where } j = 2,3, \ldots, (J-1) \text{ and } k = 2,3, \ldots, (K-1) \qquad \ldots \textit{(3.66)}$$

The above equations allow a different number of integration points in each direction which is necessary in the pipe bend problem which has widely differing behaviour in the θ and ϕ directions.

3.4.5 Solution of matrix equation

Many solution methods are available for linear equations, and where a small number only is involved the method chosen is immaterial. For large numbers, however, it is important to choose the most economical in computer time and storage, and that best suited to take advantage of any special properties the equations may possess. A typical matrix for the present problem has 130 rows which requires at least thirteen thousand storage locations in a computer for the [A] matrix.

The two classes of solution method available are termed direct and indirect methods. In the former a single set of operations is carried out on the equations and the results are obtained, while in the latter, solution is attempted by a series of successive approximations. MEYER [230] examined all of the major matrix solution routines in the context of structural analysis. He states that no method exists which requires less arithmetic operations than Gaussian elimination. Most systems of linear equations arising from problems in linear elasticity are positive definite and well-posed in the mathematical sense. Further, the accuracy of the solution from the Gauss algorithm is usually sufficient.

The Gaussian elimination method will be used herein.

The standard Gauss algorithm, which dates as far back as 1826, is given in APPENDIX (2). This method can be adapted to use the symmetry of the matrix and thus reduce the solution time. It is in this form that the algorithm is presented in APPENDIX (2). On the computer, the matrix can be solved in its own storage, hence reducing storage requirements. The storage requirement can be further reduced by taking advantage of the banded nature [231] of the [A] matrix. The band width "b" of the symmetric matrix [A] is defined as the largest number of elements in any row from the diagonal to the extreme right-hand non-zero element, inclusive. Matrices for which b is much less than the order N of the matrix are said to be banded. In this particular problem the matrix [A] was found to be well-populated, i.e. b approaches N. However, the author was still able to improve the storage requirement and to some extent the efficiency of the program by storing the upper triangle of the [A] matrix in a vector form. The reduction in storage using a vector form is shown in Figure (3.9). The efficiency

of the program is improved by having only one location reference for elements in the vector form, whereas two are required for the array form.

3.4.6 *Total potential energy*

The total potential energy expression is:

$$V = \frac{C}{2}\int_0^{2\pi}\int_0^{\alpha}[(\varepsilon_\phi+\varepsilon_\theta)^2 - 2(1-\nu)(\varepsilon_\phi\varepsilon_\theta-\frac{1}{4}\gamma_{\theta\phi}^2)]rR'd\theta d\phi$$
$$+\frac{D}{2}\int_0^{2\pi}\int_0^{\alpha}[(K_\phi+K_\theta)^2 - 2(1-\nu)(K_\phi K_\theta - K_{\theta\phi}^2)]rR'd\theta d\phi - M\gamma \quad \ldots (3.67)$$

where $C = \frac{Et}{(1-\nu^2)}$, $D = \frac{Et^3}{12(1-\nu^2)}$, $R' = R + r\sin\phi$

γ is the rotation between the ends of the bend which is found from the displacement equation (3.16):

$$\gamma = -\frac{1}{R}\sum_{j=1}^{JT} A_j \left(\frac{j\pi}{2\alpha}\right)\sin\left(\frac{j\pi\theta}{2\alpha}\right)$$

The strains and curvatures from equations (3.52) can be substituted in equation (3.67) to give the complete total potential energy function. This needs to be non-dimensionalised so that the solution can be in terms of as few characterising parameters as possible. Moreover, it can also be used to simplify the function and improve the numerical condition of the matrix. The T.P.E. will be non-dimensional using:

$$\bar{V} = V \Big/ \left[\frac{M\gamma_0}{2\pi\alpha(1-\nu^2)}\right] \quad \ldots (3.68)$$

This form of non-dimensionalisation is the same as that used by Thomson. Here, however, the factor of 2.0 appears in the numerator of $\overline{V}$ due to the lack of symmetry in integration displayed by the loading condition of out-of-plane bending.

Note that the $(1-\nu^2)$ term, omitted by many of the earlier authors using a lower bound approach, has been included in the present work. This will mean that the end rotation will tend towards the value of $(1-\nu^2)\gamma_o$ and not γ_o at high values of $\lambda(\lambda > 2)$. A full discussion of the implications of this was given by Spence [4]. A true lower bound is only achieved if it is included.

The nominal rotation γ_o, is the rotation of an equivalent length $(R\alpha)$ of straight pipe under the same load M, as found from simple bending theory:

$$\gamma_o = \frac{MR\alpha}{EI} \quad , \quad I = \pi r^3 t \qquad \ldots (3.69)$$

Using the non-dimensionalisation given by equation (3.68) the T.P.E. becomes:

$$\overline{V} = \frac{Et}{2(1-\nu^2)} \cdot \frac{2\pi\alpha(1-\nu^2)}{M\gamma_o} \cdot \Phi - 2\pi\alpha(1-\nu^2)\frac{\gamma}{\gamma_o}$$

where in this case

$$\Phi = \int_0^{2\pi}\int_0^{\alpha} [(\varepsilon_\phi + \varepsilon_\theta)^2 - 2(1-\nu)(\varepsilon_\phi\varepsilon_\theta - \tfrac{1}{4}\gamma_{\theta\phi}^2)]$$
$$+ \frac{\lambda^2}{12}\frac{r^4}{R^2}[(K_\phi + K_\theta)^2 - 2(1-\nu)(K_\phi K_\theta - K_{\theta\phi}^2)]\, rR'd\theta d\phi \qquad \ldots (3.70)$$

on re-arranging this gives:

$$\bar{V} = \bar{\Phi} - 2\pi\alpha(1-\nu^2)\frac{\gamma}{\gamma_o}$$

where $\bar{\Phi} = \int_0^{2\pi}\int_0^{\alpha} [(\bar{\varepsilon}_\phi + \bar{\varepsilon}_\theta)^2 - 2(1-\nu)(\bar{\varepsilon}_\phi\bar{\varepsilon}_\theta - \frac{1-2}{4}\gamma_{\theta\phi})]$

$$+ \frac{\lambda^2}{12}[(\bar{K}_\phi + \bar{K}_\theta)^2 - 2(1-\nu)(\bar{K}_\phi\bar{K}_\theta - \bar{K}^2_{\theta\phi})]\, Z d\theta d\phi$$

and

$$\bar{\varepsilon}_\phi = \varepsilon_\phi.(\frac{R\alpha}{r\gamma_o}) \quad , \quad \bar{\varepsilon}_\theta = \varepsilon_\theta.(\frac{R\alpha}{r\gamma_o}) \quad , \quad \bar{\gamma}_{\theta\phi} = \gamma_{\theta\phi}.(\frac{R\alpha}{r\gamma_o})$$

$$\bar{K}_\phi = K_\phi.(\frac{r\alpha}{\gamma_o}) \quad , \quad \bar{K}_\theta = K_\theta.(\frac{r\alpha}{\gamma_o}) \quad , \quad \bar{K}_{\theta\phi} = K_{\theta\phi}.(\frac{r\alpha}{\gamma_o})$$

$$Z = (1 + \frac{r}{R}\sin\phi) \quad , \quad \lambda = \frac{Rt}{r^2} \qquad \ldots (3.71)$$

The distortion coefficients will be non-dimensionalised using:

$$\bar{A1}_{mn} = A1_{mn}.(\frac{\alpha}{r\gamma_o}) \quad , \quad \bar{A2}_{mn} = A2_{mn}.(\frac{\alpha}{r\gamma_o})$$

$$\bar{B}_{mn} = B_{mn}.(\frac{\alpha}{r\gamma_o}) \quad , \quad \bar{C}_{mn} = C_{mn}.(\frac{\alpha}{r\gamma_o}) \qquad \ldots (3.72)$$

The same form of non-dimensionalisation can be applied to the rigid section displacements A_j and B_j. An alternative form is:

$$\bar{A}_j = A_j\frac{1}{R\gamma_o} \quad , \quad \bar{B}_j = B_j.\frac{1}{R\gamma_o} \qquad \ldots (3.73)$$

No significant difference was found between the form given by equation (3.72) and (3.73). As equation (3.73) represents a more direct form, this type was chosen for the rigid section displacement coefficients.

The strains as given in equations (3.52) can be arranged using the non-dimensional forms given by equations (3.71), (3.72) and (3.73) into a form suitable for computer application. These strains are given in Appendix (3).

A computer program which incorporates all the techniques just explained is given in Appendix (1). This program is written in FORTRAN [232] and uses double precision throughout. Values of the characterising parameters, α, $R/_r$, λ and ν are required for each run. A typical, fully converged, run, for a 90° bend takes around 25 minutes on the ICL 2980 computer.

3.4.7 *Deformations*

By minimising the total potential energy function in equation (3.71), using the procedure just outlined, numerical values are obtained for the $\bar{A}1_{mn}$, $\bar{A}2_{mn}$, $\bar{B}_{mn}$, $\bar{C}_{mn}$, $\bar{A}_j$ and $\bar{B}_j$ coefficients for any particular values of α, $R/_r$, λ and ν.

It is then a relatively simple task to determine the mid-surface displacements, w, v and u at any circumferential (θ) and meridional (ϕ) position on the bend from equations (3.51).

3.4.8 *Flexibility factor*

From the definition of the flexibility factor given in the introduction to CHAPTER (1), it follows from equations (3.16) and (3.73) that the flexibility factor K is given by:

$$K = -\sum_{j=1}^{JT} A_j \left(\frac{j\pi}{2\alpha}\right) \sin\left(\frac{j\pi\theta}{2\alpha}\right) \qquad \ldots (3.74)$$

where $\theta = \alpha$

This factor K corresponds to the overall rotation between the flanged ends of the bend and is based on the nominal rotation defined by equation (3.69). The overall rotation γ is that compatible with a pure out-of-plane bending moment.

3.4.9 Stress concentration factors

Once the displacement coefficients have been determined, it is then a relatively straightforward task to calculate the strains using equations (3.52). From the stress/strain relationships for a linear elastic isotropic material given in equations (2.14) the stresses at any point on the bend can be found.

The stresses are normally examined using stress concentration factors (S.C.F.). These have been defined generally in CHAPTER (1). They are written as:

$$\text{S.C.F.} = \text{stress} \;/\; \left[\frac{Mr}{I}\right] \qquad \ldots (3.75)$$

where [Mr/I] is the maximum stress in an equivalent straight pipe under a bending moment, M, from simple bending theory. The use of S.C.F.'s is particularly useful, for example in the case of tangent pipes under a constant bending moment where the circumferential S.C.F. approaches unity.

The strain S.C.F.'s are defined in a similar manner:

$$\text{S.C.F.} = \text{strain} \;/\; \left[\frac{Mr}{EI}\right] \qquad \ldots (3.76)$$

where [Mr/EI] is the maximum strain in an equivalent straight pipe under a bending moment, M. Note that this maximum strain can be written as:

$$\frac{Mr}{EI} = \frac{r\gamma_o}{R\alpha} \qquad \ldots (3.77)$$

If the strains are found in their non-dimensional form as given by equations (3.71) the S.C.F.'s in stress can be written as:

$$\bar{\sigma}_\phi = \frac{1}{(1-\nu^2)}\left[(\bar{\varepsilon}_\phi + \nu\bar{\varepsilon}_\theta) \mp \frac{\lambda}{2}(\bar{K}_\phi + \nu\bar{K}_\theta)\right]$$

$$\bar{\sigma}_\theta = \frac{1}{(1-\nu^2)}\left[(\bar{\varepsilon}_\theta + \nu\bar{\varepsilon}_\phi) \mp \frac{\lambda}{2}(\bar{K}_\theta + \nu\bar{K}_\phi)\right] \qquad \ldots (3.78)$$

where $\bar{\sigma}_\phi$ is the meridional stress S.C.F. and $\bar{\sigma}_\theta$ the circumferential stress S.C.F. The "+" and "-" signs in the above equations, correspond to the stresses at the outside and inside surfaces of the shell, respectively.

The shear stress concentration factor $\bar{\tau}_{\theta\phi}$ can be found from a similar method as:

$$\bar{\tau}_{\theta\phi} = \frac{1}{(1+\nu)}\left[\bar{\gamma}_{\theta\phi} \mp \lambda\bar{K}_{\theta\phi}\right] \qquad \ldots (3.79)$$

The above expression for shear stress, as explained in CHAPTER (2), is approximate. The degree of approximation is of the same order as the basic assumptions of thin shell theory and can be ignored.

3.5 Theoretical Results

3.5.1 Introduction

In this section, a comprehensive set of results covering a wide range of the characterising parameters are presented along with a comparison with theoretical results given by other authors.

In CHAPTER (4), the theory will be compared with experimental results.

The final solution adopted, as given by equations (3.51), was based on the results of a large number of solutions developed during the course of the study. The principal form of these solutions in terms of their displacement series and convergence characteristics are presented in APPENDIX (4) and (5). The results of these solutions will be referred to in the course of this section.

3.5.2 Solution convergence

In the typical Kármán type analysis, with no-end effects, the solution is characterised by one parameter - the pipe factor (λ). Here, however, convergence of the solution was found to vary with the bend parameters - λ, bend angle (α) and radius ratio ($\frac{R}{r}$). The number of displacement terms (MT, NT, JT) required for a bend angle of 45° was found to be inadequate for a larger bend angle of 180°. This trend became more evident as the radius ratio increased and the λ value reduced. The behaviour can be explained by the fact that as the flexibility of the bend increases so also does the distortion of the cross-section. Hence, more terms will be necessary to describe the displacement of the cross-section. The more flexible bend will be defined by

a large bend angle and radius ratio and low λ value. Using such values for checking convergence of the solution should then allow the solution to be applicable to a large range of bend parameters and thus dispense with the inordinate task of examining convergence for a large number of λ, α and $(\frac{R}{r})$ values.

For this purpose the following parameters were chosen to check convergence:

$$\alpha = 180°$$
$$\lambda = 0.07$$
$$(\frac{R}{r}) = 10.0$$

In choosing a bend angle of 180° a further aspect was introduced in convergence of the solution, namely - the symmetries displayed by this bend angle when subjected to an out-of-plane bending moment. In the study of in-plane bending, Thomson was able to adopt two planes of symmetry - a circumferential symmetry taken through the bend centre and a meridional symmetry about $\phi = +90°$ and $\phi = -90°$. By prescribing such symmetries in his displacements, Thomson was able to ensure symmetry in his results. This also led to a significant reduction in program running time due to the reduced integration limits.

For out-of-plane bending the use of a circumferential symmetry through the bend centre was only possible for a bend angle of 180°. However, as can be seen in APPENDIX (5), this particular solution gave poor convergence. Hence the general solution as given by equations (3.51) had to be examined to ensure that the necessary symmetries were present.

3.5.2.1 Integration convergence

The accuracy obtained using a large number of integration points has to be balanced against program running time. For in-plane bending Thomson used the values of $\bar{N}_\theta = 9$ and $\bar{N}_\phi = 17$. He was able to show that these values gave a difference of less than 1% for flexibility factor when compared against $\bar{N}_\theta = 15$ and $\bar{N}_\phi = 25$ with less than half the program running time*. From the two symmetries employed in his analysis, Thomson was able to use the following integration limits:

$$0 \leq \theta \leq \frac{\pi}{2} \quad , \quad -\frac{\pi}{2} \leq \phi \leq \frac{\pi}{2} \quad (\text{for } \alpha = \pi)$$

Under out-of-plane bending the integration limits are doubled:

$$0 \leq \theta \leq \pi \quad , \quad 0 \leq \phi \leq 2\pi \quad (\text{for } \alpha = \pi)$$

Hence it is to be expected that the number of integration points will increase significantly. The results using different methods of integration with $\bar{N}_\theta = 17$ and $\bar{N}_\phi = 33$ for the bend parameters of $\alpha = 180°$, $\lambda = 0.1$, $(\frac{R}{r}) = 10.0$ and $\nu = 0.3$ are shown in Figure (3.10). These results show that the maximum program running time of 7200 CPU seconds was reached before the solution had begun to converge to within anywhere near the limits obtained by Thomson.

In order to achieve a practical solution in terms of program running time the optimum number of integration points were chosen as:

for $\alpha = 180°$; $\bar{N}_\theta = 13$ and $\bar{N}_\phi = 33$

for $\alpha \leq 90°$; $\bar{N}_\theta = 9$ and $\bar{N}_\phi = 33$

---

*A reduction in program running time from 412 to 171 CPU seconds, for bend parameters of $\alpha = 180°$, $\lambda = 0.05$, $(\frac{R}{r}) = 10$ and $\nu = 0.3$ using Simpson's rule.

The large value of $\bar{N}_\phi$ was maintained to cope with the more rapidly varying displacements in this direction. For the bend parameters of $\alpha = 180°$, $\lambda = 0.05$, $(\frac{R}{r}) = 10.0$ and $\nu = 0.3$, the variation in $\bar{N}_\theta$ is shown in Figure (3.11). From Figure (3.11) it can be seen that an increase in $\bar{N}_\theta$ did not as expected result in an increase in flexibility factor. It was also found that as the value of $\bar{N}_\theta$ approached MT, the solution became numerically unstable. These aspects are discussed earlier in section (3.1.1).

For $\alpha = 180°$ using the displacement terms of NT = MT = JT = 6, the reduction in $\bar{N}_\theta$ from 17 to 13 resulted in only a small reduction in program running time - from 3000 to 2750 CPU seconds. Nevertheless it had the distinct effect of providing convergence in flexibility factor. This is clearly seen in the results of the solutions given in APPENDIX (4) and in section (3.5.2.2) where series convergence is considered. Although series and integration convergence of the solution are presented separately, in practice they were conducted simultaneously due to the non-linear relationship displayed between $\bar{N}_\theta$ and MT.

3.5.2.2 Series convergence

Series convergence of the solution was performed using the parameters given earlier of:

$$\alpha = 180° \qquad (\frac{R}{r}) = 10.0$$
$$\lambda = 0.07 \qquad \nu = 0.3$$
$$\bar{N}_\theta = 13 \qquad \bar{N}_\phi = 33$$

The variation of flexibility with the displacement terms MT, NT and JT for this bend angle and a bend angle of 90° using $\bar{N}_\theta = 9$, are shown in Figure (3.12). These values are also given in TABLE (3.1). As discovered in earlier solutions, convergence of the 90° bend was found

to be better than the 180° bend. Further, the behaviour of the 90° bend was more monotonic although it can be seen from Figure (3.12) that as MT approaches $\bar{N}_\theta$ the solution becomes unstable. This behaviour was not so pronounced on the 180° bend due to the larger value of $\bar{N}_\theta$.

For an increase in the displacement terms of NT = MT = JT = 6 to NT = MT = JT = 7, the flexibility factor increased by 3% for both bend angles. The corresponding difference in program running time for the 180° bend was more than two-fold, increasing from 2750 to approximately 6000 CPU seconds.

For the 180° bend the variation in meridional stress with MT, NT and JT is shown in Figure (3.13). Here the maximum difference with NT, MT and JT changing from 6 to 7 was 7.5%.

In view of the high computation time these levels of accuracy were considered sufficient for a converged solution. Accordingly, the following values were adopted for the converged solution:

$$NT = MT = JT = 6$$

Similar values of the displacement terms were used by Thomson in his converged solution: NT = MT = JT = 5. Thomson's solution required the evaluation of 105 coefficients. Here, 156 coefficients were required to be evaluated. Variations within MT, NT and JT were not actively pursued. However, variations around the converged values indicated no improvement in accuracy or computation time.

The level of accuracy presented by this solution does however require further work to ensure that the present results are close to the fully converged results.

TABLE (3.1): Convergence of flexibility factors.
$\lambda = 0.07$, $(\frac{R}{r}) = 10$, $\nu = 0.3$, $\alpha = 90°$ and $180°$

Bend angle	Value of NT, MT, JT							
	1	2	3	4	5	6	7	8
180°	0.285	0.941	1.218	1.949	4.465	4.916	5.063	5.278
90°	0.650	1.203	2.051	2.318	2.433	2.479	2.546	3.503

3.5.2.3 Displacement coefficients

Displacement coefficients for a bend angle of 180° and 90° with $\lambda = 0.07$, $(\frac{R}{r}) = 10.0$ and $\nu = 0.3$ are given in TABLE (3.2) and (3.3) respectively. These illustrate several interesting features of the flanged pipe bend problem.

The Kármán solution for a pipe bend without end effects uses only the even fourier terms ($n = 2,4,6, \ldots$) in the series for w_D. For both bend angles, TABLE (3.2) and (3.3) show that these are the significant terms but the odd terms ($n = 3,5,7, \ldots$) are not negligible. In the analysis of the 180° bend the $\bar{A2}_{mn}$ coefficients are the most significant. These coefficients represent the odd terms ($m = 1,3,5,\ldots$) in the fourier series for the displacement w_D (3.36). The even terms ($m = 2,4,6, \ldots$) of this series are represented by the $\bar{A1}_{mn}$ coefficients which are smaller by several orders of magnitude. The displacement w_D is anti-symmetrical about the bend centre (see APPENDIX (5)) which explains the importance of the odd $\bar{A2}_{mn}$ coefficients. For the 90° bend there is no symmetry in this displacement. Here, the coefficients $\bar{A1}_{mn}$ and $\bar{A2}_{mn}$ are of a similar order.

For the 180° bend the even terms ($m = 2,4,6, \ldots$) in the $\bar{B}_{mn}$ coefficients and the odd terms ($m = 1,3,5, \ldots$) in the $\bar{C}_{mn}$ coefficients are larger by several orders of magnitude when compared to their corresponding odd and even terms, respectively. This trend is not reflected in the coefficients for the 90° bend. It is interesting to note that in the analysis of the 180° bend neglecting the $\bar{A1}_{mn}$ coefficients ($m = 1,2,3, \ldots$), the odd $\bar{B}_{mn}$ coefficients ($m = 1,3,5, \ldots$) and the even $\bar{C}_{mn}$ coefficients ($m = 2,4,6, \ldots$) resulted in a significant reduction in flexibility and stress together with a loss in symmetry around the bend.

Convergence of the distortion series is easily seen from the table of coefficients. There is, however, a significant difference between the first and last terms of the $\bar{A1}_{mn}$, $\bar{A2}_{mn}$, $\bar{B}_{mn}$ and $\bar{C}_{mn}$ series. For example, in the $\bar{A2}_{mn}$ series (TABLE (3.2)), $\bar{A2}_{11} = -9.70174$ and $\bar{A2}_{66} = 0.00281$. These coefficients differ by a factor of over 3000.

In the rigid section coefficients the large difference between the first and last term persists although to a lesser degree. However, in the analysis of the 180° bend the coefficients $\bar{A}_1$ and $\bar{A}_6$ differ only by a factor of 3. Here, the convergence is poor when compared to the $\bar{A}_j$ coefficients in the 90° bend. Convergence of the coefficients was improved significantly as λ increased and $(\frac{R}{r})$ and α reduced. The numerical instability observed in the solution as MT approached $\bar{N}_\theta$ was characterised by an increase in the magnitude of the $\bar{A}_j$ coefficients. For the 90° bend, the first coefficient $\bar{A}_1$ increased to 944.09 when MT = 8. No significant difference was displayed by the distortion coefficients $\bar{A1}_{mn}$, $\bar{A2}_{mn}$, $\bar{B}_{mn}$ and $\bar{C}_{mn}$. This increase in $\bar{A}_j$ increases significantly the large difference already displayed by the distortion coefficients leading to obvious numerical difficulties in inversion of the coefficient matrix. The use of different non-dimensionalisation of the coefficients did little to improve their problem (see APPENDIX (4)).

TABLE (3.2): Displacement coefficients.

$\alpha = 180°$, $\lambda = 0.07$, $(\frac{R}{r}) = 10.0$, $\nu = 0.3$

$MT = NT = JT = 6$

$\bar{N}_\theta = 13$, $\bar{N}_\phi = 33$

j	1	2	3	4	5	6
$\bar{A}_j$	-0.942791	-1.596077	3.634720	-1.298545	0.402856	-0.363247
$\bar{B}_j$	0.246651	-0.128434	-0.000497	0.004221	0.000179	-0.000205

$\bar{A1}_{mn}$

n \ m	1	2	3	4	5	6
2	0.08261	-0.16229	0.04391	0.00907	0.00471	0.00194
3	0.02117	-0.07459	0.03172	0.00869	0.00537	0.00234
4	0.02026	-0.02642	0.00244	-0.00045	-0.00060	-0.00030
5	0.00695	-0.02164	0.00863	0.00228	0.00138	0.00060
6	0.00389	-0.00402	-0.00019	-0.00029	-0.00025	-0.00012
7	0.00114	-0.00318	0.00119	0.00030	0.00018	0.00008

$\bar{A2}_{mn}$

n \ m	1	2	3	4	5	6
2	-9.70174	0.00622	-0.01100	-0.17690	-0.25532	0.07261
3	-2.17737	0.84292	0.22148	0.12760	0.04702	0.05482
4	-2.29661	-0.24354	0.01554	-0.05207	-0.07989	0.02542
5	-0.67289	0.23091	0.06864	0.03706	0.01136	0.01778
6	-0.44108	-0.06865	0.00184	-0.01216	-0.01733	0.00489
7	-0.11058	0.02974	0.01050	0.00510	0.00109	0.00281

TABLE (3.2) cont.

$\bar{B}_{mn}$

n \ m	1	2	3	4	5	6
2	0.00117	6.75344	0.07653	-1.80889	-0.05638	-0.23798
3	-0.00087	-0.56769	-0.01776	0.60368	0.02185	0.00185
4	0.00001	0.86223	0.00803	-0.16046	-0.00321	-0.05852
5	-0.00016	-0.10876	-0.00324	0.10577	0.00366	0.00259
6	-0.00001	0.11551	0.00097	-0.01740	-0.00023	-0.00881
7	-0.00002	-0.01370	-0.00035	0.01116	0.00037	0.00062

$\bar{C}_{mn}$

n \ m	1	2	3	4	5	6
2	0.25739	0.00429	-0.71437	-0.01600	0.04149	0.00623
3	0.01488	0.00056	-0.08684	-0.00361	0.04798	0.00199
4	0.01623	0.00024	-0.03896	-0.00050	-0.00694	0.00005
5	0.00223	0.00007	-0.01059	-0.00038	0.00422	0.00019
6	0.00137	0.00002	-0.00286	-0.00001	-0.00106	-0.00001
7	0.00028	0.00001	-0.00102	-0.00003	0.00020	0.00001

TABLE (3.3): Displacement coefficients.

$\alpha = 90°$, $\lambda = 0.07$, $(\frac{R}{r}) = 10.0$, $\nu = 0.3$

$MT = NT = JT = 6$

$\bar{N}_\theta = 9$, $\bar{N}_\phi = 33$

j	1	2	3	4	5	6
$\bar{A}_j$	-0.706506	-0.782449	0.830049	-0.331317	0.143456	-0.043563
$\bar{B}_j$	0.070649	-0.012023	-0.001030	-0.000605	0.000154	-0.000670

$\bar{A1}_{mn}$

n \ m	1	2	3	4	5	6
2	2.23076	-0.13798	-0.09125	0.01251	0.09917	-0.00459
3	0.77634	-0.47212	-0.05444	-0.02579	0.02830	-0.07951
4	0.35246	0.24484	-0.06747	-0.00498	0.00259	0.04982
5	0.19712	-0.04609	-0.04744	-0.01684	-0.00488	-0.00970
6	0.05657	0.04956	-0.00545	0.00208	0.00264	0.01120
7	0.02770	-0.00197	-0.00736	-0.00245	-0.00102	-0.00041

$\bar{A2}_{mn}$

n \ m	1	2	3	4	5	6
2	-1.25171	0.00732	-0.05630	0.01183	-0.09291	0.01431
3	-0.85421	0.25773	0.02484	0.03689	-0.02938	0.01019
4	0.04124	-0.21987	-0.01028	0.00387	-0.04493	-0.01697
5	-0.16070	-0.02574	0.01269	0.01667	-0.02238	-0.00622
6	0.01672	-0.03555	-0.00476	-0.00150	-0.00718	-0.00265
7	-0.01934	-0.00792	0.00190	0.00262	-0.00402	-0.00132

TABLE (3.3) cont.

$\bar{B}_{mn}$

n \ m	1	2	3	4	5	6
2	-1.81072	0.90469	0.44438	-0.18859	0.01359	-0.03435
3	0.16372	-0.28814	-0.27730	0.19011	0.05714	0.00076
4	-0.22772	0.05914	-0.03113	0.06404	0.05129	-0.02750
5	0.03228	-0.04917	-0.03248	0.00742	-0.00768	0.01136
6	-0.02996	0.00514	-0.00641	0.00803	0.00516	-0.00213
7	0.00393	-0.00507	-0.00265	-0.00002	-0.00123	0.00150

$\bar{C}_{mn}$

n \ m	1	2	3	4	5	6
2	0.07684	0.21397	-0.16871	-0.03964	-0.00575	0.00242
3	0.01477	0.04127	-0.05890	-0.04597	0.02077	0.00131
4	0.00361	0.00627	0.00441	0.01572	-0.01596	-0.00320
5	0.00205	0.00407	-0.00350	-0.00048	-0.00315	-0.00190
6	0.00011	0.00014	0.00060	0.00129	-0.00095	0.00022
7	0.00016	0.00031	-0.00016	0.00010	-0.00039	-0.00017

3.5.3 *Flexibility factors*

Flexibility factors for flanged bends under out-of-plane bending are given in Figures (3.14), (3.15) and (3.16) for 180°, 90° and 45° bends, respectively. In each figure the variation with radius ratio $(\frac{R}{r})$ is shown for the range of values 2, 3, 5 and 10. The results were obtained using NT = MT = JT = 6 with $\bar{N}_\theta = 9$ and $\bar{N}_\phi = 33$. For the bend angle of 180° the number of integration points in the circumferential direction $(\bar{N}_\theta)$ was increased to 13. In all cases, poissons ratio $(\nu)^*$ was taken as 0.3.

The results show clearly that flanged bends of smaller subtended angles and shorter radius have the lowest flexibility. As the pipe factor (λ) reduces the flexibility increases. However, unlike the Kármán converged solution, the present results are not straight lines on a log-log graph. This means that simple formulae cannot be derived easily covering a wide range of parameters.

The typical variation with bend angle for $\lambda = 0.1$ is shown in Figure (3.17). This demonstrates how the flexibility reduces with bend angle. It can also be seen that flanged bends with a subtended angle of less than 45° behave almost like an equivalent straight pipe. The variation with radius ratio $(\frac{R}{r})$ is also shown in Figure (3.17). Here the fall in flexibility as the radius ratio $(\frac{R}{r})$ reduces is clearly illustrated.

In Figure (3.18) and (3.19) a comparison is given with Whatham's flexibility factors using the present definition of flexibility factor. For a bend angle of 180° (Figure (3.18)) Whatham's results are around

---

* Unless otherwise stated, poissons ratio $(\nu) = 0.3$.

10% higher whereas for a bend angle of 90° (Figure (3.19)) the difference increases to around 20%. As explained in CHAPTER (2), the present flexibility factors are lower bounds. Whatham's results [171] for an unflanged bend agree with solutions obtained from an upper bound analysis of the same problem. Therefore, it is to be expected that if Whatham's results for a flanged bend are valid then they will be greater than the present lower bounds. If the $(1-\nu^2)$ term in the total potential energy of the present solution is neglected, in the way it was by many previous authors (see [4]), then the present flexibility factors will agree closer with Whatham's results. For the 180° and 90° bend, Whatham presented his results for a λ range (0.02 - 0.3) extending outwith the range of the present solution ($\lambda \nmid 0.07$). Hence at λ values less than 0.07 good comparison is not expected.

If the scale of Figure (3.17) is altered as in Figure (3.20), a comparison with Thomson's results for in-plane bending shows that the effect of the radius ratio $(\frac{R}{r})$ is not so pronounced. Thomson's flexibility factors for in-plane bending are larger by a factor of approximately 3. For a value of $\lambda = 0.1$ the flexibility from a typical no-end effect theory such as Elbow [48] is 17.3. Hence, it is clear that the use of a no-end effect theory particularly for the case of out-of-plane bending of flanged bends greatly overestimates the flexibility factor.

3.5.4 Stress concentration factors

For a pipe bend with end effects, the stress concentration factors (S.C.F.) vary in the meridional and circumferential directions and through the thickness. This makes it difficult to present a comprehensive stress distribution for all points on a bend. The problem is further

complicated by the maximum stresses not being at the same position for all bend geometries, making it necessary to examine more than a single bend section. Therefore only some typical stress distributions will be examined together with the peak stresses for a range of bend geometries.

Due to the lack of available theoretical results, no attempt has been made to compare the present results with those of other authors. Whatham presented flexibility factors for a limited range of bend geometries but failed to present any stress results for out-of-plane bending. Comparisons that are made include the A.S.M.E. code for peak stress given by equation (1.25):

$$\hat{\bar{\sigma}} = \frac{0.9}{\lambda^{\frac{1}{3}}}$$

3.5.4.1 Meridional stress distribution

The effect of the radius ratio $(\frac{R}{r})$ on the distribution of the meridional S.C.F. $(\bar{\sigma}_\phi)$ at the centre of the bend $(\theta = 45°)$ for $\alpha = 90°$ and $\lambda = 0.2$ is shown in Figure (3.21). As in the Kármán analysis, the distribution shows four distinct peaks. For $(\frac{R}{r}) = 10$, the maximum meridional S.C.F. $(\hat{\bar{\sigma}}_\phi)$ occurs on the outside surface, in the latter two quadrants at $\phi = 214°$ and $\phi = 326°$. The Kármán analysis for a bend with no end effects predicted the maximum meridional S.C.F. at around the same locations (approximately $\phi = 204°$ and $\phi = 336°$) together with two other locations positioned diametrically opposite. The present solution removes the equality of the four stress peaks displayed by the Kármán solution and introduces a difference in those appearing between $\phi = 0°$ and $180°$ and $\phi = 180°$ and $360°$. The value of zero stress (and strain) at $\phi = 90°$ and $\phi = 270°$ arises from

coincidence of the two symmetries prescribed for the rigid section and distortion displacements. As the radius ratio reduces (Figure (3.21)) the position of the maximum meridional S.C.F. remains essentially unaltered however the magnitude of $\hat{\bar{\sigma}}_\phi$ is reduced.

The distribution of $\bar{\sigma}_\phi$ at the loaded flange ($\theta = 90°$) for a bend angle of 90° is shown in Figure (3.22). As the radius ratio increases from $(\frac{R}{r}) = 2$ to $(\frac{R}{r}) = 10$ the stress at the flange increase slightly. At $(\frac{R}{r}) = 2$ the stresses at the fixed flange ($\theta = 0°$) were comparable with those at the loaded flange. Here, however, an increase in $(\frac{R}{r})$ resulted in a reduction of $\hat{\bar{\sigma}}_\phi$ at the fixed flange.

For a 90° bend the position of the maximum $\hat{\bar{\sigma}}_\phi$ was found to lie away from the flanged ends at between $\theta = 45°$ and $\theta = 67°$. For a 90° bend the fixed flange is subjected to a pure torsional moment whereas at the loaded flange a pure out-of-plane bending moment exists. This will give rise to less distortion at the fixed flange and explain the smaller value of $\hat{\bar{\sigma}}_\phi$ displayed at this section.

The circumferential variation of $\hat{\bar{\sigma}}_\phi$ for $\alpha = 180°$ and $\lambda = 0.1$ at $\phi = 202.5°$ is shown in Figure (3.23). Here $\hat{\bar{\sigma}}_\phi$ occurs at approximately $\theta = 50°$ and $\theta = 130°$ from a symmetrical distribution about the bend centre ($\theta = 90°$). Some indication of the symmetry achieved in the circumferential direction for $\bar{\sigma}_\phi$ is also shown in Figures (3.24) and (3.25). Here, it can be seen that as the bend angle and radius ratio increase the magnitude of $\hat{\bar{\sigma}}_\phi$ increases significantly and the magnitude of the four stress peaks $\hat{\bar{\sigma}}_\phi$ become similar. They are, however, less by a factor of 50% when compared to the Kármán type solution [48]. For the 180° bend the mid-section ($\theta = 90°$) is under a pure torsional moment. Around this section the value of $\bar{\sigma}_\phi$ was negligible.

As in the case of the 90° bend, the position of the maximum $\hat{\bar{\sigma}}_\phi$ was found to lie away from the flanged ends at between $\theta = 45°$ and 67° and $\theta = 135°$ and 157°.

3.5.4.2 Circumferential stress distribution

Figure (3.26) illustrates the variation of the circumferential S.C.F. ($\bar{\sigma}_\theta$) with radius ratio ($\frac{R}{r}$) around the bend mid-section ($\theta = 45°$) for $\alpha = 90°$ and $\lambda = 0.2$. For ($\frac{R}{r}$) = 10, the maximum circumferential S.C.F. ($\hat{\bar{\sigma}}_\theta$) occurs at the outside surface at $\phi = 214°$ and $\phi = 326°$. These locations correspond with the position of $\hat{\bar{\sigma}}_\phi$ (see Figure (3.21)). Again the points of zero stress (and strain) can be identified at $\phi = 90°$ and $\phi = 270°$. As ($\frac{R}{r}$) reduces the value of $\hat{\bar{\sigma}}_\theta$ decreases and moves out from the intrados toward the neutral axis of the section.

A typical distribution around the loaded flange ($\theta = 90°$) for a 90° bend is shown in Figure (3.27). For ($\frac{R}{r}$) = 2 the variation around both the fixed flange ($\theta = 0°$) and the loaded flange ($\theta = 90°$) was similar. As ($\frac{R}{r}$) increased, the magnitude of $\hat{\bar{\sigma}}_\theta$ around the loaded flange increased significantly when compared to the fixed flange or locations along the bend. However, as in the behaviour of $\hat{\bar{\sigma}}_\phi$ this increase in ($\frac{R}{r}$) reduced the magnitude of $\hat{\bar{\sigma}}_\theta$ at the fixed flange.

A typical variation of $\bar{\sigma}_\theta$ in the circumferential direction for $\alpha = 180°$, $\lambda = 0.1$ and ($\frac{R}{r}$) = 10 at $\phi = 202.5°$ is shown in Figure (3.28). A further illustration of the symmetry achieved in the solution is shown in Figures (3.29) and (3.30).

The position of the maximum $\hat{\bar{\sigma}}_\theta$ was found to be dependent on the bend geometry. For large values of ($\frac{R}{r}$) and low λ values the position of the maximum $\hat{\bar{\sigma}}_\theta$ for a bend angle of 90° or less was found

to be at the loaded flange. In the case of a 180° bend these parameters caused $\hat{\bar{\sigma}}_\theta$ to occur away from the flanges at a position of approximately $\theta = 45°$ and $\theta = 135°$ along the bend. For all bend angles a small value of $(\frac{R}{r})$ resulted in comparable values of $\hat{\bar{\sigma}}_\theta$ at the flanges and along the bend. In some instances, however, the maximum value of $\hat{\bar{\sigma}}_\theta$ remained at the flanges. The changing position of $\hat{\bar{\sigma}}_\theta$ from the outside surface to the inside surface further complicated matters. So that although a clear trend could be identified for the particular range of parameters of large $(\frac{R}{r})$ and small λ, at values outwith this range no clear trend was evident.

3.5.4.3 Shear stress distribution

The distribution of shear S.C.F. $(\bar{\tau}_{\theta\phi})$ at $\theta = 45°$ for $\alpha = 90°$ and $\lambda = 0.2$ is shown in Figure (3.31). For $(\frac{R}{r}) = 10$ and $(\frac{R}{r}) = 2$ the peak shear S.C.F. $(\bar{\tau}_{\theta\phi})$ differ very little. When compared to $\hat{\bar{\sigma}}_\phi$ they are less by a factor of approximately 2. At the fixed flange ($\theta = 0°$) the distribution of $\bar{\tau}_{\theta\phi}$ is similar (Figure (3.32)). However, at the loaded flange ($\theta = 90°$) the distribution of $\bar{\tau}_{\theta\phi}$ (Figure (3.33)) changes to give positive and negative values around the section. Here the magnitude of $\hat{\bar{\tau}}_{\theta\phi}$ is greater than $\hat{\bar{\sigma}}_\phi$ by a factor of approximately 2.

For a bend angle of 180°, $\lambda = 0.1$ and $(\frac{R}{r}) = 10$, the distribution of $\bar{\tau}_{\theta\phi}$ at the fixed and loaded flanges, at $\theta = 45°$ and 135° and at the bend mid-section ($\theta = 90°$) is shown in Figures (3.34) to (3.36), respectively. Here the maximum $\hat{\bar{\tau}}_{\theta\phi}$ occurs at the flanges and is comparable with the magnitude of $\hat{\bar{\sigma}}_\phi$.

It is interesting to note that at sections where the torsional moment predominates the distribution of $\bar{\tau}_{\theta\phi}$ is essentially uniform

around the section whereas at locations where the out-of-plane bending moment predominates, such as at the loaded flange of a 90° bend and both flanges on a 180° bend, the distribution of $\bar{\tau}_{\theta\phi}$ becomes cyclic around the section.

3.5.4.4 Maximum S.C.F.

Maximum meridional S.C.F.

Maximum meridional S.C.F. ($\hat{\bar{\sigma}}_{\phi}$) for bend angles of 180°, 90° and 45° are given in Figures (3.37) to (3.39). Each figure contains curves for $(\frac{R}{r})$ = 10, 5, 3 and 2. The values of $\hat{\bar{\sigma}}_{\phi}$ occurred at between approximately θ = 45° and θ = 67°. For a bend angle of 180° these values appeared symmetric about the bend centre (θ = 90°). Note that for α = 45° the position of $\hat{\bar{\sigma}}_{\phi}$ occurred at approximately θ = 30°. For α = 180° at low values of $(\frac{R}{r})$ the magnitude of $\hat{\bar{\sigma}}_{\phi}$ decreases once λ is less than approximately 0.2. As the bend angle reduced this behaviour became more evident over a larger $(\frac{R}{r})$ and λ range. For most bend geometries the A.S.M.E. code for peak stress is lower than the present results.

Maximum circumferential S.C.F.

The maximum circumferential S.C.F. ($\hat{\bar{\sigma}}_{\theta}$) for a variety of locations around the bend are given in Figures (3.40) to (3.42) for bend angles of 180°, 90° and 45°, respectively. Unlike the curves for flexibility factor and maximum meridional S.C.F. ($\hat{\bar{\sigma}}_{\phi}$) the curves for $\hat{\bar{\sigma}}_{\theta}$ cross each other. This change over in position arises from a change in the meridional and circumferential position of the maximum $\hat{\bar{\sigma}}_{\theta}$. For α = 90° the value of $\hat{\bar{\sigma}}_{\theta}$ changed little with $(\frac{R}{r})$ at λ values less than

0.2. For $\alpha = 45°$ this was also the case although here at low values of $(\frac{R}{r})$ a reduction in λ caused a reduction in $\hat{\bar{\sigma}}_\theta$. Again, for most bend geometries the peak stress given by the A.S.M.E. code was found to underestimate $\hat{\bar{\sigma}}_\theta$.

3.6 General Comments on the Results

The results presented in this section were based on a solution employing essentially only the assumptions of thin shell theory to solve the problem of a smooth pipe bend with rigid flanges under out-of-plane bending. The resulting flexibility factors are a lower bound on the stated problem. In practice, however, flanges are not completely rigid, making the bend flexibility slightly higher. Hence the present results should also be a lower bound on the "real" problem. Further comment regarding the rigidity of the flanges will be made in CHAPTER (4) where the present results for flexibility and stress are compared with experiment. The results clearly show that for out-of-plane bending the flexibility factor is greatly reduced when compared to Thomson's results for in-plane bending for the same problem. A typical comparison of the stress distributions for the present solution and that of Thomson's (Figure (3.43)) also shows that in out-of-plane bending the peak stresses can be reduced by approximately half. Pure torsion of a thin walled cylinder results in a shear stress and a circumferential stress tending to shorten the length. In a curved tube with both bending and torsion varying along the length the behaviour is more complicated. However, the general trend of the stress distributions found by Thomson is also reflected in the present results. For both loading cases, $\hat{\bar{\sigma}}_\phi$ was found to lie along the bend whereas the position of $\hat{\bar{\sigma}}_\theta$ was dependent on the bend geometry. This latter aspect has important implications in design as the maximum value of $\hat{\bar{\sigma}}_\theta$ occurring along the bend does not necessarily represent the true maximum.

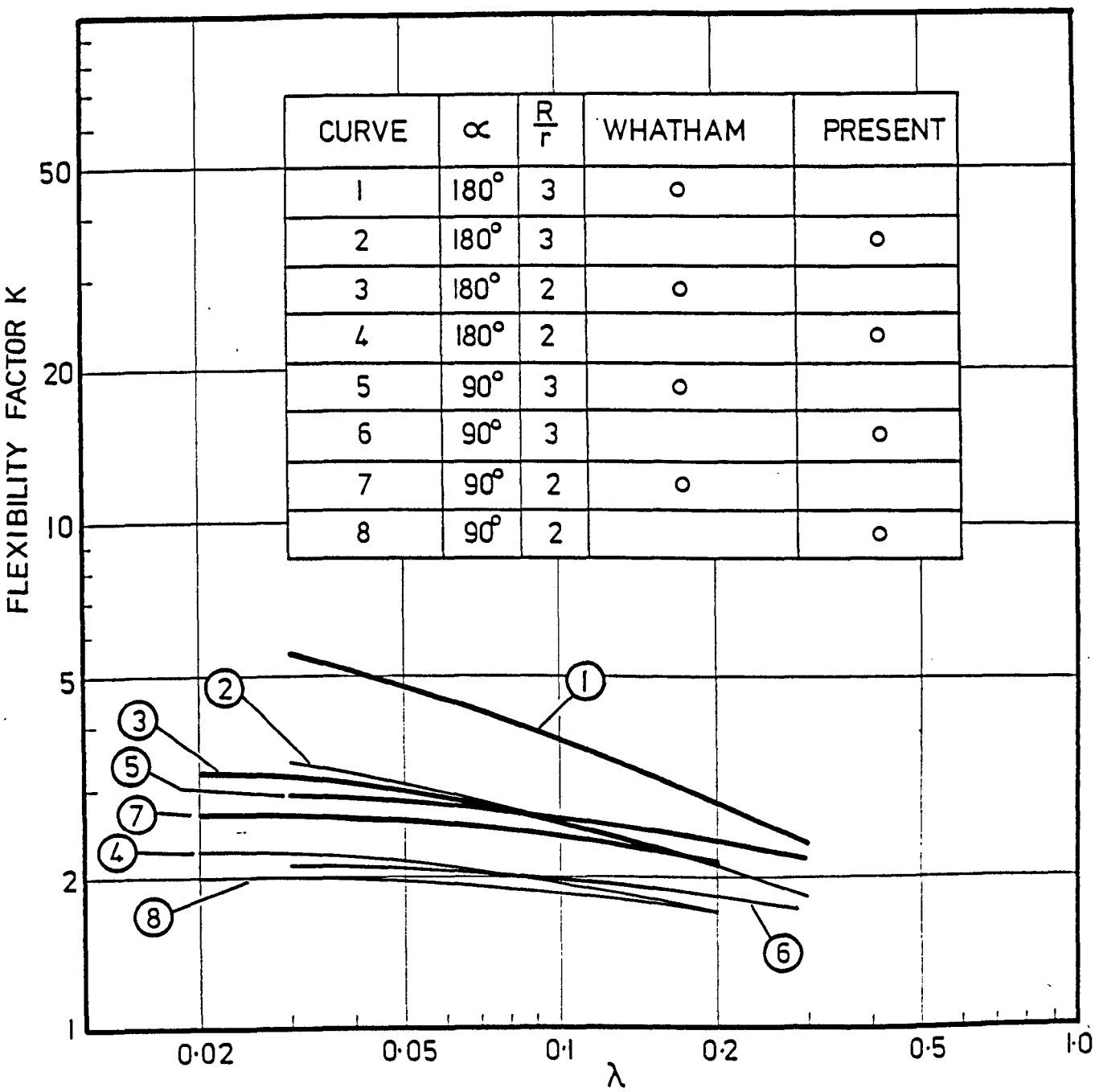

COMPARISON OF
FLEXIBILITY FACTOR DEFINITION
WHATHAM [170]
OUT-OF-PLANE BENDING

FIG. 3·1

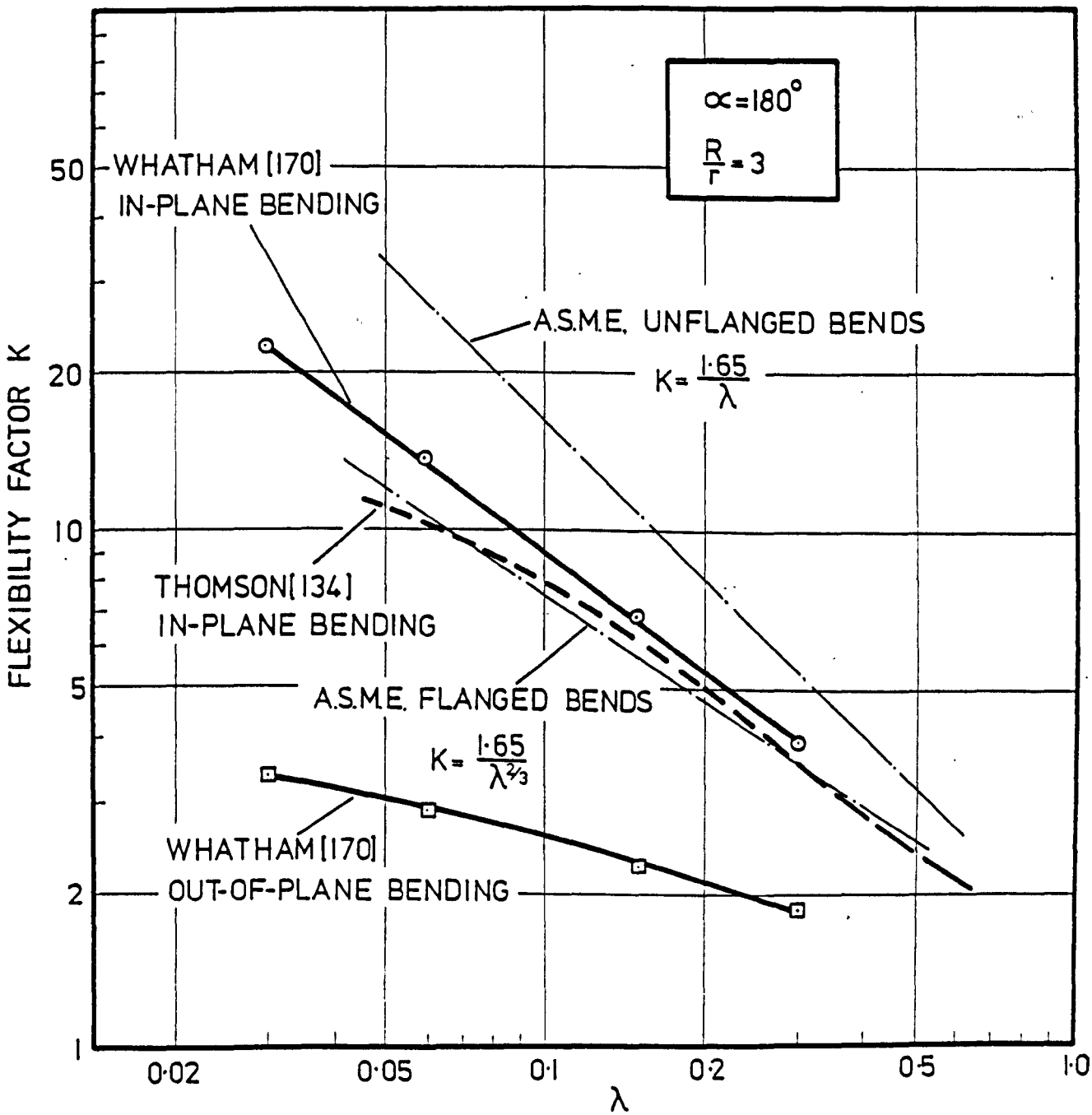

FLEXIBILITY FACTORS
IN & OUT-OF-PLANE BENDING

FIG. 3·2

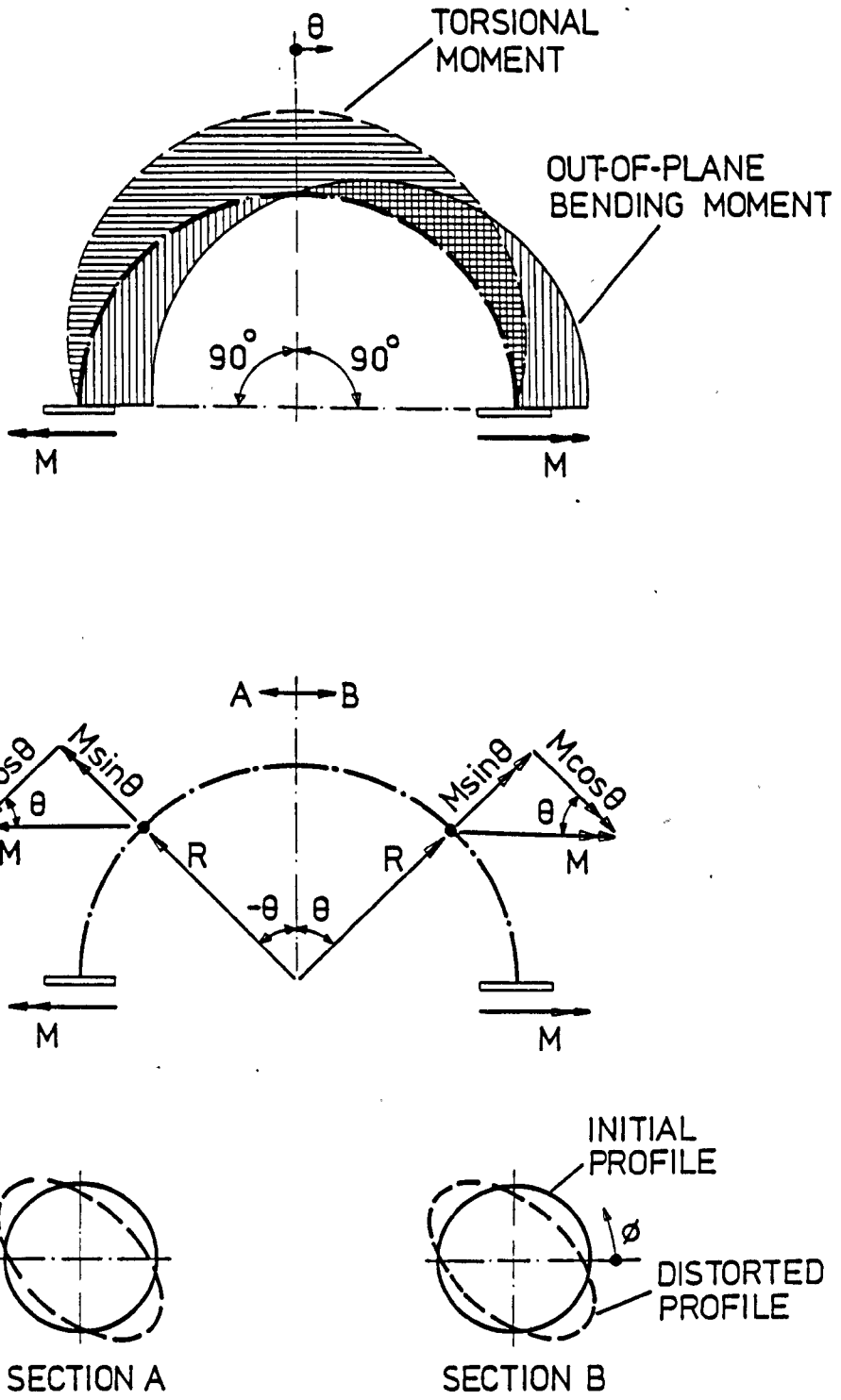

GENERAL LOADING AND DISTORTION
180° BEND

FIG.3·3

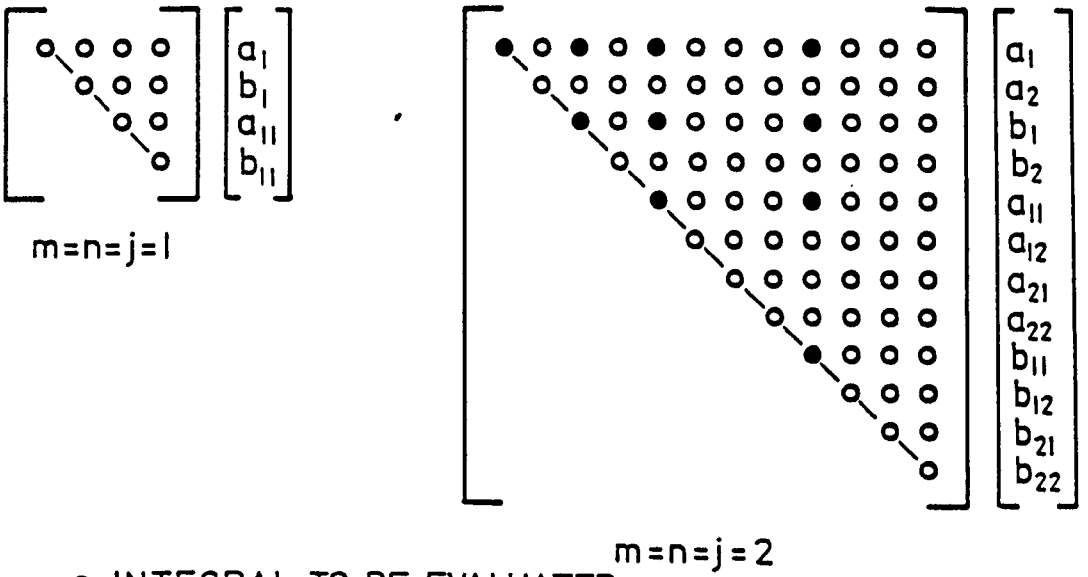

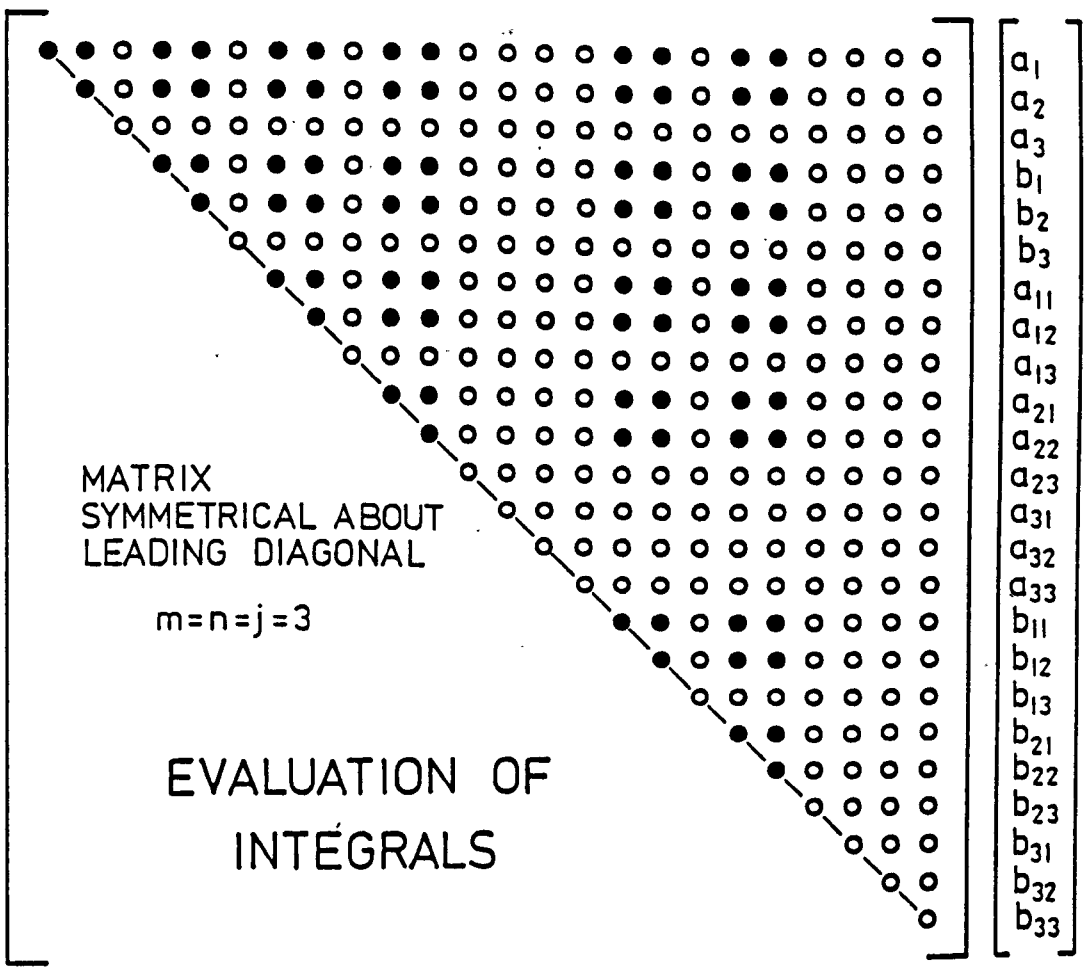

a_j . b_j : RIGID SECTION COEFFICIENTS

a_{mn} . b_{mn} : DISTORTION COEFFICIENTS

FIG.3·4

REDUCTION IN COMPUTATION USING STORED INTEGRALS

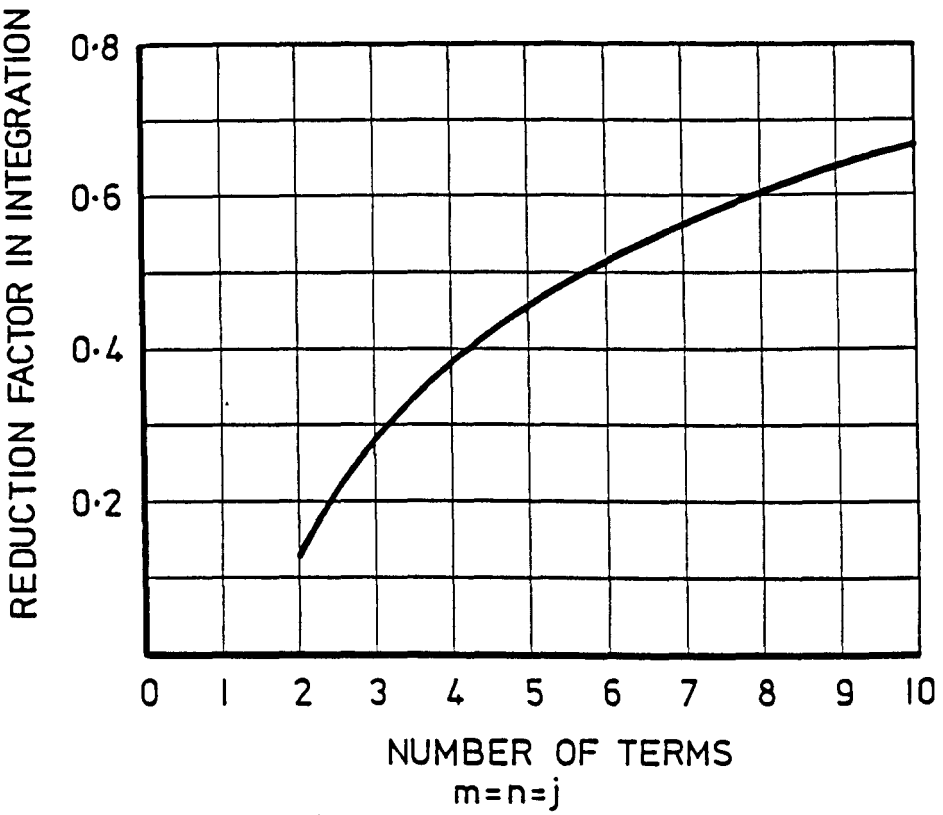

$$\text{REDUCTION FACTOR} = \frac{\left[\sum_{i=1}^{n_2} n_4 + n_6 - (i-1)\right] - (n_6 - 1)}{\left[\sum_{i=1}^{n_1} n_3 + n_5 - (i-1)\right] - (n_5 - 1)}$$

where: $n_6 = 2j + 2.m.n$: $n_5 = 2.(j+1) + 2(m+1)(n+$

$n_4 = n_6 + 2$: $n_3 = n_5 + 2$

$n_2 = n_6 - 2$: $n_1 = n_5 - 2$

FIG. 3·5

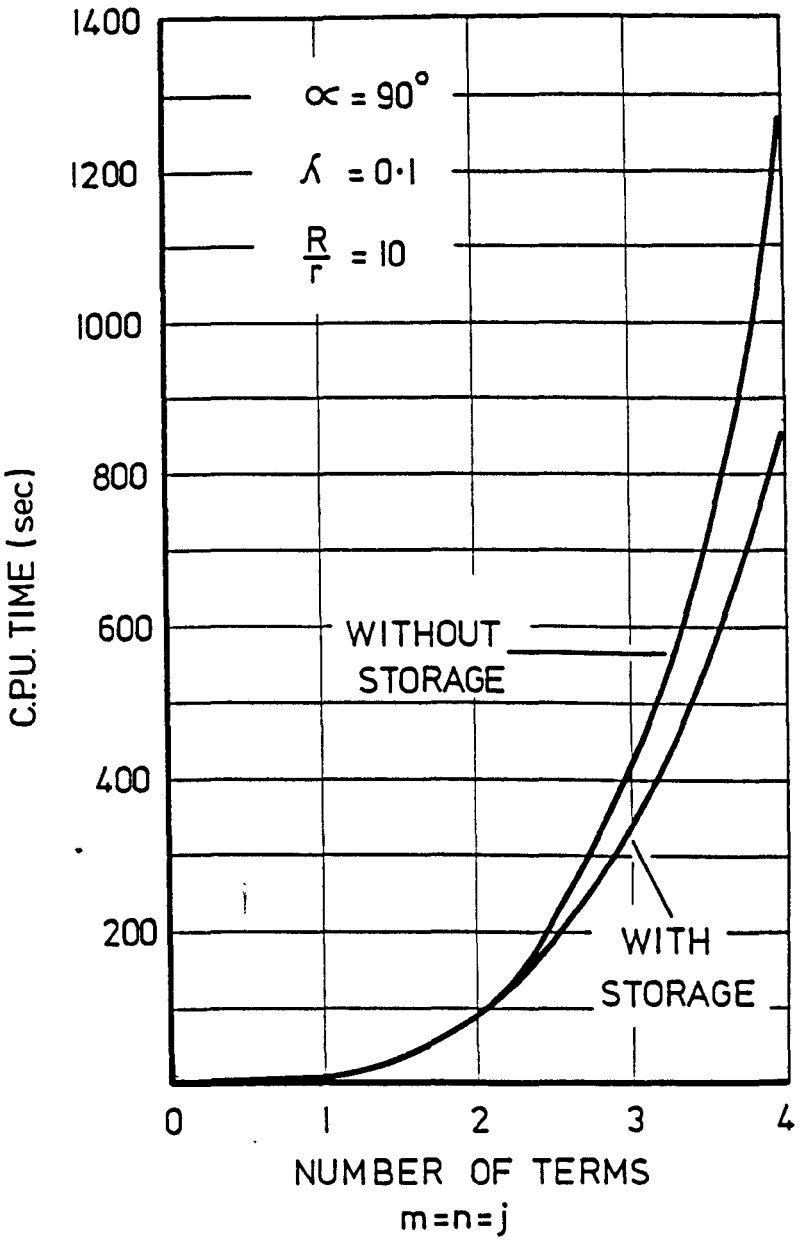

INTEGRATION : GAUSSIAN QUADRATURE
where $\bar{N}_\theta = 10$ and $\bar{N}_\phi = 15$

REDUCTION IN CPU TIME

FIG. 3·6

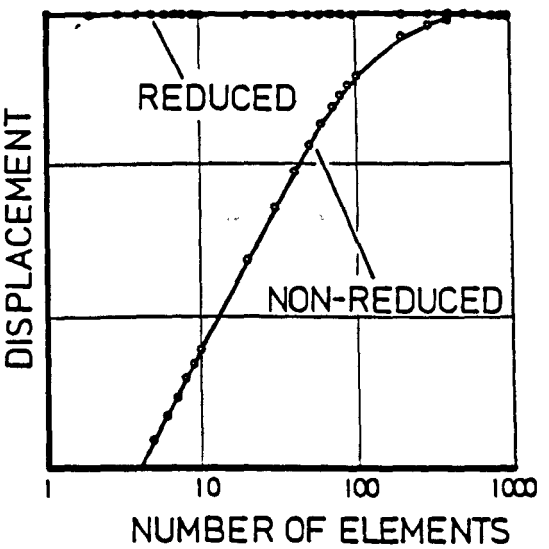

REDUCED INTEGRATION

TAKEDA & ISHA [222]

FIG.3·7

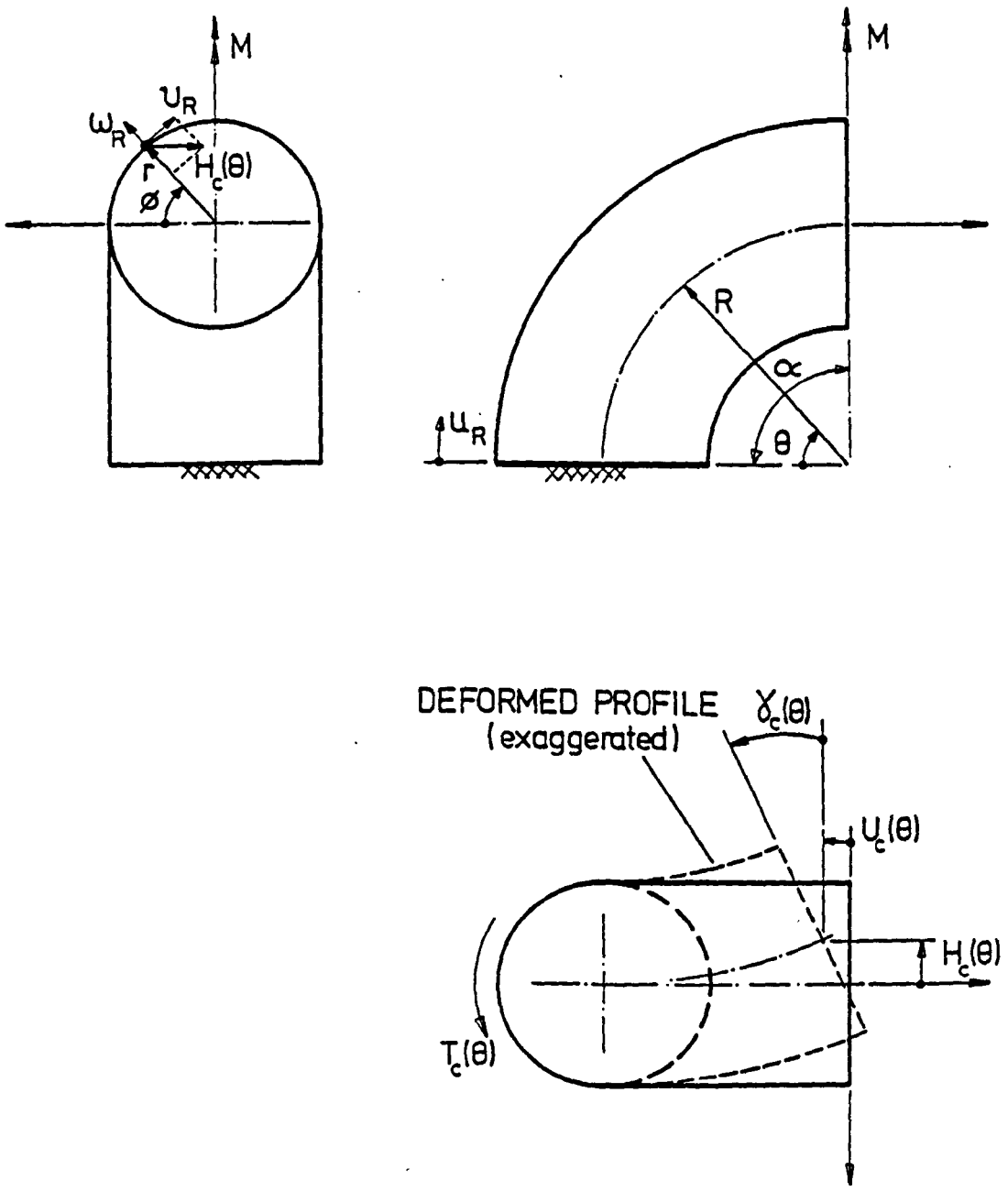

RIGID SECTION DISPLACEMENTS

FIG. 3·8

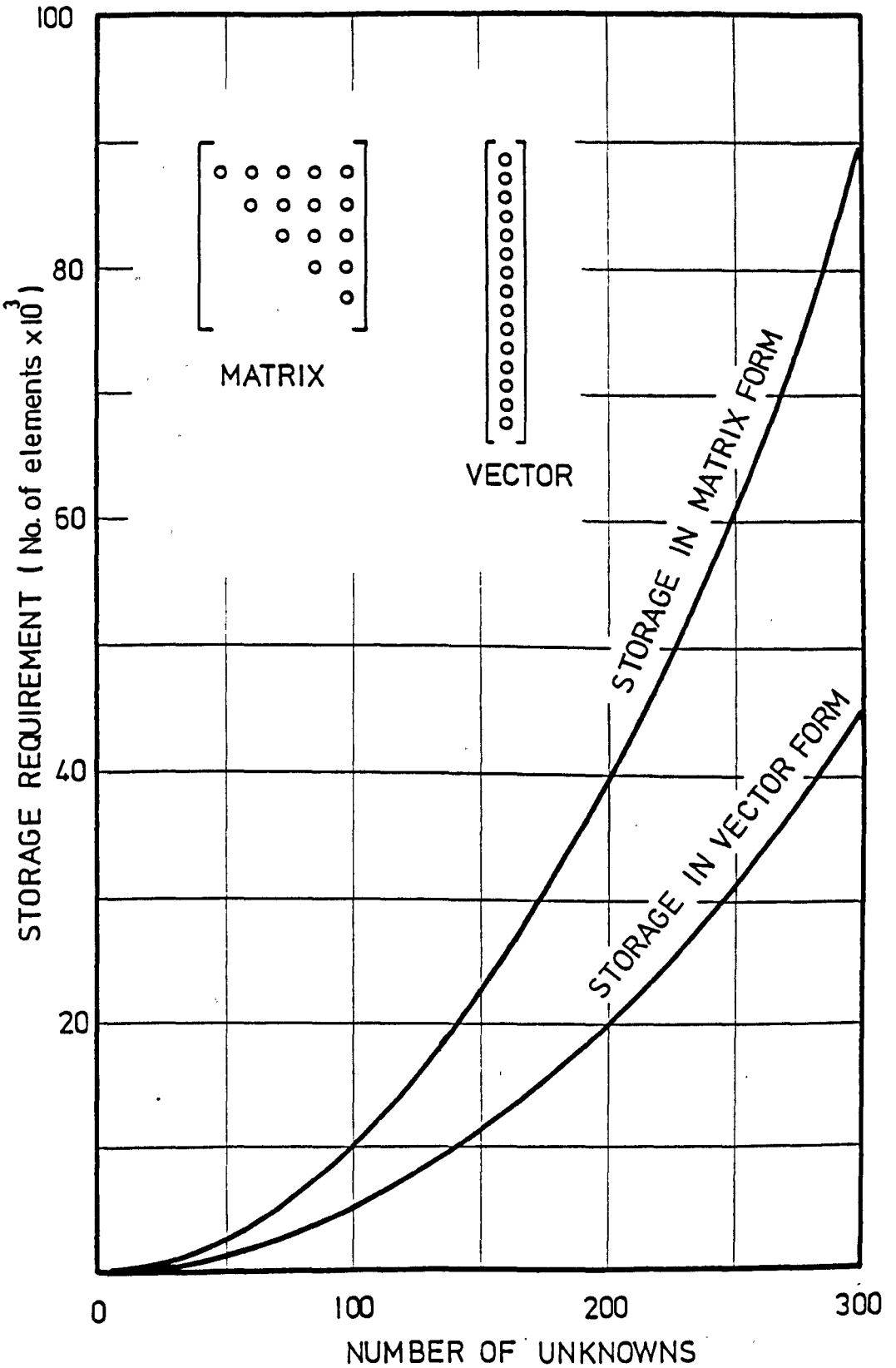

STORAGE OF INTEGRALS

FIG. 3·9

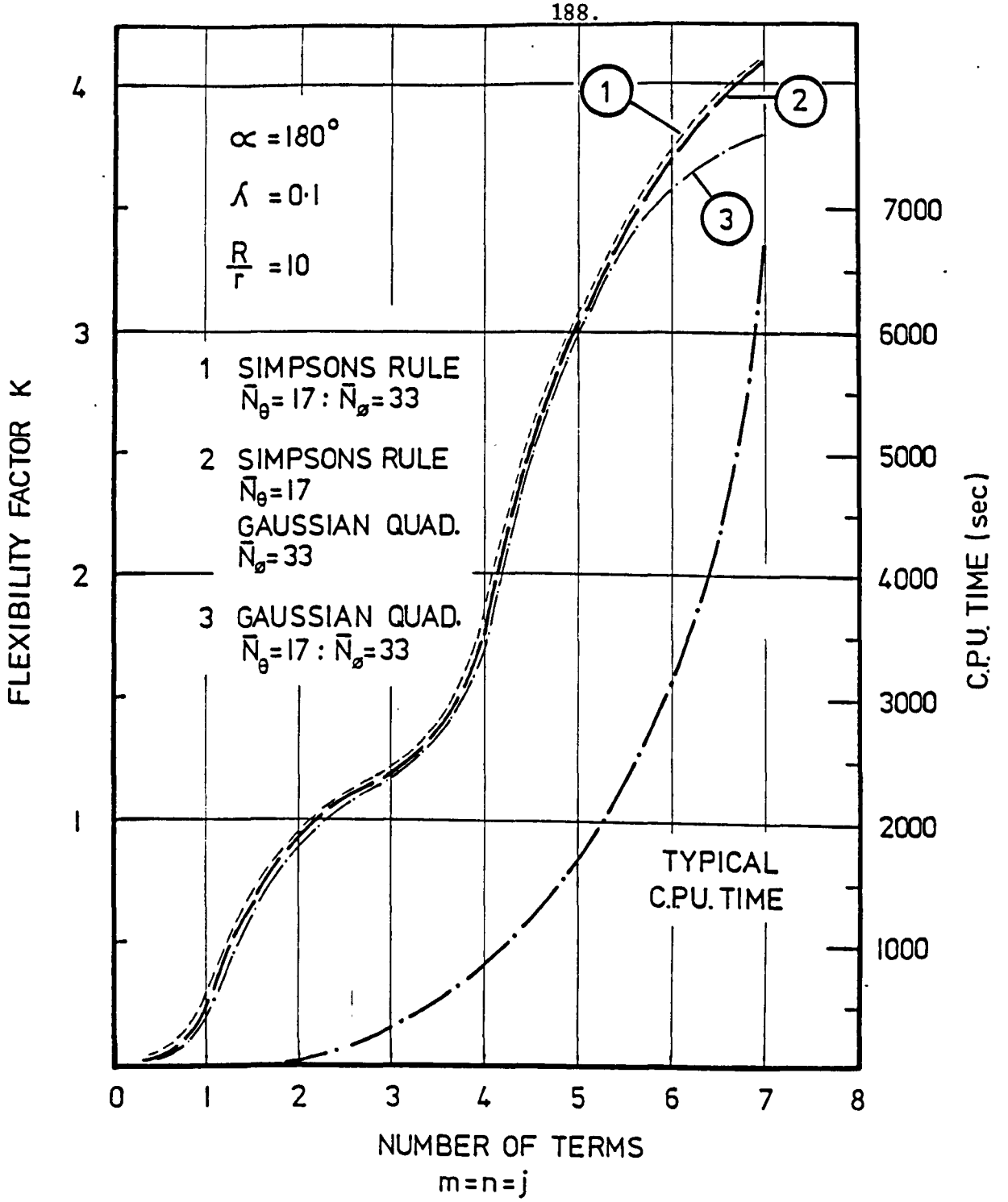

FOR m = n = j = 8 C.P.U. TIME > 7200 sec

CONVERGENCE
USING DIFFERENT INTEGRATION METHODS
FIG. 3·10

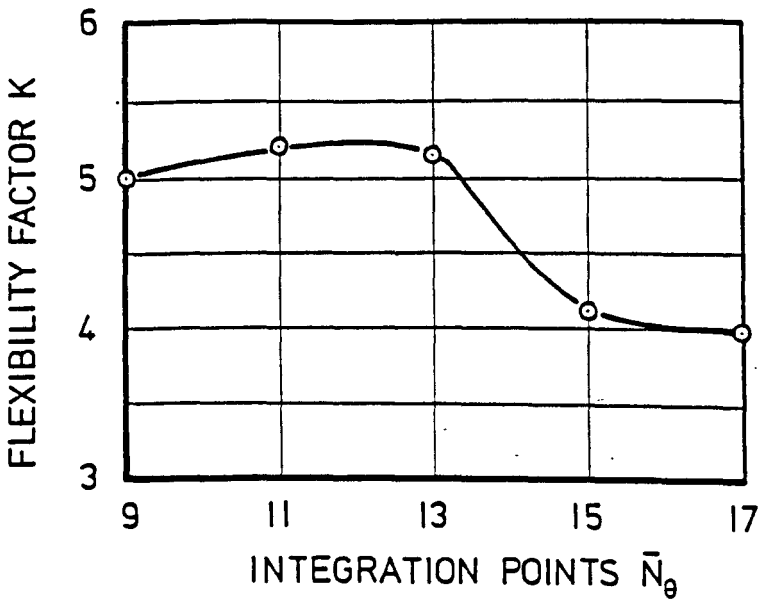

$\alpha = 180^\circ$

$\lambda = 0.05$

$\frac{R}{r} = 10$

$m = n = j = 5$

INTEGRATION : SIMPSONS RULE

$\bar{N}_\alpha = 33$

INTEGRATION

FIG.3·11

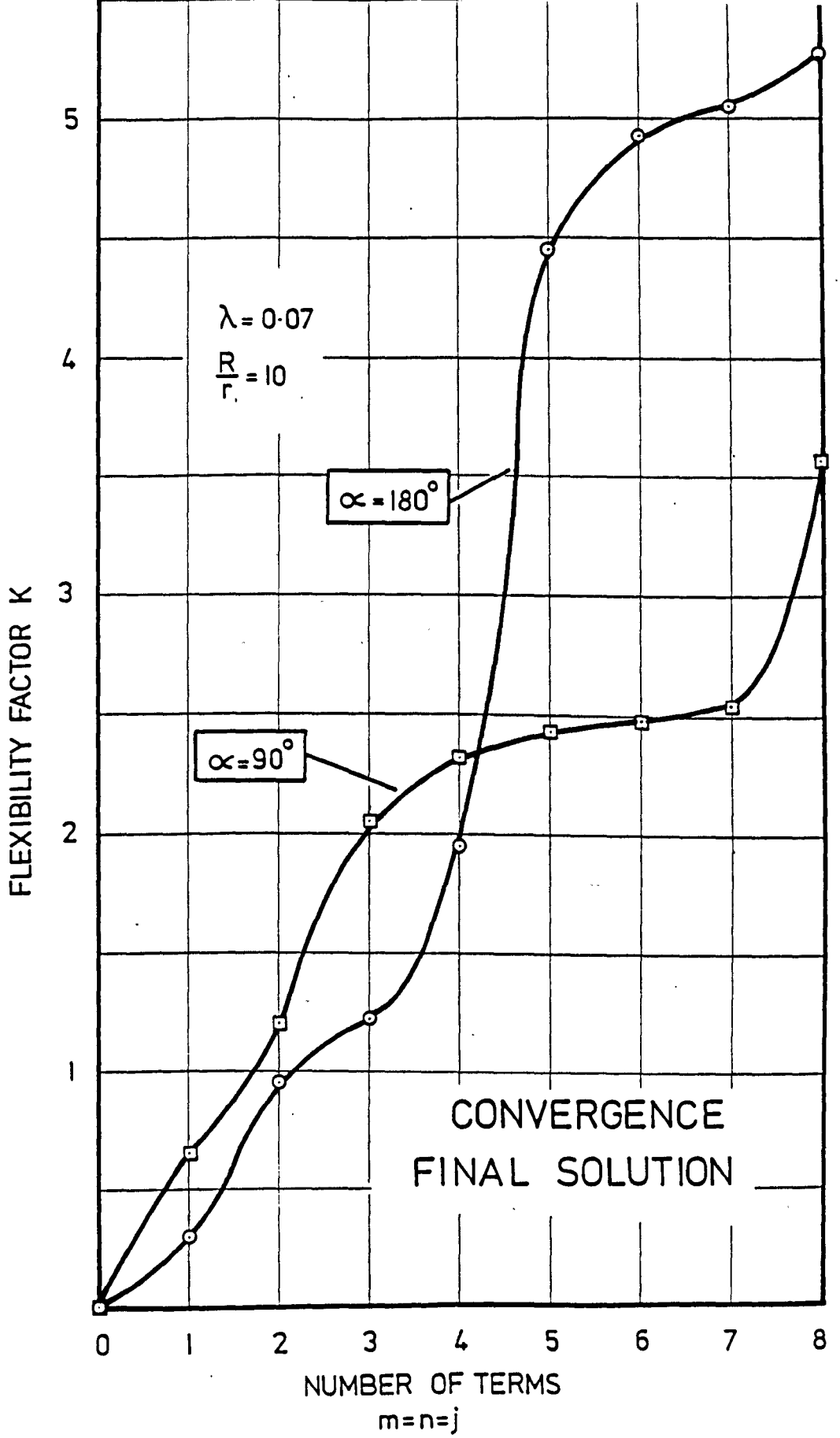
FLEXIBILITY FACTOR K
NUMBER OF TERMS
m=n=j
λ = 0·07
R/r = 10
∝ = 180°
∝ = 90°
CONVERGENCE
FINAL SOLUTION
0
1
2
3
4
5
6
7
8

FIG.3·12

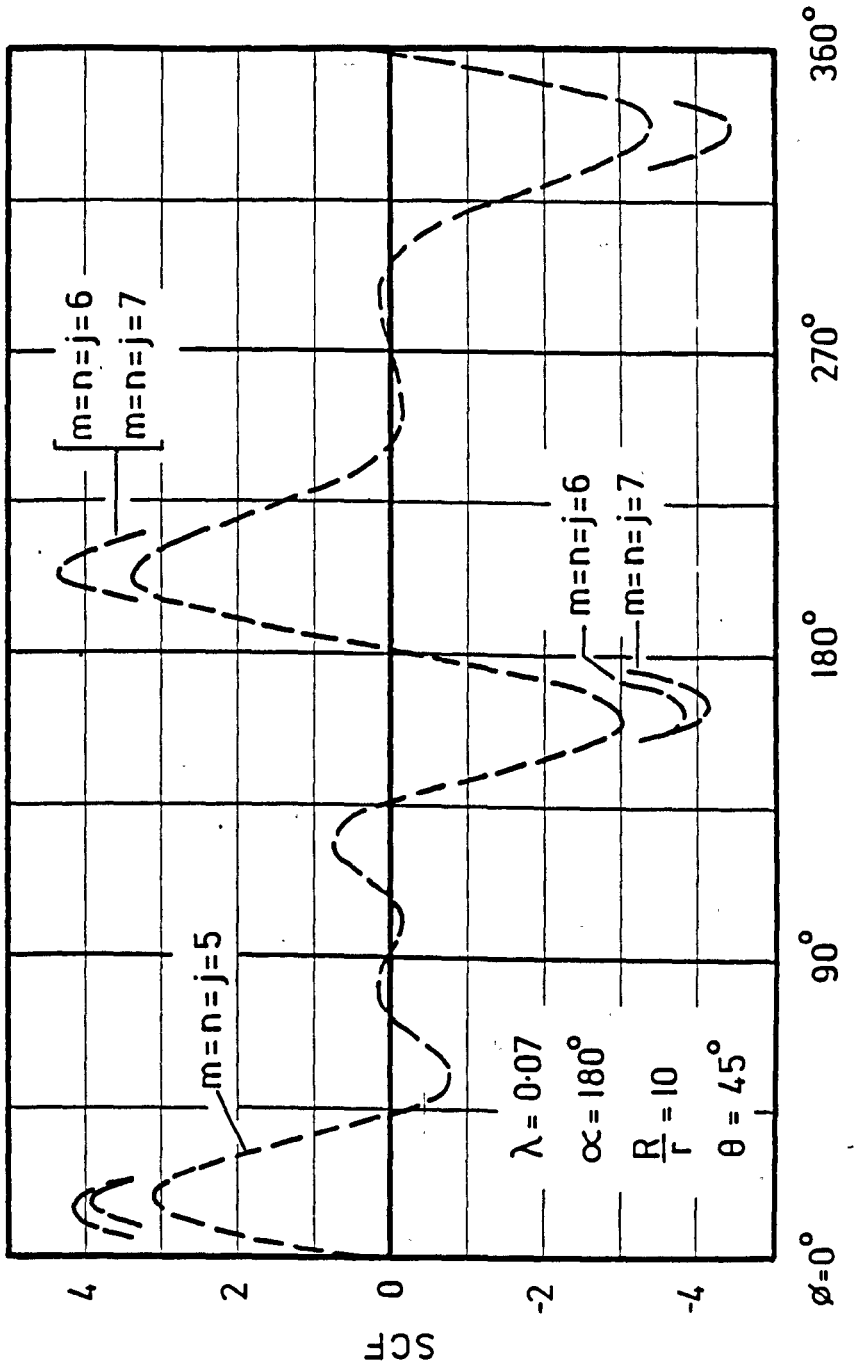

MERIDIONAL STRESS AT θ=45°

VARIATION WITH m, n and j

FIG. 3·13

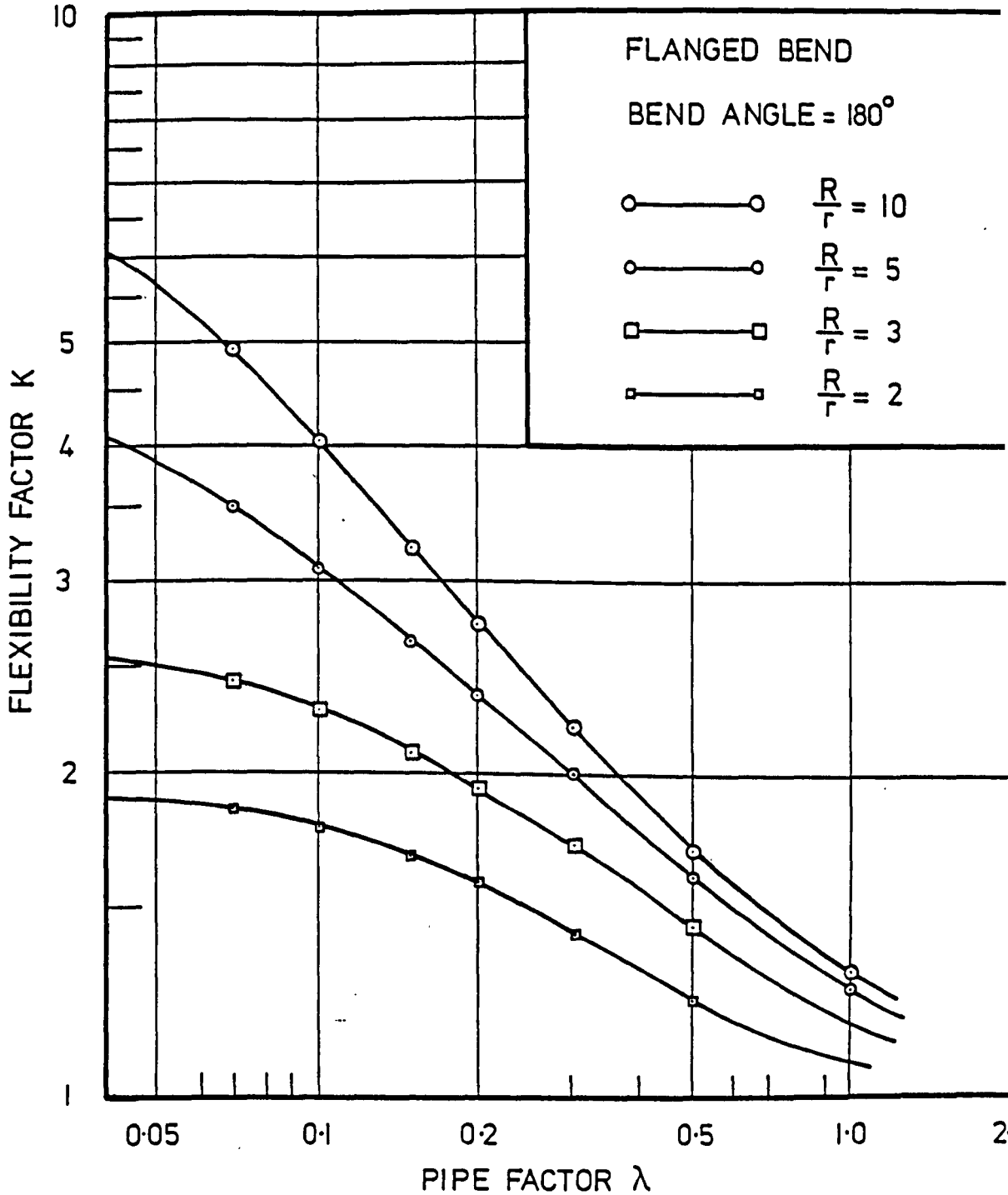

THEORETICAL FLEXIBILITY FACTORS

FIG. 3·14

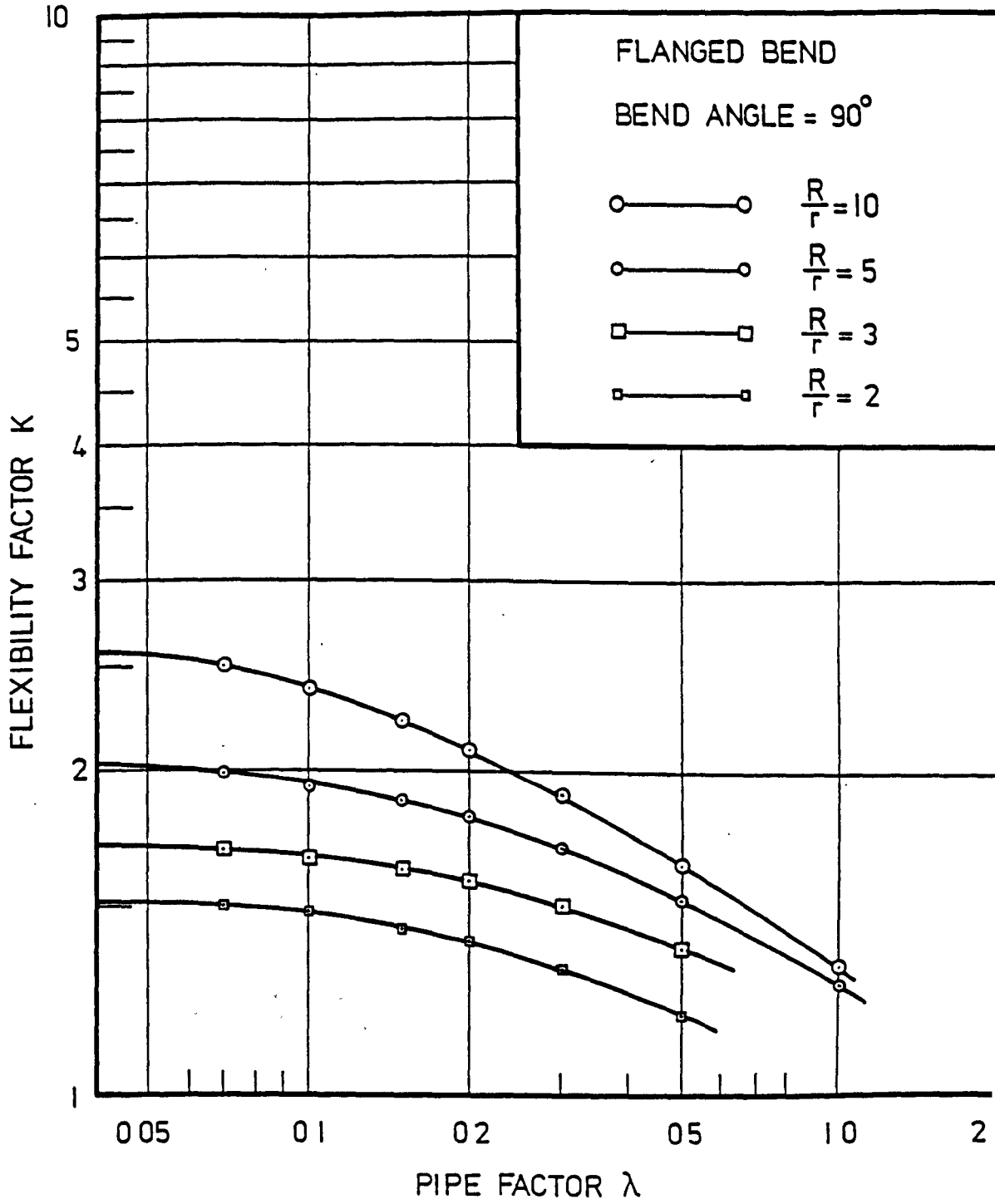

THEORETICAL FLEXIBILITY FACTORS

FIG.3·15

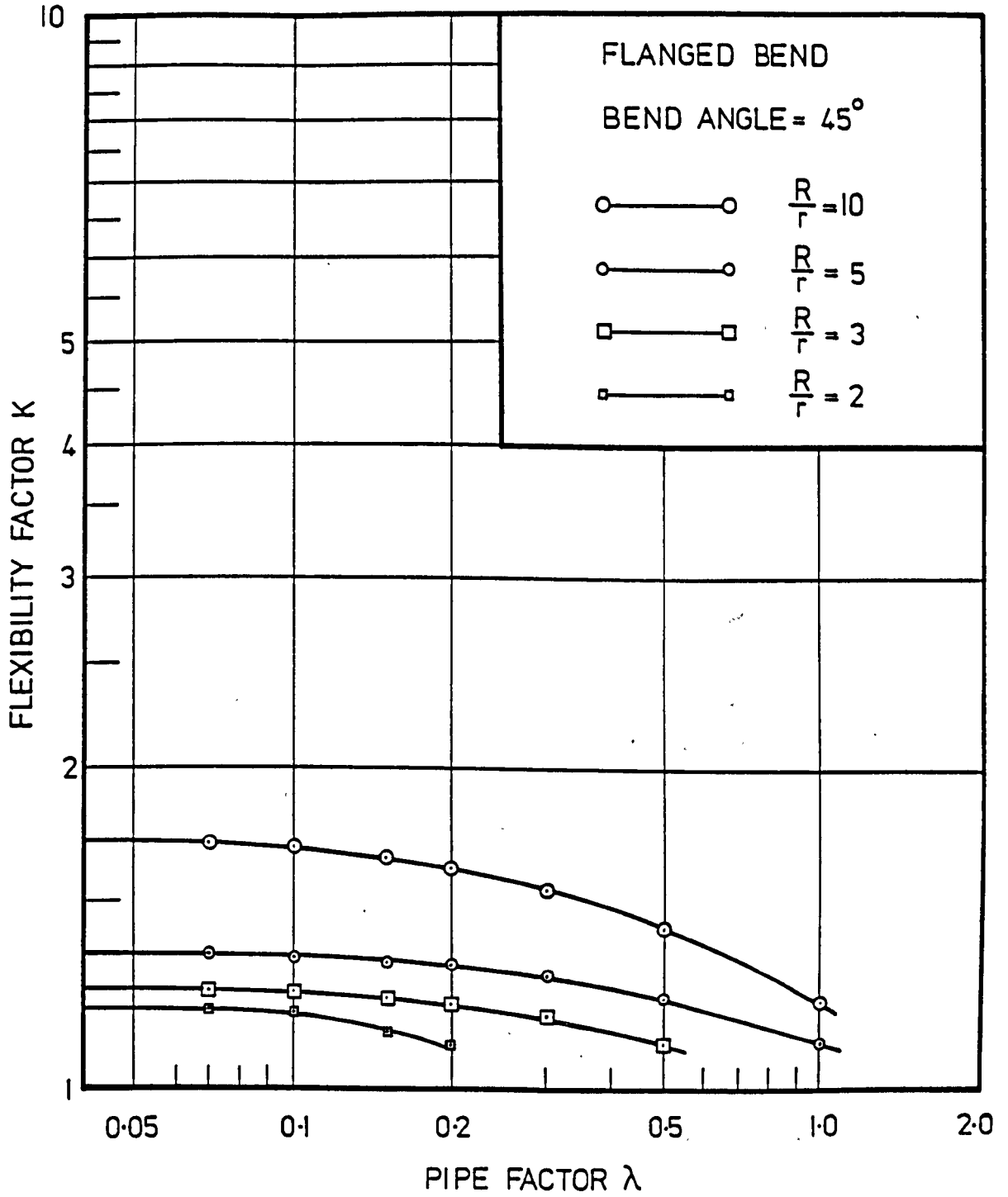

THEORETICAL FLEXIBILITY FACTORS

FIG.3·16

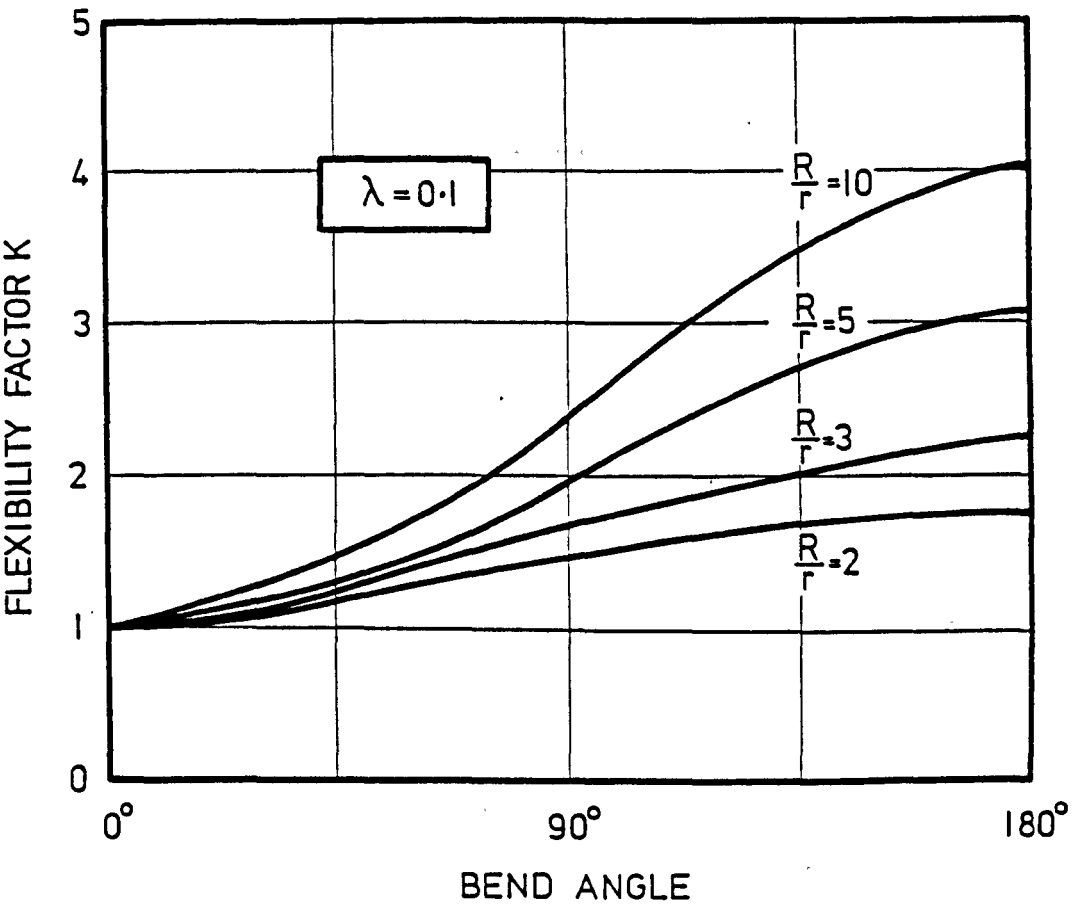

VARIATION OF FLEXIBILITY FACTOR WITH BEND ANGLE

FIG.3·17

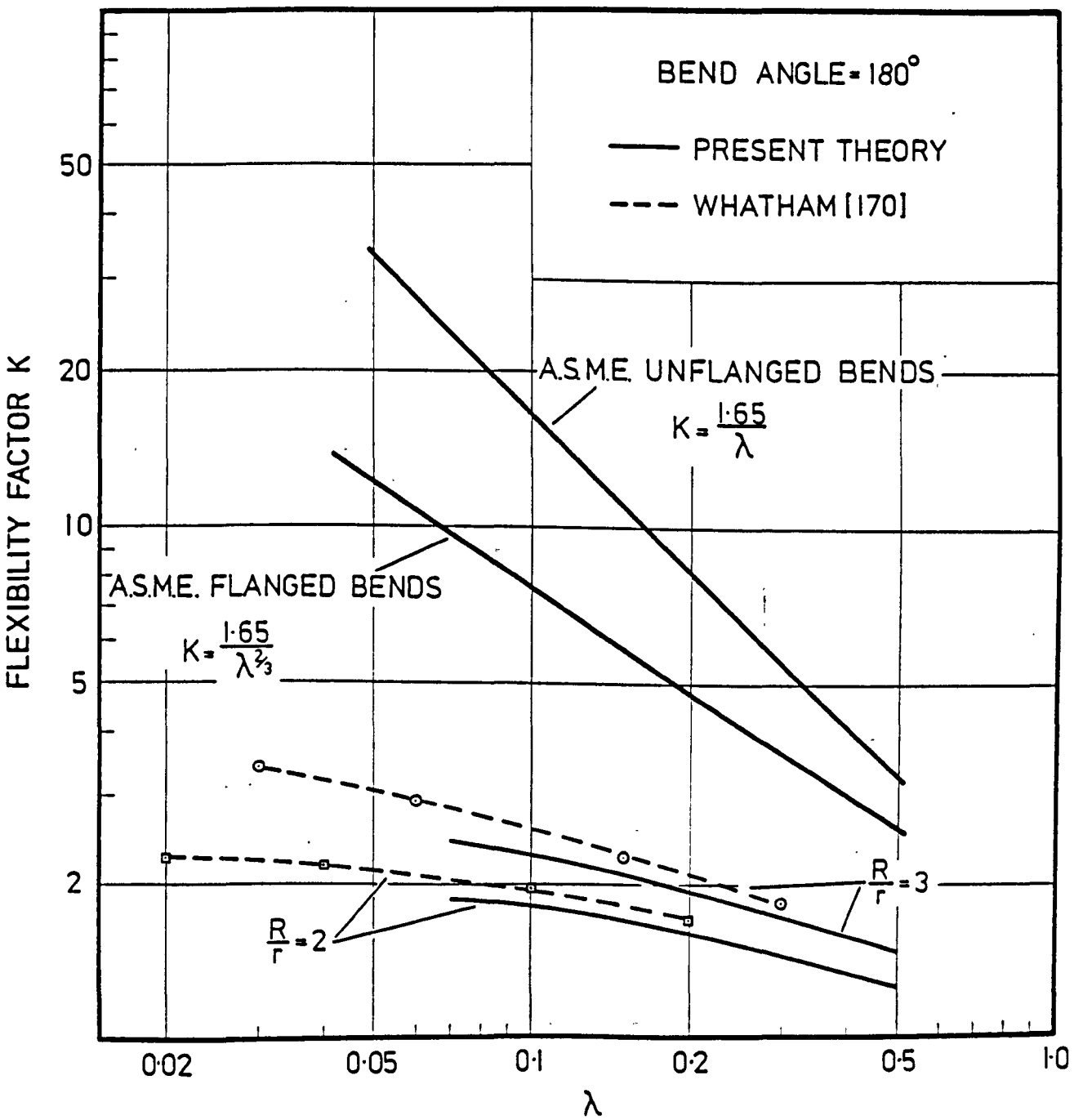

FLEXIBILITY FACTORS
THEORETICAL COMPARISON
FIG. 3·18

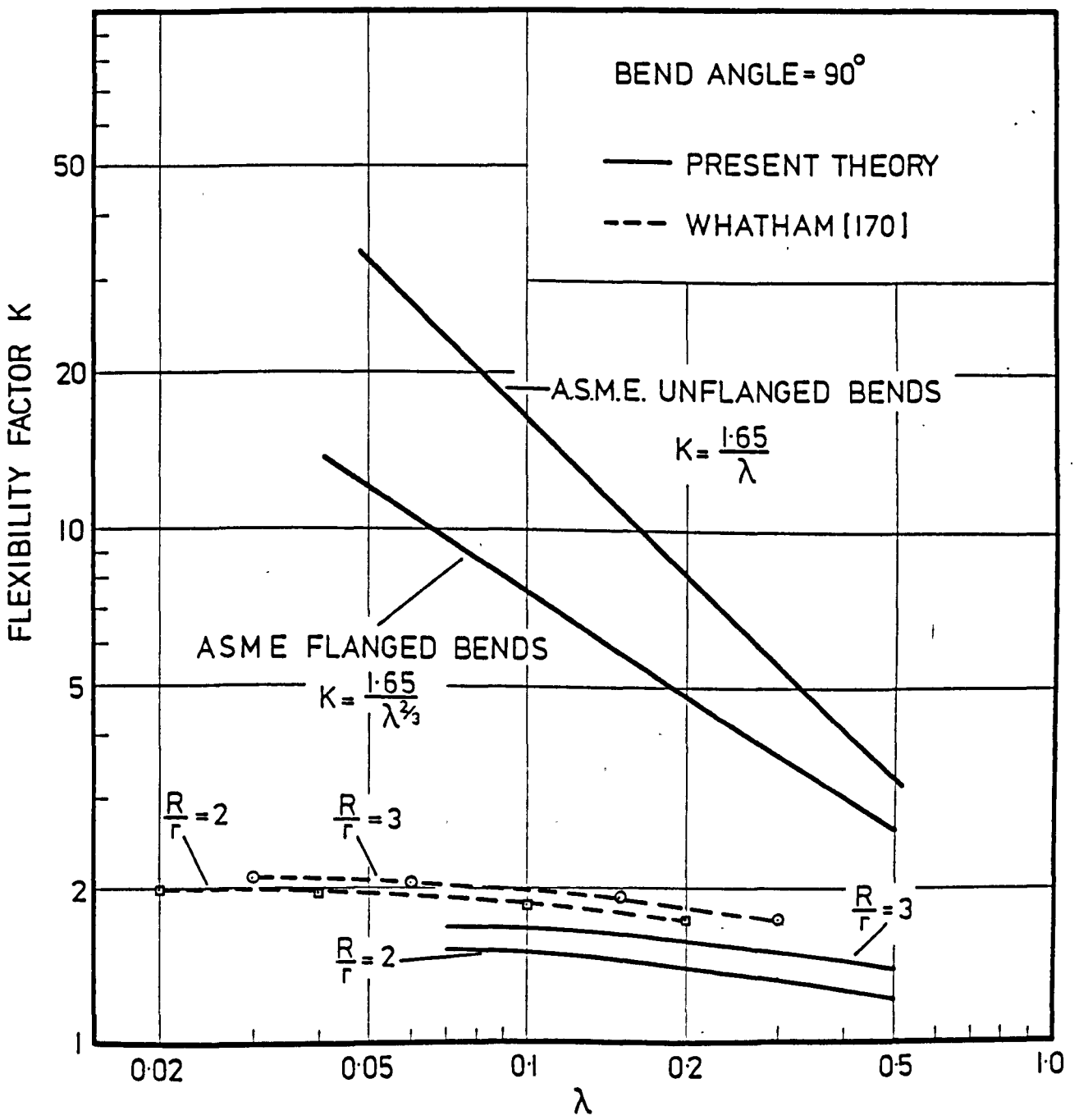

FLEXIBILITY FACTORS
THEORETICAL COMPARISON

FIG. 3·19

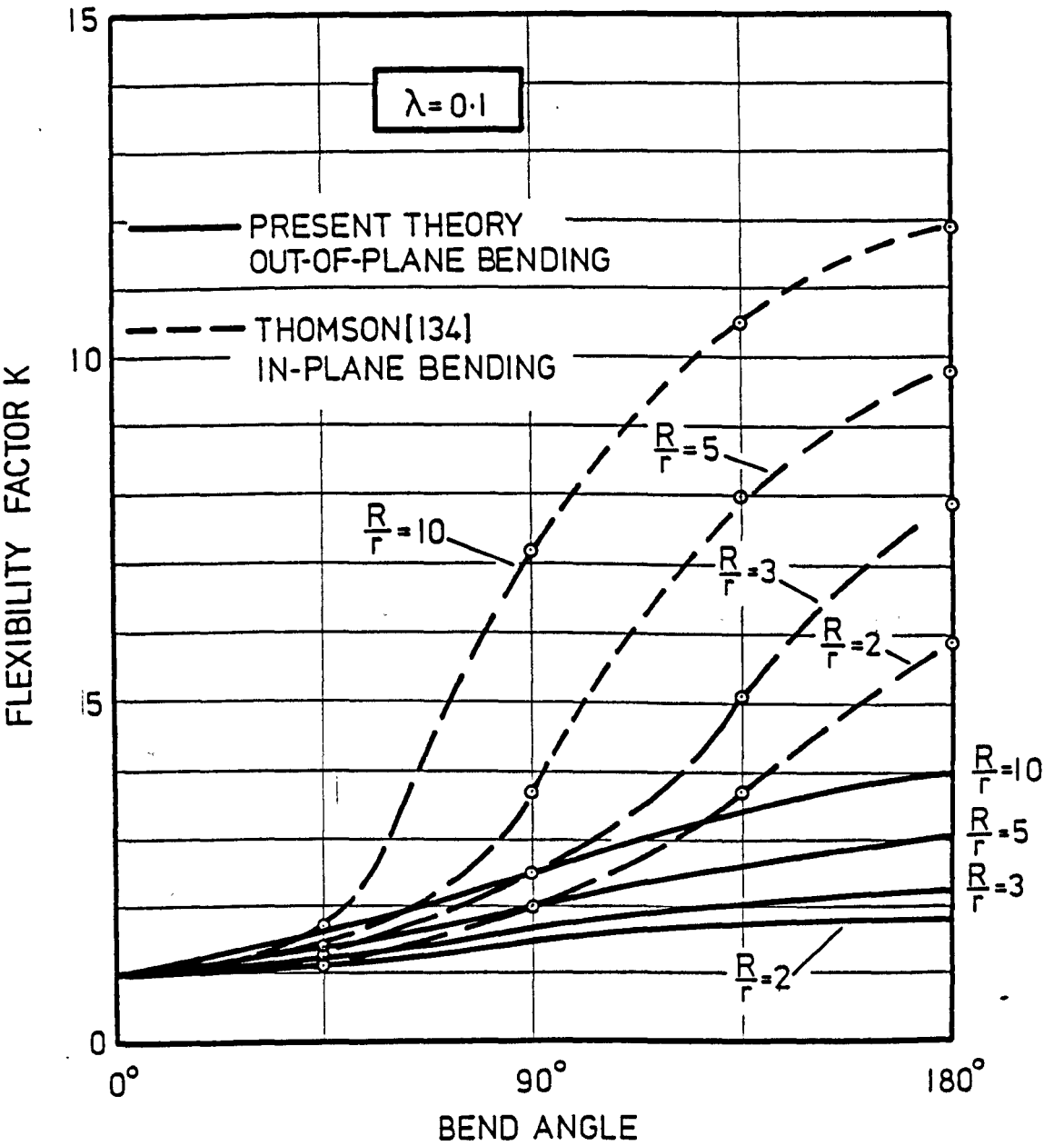

THEORETICAL COMPARISON
OF
FLEXIBILITY FACTOR

FIG.3·20

THEORETICAL MERIDIONAL STRESS AT $\theta = 45^\circ$

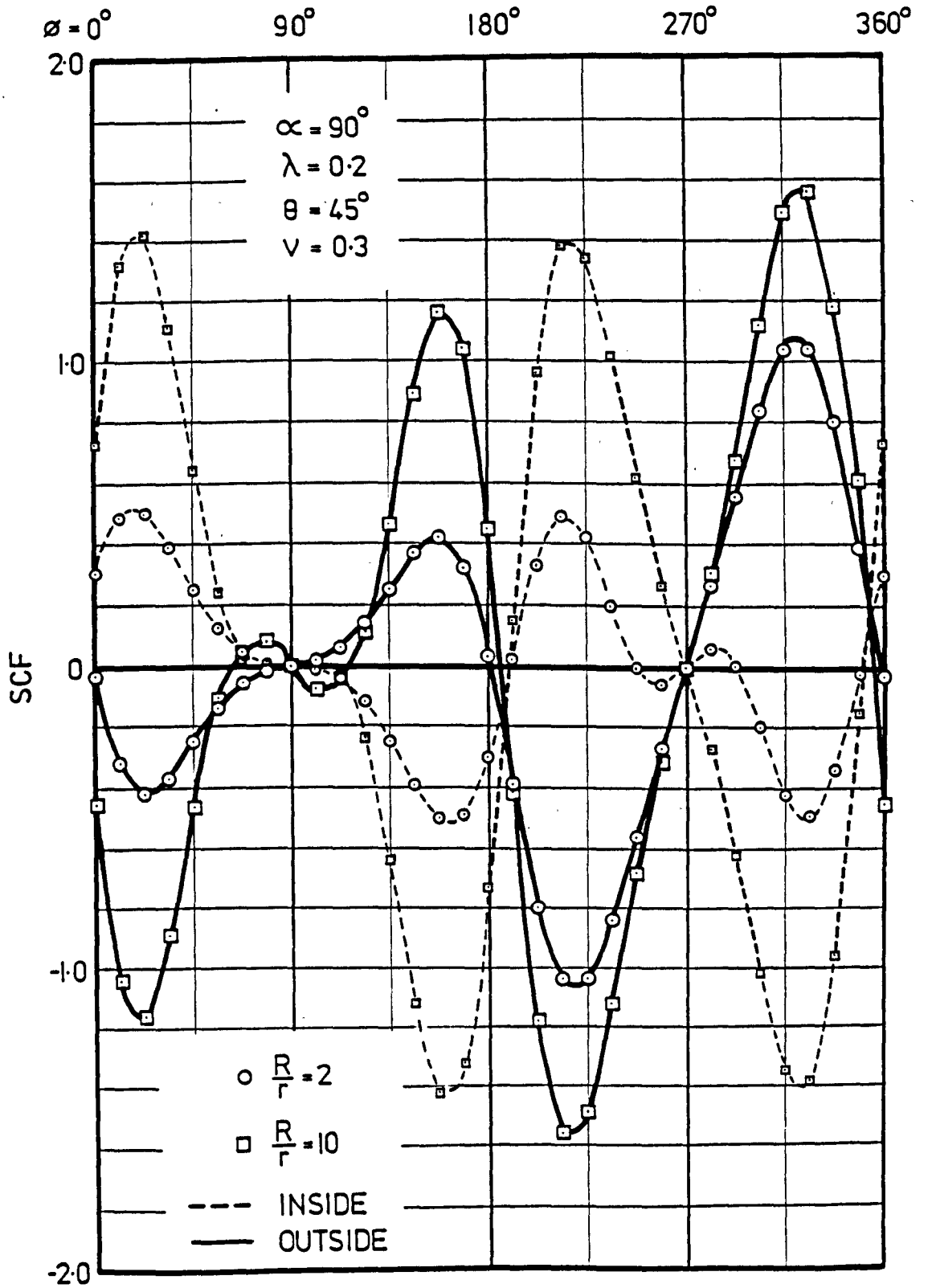

FIG. 3·21

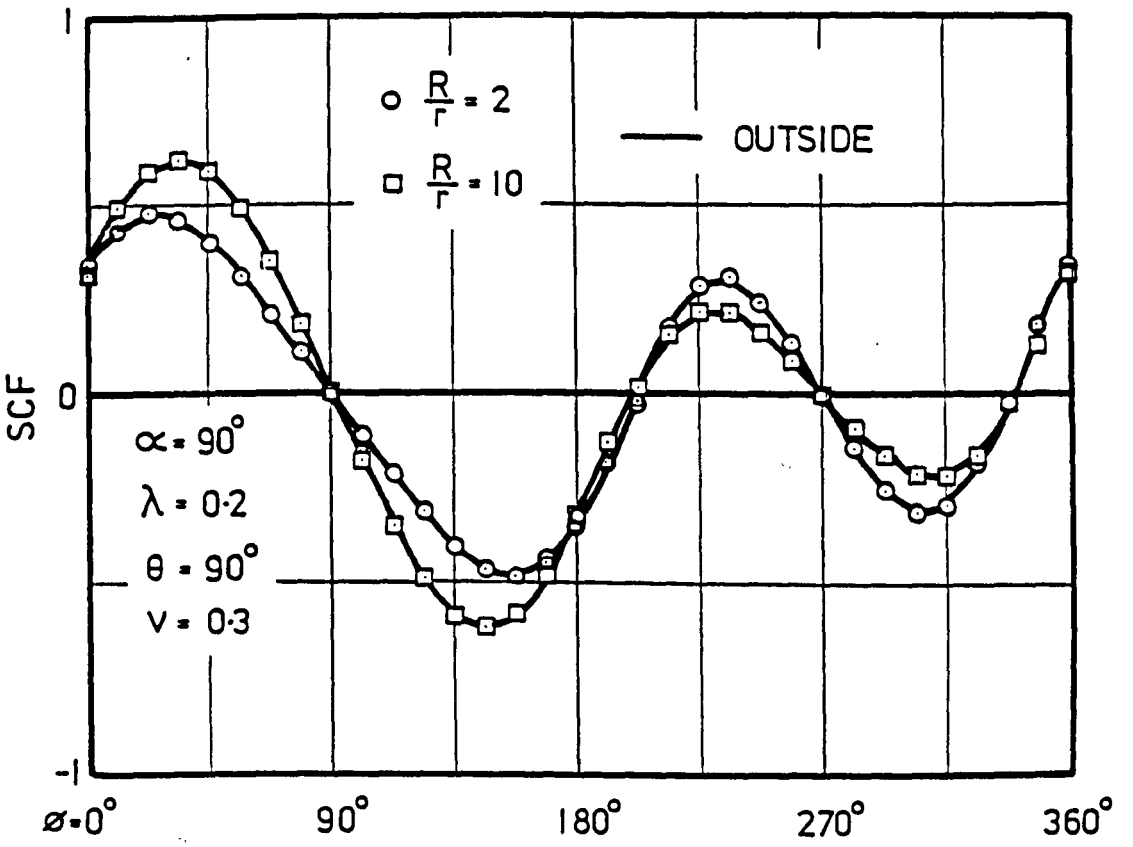

THEORETICAL
MERIDIONAL STRESS
AT $\theta=90^\circ$

FIG.3·22

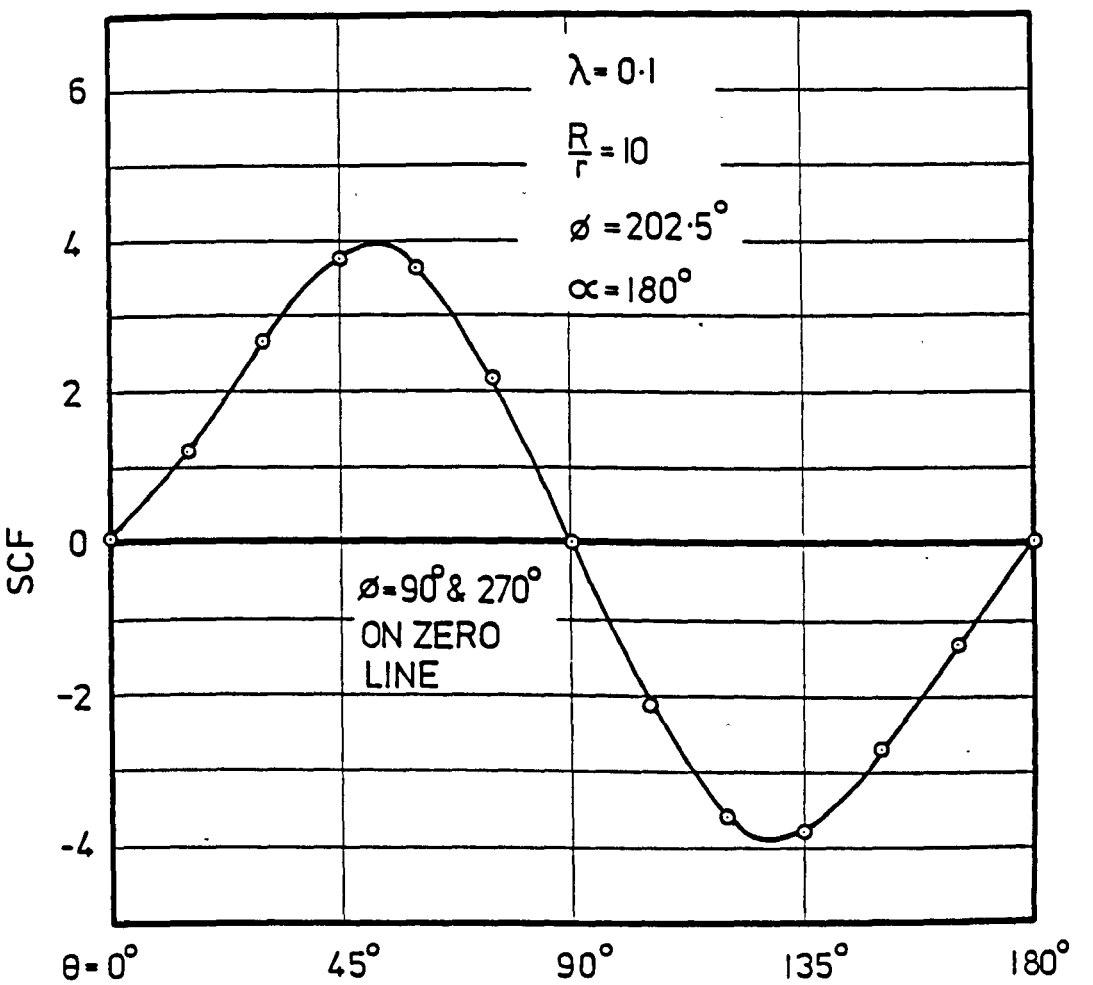

CIRCUMFERENTIAL VARIATION
OF MERIDIONAL STRESS

FIG.3·23

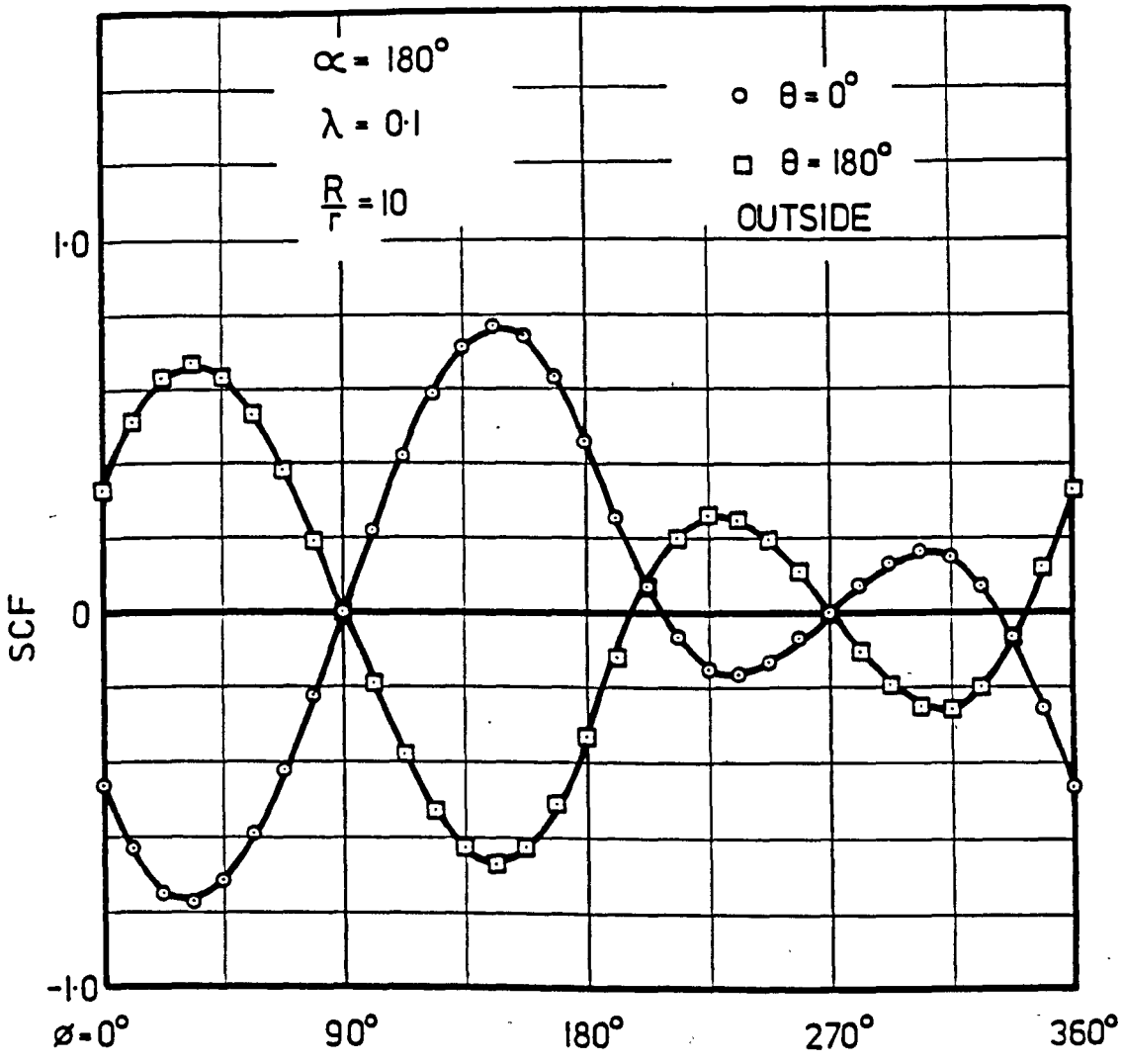

THEORETICAL MERIDIONAL STRESS AT θ = 0° AND θ = 180°

FIG. 3·25

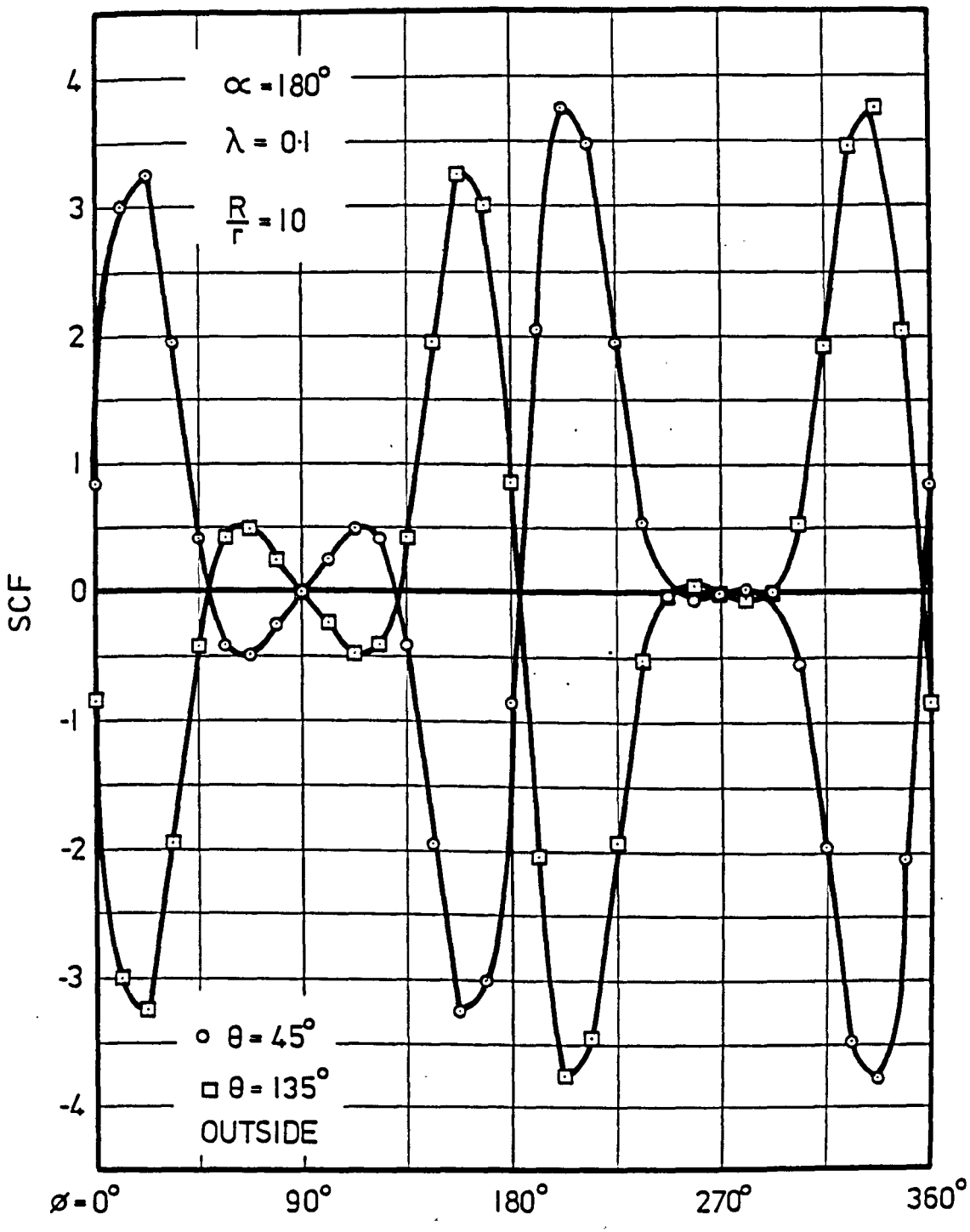

THEORETICAL MERIDIONAL STRESS AT θ=45° AND θ=135°

FIG.3·24

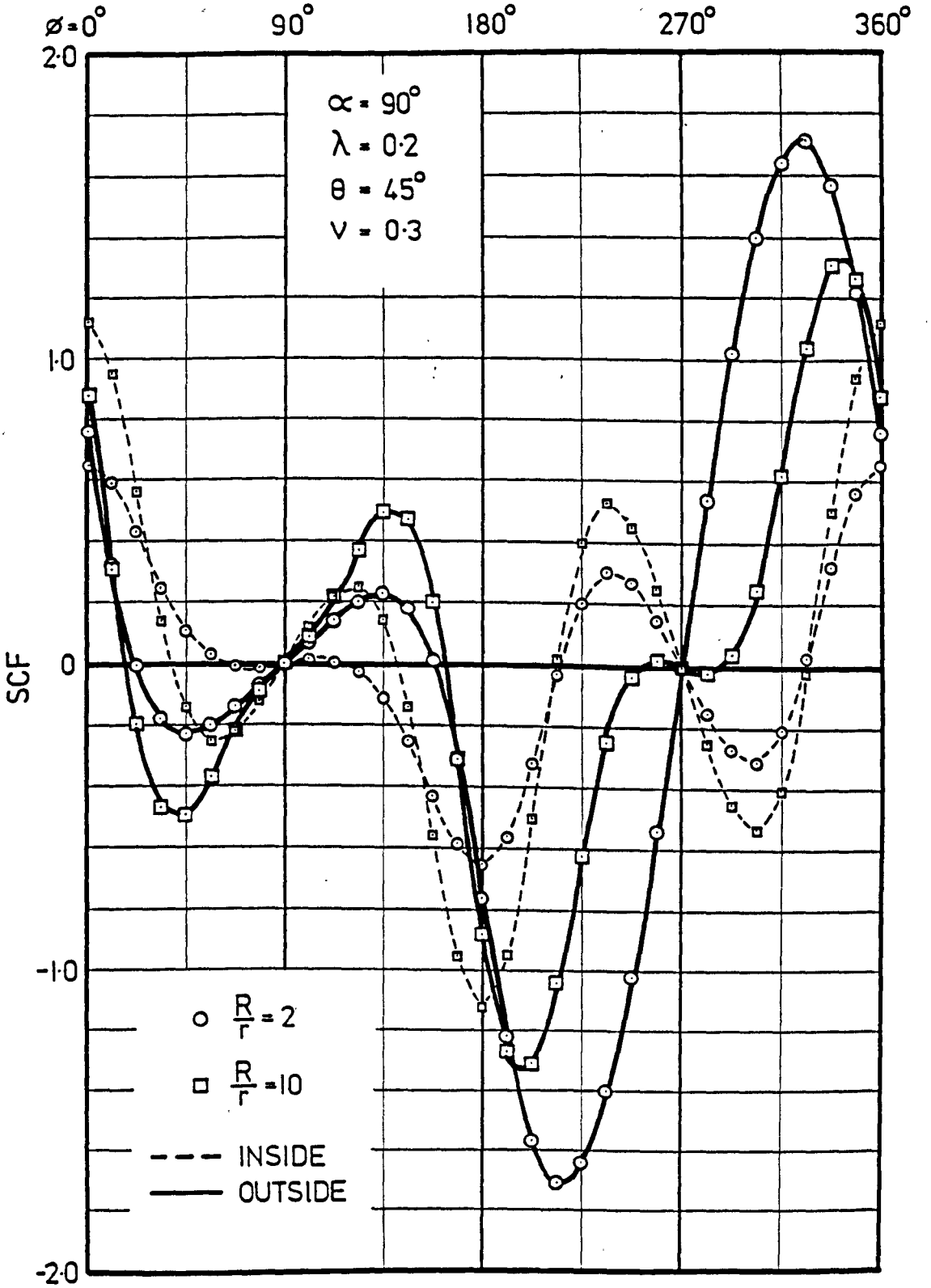

THEORETICAL CIRCUMFERENTIAL STRESS AT θ=45°

FIG. 3·26

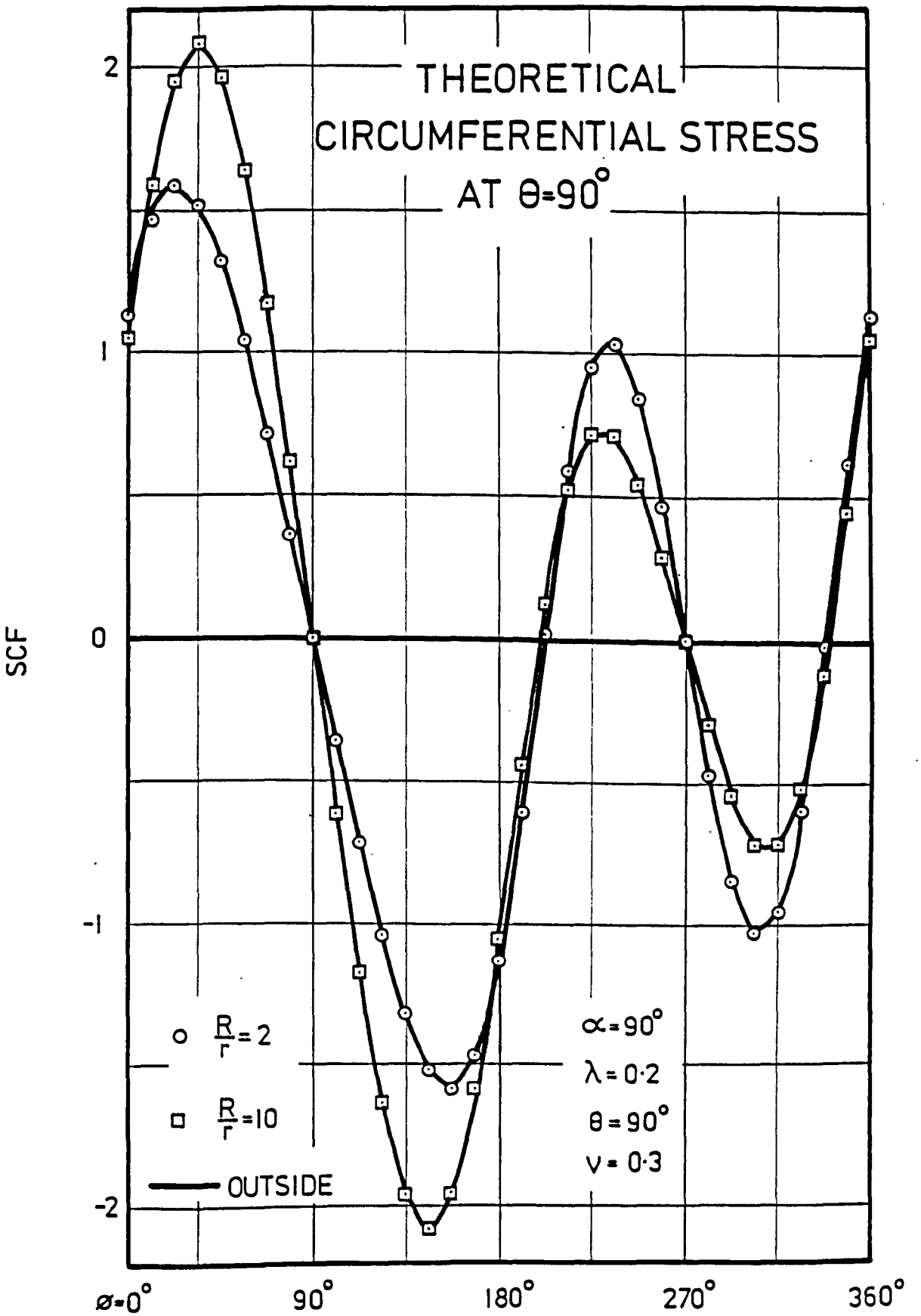
THEORETICAL
CIRCUMFERENTIAL STRESS
AT θ=90°
SCF
2
1
0
-1
-2
ø=0°
90°
180°
270°
360°
R/r=2
R/r=10
OUTSIDE
α=90°
λ=0·2
θ=90°
ν=0·3

FIG. 3·27

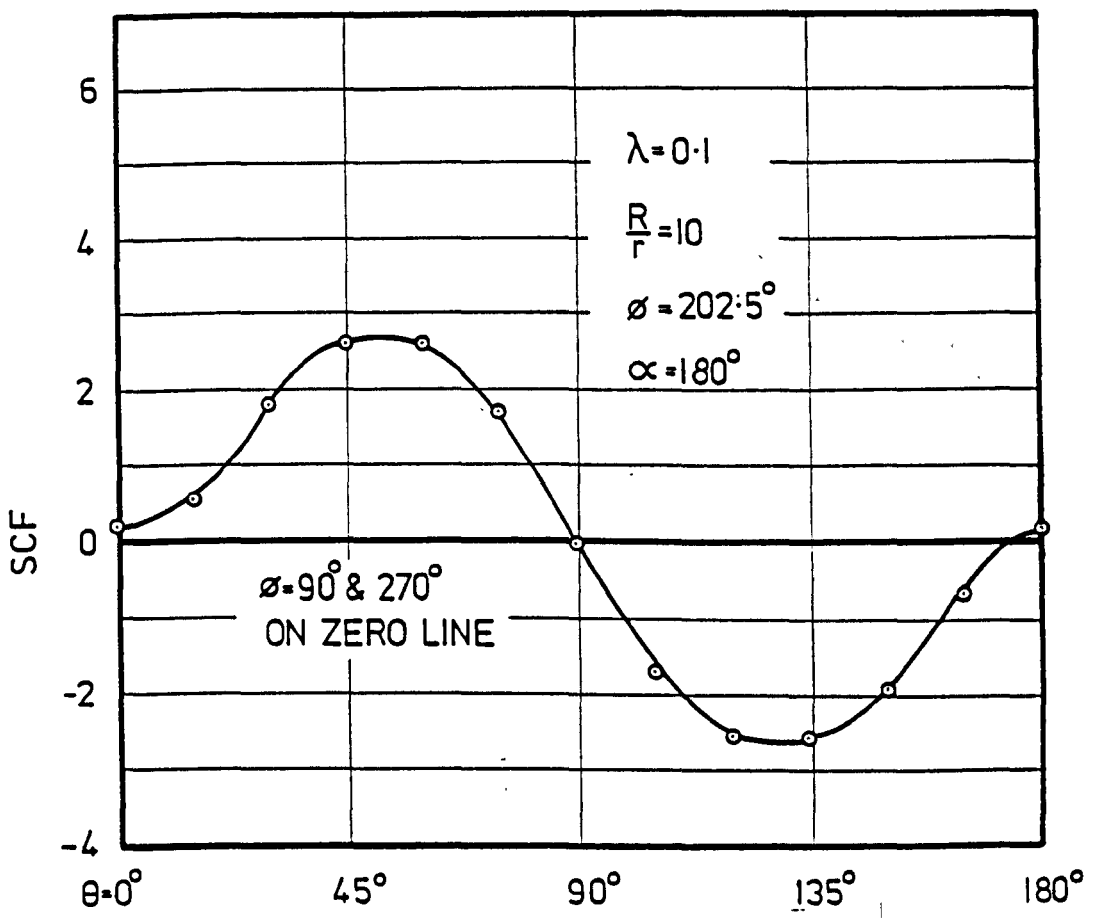

CIRCUMFERENTIAL VARIATION
OF CIRCUMFERENTIAL STRESS

FIG. 3·28

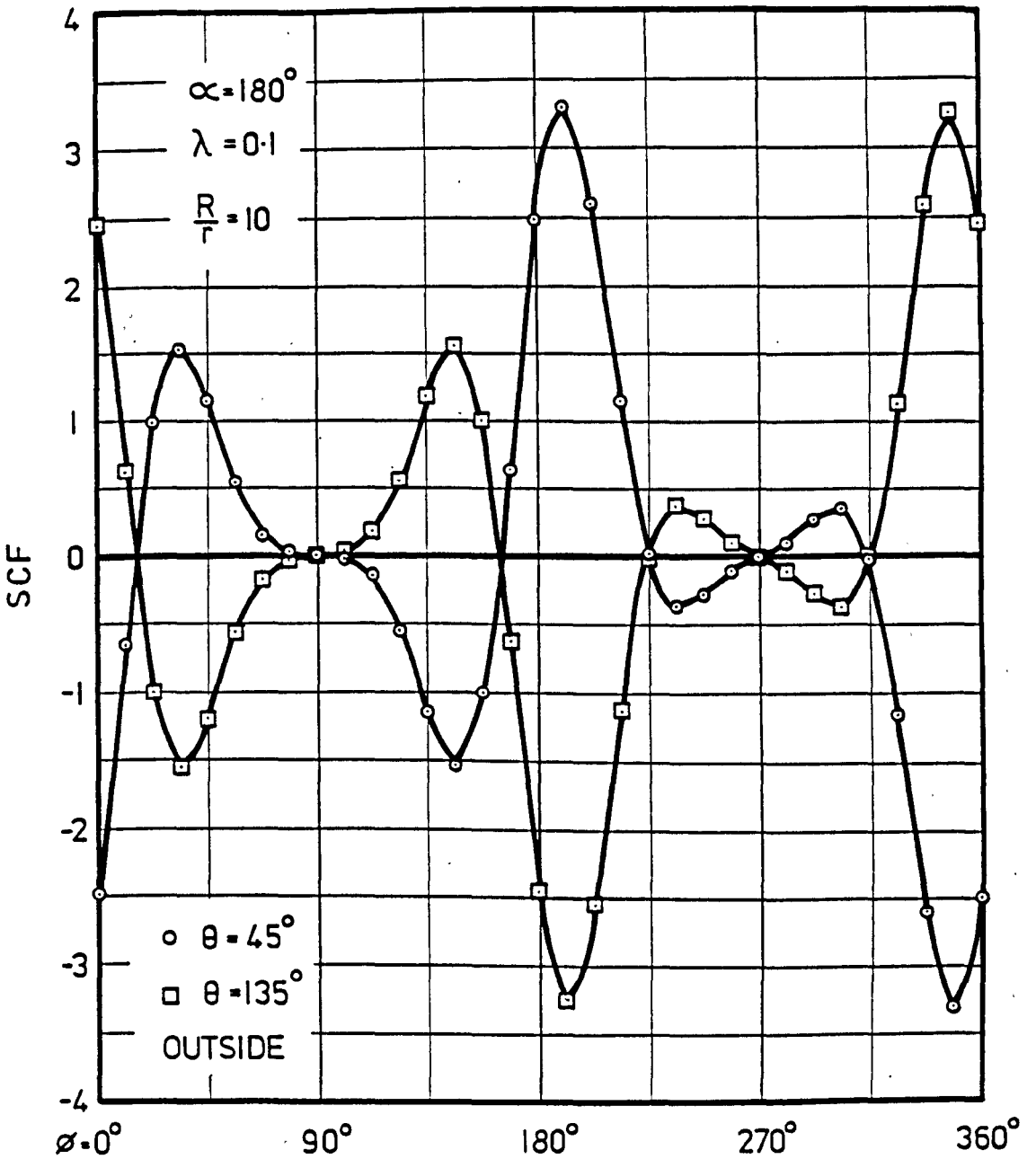

THEORETICAL CIRCUMFERENTIAL STRESS AT θ=45° AND θ=135°

FIG. 3·29

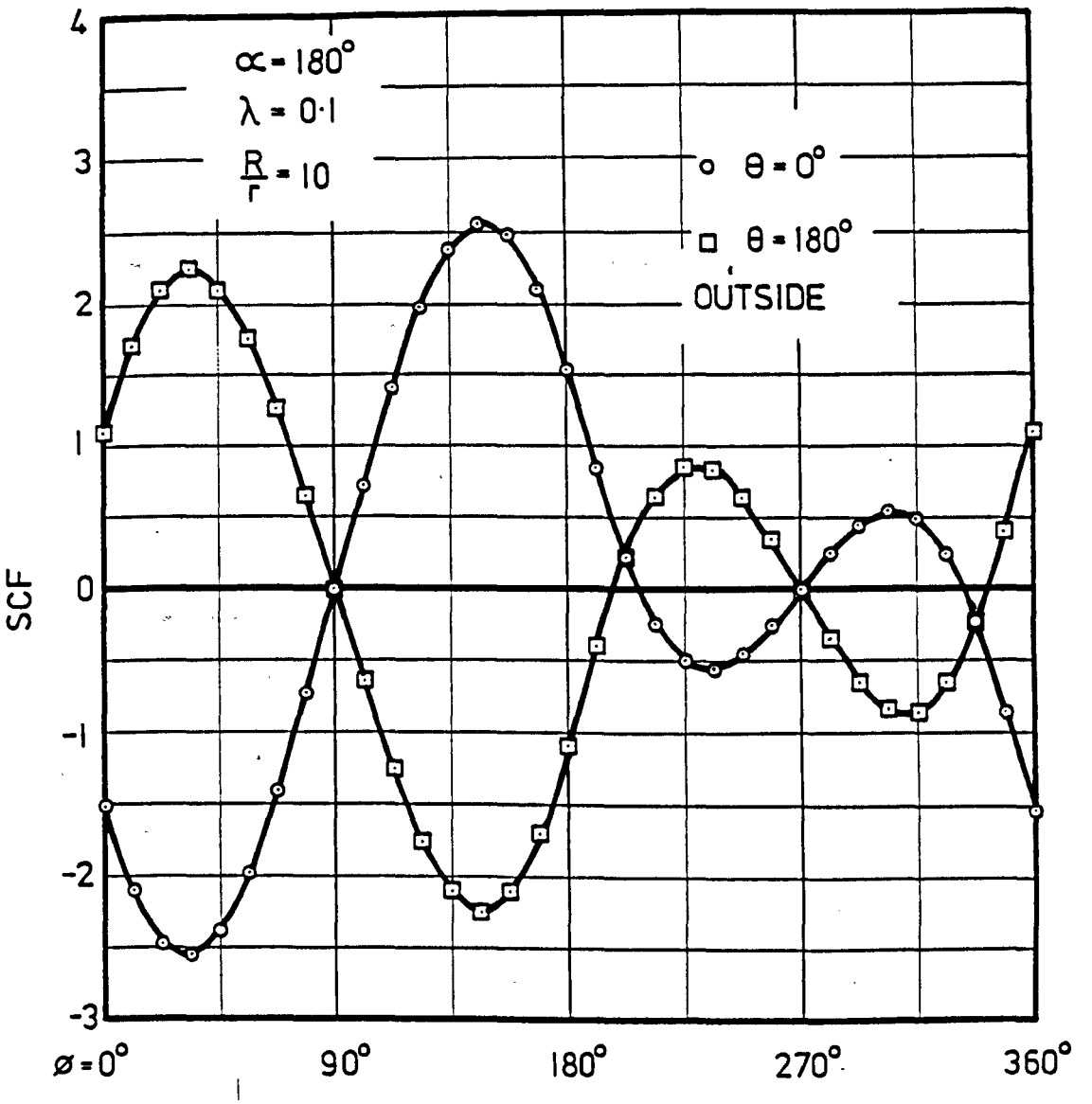

THEORETICAL CIRCUMFERENTIAL STRESS AT θ = 0° AND θ = 180°

FIG. 3·30

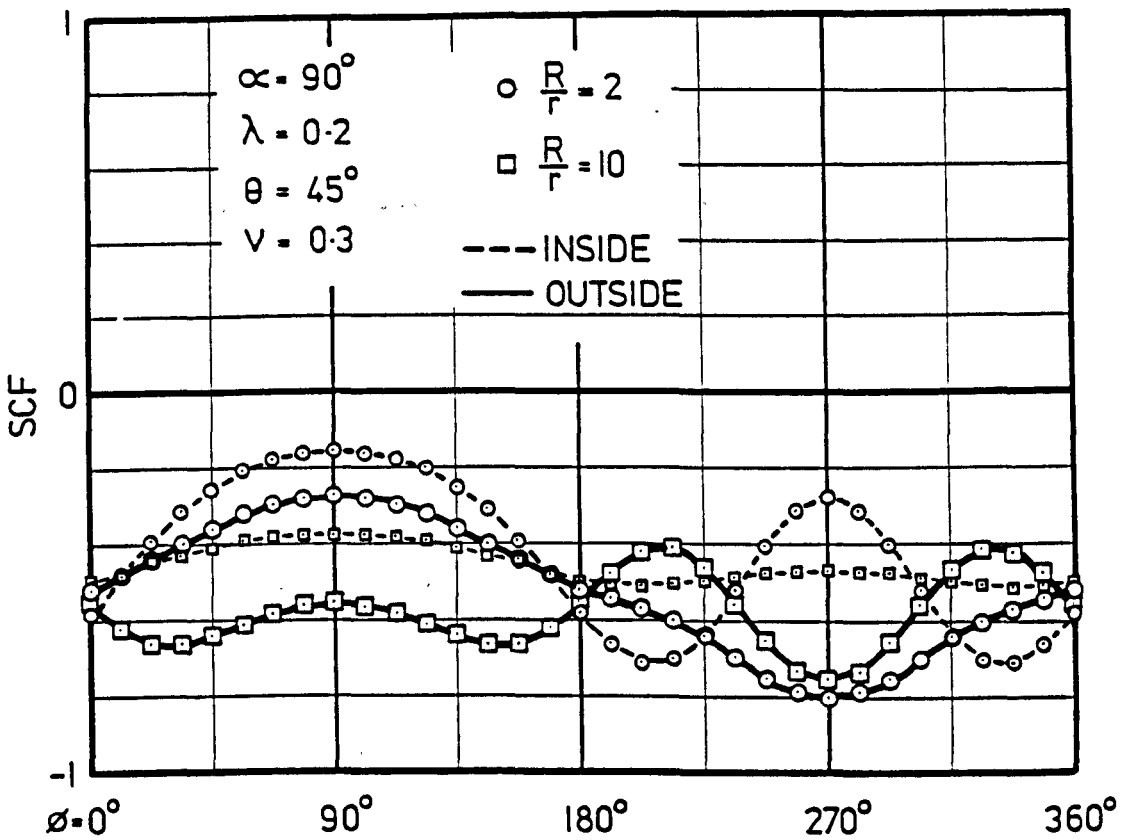

THEORETICAL
SHEAR STRESS
AT θ=45°

FIG. 3·31

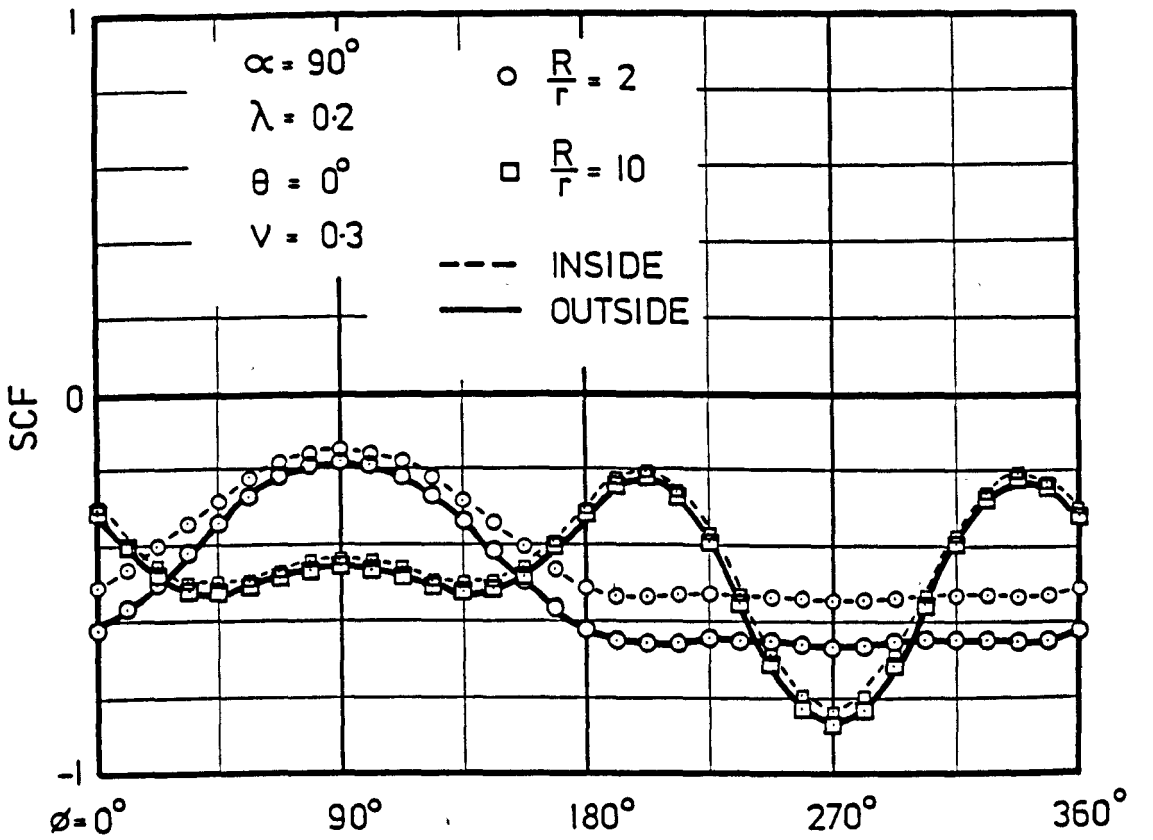

THEORETICAL
SHEAR STRESS
AT θ=0°

FIG. 3·32

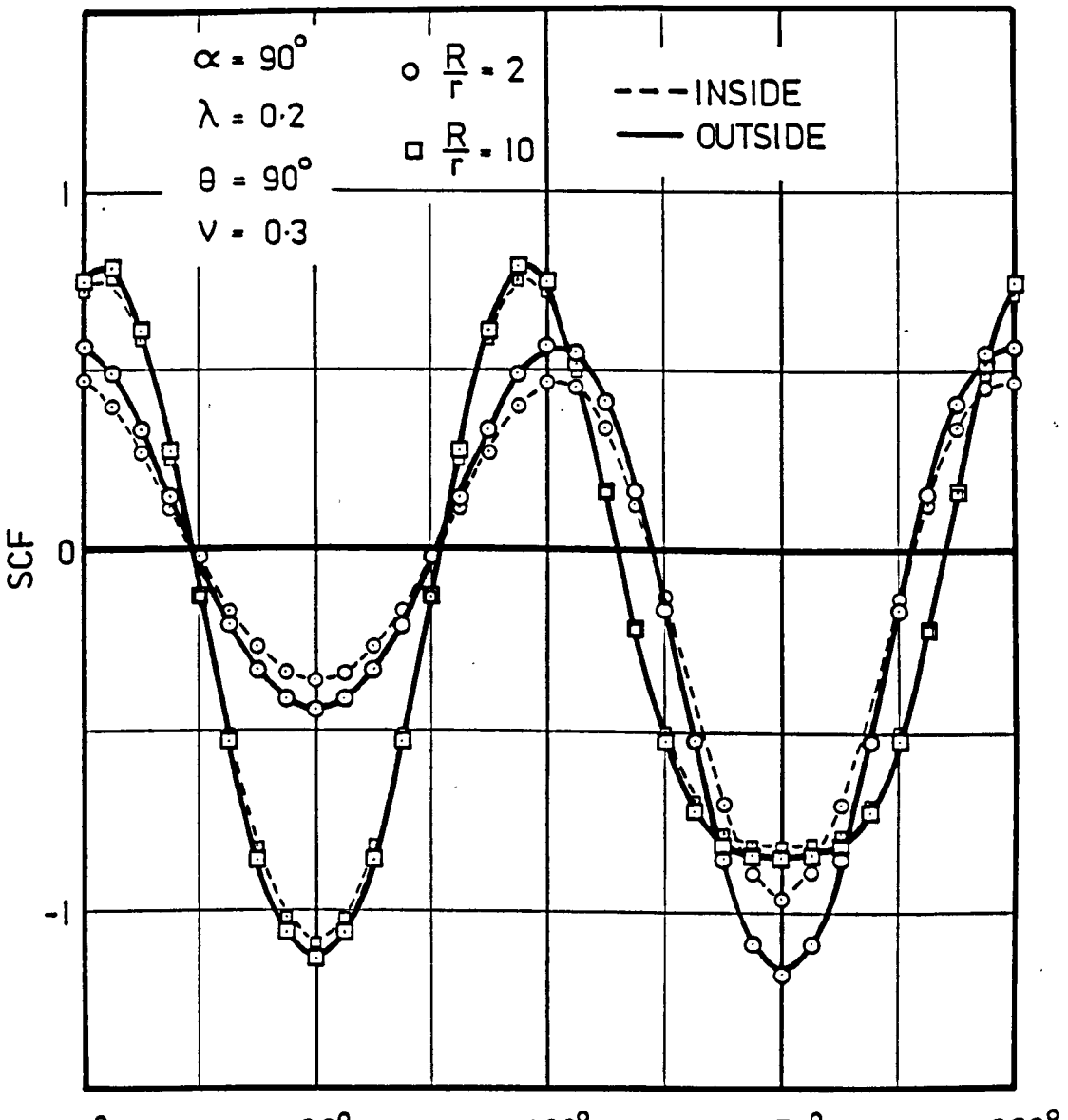

THEORETICAL
SHEAR STRESS
AT θ=90°

FIG. 3·33

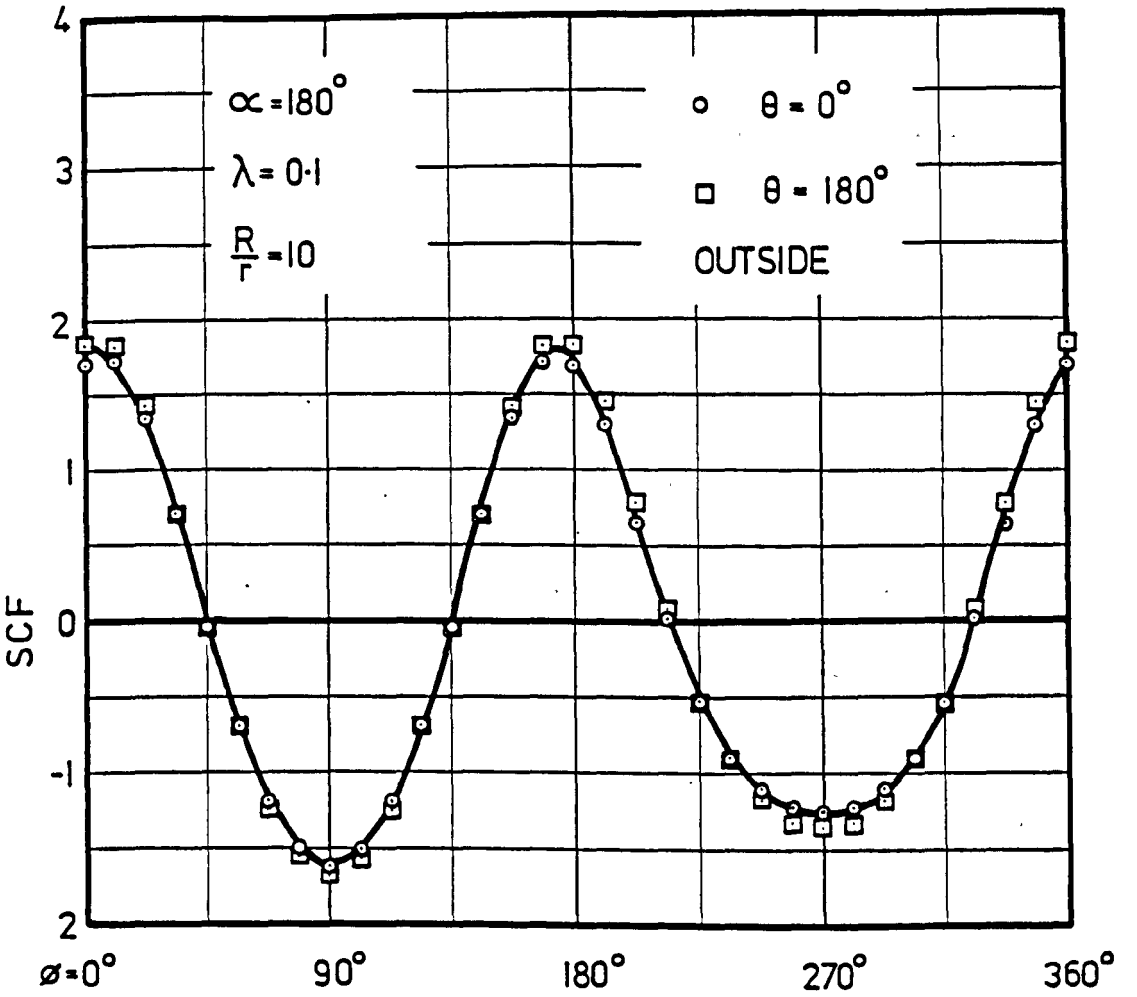

THEORETICAL SHEAR STRESS
AT θ=0° AND θ=180°

FIG.3·34

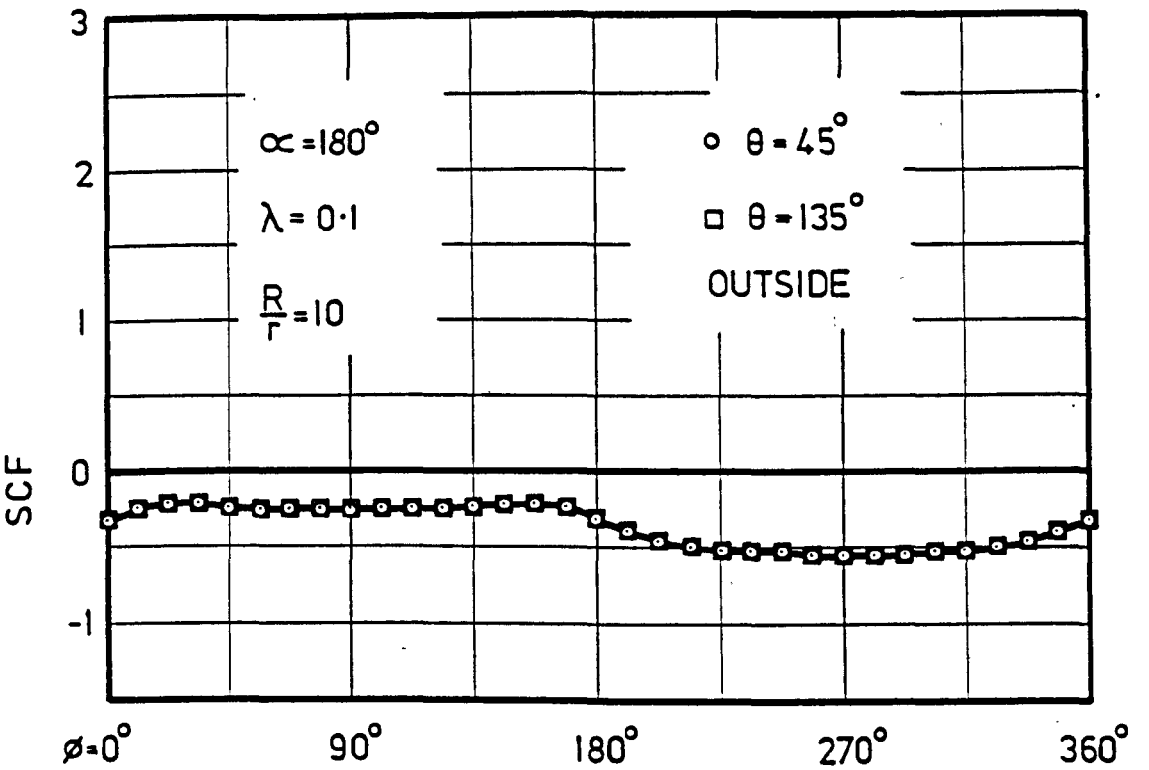

THEORETICAL SHEAR STRESS
AT $\theta = 45^\circ$ AND $\theta = 135^\circ$

FIG. 3·35

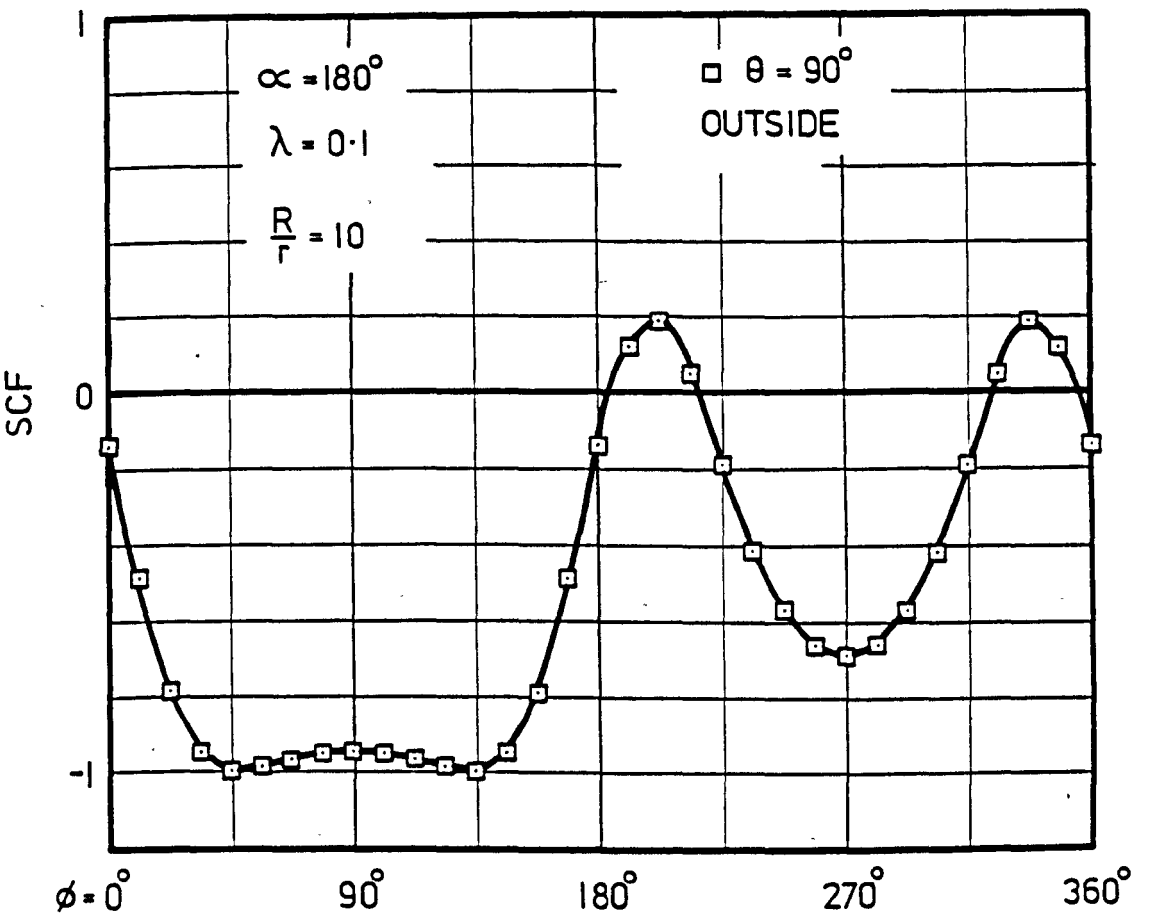

THEORETICAL SHEAR STRESS
AT θ=90°

FIG. 3·36

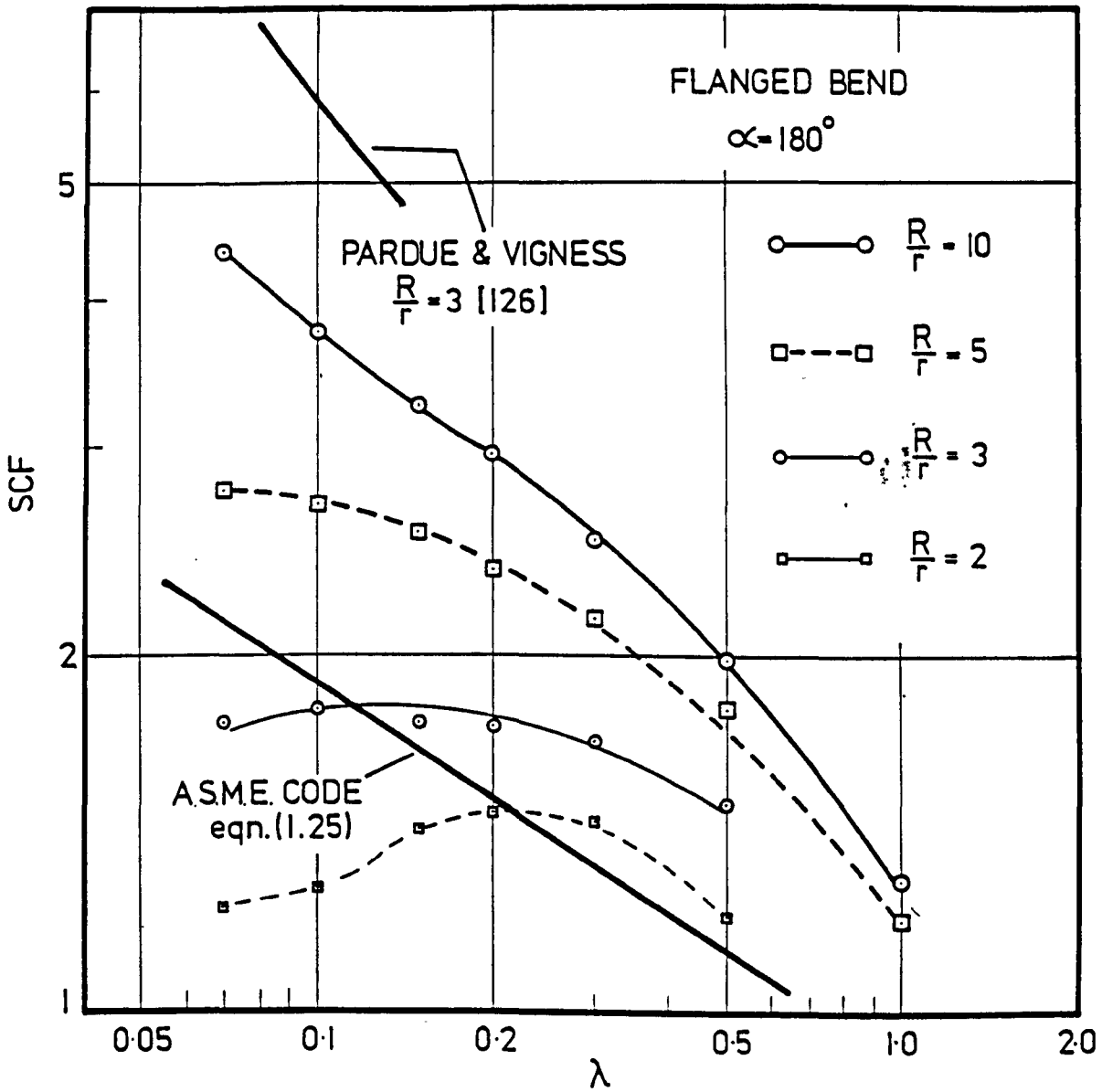

MAXIMUM MERIDIONAL STRESS

FIG. 3·37

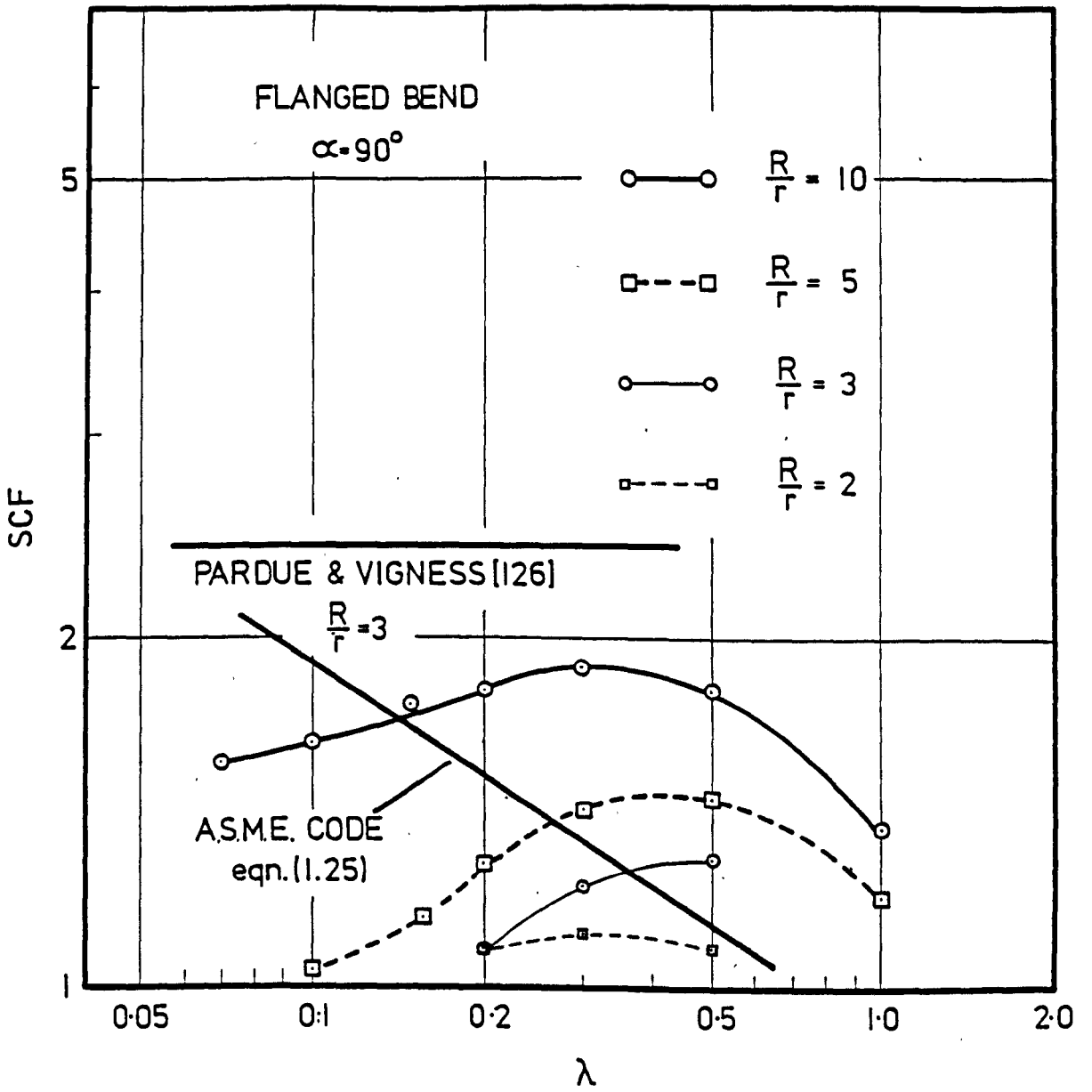

MAXIMUM MERIDIONAL STRESS

FIG. 3·38

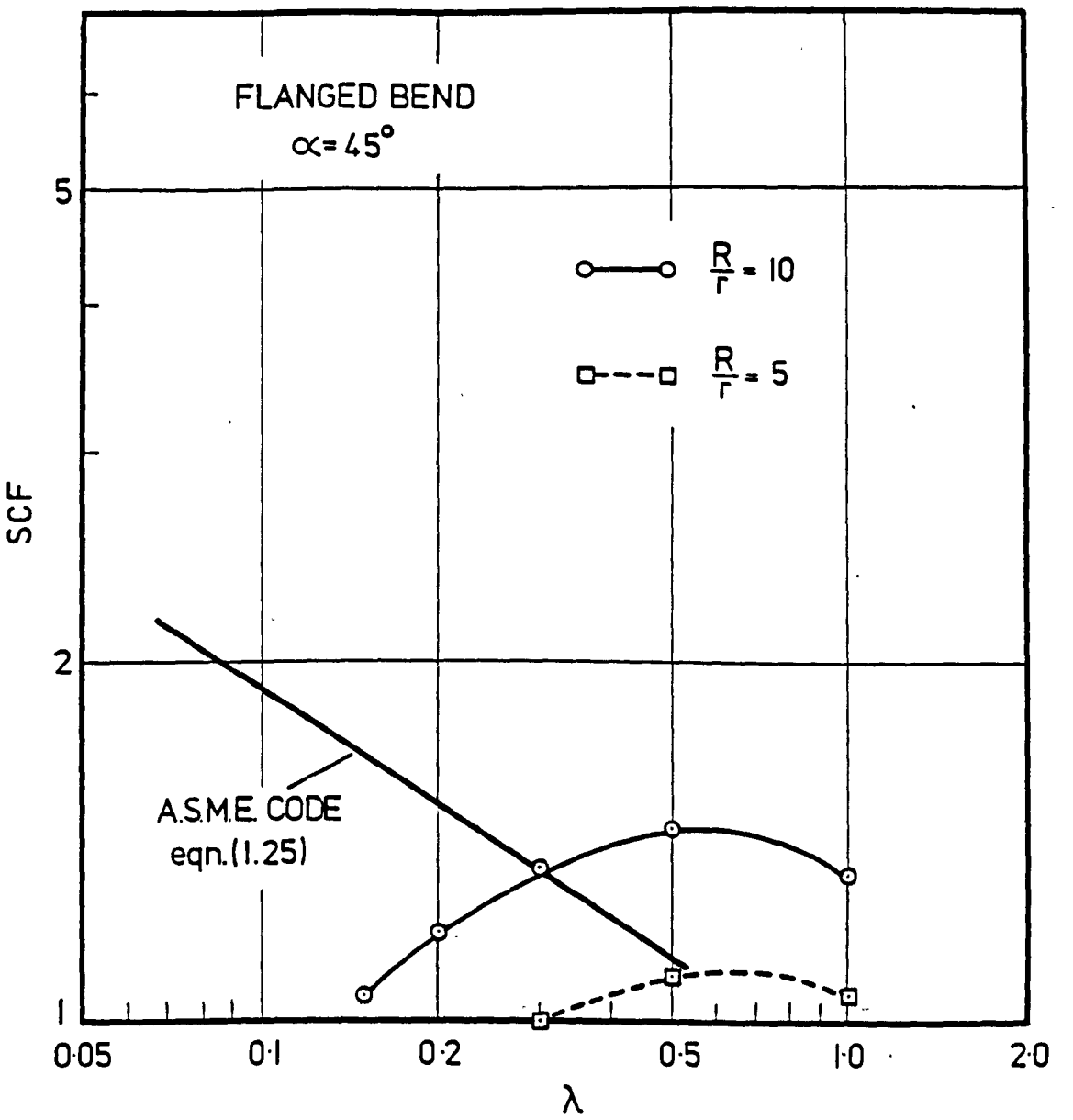

MAXIMUM MERIDIONAL STRESS

FIG. 3·39

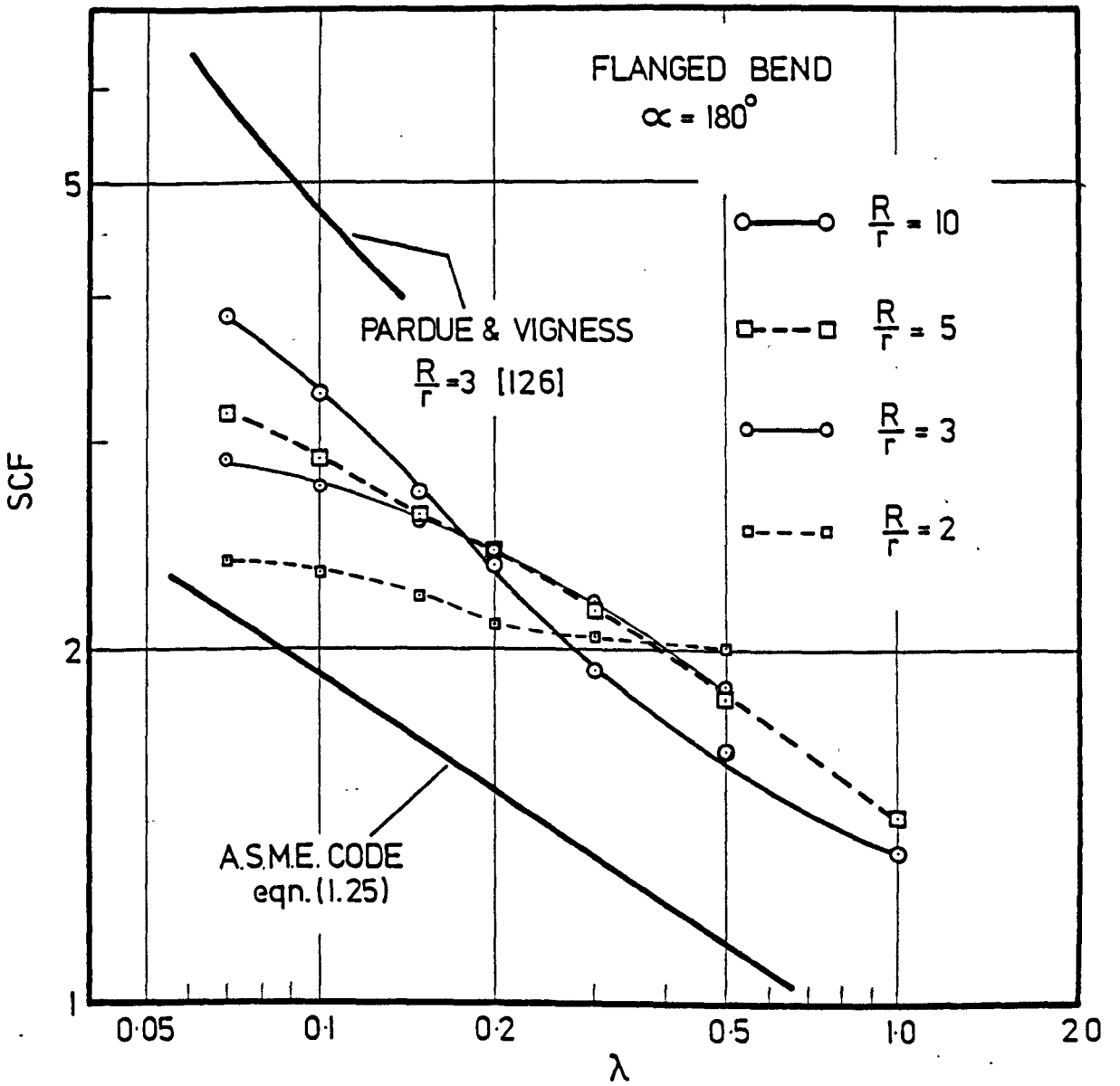

MAXIMUM CIRCUMFERENTIAL STRESS

FIG. 3·40

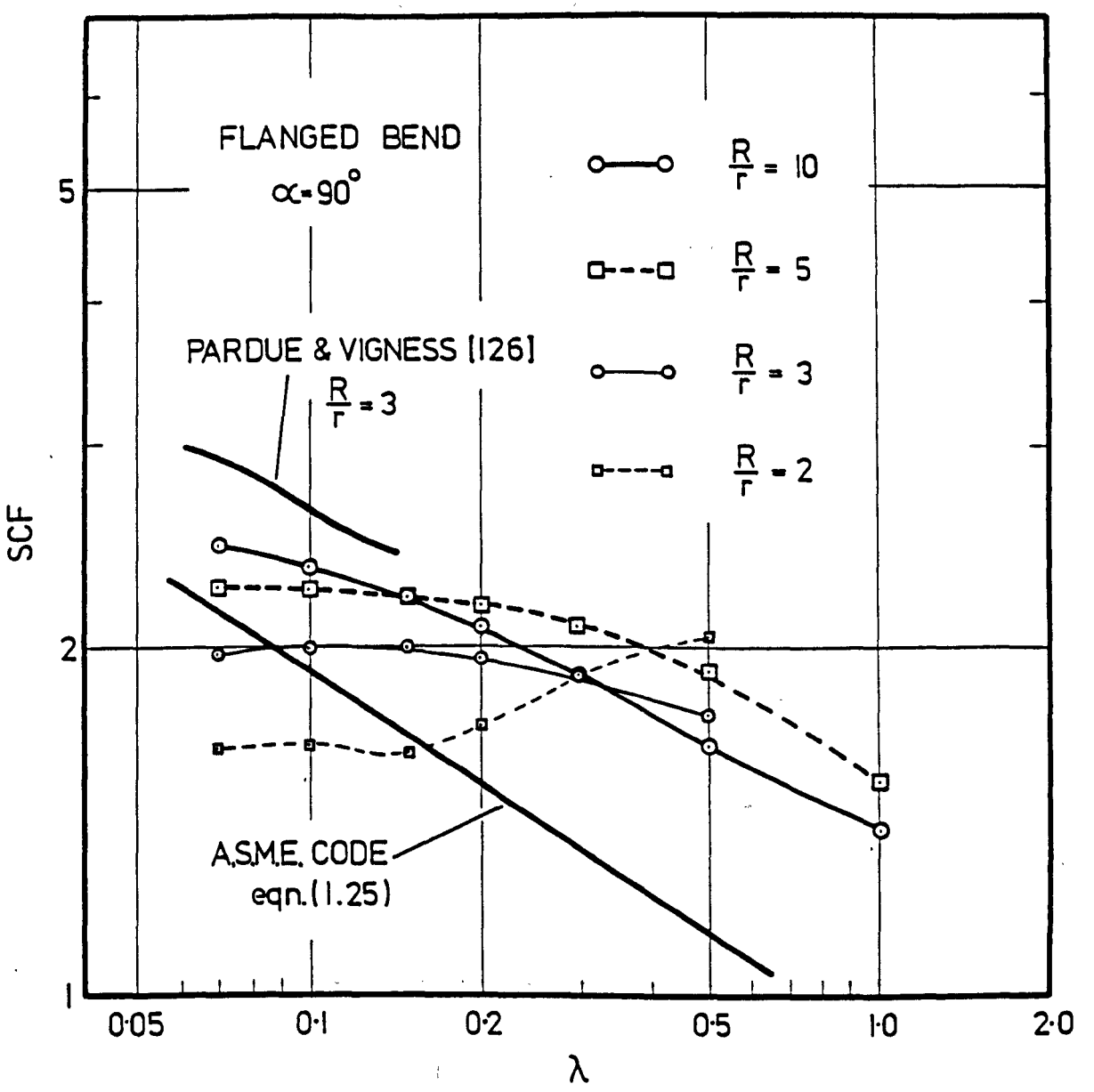

MAXIMUM CIRCUMFERENTIAL STRESS

FIG. 3·41

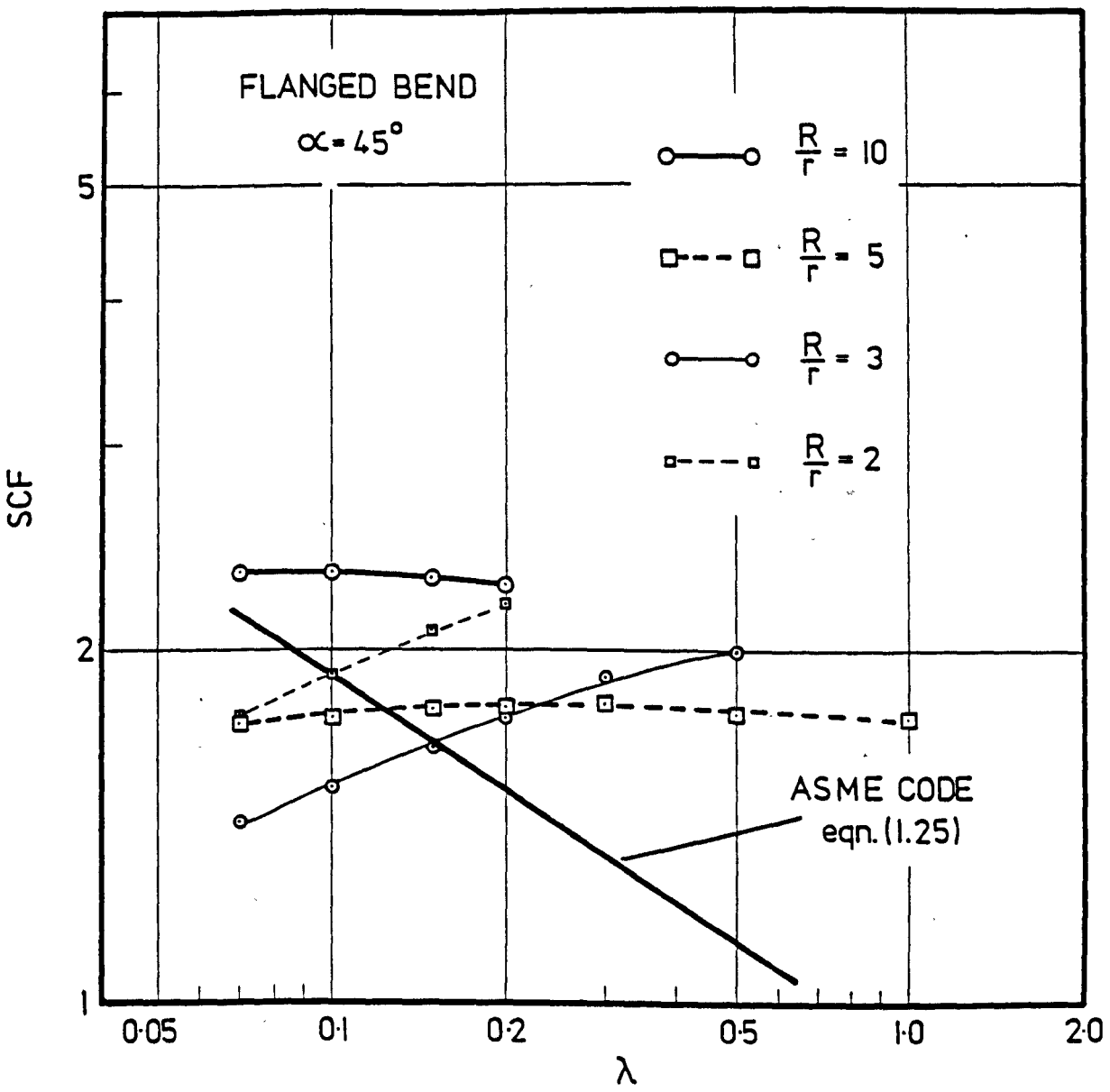

MAXIMUM CIRCUMFERENTIAL STRESS

FIG. 3·42

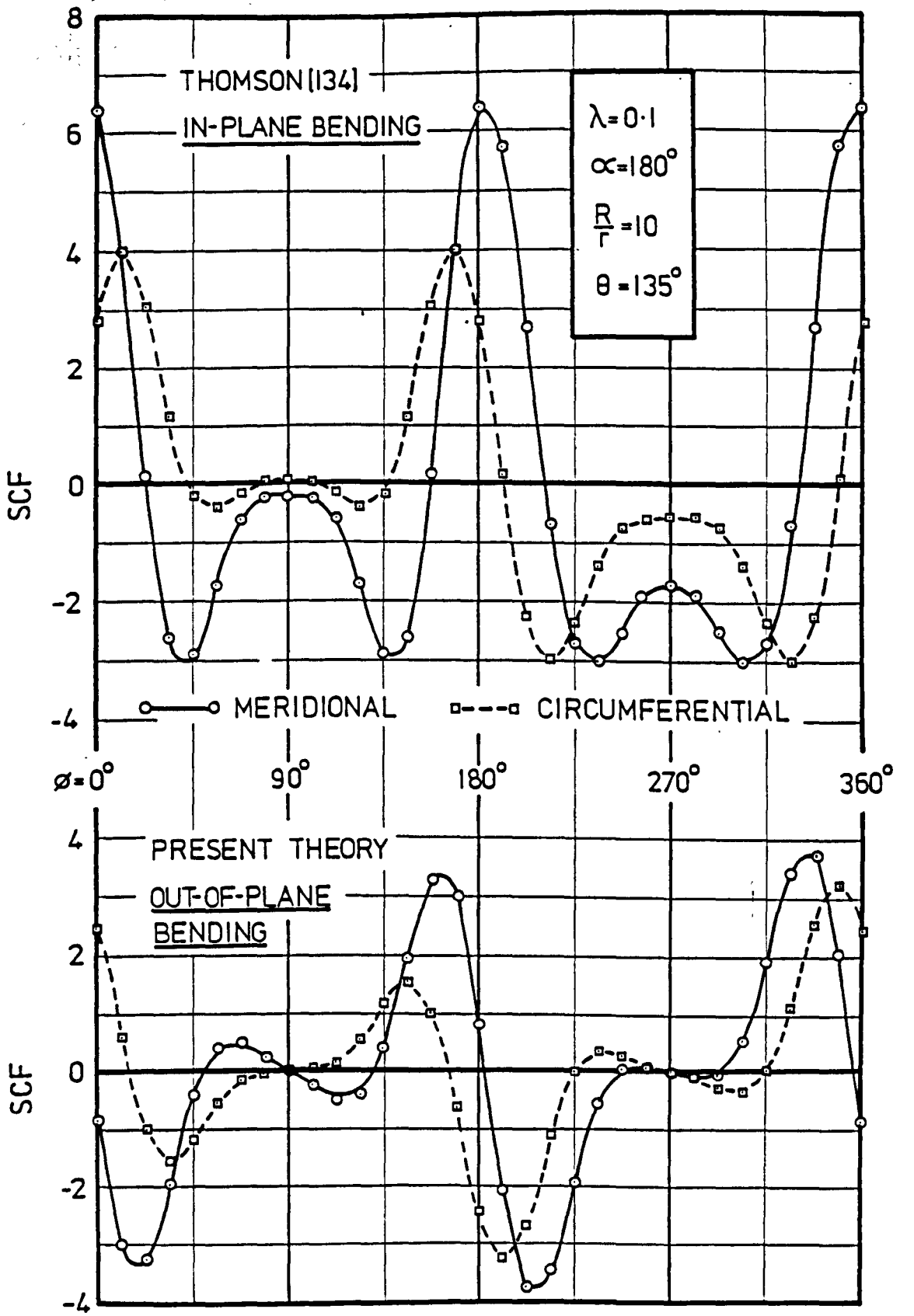

THEORETICAL STRESS COMPARISON
IN & OUT-OF-PLANE BENDING

FIG. 3·43

CHAPTER 4

Experiments on Flanged Bends and Comparison with Theory

ABSTRACT

Details are given of out-of-plane bending tests performed on a 90° and a 180° flanged bend.

The theory developed in CHAPTER (3) is compared against the experimental flexibility and stress factors obtained by present and past authors.

CHAPTER (4)

EXPERIMENTS ON FLANGED BENDS AND COMPARISON WITH THEORY

4.1 Present Experiments

4.1.1 Introduction

This chapter presents the results of experiments conducted on flanged bends subjected to out-of-plane bending. The main purpose of the work was to confirm the theoretical general solution presented in CHAPTER (3). However, as a result of the lack of detailed experimental results on flanged bends under out-of-plane bending, no serious attempt has been made to compare the present results with that of other work. Ideally, this necessitates a test program considering a comprehensive set of bend parameters and as this was not possible careful consideration had to be given to the choice in bend configuration.

In the manufacture of the bends, forged bends were chosen because of their small manufacturing tolerances for out-of-roundness and thickness variations. From practical considerations in testing the pipe diameters and bend radii had to be sufficiently large to allow attachment and accurate positioning of strain gauges in the meridional (ϕ) and circumferential (θ) directions. Further, to confirm convergence of the theoretical solution low pipe factors (λ) and different bend angles (α) were required.

From these considerations, two carbon steel bends were selected:

1. Bend No. 1 : $\alpha = 90°$, $\lambda = 0.17$, $\frac{R}{r} = 1.89$
2. Bend No. 2 : $\alpha = 180°$, $\lambda = 0.25$, $\frac{R}{r} = 2.84$

4.1.2 Specimen details

The two bend types chosen were supplied by MUNRO and MILLER [233] and manufactured in accordance with British Standard, BS 1640 [234] and American Standard, ANSI B16.9 [235]. All welds were x-rayed and both assemblies were stress relieved.

Details of each bend are shown in Figure (4.1) and Figure (4.2). The use of a "taper" or "weld-neck" flange and the "slip-on" flange commonly used on straight pipes was based upon advice suggested by the manufacturer. Industrial practice tends to favour the taper flange for direct connection to pipe bends. The theoretical solution, however, relates more to the slip-on flange termination. As such, both types of termination were incorporated in each bend.

The external pipe diameters between $\phi = 0°$ and $\phi = 180°$ and between $\phi = 90°$ and $\phi = 270°$, at the bend mid-section ($\theta = 90°$), were measured with a micrometer and found to be 6.625 in. and 6.617 in. respectively for bend No. 2. These are well within the permitted tolerance from the above codes of +0.094 in. and -0.0625 in. and give an ovality of better than 0.998.

Wall thicknesses were measured around a section at approximately $\theta = 130°$ (close to the slip-on flange) for bend No. 2 and are given in the following table:

ϕ	Thickness (in)	ϕ	Thickness (in)
0°	0.280	180°	0.285
45°	0.285	225°	0.280
90°	0.290	270°	0.280
135°	0.285	315°	0.280

These are well within the limits of ∓ 0.0625 in. on wall thickness allowed by the codes.

A similar dimensional survey was carried out on bend No. 1, which was also found to be within the above variations.

Accordingly, results presented herein will be based on the manufacturer's nominal dimensions which are as follows:

Bend No.	Outside pipe diameter	Bend radius	Wall thickness	$\frac{R}{r}$	α	λ
	(in)	(in)	(in)			
1	6.625	6	0.28	1.89	90°	0.17
2	6.625	9	0.28	2.84	180°	0.25

4.1.3 Details of test rigs

The test rigs were intended primarily for elevated temperature tests on tangent bend assemblies and are described more fully in CHAPTER (5). However, in the design of the test rigs consideration was also given to the testing of flanged bends so that both types could be easily accommodated.

The general layout for bend No. 1 is shown in Figure (4.3). The bend was bolted to a 1 in. thick plate mounted on two channel sections secured to the floor. A 6 ft and 4 ft long straight pipe with flanged ends were bolted to the free end of the bend. The use of two straight sections was to allow the standard out-of-plane loading points to be adopted. Loading of the bend was achieved using turn-buckles and previously calibrated load cells attached to the straight pipe at

two points as shown in Figures (4.3) and (4.4). This configuration allowed the application of two equal and opposite forces resulting in a pure out-of-plane bending moment.

For bend No. 2 the general layout is shown in Figure (4.5). Here the bend was bolted to a substantial base incorporated in the test rig (Figure (4.6)). The loading system was essentially the same as that used in bend No. 1 giving a pure out-of-plane bending moment.

4.1.4 Strain gauging and instrumentation

The measurement of surface strains, for both bends, was accomplished using electrical resistance strain gauges temperature compensated for mild steel. Details of the gauges were as follows:

Type:	SHOWA NII-FA5-120-16
Gauge length:	5 mm
Nominal resistance:	120 Ω
Gauge factor:	2.10

In order to obtain a reasonable experimental stress distribution from bend No. 1, a total of 86 strain gauges were employed. These were located in pairs on the outside surface of the bend, orientated along the principal bend axes, at the positions shown in Figure (4.7).

For bend No. 2, a total of 54 strain gauges were employed at the positions shown in Figure (4.8).

The strain gauges were read at each load step using an ELCOMATIC data logger linked to an APPLE computer. The gauge readings obtained from the data logger in $\Omega/\Omega \times 10^{-5}$ were stored in the computer for subsequent use. Correct strain values were obtained by dividing the gauge reading by the gauge factor x 10 (to give $\mu\varepsilon$).

4.1.5 Evaluation of stresses

The actual value of strain was computed from the slope of a best fit straight line. This was accomplished using the APPLE computer on the stored data. The method was not relied on completely and each set of gauge readings were checked visually using a graphics routine, removing spurious readings where required. The first point at zero load was frequently found to effect the slope of the best fit line and as there was no requirement for this line to pass through the origin this point was neglected.

A typical example of the response of a pair of gauges from bend No. 1 is shown in Figure (4.9).

The software employed on the APPLE computer used a regression analysis [216] whereby the linear equation between strain ε and moment M at "n" points is written as:

$$\varepsilon = a + bM \qquad \ldots (4.1)$$

where $$b = \frac{\sum_{i=1}^{n} [M_i - \bar{M}]\,[\varepsilon_i - \bar{\varepsilon}]}{\sum_{i=1}^{n} [M_i - \bar{M}]^2}$$

$$a = \frac{[\sum_{i=1}^{n} \varepsilon_i - b \sum_{i=1}^{n} M_i]}{n}$$

$$\bar{M} = \sum_{i=1}^{n} \frac{M_i}{n} \quad , \quad \bar{\varepsilon} = \sum_{i=1}^{n} \frac{\varepsilon_i}{n} \qquad \ldots (4.2)$$

The strain at any load level is found from the product of M and b.

The corresponding stresses for each gauge was obtained from the normal stress-strain relationships for a thin shell, e.g.:

$$\sigma_1 = \frac{E}{(1-\nu^2)} [\varepsilon_1 + \nu\varepsilon_2] \quad \ldots (4.3)$$

where Young's Modulus, E, was taken a $30.0 * 10^6$ lbf/in^2 and poisson's ratio, ν, as 0.3 [236]. The stress concentration factors (S.C.F.) were then found from:

$$S.C.F. = \frac{\sigma}{[\frac{Mr}{I}]} \quad \ldots (4.4)$$

The out-of-plane bending moment, M, was taken as that at the loaded flange. For both bends this was defined as:

$$M = P \times L$$

where P = applied load (lbf)

L = distance between applied loads = 43 in. $\ldots (4.5)$

4.1.6 *Flexibility measurement*

The flexibility of the bends was determined by measuring the rotation between the flanged ends using dial gauges.

On bend No. 1 this method employed two dial gauges bearing on an extended arm attached to the loaded flange as shown in Figure (4.10). For the loaded end, which is subject to a pure out-of-plane bending moment, the end rotation can (γ_L) be evaluated from:

$$\gamma_L = \tan^{-1} [\frac{\Delta d_1 - \Delta d_2}{L_L}] \quad \text{radians}$$

where Δd_1 = displacement recorded by dial gauge No. 1

Δd_2 = displacement recorded by dial gauge No. 2

L_L = fixed distance between dial gauges. $\ldots (4.6)$

The fixed end on bend No. 1 is subject to pure torsion. Here the rotation was measured using one dial gauge as shown in Figure (4.10). This rotation (γ_F) was determined from:

$$\gamma_F = \frac{\Delta d_3}{L_F} \quad \text{radians}$$

where Δd_3 = displacement recorded by dial gauge No. 3

L_F = distance from centre of bend section to point of measurement . . . *(4.7)*

The overall rotation (γ) of the bend was then found from:

$$\gamma = \gamma_L - \gamma_F \quad \ldots \textit{(4.8)}$$

The flexibility factor, K, was calculated from:

$$K = \frac{\gamma}{[\frac{MR\alpha}{EI}]} \quad \ldots \textit{(4.9)}$$

where M is that given by equation (4.5).

The rotation between the ends of bend No. 2 was measured using a similar technique. Here, however, both ends of the bend are subjected to a pure out-of-plane bending moment so that the method given by equation (4.6) is applied at both ends of the bend.

In the measurement of rotation on bend No. 1 the small rotation of the loaded end was comparable to that of the fixed end. As such some doubt exists about the accuracy of the flexibility factor although it is given later.

4.1.7 Results

The stress and strain factors evaluated for bends No. 1 and No. 2 are given in Tables (4.1) and (4.2) respectively.

The experimental value of flexibility factor for both bends was determined as:

Bend No. 1 , $K = 0.33$

Bend No. 2 , $K = 2.34$

These values are based on best fit straight lines for bends No. 1 and No. 2 as shown in Figure (4.11) and Figure (4.12) respectively. Detailed comparison of the results with the theory will be made in the following sections.

TABLE (4.1): Experimental results for bend No. 1.
(*** = faulty gauge)

Strain gauge number	Meridional S.C.F. $\bar{\varepsilon}_\phi$	$\bar{\sigma}_\phi$	Strain gauge number	Circumferential S.C.F. $\bar{\varepsilon}_\theta$	$\bar{\sigma}_\theta$
1	+0.01	-0.01	0	-0.01	+0.01
3	+0.60	+0.06	2	-0.13	+0.62
5	0.00	+0.09	4	+0.08	+0.03
7	-0.12	-0.09	6	-0.05	-0.14
9	+1.44	+0.19	8	-0.26	+1.15
11	-0.05	+0.01	10	+0.02	-0.05
13	+0.88	+0.37	12	-0.60	+0.77
15	-0.65	-0.21	14	0:00	+0.71
17	+1.39	-0.22	16	-0.62	+1.33
19	-0.13	-0.37	18	-0.29	-0.24
21	+0.49	+0.32	20	+0.14	+0.59
23	+1.22	+1.27	22	+0.79	+1.60
25	***	***	24	***	***
27	+1.25	-0.19	26	-0.55	+1.19
29	+0.27	-0.81	28	-0.81	+0.03
31	-0.36	-0.32	30	-0.19	-0.45
33	-0.03	-0.18	32	-0.15	-0.09
35	-0.08	+0.02	34	+0.04	-0.07
37	+1.09	-0.07	36	-0.39	+1.08
39	+1.03	0.00	38	-0.31	+1.03
41	+0.63	+0.09	40	-0.11	+0.66
43	+0.09	-0.15	42	-0.16	+0.04
45	-0.84	-0.59	44	-0.28	-1.02
47	+0.38	+0.20	46	+0.06	+0.44
49	***	***	48	+0.23	***
51	+0.09	+0.19	50	+0.14	+0.15
53	-0.60	-0.45	52	-0.23	-0.74
55	+0.05	-0.02	54	-0.03	+0.05
57	-0.52	+0.04	56	+0.19	-0.51
59	+0.05	-0.02	58	-0.03	+0.05
61	-0.57	+0.27	60	+0.41	-0.49
63	0.00	-0.07	62	-0.06	-0.02
65	-0.73	+0.45	64	+0.63	-0.60
67	+0.39	+0.27	66	+0.78	-0.59
69	-0.76	+0.61	68	+0.78	-0.59
71	-1.38	-1.55	70	-0.99	-1.85
73	+0.04	-0.06	72	-0.06	+0.02
75	***	***	74	+0.85	***
77	+0.05	-0.03	76	-0.04	+0.04
79	-1.19	+0.61	78	+0.91	-1.02
81	+0.05	-0.04	80	-0.05	+0.04
83	-1.49	+0.39	82	+0.80	-1.38
85	-1.38	+0.01	84	+0.42	-1.37

TABLE (4.2): Experimental results for bend No. 2.

Strain gauge number	Meridional S.C.F. $\bar{\varepsilon}_\phi$	$\bar{\sigma}_\phi$	Strain gauge number	Circumferential S.C.F. $\bar{\varepsilon}_\theta$	$\bar{\sigma}_\theta$
0	+0.14	+0.17	1	+0.05	+0.10
2	+0.22	+0.23	3	-0.05	+0.02
4	+0.29	+0.28	5	-0.11	-0.02
6	0.00	-0.10	7	-0.31	-0.34
8	-0.27	-0.36	9	-0.19	-0.31
10	-0.27	-0.25	11	+0.15	+0.08
12	+0.15	+0.25	13	+0.26	+0.34
14	+0.28	+0.36	15	+0.14	+0.25
16	+0.23	+0.28	17	+0.09	+0.18
18	0.00	-0.02	19	-0.04	-0.04
20	+0.50	+1.21	21	+2.44	+2.63
22	+0.07	+0.07	23	-0.03	-0.01
24	+0.11	+0.10	25	-0.06	-0.04
26	-1.23	-0.85	27	+1.53	+1.28
28	+0.08	+0.03	29	-0.18	-0.18
30	-0.39	-0.43	31	0.00	-0.13
32	+0.05	+0.12	33	+0.20	+0.24
34	+0.13	+0.14	35	0.00	+0.04
36	+0.57	+0.73	37	+0.31	+0.53
38	+0.88	+0.51	39	-1.41	-1.26
40	-1.57	-2.04	41	-0.92	-1.53
42	+0.18	+0.22	43	+0.08	+0.15
44	+1.64	+2.22	45	+1.24	+1.91
46	-1.33	-1.06	47	+1.20	+0.89
48	-0.32	-0.56	49	-0.63	-0.80
50	+0.06	+0.05	51	-0.05	-0.04
52	+0.16	-0.27	53	-1.36	-1.44

4.2 Comparison of Flexibility Factors from Theory and Experiment

A comparison of the experimental flexibility factors for bend No. 1 and No. 2 with that of the present solution is given in Table (4.3). The experimental flexibility factor for bend No. 1 ($\alpha = 90°$) is much lower than the present theory. As explained earlier some doubt exists about its accuracy. For bend No. 2 ($\alpha = 180°$) the experimental value is around 30% higher than that predicted by the present theory.

TABLE (4.3): Comparison of experimental and theoretical flexibility factors.

Bend No.	α	λ	$(\frac{R}{r})$	K Experiment	K Present theory
1	90°	0.17	1.89	0.33	1.38
2	180°	0.25	2.84	2.34	1.77

Differences between the "real" flange and that employed in the mathematical model of the bend can give rise to the experimental value being higher. It is difficult, however, to estimate the degree of restraint provided by the flanges in the present experiments although the use of a taper flange is expected to result in some reduction in restraint with a consequent increase in flexibility. With this in mind, and also the fact that the present solution represents a lower bound, it is considered that the comparison with theory and experiment for bend No. 2 is favourable.

Although no valid experimental result is presented for bend No. 1 ($\alpha = 90°$) a comparison (Figure (4.13)) with Whatham's theory, the present solution and the experimental results of Pardue and Vigness

[126] for $\alpha = 90°$ and $(\frac{R}{r}) = 3$ show a similar trend to that found here for bend No. 2. In [126] only the flexibility results for a flanged 90° bend were presented. The results of Pardue and Vigness are between 20-30% higher than Whatham's theory, which in turn is around 20% higher than the present solution. The higher experimental results can be explained partly by the fact that the results of Pardue and Vigness were based on average values. In [134], however, Thomson expresses some doubt regarding the effectivness of their flanges which for certain geometries must have been little thicker than the bend wall.

4.3 Stress Distributions

4.3.1 Bend No. 1 ($\alpha = 90°$)

The experimental meridional ($\bar{\sigma}_\phi$) and circumferential ($\bar{\sigma}_\theta$) S.C.F. around the bend mid-section ($\theta = 45°$) are shown in Figures (4.14) and (4.15) respectively. Both show good agreement with the present theory. A comparison of these results and that from a typical no-end effect theory [48] is shown in Figure (4.16). This clearly illustrates the over-estimation in stress levels predicted by the no-end effect theory which for $\hat{\bar{\sigma}}_\phi$ is greater than a factor of 3.

The distribution around the fixed ($\theta = 0°$) and the loaded end ($\theta = 90°$) is shown in Figures (4.17) and (4.18) respectively. In both cases the results show remarkable agreement with the present theory being apparently unaffected by the different type of flange restraints at each end of the bend.

4.3.2 Bend No. 2 ($\alpha = 180°$)

The experimental meridional ($\bar{\sigma}_\phi$) and circumferential ($\bar{\sigma}_\theta$) S.C.F. around the bend section at $\theta = 45°$ are shown in Figures (4.19) and (4.20) respectively. As in the case of bend No. 1, both show good agreement with the present theory. Due to the larger λ value these results show a better comparison (Figure (4.21)) with that of a typical no-end effect theory [48] which is dependent totally on λ.

The distribution of $\bar{\sigma}_\phi$ and $\bar{\sigma}_\theta$ around the fixed end and the loaded end is shown in Figures (4.22) and (4.23) respectively. These results also show good agreement with the present theory.

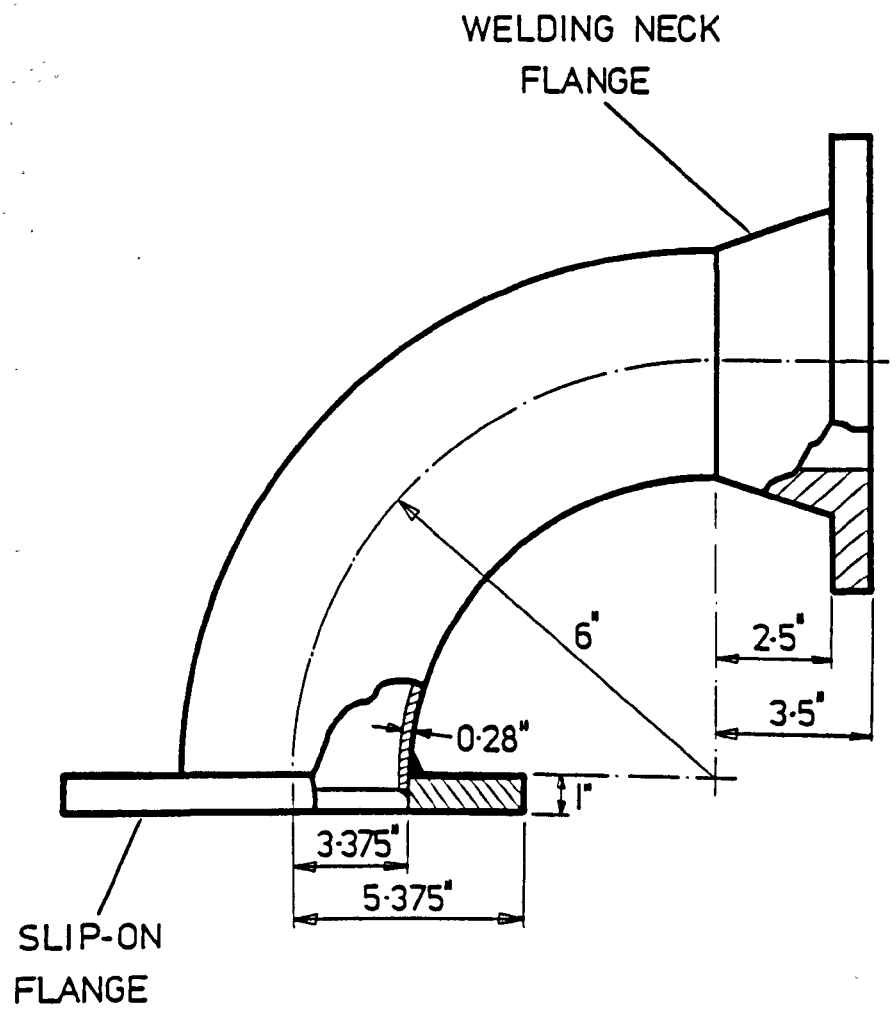

BEND No. 1

FIG. 4.1

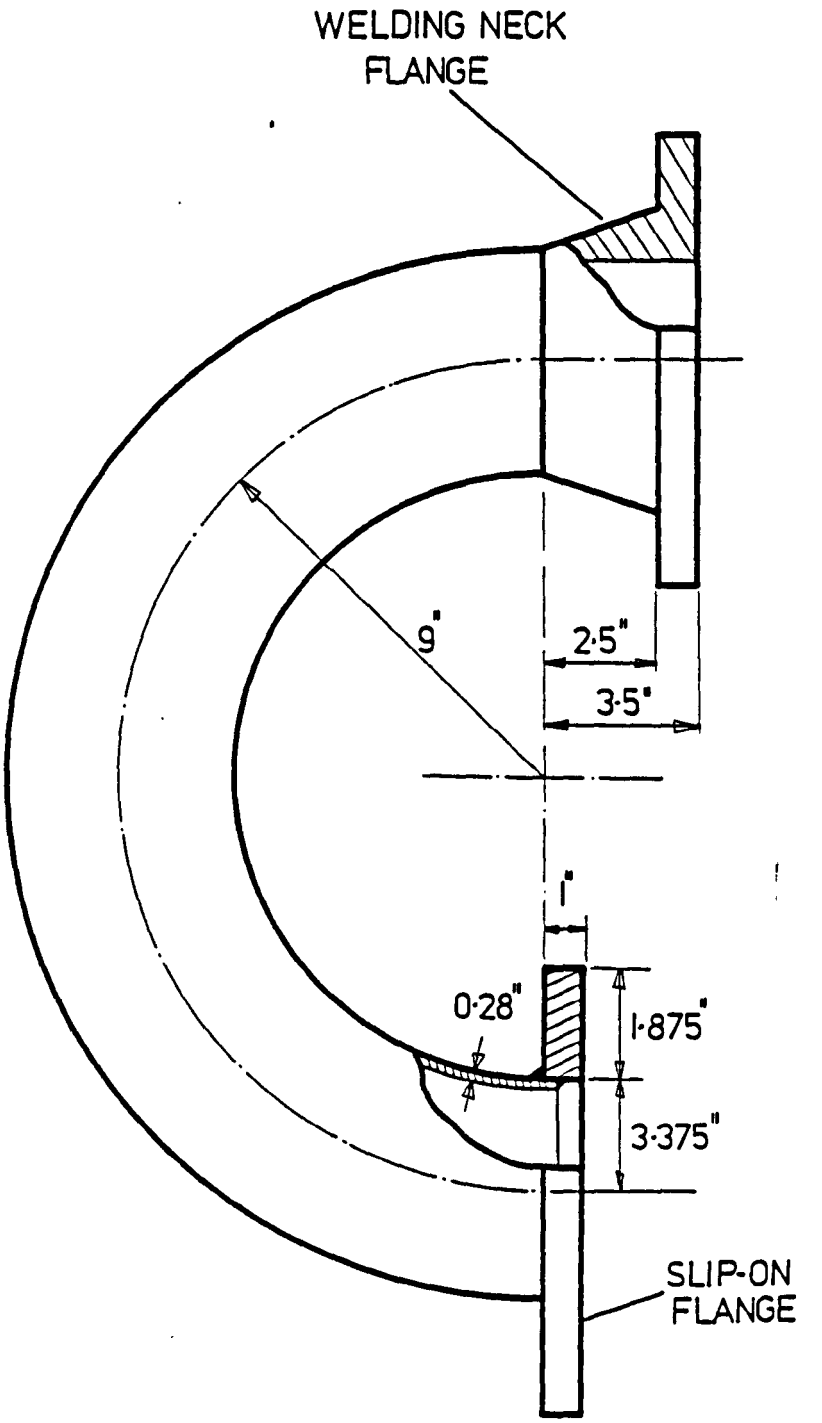

BEND No. 2

FIG. 4.2

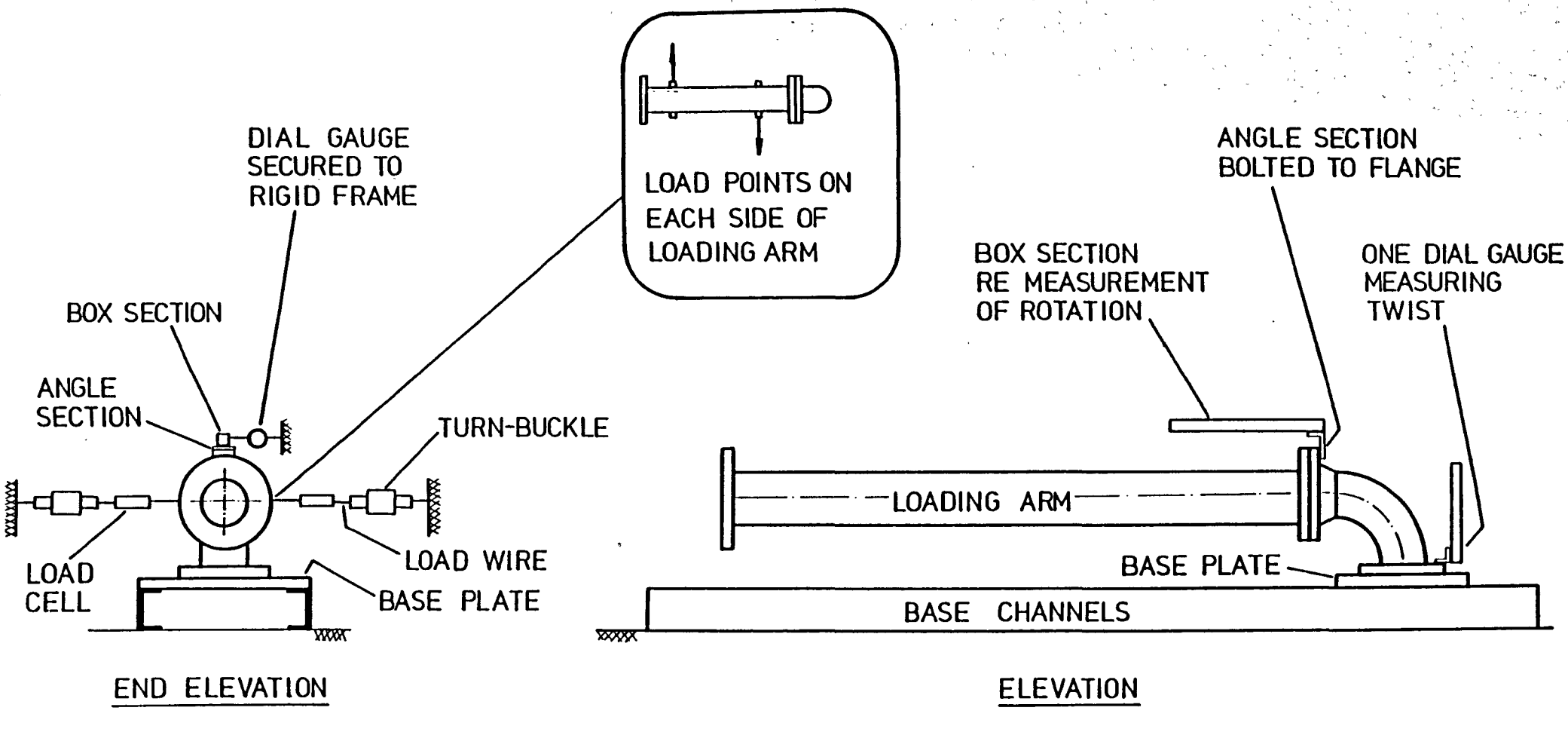

BEND No.1
GENERAL LAYOUT
FIG. 4.3

BEND No.1
OUT-OF-PLANE LOADING

FIG.4.4

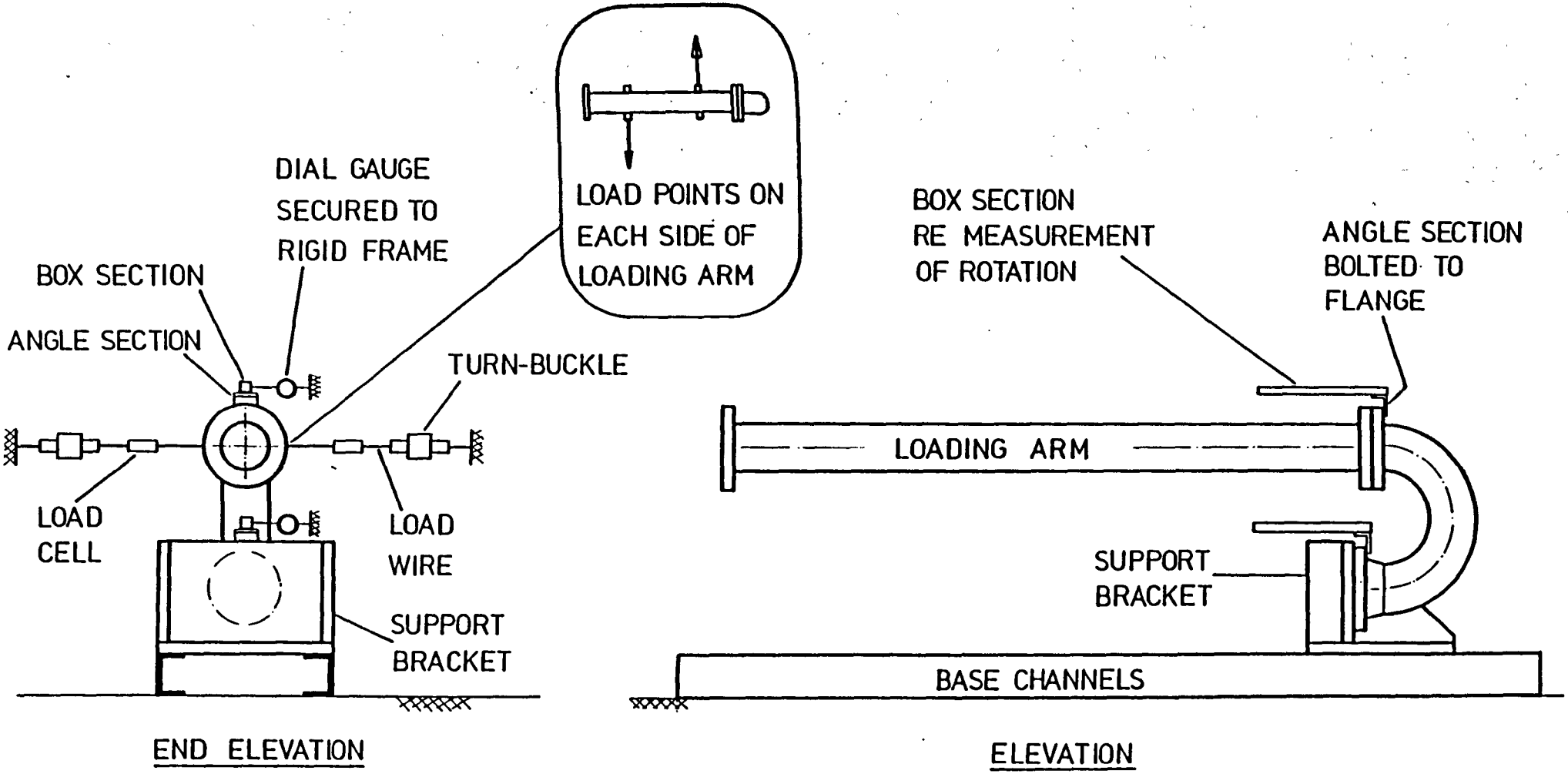

BEND No.2

GENERAL LAYOUT

FIG. 4.5

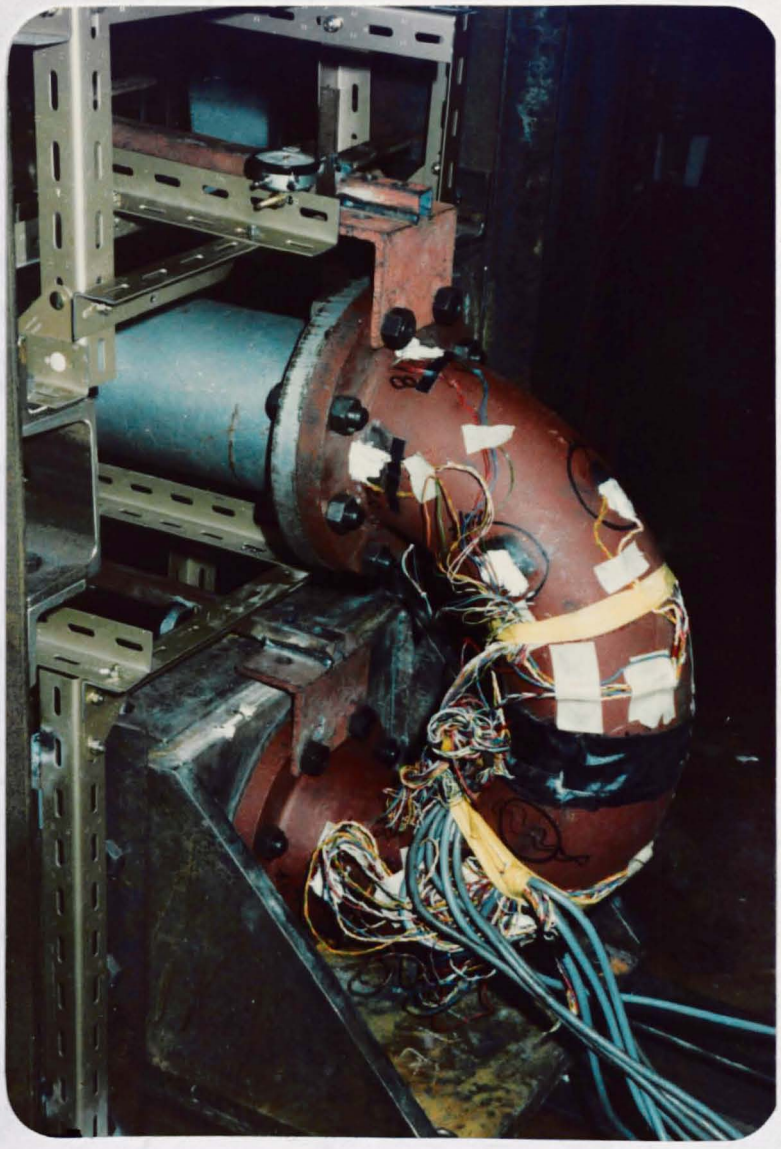

BEND No.2
BASE SUPPORT

FIG. 4.6

o GAUGE PAIR

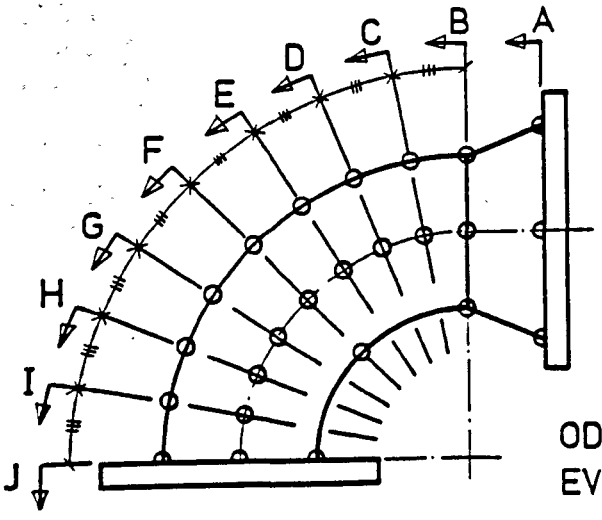

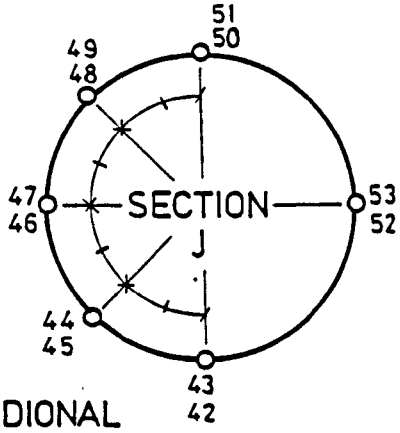

ODD Nos. MERIDIONAL
EVEN Nos. CIRCUMFERENTIAL

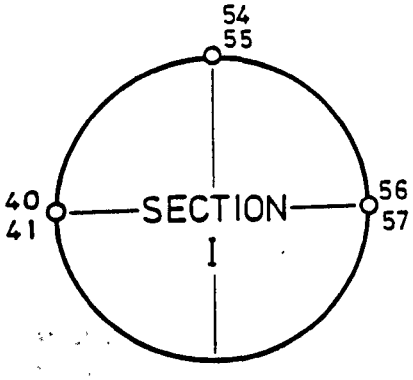

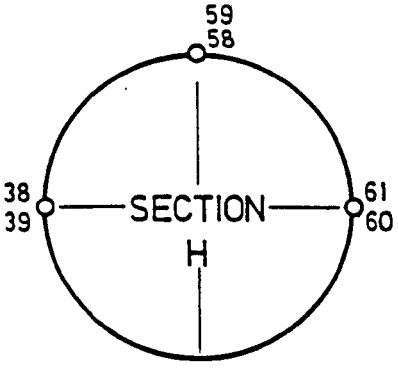

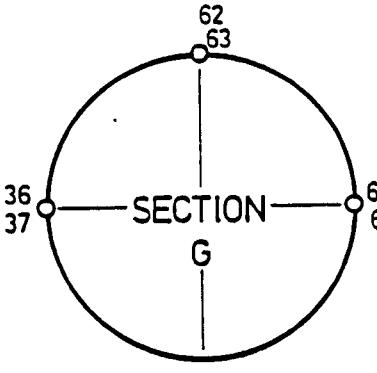

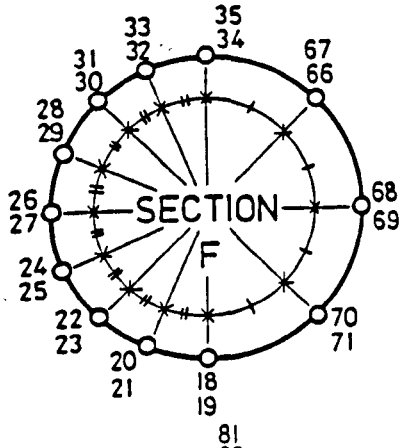

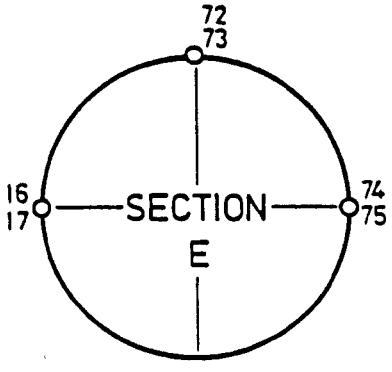

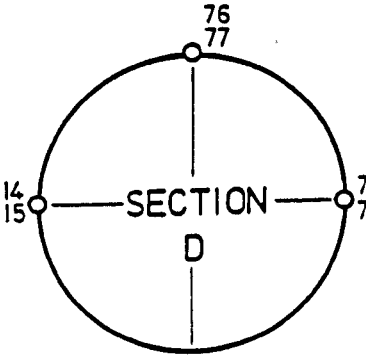

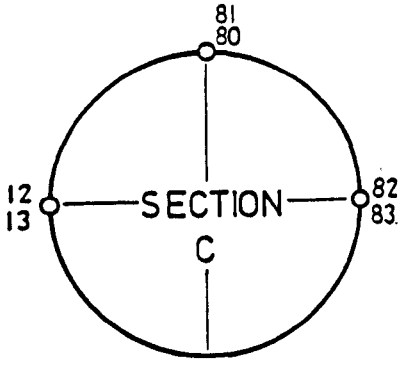

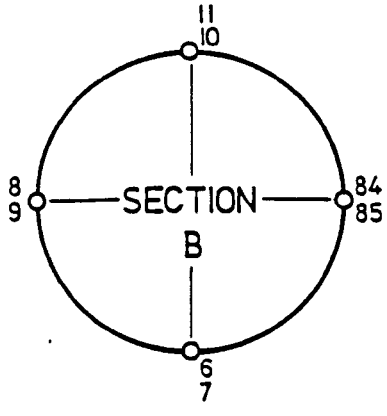

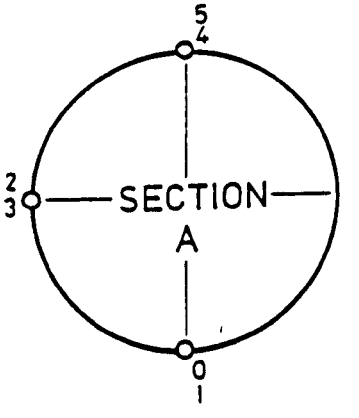

BEND No.1 STRAIN GAUGE LAYOUT

FIG. 4.7

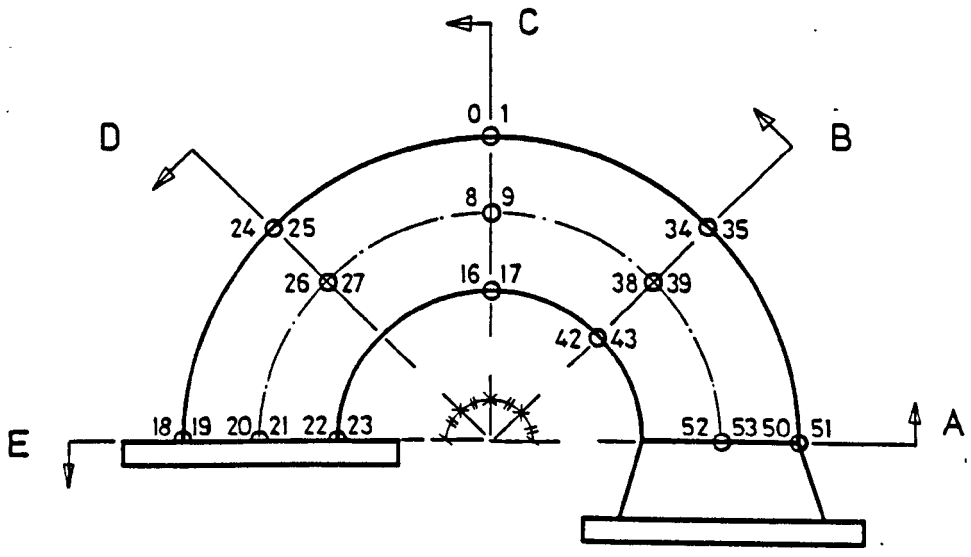

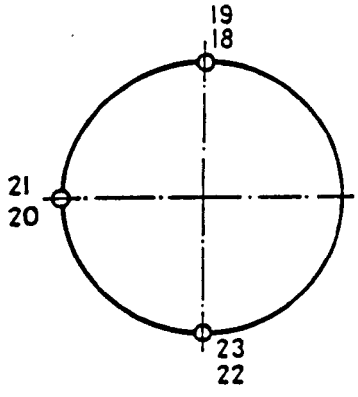

SECTION E

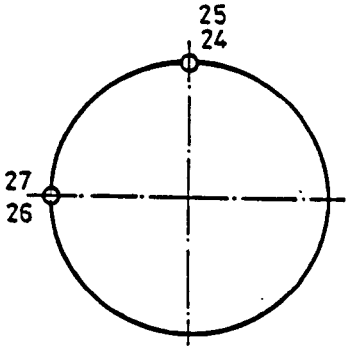

SECTION D

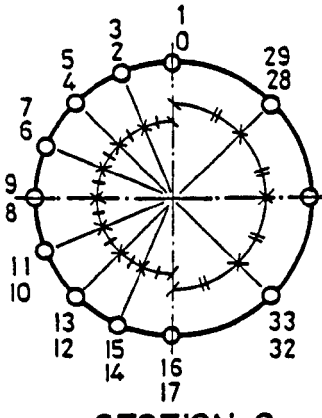

SECTION C

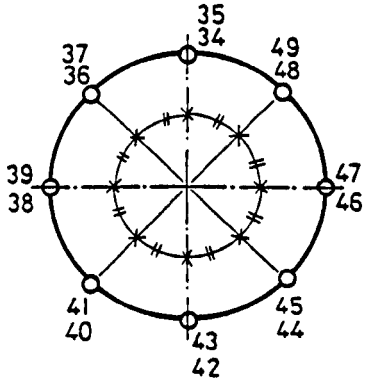

SECTION B

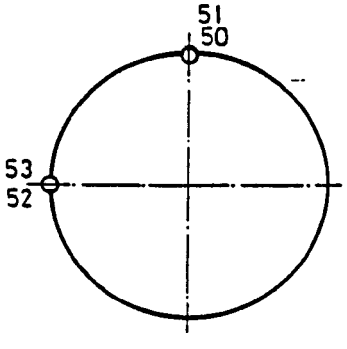

SECTION A

o GAUGE PAIR

EVEN Nos. MERIDIONAL
ODD Nos. CIRCUMFERENTIAL

BEND No.2 STRAIN GAUGE LAYOUT

FIG. 4.8

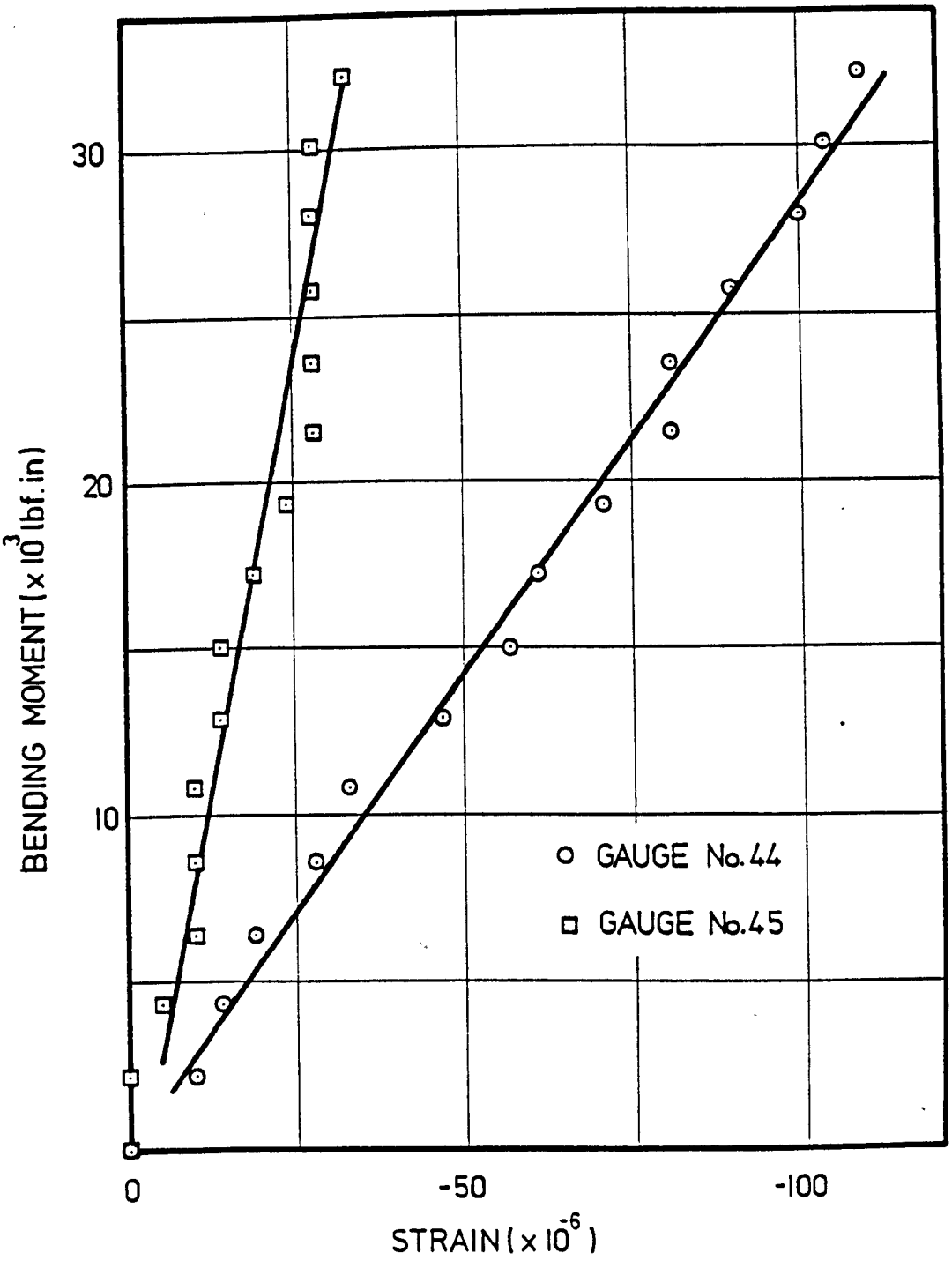

BEND No.1
STRAIN GAUGE PLOT

FIG. 4.9

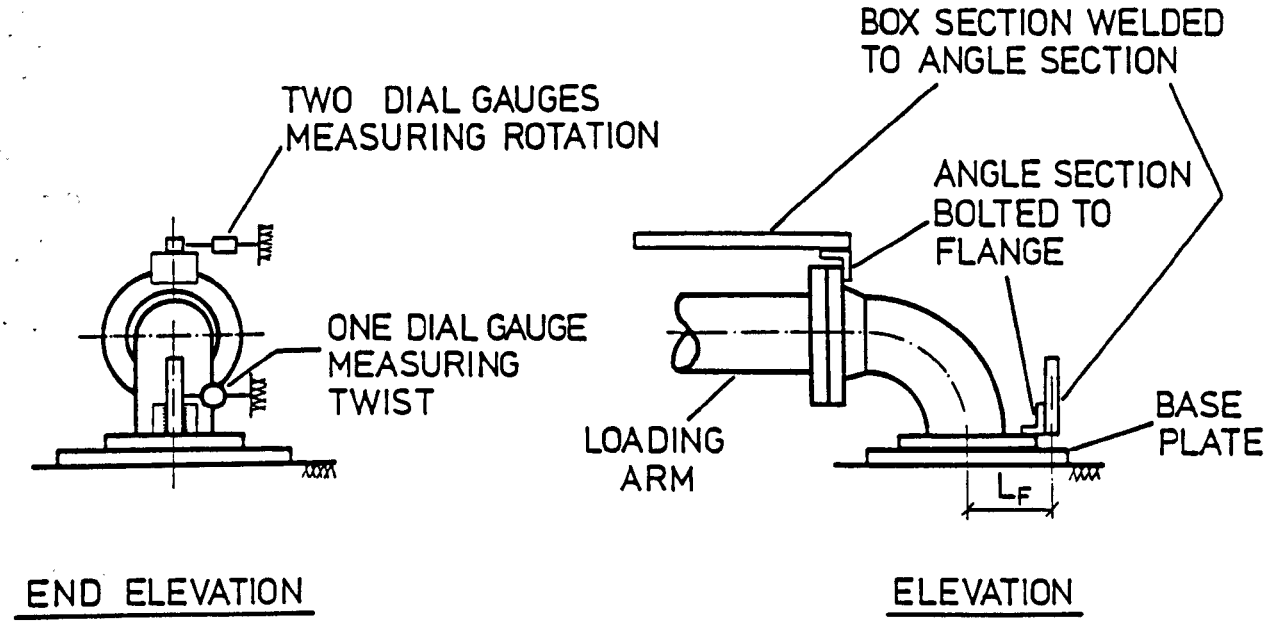

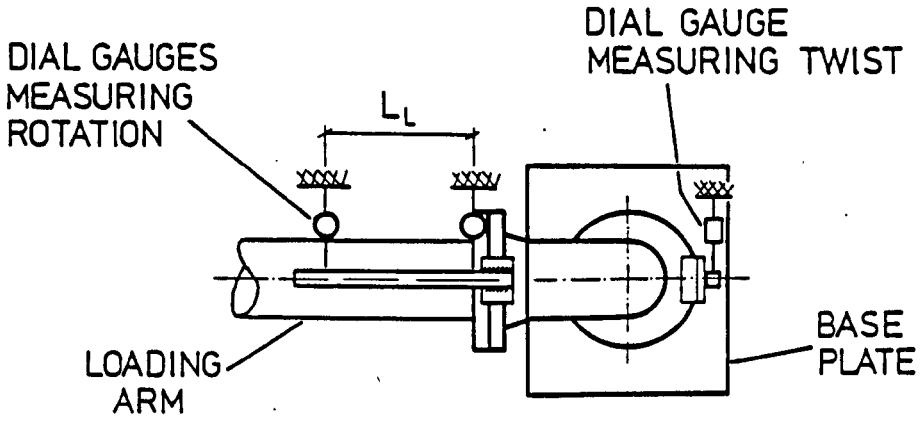

BEND No. 1

MEASUREMENT OF ROTATION

FIG. 4.10

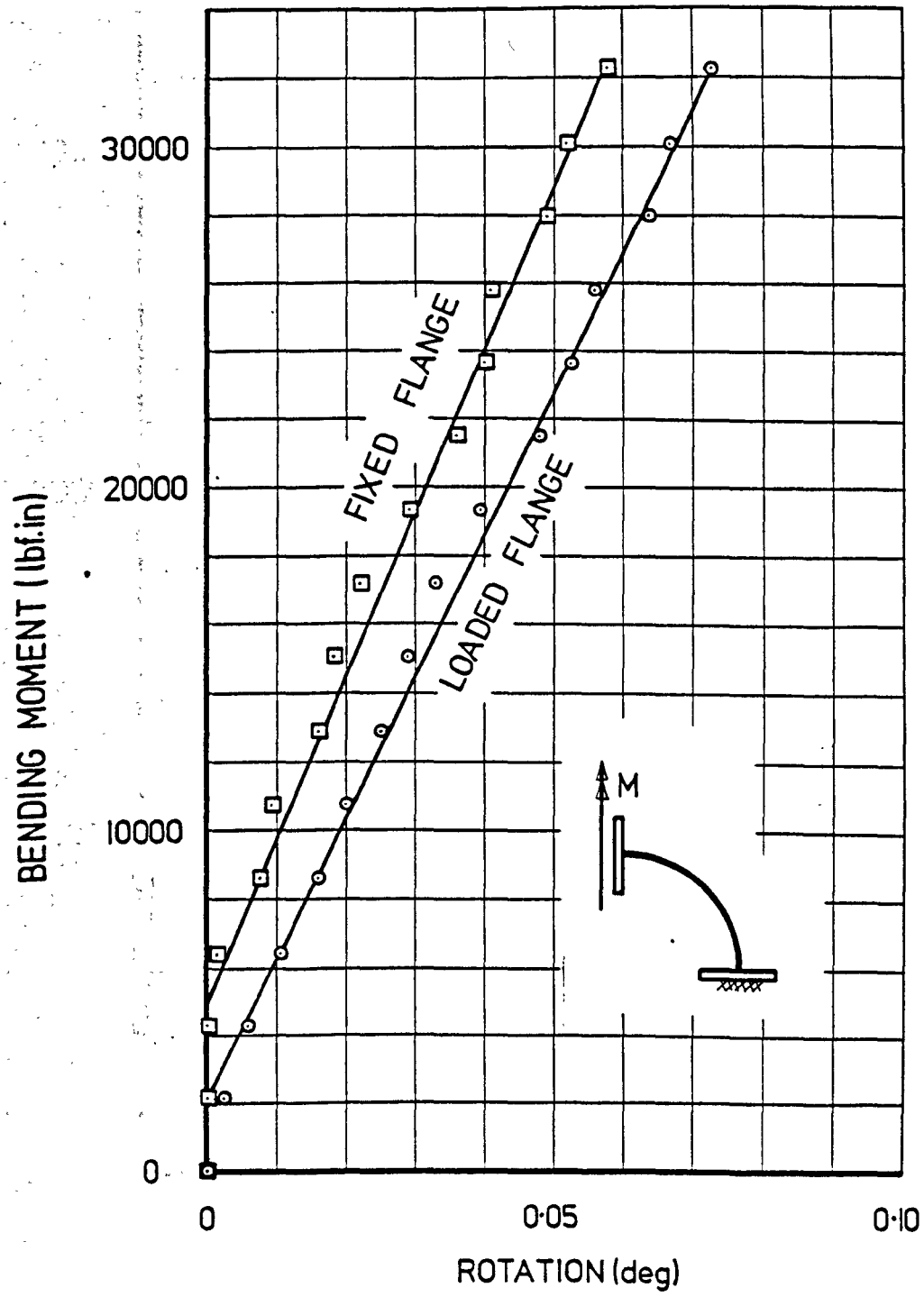

FIXED FLANGE:

$\gamma_F = a + bM$

$a = -0{\cdot}0131$

$b = 2{\cdot}1886 \times 10^{-6}$

LOADED FLANGE:

$\gamma_L = a + bM$

$a = -0{\cdot}0052$

$b = 2{\cdot}3995 \times 10^{-6}$

BEND No.1

EXPERIMENTAL ROTATION

FIG. 4.11

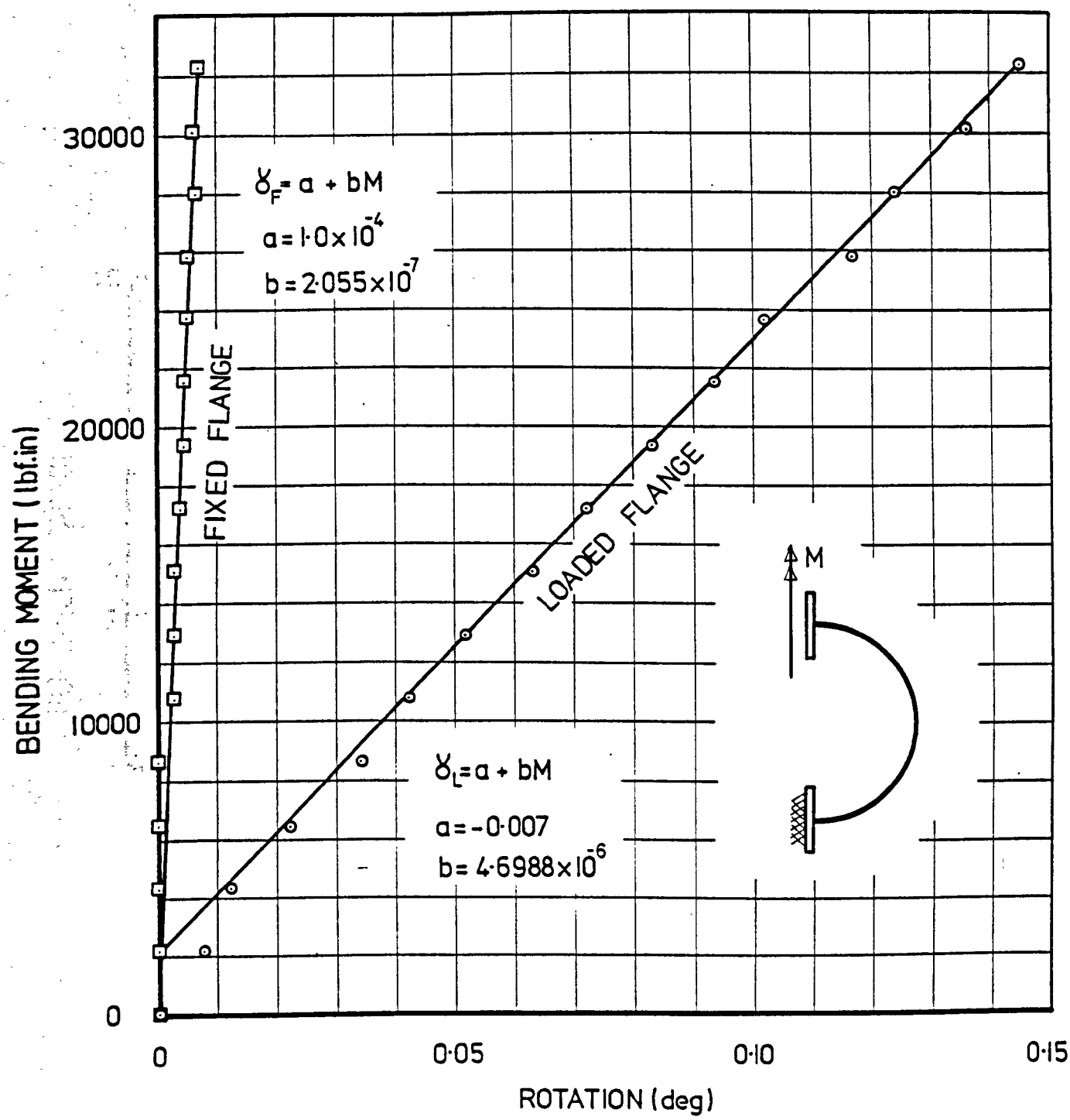

BEND No. 2
EXPERIMENTAL ROTATION

FIG. 4.12

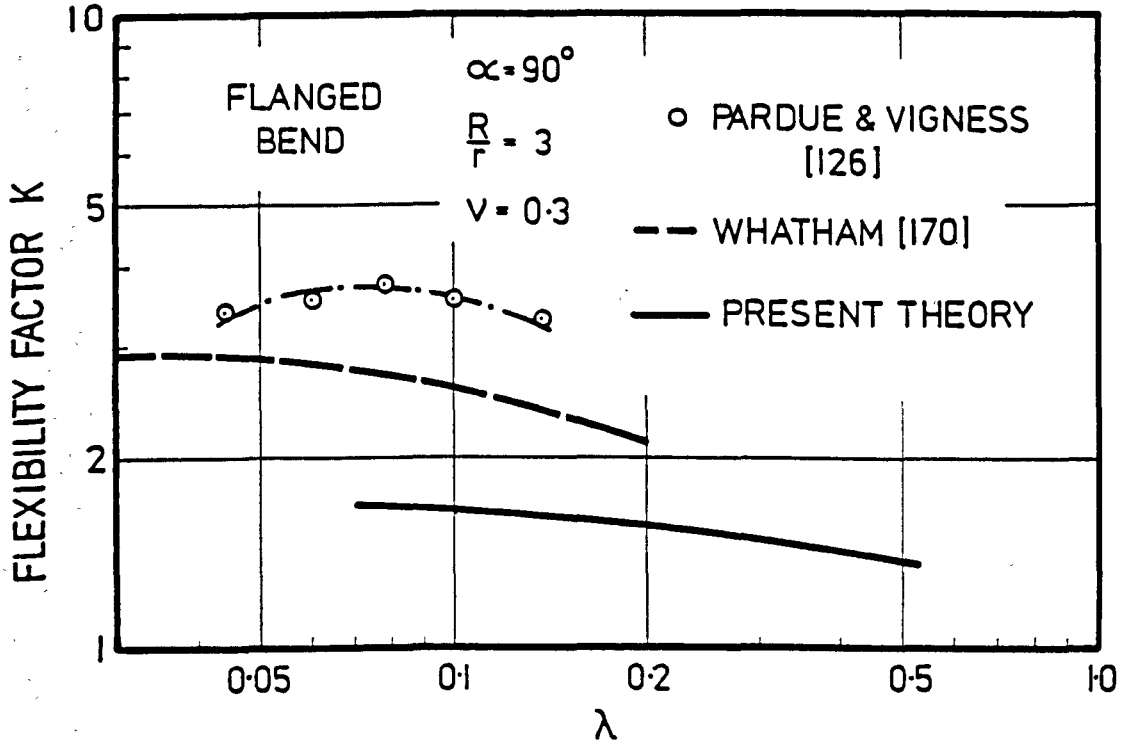

THEORETICAL & EXPERIMENTAL
FLEXIBILITY FACTORS
OUT-OF-PLANE BENDING

FIG. 4·13

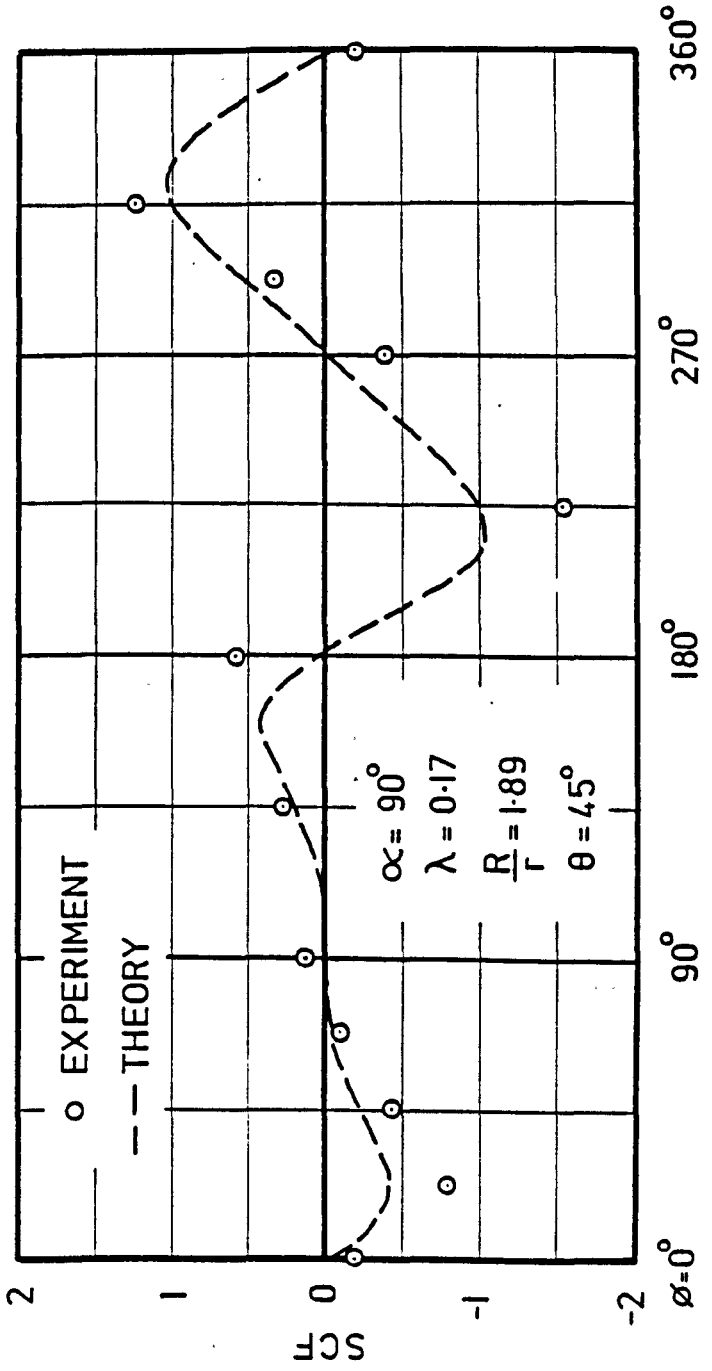

EXPERIMENTAL MERIDIONAL STRESS
AT θ=45°
BEND No. 1

FIG. 4·14

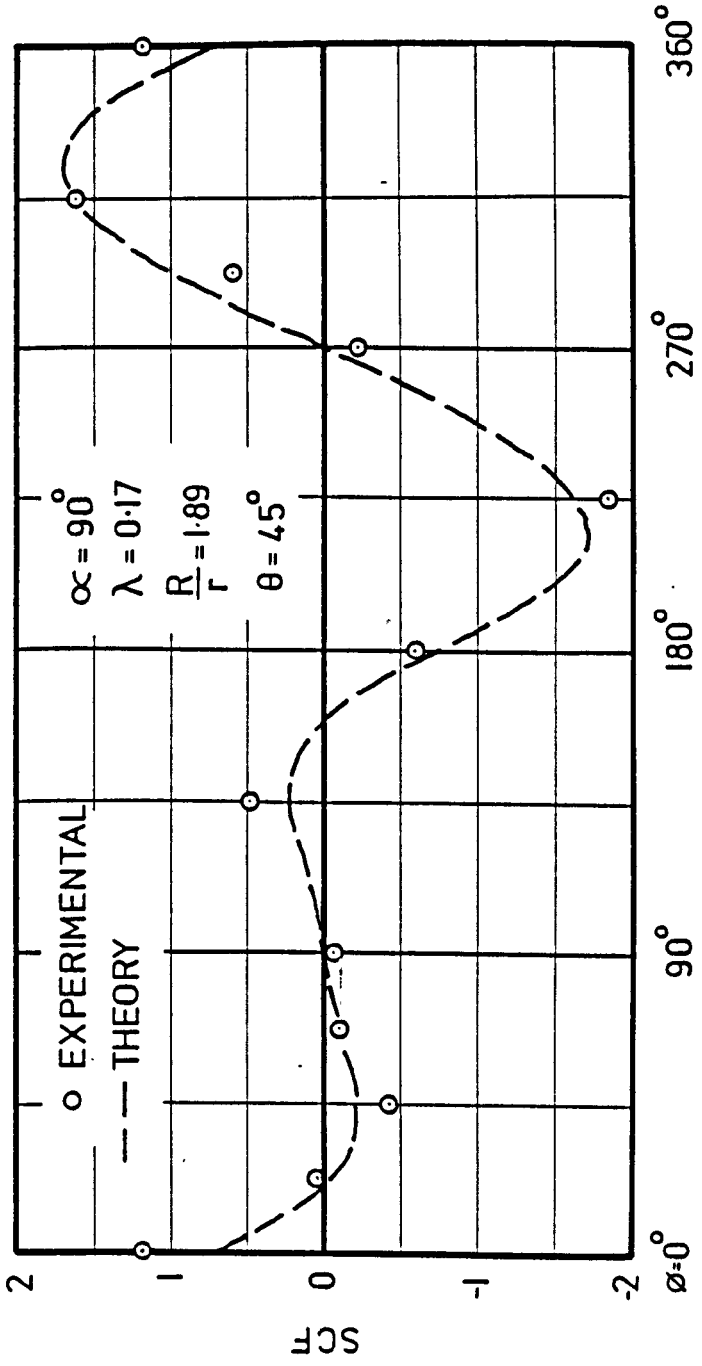

EXPERIMENTAL CIRCUMFERENTIAL STRESS AT θ=45°

BEND No.1

FIG. 4·15

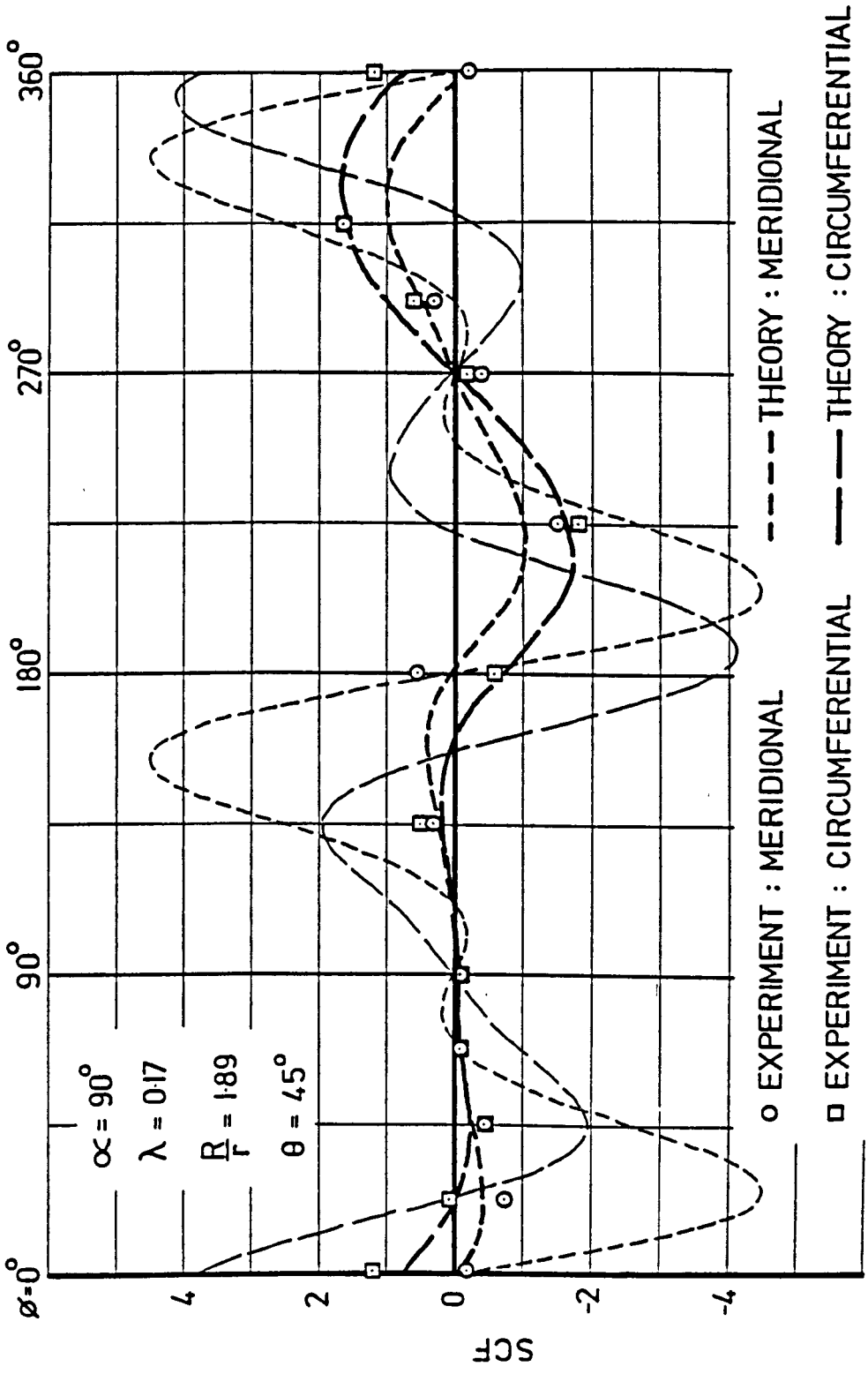

STRESS VARIATION AT θ=45°

BEND No. 1

COMPARISON OF

THEORY AND EXPERIMENT

FIG. 4·16

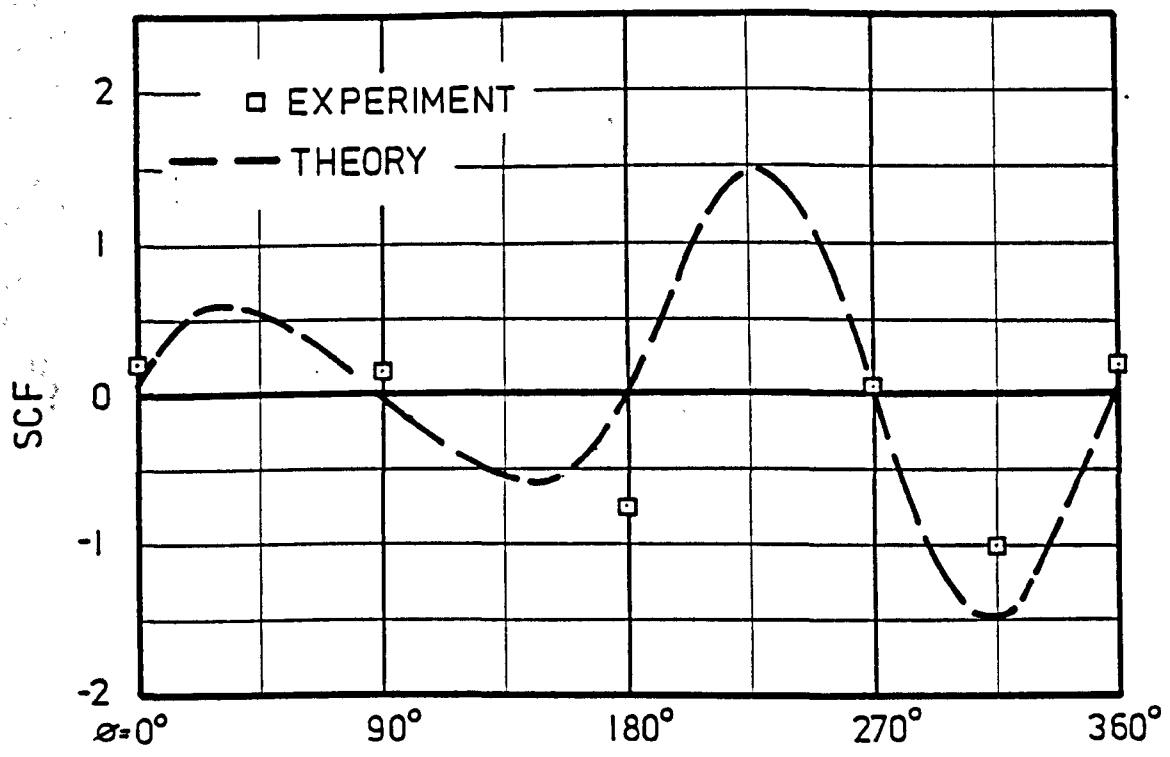

CIRCUMFERENTIAL STRESS AT $\theta=0^\circ$

$\alpha=90^\circ$: $\lambda=0.17$: $\frac{R}{r}=1.89$.

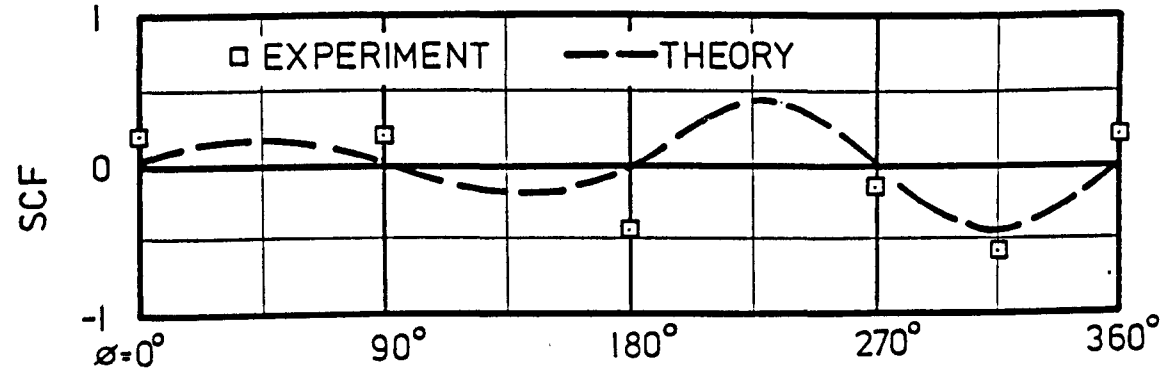

MERIDIONAL STRESS AT $\theta=0^\circ$

STRESS DISTRIBUTION AT FIXED END

(SLIP ON FLANGE)

BEND No. 1

FIG. 4·17

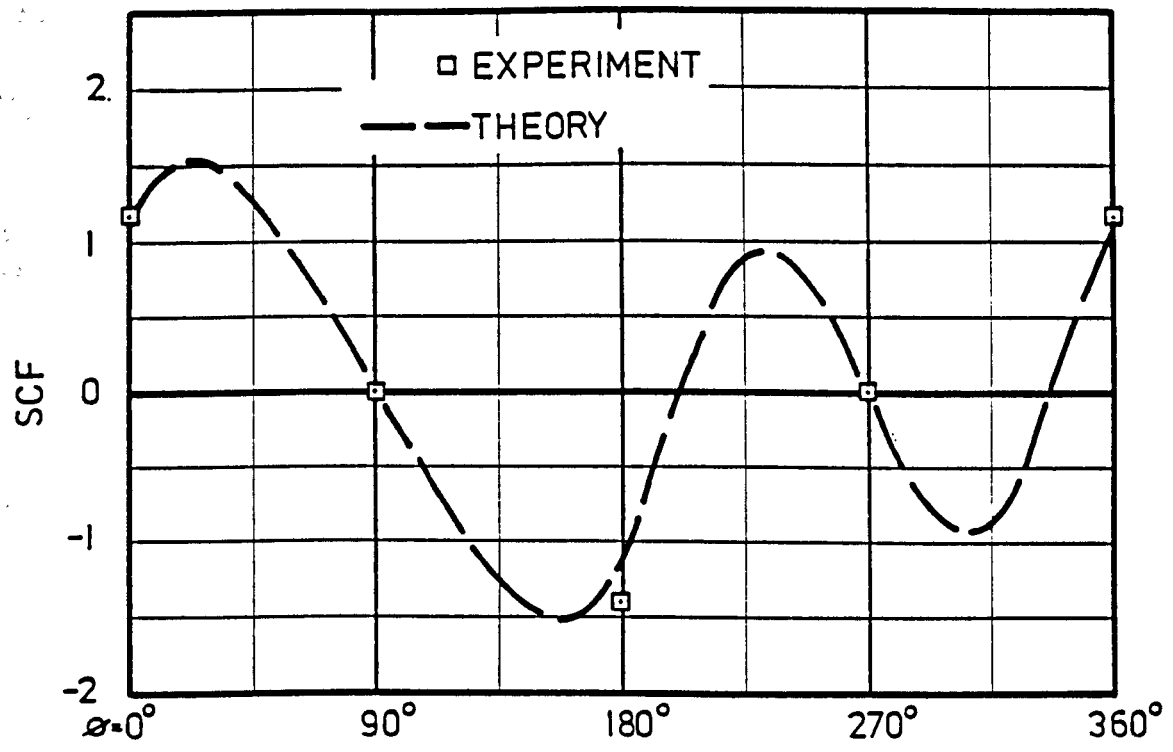

CIRCUMFERENTIAL STRESS AT θ=90°

$\alpha = 90^\circ : \lambda = 0.17 : \frac{R}{r} = 1.89.$

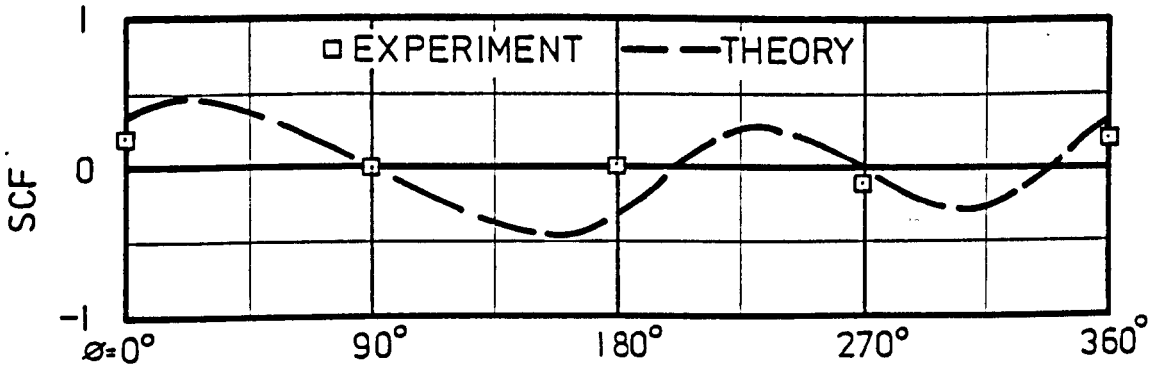

MERIDIONAL STRESS AT θ=90°

STRESS DISTRIBUTION AT LOADED END

(TAPER FLANGE)

BEND No. 1

FIG. 4·18

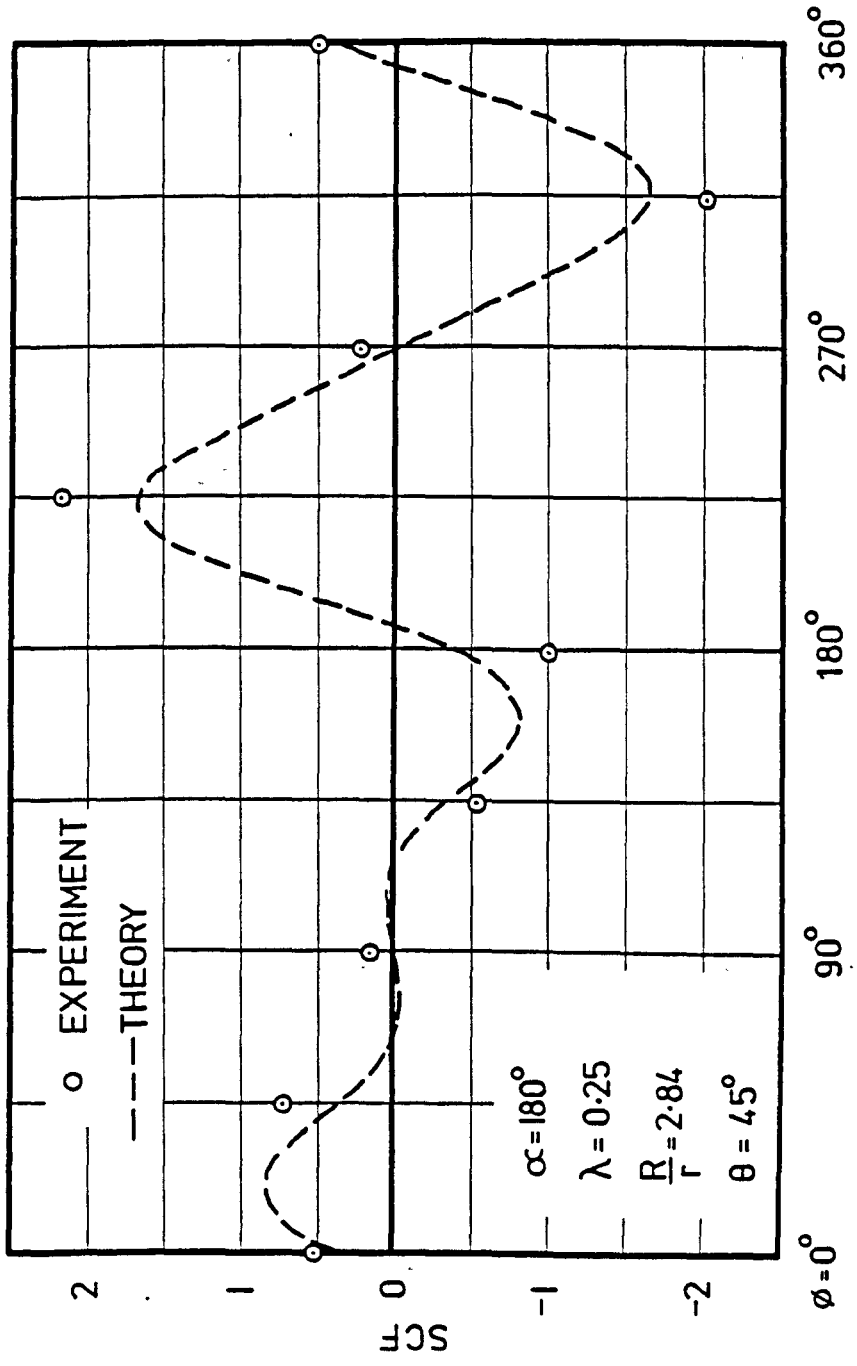

EXPERIMENTAL MERIDIONAL STRESS AT θ=45°
BEND No. 2

FIG. 4·19

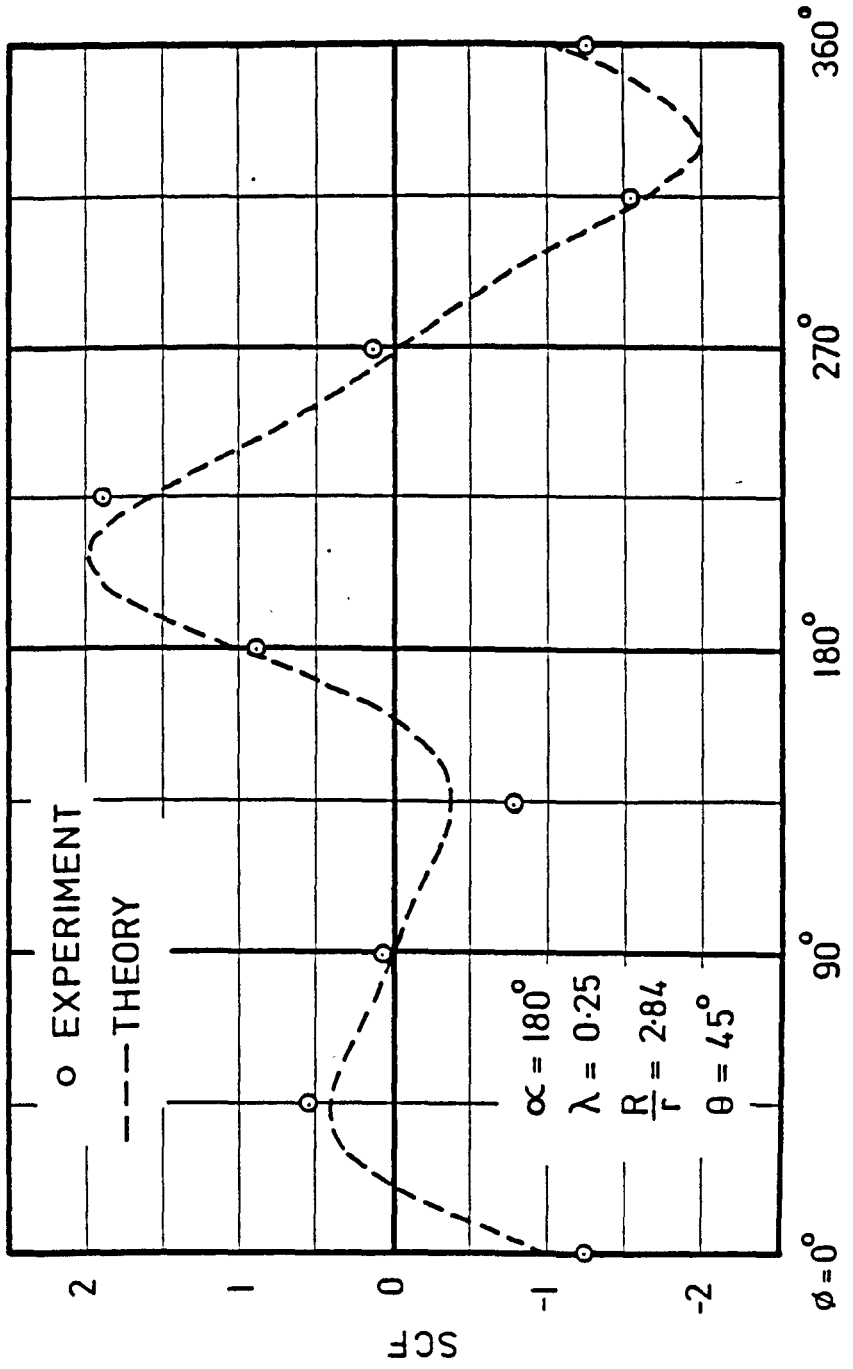

EXPERIMENTAL CIRCUMFERENTIAL STRESS AT $\theta = 45^\circ$

BEND No.2

FIG. 4·20

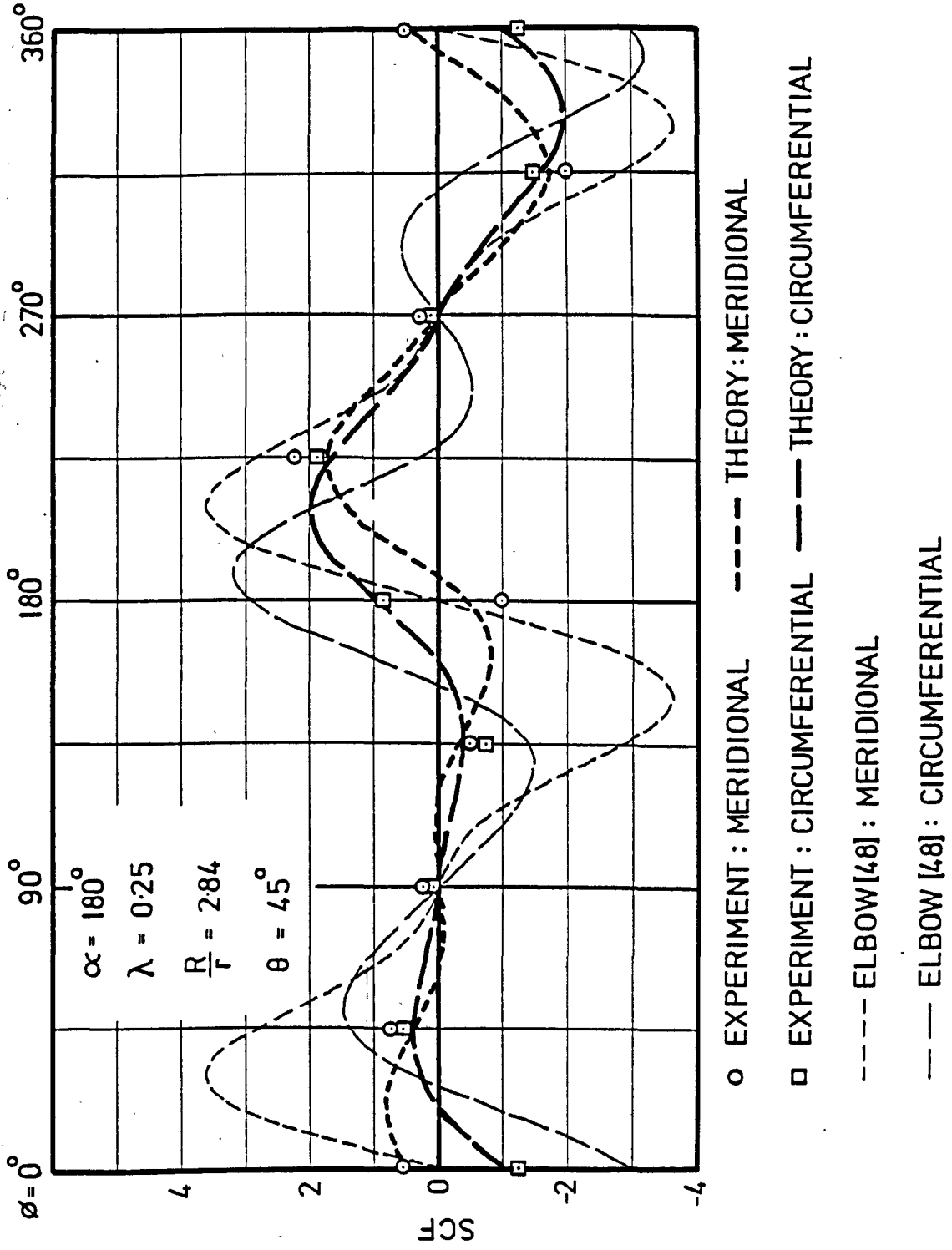

STRESS VARIATION AT θ=45°
BEND No. 2

COMPARISON OF
THEORY AND EXPERIMENT

FIG. 4·21

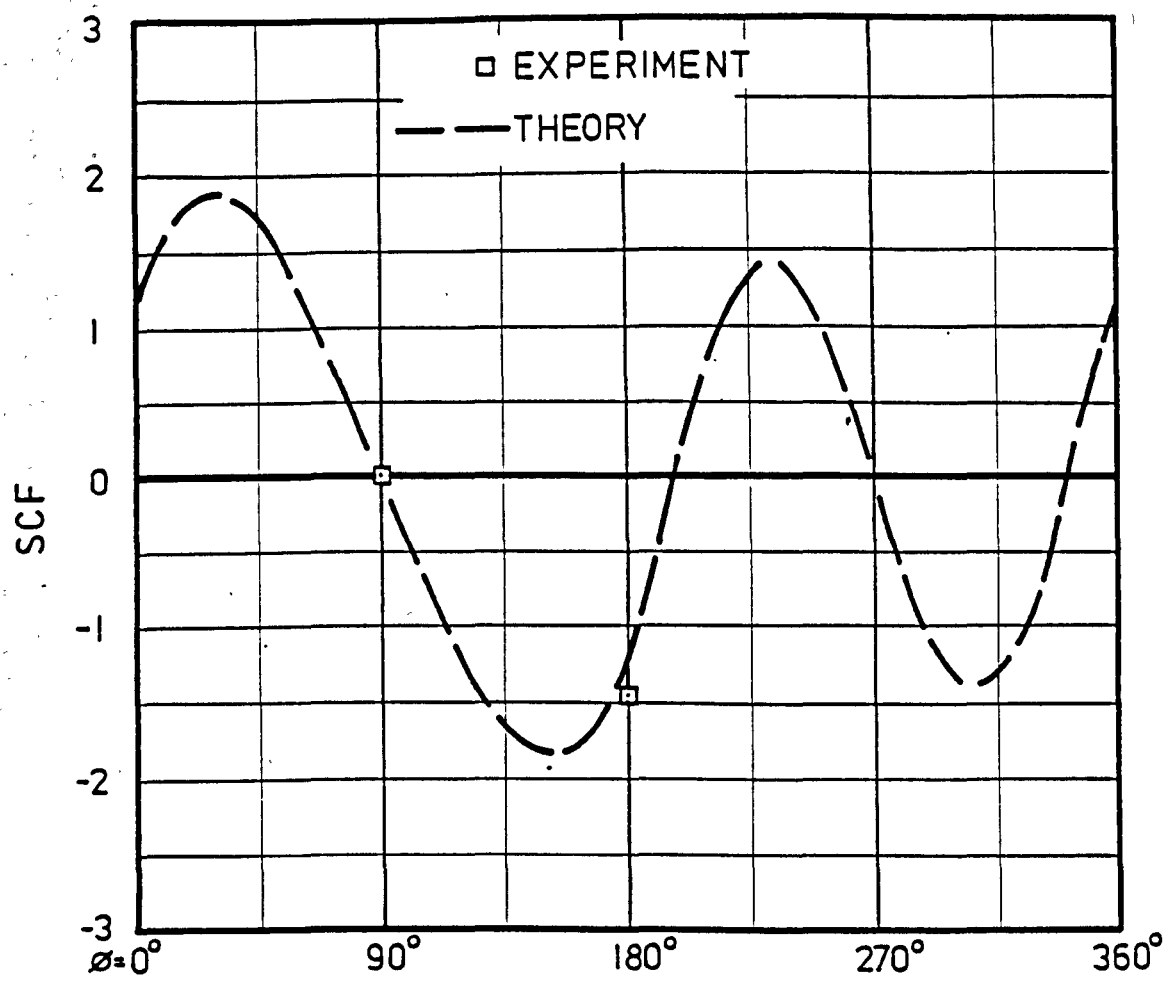

CIRCUMFERENTIAL STRESS AT θ=0°

$\alpha = 180°$; $\lambda = 0{\cdot}25$; $\frac{R}{r} = 2{\cdot}84$.

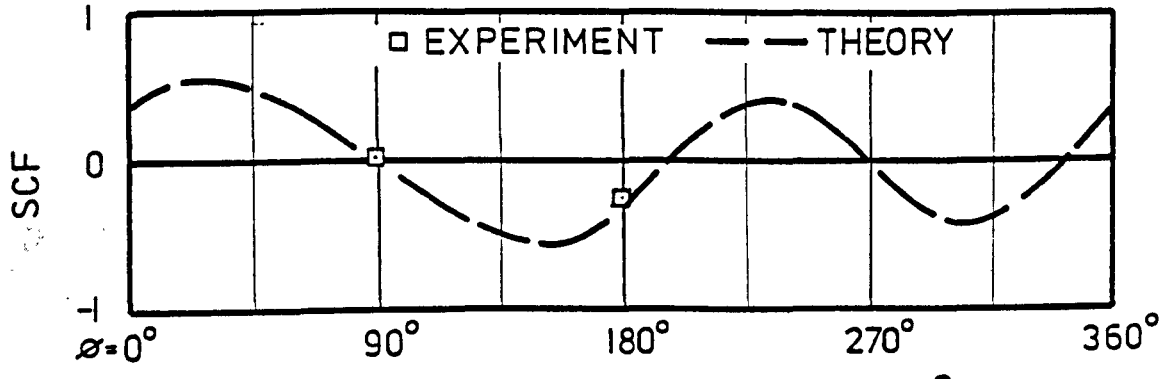

MERIDIONAL STRESS AT θ=0°

STRESS DISTRIBUTION AT FIXED END

(TAPER FLANGE)

BEND No. 2

FIG. 4·22

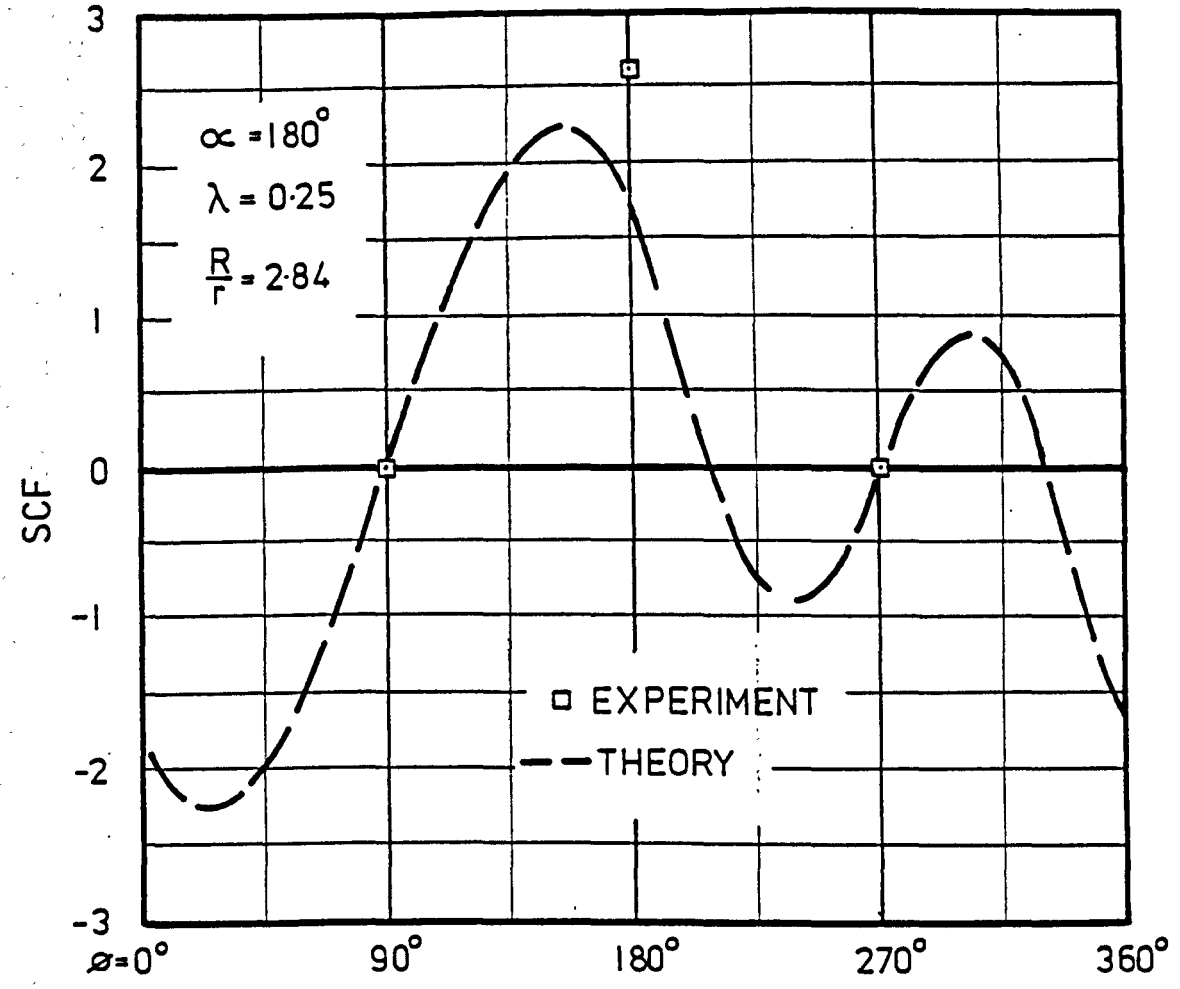

CIRCUMFERENTIAL STRESS AT θ=180°

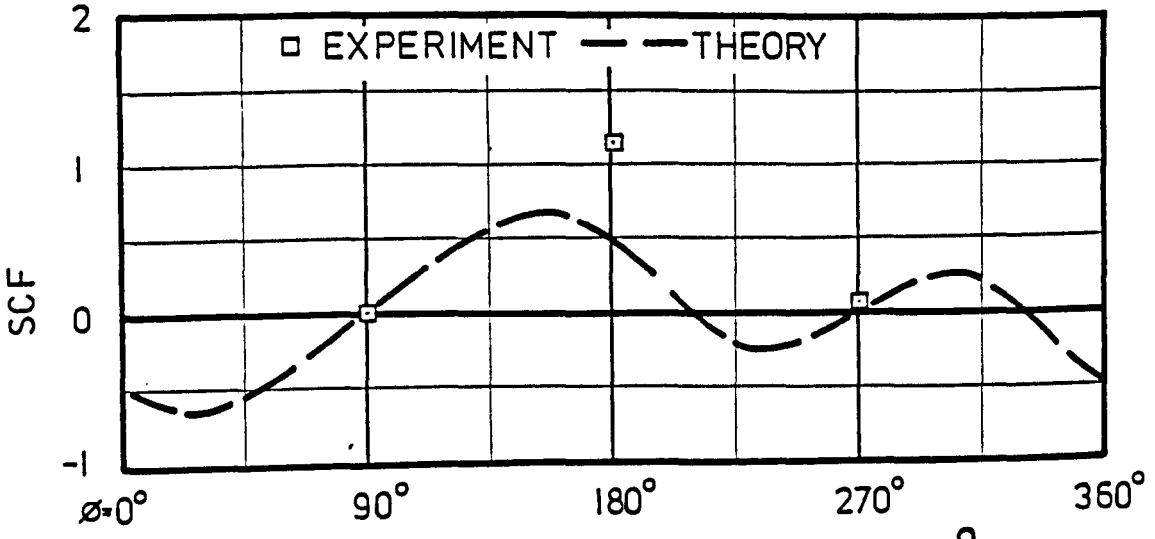

MERIDIONAL STRESS AT θ=180°

STRESS DISTRIBUTION AT LOADED END

(SLIP ON FLANGE)

BEND No.2

FIG. 4·23

PART 2

EXPERIMENTAL WORK AT ELEVATED TEMPERATURE ON PIPE BENDS WITH TANGENT END CONSTRAINTS

CHAPTER 5

General Description of Experimental Creep Programme

ABSTRACT

A general description is given of an experimental creep programme conducted on a number of stainless steel pipe bend assemblies.

Details of the test programme and the results of a mensuration exercise carried out on the pipe bend are presented.

A description is then given of the test equipment covering the measurement of displacement and strain at room temperature and elevated temperature (570°C).

Problems encountered in the experimental field are highlighted and a brief description is given of the development in experimental techniques.

CHAPTER (5)

GENERAL DESCRIPTION OF EXPERIMENTAL CREEP PROGRAMME

5.1 General Purpose and Background of the Test Programme

5.1.1 Introduction

This chapter presents a general description of the work undertaken by this author on an extensive experimental creep programme on pipe bends. The experimental work represents a continuation of earlier work carried out at the University by SPENCE and BOYLE [237] and later in a pilot scheme by SPENCE, BOYLE and RAE [238] and is largely a consequence of the theoretical work of Spence and Boyle typified in [121] and more recently in [239] and [240].

The main interest in this text will be focussed on the establishment of testing facilities and the development and application of new and existing techniques in the measurement of strain and other related aspects, at elevated temperature.

During the pilot scheme [238], which employed seven stainless steel, type 316, schedule 10 and 40 pipe bend assemblies, only a few creep tests were conducted. In this programme the emphasis was placed on the development and establishment of experimental techniques. However, a large number of room temperature elastic tests were conducted on these assemblies. In these tests the loading conditions covered in-plane and out-of-plane bending, internal pressure and a combination of these three loadings.

In the main creep programme, which utilised the techniques developed during the pilot scheme, a total of ten stainless steel, type 316, schedule 10 and 40 pipe bend assemblies were used. In this test programme a variety of elevated temperature tests were performed. These comprised forward creep tests under in-plane bending, out-of-plane bending and combined bending and creep relaxation tests

under in-plane bending. Elevated temperature plastic collapse tests were also performed on a number of the bend assemblies. This creep programme is still in progress and it is expected that all the pipe bend assemblies will be tested at elevated temperature.

As an integral and important part of both test programmes a series of uni-axial tensile tests at elevated temperature was also initiated. The purpose of these tests is to provide data on the material properties at temperature. This in turn permits suitable constitutive equations to be employed in the analytical work. The importance of these tests cannot be over-emphasised as the use of improper parameters in the constitutive equation in even the most sophisticated of analytical methods can lead to spurious results and poor comparison with experiment.

In both the pilot scheme and the main creep programme three bend angles of 180°, 90° and 45° were used having λ values of 0.11 and 0.25. The test temperature adopted was 570°C.

The experimental work was closely associated with the nuclear industry being funded by the United Kingdom Atomic Energy Authority (UKAEA).

5.1.2 Purpose of the tests

As mentioned briefly in CHAPTER (1), the public demand for increased safety and the inherent danger of failure of a component in a nuclear piping system has led to the need for a more detailed understanding of the stress and resulting failure mechanisms in these components under load [241]. This is further complicated by the fact that these components are operating at a temperature where material creep becomes a problem.

The analysis of the pipe work system associated with the heat transport system poses particular problems for the engineer over and above those of thermal and fluid dynamics (see [242-247]). This is due not only to the geometrical complexity of the piping system but also to the unavoidable variation in material properties throughout.

Apart from the general problem of creep, this desire for high structural integrity in the piping system has introduced a variety of further failure mechanisms and ultimate load criteria. Typical examples of this are the "pipe whip" problem, aircraft impact on a nuclear power installation and seismic loading effects (see [248-252]).

The bend assemblies employed herein on the creep programme are in fact one-fifth scale models of the components used in the secondary sodium circuit of a typical Liquid Metal Fast Breeder Reactor (LMFBR).

Pipe bends introduced in such systems for practical convenience in the layout or specifically to absorb expansion in the system will obviously require particular attention due to the high stress concentrations set up in such components under load. Indeed, they play an important and critical role in the operation of the system representing in many instances a substantial proportion of the capital cost of the plant.

The diversity in loading experienced by these components and the severe consequences of failure gives some indication of the complexities facing today's engineer in the design of a nuclear power installation piping system. The complexity and size of the problem naturally calls for considerable simplifying assumptions to be made. The results from such a simplified analysis require to be validated in some manner to ensure that the predicted behaviour of a single component, such as

the pipe bend case considered herein or a more sophisticated and realistic combination, is representative of the actual behaviour of the component. This in essence is the purpose of the creep tests described herein. The experimental work itself, however, also requires some form of validation, i.e. is the strain being measured accurately, is the temperature distribution and loading representative of the actual situation and furthermore, and perhaps more importantly, does the pipe bend model under test correspond to the mathematical model employed in the simplified analysis.

Thus the object of the creep testing is seen to be essentially two-fold and can be summarised as follows:

1. The techniques of creep testing were to be fully investigated and established. This task was accomplished during the pilot scheme.

2. Preliminary information, based on sound experimental results was to be obtained to aid further the development of simplified analytical methods. This data would be sought from the main creep programme.

5. 1. 3 Current developments in theory and experiment

In the analysis of piping systems subject to plasticity and creep, two distinct approaches to the problem are currently being pursued. These are discussed more fully in the work of Boyle and Spence [121]. In the first method, the finite element method is employed with beam elements representing the straight sections of pipe and special "pipe bend elements" representing the elbows. This approach was pioneered in the Marc [66] general purpose finite element package. The pipe bend element employed was, however, the subject of much criticism, for example, it did not account for the restraining effect of tangent pipes. Following this a number of improved elements were developed. These are employed in the Abaqus [108] system, in Adina [81] and Paula 82 [82].

The second approach attempts to extend the well-established linear elastic techniques which employ factors on beam elements to account for the additional flexibility of the pipe bends. However, early attempts at general purpose computer codes using this approach are deficient in several respects. For example, PACE 2 [253] addresses only the two anchor problem and simple loading cases, PIRAX 2 [254] is based on an inadmissable assumption regarding decomposition of the loading effects. Nevertheless, in terms of cost this approach is attractive and is being pursued at an international level by the French with the TEDEL [255] program and by the Japanese with PISAC [256]. The method, however, is not yet at a stage where localised accumulation of strain can be accurately quantified.

As discussed earlier, these simplified forms of analysis require some form of validation. The accuracy of the analysis must be gauged

by verification and qualification against what has become termed "benchmark" solutions, these being good experimental results on piping components under load at elevated temperature. However, owing to the high cost and inherent difficulties only a few tests have been conducted on pipe bends. The bulk of those that have been performed have been aimed principally at benchmark solutions. For example, the tests conducted by Griffith and Rodabaugh [115] were aimed at verifying the program Pirax 2.

In an attempt to co-ordinate the efforts of the various countries involved in this work, several organisations have been set up such as the International Working Group on Fast Reactors (IWGFR) and the Pressure Vessel Research Committee (PVRC), both based in the U.S.A. Working in collaboration with Commissarait à l'Énergie Atomique Centre d'Études Nucléaires in France (CEA), Power Reactor and Nuclear Fuel Development Corporation in Japan (PNC), Central Electricity Generating Board in the U.K. (CEGB) and Battele Laboratries, U.S.A., these organisations have established a series of benchmark problems to be used in the development of suitable analytical procedures and techniques in the analysis of piping systems.

In a recent IWGFR study compiled by Oak Ridge National Laboratory [257], three tests on in-plane bending were considered. Two of these tests [115] and [116] were conducted at elevated temperature on 90° bends. In the third test, contributed by BROUARD, ROCHE and VRILLON, the room temperature elastic-plastic in-plane bending of a 180° bend was examined. A similar task was performed by PVRC [124]. In this study, the elastic-plastic-creep analysis of piping elbows was identified as one of four critical problems in the field of elevated temperature design. A report on this study is to be published shortly.

In a recent report by IMAZU, NAGATA and SATO [258] a large number of elevated temperature tests on piping components, completed and proposed, are presented. This work is part of an extensive research and development program currently being undertaken by PNC for the requirements of the LMFBR.

More recently in a paper by FORTMANN [259] a general description is given of the experimental set-up for proposed elevated temperature tests on a full size 90° bend. This work is part of a research programme being undertaken by Internationale Atomreaktorbau (INTERATOM) in West Germany.

The introduction of nuclear power has clearly resulted in significant development in the theoretical and experiment field of piping systems. This increased activity in research is also expected to be reflected in the design of the more conventional, low temperature pipework systems. However, in the continuing development of an analysis procedure, Boyle and Spence [121] express a word of caution in the use of benchmark solutions. Benchmarks are considered as necessary but not sufficient to establish the validity of an analysis and care should be exercised in the comparison between different analysis, which from the theoretical standpoint could be totally different.

5.2 Details of Pipe Bend Assemblies

5.2.1 General description

In order to satisfy the interest of the fast reactor secondary sodium circuit pipework, the bend geometries were required to lie within the range of diameter / thickness ratio of 40 to 80 and λ values in the range 0.1 to 0.3. For this purpose two bend types of schedule 10 ($\lambda = 0.11$) and schedule 40 ($\lambda = 0.25$) were chosen with bend angles of 180°, 90° and 45°.

The pipe bend assemblies were made up of a 24 in. tangent (straight) - a 6 in. nominal bore bend - 24 in. tangent, manufactured from stainless steel type 316, each tangent being terminated by 1 in. thick carbon steel flanges. An illustration of the bend assemblies is shown in Figure (5.1).

Based on nominal dimensions, the sectional properties of the two bend types of schedule 10 and schedule 40 were as follows:

1. Schedule 10

bend radius	R	= 9 in.
outside pipe section diameter	D	= 6.625 in.
wall thickness	t	= 0.134 in.
nominal pipe section radius	r	= 3.2455 in.
second moment of area	I	= 14.39 in^4
section modulus	Z	= 4.34 in^3
pipe factor	λ	= 0.11
radius ratio	$\frac{R}{r}$	= 2.77
tangent length/r		= 7.39

2. Schedule 40

bend radius	R	= 9 in.
outside pipe section diameter	D	= 6.625 in.
wall thickness	t	= 0.28 in.
nominal pipe section radius	r	= 3.1725 in.
second moment of area	I	= 28.09 $in.^4$
section modulus	Z	= 8.48 $in.^3$
pipe factor		= 0.25
radius ratio	$\frac{R}{r}$	= 2.84
tangent length/r		= 7.56

Details of the bend assemblies chosen for the pilot scheme and the main creep programme were as follows:

1. Pilot scheme

Bend number	1	2	3	4	5	6	7
Bend angle	180°	180°	90°	90°	180°	90°	45°
Schedule	40	40	40	40	10	10	10

TABLE (5.1):

2. Main creep programme

Bend number	1	2	3	4	5	6	7	8	9	10
Bend angle	180°	180°	90°	90°	180°	180°	90°	90°	45°	45°
Schedule	40	40	40	40	10	10	10	10	10	10

TABLE (5.2):

The bend assemblies were manufactured by Munro and Miller Fittings Ltd [233] from commercial straight and curved tubes using maximum curved segments of 90°. The quality control on fabrication and subsequent heat treatment were defined as follows:

1. All welding in accordance with A.S.M.E. Section 3.
2. All external welds except fillet welds to be ground flush.
3. Penetration of inside weld bead to be kept to a minimum.
4. Fillet welds between flanges and pipe to be dye-penetrant checked.
5. Assembly to be heat treated to 1050°C for 20 mins then cooled in air and pickled prior to fitting of the flanges.
6. 100% x-ray on all stainless steel butt welds.

5.2.2 Mensuration of bend assemblies

During the fabrication of the bend assemblies for the pilot scheme there was no special liaison between the manufacturer and the University. This arose from a lack of full-time staff employed on this particular research contract during the early stages. As a result of this, significant distortion was observed on some of the bend assemblies. This was particularly evident around the butt welds and arose from the welding and bad matching of the straight and curved components.

In the main creep programme on which two full-time staff were employed, every effort was made to avoid this problem. This was accomplished in a bend matching exercise prior to fabrication of the assemblies. This operation, carried out at the manufacturer's, resulted in a significant improvement of the bend profile, particularly around the butt welds. Initially, it was intended that wall thickness and diameter

measurements taken by the manufacturer would be the basis of this matching exercise, but it was found to be more practical to physically match each bend component on the work bench. As a result of the good fit obtained on the first 180° bend assembly, using two 90° curved segments, it was decided to adopt this option as opposed to employing two 45° and one 90° curved segments. Although this option retained the central butt weld it was hoped that careful supervision of the final grinding would produce a minimal discontinuity and possible use of this section for instrumentation. Fuller details of this work are reported in [260].

Following the fabrication and delivery of these bend assemblies, a comprehensive mensuration exercise [261] was carried out. The main measurements taken along the bend and the tangent included:

1. ovality
2. wall thickness
3. outside diameter

In the measurement of each bend assembly the work was divided into two main stages:

1. the marking off and measurement of ovality;
2. the measurement of outside diameter and wall thickness.

Using a surface table, the marking off operation was carried out by laying out each bend upon a template shape drawn on hardboard. This allowed a best fit to be obtained in terms of the bend angle and length together with section marks at $\phi = 90°$ and $\phi = 270°$ along the extrados and intrados, respectively. To establish the corresponding section marks at $\phi = 0°$ and $\phi = 180°$, the instrument used in measuring ovality

was employed (Figure (5.2)). Scoring of the outside surface was prevented by painting each assembly with a white emulsion. Following this the outside diameter was measured using a 7 in. micrometer. Wall thickness measurements were taken using an ultrasonic instrument - KRAUTKRAMER-BRANSON Model CL204.

In order to achieve the correct orientation regarding dimensions and also identification, each assembly was clearly marked on the outside edge of one flange.

Ovality measurements made were via the special instrument which is shown in Figure (5.2). These were taken around each bend at 15° intervals circumferentially and at 10° intervals meridionally. On the tangents this was done at 10° intervals meridionally and at the following circumferential sections:

1. For a 180° assembly, at sections 2,4,18,20 (see Figure (5.3)).
2. For a 90° assembly, at sections 2,4,12,14 (see Figure (5.4)).
3. For a 45° assembly, at sections 2,4, 9,11 (see Figure (5.5)).

The measurement of wall thickness was taken at 15° intervals circumferentially and 45° intervals meridionally. On the tangents this was done again at 45° intervals meridionally and on the same sections used in ovality.

Outside diameters were measured at 15° intervals circumferentially and on the principal diamters of $\phi = 0°/180°$ and $\phi = 90°/270°$. The same procedure was carried out on the tangents at the same sections used in ovality measurements. The ovality measurements enabled a further 16 diameters to be derived at 10° intervals meridionally.

In order to cope with this vast amount of data, e.g. nearly 800 readings for a 180° bend assembly, the information was computerised using a TEKTRONIX 4051. This allowed a graphical representation of the ovality measurements and a clearer presentation of the results overall. Typical results from a 180° bend are given in APPENDIX (6).

A general indication of the dimension tolerances achieved is given in Table (5.3). To some extent these values represent a "worst case", bearing in mind that they are for the centre section of each bend, where for example in a 180° assembly this section is represented by a meridional butt weld.

Overall the circularity was good and appeared satisfactory, particularly around the bend. This was due in part to the method of manufacture using rolled plate and a circumferential weld to form the bend. In wall thickness the variation was generally above the nominal. The worst cases as mentioned were invariable at the meridional butt welds where the actual measurement became less certain.

TABLE (5.3): Mid-bend dimensions.

Bend number	** Ovality %	Outside diameter % difference of average & nominal	*Wall thickness* % difference of max & min to average		*Wall thickness* % difference of max & min to nominal	
			Minimum	Maximum	Minimum	Maximum
No. 1 - 180° - Sch 40 Section No. 11	1.08	+0.22	-10.02	+ 6.21	-6.32	+10.56
No. 2 - 180° - Sch 40 Section No. 11	2.27	-0.44	-17.81	+ 8.19	-7.21	+22.14
No. 3 - 90° - Sch 40 Section No. 8	0.99	+0.36	+ 6.36	- 4.86	-6.43	+ 4.78
No. 4 - 90° - Sch 40 Section No. 8	0.84	+0.72	- 4.84	+ 4.38	-5.28	+ 3.89
No. 5 - 180° - Sch 10 Section No. 11	3.72	-0.93	- 9.20	+ 4.60	+3.06	+18.73
No. 6 - 180° - Sch 10 Section No. 11	2.52	-0.71	-18.03	+ 9.21	-7.01	+23.88
No. 7 - 90° - Sch 10 Section No. 8	1.34	+0.28	- 8.80	+10.69	-2.61	+18.21
No. 8 - 90° - Sch 10 Section No. 8	0.90	+0.29	- 8.48	+ 8.41	-0.97	+17.31
No. 9 - 45° - Sch 10 Section No. 6	2.90	+0.50	- 7.36	+ 2.23	+2.31	+12.91
No. 10 - 45° - Sch 10 Section No. 6	2.80	+0.60	- 5.71	+ 2.38	+3.43	+12.31

** Ovality measured as: $\frac{(D_{max} - D_{min}) \times 100}{D_{av}}$

where D_{max} = maximum outside diameter
D_{min} = minimum outside diameter
D_{av} = average outside diameter based on 18 values

5.3 Test Programme

5.3.1 Pilot scheme

In the pilot scheme it was initially envisaged that most of the seven pipe bend assemblies would be tested at temperature. However, due to difficulties encountered in the experimental work this was not possible. Several of the bend assemblies were employed in the development of experimental techniques during the course of which a large number of room temperature elastic tests were conducted. The main difficulties centred around the reliable measurement of strain at elevated temperature using the CERL-PLANER [262] capacitance strain gauge and the provision of a reasonable temperature distribution around the bend, particularly in the meridional direction. As a result, the test programme was altered to one of research and development.

5.3.2 Main creep programme

Apart from the theoretical considerations discussed earlier, the preparation of this test programme was also influenced by many practical considerations. The layout of the actual test facilities, for example, which dictated the number of bends that could be tested simultaneously, was in itself an important factor. A typical forward creep test could rate around 6 months and although this would indicate that a more than sufficient time was available for integration of the tests it should be borne in mind that the preparation time, prior to testing, could take upwards of 8 weeks. Considering only forward creep and creep relaxation test types, it can be seen from Table (5.4) that for the 10 bend geometries chosen there is a possible

TABLE (5.4): Possible and actual creep tests.

Forward creep			*Creep relaxation*			
In-plane bending	Out-of-plane bending	Combined bending	In-plane bending	Out-of-plane bending	Combined bending	Bend angle and schedule
No.	No.	No.	No.			
		5 & 6				180° - Sch 10
	1		2*			180° - Sch 40
7*			8*			90° - Sch 10
3	3	4				90° - Sch 40
9*			10			45° - Sch 10

* tests completed

30 test types. If the in-plane bending and the combined bending case is expanded to include the options of opening and closing, then the range of possibilities increases to 500. Naturally, all these options could not be exercised so that care was required in choosing the appropriate test types.

The proposed tests are shown in Table (5.4). Due to the long period of preparation required for one creep test, plastic collapse test were normally conducted at the end of the creep test.

5.4 Test Equipment

5.4.1 Test rigs - general description

In the pilot scheme three simple test rigs were employed. Of these, two were capable of testing a 45° and 90° bend only (Figure (5.6)). They were made up simply of two channel sections bolted to the floor and connected on top at one end by a 1 in. thick flat plate on to which the bend was mounted. In-plane and out-of-plane loading was catered for but only forward creep tests could be performed. The third test rig (Figure (5.7)) was designed specifically for a 180° bend and although slightly more complex in construction it could only cope with in-plane bending on forward creep tests.

The severe restrictions in loading types imposed by these test rigs was to warrant considerable attention in the design of a new test rig. By being limited in space to at most three test rigs it was essential that a new design should be capable of dealing with more than one bend angle. Further, the test types of forward creep and creep relaxation in any loading direction should be incorporated as essential features. Two test rigs designed to meet these specific requirements were designed and constructed. Both test rigs were designed in accordance with BS 449 [263] using bolted connections wherever possible to ease construction. The general layout of the rig is given in Figure (5.8) showing the various loading systems for a 180° bend. The structure comprises essentially a portal frame which encloses the loading arm of the bend. As in the earlier designs the rig is secured by two channels bolted to the floor. The provision for a 180° bend is given by a substantial 1 in. thick support bracket (Figure (5.9)) mounted on the channels. This also provides additional rigidity and guides for the creep relaxation

rods. Accommodation for a 90° or 45° bend is provided by a 1 in. thick flat plate mounted to the rear (Figure (5.10).

To retain the compliment of three test rigs one of the original designs as shown in Figure (5.6) was employed.

In the sections that follow, details of the equipment relate to those currently in use. Their development and application are discussed more fully in CHAPTER (6).

5.4.2 Test rigs - loading

5.4.2.1 Forward creep - in and out-of-plane loading

In-plane loading of the bend was accomplished simply by attaching a cradle of dead weights at the end of the moment arm. This would produce an in-plane closing mode. An opening mode was performed using made up lengths of steel wire running through a system of pulleys incorporating precision bearings. Here, again, dead weights could be applied on a cradle attached to the end of the wire. The application of a pure in-plane bending moment, i.e. "shear force negated", was achieved by suitable arrangement via the pulley system giving two equal and opposite forces.

Out-of-plane loading, in either direction, was achieved using a small portal frame mounted adjacent to the test rig (Figure (5.11)). As the new test rigs were mounted side by side,three of these frames were all that was required to serve the needs of both rigs. Here the main types of loading was by dead weights or turnbuckle, the dead weight load wire running over a precision bearing mounted on the out-of-plane portal. The option of shear force negated was available via diagonally placed attachments on the portals.

In most instances, the loading was accomplished using dead weights as this proved to be the easiest and most direct method. Needless to say, there was to hand an abundant supply of 50 lbf and 22.4 lbf weights. Turnbuckles were used mainly in short term tests, such as the elastic room temperature tests. They were found particularly helpful in tests of shear force negated where their high sensitivity proved useful in the application of two equal and opposite forces. Other forms of loading were available such as hydraulic rams and "TIRFORS". Tirfor is the trade name given to a mechanical rachet device which employs friction as its principal force, and is used extensively in Civil Engineering Works. However, both these forms of loading were found to be awkward to install and use.

In the elevated temperature tests, every attempt was mde to use dead weight loadings. Each test performed used a single point loading to represent the loadings of in-plane and out-of-plane bending. Earlier elastic room temperature tests had indicated no significant difference between the case of a point load and pure bending. Further, in each test, a counter-balance was employed to negate the bending moment at the loaded flange arising from the weight of the moment arm.

A general illustration of the layout of an in-plane loading test is given in Figure (5.12).

Where applicable, measurement of the applied load was achieved using load cells designed with the appropriate end attachments to operate in the range of 0-2000 lbf (Figure (5.13)). These were manufactured from 1 in. diameter EN8 steel bar, turned down and drilled through to give an adequate degree of sensitivity. In order to cope with the large number of possible loadings, a series of ten load cells

were manufactured and calibrated. These were suitably strain gauged in a half bridge configuration such that only axially applied load was measured. Measurement of the load cells was accomplished using a BUDD strain recorder.

5.4.2.2 Creep relaxation in and out-of-plane loading

Under in-plane loading the restraint in displacement was effected by a cross-head running down two threaded bars on each side of the loading arm (Figures (5.14) and (5.15)). The cross-head bearing on the loading arm was at a small distance from the pipe flange and was capable of holding the bend down in a closing mode or up in an opening mode. A "beam" type load cell (Figure (5.16)) mounted on the cross-head with a ball-bearing contact on an extended part of the loading arm enabled the measurement of load reduction. This beam was manufactured from 1 in. diameter EN24T steel bar turned down with flats on two opposite sides. The beam was strain gauged and calibrated in bending giving a sensitivity similar to that of the load cells. In addition to this the two tension rods supporting the cross-head were strain gauged and calibrated in tension to provide a back-up in the event of malfunction of the beam load cell.

In the case of out-of-plane loading the restraint was provided by a threaded bar, strain gauged and calibrated in tension, running horizontally through the loading arm and secured at the two main rear columns.

All the load cells here including the beam type were measured using a BUDD strain recorder.

Again a counter-balance weight was attached to the loading arm to negate its bending moment at the loaded flange.

5.4.3 Measurement of strain

5.4.3.1 Room temperature elastic tests

In the room temperature elastic tests electrical resistance strain gauges (ERSG) of 2 mm, 5 mm and strip gauges of 2 mm gauge length were employed, temperature compensated for stainless steel. Strain readings from the ERSG were recorded using an ELCOMATIC data logger linked to an APPLE computer (Figure (5.17)). The gauges were wired to the internal quarter Wheastone bridge of the unit using the standard three wire technique, minimising the effect of changes in gauge lead resistance [264,265]. By the development of a specific interface card and suitable software, the strain readings were passed to the computer and stored on diskette for subsequent use. The use of the Apple computer did not allow a two-way interface, i.e. the data logger was not controlled by the computer.

Actual values of strain were obtained from the computer via a best fit straight line program.

5.4.3.2 Elevated temperature tests

In the elevated temperature tests, the measurement of strain was accomplished using the CERL-Planer capacitance strain gauge (Figure (5.18)).

During the pilot scheme, a totally manual system of recording the strain was employed. The layout of this system, manufactured by Automatic Systems Laboratries (ASL) [266] is shown in Figure (5.19). For the main creep programme a more sophisticated system was introduced (Figure (5.20)). This comprised an automatic ASL balancing capacitance bridge linked to an Apple computer using a specially

developed interface card allowing a two-way interface between the ASL equipment and the computer (Figure (5.21)). Using the appropriate software the computer reads through each selected channel on the ASL balancing bridge, balancing in sequence. After acceptance on the third balance on each channel the reading is converted to strain using a 5-degree polynomial based on the manufacturer's standard 21 point calibration. The true strain is obtained by the product of this strain and a calibration factor F. This calibration factor arises from the inaccuracy in using the standard calibration to measure bending strains, and was the result of an intensive research programme carried out at the University. This is discussed more fully in CHAPTER (6).

The introduction of a computer linked measurement system helped significantly in the problem of data retrieval. It was also useful during the initial loading of bends at temperature. Here the linearity or non-linearity could be checked at a glance using a graphics routine incorporated in the software.

5.4.4 Measurement of displacement

5.4.4.1 Rotation

As defined in CHAPTER (1), the flexibility factor of a pipe bend with connected tangents can be written as:

$$K = \frac{\gamma - \gamma_T}{\gamma_o}$$

where γ = the overall rotation of the bend assembly as measured between both flanges

γ_T = the relevant rotation of both tangents

γ_o = the nominal rotation . . . *(5.1)*

For both in-plane and out-of-plane loading measurement of the overall rotation was accomplished using dial gauges measuring the displacement at two fixed points of an angle or box section bolted to both flanges (Figure (5.22)). Using this method the overall rotation can be determined from:

$$\gamma = \tan^{-1}\left[\frac{d}{\ell}\right]$$

where d = difference in travel between two associated dial gauges

ℓ = fixed distance between dial gauges . . . (5.2)

For a 90° and a 45° bend under out-of-plane loading only one dial gauge at the fixed flange was required to measure the rotation as at this point the primary displacement arises from torsion. This is discussed earlier in CHAPTER (4) on the out-of-plane loading on flanged bends.

A summary of the flexibility factors for both the case of in-plane and out-of-plane loading, for bend angles of 180°, 90° and 45° is given in APPENDIX (7).

5.4.4.2 Distortion

The method of measurement finally adopted for measurement of distortion of the cross-section involved the use of eight 3 in. lengths of $\frac{1}{4}$ in. square stainless steel type 316 welded to the surface of the bend (Figure (5.23)). These rods, pointing radially outwards, were spaced equidistantly around the bend cross-section, beginning at $\phi = 0$, and were of sufficient length to be just visible above the insulation. The actual measurement of distortion was accomplished by measuring the displacement between two diametrically opposite rods using

a specially manufactured U-shaped steel bar incorporating a dial gauge (Figure (5.24)). The dial gauge was eventually replaced by a displacement transducer which allowed the operation to be performed by one person. Measurement of distortion was performed normally at one section only, as close as possible to the bend centre. This particular method allowed the measurements to be taken at various locations along the bend and removed the problem of relative movement between the bend and the measuring system displayed by earlier methods. This is discussed in section (6.2.2).

5.4.5 Heating system and control

Heating of the bend assembly was accomplished by encasing both tangents and the bend section in a pre-fabricated copper sheath $\frac{1}{8}$ in. thick. The sheath was manufactured by hand in two halves for each part to enable ease of attachment and removal. Three heating tapes (ITQ-250-ISOPAD [267]) providing the heat source were then wound along the length of the bend. A typical layout is shown in Figure (5.25). Temperature control was by a thermocouple activated zero crossing switch box (CSW/1000 ISOPAD), using a thermocouple from the central section of the bend. Measurement of the temperature variation was done using a number of thermocouples (CHROMEL ALUMEN DKIO) spot welded to the outside surface at various locations around the bend as shown in Figure (5.26).

Insulation of the bend was provided by two layers of 8 lbf/ft^3 blanket (TRITON KAOWOOL [268]) on the exterior. The interior of the bend was left empty. Heat losses at the flanges were minimised using a heat barrier gasket (TRITON KAOWOOL STRONG BOARD) and a $\frac{1}{2}$ in. thick blank flange to prevent plugging of the gasket.

The use of the copper sheath in heating the bend removes the discrete form of heating produced by the heating tapes leading to an improved and more uniform temperature distribution. Its implementation was the result of development work carried out at the University reported in [269].

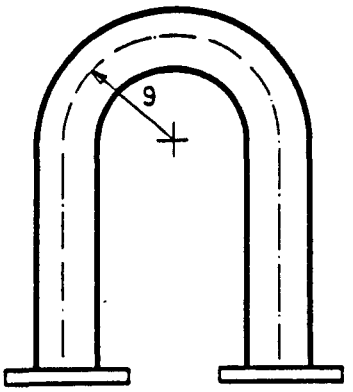

180° BEND

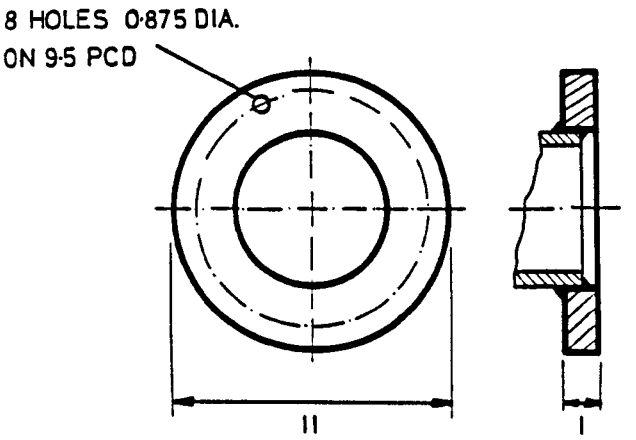

FLANGE DETAIL

DIMENSIONS IN in

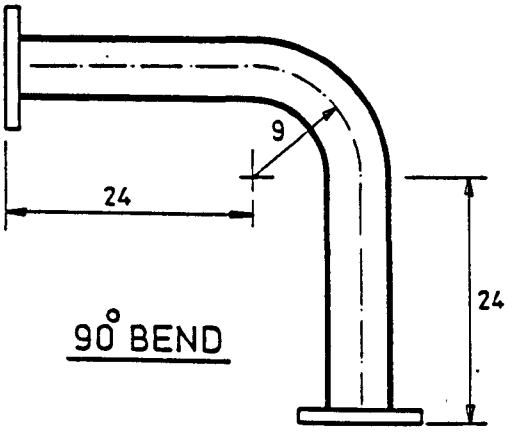

90° BEND

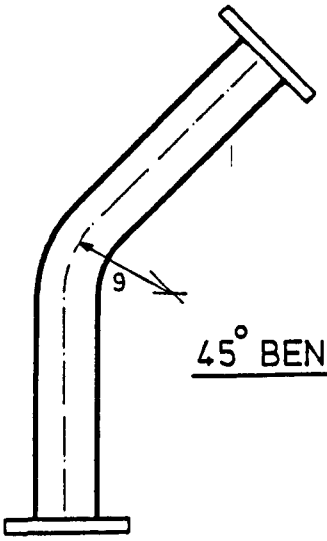

45° BEND

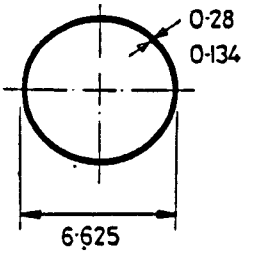

CROSS-SECTION

BEND ASSEMBLIES

FIG. 5.1

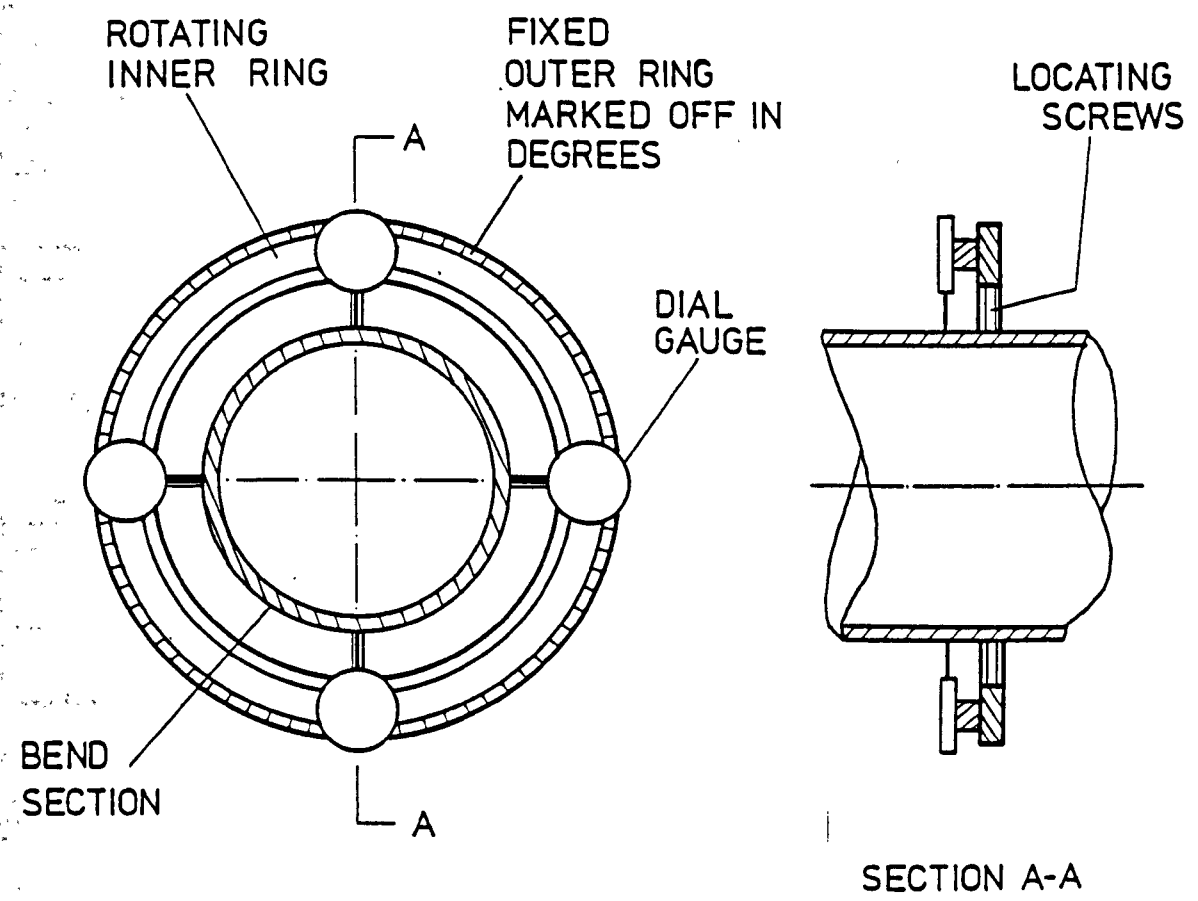

MEASUREMENT OF OVALITY

SIGN CONVENTION :- DIAL GAUGE READING INCREASES (+ve)
RADIUS INCREASES

FIG. 5.2

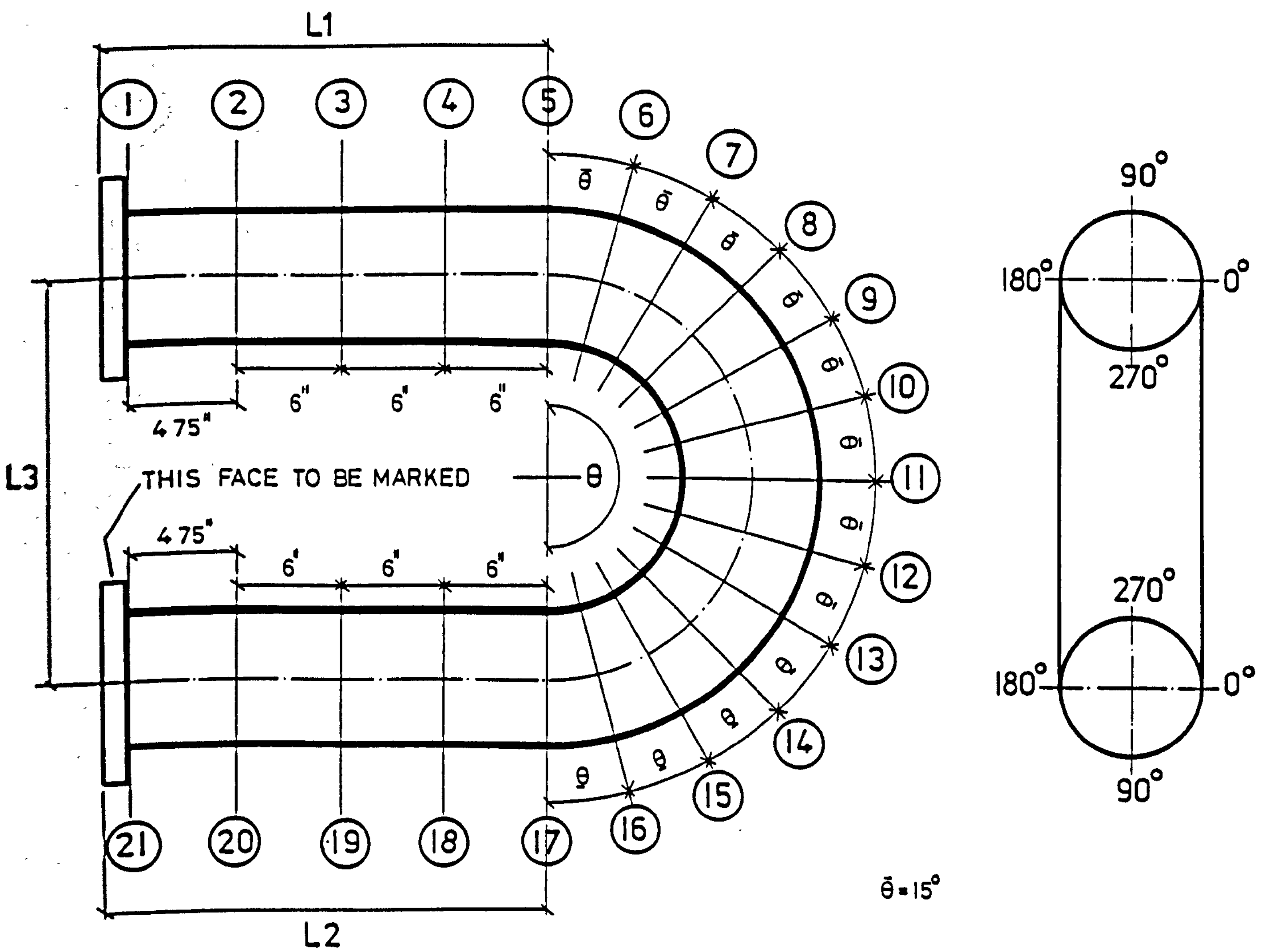

180° BEND ASSEMBLY

FIG. 5.3

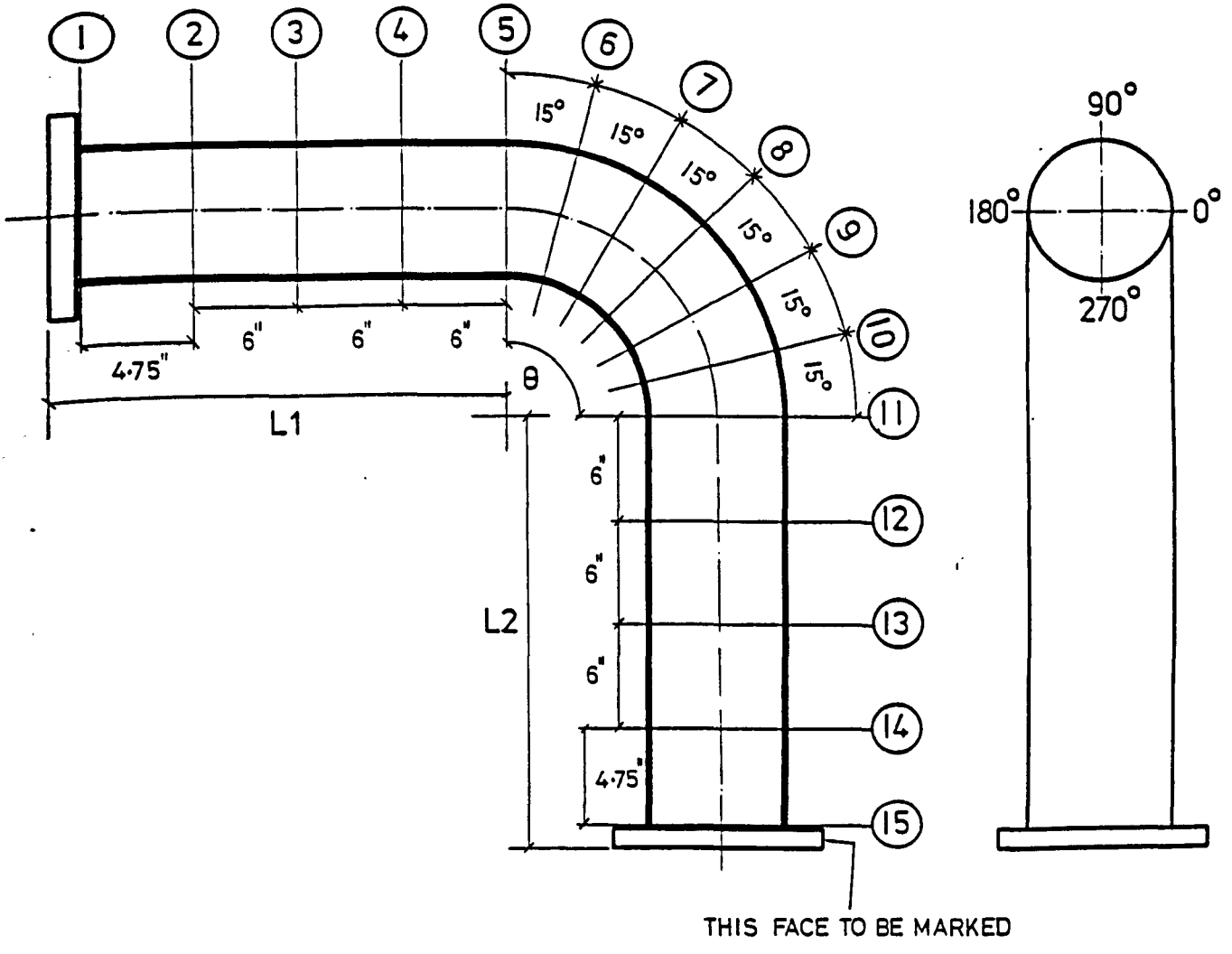

90° BEND ASSEMBLY

FIG. 5.4

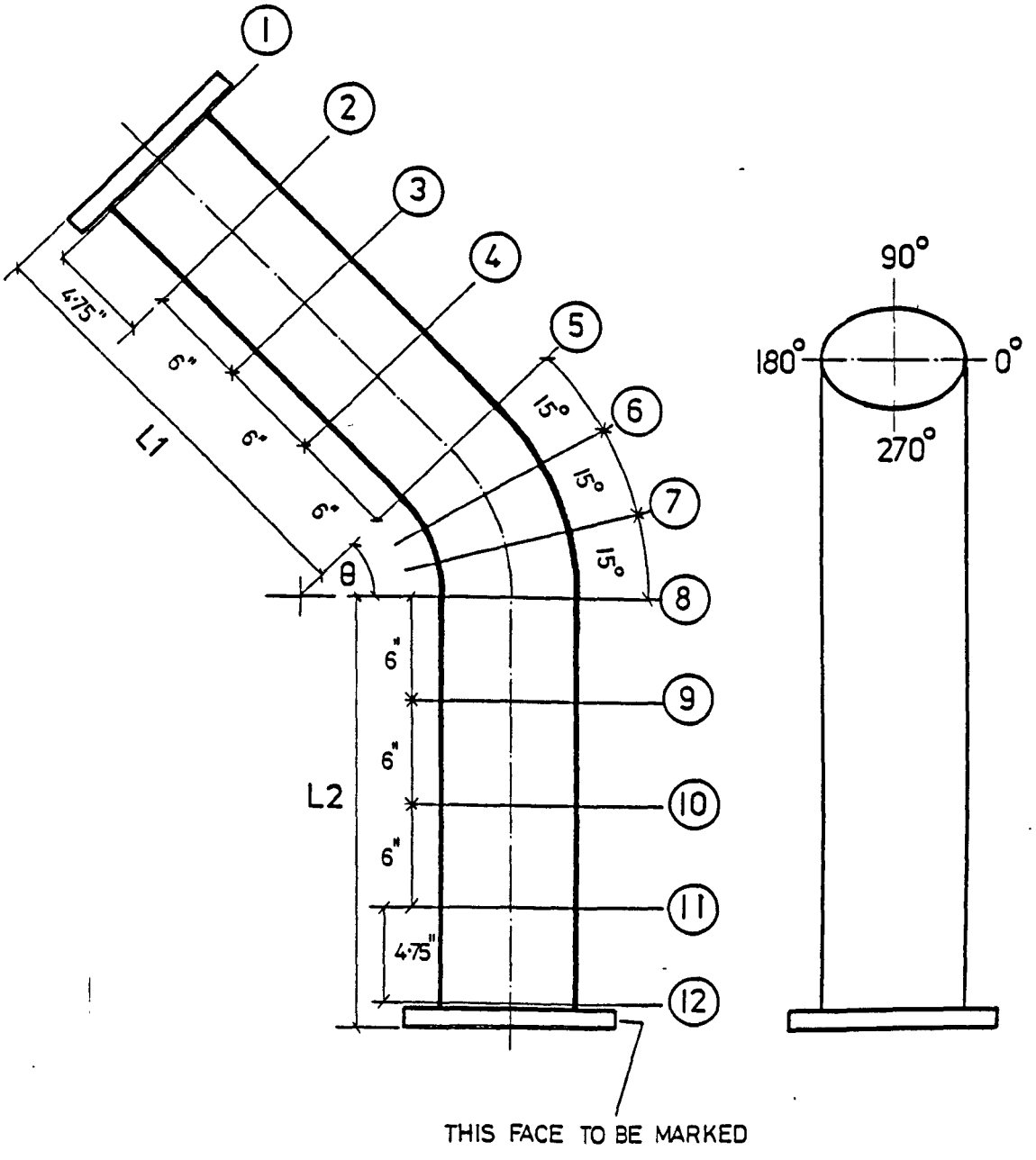

45° BEND ASSEMBLY

FIG. 5.5

45° & 90° TEST RIG

FIG.5.6

180° TEST RIG

FIG. 5.7

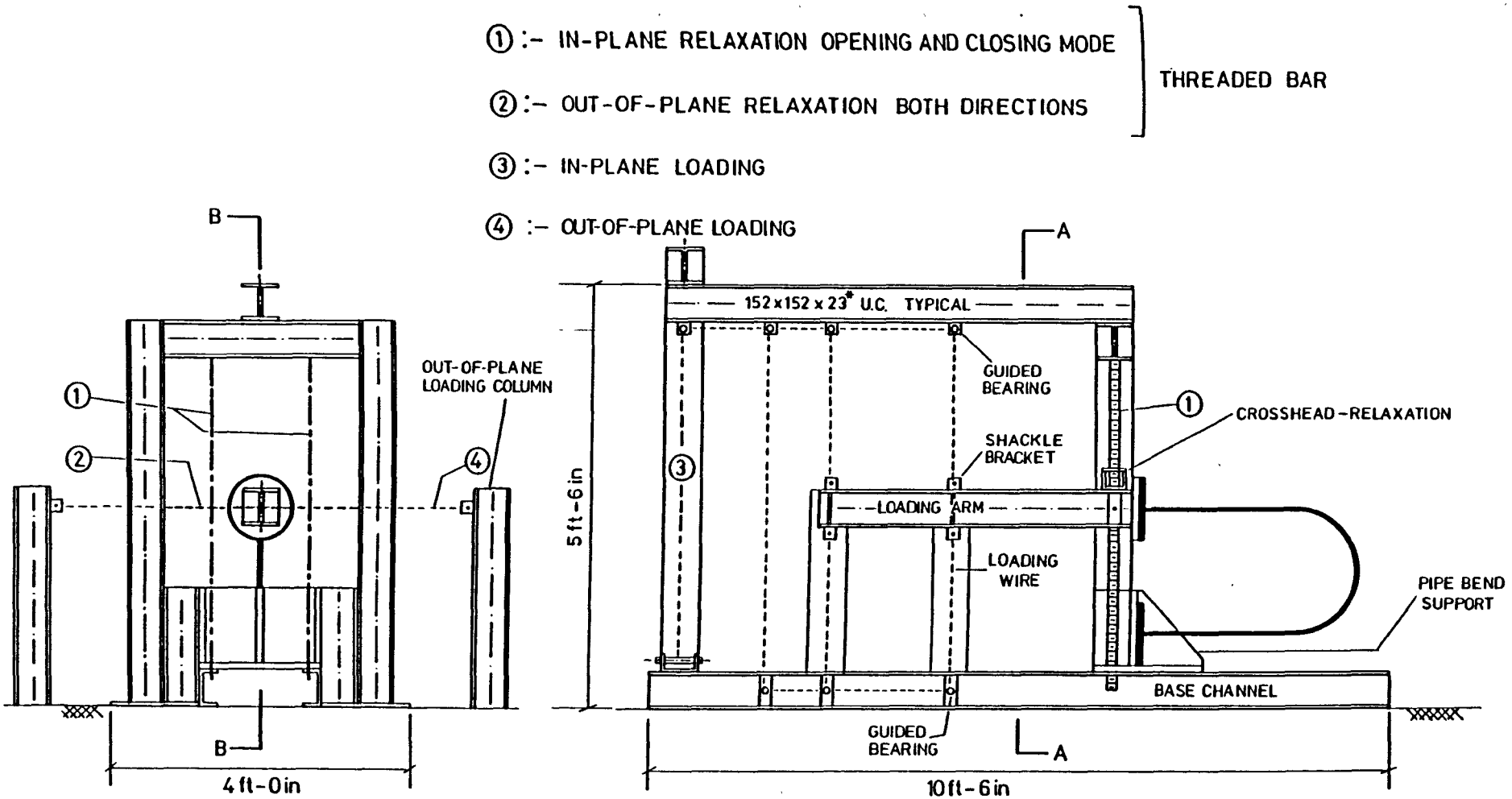

FIG. 5.8

LAYOUT OF TEST RIG

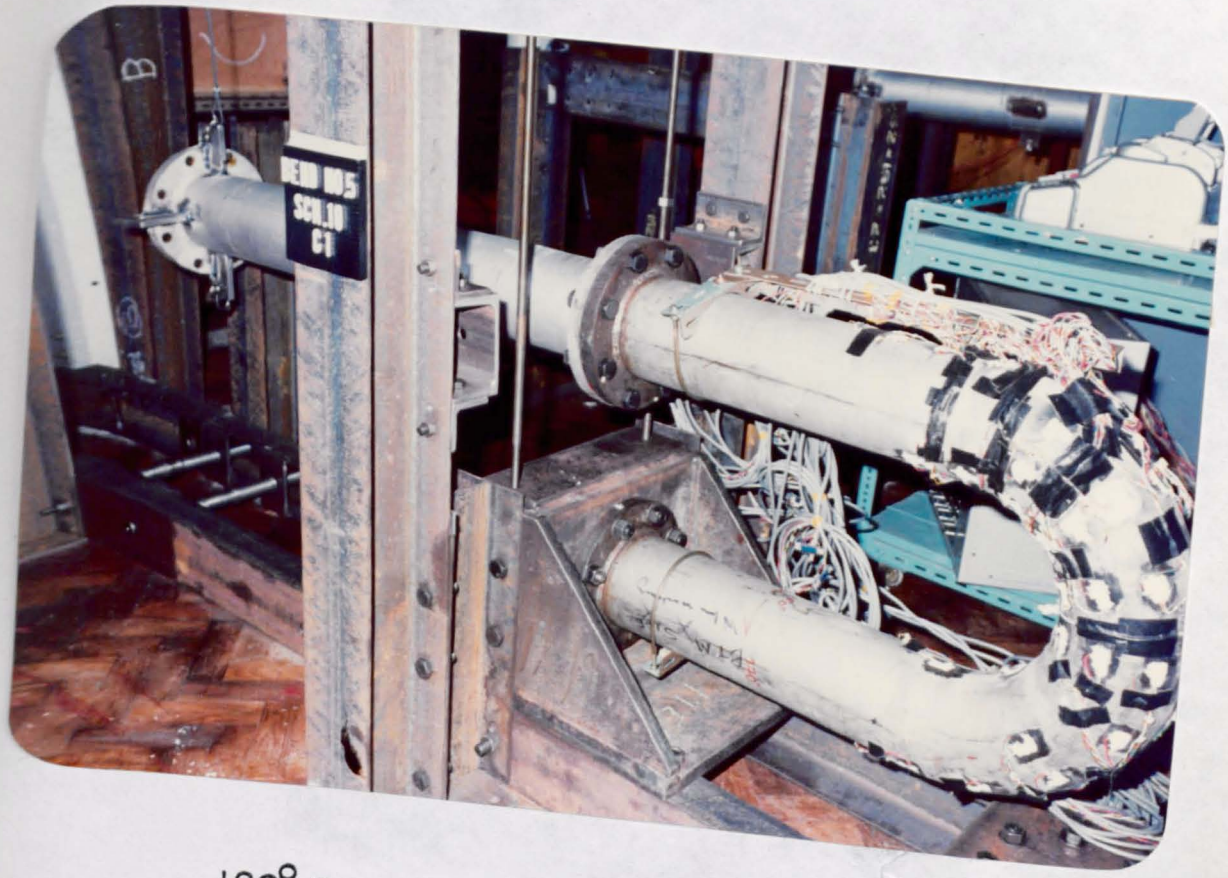

180° BEND BASE SUPPORT

FIG. 5.9

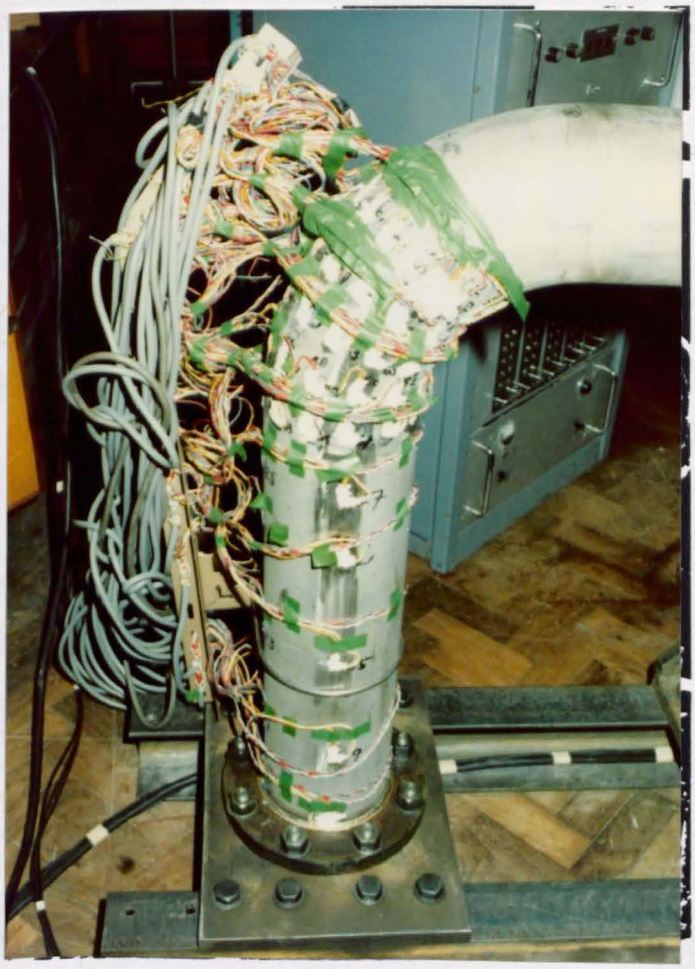

90° BEND BASE SUPPORT

FIG.5.10

OUT-OF-PLANE PORTALS

FIG. 5.11

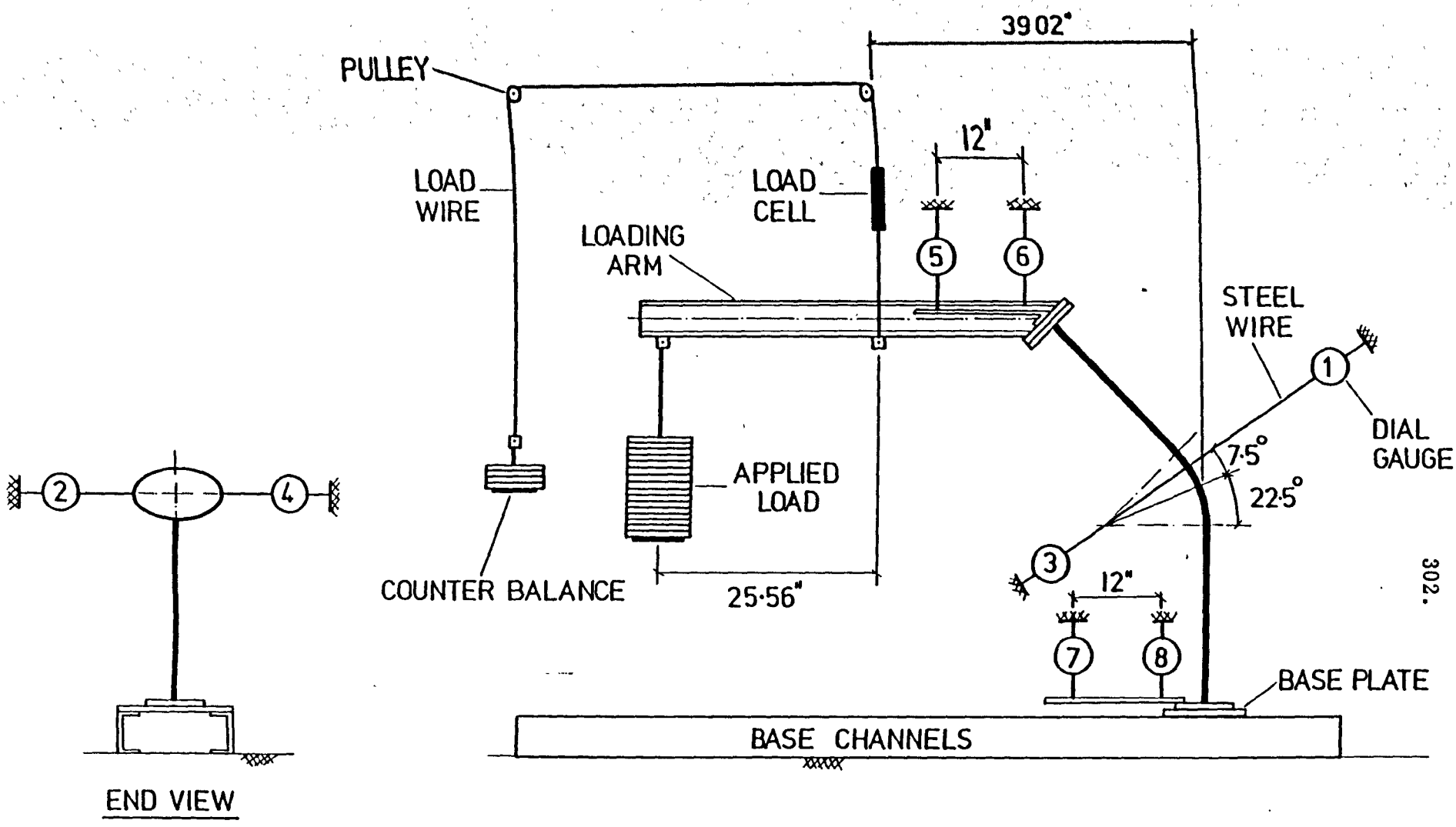

FIG. 5.12 TEST LAYOUT

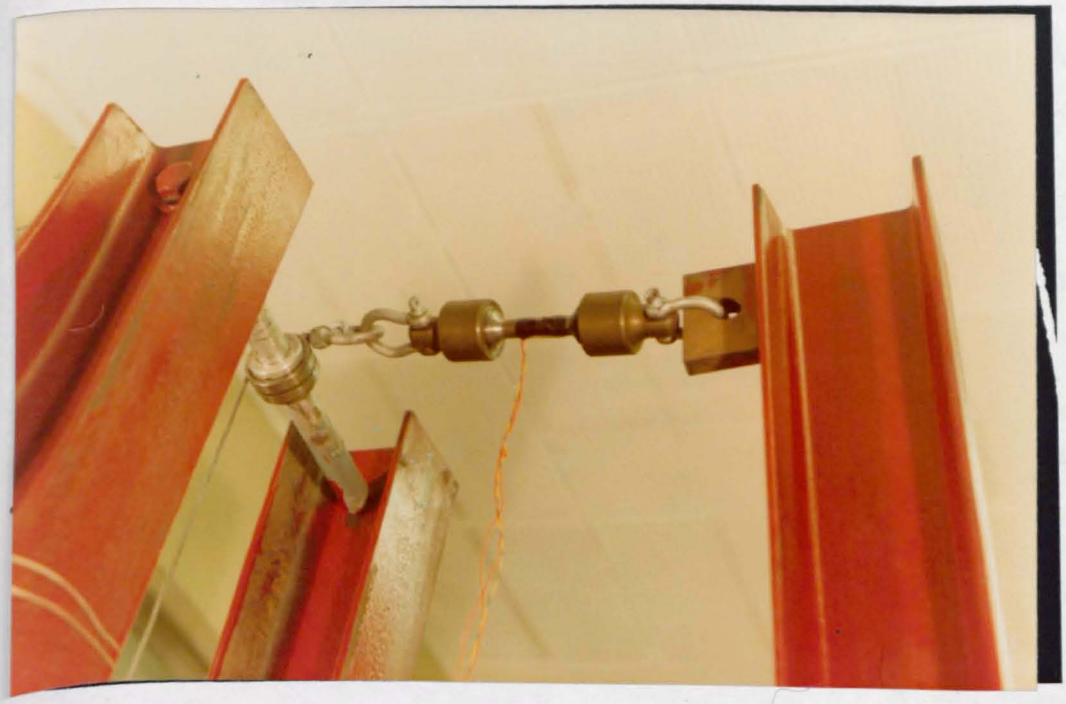

LOAD CELL

FIG. 5.13

IN-PLANE RELAXATION TEST

FIG.5.14

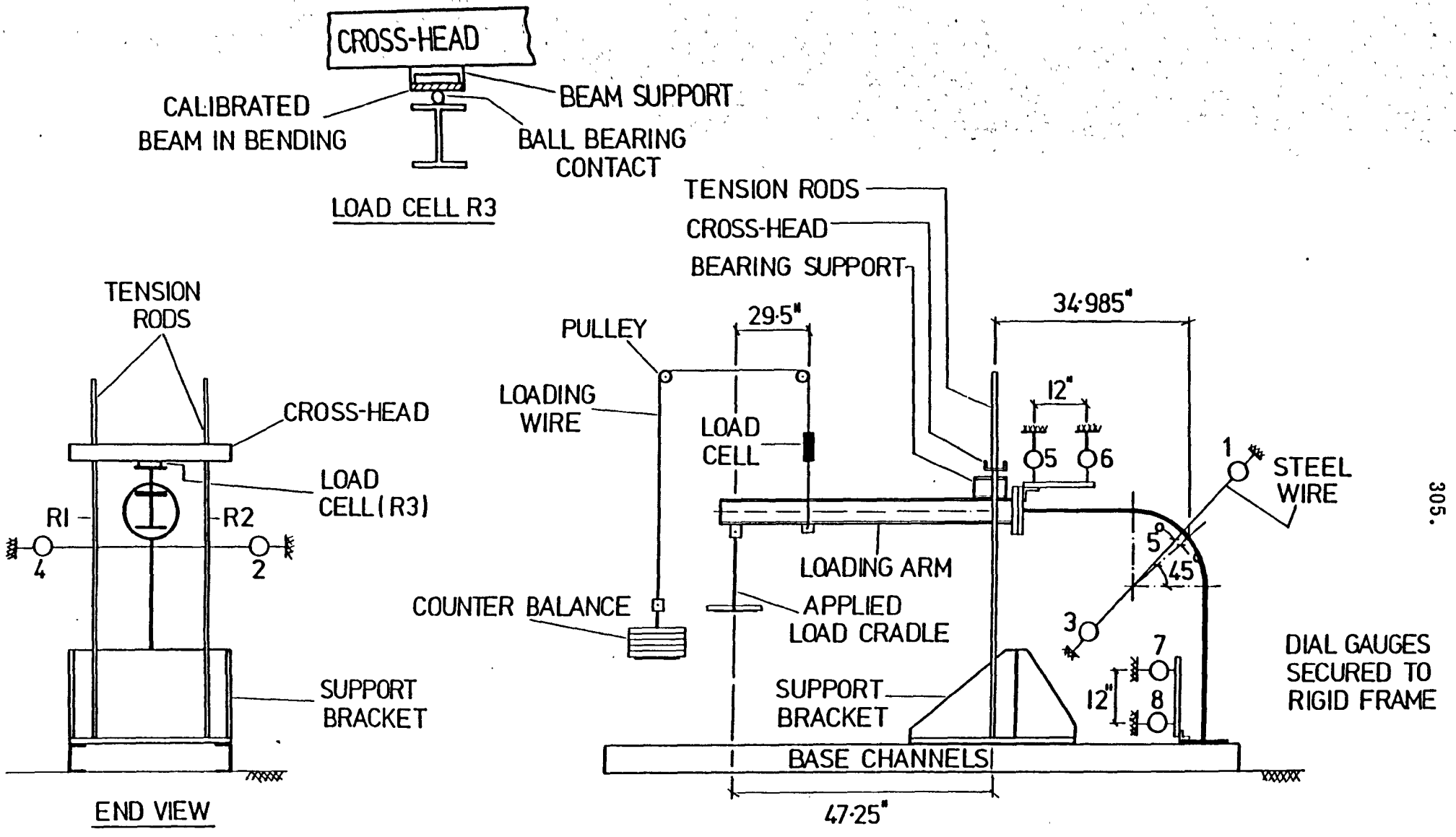

FIG.5.15 TEST LAYOUT

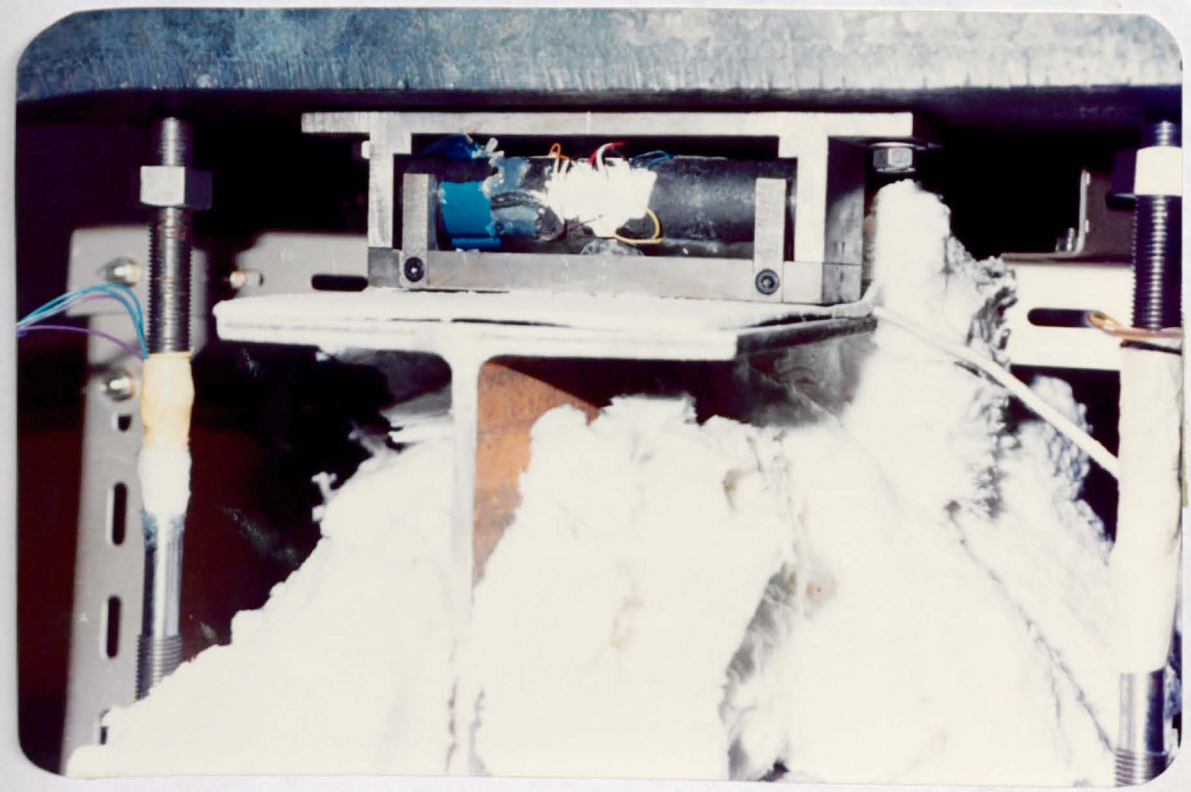

RELAXATION LOAD CELL

FIG. 5.16

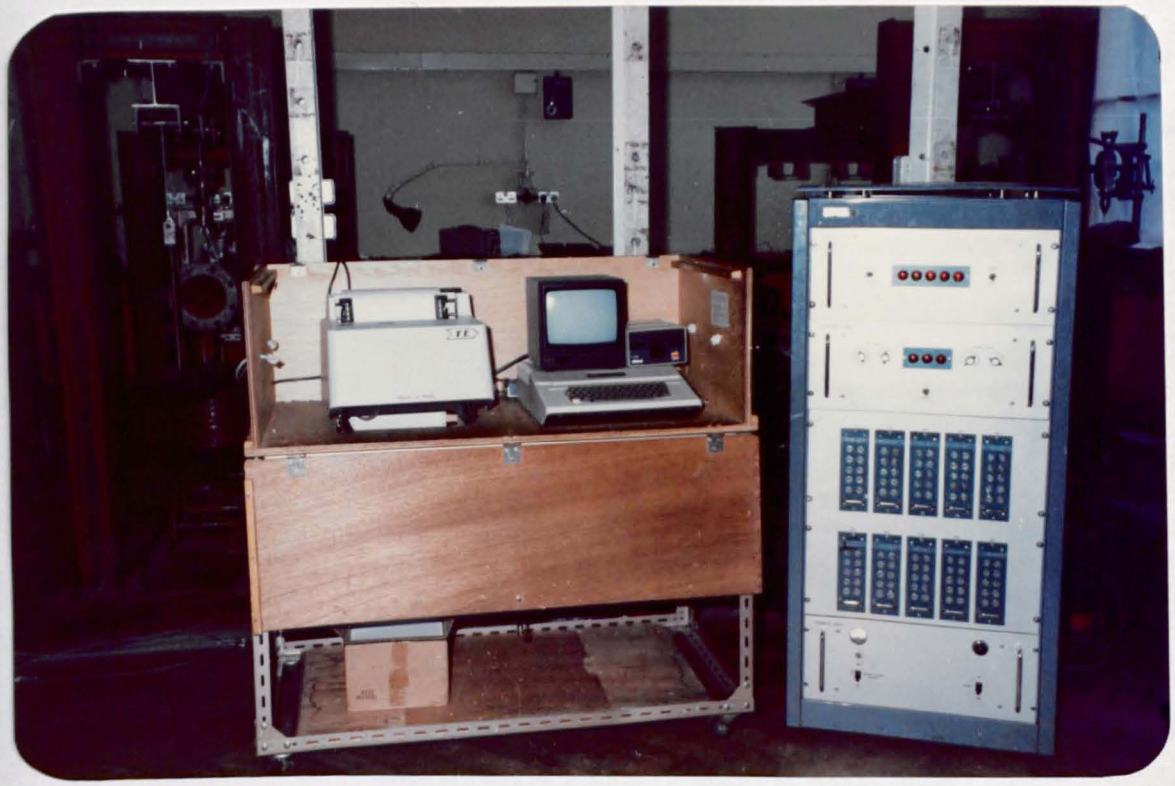

APPLE-ELCOMATIC UNIT

FIG. 5.17

C.E.R.L.-PLANER
CAPACITANCE STRAIN GAUGE

FIG. 5.18

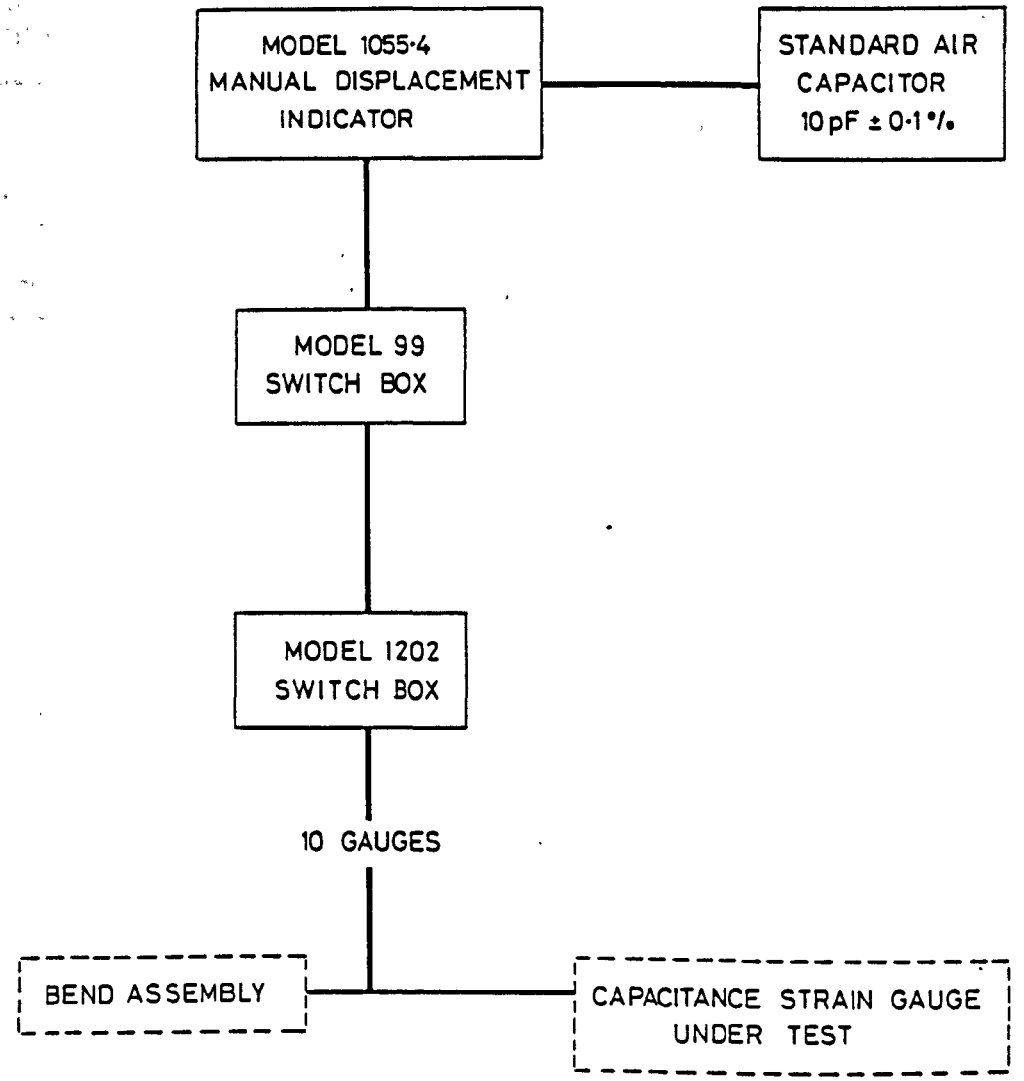

MANUAL SYSTEM
OF
CAPACITANCE STRAIN GAUGE
MEASUREMENT

FIG. 5.19

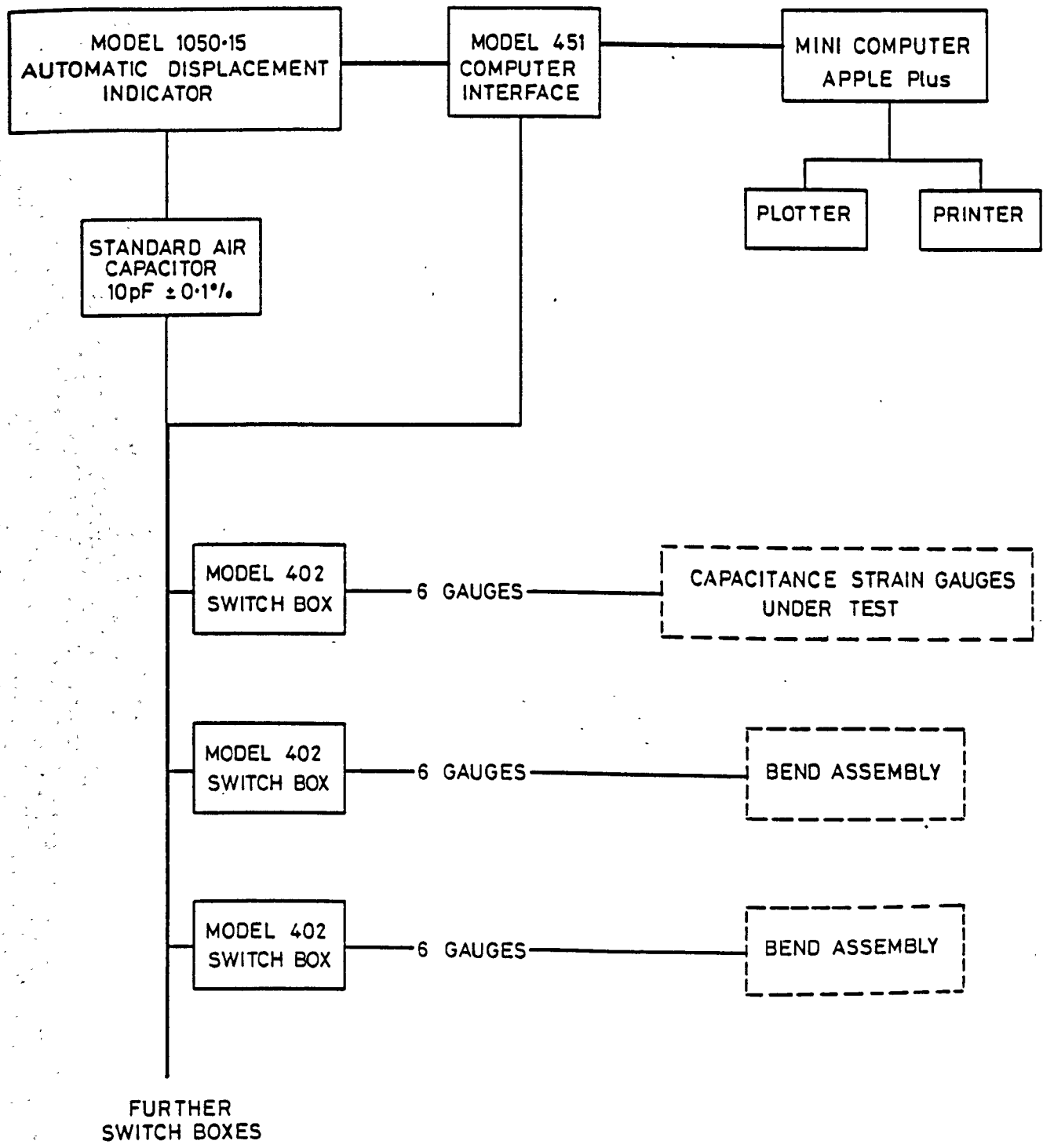

AUTOMATED
CAPACITANCE STRAIN GAUGE
MEASUREMENT
FIG.5.20

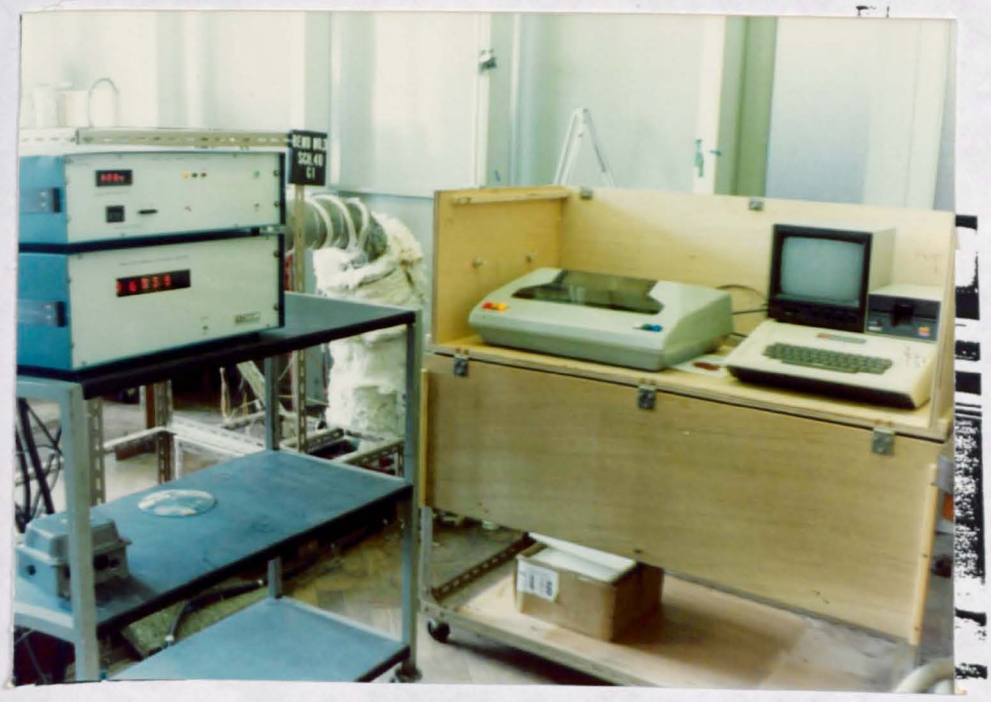

APPLE A.S.L. UNIT

FIG. 5.21

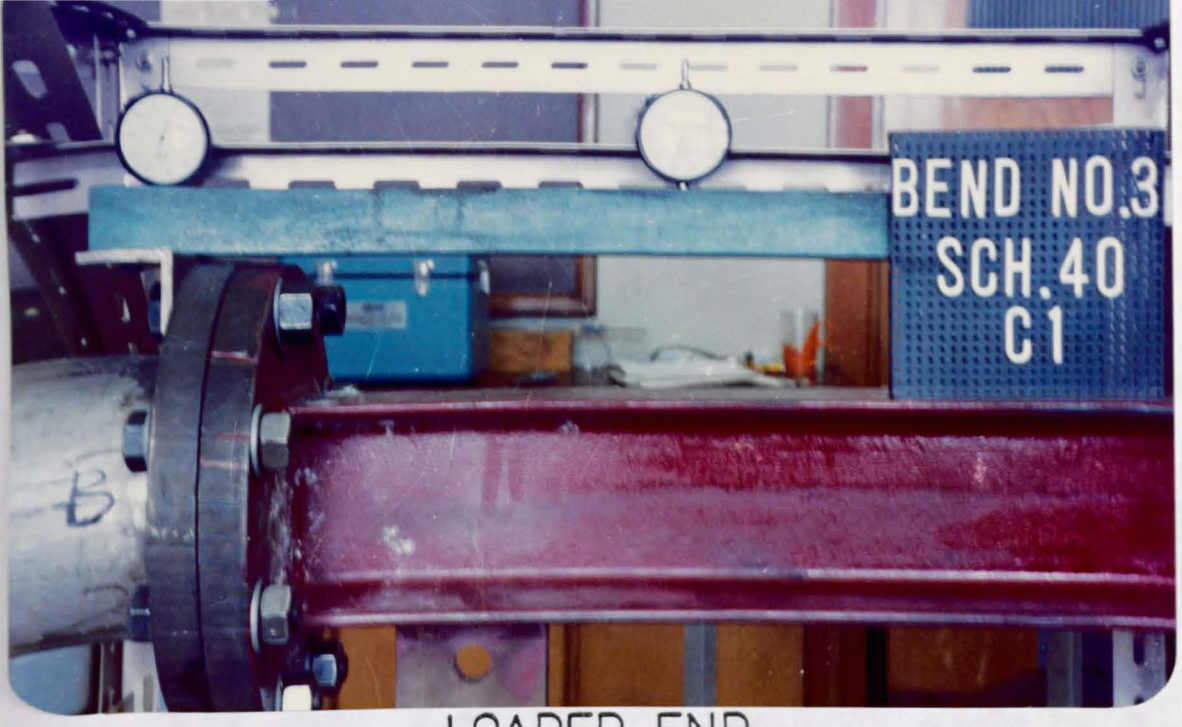

LOADED END

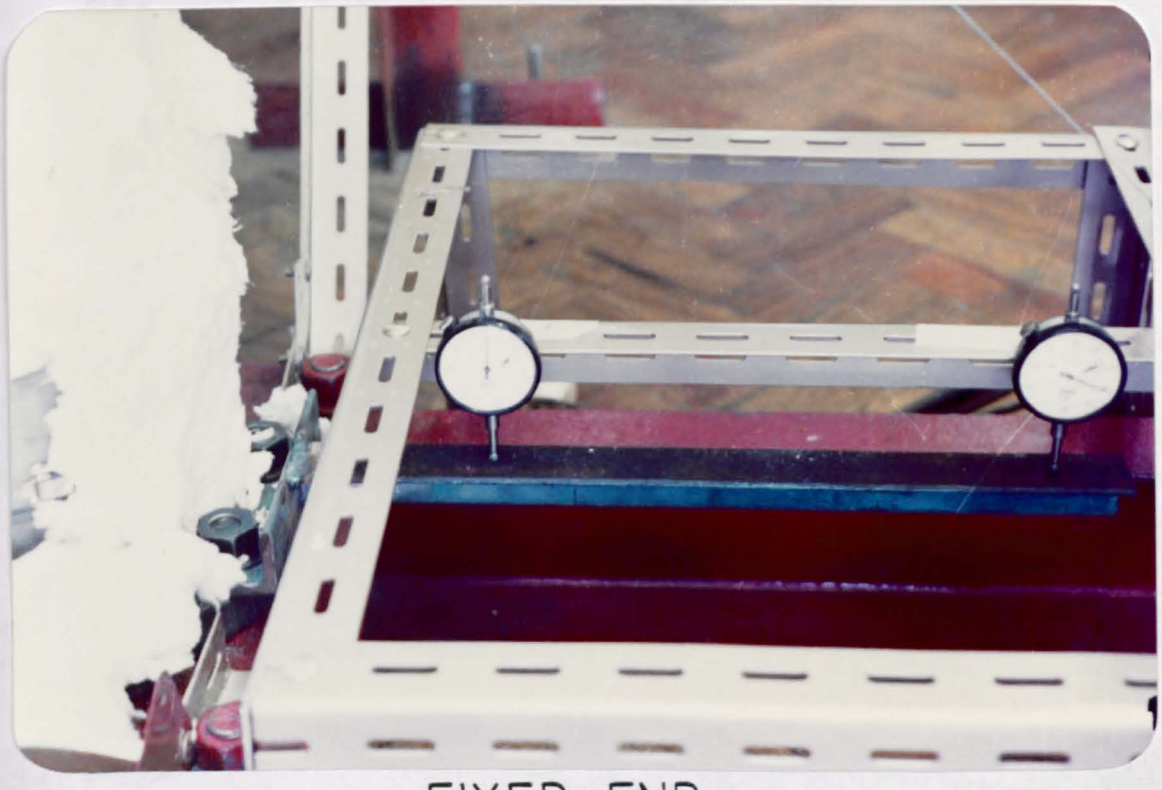

FIXED END

MEASUREMENT OF ROTATION

FIG. 5.22

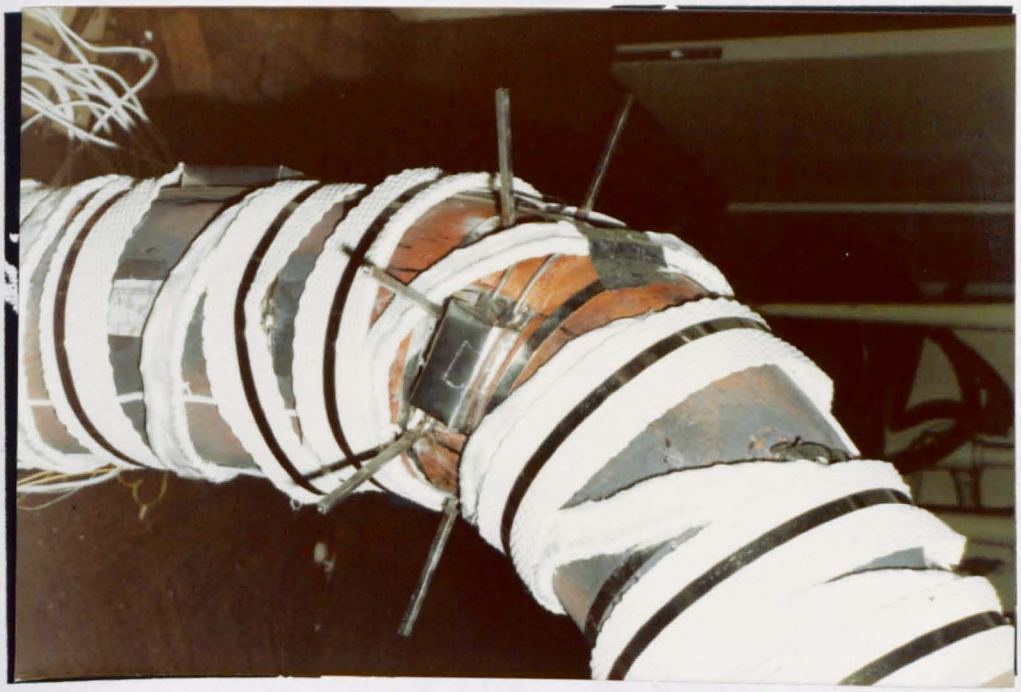

MEASUREMENT OF DISTORTION

FIG. 5.23

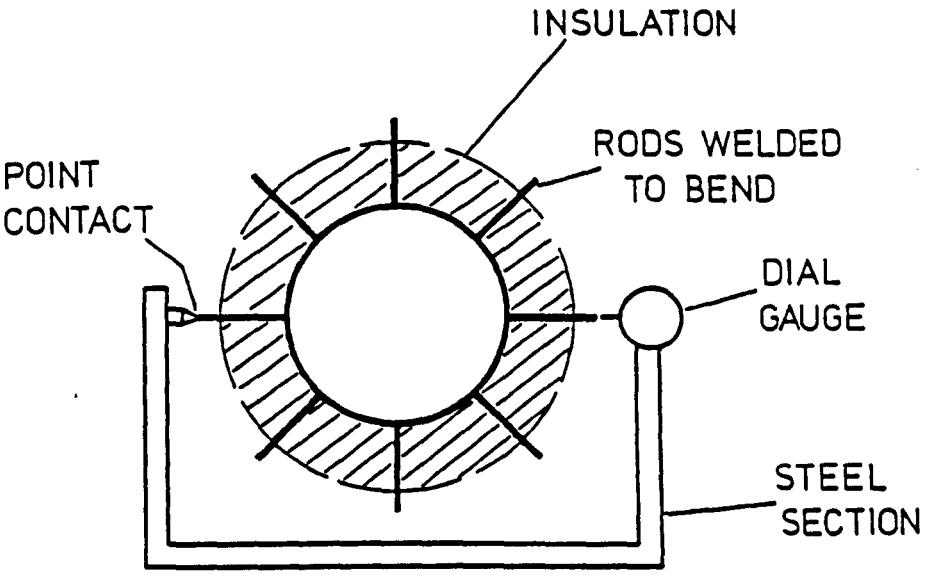

MEASUREMENT OF DISTORTION

FIG.5.24

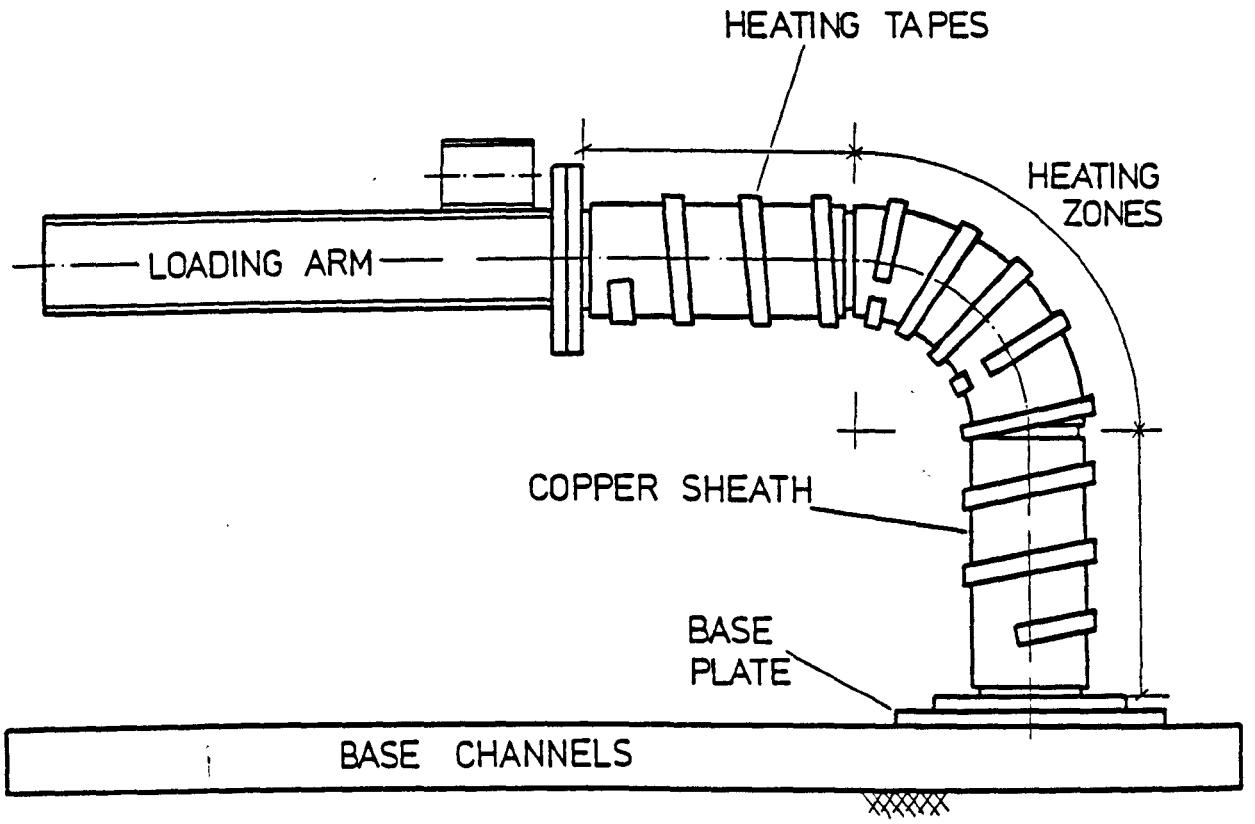

GENERAL LAYOUT OF HEATING SYSTEM

FIG. 5.25

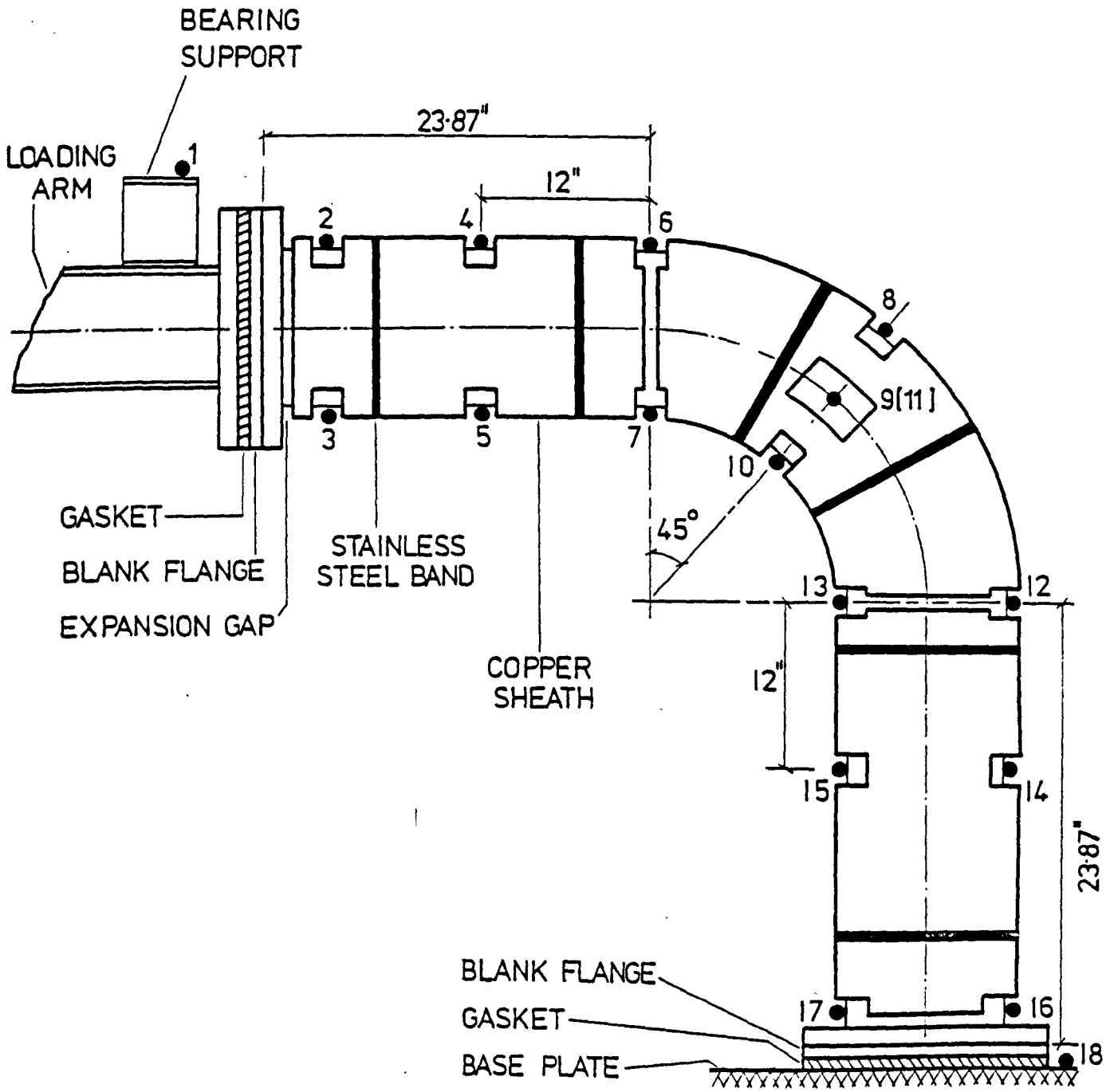

LAYOUT OF THERMOCOUPLES

FIG. 5.26

CHAPTER 6

Development of Experimental Techniques

ABSTRACT

The theory, and application of the capacitance strain gauge to the measurement of strain on pipe bends is discussed. From development work conducted on the CERL-Planer capacitance gauge experimental techniques are presented to ensure accurate results.

The development of methods of displacement measurement for distortion and rotation are presented.

Details are also presented on a novel and economic bend heating system designed to give a uniform temperature distribution around the bend.

Finally, the experimental results from a number of tests performed on the pipe bends at room temperature and elevated temperature are given.

CHAPTER (6)

DEVELOPMENT OF EXPERIMENTAL TECHNIQUES

6.1 Application of the CERL-Planer Capacitance Strain Gauge

6.1.1 Development of the capacitance strain gauge

The variation of electrical resistance as a means of measuring strain was first developed by BRIDGMAN [270] in 1912. Since then the techniques in the use of the electrical resistance strain gauge (ERSG) have become well-established. Their general application is, however, limited to temperatures in the range 10°C to 200°C [271]. At temperatures above this range the invariant nature of the gauge characteristics can no longer be guaranteed. Attempts to increase the temperature range have been the subject of extensive research by several investigators, each with varying degrees of success [272-275].

In the measurement of dynamic strains at temperatures around 1000°C, the weldable ERSG-AILTECH [276], has achieved a limited degree of success. However, the unpredictable response of the ERSG under prolonged use makes them unsuitable for creep measurements. The main problem arises from the fact that it has not been possible to find a resistance alloy having basically stable and repeatable resistance-temperature characteristics. Further, the materials suitable for bonding the resistance wires to the test surface, whether directly or indirectly, have limited insulation capabilities at higher temperatures. This particular problem is eliminated in the weldable ERSG.

In 1945, CARTER, SHANNON and FORSHAW [277] proposed an alternative method of strain measurement using capacitance as opposed to electrical resistance. Two types of capacitance gauge were developed which they termed "varying-gap" and "varying-area pick ups". They suggested that these devices could have a useful application where

the temperature was beyond the limits of the ERSG. In fact, a consideration of the principle of capacitance devices shows that the fundamental problems inherent in the use of the ERSG can be avoided. For a simple parallel plate capacitor:

$$c \alpha akt$$

where c = capacitance

a = area of the plate

k = dielectric constant

t = distance between the plates . . . *(6.1)*

Thus the capacitance can be varied by changing the area a, or the gap t. Further, in using air as the gap the dielectric constant is only marginally effected by changes in temperature. This means that capacitance devices can be made to depend only on geometrical features. Provided the capacitor terminals are isolated from earth, the electrical properties of the materials used are relatively unimportant, so that they can be chosen to meet the mechanical requirements. This provides a significant advantage over resistance wires.

However, progress in the development of the capacitance strain gauge was severely hindered by the inability to measure the small values of capacitance associated with such devices and it is only in recent years that such problems have been overcome. Using what is termed the "three terminal method" it is now relatively easy to measure gauge capacitance of less than 1 pF with a sensitivity of the order of 10^{-4} pF and a resolution of similar order. A major problem in the measurement of capacitance was that the capacitance instabilities of the connecting cables, which were significant in terms of the gauge capacitance, could

not be isolated from the gauge signal. Some idea of the small values of capacitance being measured can be seen by considering a simple parallel square plate capacitor with a gap (in air) of 1 mm. To have a capacitance of 1.0 F (10^{12} pF) the side of each plate must measure 1.06×10^{4} m (6.6 miles). Thus the "pico-farad" is an extremely small measure of capacitance.

Where small movements are to be translated into changes of electrical capacitance it is usual for the variable to be the gap of the parallel plate capacitor. The sensitivity of such a change can be increased if the initial gap is small. If mechanical amplification can be introduced, further increases in sensitivity result, with an additional increase in stability. Such a mechanical amplification can be devised by using two small arches made of thin metal strip. The arches are of equal span but differing heights, giving a gap between the two arches. Tangential capacitor plates are fixed to the crowns of the arches inside the gap. The ends of the gauge are welded to the surface under test and as the surface strains, the movement across the ends of the arches is converted into a larger movement, normal to the surface, across the capacitor plates. This is the principal of the CERL-Planer capacitance gauge (Figure (6.1)) developed by NOLTINGK *et al* [278,279]. The gauge was developed with particular application to the power generation industry being funded by the CEGB and G.V. Planer Ltd. It is designed to operate in air at a temperature of 650°C and is manufactured from a nimonic alloy in such a fashion that in its "free" unmounted form it has approximately equal range in two directions of at least $\mp 0.5\%$ strain. On attachment to the surface under test the gauge can be offset from this free position to give the full 1% strain

measuring capability in the chosen direction. As can be seen in Figure (6.2) a horizontal displacement of the feet of the gauge results in a non-linear relation between capacitance and strain. This is the form of calibration normally supplied by the manufacturer. However, due to the dimensional tolerances employed in production each gauge will have a different capacitance-strain relation, hence each gauge must be calibrated prior to use. Changes in material, heat treatment and improvements in construction has led to two gauge types designated C4 and C5 for use on ferritic and austenitic materials, respectively. Each gauge has a nominal gauge length of 19.0 mm although a smaller gauge length is currently being developed.

Two other capacitance gauges have been developed, namely, the HUGHES gauge and the BOEING/HITEC (BH) gauge. Due in part to its restricted application the Hughes gauge is no longer available. Application of the BH gauge has also been restricted to some extent, as a result of the high cost. For completeness, a brief description of these gauges is given.

The Hughes [280] capacitance gauge was developed to measure strains induced by aerodynamic forces and temperature changes over a relatively short period of time. The gauge comprised a rhombic frame (Figure (6.3)) incorporating a multi-plate design of capacitance plates and was designed to operate for 30 mins at a temperature of 1100°C. The working range in strain at 950°C was given as $\mp 0.2\%$.

The BH capacitance gauge was a joint development of the Boeing Company and the NASA Flight Research Centre [281]. The design of this gauge differs considerable from the Hughes and the CERL-Planer gauge. As the dimensions of the test surface change due to

strain the outer cylinder (Figure (6.4)) moves axially with respect to the two inner cylinders, changing the differential capacitance. The working temperature is given as 800°C with a corresponding strain range of ∓2.0% with a gauge length of 25 mm. A reduced gauge length of 6 mm results in an increased strain range of ∓8.0%.

A further development in the capacitance gauge has appeared recently from work being conducted by INTERATOM [259], mentioned earlier in CHAPTER (5). Details of this development are not clear as the publication (in German) has only recently come to the author's attention. It would appear, however, that the gauge gives a working strain range of ∓1.1% at a temperature of 650°C.

Recent comparisons [282-284] of the capacitance and resistance gauge suggest that the capacitance strain gauge offers the most promise for the measurement of prolonged strain at elevated temperature. They are, however, expensive. For the CERL-Planer gauge, the cost of one gauge and two mineral insulated leads approaches £300.00. The cost of the BH gauge is not known, although it is believed to be around two to three times that of the CERL-Planer gauge. Resistance gauges, particularly encapsulated weldable ones [285], show promise though their erratic behaviour makes them suspect for creep measurements. It is of interest to note that this gauge type is being used extensively on the elevated temperature tests on pipework components by PNC [258]. However, it is likely that because of their convenience and economy, research will continue to develop techniques to make them more reliable.

6.1.2 *Measurement of strain in pipe bends*

The CERL-Planer capacitance gauge has been used extensively by CEGB in a variety of "in-situ" and laboratory applications at normal and elevated temperatures with apparent success. However, most of the published literature deals with their performance and drift characteristics over prolonged periods, which for the most part have been shown to be satisfactory [286-289].

In the application to pipe bends it is evident from the previous chapters in PART (1) of this text that meridional bending strains will predominate when the pipe bend is subject to moment loadings. In [278] Noltingk *et al.* discussed the sensitivity of the gauge to bending strains and to account for this he suggested that the gauge be considered as 0.05 mm above the surface. Essentially, this was an attempt to increase the measured strain and was the result of two tests carried out on different beam sections. Apart from this work, the author has been unable to discover any other work dealing specifically with this application.

During the pilot scheme it was found that, under room temperature elastic conditions, the measurement of these strains using the CERL-Planer gauge led consistently to an underestimation in strain of between 20% to 30%[*1]. This level of inaccuracy, assuming it remains the same at elevated temperature, has been considered acceptable in the measurement of creep strain [290]. As this invariance with temperature could not be firmly established an attempt was made at improving the comparison. However, in doing so further problems[*2] were encountered and

---

[*1] Based on tests conducted on schedule 40 bends.
[*2] Tests conducted on schedule 10 bends showed that this comparison deteriorated even further to values around 70%.

as a result an intensive investigation into the behaviour of the gauge was begun. This work was considered in two parts. The first part, which was reported in [291] and is presented in APPENDIX (8), dealt with the behaviour and response of the gauge under room temperature elastic conditions. The second part, and perhaps the most difficult in terms of experimental work, was intended to examine the behaviour of the gauge at elevated temperature and in so doing establish the validity of the room temperature gauge calibration. Unfortunately, due to limitations in cost and time this work was not completed. However, it is hoped that the work reported in [291] will act as a stimulus for other researchers in the field.

From the room temperature study two main conclusions can be drawn:

1. In mounting the gauge on curved surfaces in which the radius of curvature is less than a nominal value of 250 mm it is preferable to bend the feet of the gauge as opposed to the use of wedges in providing an adequate contact area.

2. Gauge calibrations conducted under in-situ conditions were shown to be essential for accurate results.

Bending the feet of the gauge is, of course, a delicate operation and a special jig was made for this purpose. There are of course limits to which the feet can be bent in order to retain operation of the gauge. These limits, however, were not explored.

The matter of gauge calibration is of a more general application and should be included where possible as normal practice. Calibration

under in-situ conditions can in some instances limit the strain range. However, with judgement and commonsense it should be possible to produce a representative model of the actual conditions.

The gauge calibration provided by the manufacturer, as mentioned earlier, is based on a horizontal displacement of the gauge feet. The calibration is performed on a flat-bed micrometer. With hindsight, it should have been obvious from the beginning that where bending strains predominate such a displacement is incapable of describing the overall movement.

6.2 Measurement of Displacement

6.2.1 Rotation

In the measurement of rotation a number of methods were examined:

1. dial gauges
2. rotating mirror
3. inclinometer

The method using dial gauges, as described in section (5.4.4.1), was the main method adopted throughout all the room temperature and elevated temperature tests. The main attraction being their ease and simplicity in use. Further, they can be adapted easily to cope with in-plane or out-of-plane loading. The replacement of the dial gauge with a transducer, in particular a capacitance transducer, to link up with the capacitance gauge measuring system was considered. However, the high cost did not justify the replacement of a perfectly adequate although perhaps unsophisticated device.

The rotating mirror was employed on a few room temperature elastic tests. The principle of this method is shown in Figure (6.5). For measurements of the overall rotation two sets of readings are required, i.e. at the loaded flange and at the fixed flange. The method was not considered suitable in the elevated temperature tests.

Inclinometers as a means of measuring rotation are being used extensively in tests being conducted by CEA [292]. Their principle in operation is generally based on a change of inductance in a pendulous, oil-damped spring-mass system. As distinct from this type a strain gauge inclinometer has been developed at Imperial College, London. The particular application of this development is not known. Details of the instrument are given in [293].

A review of the currently available types [294,295] indicated that the cost would be prohibitive. As a consequence of this the development of an in-house strain gauge inclinometer was begun. A prototype of this instrument is shown in Figure (6.6). The idea is based on a cantilever beam attached to the specimen at the fixed end and loaded at the free end by a small weight. Rotation of the fixed end is calibrated against the longitudinal strain developed in the beam. Using a hack-saw blade the cost is reduced to a fraction of the commercially available types. The principle in operation, however, limits the application to in-plane bending.

6.2.2 Distortion

The distortion of the bend cross-section plays an important part in the overall displacement of the bend. In fact, in the typical Kármán type analysis, without end effects, it can be seen that representation of the distortion, be it by fourier series or a simple trigonometric function, constitutes the basis of the analysis. The experimental measurement of distortion can be considered as essentially a further means of verifying the analysis.

In the room temperature elastic tests, this task is accomplished easily. Here, small steel ball-bearings, attached by a suitable adhesive to the bend surface, are positioned at diametrically opposite locations around the bend cross-section. Measurement of displacement across the ball-bearings is done using a micrometer. This is a well-established tecnique and although time consuming, can be extended easily to examine various cross-sections around the bend.

For the elevated temperature tests, a number of methods were examined. In an attempt to cope with the continually changing and irreversible conditions displayed in such tests these methods were incoprorated as an integral part of the experimental set-up.

During the course of the work two main methods were investigated. The first method (Figure (6.7)) employed a "comparator ring" attached to the bend by a large bolt welded to the bend at the intrados. Four steel rods sliding through guides incorporated in the comparator ring and bearing on the bend surface were positioned at the four cardinal points around the bend section. Distortion of the cross-section was measured using dial gauges bearing on the opposite end of the rods.

This method was significantly affected by relative movement between the ring and the bend. As distortion proceeded so also did rotation of the bend to the extent that the rods were no longer bearing on the circumferential section initially located on. The errors incurred by this movement were further exaggerated by the curved geometry of the bend.

In tests conducted at PNC [258] a similar method was adopted. Here, however, the relative movement was inhibited by a universal joint attachment of the steel rods to the bend. The uncertainties in the method and, moreover, the time involved in the manufacture of such joints, was not considered justified and a simpler method, dispensing with the comparator ring, was sought.

In the revised system, measurement of the displacements was achieved by tensioned lengths of steel wire attached to stainless steel lugs welded to the bend (Figure (6.8)). Each wire, running normal to the bend surface and approximately 1 m in length was tensioned

by means of additional springs incorporated in the dial gauge connection. A typical layout of the system incorporated in a forward creep test on a 90° bend under in-plane loading is shown in Figure (6.9). In this method, the problem of rigid body motion of the bend could be accommodated. Under in-plane loading the problem was particularly evident on the dial gauges marked No. 1 and No. 3 in Figure (6.9), their line of measurement coinciding with the plane of rotation of the bend. Distortion in this direction was evaluated from the difference in displacement recorded by these two dial gauges. The response of this system during an in-plane loading test [296] is shown in Figure (6.10) to Figure (6.12). During the room temperature elastic test (Figure (6.10)) and the initial loading at temperature (Figure (6.11)) the system operated satisfactorily giving approximate symmetry in displacements. However, during the creep period (Figure (6.12)), the vertical displacements were much smaller than the horizontal displacements. This was found later to be the result of dial gauge No. 1 operating outwith its range. This problem was encountered often and it was not uncommon for the wire under tension to break in this plane.

In order to have a system of measurement independent of the rotation of the bend and further be a practical set-up for out-of-plane loading it was decided to adopt a system similar to that used in the room temperature elastic tests mentioned earlier. Here, the ball bearing contacts were replaced by steel rods radiating outwards from the bend surface. This method is described more fully in section (5.4.4.2). The continual process of development in the measurement of distortion has meant that this system of measurement has been only recently introduced and as such no long-term results are available.

6.3 Heating System

The basic heating system, which was similar to that used by Griffith and Rodabaugh [114] consisted essentially of electrical resistance heating elements wound around the bend and fixed in place by stainless steel bands (Figure (6.13)). A ceramic blanket completely surrounding the installation provided the thermal insulation (Figure (6.14)).

This system was found to be deficient in two main aspects:

1. By virtue of the discrete form of heating, the poor conductivity of the stainless steel and the geometry of the bend a differential of around ∓30°C at 570°C could exist between the intrados and extrados of the bend mid-section, the latter being the sink.

2. In loading the bend, a moment arm is fixed to the bend. This is an efficient means of cooling the bend and hence a variation in temperature occurred along the bend. The base fixture of the bend would also act as a sink.

In tests conducted by IMAZU *et al.* [116] the bend was enclosed in a purpose built furnace. Hot air circulated through the bend resulted in a maximum differential of ∓5°C at 600°C around the bend section. Further work reported in [258] employed specially shaped internal heating elements and in another case sodium circulated through the bend.

Purpose built systems to heat the bend were examined. However, the cost of such installations was found to be prohibitive.

In an attempt to minimise the deficiencies inherent in the heating system an investigation was begun into the ways and means by which the existing system could be improved.

The results of this work were reported in [269] and are presented in APPENDIX (9). By encasing the bend in prefabricated sheets of copper the differential across the intrados and extrados was reduced to ∓3°C at 570°C. The differential along the length of the bend was minimised using insulation gaskets between the flanges at the loaded and fixed ends of the bend.

6.4 Test Procedure

6.4.1 Introduction

The experience gained during the development work and the tests conducted during the pilot scheme provided a sound breadth of knowledge on which the bulk of the main creep programme was based. Although development work continued throughout the main programme, the principal features remained unchanged and it became a relatively straightforward task in establishing a standard test procedure for each test. This consistency in approach was expected to be reflected in the quality and standard of the results.

The elevated temperature test, be it forward creep or creep relaxation, can be considered to comprise three main stages.

1. Room temperature calibration tests
2. Heating up period
3. Creep period

This section presents a brief description of each stage using the results of tests conducted by the author, reported in [296,297,298, 299].

6.4.2 Room temperature elastic calibration tests

Essentially these tests were performed to evaluate the capacitance gauge calibration factor F using electrical resistance strain gauges for comparison. As a secondary function the tests ensure that the measurement system as a whole is working properly. They also provide further experimental data on the restraining effect of tangent pipes under elastic conditions.

The calibration factor F is defined as:

$$F = \frac{B_E}{B_C} \qquad \ldots (6.2)$$

where B_E and B_C are simply the slope of best fit straight lines for the electrical resistance and capacitance gauge, respectively.

The first stage in calibration of the capacitance strain gauge is an examination of the strain distribution. Here, using electrical resistance gauges of single and strip form (Figure (6.15)), the points of maximum strain are determined around the desired section. For the case of in-plane loading [296] a comparison of these strains (Figure (6.16)) with Thomson's [133] theory shows good agreement (Figure (6.17)).

For convenience the copper heating sheath is fitted following completion of this test. Thereafter, resistance gauges of comparable gauge length (20 mm) to the capacitance gauge were mounted at these points of maximum strain, and a test conducted. These gauges were then removed and replaced with capacitance gauges using location marks for accuracy in position and the assembly re-tested to the same level as before.

Due to the high cost of the capacitance gauge only three are normally employed - two active gauges measuring strain in the meridional direction and one "dummy" gauge mounted on a load free plate measuring the drift characteristics which is taken to be representative of the two active gauges.

In mounting the capacitance gauge the main points in the technique developed were:

1. For gauges mounted in the meridional direction the feet are bent to accommodate the curvature of the bend section using the jig shown in Figure (6.18).

2. To minimise the effect of gauge lead movement being transmitted to the gauge, a behaviour peculiar to pipe bends, all gauge leads were attached securely to the bend at apertures provided in the copper sheath. Each lead on the active gauges was bent through 90° prior to entering the gauge area, with the minimum of gauge lead exposed (Figure (6.19)). The problem of gauge lead movement has not been reported by any other researchers. This, however, may be due to the fact that the few reported results of this gauge have dealt with large stiff structures [300]. The problem as shown in Figure (6.20) arises essentially from the inability of the nichrome leads to prevent movement of the gauge leads being transmitted to the gauge.

3. From location marks given by the strain distribution, the gauge was positioned and one foot spot welded.

4. Following attachment of the nichrome coiled leads the remaining foot was spot welded allowing if necessary for off-set to provide a large positive or negative strain capability.

5. Finally, to prevent the inclusion of dust the gauge is enclosed in a stainless steel cover, immediately following mounting.

The results of a typical calibration test [296] are shown in Figure (6.21). From this, the calibration factor F defined by equation (6.2) can be determined for each gauge as 1.30 and 1.48. The true strain is thus obtained by the product of F and that determined from the manufacturer's standard calibration. This assumes, of course, that the standard calibration is valid at elevated temperature.

6.4.3 Heating up period

This stage of the test, although having the main function of gradually increasing the temperature to the test state of 570°C also serves as a further check on the instrumentation. In particular, the capacitance circuit needs checked because it is not uncommon, for example, for a gauge lead exhibiting the nominal resistance of 20MΩ at room temperature to break down partially or totally at temperature [301]. In the measurement of displacement, however, the mechanisms employed in measuring the displacement themselves undergo a temperature change so that no great significance can be attached to their values. Suffice to say that on reaching temperature a degree of stability in behaviour should be apparent.

Results for the temperature variation throughout a whole test [299] are shown in Figure (6.22). Around the bend section (Figure 6.23)) this resulted in an average temperature of 578°C with a maximum variation of ∓ 3°C.

6.4.4 Creep period

In order to obtain a reasonable value of strain rate in the forward creep test, the initial loading was required to provide an optimum amount of plastic strain. This proved to be a skilled operation as too much plastic strain could easily lead to premature collapse whilst too little resulted in little or no measurable creep strain. The rate of load relaxation in the creep relaxation test was also effected in the same manner.

Results taken from an in-plane forward creep test [296] conducted on a 90° bend are shown in Figure (6.24), (6.25) and (6.26). This test was run for a period of over 3800 hr and completed with plastic collapse. An optimum level of plastic strain was obtained during the initial loading (Figure(6.24)) resulting in a well-defined creep curve (Figure (6.25)). The accumulated creep strain was around +1700 x 10^{-6} which was comparable to that of the elastic-plastic loading strain. In this test the total strains (Figure (6.26)) recorded of around +8000 x 10^{-6} indicates clearly the need for off-set in mounting the capacitance gauge. During the loading stages the response of the capacitance gauge was found in most cases to be satisfactory. If difficulties were to be encountered then this was usually during the creep period. The failure of a heating tape or breakdown in gauge lead resistance were a common cause of complaint, although as can be seen from the creep curve in Figure (6.25) the system was able to recover. In the event of failure of one active capacitance gauge dismantling of the test was found to introduce further problems and the test was normally continued.

In the creep relaxation tests the method of displacement restraint and measurement of load relaxation operated successfully. The results

of such a test [297] conducted in an in-plane mode are shown in Figures (6.27) and (6.28).

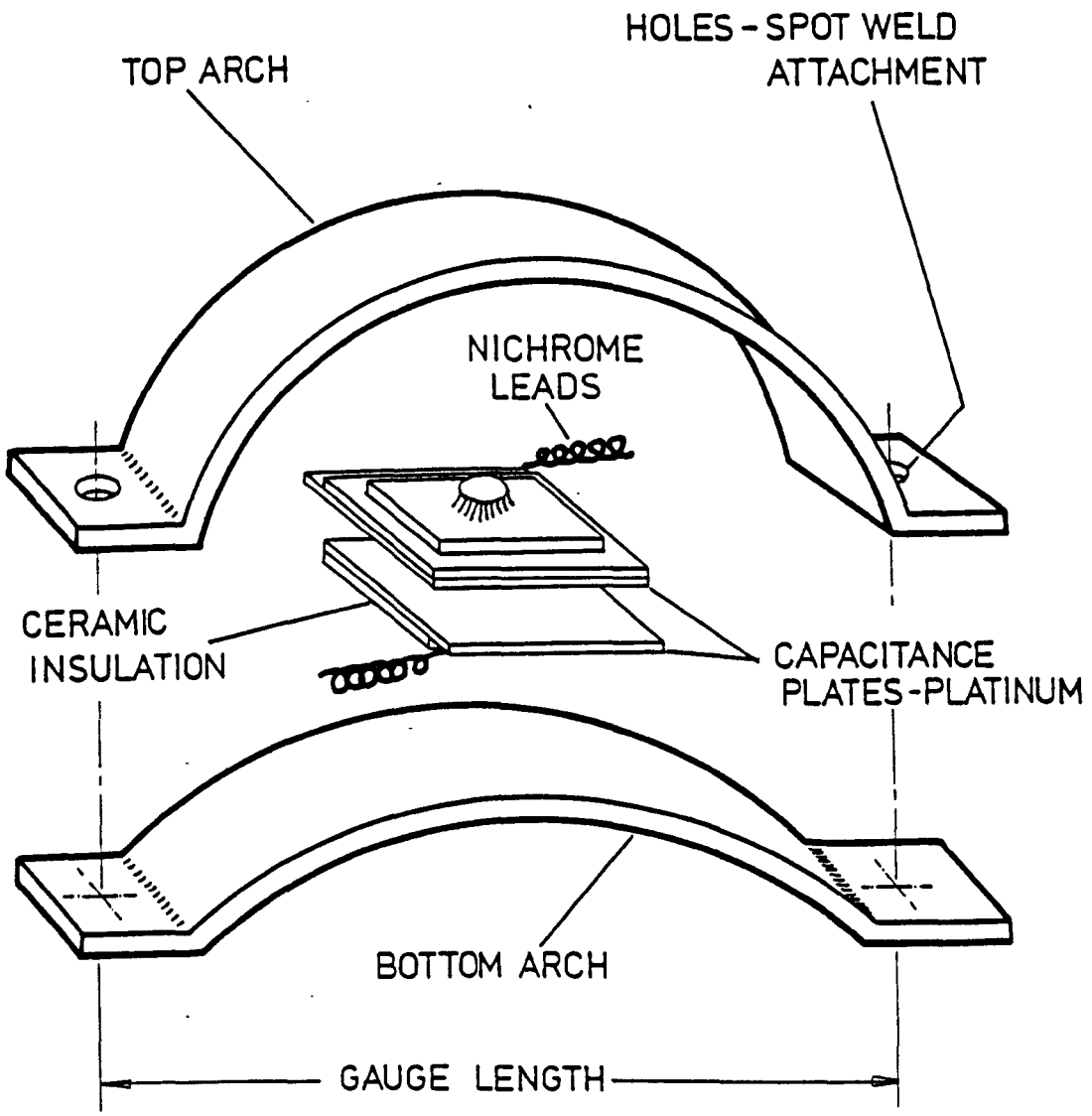

C.E.R.L. PLANER
CAPACITANCE STRAIN GAUGE

FIG. 6.1

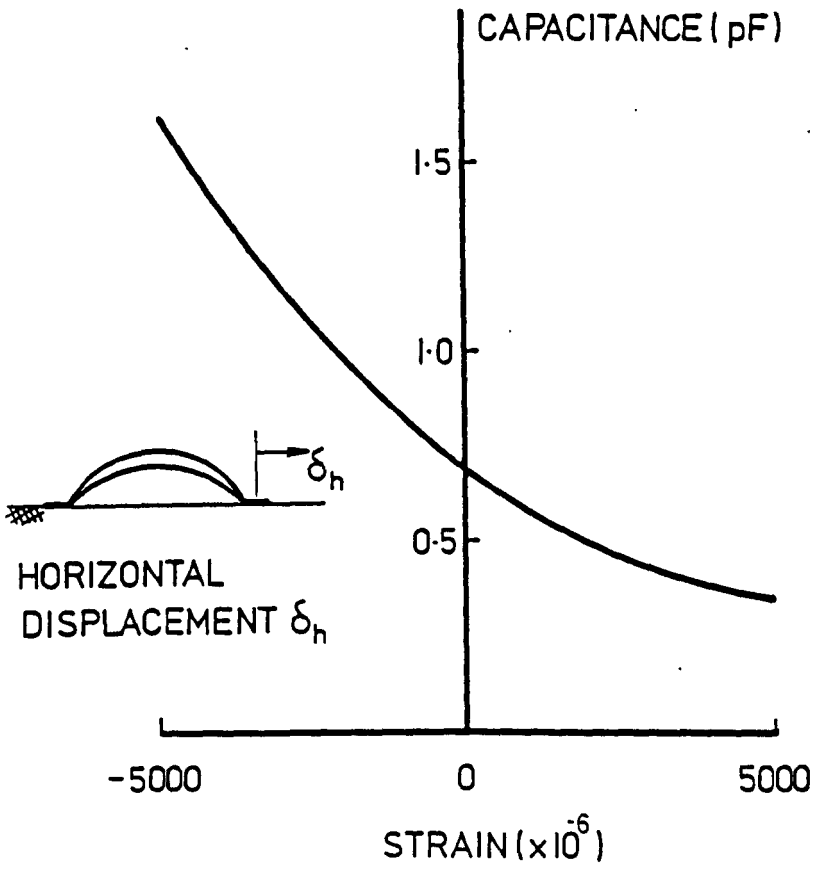

CALIBRATION CURVE

C.E.R.L. PLANER GAUGE

FIG. 6.2

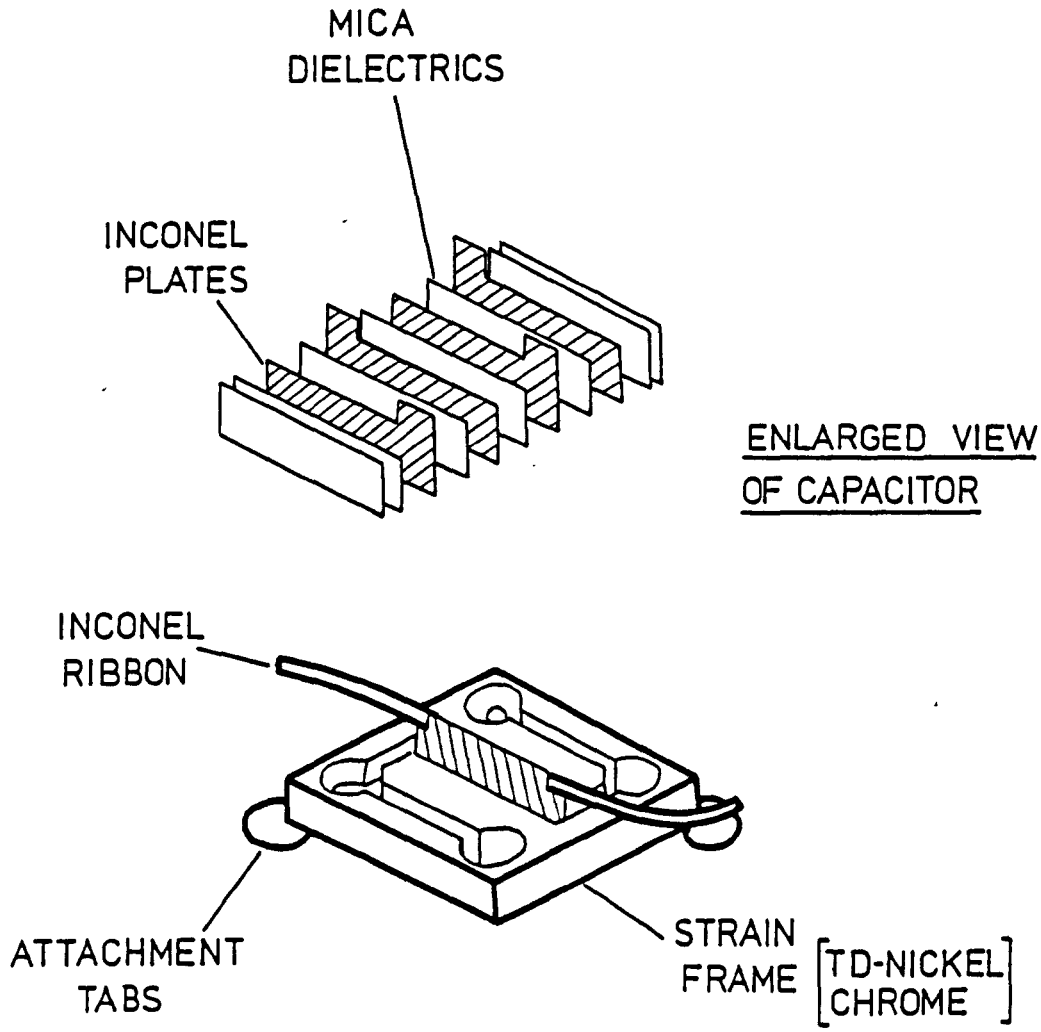

HUGHES CAPACITANCE
GAUGE

FIG.6.3

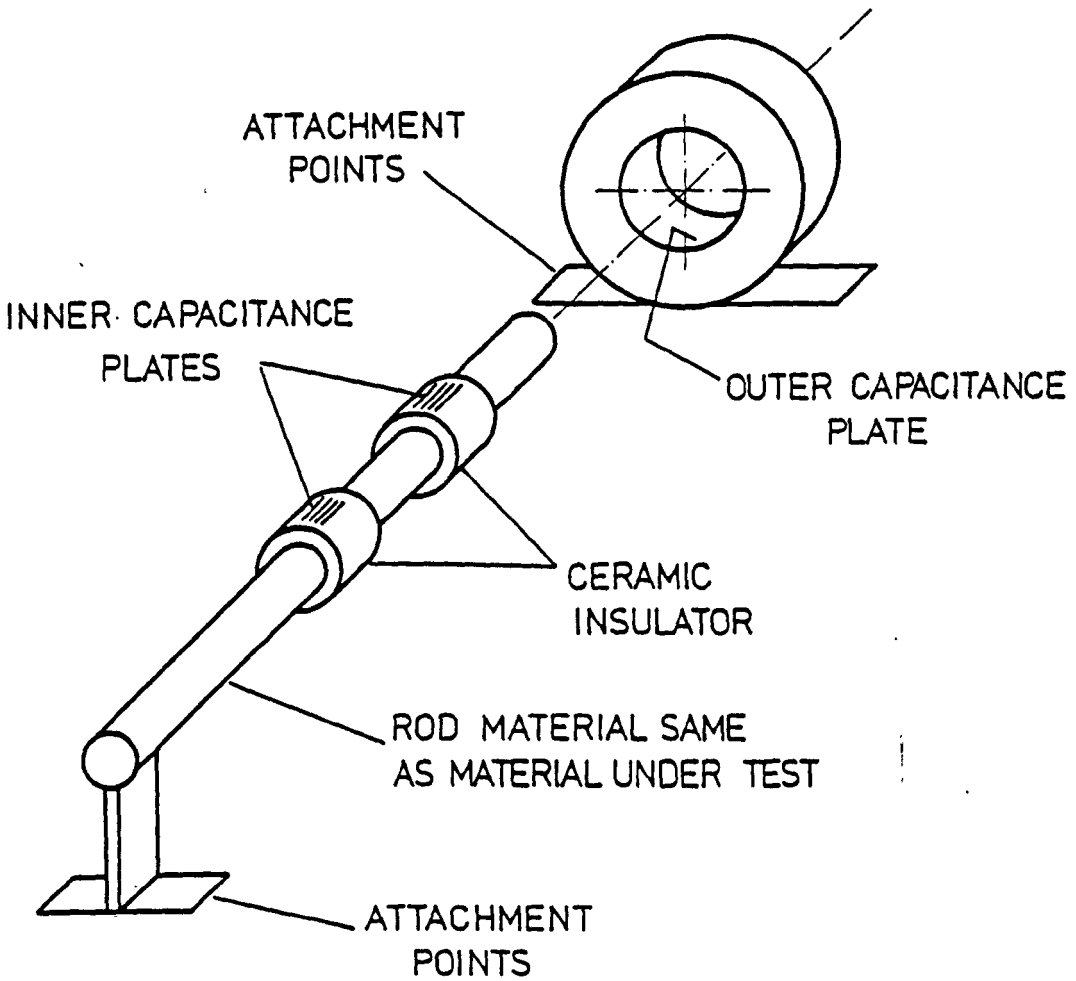

BOEING-HITEC
CAPACITANCE GAUGE

FIG. 6.4

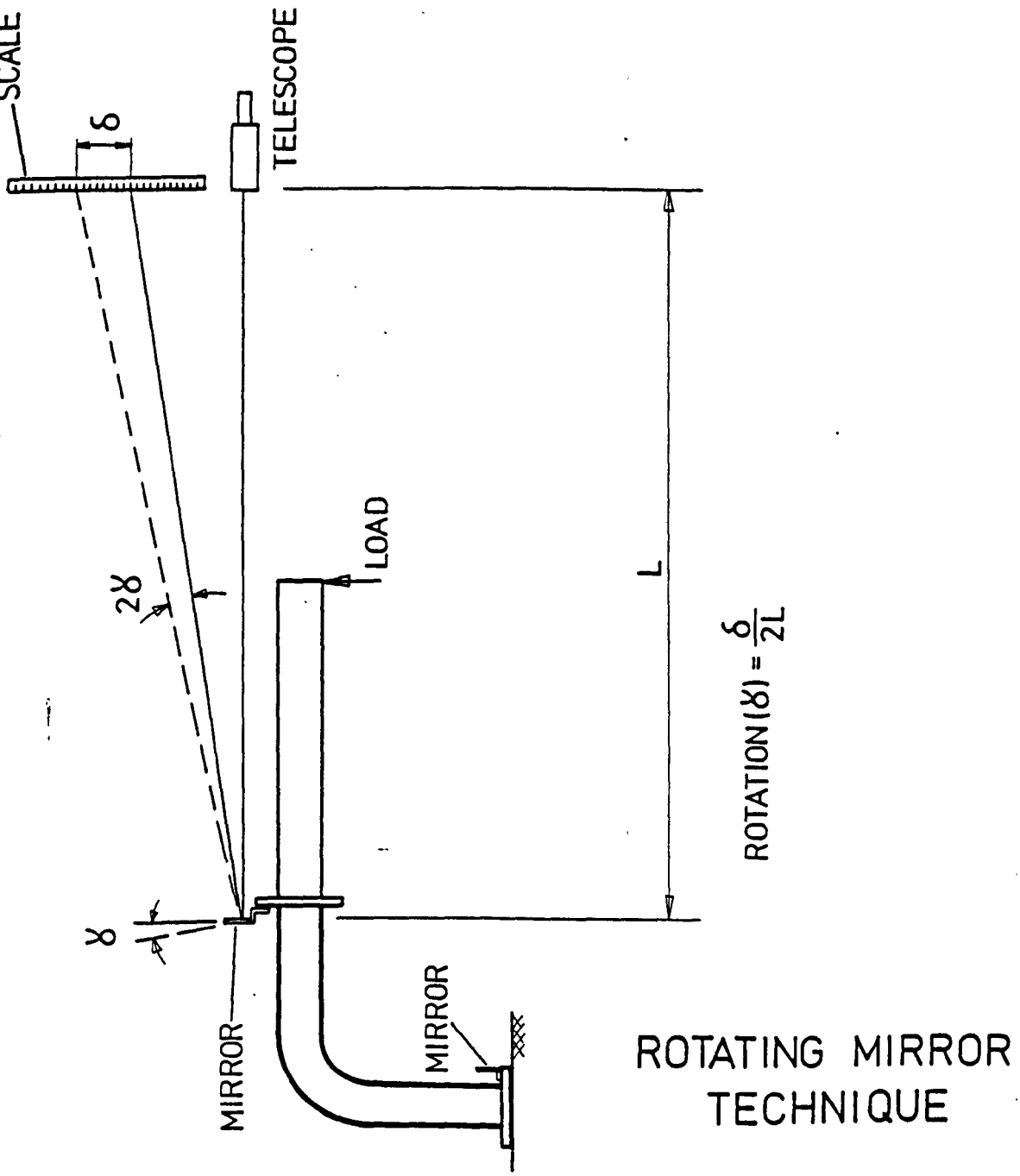
SCALE
δ
TELESCOPE
LOAD
2α
L
ROTATION (θ) = δ/2L
α
MIRROR
MIRROR
ROTATING MIRROR
TECHNIQUE

FIG. 6.5

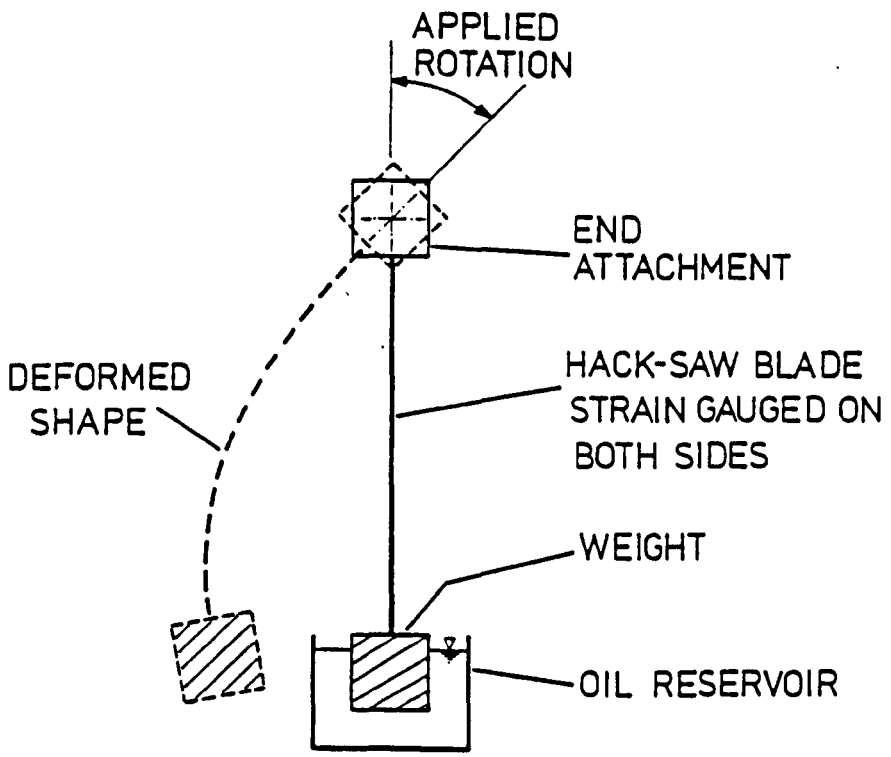

STRAIN GAUGE INCLINOMETER

FIG. 6.6

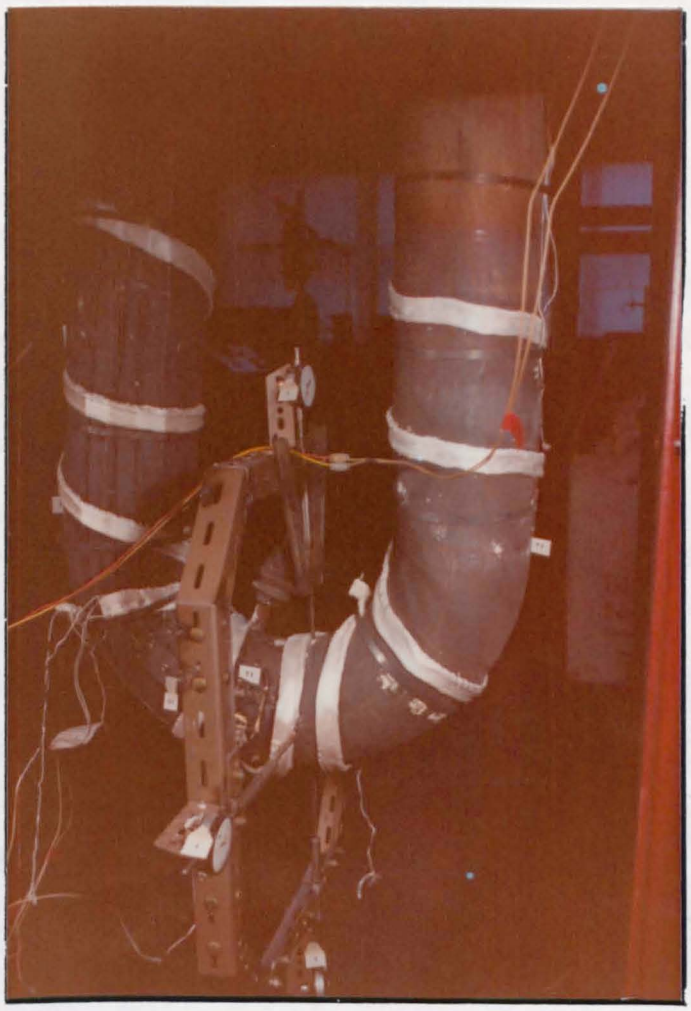

COMPARATOR RING

FIG. 6.7

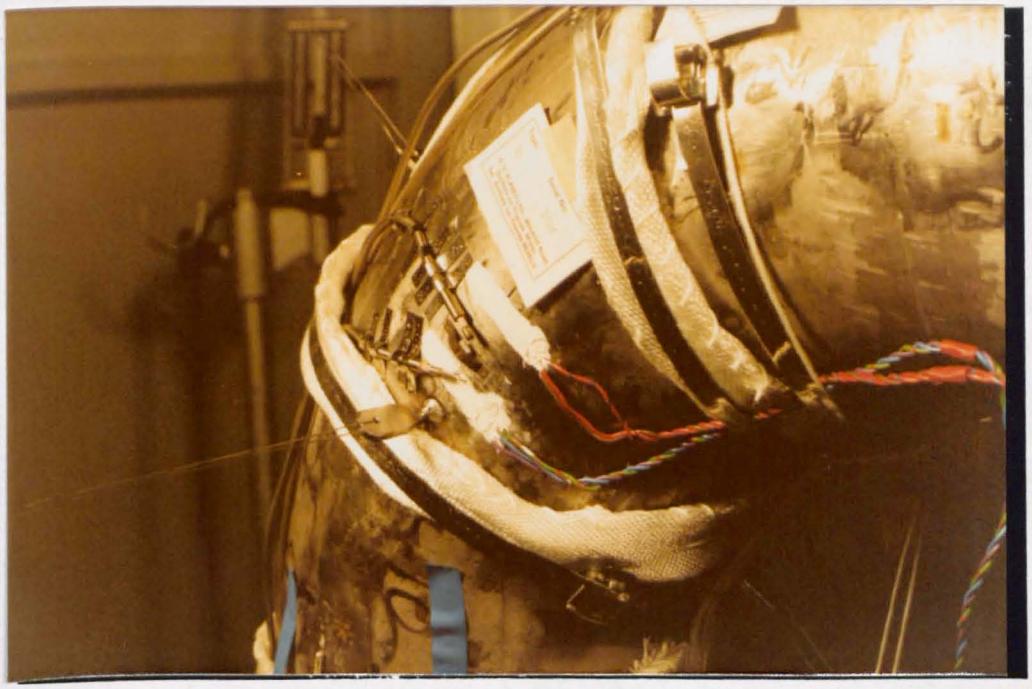

DISTORTION LUGS

FIG. 6.8

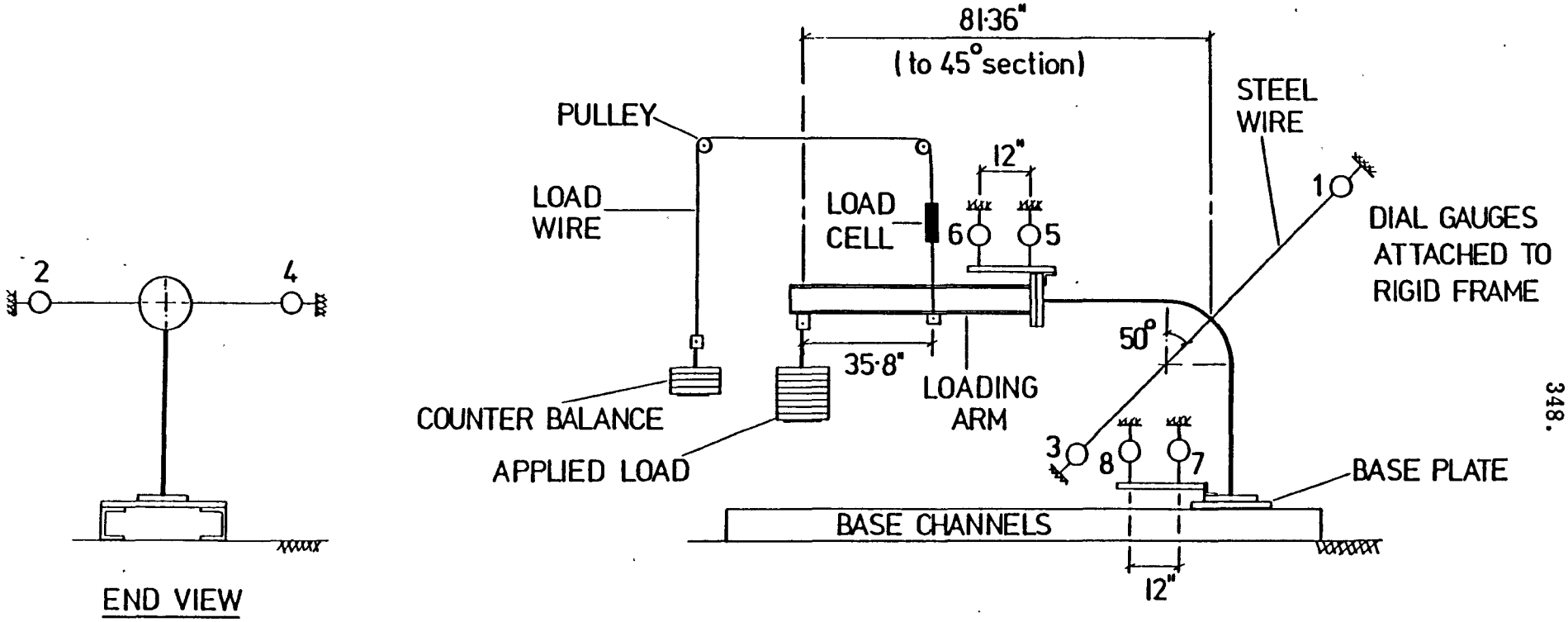

FIG.6.9 TEST LAYOUT

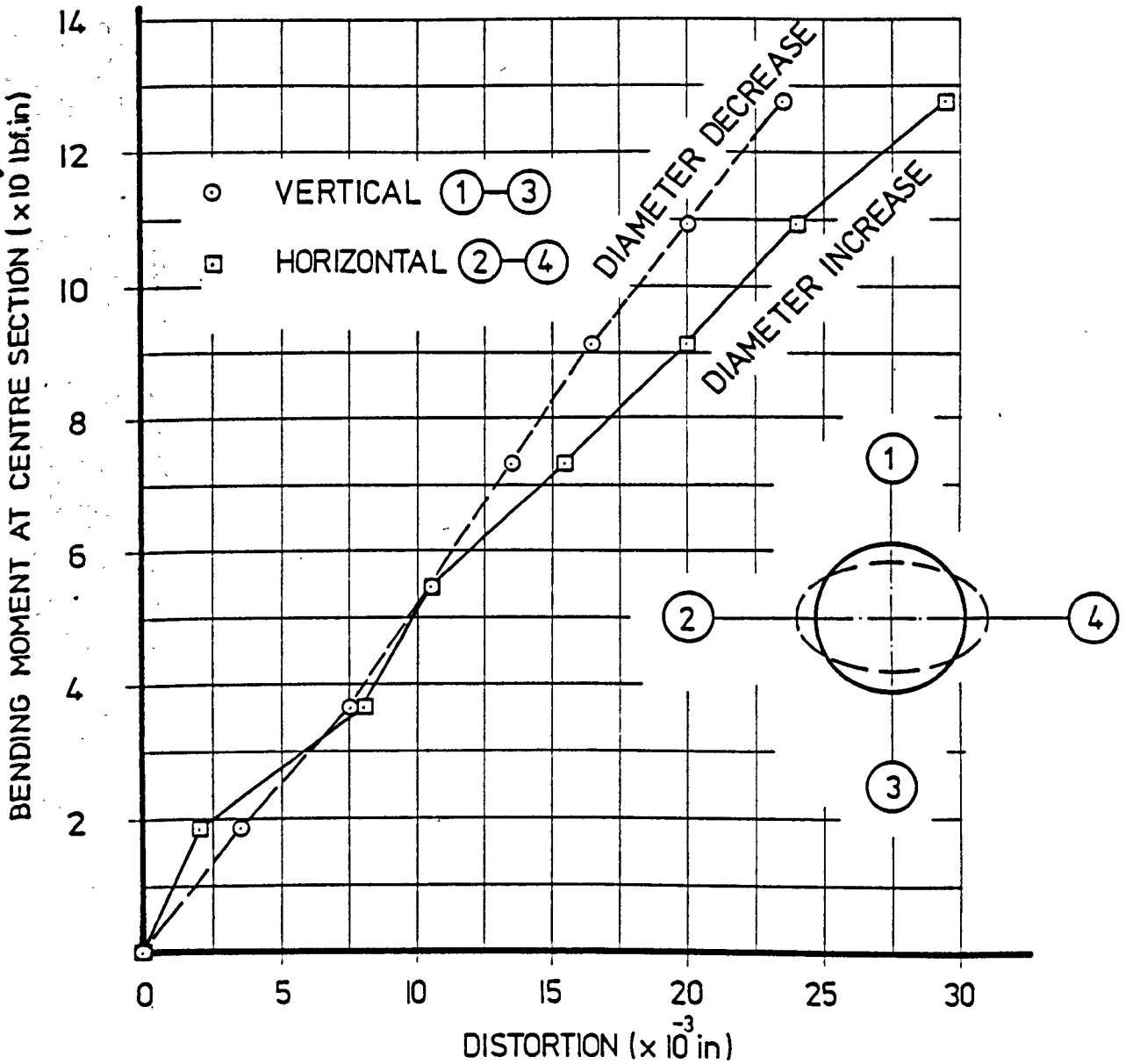

ROOM TEMPERATURE ELASTIC DISTORTION

FIG. 6.10

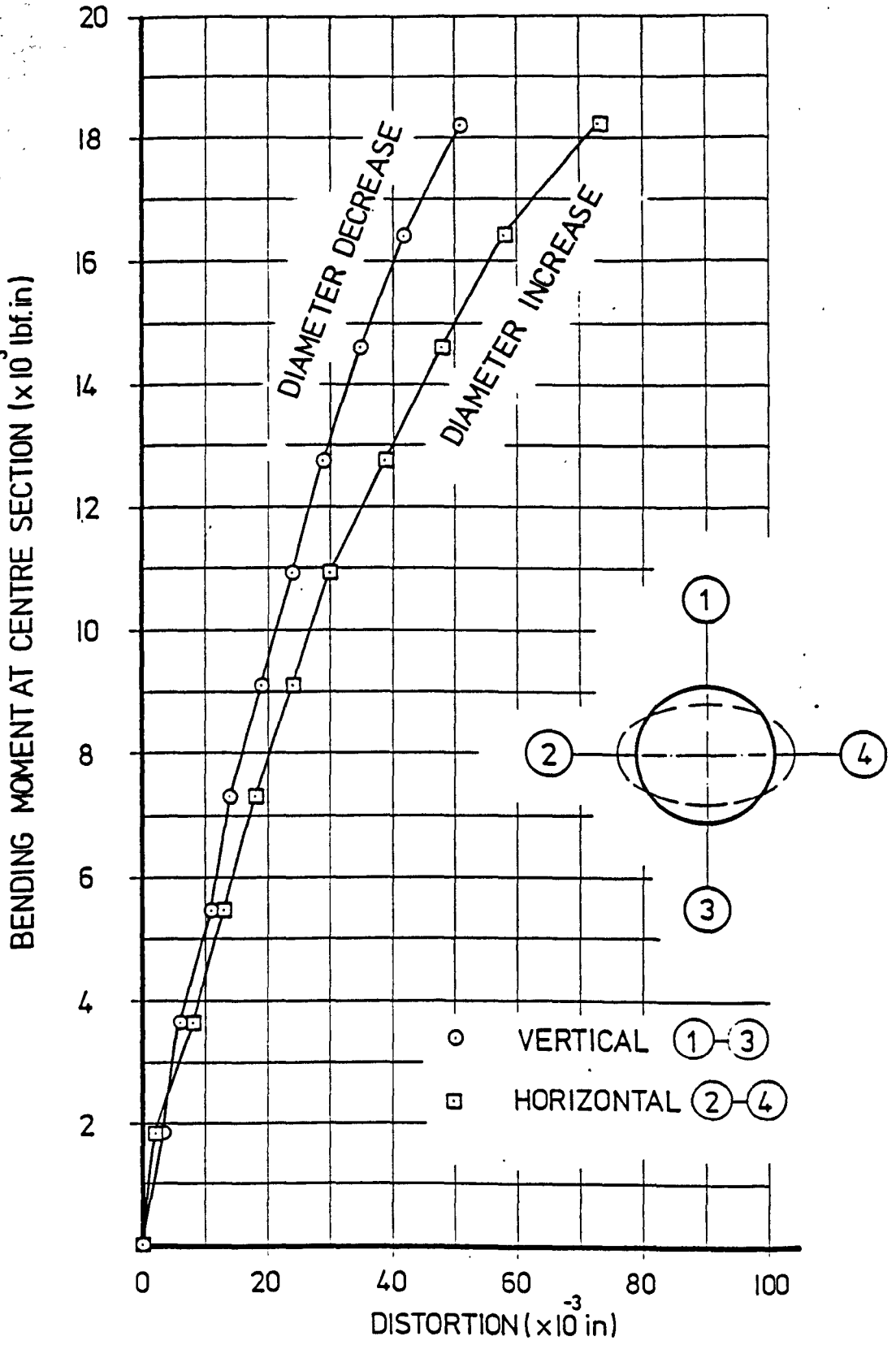

INITIAL LOADING AT TEMPERATURE

DISTORTION

FIG. 6.11

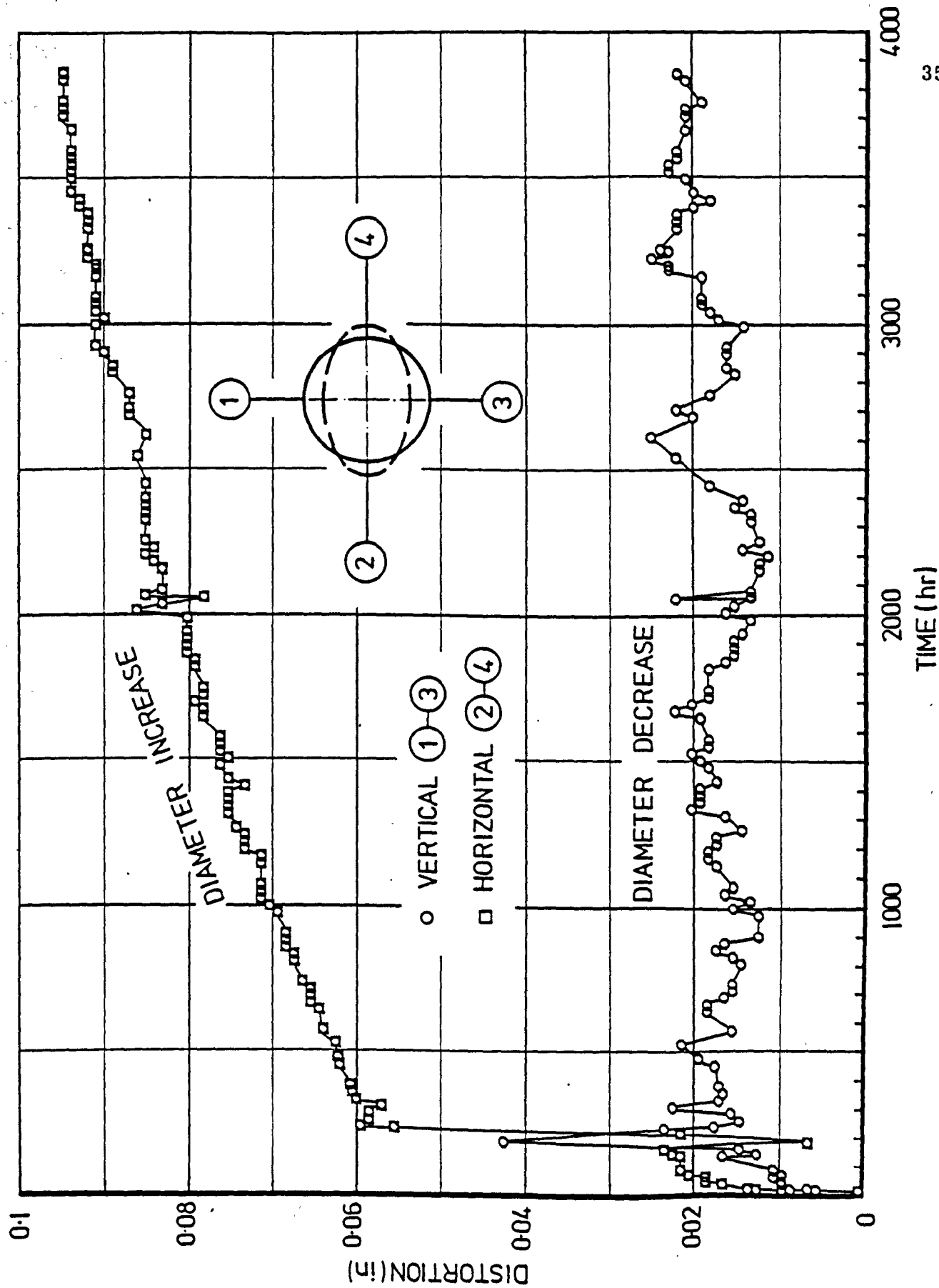

CREEP PERIOD
DISTORTION

FIG. 6.12

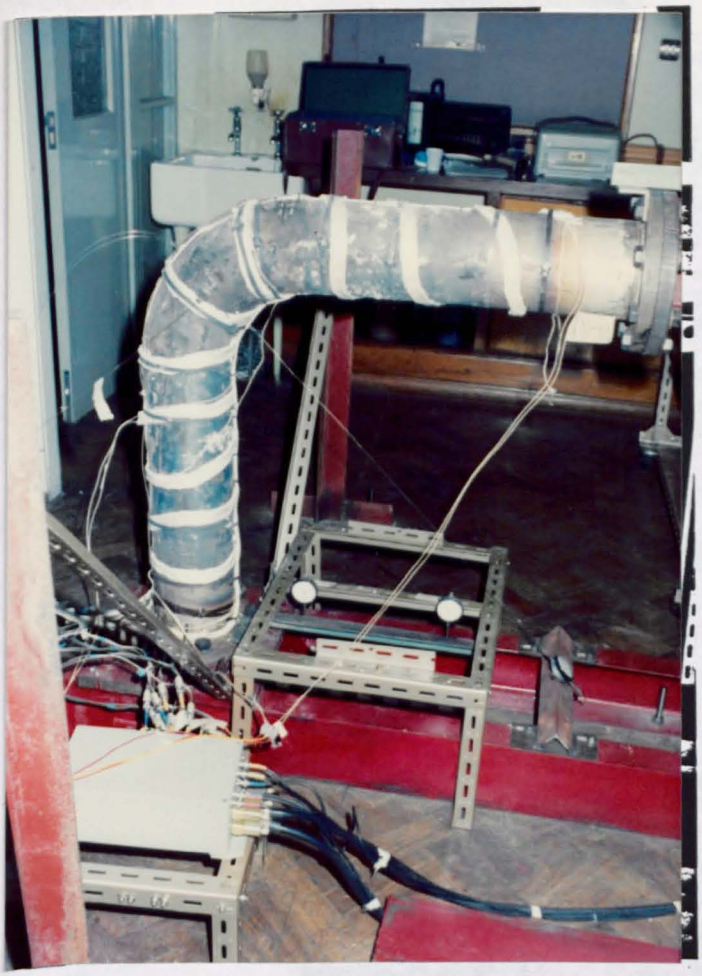

HEATING
SYSTEM

FIG. 6.13

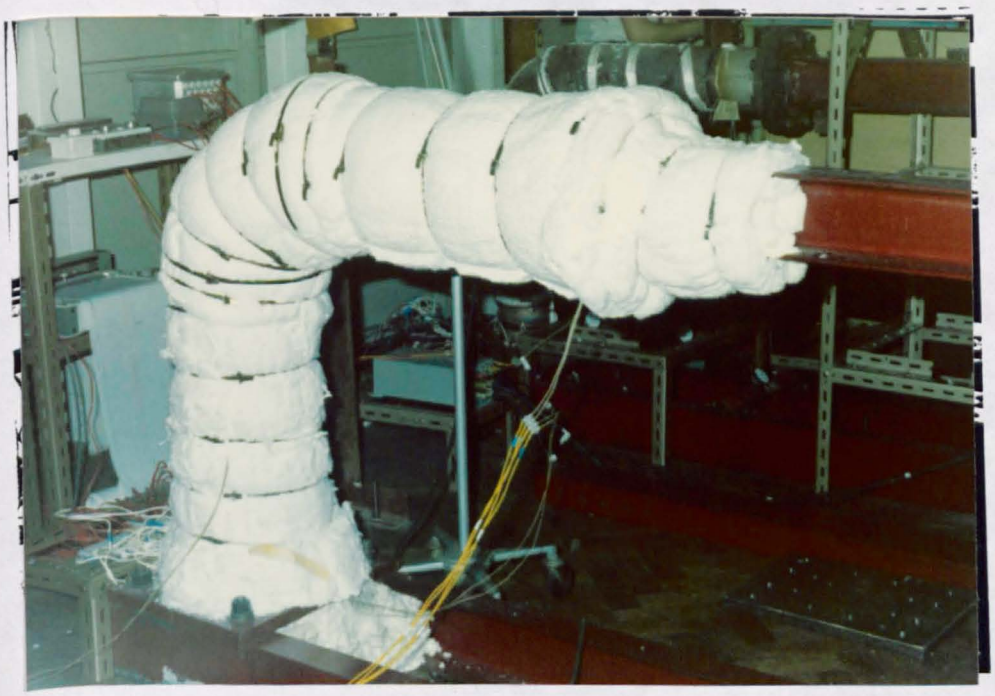

BEND INSULATION

FIG. 6.14

GAUGE LAYOUT
ROOM TEMPERATURE ELASTIC
CALIBRATION TEST

FIG. 6.15

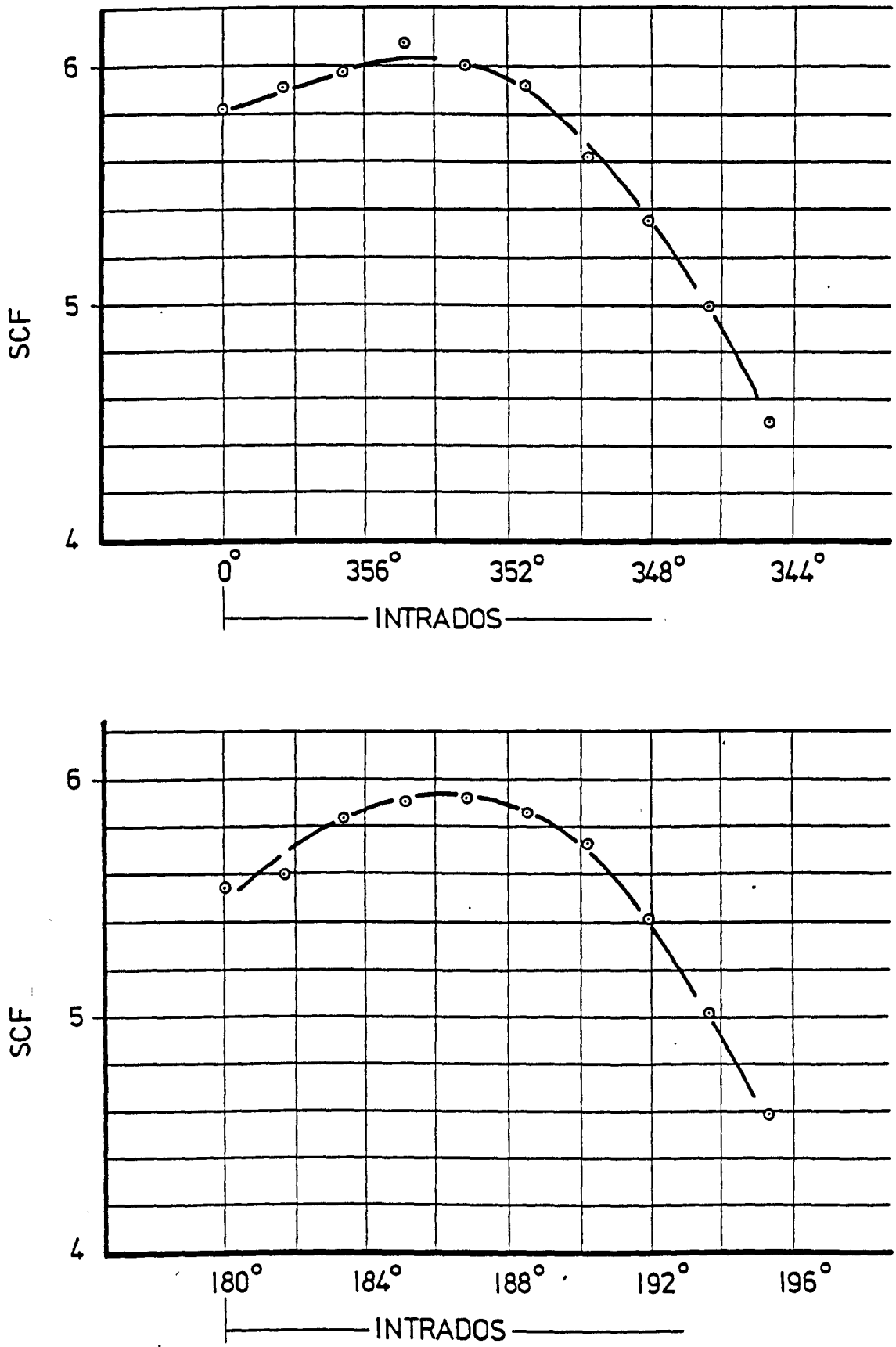

R.T. ELASTIC
IN-PLANE BENDING CLOSING MODE

MERIDIONAL STRAIN

FIG. 6.16

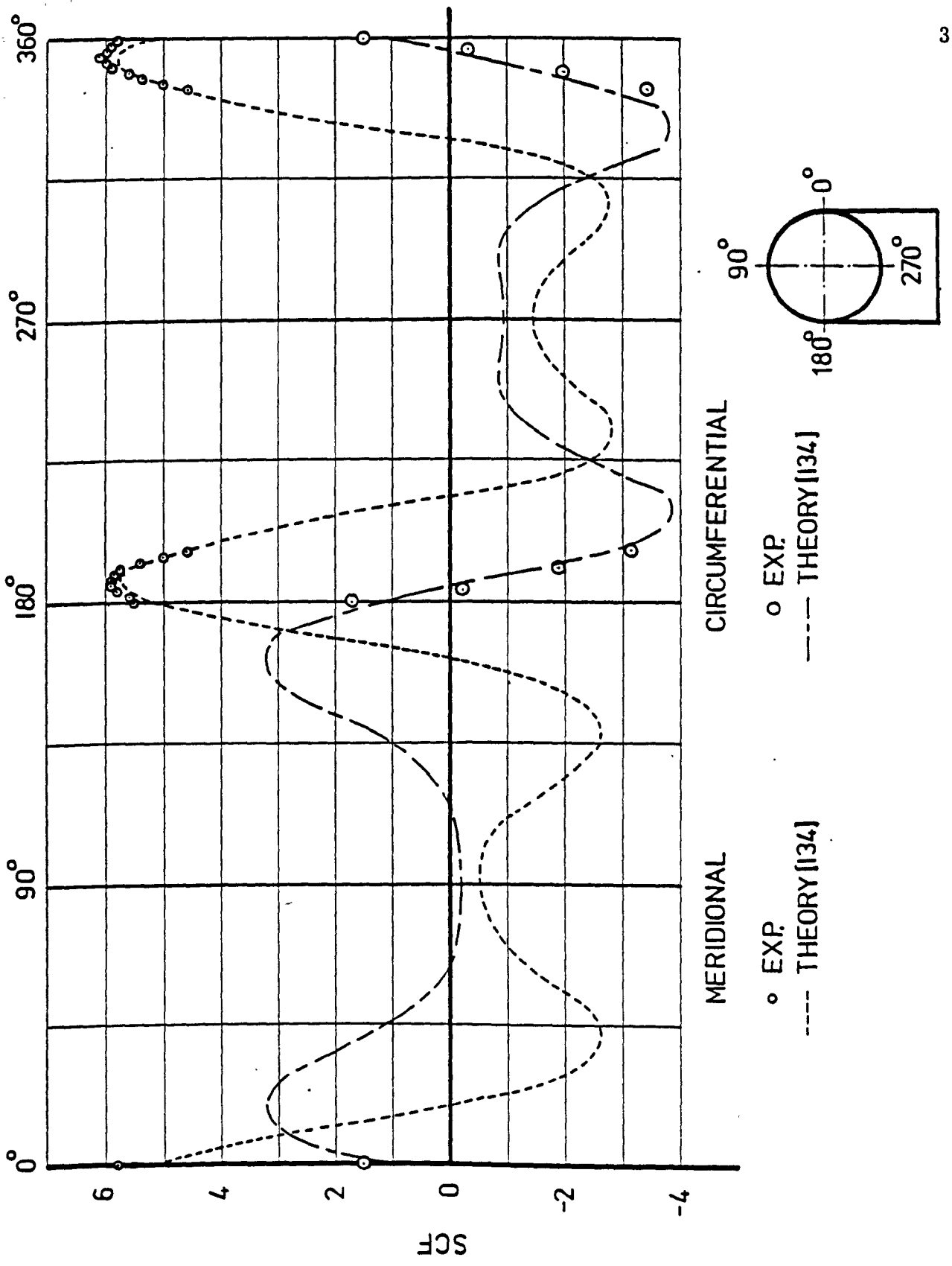

R. T. ELASTIC - STRAIN

FIG. 6.17

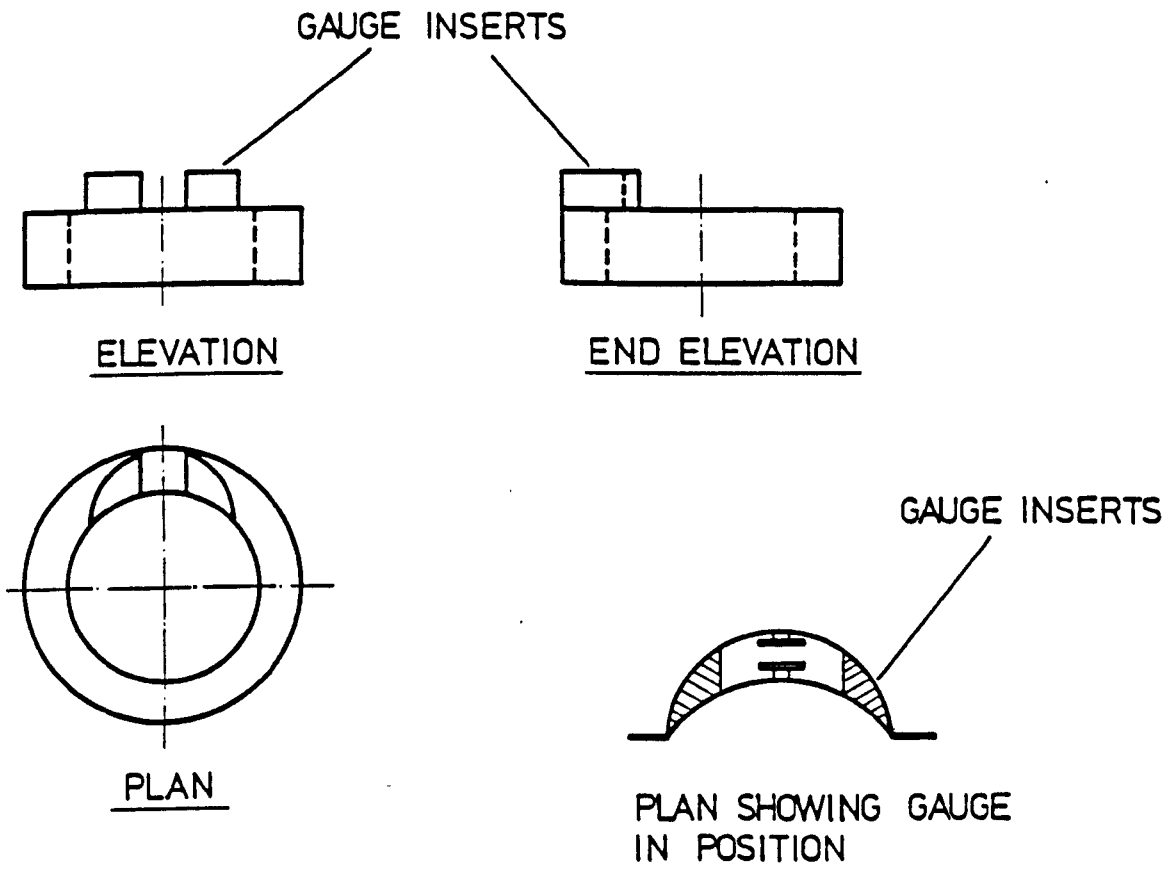

CAPACITANCE GAUGE
FEET BENDING

FIG. 6.18

CAPACITANCE GAUGE
LAYOUT

FIG. 6.19

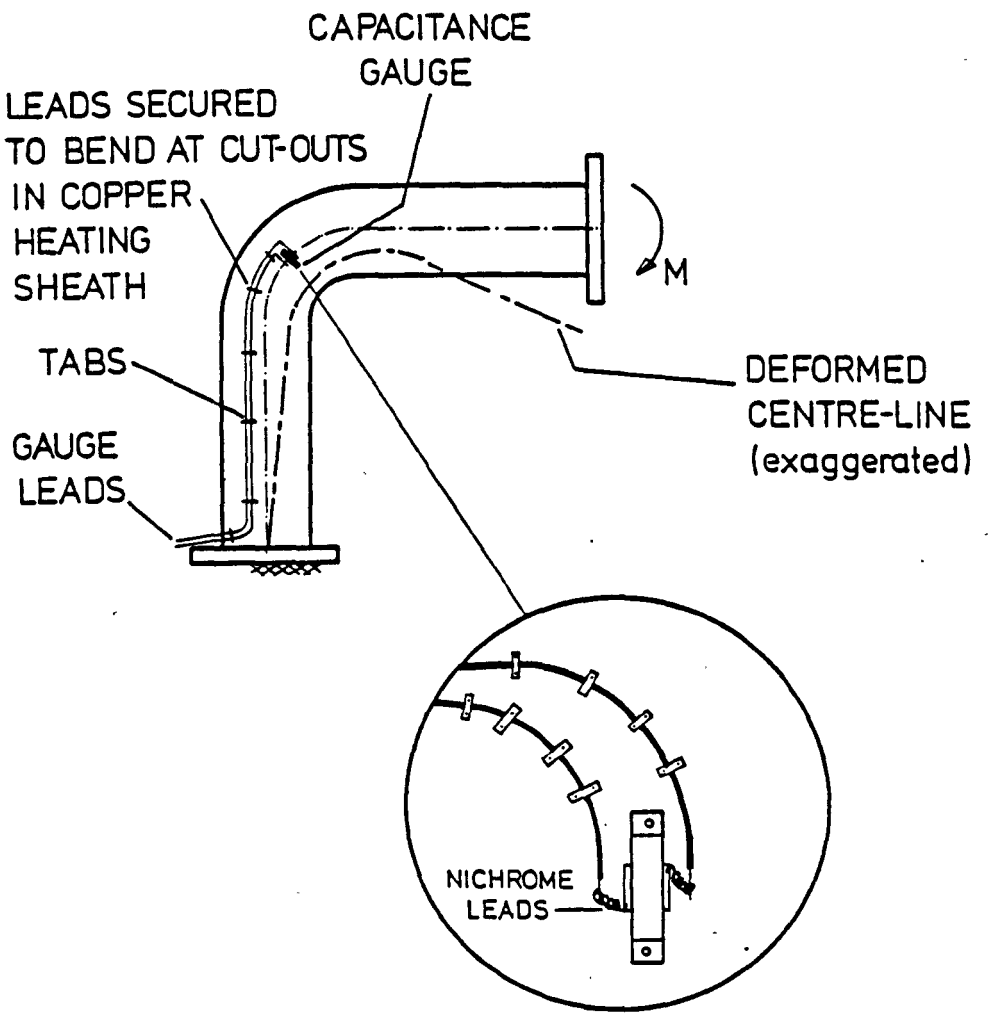

GAUGE LEAD MOVEMENT

FIG. 6.20

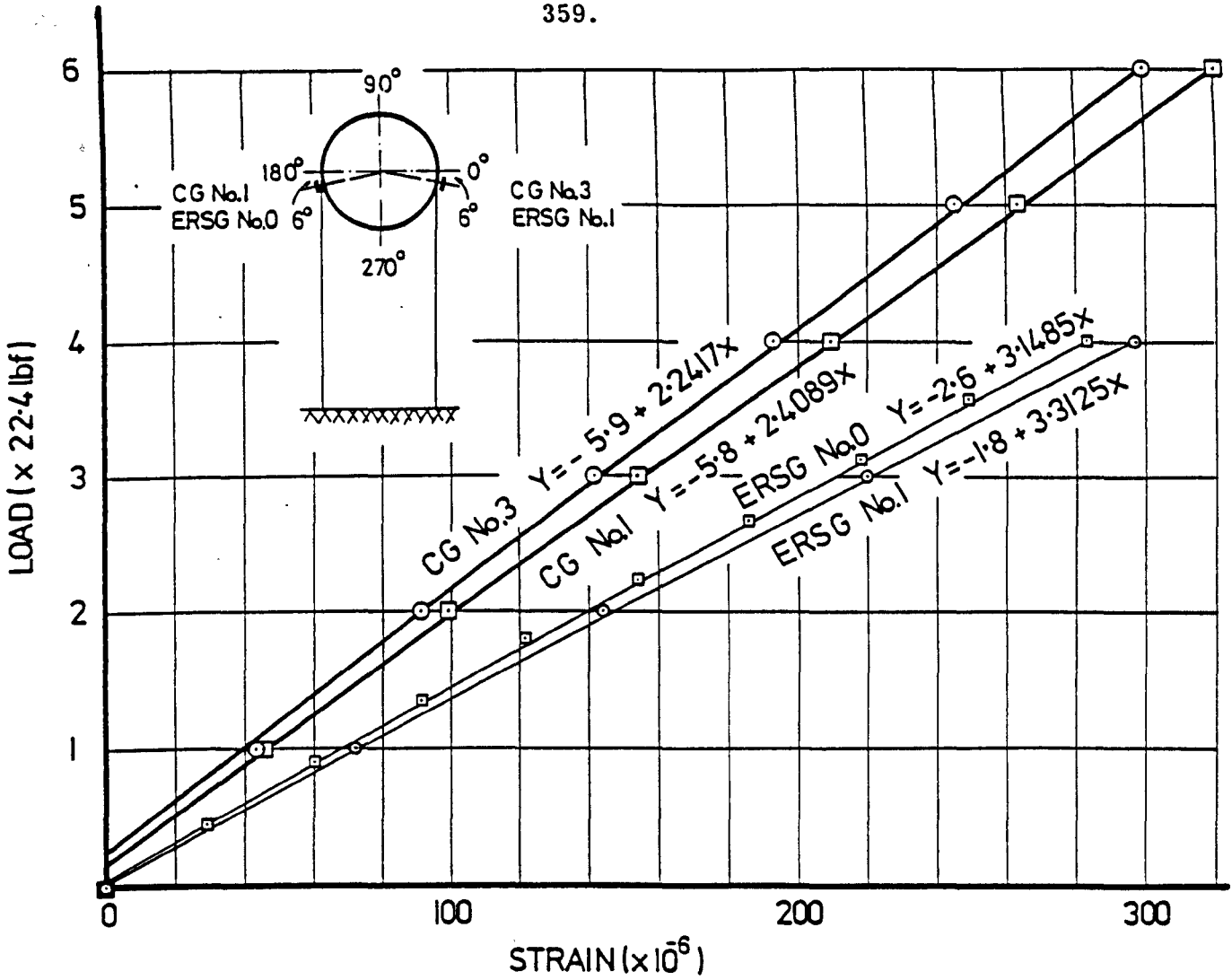

best line fit $Y = A + Bx$ where Y = strain x 10^{-6}
x = load - lbf

ERSG:- GL=20mm, GF= 2·14

R.T. ELASTIC CALIBRATION
IN-PLANE BENDING CLOSING MODE

FIG. 6.21

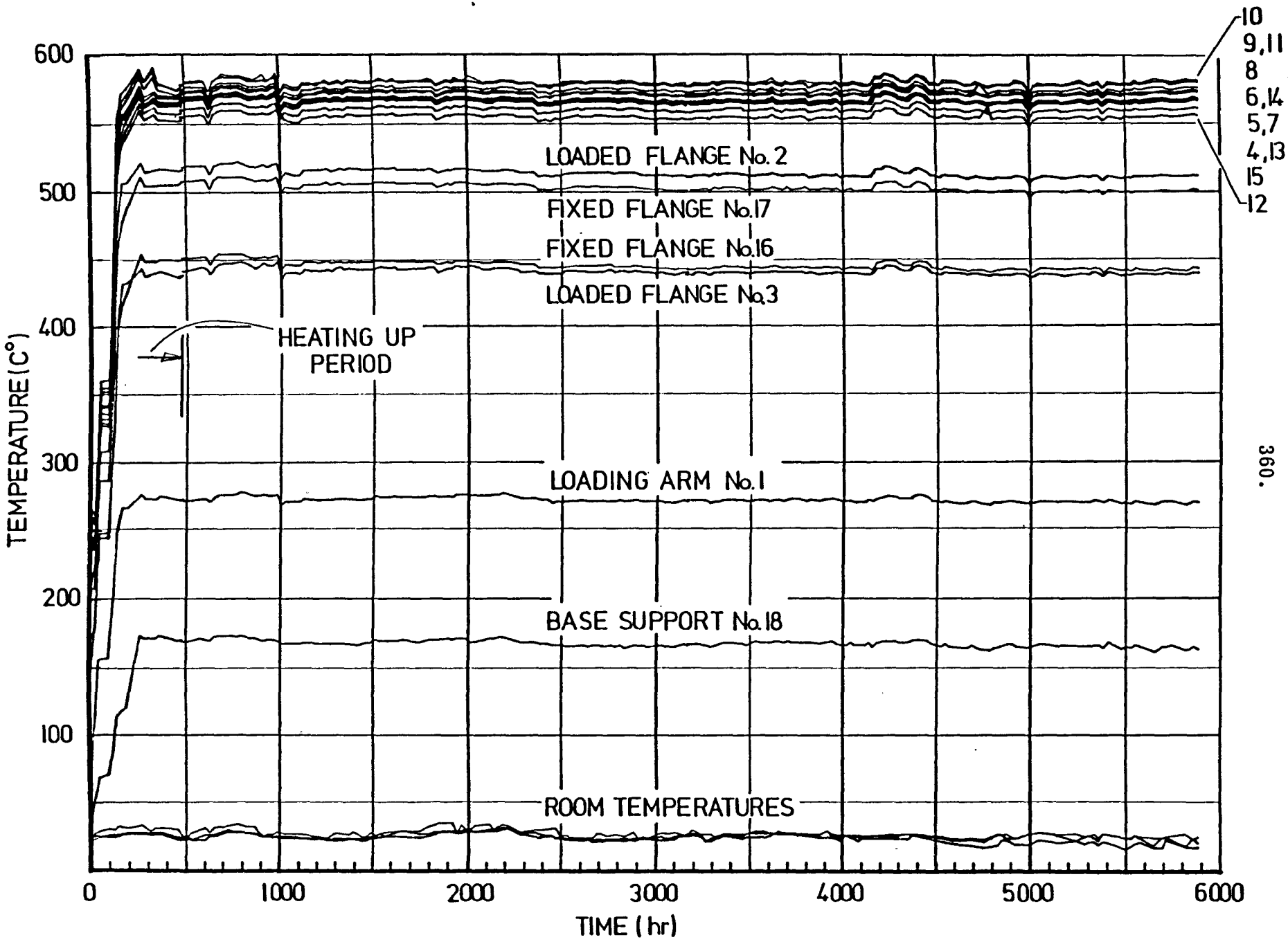

TEMPERATURE VARIATION

FIG. 6.22

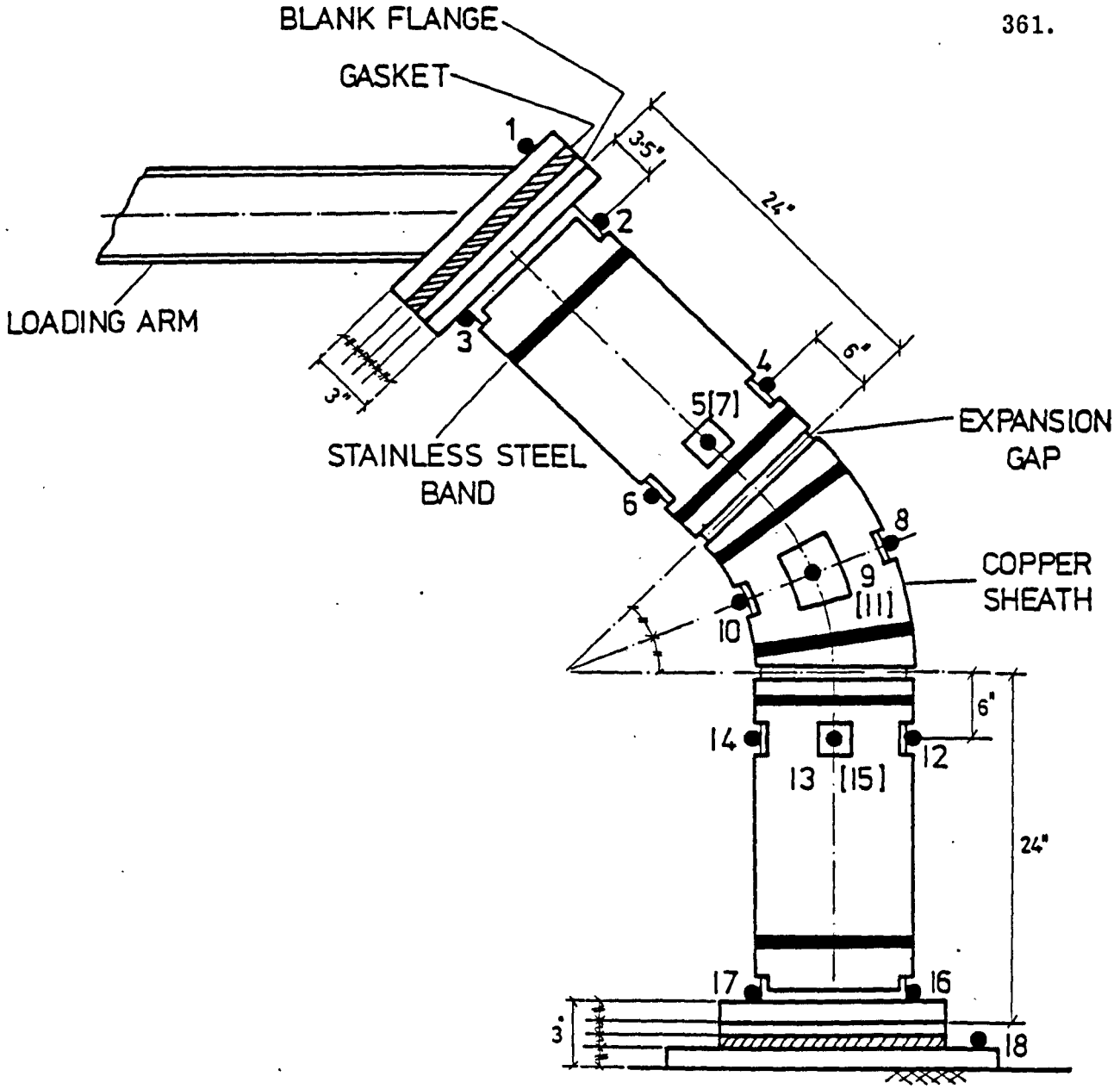

LAYOUT OF THERMOCOUPLES

FIG. 6.23

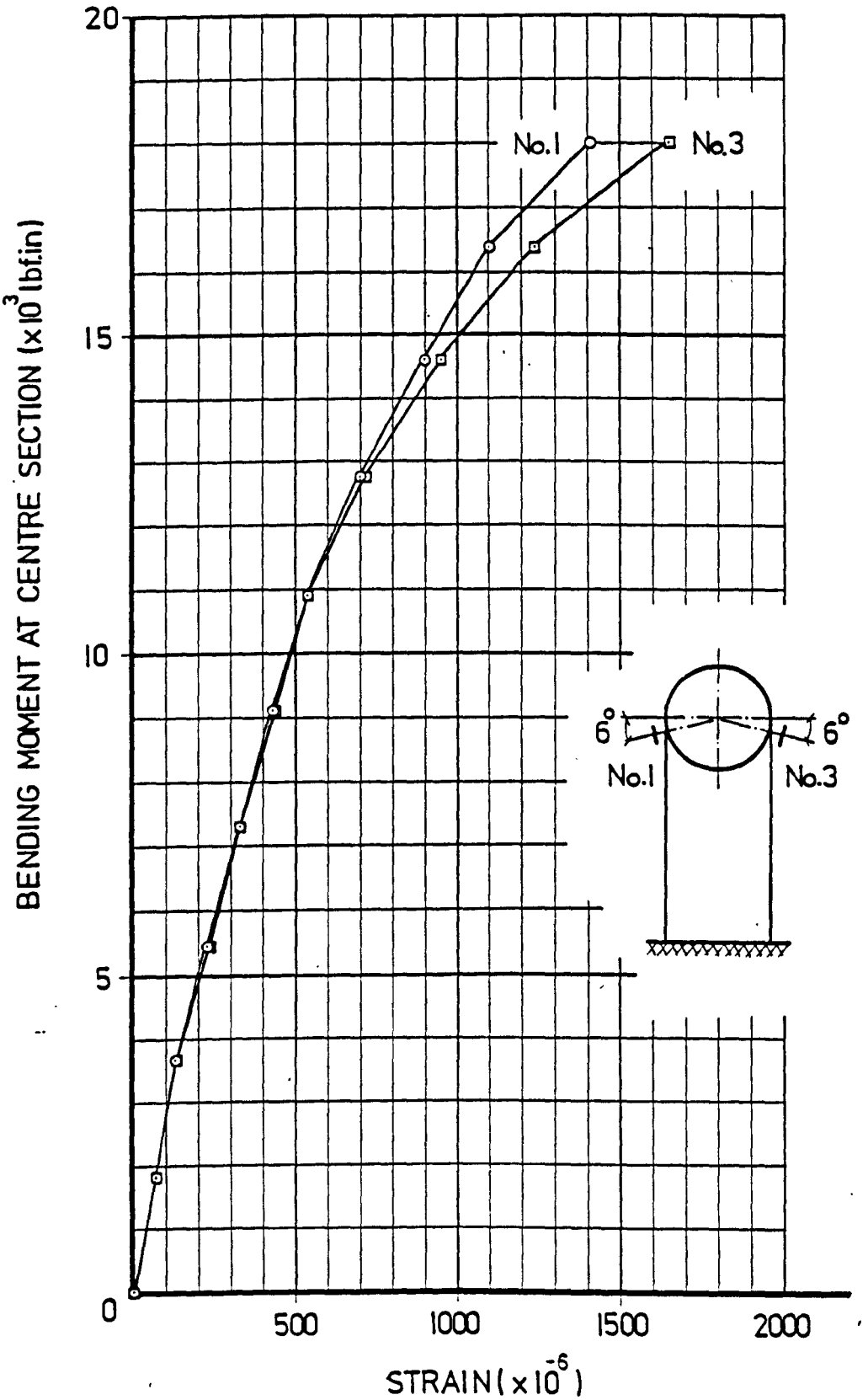

INITIAL LOADING AT TEMPERATURE STRAIN

FIG. 6.24

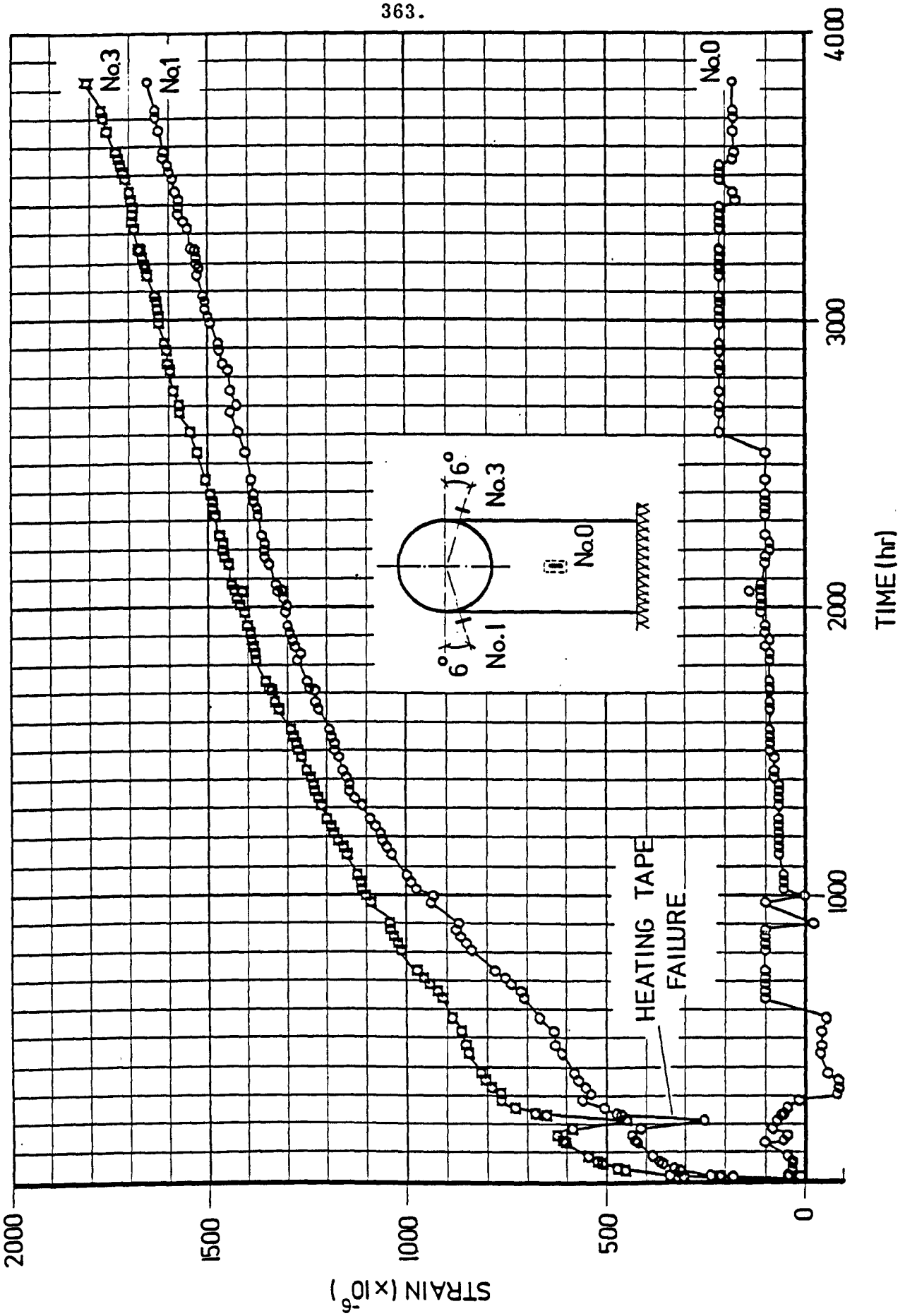

CREEP STRAIN

FIG. 6.25

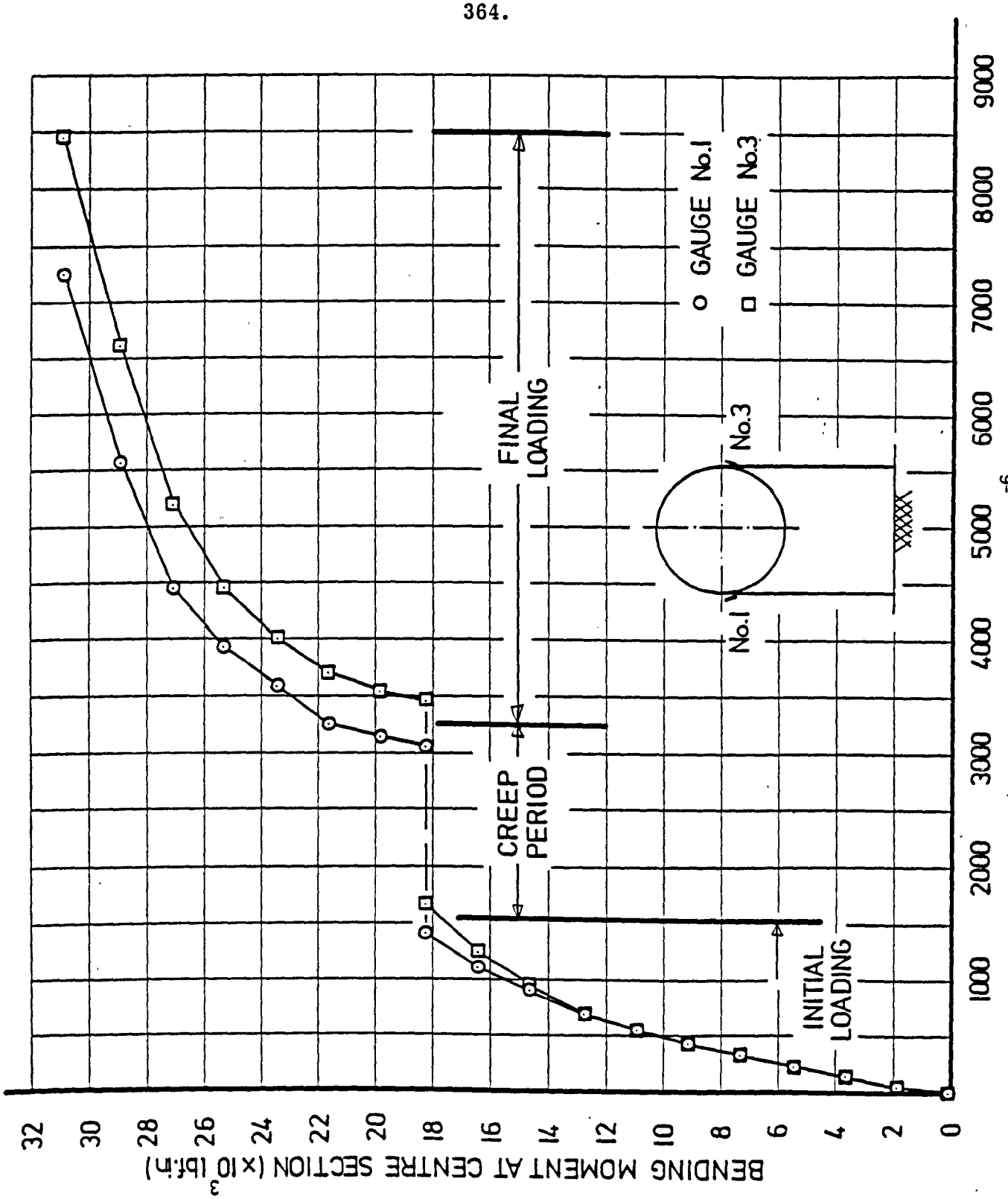

TOTAL STRAIN

FIG. 6.26

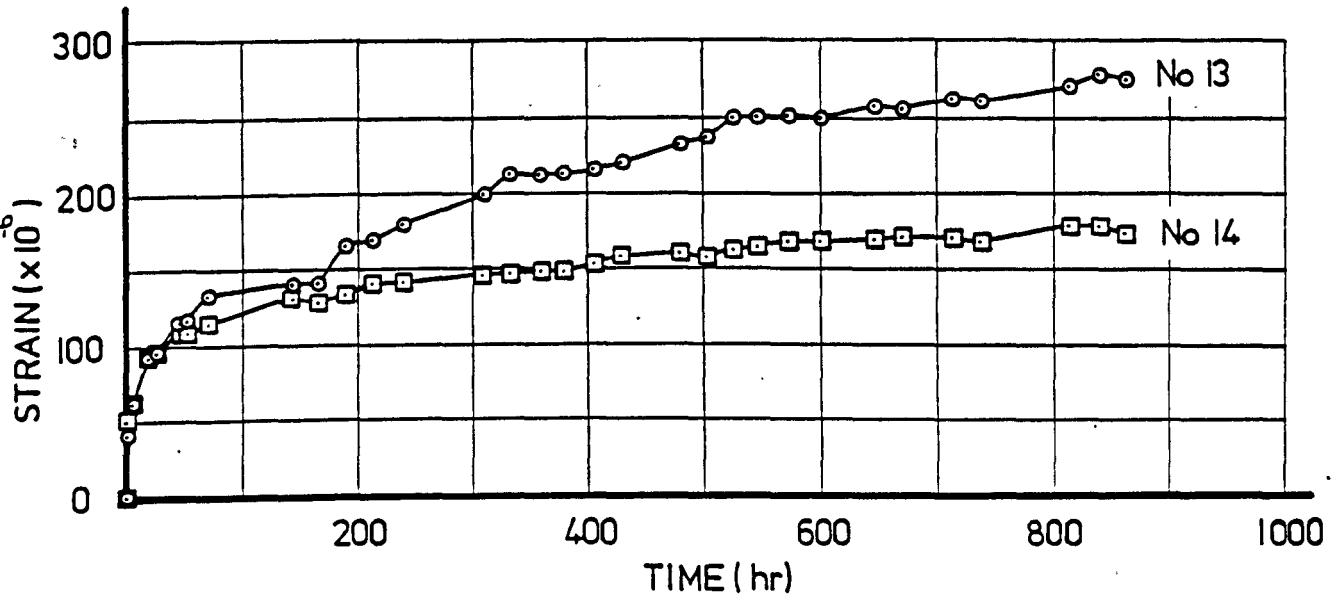

ACTIVE GAUGES

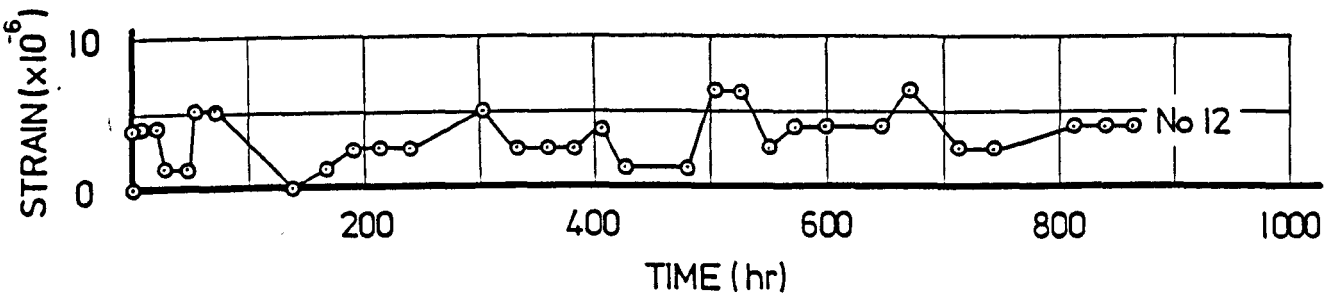

DUMMY GAUGE

FIRST RELAXATION PERIOD

STRAIN

FIG. 6.27

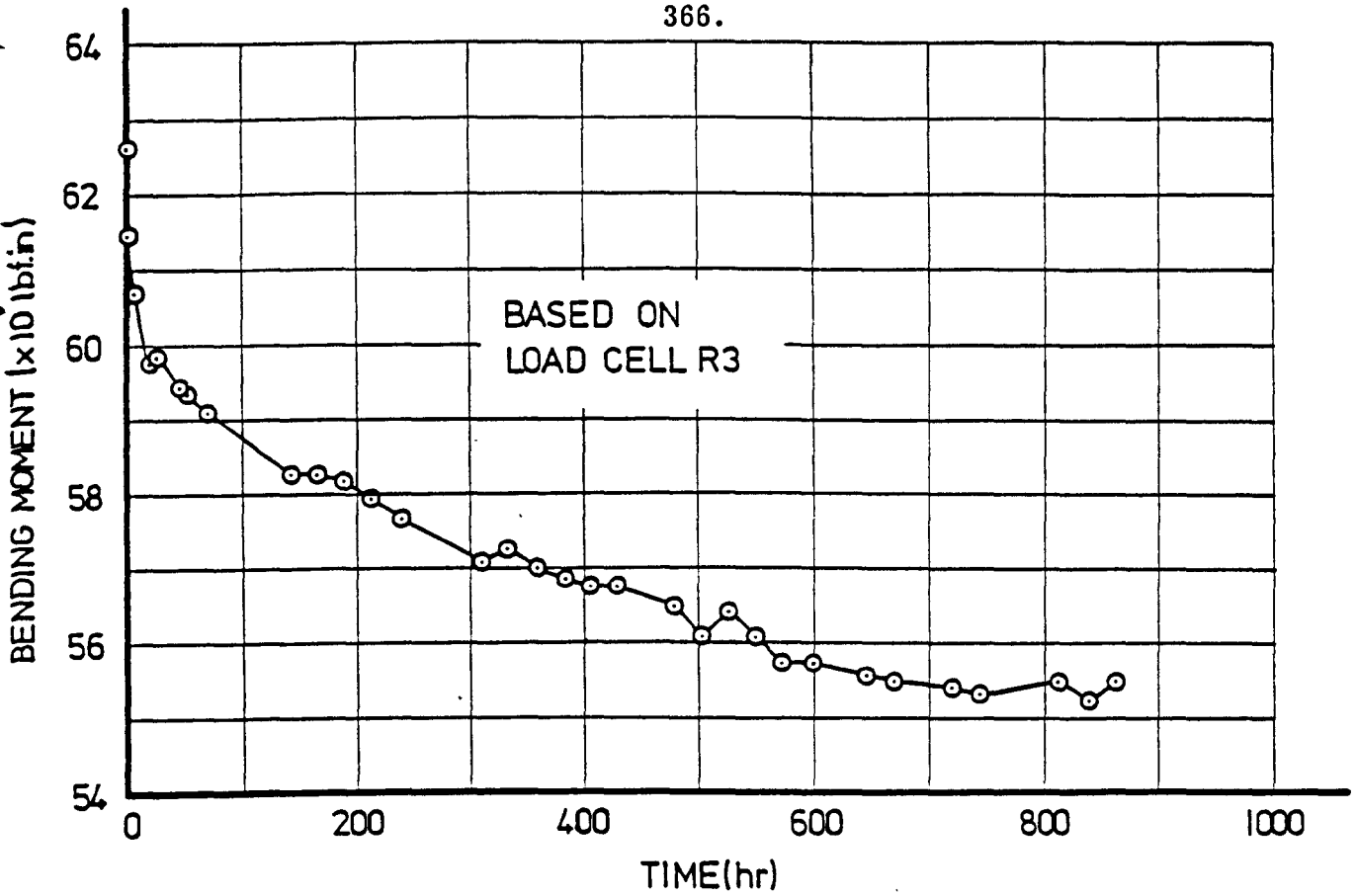

FIRST RELAXATION PERIOD
BENDING MOMENT

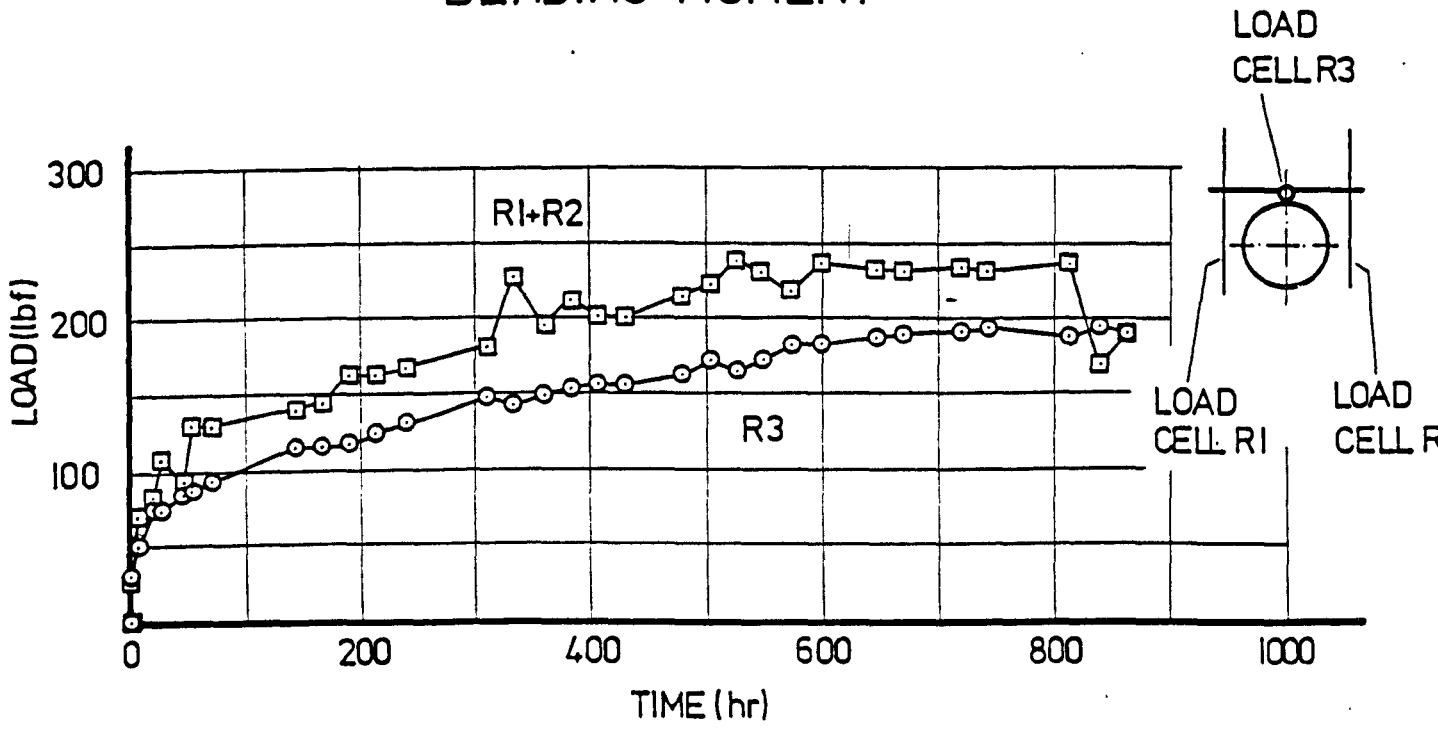

FIRST RELAXATION PERIOD
LOAD REDUCTION

FIG. 6.28

CHAPTER 7

General Conclusions

A theoretical analysis of the flanged bend problem under out-of-plane bending has been presented in PART (1) of this thesis. The analysis represents an optimum lower bound solution based on the results of earlier solutions obtained during the study. A comparison with these earlier results shows that the chosen solution gives the highest (and hence best) flexibility factor with the minimum level of computation.

The results clearly demonstrate that the incorporation of rigid flanges on the ends of a bend can cause a significant reduction in its flexibility factor, the flexibility reducing with bend angle and radius ratio and increasing as the pipe factor reduces. The location and magnitude of the maximum stress on a flanged bend was shown to be dependent on the bend angle, radius ratio and pipe factor, but without any simple trend. The maximum stresses may occur along the bend or at the flange, on the inside or outside surface and may be in the direction of either of the principal axes.

A comparison with the theoretical results of Whatham [170] gave good general agreement, his flexibility factors being between 10% to 20% higher. Although a variety of finite element results have been published for various combinations of end constraints, Whatham appears to be the only author who has published theoretical results on the out-of-plane bending of flanged bends. A similar trend is evident in the experimental field and it is unfortunate that perhaps the most comprehensive set of experimental results conducted by Pardue and Vigness [126] dates back to 1952. Their results for flexibility and stress factors were shown to be higher than both the present theory and Whatham's results. Although Pardue and Vigness performed a comprehensive set

of experiments the actual details of their tests are not completely clear and as such have not been considered as valid comparison. Experiments conducted by this author, however, were shown to compare favourably with the present theory.

A comparison with the results of Thomson [134] for in-plane bending showed that the flexibility and stress factors are greatly reduced when the bend is subjected to an out-of-plane moment. It is expected that this trend will also prevail when tangent pipe end constraints are considered. However, due to the high level of computation time demanded by the solution this extension to the theory was not actively pursued although it was incorporated as an optional feature in the computer program.

In the light of the current work it is evident that little attention has been paid to the problem of out-of-plane bending. The current design codes are seen to be inadequate and require some modification, particularly in regard to the end constraints of flanges.

In PART (2) of this thesis a description of the work undertaken during an experimental creep programme on pipe bends has been presented. This programme of work was aimed primarily at obtaining long-term static creep strain measurements at elevated temperature (570°C) on a variety of stainless steel pipe bend assemblies under bending loads.

In presentation the emphasis has been placed upon the experimental techniques employed and the development of new techniques arising from problems encountered during the course of the work. As in all experimental studies, by virtue of the diverse nature of the

problems encountered, the work encroached into many other fields. The results of the work highlighted a number of features regarding the performance and operation of a variety of techniques and devices. These were seen to cover the three broad areas of:

(a) measurement of strain at elevated temperature

(b) measurement of displacement at elevated temperature

(c) heating and control system.

In the measurement of strain at elevated temperature the accuracy of the CERL-Planer capacitance strain gauge was shown to be dependent on a representative in-situ calibration. Calibrations not compatible with the in-situ conditions were shown to underestimate the strain by at least 20% to 30%. Other aspects such as the use of wedges for mounting of the gauge on curved surfaces, electrical interference between component parts of the gauge and insulation breakdown on the gauge leads, were shown to influence the response of the gauge by varying degrees.

The CERL gauge has been in use, with apparent success, for a number of years in several laboratory establishments at home and abroad, and it is only in the course of this study that these problems have come to light.

A number of methods of measurement of distortion of the cross-section and rotation of the bend assembly were examined during the course of the work. Each method incorporated dial gauges as the prime means of measuring displacement, and although other devices were examined the dial gauge was retained for its versatility and low cost.

In the provision of a heating system resulting in a more uniform temperature distribution a novel heating system was developed using a copper sheath enclosing the bend assembly. This was shown to provide an improved temperature distribution in both the meridional and circumferential direction at a significant saving to commercially available systems.

From all the development work conducted during the study, the essential feature was seen to be the establishment of a testing procedure using proven techniques to give accurate and perhaps more importantly, results which could be considered as "sound experimental data" to aid in substantiating present and developing theories.

In view of the difficulties encountered during the theoretical work, it is important to recognise that any further work undertaken would require a convergence check on the final solution before proceeding.

BIBLIOGRAPHY

1. KÁRMÁN, Von T. "Uber die Formanderung Dunnwandiger Röhre insb esonders Federnder Ausgleich-rohre". Zeits V.D.I., Vol. 55, pp. 1889-1895, 1911.

2. BANTLIN, A. "Formanderung und Beanspruchung Febernder Ausfleichrochen". Zeits V.D.I., Vol. 2, pp. 43-49, 1910.

3. MARBEC, M. "Flexibilité des tubes". Bull. Assoc. Techn. Maritime Aeronaut, Vol. 22, pp. 441-475, 1911.

4. SPENCE, J. "On the Bounding of Pipe Bend Flexibility Factors". Nuc. Eng. and Design, Vol. 12, No. 1, pp. 39-47, 1970.

5. LORENZ, H. "Die Biegung Krummer Röhre". Physik Zeits, Vol. 13, pp. 768-774, 1912.

6. TIMOSHENKO, S. "Bending Stresses in Curved Tubes of Rectangular Cross-sections". Trans. A.S.M.E., Vol. 45, pp. 135-140. 1923.

7. HOVGAARD, W. "The Elastic Deformation of Pipe Bends". J. of Math. and Phys. of M.I.T., Vol. VI, No. 2, pp. 69-118, 1926.

8. HOVGAARD, W. "Deformation of Plane Pipes". J. of Math. and Phys. of M.I.T., Vol. VII, pp. 198-238, 1928.

9. WAHL, A.M. "Stresses and Reactions in Expansion Pipe Bends". Trans. A.S.M.E., Vol. 50, pp. 241-262, 1928.

10. JENKS, H.E. "Design of Steam Piping to Care for Expansion". Trans. A.S.M.E., Vol. 51, pp. 443-444, 1929.

11. HOVGAARD, W. "Stresses in Three-Dimensional Pipe Bends". Trans. A.S.M.E., Vol. 57, pp. 401-415, 1935.

12. HOVGAARD, W. "Further Studies of Three-Dimensional Pipe Bends". *ibid.*, Vol. 60, pp. 647-650, 1938.

13. MARKL, A.R.C. "Piping Flexibility Analysis". Trans. A.S.M.E., Vol. 77, pp. 419-441, 1955.

14. THULOUP, M.A. "Essai sur la Fatigue des Tuyaux Minces à Fibre moyenne plane au gauche". Bull. Assoc. Techn. Maritime Aeronaut, Vol. 32, p. 643, 1928.

15. THULOUP, M.A. "Sur la Deformation et les Tensions Internes des Tuyaux à Ligne Moyenne Plane". *ibid.*, Vol. 36, 1932.

16. THULOUP, M.A. "Remarques sur le calcul des Tuyaux Minces sous Pression". *ibid.*, Vol. 41, 1937.

17. TUEDA, M. "Mathematical Theories of Bourdon Pressure Tubes and Bending of Curved Pipes". Mem. Coll. Eng., Kyoto Imperial Univ., First Rep., Vol. 8, p. 102, 1934. Second Rep., Vol. 9, p. 132, 1936.

18. KARL, H. "Biegung geKrümmter, dünnwandiger Röhre". Zeits Angew. Math. Mech., Vol. 23, pp. 331-345, 1943.

19. VIGNESS, I. "Elastic Properties of Curved Tubes". Trans. A.S.M.E., Vol. 65, pp. 105-120, 1943.

20. BESKIN, L. "Bending of Curved Thin Tubes". Trans. A.S.M.E., Vol. 67, p. A-1, 1945.

21. BARTHELEMY, J. "Étude de la Déformation et des Tensions Internes des Tuyaux à Ligne Moyenne Plane, sans Pression Interne". Bull. Assoc. Techn. Maritime Aeronaut, Vol. 45, p. 139, 1946.

22. BARTHELEMY, J. "Étude de la Deformation et des Tensions Internes des Tuyaux à Ligne Moyenne Plane soumis à des Efforts Extériéurs et à une Pression Interne". *ibid.*, Vol. 46, p. 411, 1947.

23. DE LEIRIS, H. BARTHELEMY, J. "Determination des Deformations et des Tensions dans un Tuyaux à Section Ovale". *ibid.*, Vol. 47, p. 147, 1948.

24. DE LEIRIS, H. BARTHELEMY, J. "Deformations et Tensions dans les Tuyaux à Ligne Moyenne Plane". French paper, source uncertain, pp. 308-321, c. 1950.

25. HUBER, M.T. — "The Bending of the Curved Tube of Elliptic Section". Proc. 7th Int. Cong. for Appl. Mech., Vol. 1, p. 322, 1949.

26. HUBER, M.T. — "Archiwum Mechaniki Stosowanej". Polish Publication, Vol. 1, No. 2, 1949.

27. REISSNER, E. — "On Bending of Curved Thin-Walled Tubes". Proc. Natl. Acad. Sci. U.S., Vol. 35, pp. 204-208, 1949.

28. CLARK, R.A. REISSNER, E. — "Bending of Curved Tubes". Adv. in Appl. Mechs., Vol. II, 1951.

29. GROSS, N. — Experiments in Short-Radius Pipe Bends". Proc. I. Mech. E., (B). Vol. 1B, p. 465, 1952-1953.

30. GROSS, N. FORD. H. — "The Flexibility of Short-Radius Pipe Bends". Proc. I. Mech. E., (B). Vol. 1B, p. 480, 1952-1953.

31. KAFKA, P.G. DUNN, M.B. — "Stiffness of Curved Circular Tubes with Internal Pressure". Trans. A.S.M.E., J. of Appl. Mechs., Vol. 78, p. 247, 1956.

32. CRANDALL, S.H. DAHL, N.C. — "The Influence of Pressure on the Bending of Curved Tubes". Proc. 9th Int. Cong. of Appl. Mechs., pp. 101-111, 1956.

33. RODABAUGH, E.C. GEORGE, H.H. — "Effect of Internal Pressure on Flexibility and Stress-Intensification Factors of Curved Pipe or Welding Elbows". Trans. A.S.M.E., Vol. 79, pp. 939-948, 1957.

34. TURNER, C.E. FORD, H. — "Examination of the Theories for Calculating the Stresses in Pipe Bends Subjected to In-Plane Bending". Proc. I. Mech. E., Vol. 171, p. 513, 1957.

35. FINDLAY, G.E. SPENCE, J. — "In-Plane Bending of a Large 90° Smooth Bend". J. of Strain Analysis, Vol. 1, No. 4, p. 290, 1966.

36. JONES, N. KITCHING, R. — "An Experimental Investigation of a Right-Angled Single Unreinforced Mitre-Bend Subjected to Various Bending Moments". J. of Strain Analysis, Vol. 1, No. 3, pp. 248-263, 1966.

37. M.W. KELLOG Co. "Design of Piping Systems". John Wiley and Sons Inc., 1956.

38. JONES, N. "On the Design of Pipe Bends". Nuc. Eng. and Design, Vol. 4, pp. 399-405, 1966.

39. JONES, N. "In-Plane Bending of a Short-Radius Curved Pipe Bend". Trans. A.S.M.E., J. of Eng. for Industry, Vol. 89, ser. B, p. 271, 1967.

40. SMITH, R.T. "Theoretical Analysis of the Stresses in Pipe Bends Subjected to Out-of-Plane Bending". J. of Mech. Eng. Sci., Vol. 9, No. 2, p. 115, 1967.

41. CHENG, D.H. THAILER, H.J. "In-Plane Bending of Curved Circular Tubes". Trans. A.S.M.E., J. of Eng. for Industry, Vol. 90, Ser. B, No. 4, p. 666, 1968.

42. CHENG, D.H. THAILER, H.J. "On the Bending of Curved Circular Tubes". *ibid.*, Vol. 92, Ser. B, No. 1, pp. 62-66, 1970.

43. BOND, M.P. KITCHING, R. "Stress and Flexibility Factors for Multi-Mitred Bends Subjected to Out-of-Plane Bending". J. of Strain Analysis, Vol. 6, No. 4, pp. 213-225, 1971.

44. KITCHING, R. "Mitre Bends Subjected to In-Plane Bending Moments". Int. J. of Mech. Eng. Sci., No. 7, p. 551, 1965.

45. FINDLAY, G.E. SPENCE, J. "Bending of Pipe Bends with Elliptic Cross-Sections". Weld. Res. Counc. Bull., No. 164, 1971.

46. SPENCE, J. FINDLAY, G.E. "The Effect of Thickness Variations on the Behaviour of Smooth Curved Pipes under External Bending". A.S.M.E./C.S.M.E. Press. Ves. and Piping Conf., Montreal, June 1978, A.S.M.E. paper No. 78-PVP-93.

47. DODGE, W.G. MOORE, S.E. "Stress Indices and Flexibility Factors for Moment Loadings on Elbows and Curved Pipes". Welding Res. Counc. Bull., No. 179, 1972.

48. DODGE, W.G.
MOORE, S.E.
"ELBOW: A Fortran Program for the Calculation of Stresses, Stress Indices and Flexibility Factors for Elbows and Curved Pipes".
Oak Ridge Nat. Lab., Rep. No. ORNL-TM-4098, April 1973.

49. BLOMFIELD, J.A.
TURNER, C.E.
"Theory of Thin Elastic Shells Applied to Pipe Bends Subjected to Bending and Internal Pressure".
J. of Strain Analysis, Vol. 7, No. 4, pp. 285-293, 1972.

50. KITCHING, R.
BOND, M.P.
"Out of Circularity Effects in a Pipe Subjected to Pressure and Bending Loads".
J. of Strain Analysis, Vol. 7, No. 4, pp. 294-302, 1972.

51. ROBERT, A.
DUFORET, C.
"Analysis of the Flexibility and the Stresses in Curved Pipes Subjected to In-Plane or Out-of-Plane Bending".
2nd Int. Conf. on Press. Ves. Tech., Part 1, San Antonio, Texas, 1973.

52. SMITH, R.T.
FORD, H.
"Experiments on Pipelines and Pipe Bends Subjected to Three-Dimensional Loading".
J. of Mech. Eng. Sc., Vol. 9, No. 2, p. 124, 1967.

53. SEAMAN, W.J.
WAN, F.Y.M.
"Lateral Bending and Twisting of Thin-Walled Curved Tubes".
Studies in Appl. Math., Vol. LIII, No. 1, pp. 73-89, 1974.

54. THOMPSON, J.J.
"Shell Theory Analysis of Pure In-Plane Bending of a Pipe Bend".
Proc. 3rd Int. Conf. Struct. Mech. in Reactor Tech., London, 1975.

55. ARAV, F.
"Evaluation of Pipe Bends having Local Corrugations".
3rd Int. Conf. on Press. Ves. Techn., Part 1, Tokyo, Japan, 1977.

56. COPE, E.T.
WERT, E.A.
"Load-Deflection Relations for Large, Plain, Corrugated, and Creased Pipe Bends".
Trans. A.S.M.E., Vol. 54, 1932.

57. MARCAL, P.V.
PILGRIM, W.R.
"A Stiffness Method for Elastic-Plastic Shells of Revolution".
J. of Strain Analysis, Vol. 1, No. 4, pp. 339-350, 1966.

58. MARCAL, P.V. "Elastic-Plastic Behaviour of Pipe Bends with In-Plane Bending". J. of Strain Analysis, Vol. 2, No. 1, pp. 84-90, 1967.

59. BOLT, S.E.
GREENSTREET, W.L. "Experimental Determination of Plastic Collapse Loads for Pipe Elbows". Press. Vess. and Piping Conf., San Francisco, 1971.

60. VRILLON, B.
ROCHE, R.
BAYLAC, G. "Comparison Between Experimental and Computer Analyses of the Behaviour Under Pressure of a 90° Bend with an Elliptical Section". 2nd Int. Conf. on Press. Ves. Techn., Part 1, San Antonio, Texas, 1973.

61. SPENCE, J.
FINDLAY, G.E. "Limit Loads for Pipe Bends Under In-Plane Bending". 2nd Int. Conf. on Press. Ves. Techn., Part 1, San Antonio, Texas, 1973.

62. MARCAL, P.V.
TURNER, C.E. "Elastic Solution in the Limit Analysis of Shells of Revolution with Special Reference to Expansion Bellows". J. of Mech. Eng. Sc., Vol. 3, No. 3, pp. 252-257, 1961.

63. SPENCE, J. "Creep Analysis of Smooth Curved Pipes Under In-Plane Bending". J. of Mech. Eng. Sc., Vol. 15, No. 4, 1973.

64. CALLADINE, C.R. "Limit Analysis of Curved Tubes". J. of Mech. Eng. Sc., Vol. 16, No. 2, pp. 85-87, 1974.

65. MELLO, R.M.
GRIFFIN, D.S. "Plastic Collapse Loads for Pipe Elbows Using Inelastic Analysis". Trans. A.S.M.E., J. of Press. Ves. Techn., Vol. 96, pp. 177-183, 1974.

66. "MARC." "MARC-CDC Nonlinear Finite Element Analysis Program". MARC Analysis Corporation and Control Data Corporation, Minneapolis, Minnesota, 1971.

67. VRILLON, B.
MONTFORT, C.
BEFRE, J. "Experimental Analysis on Piping Components of Fast Breeder Reactors". Trans. of 3rd Int. Conf. Struct. Mech. in Reactor Tech., Vol. 2, London, 1975.

68. SPENCE, J.
FINDLAY, G.E.
"Limit Moments for Non-Circular Cross-Sections (Elliptical) Pipe Bends".
Trans. of 4th Int. Conf. Struct. Mech. in Reactor Tech., San Francisco, 1977.

69. SOBEL, L.H.
NEWMAN, S.Z.
"Comparison of Experimental and Simplified Analytical Results for the In-Plane Plastic Bending and Buckling of an Elbow".
Trans. A.S.M.E., J. of Press. Ves. Tech., Vol. 102, pp. 400-409, 1980.

70. MOORE, M.A.
"In-Plane Flexural Behaviour of Smooth Pipe Bends under Elastic and Plastic Conditions".
Doctoral Dissertation, Univ. of Manchester, 1978.

71. PROST, J.P.
AMZALLAG, C.
"Experimental Study of Carbon Steel Straight Pipes and Elbows under Moment Loadings".
Trans. of 6th Int. Conf. on Struct. Mech. in Reactor Tech., Paris, France, 1981.

72. BRASCHEL, R.A.
RICHTER, Th.
ZEITNER, W.H.
RICHTER, G.
"Calculation of the Load Carrying Capacity of Pipe Elbows with the help of the Method of Approximation".
Trans. of 7th Int. Conf. on Struct. Mech. in Reactor Tech., Chicago, Illinois, U.S.A., 1983.

73. "NISA".
"NISA Benutzerhandbuch".
Institut für Baustatik, Univ. of Stuttgart, W. Germany.

74. PROST, J.P.
TAUPIN, Ph.
DELIDAIS, M.
"Experimental Study of Austenitic Stainless Steel Pipes and Elbows under Pressure and Moment Loadings".
Trans. of 7th Int. Conf. on Struct. Mech. in Reactor Tech., Chicago, Illinois, U.S.A., 1983.

75. SOBEL, L.H.
"The Southwell Method for Predicting Plastic Buckling Loads for Elbows".
Trans. A.S.M.E., J. of Press. Ves. Tech., Vol. 105, pp. 2-8, 1983.

76. SOUTHWELL, R.V.
"On the Analysis of Experimental Observations in Problems of Elastic Stability".
Proc. of Royal Soc., Series A, Vol. 135, pp. 601-616, 1932.

77. PAN, Y.
YETTER, R.
"Inelastic Analysis of Pipelines in the F.F.T.F. C.L.S. Module".
A.S.M.E. Conf. on Press. Ves. and Piping Analysis and Computers, Miami, 1974.

78. LARSON, L.D.
STOKEY, W.F.
FRANZEN, W.E.
"An Approximate Model for an Elastic Plastic Pipe Element under Combined Loading".
Trans. A.S.M.E., Ser. J., J. of Press. Ves. Tech., 97, pp. 22-28, 1975.

79. LAZZERI, L.
"An Elastoplastic Elbow Element, Theory and Applications".
5th Int. Conf. on Struct. Mech. in Reactor Tech., Berlin, 1979.

80. LAZZERI, L.
"A Model for a Strain Hardening Pipe Element".
A.S.M.E. paper No. 77-PVP-47.

81. BATHE, K-J.
ALMEIDA, C.A.
HO, L.W.
"A Simple and Effective Pipe Elbow Element - some Nonlinear Capabilities".
Comp. and Struct., Vol. 17, No. 5-6, pp. 659-667, 1983.

82. LAZZERI, L.
"PAULA 82: A Code for Nonlinear Analysis of Pipes and Shells".
Trans. 7th Int. Conf. on Struct. Mech. in Reactor Tech., Chicago, Illinois, U.S.A., 1983.

83. DENNISON, R.L.
"The Strength and Flexibility of Corrugated and Creased Bend Piping".
J. of Am. Soc. Naval Eng., Vol. 47, pp. 343-432, 1935.

84. ROSSHEIM, R.B.
MARKL, A.R.C.
"The Significance of and Suggested Limits for the Stresses in Pipe Lines due to the Combined Effects of Pressure and Expansion".
Trans A.S.M.E., Vol. 62, pp. 443-464, 1940.

85. MARKL, A.R.C.
"Fatigue Tests of Welding Elbows and Comparable Double-Mitre Bends".
Trans. A.S.M.E., Vol. 69, pp. 869-879, 1947.

86. MARKL, A.R.C.
"Fatigue Tests of Piping Components".
Trans. A.S.M.E., Vol. 74, p. 287, 1952.

87. LANE, P.H.R.
"Fatigue Tests on Seamless Mild Steel Pipe Bends".
B.W.R.A. (Confidential Report) No. 16/41/56, 1956.

88. BLOMFIELD, J.A.
JACKSON, P.B.M.
"Fatigue Tests on some Cupro-Nickel Pipe Bends and a Comparison of some Failure Prediction Methods".
1st Int. Conf. on Press. Ves. Tech., Deltf, 1969.

89. BLOMFIELD, J.A.
"The Elastic Plastic Behaviour of Pipe Bends Subjected to Cyclic Loading".
Doctoral Dissertation, Univ. of London, 1970.

90. UDOGUCHI, T.
ASADA, Y.
"Investigation on Low-Cycle Fatigue Strength of Piping Components".
2nd Int. Conf. on Press. Ves. Tech., Part 2, San Antonio, Texas, 1973.

91. ANDO, Y.
YAGAWA, G.
KAWAGUCHI, O.
OKABAYASHI, K.
UEDA, S.
NAGATA, T.
"Low-Cycle Fatigue Strength of Piping Components".
2nd Int. Conf. on Press. Ves. Tech., Part 2, San Antonio, Texas, 1973.

92. HEALD, J.D.
KISS, E.
"Low-Cycle Fatigue of Nuclear Pipe Components".
Trans. A.S.M.E., J. of Press. Ves. Tech., 1974.

93. JAMES, L.A.
"Estimation of Crack Extension in a Piping Elbow using Fracture Mechanics Techniques".
Trans. A.S.M.E., J. of Press. Ves. Tech., 1974.

94. DOYEN, J.J.
MARINI, J.
"Propagation of Inadequate Joint Penetration Defects of Welded Elbows".
4th Int. Conf. on Struct. Mech. in Reactor Tech., San Francisco, 1977.

95. KACHANOV, L.M.
"O PlastichensKom Izgibe Krivgich FunKostennyich Trub".
Igv. Akad. Wauk S.S.R. OTD, Vol. 5, p. 42, 1957.

96. SPENCE, J.
MACKENZIE, A.C.
"Stationary Creep Deformation of a Smooth Pipe Bend under In-Plane Bending Moments".
Int. J. of Mech. Sc., Vol. 11, pp. 387-394, 1969.

97. NORTON, F.H. "The Creep of Steel at High Temperatures". McGraw-Hill, London, 1929.

98. SPENCE, J. "Creep Behaviour of Smooth Curved Pipes under Bending". 1st Int. Conf. on Press. Ves. Tech., Delft, 1969.

99. SPENCE, J. "An Upper Bound Analysis for the Deformation of Smooth Pipe Bends in Creep". 2nd Int. Union of Theo. and Appl. Mech. Sym. on Creep in Structures, Gottenburg, 1970.

100. SPENCE, J. "Creep of Pipe Bends". Doctoral Dissertation, Univ. of Strathclyde, 1971.

101. SPENCE, J. "An Analysis for Pipework Systems under Creep Conditions". Proc. 1st Int. Conf. on Struct. Mech. in Reactor Tech., 1971.

102. SPENCE, J. "Stationary Creep Stresses for Elliptical Cross-Section Pipe Bends Subject to In-Plane Bending". A.S.M.E., J. of Press. Ves. Tech., Vol. 96, pp. 162-171, 1974.

103. SPENCE, J. "A Note on the Gross Correction for Non-circular Inelastic Pipe Bends under In-Plane Bending". A.S.M.E., J. of Press. Ves. Tech., Vol. 101, pp. 102-104, 1979.

104. SPENCE, J. "The Creep Deformation of Elliptical Cross-Section Pipe Bends under In-Plane Bending". Int. Conf. on Creep and Fatigue, A.S.M.E./ I.Mech.E., Philadelphia, 1974.

105. SPENCE, J. "The Creep Behaviour of Short Radius Pipe Bends". 3rd Int. Conf. on Struct. Mech. in Reactor Tech., London, 1975.

106. WORKMAN, G.H. RODABAUGH, E.C. "Strain Concentration in an Elbow in a Piping System under High Temperature Relaxation Conditions". A.S.M.E., 2nd Int. Conf. Press. Ves. Tech., San Antonio, Texas, 1973.

107. WORKMAN, G.H.
RODABAUGH, E.C.
"Simplified Second Stage Creep/Relaxation Analysis of Moderately Complex Spatially Three-Dimensional Piping Systems". J. of Press. Ves. Tech., Trans. A.S.M.E., Vol. 94, pp. 184-192, 1974.

108. HIBBITT, H.D.
SORENSON, E.P.
MARCAL, P.V.
"The Elastic-Plastic and Creep Analysis of Pipelines by Finite Elements". 2nd Int. Conf. Press. Ves. Tech., San Antonio, Texas, 1973.

109. MELLOW, R.M.
SCHELLER, J.D.
"Simplified Inelastic (Plastic and Creep) Analysis of Pipe Elbows Subjected to In-Plane and Out-of-Plane Bending". A.S.M.E., 2nd Nat. Cong. on Press. Ves. and Piping, San Francisco, 1975.

110. BOYLE, J.T.
"Rational Creep Mechanics". Doctoral Dissertation, Univ. of Strathclyde, 1975.

111. BOYLE, J.T.
SPENCE, J.
"The Nonlinear Analysis of Pressurised Curved Pipes". 3rd Int. Conf. Press. Ves. Tech., Tokyo, Japan, 1977.

112. BOYLE, J.T.
SPENCE, J.
"An Analysis of Out-of-Plane Bending of Curved Pipes in Creep". Proc. I.W.G.F.R. Conf. Fast Breeder Reactors, Pittsburgh, U.S.A., 1976.

113. BOYLE, J.T.
SPENCE, J.
"The Flexibility of Curved Pipes in Creep". Trans. A.S.M.E., J. of Press. Ves. Tech., Vol. 99, pp. 844-853, 1977.

114. BOYLE, J.T.
SPENCE, J.
"The Analysis of Piping Systems for Creep". 4th Int. Conf. on Struct. Mech. in Reactor Tech., San Francisco, 1977.

115. GRIFFITH, W.I.
RODABAUGH, E.C.
"Tests at Room Temperature and 1100°F on a 4 in. Sch. 10 Elbow-Pipe Assembly Subjected to In-Plane Moment Loading". Press. Ves. and Piping: Verification and Qualification of Inelastic Analysis Computer Programs, A.S.M.E., pp. 59-78, 1975.

116. IMAZU, A.
MIURA, R.
NAKUMARA, K.
NAGATA, T.
OKABOYASHI, K.
"Elevated Temperature Elastic-Plastic Creep Tests of an Elbow Subjected to In-Plane Moment Loading". Press. Ves. and Piping Conf., A.S.M.E., Mexico, 1976.

117. IMAZU, A.
NAKAMURA, K.
"Simplified Creep Buckling Analysis of Elbows under In-Plane Bending".
5th Int. Conf. on Struct. Mech. in Reactor Tech., Berlin, 1979.

118. WATANABE, O.
OHTSUBO, H.
"Inelastic Flexibility and Strain Concentration of Pipe Bends in Creep Range with Plastic Effects".
Trans. A.S.M.E., J. of Press. Ves. Tech., Vol. 102, pp. 271-277, 1980.

119. KRAUS, H.
"International Benchmark Project on Simplified Methods for Elevated Temperature Design and Analysis".
WRC Bull. 258, 1980.

120. KRAUS, H.
"International Benchmark Project on Simplified Methods for Elevated Temperature Design and Analysis".
WRC Bull. 274, 1982.

121. BOYLE, J.T.
SPENCE, J.
"Inelastic Analysis Methods for Piping Systems".
Nuc. Eng. and Design, 57, pp. 369-390, 1980.

122. BOYLE, J.T.
SPENCE, J.
"A Comparison of Approximate Methods for Estimation of the Creep Relaxation of a Curved Pipe".
Int. J. of Press. Ves. and Piping, 4, pp. 221-252, 1976.

123. SEVERUD, L.K.
"Experience with Simplified Inelastic Analysis of Piping Designed for Elevated Temperature Services".
Trans. A.S.M.E., J. of Press. Ves. Tech., Vol. 103, pp. 267-280, 1981.

124. PAI, D.H.
"The PVRC International Benchmark Project on Simplified Methods for Elevated Temperature Design and Analysis - An Up date".
Trans. A.S.M.E., J. of Press. Ves. Tech., Vol. 105, pp. 85-90, 1983.

125. CESARI, F.
REGIS, V.
MENGHINI, S.
"Inelastic Analysis and Material Tests Comparison in High Temperature Steam Piping Life Verification".
Trans. of 7th Int. Conf. on Struct. Mech. in Reactor Tech., Chicago, Illinois, 1983.

126. PARDUE, T.E.
VIGNESS, I.
"Properties of Thin-Walled Curved Tubes of Short-Bend Radius".
Trans. A.S.M.E., Vol. 73, pp. 77-87, 1951.

127. PARDUE, T.E.
VIGNESS, I.
"Characteristics of Pipe Bends under Applied Moments".
Naval Research Lab., Rep. No. 111292, 1953.

128. VISSAT, P.L.
DEL BUONO, A.J.
"In-Plane Bending Properties of Welding Elbows".
Trans. A.S.M.E., Vol. 77, pp. 161-175, 1955.

129. KALNINS, A.
"Analysis of Shells of Revolution Subjected to Symmetrical and Non-symmetrical Loads".
J. of App. Mech., Vol. 31, pp. 467-476, 1964.

130. KALNINS, A.
"Analysis of Curved Thin Walled Shells of Revolution".
A.I.A.A. J., Vol. 6, No. 4., pp. 584-588, 1968.

131. KALNINS, A.
"Stress Analysis of Curved Tubes".
1st Int. Conf. on Press. Ves. Tech., Delft, 1969.

132. JACOBS, R.L.
SUROSKY, H.
"Experimental Investigation of the Effect of End Conditions and Bend Angle on the Stress Distribution of Welding Elbows".
MACHLAB Rep. No. 66, Naval Ship Research and Dev. Centre, Maryland, 1968.

133. THAILER, H.J.
CHENG, D.H.
"In-Plane Bending of a U-Shaped Circular Tube with End Constraints".
J. Eng. for Industry, Vol. 92, No. 4, pp. 792-796, 1970.

134. THOMSON, G.
"The Influence of End Constraints on Pipe Bends".
Doctoral Dissertation, Univ. of Strathclyde, 1980.

135. NATARAJAN, R.
"Finite Element Analysis of Pipe Bends using Doubly Curved Shell Elements".
Doctoral Dissertation, Univ. of London, 1971.

136. BLOMFIELD, J.A.
NATARAJAN, R.
"Piping Analysis - The Need to Establish Correct Flexibility Factors for Bends".
Conf. on "The Use of Computers in Pressure Vessel Design", I. Mech. Eng., 1971.

137. NATARAJAN, R.
BLOMFIELD, J.A.
"Stress Analysis of Curved Pipes with End Constraints".
Comp. and Struct., Vol. 5, pp. 187-196, 1975.

138. IMAMASA, J.
URAGAMI, K.
"Experimental Study of Flexibility Factors and Stresses of Welding Elbows with End Effects".
2nd Int. Conf. on Press. Ves. Tech., Part 1, San Antonio, Texas, 1973.

139. ARAI, K.
"Finite Element Method with Consideration to the Continuity of Normal Slope".
Mitsubishi Tech. Bull. No. 79, 1972.

140. FINDLAY, G.E.
"A Study of Smooth Pipe Bends under In-Plane Bending with Reference to End Constraints".
Doctoral Dissertation, Univ. of London, 1973.

141. FINDLAY, G.E.
SPENCE, J.
"The Effects of Flanges on Smooth Pipe Bends in Piping Systems".
2nd Int. Conf. on Struct. Mech. in Reactor Tech., Berlin, 1973.

142. FINDLAY, G.E.
SPENCE, J.
"Flexibility of Smooth Circular Curved Tubes with Flanged End Constraints".
Int. J. of Press. Ves. and Piping, Vol. 7, pp. 13-29, 1970.

143. FINDLAY, G.E.
SPENCE, J.
"Stress Analysis of Smooth Curved Tubes with Flanged End Constraints".
Int. J. of Press. Ves. and Piping, 1979.

144. AKSEL'RAD, E.L.
KVASNIKOV, B.N.
"Semi-zero-moment Theory of Curvilinear Bar Shells".
Izv. AN SSSR., Mekhanika Tverdogo Tela, Vol. 9, No. 2, pp. 139-147, 1974.
Translation: Mech. of Solids, pp. 125-133, 1974.

145 AXELRAD, E.
"Flexible Shell Theory and Buckling of Toroidal Shells and Tubes".
Ingenieur Archiv, pp. 95-104, 1978.

146. WRIGHT, W.B.
RODABAUGH, E.C.
THAILER, H.J.
"Influence of End Effects on Stresses and Flexibility of a Piping Elbow with In-Plane Moment".
Conf. on Press. Ves. and Piping, Analysis and Computers, Miami, 1974.

147. SOBEL, L.H.
"In-Plane Bending of Elbows".
Computers and Structures, Vol. 7, pp. 701-715, 1977.

148. RODABAUGH, E.C.
ISKANDER, S.K.
MOORE, S.E.
"End Effects on Elbows Subjected to Moment Loadings".
ORNL/Sub-2913/7, 1978.

149. "EPACA"
"Theory and Users Manual for EPACA, General Purpose Finite Element Analysis Program for Three-Dimensional Thick Shell Structures".
Argonne Code Centre, Argonne National Laboratory, Argonne.
Also: Nuc. Eng. and Design, 28, pp. 414-445, 1974.

150. KANO, T.
IWATA, K.
ASAKURA, J.
TAKEDA, H.
"Stress Distributions of an Elbow with Straight Pipes".
4th Int. Conf. on Struct. Mech. in Reactor Tech., San Francisco, 1977.

151. DE SALVO, G.J.
SWANSON, J.A.
"ANSYS Users Manual".
1972.

152. "ASKA"
"ASKA part 1 - Linear Static Analysis Users Reference Manual".
ISD - Rep. No. 73, Univ. of Stuttgart, 1971.

153. OHTSUBO, H.
WATANABE, O.
"Flexibility and Stress Factors of Pipe Bends - An Analysis by the Finite Ring Method".
Trans. A.S.M.E., J. of Press. Ves. Tech., pp. 281-290, 1977.

154. OHTSUBO, H.
WATANABE, O.
"Stress Analysis of Pipe Bends by Ring Elements".
Trans. A.S.M.E., J. of Press. Ves. Tech., Vol. 100, pp. 112-122, 1978.

155. WHATHAM, J.F.
"In-Plane Bending of Flanged Pipe Elbows".
Metal Struct. Conf., Inst. of Eng., Perth, Australia, 1978.

156. NOVOZHILOV, V.V.
"Thin Shell Theory".
Wolters-Noordhoff, Groningen, The Netherlands, 1970.

157. WHATHAM, J.F.
THOMPSON, J.J.
"The Bending and Pressurising of Pipe Bends with Flanged Tangents".
Nuc. Eng. and Design, Vol. 54, pp. 17-28, 1979.

158. BROUARD, D.
TREMBLAIS, A.
VRILLON, B.
"In-Plane and Out-of-Plane Bending Tests on Carbon Steel Pipe Bends".
Trans. 5th Int. Conf. on Struct. Mech. in Reactor Tech., Berlin, 1979.

159. KANO, T.
IWATO, K.
et al.
"Detailed Analysis of Three Elbow Pipe Assemblies".
Trans. of 5th Int. Conf. on Struct. Mech. in Reactor Tech., Berlin, 1979.

160. "FINAS"
"Development for FBR. Inelastic Structural Analysis System FINAS (II)".
SJ 240 78-01, Power Reactors and Nuclear Fuel Dev. Corp., 1978.

161. TAKEDA, H.
ASAI, S.
IWATA, K.
"A New Finite Element for Structural Analysis of Piping Systems".
Trans. of 5th Int. Conf. on Struct. Mech. in Reactor Tech., Berlin, 1979.

162. BATHE, K.J.
ALMEIDA, C.A.
"A Simple and Effective Pipe Elbow Element-Linear Analysis".
Trans. A.S.M.E., J. of App. Mech., Vol. 47, pp. 93-100, 1980.

163. KWEE, H.K.
"Stress Distributions and Flexibility of the Suction Bend of the Primary Sodium/Pump LMFBR-SNR 300".
Trans. of 5th Int. Conf. on Struct. Mech. in Reactor Tech., Berlin, 1979.

164. THOMSON, G.
SPENCE, J.
"The Influence of End Constraints on Smooth Pipe Bends".
Trans. of 6th Int. Conf. on Struct. Mech. in Reactor Tech., Paris, 1981.

165. NATARAJAN, R.
MIRZA, S.
"Stress Analysis of Curved Pipes with End Restraints Subjected to Out-of-Plane Moments".
Trans. of 6th Int. Conf. on Struct. Mech. in Reactor Tech., Paris, 1981.

166. THOMAS, K.
"Stiffening Effects on Thin-Walled Piping Elbows of Adjacent Piping and Nozzle Constraints".
Trans. A.S.M.E., J. of Press. Ves. Tech., Vol. 104, pp. 180-187, 1982.

167. ALMROTH, B.O.
BROGAN, F.H.
STANLEY, G.M.
"Structural Analysis of General Shells - Vol. III - User Instructions for STAGSC".
1975.

168. WHATHAM, J.F.
"Thin Shell Equations for Circular Pipe Bends".
Nuc. Eng. and Design, 65, pp. 77-89, 1981.

169. WHATHAM, J.F.
"Thin Shell Analysis of Circular Pipe Bends".
Trans. I. Aus. Eng., CE23, No. 4, 1981.

170. WHATHAM, J.F. "Analysis of Circular Pipe Bends with Flanged Ends". Nuc. Eng. and Design, 71, 1982.

171. WHATHAM, J.F. "Thin Shell Analysis of Flanged Pipe Bends". Trans. I. Aus. Eng., CE25, No. 1, 1983.

172. WHATHAM, J.F. "The use of Computer Codes BENDEF and PRESEF". M98, Australian Atomic Energy Commission, 1982.

173. WHATHAM, J.F. "The use of Computer Codes FLEXIN and FLEXOT". M99, Australian Atomic Energy Commission, 1982.

174. WHATHAM, J.F. "The use of Computer Codes SHEREF, COILEF and TURNEF". M100, Australian Atomic Energy Commission, 1982.

175. ÖRY, H.
WILCZEK, E. "Stress and Stiffness Calculation of Thin-Walled Curved Pipes with Realistic Boundary Conditions being Loaded in the Plane of Curvature". Int. J. Press. Ves. and Piping, 12, pp. 167-189, 1983.

176. ÖRY, H.
HORNUNG, E.
FAHLBUSCH, G. "A Simplified Matrix Method for the Dynamic Calculation of Different Shells of Revolution". AIAA - Symposium, Boston, 1965.

177. THOMSON, G.
SPENCE, J. "Combined Pressure and In-Plane Bending on Pipe Bends with Flanges". Trans. of 7th Int. Conf. on Struct. Mech. in Reactor Tech., Chicago, Illinois, 1983.

178. NATARAJAN, R.
MIRZA, S. "Effect of Internal Pressure on the Flexibility and Stresses in Pipe Elbows with End Constraints". Trans. of 7th Int. Conf. on Struct. Mech. in Reactor Tech., Chicago, Illinois, 1983.

179. MILLARD, A.
RICARD, A. "Accounting for Straight Parts Effects on Elbow's Flexibilities in a Beam Type Finite Element Program". Trans. of 7th Int. Conf. on Struct. Mech. in Reactor Tech., Chicago, Illinois, 1983.

180. MILLARD, A.
HOFFMANN, A.
ROCHE, R. "Program TEDEL - Analyse Élastique et Plastique de coudes". Note CEA, N-2116, 1980.

181. BRITISH STANDARD — "BS 806: Ferrous Pipes and Piping Installations for and in Connection with Land Boilers". 1975.

182. BRITISH STANDARD — "BS 3351: Piping Systems for Petroleum Refineries and Petrochemical Plant". 1971.

183. E.S.D.U. — "Flexibilities of and Stresses in Thin Pipe Bends under In-Plane Bending: Influence of Bend Angle and Tangent Pipe Ends". Item No. 75014, Eng. Sc. Data Unit, 1975.

184. E.S.D.U. — "Flexibilities of and Stresses in Thin Unpressurised Pipe Bends with Flanged Ends under In-Plane Bending: Influence of Bend Angle". Item No. 81041, Eng. Sc. Data Unit, 1981.

185. A.S.A. — "A.S.A. B.31.3 - 1966: Petroleum Refinery Piping".

186. U.S.A.S. — "U.S.A.S. B.31.10: Power Piping".

187. U.S.A.S. — "U.S.A.S. B.31.7: Nuclear Power Piping".

188. A.S.M.E. — "A.S.M.E. Boiler and Pressure Vessel Codes: Section 3, Nuclear Power Plant, Components". 1974.

189. SYMONDS, P.S. PARDUE, T.E. — "Characteristics of Short Radius Tube Bends". Naval Research Laboratory, Report O-2761, 1946.

190. PARDUE, T.E. VIGNESS, I. — "In-Plane Bending Properties of Welding Elbows". Trans. A.S.M.E., 77, p. 161, 1955.

191. BROUARD, D. MILLARD, A. TOMASSIAN, R. — "Experiments on 316L Pipe Bends under In-Plane Bending". Trans. 6th Int. Conf. on Struct. Mech. in Reactor Tech., Paris, 1981.

192. MILLARD, A. ROCHE, R. — "Propagation of Ovalisation along straight Pipes and Elbows". Trans. 6th Int. Conf. on Struct. Mech. in Reactor Tech., Paris, 1981.

193. LOVE, A.E.H. — "The Mathematical Theory of Elasticity". Dover Publications, N.Y., 1944.

194. REISSNER, E. "A New Derivation of the Equations for the Deformation of Elastic Shells". Am. J. of Math., Vol. LXIII, No. 1, pp. 177-184, 1941.

195. SANDERS, J.L. "Nonlinear Theories for Thin Shells". Quart. of App. Math., Vol. XXI, No. 1, pp. 21-36, 1963.

196. KOITER, W.T. "On the Nonlinear Theory of Thin Elastic Shells". Proc. Kon. Akad. Weben, Vol. 69, pp. 1-54, 1966.

197. KRAUSS, H. "Thin Elastic Shells". John Wiley and Sons, 1967.

198. SANDERS, J.L. "An Improved First Approximation Theory for Thin Shells". N.A.S.A., Rep. 24, June, 1959.

199. KOITER, W.T. "The Theory of Thin Elastic Shells". Int. Union of Theo. and App. Mechs. Proc. Sym., Delft, 1959.

200. FLÜGGE, W. "Stresses in Shells". Springer-Verlag, 1973.

201. DYM, C.L. "Introduction to the Theory of Shells". Pergamon Press, 1974.

202. GOLDENVEIZER, A.L. "Theory of Elastic Thin Shells". Trans. E. Herrmann, N.Y., 1961.

203. DONNELL, L. "A Discussion of Thin Shell Theory". Proc. Fifth Cong. on App. Mech., 1939.

204. MUSHTARI, K.M. "Certain Generalizations of the Theory of Thin Shells". Izv. fiz. Mat. Ob-va Pri Kaz. Un-te., XI, 1938.

205. VLASOV, V.Z. "On the Theory of Elastic Shells". D.A.N., S.S.S.R., Vol. 68, 1949.

206. STOKER, J.J. "Differential Geometry". Wiley-Interscience, N.Y., 1969.

207. KREYSZIG, E. "Differential Geometry". Univ. of Toronto Press, Toronto, 1959.

208. RITZ, W. "Über eine neve Methode zur Lösung gewisser Variationsprobleme der mathematischen Physik". J.f. Reine u. Angew. Math., 135, pp. 1-61, 1908.

209. RAYLEIGH, J.W. "The Theory of Sound". 2nd Ed., Dover Publications, N.Y., 1945.

210. RITZ, W. "Theorie der Transversalschwingungen einer quadratischen Platte mit freien Randern". Ann. Phys., 28, pp. 737-786, 1909.

211. GALERKIN, B.G. "Series Solutions of Some Cases of Equilibrium of Elastic Beams and Plates". Vestnik. Inshenernov, 1, pp. 879-903, 1915.

212. VLASOV, V.Z. "Some New Problems on Shells and Thin Structures". Nat. Adv. Comn. Aeron., NACA Tech. Memo, No. 1204, 1949.

213. LANGHAAR, H.L. "Energy Methods in Applied Mechanics". John Wiley and Sons, N.Y., 1962.

214. SZILARD, R. "Theory and Analysis of Plates". Prentice-Hall Inc., 1974.

215. ZAANEN, A.C. "An Introduction to the Theory of Integration". North Holland Pub. Co., Amsterdam, 1958.

216. GERALD, C.F. "Applied Numerical Analysis". Addison-Wesley Pub. Co., 1973.

217. H.M. NAUTICAL ALMANAC OFFICE "Interpolation and Allied Tables". H.M.S., London, 1956.

218. DORN, W.S. McCRACKEN, D.D. "Numerical Methods with Fortran IV Case Studies". John Wiley and Sons Inc.

219. STROUD, A.H. "Gaussian Quadrature Formulas". Prentice-Hall Inc.

220. KRONROD, A.S. "Nodes and Weights of Quadrature Formulas". Consultants Bureau, N.Y., 1965.

221. ZIENKIEWICZ, O.C. "The Finite Element Method". McGraw-Hill, London, 1977.

222. TAKEDA, H.
ISHA, H.
"Some Considerations on Displacement Assumed Finite Elements with the Reduced Numerical Integration Technique".
Century Research Centre Corp., Tokyo.

223. DEN HARTOG
"Advanced Strength of Materials".
McGraw-Hill, N.Y., 1952.

224. KREYSZIG, E.
"Advanced Engineering Mathematics".
3rd Ed., John Wiley and Sons, 1972.

225. NELDER, J.A.
MEAD, R.
"A Simplex Method for Function Minimisation".
Comp. J., Vol. 7, pp. 308-313, 1965.

226. HOOKE, R.
JEEVES, T.A.
"Direct Search Solution of Numerical and Statistical Problems".
J. Assoc. Comp. Mach., Vol. 8, No. 2, pp. 212-229, 1961.

227. SYMONDS, P.S.
Appendix to [126].

228. FOX, L.
MAYERS, D.F.
"Computing Methods for Scientists and Engineers".
Clarendon Press, Oxford, 1968.

229. TIERNAY, J.A.
"Calculas and Analytic Geometry".
Allyn and Bacon, 1969.

230. MEYER, C.
"Solution of Linear Equations - State of the Art".
Proc. A.S.C.E., J. of Struct. Div., Vol. 99, No. 5T7, 1973.

231. COATES, R.C.
COUTIE, M.G.
"Structural Analysis".
Nelson, 1972.

232. CALDERBANK, V.J.
"A Course on Programming in Fortron IV".
Chapman and Hall Ltd, 1974.

233. MANUFACTURER
Munro and Miller Fittings Ltd, Sighthill, Edinburgh.

234. BRITISH STANDARD
"BS 1640: Part, Steel Butt Welding Pipe Fittings for the Petroleum Industry".
1967.

235. ANSI
"ANSI B16.9 - W58: Wrought Steel Butt Welding Fittings".

236. BOLTZ, R.E.
TUVE, G.L.
"Handbook of Tables for Applied Engineering Science".
2nd Edition C.R.C.

237. SPENCE, J.
BOYLE, J.T.
"An Investigation into the Creep Behaviour of Certain Pipework Components".
Rep. to the S.E.R.C., 1980.

238. SPENCE, J.
BOYLE, J.T.
RAE, K.
"Experimental Creep Programme on Pipe Bend Specimens".
Final Rep., Reactor Group, Agreement No. 4R 52952B, U.K.A.E.A., 1983.

239. BOYLE, J.T.
SPENCE, J.
"Stress Analysis for Creep".
Buttworths, 1983.

240. SPENCE, J.
"On Simplified Methods of Inelastic Analysis with Application to Piping Systems".
Analysis of Struct. Components at Elevated Temperature, Rio de Janeiro, 1983.

241. SMITH, T.A.
WARWICK, R.G.
"A Survey of Defects in Pressure Vessels in the U.K. for the period 1962-1978 and its Relevance to Nuclear Primary Circuits".
Int. J. of Press. Ves. and Piping, 11, pp. 127-166, 1983.

242. HU, C.K.
PHILLIPS, J.W.
"Pulse Propagation in Fluid-Filled Elastic Curved Tubes".
Trans. A.S.M.E., J. of Press. Ves. Tech., Vol. 103, pp. 43-49, 1981.

243. STRONG, B.R.
SLAGIS, G.C.
"TRANS2A: An Unconditionally Stable Code for Thermal Transient Stress Analysis in Piping".
Trans. A.S.M.E., J. of Press. Ves. Tech., Vol. 103, pp. 50-58, 1981.

244. YOUNGDAHL, C.K.
KOT, C.A.
VALENTIN, R.A.
"Pressure Transient Analysis of Elbow-Pipe Experiments Using the PTA-2 Computer Code".
Trans. A.S.M.E., J. of Press. Ves. Tech., Vol. 103, pp. 33-42, 1981.

245. WARE, A.G.
"Moment Loads Induced by Pressure and Momentum Forces in Piping".
Trans. A.S.M.E., J. of Press. Ves. Tech., Vol. 104, pp. 268-271, 1982.

246. STRONG, B.R.
BASCHIERE, R.J.
"Pipe Rupture and Steam/Water Hammer Design Loads for Dynamic Analysis of Piping Systems".
Nuc. Eng. and Design, Vol. 45, 1978.

247. McGEORGE, R.
SWEC, L.F.
"The Steam Hammer Problem: Dynamic Shock Loading of Critical Reactor Piping Systems".
Nuc. Eng. and Design, Vol. 32, 1975.

248. MA, S.M.
BATHIE, K.J.
"On Finite Element Analysis of Pipe Whip Problems".
Nuc. Eng. and Design, Vol. 37, 1976.

249. FISTEDIS, S.H.
"Structural Response of Fast Breeder Reactors to Hypothetical Core Disruptive Accidents".
Nuc. Eng. and Design, Vol. 38, 1976.

250. HURÉ, D.
MORYSSE, M.
"Comparative Methods for Analysis of Piping Systems Subjected to Seismic Motion".
Nuc. Eng. and Design, Vol. 38, 1976.

251. SLAGIS, G.C.
HAHN, W.
"Piping System Seismic Capacity".
Trans. of 7th Int. Conf. on Struct. Mech. in Reactor Tech., Chicago, Illinois, 1983.

252. SCHNEIDER, S.
LEE, H.M.
GODDEN, W.G.
"Response of a Piping System under Seismic and Thermal Loading".
Trans. of 7th Int. Conf. on Struct. Mech. in Reactor Tech., Chicago, Illinois, 1983.

253. BOYLE, J.T.
SPENCE, J.
"PACE 2: An extended Version of the Inelastic Piping Programe PACE".
Rep. to U.K.A.E.A., 1978.

254. WORKMAN, G.H.
RODABAUGH, E.C.
"Development of a Simplified Analytical Procedure for Determining the Inelastic Response of Piping Systems".
O.R.N.L. Sub-3651-1, 1974.

255. ROCHE, R.
HOFFMAN, A.
VRILLON, B.
"Piping Systems, Inelastic Analysis - a Simplified Numerical Method".
Proc. 3rd Int. Conf. on Press. Ves. Tech., Tokyo, 1977.

256. YAMASATO, K.
IMAZU, A.
"Simplified Creep Analyses of Elbows Subjected to Three-Directional Moment Loading".
Proc. Japan Soc. Mech. Eng., No. 790-13, pp. 15-18, 1979.

257.
"International Piping Benchmark Problems".
Compiled by O.R.N.L., 1977.

258. IMAZU, A.
NAGATA, T.
SATO, M.
"Piping Components Test and Related Analytical Work at Steam Generator Safety Section in O-Arai Engineering Centre of PNC".
B-043 81-01(11), PNC, 1981.

259. FORTMANN, M. "Verformungsmessung an Rohrleitungs-Komponenten bis 650°C zur Lebensdaverüberwachung". VDI - Berichte No. 480, pp. 171-174, 1983.

260. RAE, K. "First Progress Report on Inelastic Behaviour of Pipework Components". Reactor Group, Agreement No. 4R53584B, U.K.A.E.A., 1979.

261. RAE, K. "Mensuration of Bend Assemblies". Rep. No. D1, Reactor Group, Agreement No. 4R53584B, U.K.A.E.A., 1981.

262. DEPARTMENT OF TRADE AND INDUSTRY "A High Temperature Capacitance Strain Gauge". Techlink No. 1052, T.R.C., 1972.

263. BRITISH STANDARD "BS 449: The Use of Structural Steel in Building, Part 2: Metric Units". 1969.

264. HOLMAN, J.P. "Experimental Methods for Engineers". 3rd Edition, McGraw-Hill, 1978.

265. POTMA, T. "Strain Gauges - Theory and Application". Philips, 1967.

266. MANUFACTURER Automatic Systems Laboratories, Construction House, Grovebury Road, Leighton Buzzard.

267. MANUFACTURER Isopad Ltd, Stirling Way, Borehamwood, Hertfordshire.

268. MANUFACTURER Morganite Ceramic Fibres Ltd, Neston, Wirral, Merseyside.

269. RAE, K. Elevated Temperature Distribution Test, Specimen No. 4 - 90°C - SCH 40". Rep. to Reactor Group, Agreement No. 4R52952B, U.K.A.E.A., 1981.

270. BRIDGMAN, P.W. "Pressure Measurements by Electrical Means". Proc. Am. Acad. Arts Sci. Vol. 48, 1912.

271. MANUFACTURER "Data Sheet on Strain Gauges". BLH Electronics, 42 Fourth Av., Waltham, M.A., U.S.A.

272. BERTODO, R. "High-Temperature High-Elongation Resistance Strain Gauges". J. of Strain Analysis, Vol. 4, No. 3, pp. 228-235, 1969.

273. BERTODO, R. "Resistance Strain Gauges for the Measurement of Steady Strains at Temperatures above 650°C". J. of StrainAnalysis, Vol. 1, No. 1, pp. 11-19, 1965.

274. DAICHIK, M. POLYAKOV, A. VASILIEV, A. "The Increase in Strain-Gage Measurement Reliability under Extreme Conditions". Proc. Soc. Exp. Stress Analysis, Vol. XXXI, No. 2, 1974.

275. EGAWA, K. "Reversible Strain Gage". Exp. Mech., pp. 161-165, 1982.

276. MANUFACTURER AILTECH, 19535.E, Walnut Drive, City of Industry, CA 91748, U.S.A.

277. CARTER, B.C. SHANNON, J.F. FORSHAW, J.R. "Measurement of Displacement and Strain by Capacity Methods". Proc. Inst. Mech. Eng., Vol. 152, pp. 215-221, 1945.

278. NOLTINGK, B.E. *et al.* "High-Stability Capacitance Strain Gauge for Use at Extreme Temperatures". Proc. Inst. Elec. Eng., Vol. 119, No. 7, pp. 897-903, 1972.

279. NOLTINGK, B.E. "Measuring Static Strains at High Temperatures". Proc. 3rd S.E.S.A. Int. Cong. on Exp. Mech., Los Angeles, 1973.

280. GILLETTE, O.L. "Measurement of Static Strain at 2000°F". Exp. Mech., pp. 316-322, 1975.

281. WINDOW, A.L. HOLISTER, G.S. "Strain Gauge Technology". Applied Science Pub. Ltd.

282. SHARPE, W.N. "Strain Gages for Long-Term High-Temperature Strain Measurement". Exp. Mech., pp. 482-488, 1975.

283. SMITH, J.E. "Assessment of Current High-Temperature Strain Gages". O.R.N.L./TM-7025, 1979.

284. SCHOFIELD, K.G. "A Literature Survey of Strain and Restraint Measurements in Welded Joints". Int. J. of Pres. Vess. and Piping, 4, pp. 1-28, 1976.

285. HOFSTOETTER, P. "Calibration of High-Temperature Strain Gages with the Aid of a Clamping Device". Exp. Mech., pp. 223-225, 1982.

286. STRONG, J.T. "The Long-Term Stability of the CERL-Planer Capacitance Strain Gauge at High Temperature". Rep. No. RD/B/N3720, C.E.G.B., 1976.

287. PROCTER, E.
STRONG, J.T. "High Temperature Creep Strain Measurements Using a Capacitance Type Strain Gauge". Conf. Transducer '77, 1977.

288. PHILLIPS, L.S. "A Capacitance Strain Transducer for High Temperature Applications". Conf. Transducer '78, 1978.

289. DOWNE, B.
FIDLER, R.
NOLTINGK, B.E.
PROCTER, E.
WILLIAMS, J.A.
PHILLIPS, L.S. "Performance and Application of the CERL-Planer Strain Transducer". B.S.S.M.-S.E.S.A. Int. Conf., 1981.

290. HENSCHEL, R.
BERMAN, I.
PAI, D.H. "Creep-Bending Facility and Tests on Large Specimens". Exp. Mech., pp. 237-243, 1974.

291. RAE, K. "Measurement of Strain on Pipe Bends under Room Temperature Elastic Conditions using the CERL-Planer Capacitance Strain Gauge". Rep. No. CGI, Reactor Group, Agreement No. 4R53584B, U.K.A.E.A., 1981.

292. VRILLON, B. Private Communication, 1981.

293. MANUFACTURER "Strain Gauge Inclinometer". Data Sheet, Shape Instruments Ltd, Transducer House, Station Approach, Wokingham, Berkshire.

294. MANUFACTURER Schaevitz em Ltd, Slough, Berkshire.

295. MANUFACTURER Kynmore Engineering Co. Ltd, 19 Buckingham Street, London.

296. RAE, K. "Elevated Temperature Test Specimen No. 7 90°-SCH10-C2". Rep. No. HT7-C2, Reactor Group, Agreement No. 4R53584B, U.K.A.E.A., 1982.

297. RAE, K. "Elevated Temperature Test Specimen No. 2 180°-SCH40-C2". Rep. No. HT2-C2, Reactor Group, Agreement No. 4R53584B, U.K.A.E.A., 1982.

298. RAE, K. "Elevated Temperature Test Specimen No. 8 90°-SCH10-C2". Rep. No. HT8-C2, Reactor Group, Agreement No. 4R53584B, U.K.A.E.A., 1983.

299. RAE, K. "Elevated Temperature Test Specimen No. 9 45°-SCH10-C2". Rep. No. HT9-C2, Reactor Group, Agreement No. 4R53584B, U.K.A.E.A., 1983.

300. FLAMAN, M.T. SHAH, N.N. "Measurements of Stresses, Forces and Moments on Nuclear Steam Generators". Proc. S.E.S.A. Hawaii, 1982.

301. PINDER, L.W. "Failures of Metal-to-Ceramic Seals on Mineral Insulated Cables: Their Causes and Prevention". Rep. No. MID/SSD/81/0033/R, C.E.G.B., 1981.

APPENDIX (1)

Computer Program for Final Solution

TEXT BOUND INTO

THE SPINE

```
PROG KOP1
OUT-OF-PLANE BENDING
PIPE BEND WITH FLANGED OR TANGENT END CONSTRAINTS
NO RESTRICTION ON BEND ANGLE
INTEGRATION DONE USING SIMPSONS RULE
COUPLING ON RIGID DISPLACEMENTS
CIRCUMFERENTIAL CENTRE-LINE RIGID DISPLACEMENT ZERO
IMPLICIT REAL*8 (A-H,O-Z)
REAL*8 LAMDA,MU,MG1,MG2,MG3,LA
REAL*8 KZ,KY,KX,KXY,LR1,LR2,LR3
REAL*8 A1(10,10),A2(10,10),A3(10,10),A4(10,10)
REAL*8 Z(35),S1(35),C1(35),T1(35),T2(35),T3(35)
REAL*8 SM1(10,35),SM2(10,35),SM3(10,35),SM4(10,35)
REAL*8 SM5(10,35),SM6(10,35),SM7(10,35)
REAL*8 SC1(10,35),SC2(10,35),SC3(10,35),SC4(10,35)
REAL*8 SC5(10,35),SC6(10,35),SC7(10,35),SC8(10,35)
REAL*8 SR1(10,35),SR2(10,35),SR3(10,35),SR4(10,35)
REAL*8 WY(35),WE(35),WET(25),QLA(7),QRR(4),QAL(3)
REAL*8 B(80000),D(425),DE(425),NA(425)
INTEGER OUT,RP,CP,E,EN,Y
COMMON/BLOCK 1/SM1,SM2,SM3,SM4,SM5,SM6,SM7
COMMON/BLOCK 2/SC1,SC2,SC3,SC4,SC5,SC6,SC7,SC8
COMMON/BLOCK 3/SR1,SR2,SR3,SR4,Z,S1,C1,T1,T2,T3
COMMON/BLOCK 4/WE,WET,WY,HE,HET,HY,NE,NET,NY,LR3
COMMON/BLOCK 5/JT1,MNT,NT,MT,JT,NTAN,MG2,RR,AL,LA

READ IN DATA

IN=5
OUT=6
READ(IN,*) JZ1
READ(IN,*) NT,MT,JT
READ(IN,*) LAMDA,ALPHA,RR,LR1
READ(IN,*) NE,NET,NY
NTAN=1
IFLAG=1
IFLAG1=1
DATA AND OTHER CONSTANTS

JZ1=1 FOR KZ ONLY
JZ1=2 FOR KZ AND COEFFS ONLY
JZ1=3 FOR KZ,COEFFS AND STRESSES AND STRAINS

KZ=OUT-OF-PLANE BENDING FLEXIBILITY FACTOR REFERRING TO THE
BEND SECTION ONLY BASED ON A NOMINAL VALUE EVALUATED FROM SIMPLE BEND

NT=NUMBER OF TERMS IN DISTORTION DISPLACEMENT - MERIDIONAL
MT=NUMBER OF TERMS IN DISTORTION DISPLACEMENT - CIRCUMFERENTIAL
JT=NUMBER OF TERMS IN RIGID SECTION DISPLACEMENT

LAMDA=BEND RADIUS*THICKNESS/(PIPE RADIUS)**2
ALPHA=PI/BEND ANGLE
RR=RADIUS RATIO=BEND RADIUS/PIPE RADIUS
LR1=TANGENT LENGTH/PIPE RADIUS
NE=NUMBER OF INTEGRATION POINTS ON BEND - CIRCUMFERENTIAL
NET=NUMBER OF INTEGRATION ON TANGENT - CIRCUMFERENTIAL
NY=NUMBER OF INTEGRATION POINTS - MERIDIONAL
MU=POISSON RATIO


THE PIPE RADIUS IS THE RADIUS OF THE TUBE BORE + HALF THE
THICKNESS OF THE TUBE SECTION
```

```
      SPECIFYING LR1 AS ZERO GIVES A BEND WITH FLANGED END CONSTRAINTS

      A POSITIVE MOMENT IS A VECTOR WITH DIRECTION FROM INTRADOS TO EXTRADOS

      JT1=JT*2
      MNT=MT*NT
      NO=JT1+MNT*4
      NOM1=NO-1
      NOM2=NO-2
      N1=NO+1
      N2=NO+2
      NA(1)=1
      NA(2)=N2
      S=N2

      ADDRESS VECTOR

      DO 50 I=1,NOM2
      S=S+NO-(I-1)
S0    NA(I+2)=S
      IA=NA(NO)+1
      PI=3.1415926536D0
      AL=ALPHA*PI
      MU=0.3
      LA=LAMDA*LAMDA/12.0
      MG1=2.0*PI*AL*(1.0-MU*MU)
      MG2=2.0*(1.0-MU)
      MG3=1.0/(1.0-MU*MU)

      INITIALISE VECTORS

      DO 100 I=1,NO
      D(I)=0.0
100   DE(I)=0.0
      DO 125 I=1,IA
125   B(I)=0.0

      INTEGRATION DATA

      IF(LR1.GT.0.0) NTAN=2
      LR2=RR/(2.0*LR1+RR*AL)
      LR3=0.0
      IF(NTAN.EQ.2) LR3=LR1/RR
      PA1=PI*LR2*0.5
      PA2=2.0*PA1
      PA3=4.0*PA1
      E1=0.0
      E2=LR3
      E3=E2+AL
      E4=1.0/LR2
      Y1=0.0
      Y2=2.0*PI
      HET=0.0
      IF(NTAN.EQ.1) NET=0
      IF(NTAN.EQ.2) HET=(E2-E1)/(NET-1)
      HE=(E3-E2)/(NE-1)
      HY=(Y2-Y1)/(NY-1)
      MTZ=JT
      IF(MT.GT.JT) MTZ=MT
```

```
      BEND SECTION
      CIRCUMFERENTIAL FUNCTIONS


801   DO 110 E=1,NE
      EN=E+NET
      EE=(E-1)*HE+E2
      IF(IFLAG1.EQ.2) GOTO 112
      WE(E)=3.0+(-1.0)**E
      IF(E.EQ.1.OR.E.EQ.NE) WE(E)=1.0
112   DO 120 M=1,MTZ

      DISTORTION

      SC1(M,EN)=SIN(M*PA2*EE)
      SC2(M,EN)=M*PA2*COS(M*PA2*EE)
      SC3(M,EN)=-2.0*SC1(M,EN)**2
      SC4(M,EN)=-2.0*SIN((M+1)*PA2*EE)*SC1(M,EN)
      SC5(M,EN)=-M*PA3*SIN(M*PA3*EE)
      SC6(M,EN)=-PA3*((M+1)*COS((M+1)*PA2*EE)*SC1(M,EN)+
     1M*SIN((M+1)*PA2*EE)*COS(M*PA2*EE))
      SC7(M,EN)=-M*M*PA3*PA3*COS(M*PA3*EE)
      SC8(M,EN)=-PA2*PA3*(-(M*M+(M+1)*(M+1))*SIN((M+1)*PA2*EE)*
     1SC1(M,EN)+2*M*(M+1)*COS((M+1)*PA2*EE)*COS(M*PA2*EE))

      RIGID SECTION

      SR1(M,EN)=SC1(M,EN)
      SR2(M,EN)=SC2(M,EN)
      SR3(M,EN)=-M*PA1*SIN(M*PA1*EE)
120   SR4(M,EN)=-M*M*PA1*PA1*COS(M*PA1*EE)
110   CONTINUE
      IF(NTAN.EQ.1) GOTO 139

      TANGENT PIPE
      CIRCUMFERENTIAL FUNCTIONS

134   DO 130 E=1,NET
      IF(IFLAG.EQ.2) GOTO 131
      EN=E
      EE=(E-1)*HET+E1
      IF(IFLAG1.EQ.2) GOTO 132
      WET(E)=3.0+(-1.0)**E
      IF(E.EQ.1.OR.E.EQ.NET) WET(E)=1.0
      GOTO 132
131   EN=E+NET+NE
      EE=(E-1)*HET+E3
132   DO 133 M=1,MTZ

      DISTORTION

      SC1(M,EN)=SIN(M*PA2*EE)
      SC2(M,EN)=M*PA2*COS(M*PA2*EE)
      SC3(M,EN)=-2.0*SC1(M,EN)**2
      SC4(M,EN)=-2.0*SIN((M+1)*PA2*EE)*SC1(M,EN)
      SC5(M,EN)=-M*PA3*SIN(M*PA3*EE)
      SC6(M,EN)=-PA3*((M+1)*COS((M+1)*PA2*EE)*SC1(M,EN)+
     1M*SIN((M+1)*PA2*EE)*COS(M*PA2*EE))
      SC7(M,EN)=-M*M*PA3*PA3*COS(M*PA3*EE)
      SC8(M,EN)=-PA2*PA3*(-(M*M+(M+1)*(M+1))*SIN((M+1)*PA2*EE)*
     1SC1(M,EN)+2*M*(M+1)*COS((M+1)*PA2*EE)*COS(M*PA2*EE))
```

```
      RIGID SECTION

      SR1(M,EN)=SC1(M,EN)
      SR2(M,EN)=SC2(M,EN)
      SR3(M,EN)=-M*PA1*SIN(M*PA1*EE)
133   SR4(M,EN)=-M*M*PA1*PA1*COS(M*PA1*EE)
130   CONTINUE
      IF(IFLAG.EQ.2) GOTO 139
      IFLAG=2
      GOTO 134

      MERIDIONAL FUNCTIONS

139   DO 140 Y=1,NY
      YY=(Y-1)*HY+Y1
      IF(IFLAG1.EQ.2) GOTO 153
      WY(Y)=3.0+(-1.0)**Y
      IF(Y.EQ.1.OR.Y.EQ.NY) WY(Y)=1.0
153   S1(Y)=SIN(YY)
      C1(Y)=COS(YY)
      Z(Y)=1.0+S1(Y)/RR
      T1(Y)=C1(Y)*RR*Z(Y)
      T2(Y)=C1(Y)/(RR*Z(Y))
      T3(Y)=C1(Y)*(S1(Y)+RR)
      DO 150 N=1,NT
      N1=N+1
      IF((-1)**N1.GT.0) GOTO 145

      ODD FUNCTIONS

      SM1(N,Y)=COS(N1*YY)
      SM2(N,Y)=SIN(N1*YY)
      SM3(N,Y)=N1*SM1(N,Y)
      SM4(N,Y)=-N1*SM2(N,Y)
      SM5(N,Y)=N1*SM3(N,Y)
      SM6(N,Y)=-C1(Y)*SM1(N,Y)+RR*Z(Y)*SM4(N,Y)
      SM7(N,Y)=T2(Y)*SM1(N,Y)-SM4(N,Y)
      GOTO 150

      EVEN FUNCTIONS

145   SM1(N,Y)=SIN(N1*YY)
      SM2(N,Y)=COS(N1*YY)
      SM3(N,Y)=-N1*SM1(N,Y)
      SM4(N,Y)=N1*SM2(N,Y)
      SM5(N,Y)=-N1*SM3(N,Y)
      SM6(N,Y)=-C1(Y)*SM1(N,Y)+RR*Z(Y)*SM4(N,Y)
      SM7(N,Y)=T2(Y)*SM1(N,Y)-SM4(N,Y)
150   CONTINUE
140   CONTINUE
      IF(IFLAG1.EQ.2) GOTO 800

      RIGHT-HAND VECTOR

      NP1=0
      DO 160 J=1,JT
      NP1=NP1+(N2-J)
160   S(NP1)=-MG1*J*PA1*SIN(J*PI/2.0)

      SUBROUTINE FUNCT MINIMISATION AND INTEGRATION
      MATRIX FORMED IN,VECTOR

      DO 170 RP=1,NO
```

```
      D(RP)=1.0
      CALL FUNCT(NO,D,F,RP,RP)
      DE(RP)=F
      NP1=NA(RP)
      B(NP1)=2.0*F
  170 D(RP)=0.0
      DO 180 RP=1,NOM1
      NP1=NA(RP)
      IRP=RP+1
      D(RP)=1.0
      DO 190 CP=IRP,NO
      D(CP)=1.0
      CALL FUNCT(NO,D,F,CP,RP)
      B(NP1+CP-RP)=F-DE(RP)-DE(CP)
  190 D(CP)=0.0
  180 D(RP)=0.0

      SOLVE MATRIX

      CALL SOLVE(NO,IA,B,D,NA)

      FLEXIBILITY FACTOR

      KZ=0.0
      DO 200 J=1,JT
      IF(NTAN.EQ.1) GOTO 201
      KZ=KZ-D(J)*J*PA1*SIN(J*PI/2.0)
      GOTO 200
  201 KZ=KZ-D(J)*J*PA1*SIN(J*PI/2.0)
  200 CONTINUE

      DISTORTION COEFFS

      DO 220 M=1,MT
      DO 220 N=1,NT
      MP=JT1+M+MT*(N-1)
      A1(M,N)=D(MP)
      A2(M,N)=D(MP+MNT)
      A3(M,N)=D(MP+MNT*2)
  220 A4(M,N)=D(MP+MNT*3)

      WRITE OUT

      WRITE(OUT,1000)
      WRITE(OUT,1002)
      WRITE(OUT,1004) LAMDA,AL,RR,LR1
      WRITE(OUT,1006) NY,NE,NET
      WRITE(OUT,1008) NO,IA,NT,MT,JT
      WRITE(OUT,1010) KZ
      IF(JZ1.EQ.1) GOTO 999
      WRITE(OUT,1012)
      DO 230 J=1,JT
  230 WRITE(OUT,1014) J,D(J),D(J+JT)
      WRITE(OUT,1016)
      DO 250 M=1,MT
      DO 250 N=1,NT
  250 WRITE(OUT,1018) N,M,A1(M,N),A2(M,N),A3(M,N),A4(M,N)
      IF(JZ1.EQ.2) GOTO 999
      WRITE(OUT,1020)

      STRESS AND STRAIN SCF

      NY=33
```

```
      NE=13
      IF(ALPHA.LT.1.0) NE=9
      HY=(Y2-Y1)/(NY-1)
      HE=(E3-E2)/(NE-1)
      NET=0
      IF(NTAN.EQ.2) NET=NE
      HET=0.0
      IF(NTAN.EQ.2) HET=(E2-E1)/(NET-1)
      IFLAG1=2
      GOTO 801
250   IF(NTAN.EQ.1) GOTO 260

      TANGENT PIPE

260   DO 270 E=1,NET
      EE=(E-1.0)/(NET-1.0)
      IF(IFLAG.EQ.2) GOTO 280
      EN=E
      WRITE(OUT,1070) EE
      GOTO 290
280   EN=E+NET+NE
      WRITE(OUT,1071) EE
290   WRITE(OUT,1072)
      V1=0.0
      V2=0.0
      DO 300 J=1,JT
      ZR2=SR2(J,EN)
      ZR4=SR4(J,EN)
      V1=V1+D(J)*ZR4*AL
      V2=V2+D(J+JT)*ZR2*RR*AL
300   CONTINUE
      DO 310 Y=1,NY
      YY=(Y-1)*HY*180.0/PI
      SZ=S1(Y)
      CZ=C1(Y)
      F1=0.0
      F2=V1*CZ
      F3=-V2
      F4=0.0
      F5=V1*RR*CZ
      F6=-V2
      DO 305 M=1,MT
      DO 305 N=1,NT
      AM1=A1(M,N)
      AM2=A2(M,N)
      BM1=A3(M,N)
      CM1=A4(M,N)
      ZS1=SM1(N,Y)
      ZS2=SM2(N,Y)
      ZS3=SM3(N,Y)
      ZS4=SM4(N,Y)
      ZS5=SM5(N,Y)
      ZS6=SM6(N,Y)
      ZS7=SM7(N,Y)
      ZC1=SC1(M,EN)
      ZC2=SC2(M,EN)
      ZC3=SC3(M,EN)
      ZC4=SC4(M,EN)
      ZC5=SC5(M,EN)
      ZC6=SC6(M,EN)
      ZC7=SC7(M,EN)
      ZC8=SC8(M,EN)
      F1=F1+(ZS1*(AM1*ZC3+AM2*ZC4)+BM1*ZS3*ZC1)
```

```
      F2=F2+(CM1*ZS1*ZC2)
      F3=F3+(BM1*ZS2*ZC2+CM1*ZS4*RR*ZC1)
      F4=F4+(ZS5*(AM1*ZC3+AM2*ZC4)+BM1*ZS3*ZC1)
      F5=F5+(-ZS1*(AM1*ZC7+AM2*ZC8))
      F6=F6+(-ZS4*(AM1*ZC5+AM2*ZC6)+BM1*ZS2*ZC2)
305   CONTINUE
      EY=F1*RR
      EX=F2
      EXY=F3
      KY=LAMDA*F4/2.0
      KX=LAMDA*F5/(2.0*RR*RR)
      KXY=LAMDA*F6/(2.0*RR)
      EXI=EX-KX
      EXO=EX+KX
      EYI=EY-KY
      EYO=EY+KY
      SXI=(EXI+MU*EYI)*MG3
      SXO=(EXO+MU*EYO)*MG3
      SYI=(EYI+MU*EXI)*MG3
      SYO=(EYO+MU*EXO)*MG3
      SXYI=(EXY/2.0-KXY)/(1.0+MU)
      SXYO=(EXY/2.0+KXY)/(1.0+MU)
310   WRITE(OUT,1080) YY,EXI,EXO,EYI,EYO,SXI,SXO,SYI,SYO,SXYI,SXYO
270   CONTINUE
      IF(IFLAG.EQ.2) GOTO 999
      IFLAG=2

C
C     BEND SECTION

250   DO 320 E=1,NE
      EN=E+NET
      EE=(E-1)*HE*180.0/PI
      WRITE(OUT,1073) EE
      WRITE(OUT,1072)
      V1=0.0
      V2=0.0
      V3=0.0
      V4=0.0
      DO 330 J=1,JT
      ZR1=SR1(J,EN)
      ZR2=SR2(J,EN)
      ZR3=SR3(J,EN)
      ZR4=SR4(J,EN)
      V1=V1+D(J)*ZR4*AL
      V2=V2+D(J+JT)*ZR1*RR*AL
      V3=V3+D(J)*ZR3*AL
      V4=V4+D(J+JT)*ZR2*RR*AL
330   CONTINUE
      DO 340 Y=1,NY
      YY=(Y-1)*HY*180.0/PI
      SZ=S1(Y)
      CZ=C1(Y)
      ZT1=T1(Y)
      ZT2=T2(Y)
      ZT3=Z(Y)
      ZT4=T3(Y)
      F1=0.0
      F2=CZ*(V1-V2)
      F3=-(V3+V4)
      F4=0.0
      F5=V1*ZT4-V2*ZT1
      F6=-(V3+V4)
      DO 350 M=1,MT
```

```
      DO 350 N=1,NT
      AM1=A1(M,N)
      AM2=A2(M,N)
      BM1=A3(M,N)
      CM1=A4(M,N)
      ZS1=SM1(N,Y)
      ZS2=SM2(N,Y)
      ZS3=SM3(N,Y)
      ZS4=SM4(N,Y)
      ZS5=SM5(N,Y)
      ZS6=SM6(N,Y)
      ZS7=SM7(N,Y)
      ZC1=SC1(M,EN)
      ZC2=SC2(M,EN)
      ZC3=SC3(M,EN)
      ZC4=SC4(M,EN)
      ZC5=SC5(M,EN)
      ZC6=SC6(M,EN)
      ZC7=SC7(M,EN)
      ZC8=SC8(M,EN)
      F1=F1+(ZS1*(AM1*ZC3+AM2*ZC4)+BM1*ZS3*ZC1)
      F2=F2+(ZS1*(SZ*(AM1*ZC3+AM2*ZC4)+CM1*ZC2)+BM1*CZ*ZS2*ZC1)
      F3=F3+(BM1*ZS2*ZC2+CM1*ZS6*ZC1)
      F4=F4+(ZS5*(AM1*ZC3+AM2*ZC4)+BM1*ZS3*ZC1)
      F5=F5+(ZS1*(CM1*SZ*ZC2-AM1*ZC7-AM2*ZC8)+
     1ZT1*(BM1*ZS2*ZC1-ZS4*(AM1*ZC3+AM2*ZC4)))
      F6=F6+(ZS7*(AM1*ZC5+AM2*ZC6-CM1*SZ*ZC1)+BM1*ZS2*ZC2)
  350 CONTINUE
      EY=F1*RR
      EX=F2/ZT3
      EXY=F3/ZT3
      KY=LAMDA*F4/2.0
      KX=LAMDA*F5/(2.0*RR*RR*ZT3*ZT3)
      KXY=LAMDA*F6/(2.0*RR*ZT3)
      EXI=EX-KX
      EXO=EX+KX
      EYI=EY-KY
      EYO=EY+KY
      SXI=(EXI+MU*EYI)*MG3
      SXO=(EXO+MU*EYO)*MG3
      SYI=(EYI+MU*EXI)*MG3
      SYO=(EYO+MU*EXO)*MG3
      SXYI=(EXY/2.0-KXY)/(1.0+MU)
      SXYO=(EXY/2.0+KXY)/(1.0+MU)
  340 WRITE(OUT,1080) YY,EXI,EXO,EYI,EYO,SXI,SXO,SYI,SYO,SXYI,SXYO
  320 CONTINUE
      IF(IFLAG.EQ.2) GOTO 360
 1000 FORMAT(//////30X,
     1'*************************************************************'/
     230X,'*',58X,'*'/30X,'*',15X,'ANALYSIS OF SMOOTH PIPE BEND',
     315X,'*'/30X,'*',16X,'UNDER OUT-OF-PLANE BENDING',16X,'*'/
     430X,'*',27X,'WITH',27X,'*'/30X,'*',12X,
     5'FLANGED OR TANGENT END CONSTRAINTS',12X,'*'/30X,'*',58X,
     6'*'/30X,
     7'*************************************************************'
     8////)
 1002 FORMAT(////30X,
     1'*************************************************************'
     2//54X,'DATA ON BEND'//30X,
     3'*************************************************************')
 1004 FORMAT(//43X,'PIPE BEND FACTOR LAMDA  = ',F6.3/55X,
     1'BEND ANGLE  = ',F6.3/53X,'RADIUS RATIO  = ',F6.3/43X,
     2'(TANGENT/RADIUS) RATIO  = ',F6.3//28X,
```

```
     3'FOR FLANGED END CONSTRAINTS THE (TANGENT/RADIUS) RATIO IS ZERO'
     4////)
1006 FORMAT(////30X,
     1'*************************************************************'
     2//51X,'INTEGRATION DATA'//30X,
     3'*************************************************************'
     4//35X,'INTEGRATION DONE USING SIMPSONS RULE WITH NO'/55X,
     5'SYMMETRY'//34X,
     6'NUMBER OF POINTS IN THE MERIDIONAL DIRECTION = ',I3/34X,
     7'CIRCUMFERENTIAL DIRECTION :-'/42X,
     8'NUMBER OF POINTS ALONG THE BEND = ',I3/39X,
     9'NUMBER OF POINTS ALONG THE TANGENT = ',I3////)
1008 FORMAT(////30X,
     1'*************************************************************'
     2//52X,'SOLUTION DATA'//30X,
     3'*************************************************************'
     4//45X,'USING GAUSSIAN ELIMINATION'//45X,
     5'TOTAL NUMBER OF UNKNOWNS = ',I6/45X,
     6'VECTOR ORDER FROM MATRIX = ',I6//68X,
     7'NT = ',I6/68X,'MT = ',I6/68X,'JT = ',I6//43X,
     8'DOUBLE PRECISION USED THROUGHOUT'////////)
1010 FORMAT(////30X,
     1'*************************************************************'
     2//45X,'FLEXIBILITY FACTOR = ',F7.3//30X,
     3'*************************************************************'
     4//31X,'THE FLEXIBILITY FACTOR REFERS TO THE BEND SECTION ALONE'
     5/36X,'AND IS BASED ON A NOMINAL ROTATION = MRAL/EI'/29X,
     6'WHERE :- M = APPLIED OUT-OF-PLANE BENDING MOMENT AT THE FLANGE'
     7/38X,'R = BEND RADIUS'/37X,'AL = BEND ANGLE'/38X,
     8'E = YOUNGS MODULUS'/38X,'I = SECOND MOMENT OF AREA')
1012 FORMAT(////////30X,
     1'*************************************************************'
     2//40X,'RIGID SECTION DISPLACEMENT COEFFICIENTS'//30X,
     3'*************************************************************'
     4//30X,'NUMBER OF',13X,'A(J) SERIES',7X,'B(J) SERIES',7X/
     532X,'TERMS'//)
1014 FORMAT(33X,I3,13X,F12.6,6X,F12.6)
1016 FORMAT(//////30X,
     1'*************************************************************'
     2//41X,'DISTORTION DISPLACEMENT COEFFICIENTS'//30X,
     3'*************************************************************'
     4//15X,'NUMBER OF TERMS',5X,'NUMBER OF TERMS',8X,
     5'AM1(M,N)',5X,'AM2(M,N)',5X,'BM1(M,N)',5X,'CM1(M,N)'/17X,
     6'MERIDIONAL',8X,'CIRCUMFERENTIAL',9X,'SERIES',7X,'SERIES',7X,
     7'SERIES',7X,'SERIES'//)
1019 FORMAT(20X,I3,17X,I3,10X,F11.5,2X,F11.5,2X,F11.5,2X,F11.5)
1020 FORMAT(/////////30X,
     1'*************************************************************'
     2//40X,'STRESS AND STRAIN CONCENTRATION FACTORS'//30X,
     3'*************************************************************'
     4//31X,'THE SCF IN STRESS AND STRAIN ARE BASED ON NOMINAL VALUES'
     5/36X,'EVALUATED FROM SIMPLE BENDING THEORY')
1070 FORMAT(////' FIXED TANGENT'//'  DISTANCE = ',F6.3//)
1071 FORMAT(////' LOADED TANGENT'//'  DISTANCE = ',F6.3//)
1072 FORMAT(//
     11X,' STRAINS',44X,'STRESSES'//'  MERID.',4X,
     2'CIRCUMFERENTIAL',6X,'MERIDIONAL'
     3,10X,'CIRCUMFERENTIAL',6X,'MERIDIONAL',10X,'SHEAR STRESSES'//
     4'  ANGLE',3X,'INSIDE',5X,'OUTSIDE',3X,'INSIDE',4X,'OUTSIDE',4X,
     5'INSIDE',5X,'OUTSIDE',3X,'INSIDE',4X,'OUTSIDE',3X,'INSIDE',
     64X,'OUTSIDE'//)
1073 FORMAT(////'  BEND SECTION'//'  THETA = ',F6.2//)
1080 FORMAT(1X,F7.2,3X,10(F7.3,3X))
```

```
999   STOP
      END
C
C
      SUBROUTINE FUNCT(NO,D,F,CP,RP)
      IMPLICIT REAL*8 (A-H,O-Z)
      REAL*8 MG2,LA,LR1,LR3
      REAL*8 A1(10,10),A2(10,10),A3(10,10),A4(10,10)
      REAL*8 Z(35),T1(35),T2(35),T3(35),S1(35),C1(35)
      REAL*8 SM1(10,35),SM2(10,35),SM3(10,35),SM4(10,35)
      REAL*8 SM5(10,35),SM6(10,35),SM7(10,35)
      REAL*8 SC1(10,35),SC2(10,35),SC3(10,35),SC4(10,35)
      REAL*8 SC5(10,35),SC6(10,35),SC7(10,35),SC8(10,35)
      REAL*8 SR1(10,35),SR2(10,35),SR3(10,35),SR4(10,35)
      REAL*8 WY(35),WE(35),WET(25),D(425)
      INTEGER RP,CP,E,E1,Y
      COMMON/BLOCK 1/SM1,SM2,SM3,SM4,SM5,SM6,SM7
      COMMON/BLOCK 2/SC1,SC2,SC3,SC4,SC5,SC6,SC7,SC8
      COMMON/BLOCK 3/SR1,SR2,SR3,SR4,Z,S1,C1,T1,T2,T3
      COMMON/BLOCK 4/WE,WET,WY,HE,HET,HY,NE,NET,NY,LR3
      COMMON/BLOCK 5/JT1,MNT,NT,MT,JT,NTAN,MG2,RR,AL,LA
      DO 100 M=1,MT
      DO 100 N=1,NT
      MJ=JT1+M+MT*(N-1)
      A1(M,N)=D(MJ)
      A2(M,N)=D(MJ+MNT)
      A3(M,N)=D(MJ+MNT*2)
100   A4(M,N)=D(MJ+MNT*3)
      F=0.0
      IFLAG=1
      IF(NTAN.EQ.1) GOTO 105
C
C     TANGENT PIPE
C
300   DO 110 E=1,NET
      E1=E
      IF(IFLAG.EQ.2) E1=E+NET+NE
      V1=0.0
      V2=0.0
      J1=0
      DO 120 K=1,2
      J=CP
      IF(K.EQ.2) J=RP
      IF(J.GT.JT1) GOTO 120
      IF(J.GT.JT) J=J-JT
      IF(J.EQ.J1) GOTO 120
      J1=J
      ZR2=SR2(J,E1)
      ZR4=SR4(J,E1)
      V1=V1+D(J)*ZR4*AL
      V2=V2+D(J+JT)*ZR2*RR*AL
120   CONTINUE
      DO 110 Y=1,NY
      SZ=S1(Y)
      CZ=C1(Y)
      F1=0.0
      F2=V1*CZ
      F3=-V2
      F4=0.0
      F5=V1*RR*CZ
      F6=-V2
      MN1=0
      DO 130 K=1,2
```

```
      MN=CP
      IF(K.EQ.2) MN=RP
      IF(MN.LE.JT1) GOTO 130
      MN=MN-JT1
      IF(MN.GT.MNT) MN=MN-MNT
      IF(MN.GT.MNT) MN=MN-MNT
      IF(MN.GT.MNT) MN=MN-MNT
      IF(MN.EQ.MN1) GOTO 130
      MN1=MN
      N=(MN-1)/MT+1
      M=MN-MT*(N-1)
      AM1=A1(M,N)
      AM2=A2(M,N)
      BM1=A3(M,N)
      CM1=A4(M,N)
      ZS1=SM1(N,Y)
      ZS2=SM2(N,Y)
      ZS3=SM3(N,Y)
      ZS4=SM4(N,Y)
      ZS5=SM5(N,Y)
      ZS6=SM6(N,Y)
      ZS7=SM7(N,Y)
      ZC1=SC1(M,E1)
      ZC2=SC2(M,E1)
      ZC3=SC3(M,E1)
      ZC4=SC4(M,E1)
      ZC5=SC5(M,E1)
      ZC6=SC6(M,E1)
      ZC7=SC7(M,E1)
      ZC8=SC8(M,E1)
      F1=F1+(ZS1*(AM1*ZC3+AM2*ZC4)+BM1*ZS3*ZC1)
      F2=F2+(CM1*ZS1*ZC2)
      F3=F3+(BM1*ZS2*ZC2+CM1*ZS4*RR*ZC1)
      F4=F4+(ZS5*(AM1*ZC3+AM2*ZC4)+BM1*ZS3*ZC1)
      F5=F5+(-ZS1*(AM1*ZC7+AM2*ZC8))
      F6=F6+(-ZS4*(AM1*ZC5+AM2*ZC6)+BM1*ZS2*ZC2)
130   CONTINUE
110   F=F+((F1*RR+F2)*(F1*RR+F2)-
     1MG2*(F1*F2*RR-F3*F3/4.0)+
     2LA*((F4+F5/(RR*RR))*(F4+F5/(RR*RR))-
     3MG2*(F4*F5-F6*F6)/(RR*RR)))*WY(Y)*WET(E)*HY*HET/9.0
      IF(IFLAG.EQ.2) GOTO 105
      IFLAG=2
      GOTO 300

      BEND SECTION

105   DO 210 E=1,NE
      E1=E+NET
      V1=0.0
      V2=0.0
      V3=0.0
      V4=0.0
      J1=0
      DO 220 K=1,2
      J=CP
      IF(K.EQ.2) J=RP
      IF(J.GT.JT1) GOTO 220
      IF(J.GT.JT) J=J-JT
      IF(J.EQ.J1) GOTO 220
      J1=J
      ZR1=SR1(J,E1)
      ZR2=SR2(J,E1)
```

```
      ZR3=SR3(J,E1)
      ZR4=SR4(J,E1)
      V1=V1+D(J)*ZR4*AL
      V2=V2+D(J+JT)*ZR1*RR*AL
      V3=V3+D(J)*ZR3*AL
      V4=V4+D(J+JT)*ZR2*RR*AL
  220 CONTINUE
      DO 210 Y=1,NY
      SZ=S1(Y)
      CZ=C1(Y)
      ZT1=T1(Y)
      ZT2=T2(Y)
      ZT3=Z(Y)
      ZT4=T3(Y)
      F1=0.0
      F2=CZ*(V1-V2)
      F3=-(V3+V4)
      F4=0.0
      F5=V1*ZT4-V2*ZT1
      F6=-(V3+V4)
      MN1=0
      DO 230 K=1,2
      MN=CP
      IF(K.EQ.2) MN=RP
      IF(MN.LE.JT1) GOTO 230
      MN=MN-JT1
      IF(MN.GT.MNT) MN=MN-MNT
      IF(MN.GT.MNT) MN=MN-MNT
      IF(MN.GT.MNT) MN=MN-MNT
      IF(MN.EQ.MN1) GOTO 230
      MN1=MN
      N=(MN-1)/MT+1
      M=MN-MT*(N-1)
      AM1=A1(M,N)
      AM2=A2(M,N)
      BM1=A3(M,N)
      CM1=A4(M,N)
      ZS1=SM1(N,Y)
      ZS2=SM2(N,Y)
      ZS3=SM3(N,Y)
      ZS4=SM4(N,Y)
      ZS5=SM5(N,Y)
      ZS6=SM6(N,Y)
      ZS7=SM7(N,Y)
      ZC1=SC1(M,E1)
      ZC2=SC2(M,E1)
      ZC3=SC3(M,E1)
      ZC4=SC4(M,E1)
      ZC5=SC5(M,E1)
      ZC6=SC6(M,E1)
      ZC7=SC7(M,E1)
      ZC8=SC8(M,E1)
      F1=F1+(ZS1*(AM1*ZC3+AM2*ZC4)+BM1*ZS3*ZC1)
      F2=F2+(ZS1*(SZ*(AM1*ZC3+AM2*ZC4)+CM1*ZC2)+BM1*CZ*ZS2*ZC1)
      F3=F3+(BM1*ZS2*ZC2+CM1*ZS6*ZC1)
      F4=F4+(ZS5*(AM1*ZC3+AM2*ZC4)+BM1*ZS3*ZC1)
      F5=F5+(ZS1*(CM1*SZ*ZC2-AM1*ZC7-AM2*ZC8)+
     1ZT1*(BM1*ZS2*ZC1-ZS4*(AM1*ZC3+AM2*ZC4)))
      F6=F6+(ZS7*(AM1*ZC5+AM2*ZC6-CM1*SZ*ZC1)+BM1*ZS2*ZC2)
  230 CONTINUE
  210 F=F+((F1*RR+F2/ZT3)*(F1*RR+F2/ZT3)*ZT3-
     1MG2*(F1*F2*RR-F3*F3/(4.0*ZT3))+
     2LA*((F4+F5/(RR*RR*ZT3*ZT3))*(F4+F5/(RR*RR*ZT3*ZT3))*ZT3-
```

```
     3MG2*(F4*F5-F6*F6)/(RR*RR*ZT3)))*WY(Y)*WE(E)*HY*HE/9.0
      RETURN
      END
      SUBROUTINE SOLVE(N,IA,B,DE,NA)
      IMPLICIT REAL*8 (A-H,O-Z)
      REAL*8 B(IA),DE(N),NA(N)
      N2=N+2
      N1=N+1
      NM1=N-1
      NM2=N-2
      DO 100 I=1,NM1
      NP1=NA(I)
      NP2=N-I
      NP3=N2-I
      P=B(NP1)
      DO 100 J=1,NP2
      NP4=NA(I+J)
      R=B(NP1+J)/P
      NP5=NP3-J
      NP6=NP2+1-NP5
      DO 100 K=1,NP5
      K1=K-1
  100 B(NP4+K1)=B(NP4+K1)-R*B(NP1+K+NP6)

      NP1=NA(N)+1
      B(NP1)=B(NP1)/B(NP1-1)

      DO 200 M=1,NM1
      I=N-M
      IP1=I+1
      NP1=NA(IP1)
      NP2=NA(I)
      T=B(NP1-1)
      DO 300 J=IP1,N
      M1=J-IP1+1
      M2=NA(J)
      M3=M-M1+1
  300 T=T-B(M2+M3)*B(NP2+M1)
  200 B(NP1-1)=T/B(NP2)

      NS=0
      DO 400 I=1,N
      NS=NS+N2-I
  400 DE(I)=B(NS)
      RETURN
      END
```

APPENDIX (2)

Solution of Linear Simultaneous Equations

Gauss Algorithm

APPENDIX 2: Solution of Linear Simultaneous Equations - Gauss Algorithm

Consider the system of equations:

$$\begin{aligned}
a_{11}x_1 + a_{12}x_2 + a_{13}x_3 + \ldots\ldots a_{1n}x_n &= b_1 \\
a_{21}x_1 + a_{22}x_2 + a_{23}x_3 + \ldots\ldots a_{2n}x_n &= b_2 \\
a_{31}x_1 + a_{32}x_2 + a_{33}x_3 + \ldots\ldots a_{3n}x_n &= b_3 \\
\text{"} \quad\quad \text{"} \quad\quad \text{"} \quad\quad\quad\quad \text{"} \quad\quad &\vdots \\
\text{"} \quad\quad \text{"} \quad\quad \text{"} \quad\quad\quad\quad \text{"} \quad\quad &\vdots \\
a_{n1}x_1 + a_{n2}x_2 + a_{n3}x_3 + \ldots\ldots a_{nn}x_n &= b_n \qquad \ldots\ldots (2.1A)
\end{aligned}$$

These can be written in matrix form as:

$$\begin{bmatrix} a_{11} & a_{12} & a_{13} & \text{"} & \text{"} & \text{"} & a_{1n} \\ a_{21} & a_{22} & a_{23} & \text{"} & \text{"} & \text{"} & a_{2n} \\ a_{31} & a_{32} & a_{33} & \text{"} & \text{"} & \text{"} & a_{3n} \\ \text{"} & \text{"} & \text{"} & & & & \\ \text{"} & \text{"} & \text{"} & & & & \\ a_{n1} & a_{n2} & a_{n3} & \text{"} & \text{"} & \text{"} & a_{nn} \end{bmatrix} \begin{bmatrix} x_1 \\ x_2 \\ x_3 \\ \vdots \\ \vdots \\ x_n \end{bmatrix} = \begin{bmatrix} b_1 \\ b_2 \\ b_3 \\ \vdots \\ \vdots \\ b_n \end{bmatrix}$$

$$\text{or} \quad [A]\lfloor x \rfloor = \lfloor b \rfloor \qquad \ldots\ldots (2.2A)$$

where [A] is the coefficient matrix, $\lfloor x \rfloor$ is the unknown solution vector and $\lfloor b \rfloor$ is the known right hand side vector. To eliminate the unknown x_i, it is necessary first to modify the coefficient matrix and right hand vector, by forward substitution, as follows:

$$a_{jk} = a_{jk} - \frac{a_{ji}\, a_{ik}}{a_{ii}} \quad , \quad j,k = i+1, \ldots\ldots, n \quad \ldots\ldots \quad (2.3A)$$

$$b_j = b_j - \frac{a_{ji}\, b_i}{a_{ii}} \quad , \quad j = i+1, \ldots\ldots, n \quad \ldots\ldots \quad (2.4A)$$

for $i = 1,2,3, \ldots\ldots, n-1$

where a_{ij} is the element in the i^{th} row and j^{th} column of the coefficient matrix and b_i is the i^{th} element of the right hand side vector. When i=n, the n^{th} equation is solved for the x_n unknown:

$$x_n = \frac{b_n}{a_{nn}} \quad \ldots\ldots \quad (2.5A)$$

The remaining unknowns, x_i, are found by back substitution using:

$$x_i = \frac{1}{a_{ii}} [b_i - \sum_{j=i+1}^{n} a_{ij} x_j] \quad , \quad i=n-1,n-2, \ldots\ldots, 1 \quad \ldots \quad (2.6A)$$

If the coefficient matrix is symmetric, i.e.: $a_{ij} = a_{ji}$, then only the elements of the upper triangle need to be operated on during the forward substitution using, instead of equation (2.3A):

$$a_{jk} = a_{jk} - \frac{a_{ij} a_{ik}}{a_{ii}} \quad , \quad \begin{matrix} k = j, j+1, \ldots\ldots, n \\ j = i+1, i+2, \ldots\ldots, n \end{matrix} \quad \ldots \quad (2.7A)$$

This requires slightly more than half of the original operations.

APPENDIX (3)

Strains for Computer Solution

APPENDIX 3: Strains for Computer Solution

The strains as given by equations (3.52) for the flanged bend problem, using the non-dimensionalisation given in equations (3.72) and (3.73) are as follows:

$$\bar{\varepsilon}_{\phi} = [\sum_{mn}\sum [ZS1*[\bar{A1}_{mn}*ZC3 + \bar{A2}_{mn}*ZC4] + \bar{B}_{mn}*ZS3*ZC1]]\frac{R}{r}$$

$$\bar{\varepsilon}_{\theta} = [\sum_{mn}\sum [ZS1*[SZ*(\bar{A1}_{mn}*ZC3 + \bar{A2}_{mn}*ZC4) + \bar{C}_{mn}*ZC2] + \bar{B}_{mn}*CZ*ZS2*ZC1] + \sum_{j} [CZ*[\bar{A}_j*ZR4 - \bar{B}_j*ZR1*\frac{R}{r}]*\alpha]]\frac{1}{Z}$$

$$\bar{\gamma}_{\theta\phi} = [\sum_{m}\sum_{n} [\bar{B}_{mn}*ZS2*ZC2 + \bar{C}_{mn}*ZS6*ZC1] - \sum_{j} [\bar{A}_j*ZR3 + \bar{B}_j*ZR2*\frac{R}{r}]*\alpha]\frac{1}{Z}$$

$$\bar{K}_{\phi} = [\sum_{m}\sum_{n} [ZS5*(\bar{A1}_{mn}*ZC3 + \bar{A2}_{mn}*ZC4) + \bar{B}_{mn}*ZS3*ZC1]]$$

$$\bar{K}_{\theta} = [\sum_{m}\sum_{n} [ZS1*[\bar{C}_{mn}*SZ*ZC2 - \bar{A1}_{mn}*ZC7 - \bar{A2}_{mn}*ZC8] + ZT1*[\bar{B}_{mn}*ZS2*ZC1 - ZS4*(\bar{A1}_{mn}*ZC3 + \bar{A2}_{mn}*ZC4)]] + \sum_{j} [\bar{A}_j*ZT3*ZR4 - \bar{B}_j*ZT1*ZR1*\frac{R}{r}]*\alpha] [\frac{r}{RZ}]^2$$

$$\bar{K}_{\theta\phi} = [\sum_{m}\sum_{n} [ZS7*[\bar{A1}_{mn}*ZC5 + \bar{A2}_{mn}*ZC6 - \bar{C}_{mn}*SZ*ZC1] + \bar{B}_{mn}*ZS2*ZC2] - \sum_{j} [\bar{A}_j*ZR3 + \bar{B}_j*ZR2*\frac{R}{r}]*\alpha] (\frac{r}{RZ})$$

where:

$$ZC1 = \sin\left(\frac{m\pi\theta}{\alpha}\right)$$

$$ZC2 = \left(\frac{m\pi}{\alpha}\right)\cos\left(\frac{m\pi\theta}{\alpha}\right)$$

$$ZC3 = -2.0*(ZC1)^2$$

$$ZC4 = -2.0*\sin\left(\frac{(m+1)\pi\theta}{\alpha}\right)*ZC1$$

$$ZC5 = -\left(\frac{2m\pi}{\alpha}\right)\sin\left(\frac{2m\pi\theta}{\alpha}\right)$$

$$ZC6 = -\left(\frac{2\pi}{\alpha}\right)*\left[(m+1)\cos\left(\frac{(m+1)\pi\theta}{\alpha}\right)*ZC1 + m\sin\left(\frac{(m+1)\pi\theta}{\alpha}\right)\cos\left(\frac{m\pi\theta}{\alpha}\right)\right]$$

$$ZC7 = -\left(\frac{2m\pi}{\alpha}\right)^2\cos\left(\frac{2m\pi\theta}{\alpha}\right)$$

$$ZC8 = -2\left(\frac{\pi}{\alpha}\right)^2\left[-(m^2+(m+1)^2)\sin\left(\frac{(m+1)\pi\theta}{\alpha}\right)*ZC1 + 2m(m+1)\cos\left(\frac{(m+1)\pi\theta}{\alpha}\right)\cos\left(\frac{m\pi\theta}{\alpha}\right)\right]$$

$$ZR1 = \sin\left(\frac{j\pi\theta}{\alpha}\right)$$

$$ZR2 = \left(\frac{j\pi}{\alpha}\right)\cos\left(\frac{j\pi\theta}{\alpha}\right)$$

$$ZR3 = -\left(\frac{j\pi}{2\alpha}\right)\sin\left(\frac{j\pi\theta}{2\alpha}\right)$$

$$ZR4 = -\left(\frac{j\pi}{2\alpha}\right)^2\cos\left(\frac{j\pi\theta}{2\alpha}\right)$$

$$SZ = \sin\phi$$

$$CZ = \cos\phi$$

$$ZT1 = \frac{R'}{r}\cos\phi$$

$$ZT2 = \frac{r}{R'}\cos\phi$$

$$ZT3 = \cos\phi(\sin\phi + \frac{R}{r})$$

$$ZS1 = \Psi_{on}\cos(n\phi) + \Psi_{en}\sin(n\phi)$$

$$ZS2 = \Psi_{on}\sin(n\phi) + \Psi_{en}\cos(n\phi)$$

$$ZS3 = \Psi_{on}n\cos(n\phi) - \Psi_{en}n\sin(n\phi)$$

$$ZS4 = -\Psi_{on}n\sin(n\phi) + \Psi_{en}n\cos(n\phi)$$

$$ZS5 = \Psi_{on}n^2\cos(n\phi) + \Psi_{en}n^2\sin(n\phi)$$

$$ZS6 = \Psi_{on}[-\cos\phi\cos(n\phi) - n\frac{R'}{r}\sin(n\phi)] + \Psi_{en}[-\cos\phi\sin(n\phi) + n\frac{R'}{r}\cos(n\phi)]$$

$$ZS7 = \Psi_{on}[\frac{r}{R'}\cos\phi\cos(n\phi) + n\sin(n\phi)] + \Psi_{en}[\frac{r}{R'}\cos\phi\sin(n\phi) - n\cos(n\phi)]$$

APPENDIX (4)

Previous Solutions

APPENDIX 4: Previous Solutions

This appendix presents a few of the earlier solutions carried out during the study. In the presentation of the solutions the displacements are given in the form of the rigid section displacements and the distortion displacements. Each solution assumes the boundary conditions of a "thick flange" at $\theta=0$ and $\theta=\alpha$, and is applicable to a bend angle α in the range $0 \leq \alpha \leq 2\pi$.

In integration the limits employed were as follows:

in the circumferential direction	$0 \leq \theta \leq \alpha$
in the meridional direction	$0 \leq \emptyset \leq 2\pi$

Typical convergence curves for each solution are given in Figures (4.1A) - (4.4A). A comparison of the stress distributions is given in Figure (4.5A).

All the solutions use double precision throughout unless otherwise stated, and were computed on a ICL 2980 computer.

All the solutions presented employ the strain equations given by (3.52) unless otherwise stated.

Solution A1

Rigid section displacements

$$w_R = \sum_{j=1}^{JT} 2\bar{A}_j \cos\phi \sin^2\left(\frac{j\pi\theta}{4\alpha}\right)$$

$$v_R = \sum_{j=1}^{JT} -2\bar{A}_j \sin\phi \sin^2\left(\frac{j\pi\theta}{4\alpha}\right) - \bar{B}_j \sin\left(\frac{j\pi\theta}{\alpha}\right)$$

$$u_R = \sum_{j=1}^{JT} -\bar{A}_j \frac{r}{j_R}\left(\frac{j\pi}{2\alpha}\right)\cos\phi \sin\left(\frac{j\pi\theta}{2\alpha}\right) - \bar{C}_j \sin\left(\frac{j\pi\theta}{2\alpha}\right)$$

where $\bar{A}_j = \left(\frac{\alpha}{r\gamma_o}\right)A_j$, $\bar{B}_j = \left(\frac{\alpha}{r\gamma_o}\right)B_j$, $\bar{C}_j = \left(\frac{\alpha}{r\gamma_o}\right)C_j$ . . *(4.1A)*

Distortion displacements

$$w_D = \sum_{m=1}^{MT}\sum_{n=1}^{NT} -2\bar{A}_{mn} \sin(n\phi)\sin^2\left(\frac{m\pi\theta}{\alpha}\right)$$

$$v_D = \sum_{m=1}^{MT}\sum_{n=1}^{NT} \bar{B}_{mn} \cos(n\phi)\sin\left(\frac{m\pi\theta}{\alpha}\right)$$

$$u_D = \sum_{m=1}^{MT}\sum_{n=1}^{NT} \bar{C}_{mn} \sin(n\phi)\sin\left(\frac{m\pi\theta}{\alpha}\right)$$

where $\bar{A}_{mn} = \left(\frac{\alpha}{r\gamma_o}\right)A_{mn}$, $\bar{B}_{mn} = \left(\frac{\alpha}{r\gamma_o}\right)B_{mn}$, $\bar{C}_{mn} = \left(\frac{\alpha}{r\gamma_o}\right)C_{mn}$

. . *(4.2A)*

Solution A2

Rigid section displacements

$$w_R = \sum_{j=1}^{JT} 2\bar{A}_j \cos\phi \sin^2\left(\frac{j\pi\theta}{4\alpha}\right)$$

$$v_R = \sum_{j=1}^{JT} -2\bar{A}_j \sin\phi \sin^2\left(\frac{j\pi\theta}{4\alpha}\right) - \bar{B}_j \sin\left(\frac{j\pi\theta}{\alpha}\right)$$

$$u_R = \sum_{j=1}^{JT} -\bar{A}_j \frac{r}{\bar{R}}\left(\frac{j\pi}{2\alpha}\right)\cos\phi \sin\left(\frac{j\pi\theta}{2\alpha}\right) - \bar{C}_j \sin\left(\frac{j\pi\theta}{2\alpha}\right)$$

where $\bar{A}_j = \left(\frac{\alpha}{r\gamma_o}\right)A_j$, $\bar{B}_j = \left(\frac{\alpha}{r\gamma_o}\right)B_j$, $\bar{C}_j = \left(\frac{\alpha}{r\gamma_o}\right)C_j$ . . *(4.3A)*

Distortion displacements

$$w_D = \sum_{m=1}^{MT}\sum_{n=1}^{NT} -2[\Psi_{on}\cos(n\phi) + \Psi_{en}\sin(n\phi)]\left[\bar{A}1_{mn}\sin^2\left(\frac{m\pi\theta}{\alpha}\right) + \bar{A}2_{mn}\sin\left(\frac{(m+1)\pi\theta}{\alpha}\right)\sin\left(\frac{m\pi\theta}{\alpha}\right)\right]$$

$$v_D = \sum_{m=1}^{MT}\sum_{n=1}^{NT} [\Psi_{on}\sin(n\phi) + \Psi_{en}\cos(n\phi)]\bar{B}_{mn}\sin\left(\frac{m\pi\theta}{\alpha}\right)$$

$$u_D = \sum_{m=1}^{MT}\sum_{n=1}^{NT} [\Psi_{on}\cos(n\phi) + \Psi_{en}\sin(n\phi)]\bar{C}_{mn}\sin\left(\frac{m\pi\theta}{\alpha}\right)$$

where $\bar{A}1_{mn} = \left(\frac{\alpha}{r\gamma_o}\right)A1_{mn}$, $\bar{A}2_{mn} = \left(\frac{\alpha}{r\gamma_o}\right)A2_{mn}$,

$\bar{B}_{mn} = \left(\frac{\alpha}{r\gamma_o}\right)B_{mn}$, $\bar{C}_{mn} = \left(\frac{\alpha}{r\gamma_o}\right)C_{mn}$ . . *(4.4A)*

Solution A3

Rigid section displacements

$$w_R = \sum_{j=1}^{JT} -\bar{A}_j \theta^{(j+1)} \cos\phi$$

$$v_R = \sum_{j=1}^{JT} \bar{A}_j \theta^{(j+1)} \sin\phi - \bar{B}_j \sin(\frac{j\pi\theta}{\alpha})$$

$$u_R = \sum_{j=1}^{JT} \bar{A}_j \frac{r}{R}(j+1)\theta^j \cos\phi - \bar{C}_j \theta^j$$

where $\bar{A}_j = (\frac{\alpha}{r\gamma_o})A_j$, $\bar{B}_j = (\frac{\alpha}{r\gamma_o})B_j$, $\bar{C}_j = (\frac{\alpha}{r\gamma_o})C_j$ . . *(4.5A)*

Distortion displacements

$$w_D = \sum_{m=1}^{MT} \sum_{n=1}^{NT} -2[\Psi_{on}\cos(n\phi) + \Psi_{en}\sin(n\phi)] [A1_{mn}\sin^2(\frac{m\pi\theta}{\alpha}) + A2_{mn}\sin(\frac{(m+1)\pi\theta}{\alpha})\sin(\frac{m\pi\theta}{\alpha})]$$

$$v_D = \sum_{m=1}^{MT} \sum_{n=1}^{NT} [\Psi_{on}\sin(n\phi) + \Psi_{en}\cos(n\phi)]B_{mn}\sin(\frac{m\pi\theta}{\alpha})$$

$$u_D = \sum_{m=1}^{MT} \sum_{n=1}^{NT} [\Psi_{on}\cos(n\phi) + \Psi_{en}\sin(n\phi)]C_{mn}\sin(\frac{m\pi\theta}{\alpha})$$

where $\bar{A1}_{mn} = (\frac{\alpha}{r\gamma_o})A1_{mn}$, $\bar{A2}_{mn} = (\frac{\alpha}{r\gamma_o})A2_{mn}$,

$\bar{B}_{mn} = (\frac{\alpha}{r\gamma_o})B_{mn}$, $\bar{C}_{mn} = (\frac{\alpha}{r\gamma_o})C_{mn}$ . . *(4.6A)*

Solution A4

Rigid section displacements

$$w_R = \sum_{j=1}^{JT} -\bar{A}_j \theta^{(j+1)} \cos\phi$$

$$v_R = \sum_{j=1}^{JT} \bar{A}_j \theta^{(j+1)} \sin\phi - \bar{B}_j \sin(\frac{j\pi\theta}{\alpha})$$

$$u_R = \sum_{j=1}^{JT} \bar{A}_j \frac{r}{R}(j+1)\theta^j \cos\phi$$

where $\bar{A}_j = (\frac{\alpha}{r\gamma_o})A_j$, $\bar{B}_j = (\frac{\alpha}{r\gamma_o})B_j$ . . *(4.7A)*

Distortion displacements

$$w_D = \sum_{m=1}^{MT}\sum_{n=1}^{NT} [\Psi_{on}\cos(n\phi) + \Psi_{en}\sin(n\phi)][\bar{A1}_{mn}[\sin(\frac{2(m+1)\pi\theta}{\alpha}) - (m+1)\sin(\frac{2\pi\theta}{\alpha})] + \bar{A2}_{mn}[\sin(\frac{(2m+1)\pi\theta}{\alpha}) - (2m+1)\sin(\frac{\pi\theta}{\alpha})]]$$

$$v_D = \sum_{m=1}^{MT}\sum_{n=1}^{NT} [-\frac{1}{n}\Psi_{on}\sin(n\phi) + \frac{1}{n}\Psi_{en}\cos(n\phi)][\bar{A1}_{mn}[\sin(\frac{2(m+1)\pi\theta}{\alpha}) - (m+1)\sin(\frac{2\pi\theta}{\alpha})] + \bar{A2}_{mn}[\sin(\frac{(2m+1)\pi\theta}{\alpha}) - (2m+1)\sin(\frac{\pi\theta}{\alpha})]]$$

$$u_D = \sum_{m=1}^{MT}\sum_{n=1}^{NT} [\Psi_{on}\cos(n\phi) + \Psi_{en}\sin(n\phi)]\bar{B}_{mn}\sin(\frac{m\pi\theta}{\alpha})$$

where $\bar{A1}_{mn} = (\frac{\alpha}{r\gamma_o})A_{mn}$, $\bar{A2}_{mn} = (\frac{\alpha}{r\gamma_o})A2_{mn}$, $\bar{B}_{mn} = (\frac{\alpha}{r\gamma_o})B_{mn}$

. . *(4.8A)*

In this section the following displacement and strains were taken as zero:

$$U_c(\theta) = 0$$

$$\epsilon_\phi = K_\theta = K_{\theta\phi} = 0$$

Solution B1

Rigid section displacements

$$w_R = \sum_{j=1}^{JT} 2\bar{A}_j \frac{R}{r} \alpha \cos\phi \sin^2\left(\frac{j\pi\theta}{4\alpha}\right)$$

$$v_R = \sum_{j=1}^{JT} -2\bar{A}_j \frac{R}{r} \alpha \sin\phi \sin^2\left(\frac{j\pi\theta}{4\alpha}\right) - \bar{B}_j \frac{R}{r} \alpha \sin\left(\frac{j\pi\theta}{\alpha}\right)$$

$$u_R = \sum_{j=1}^{JT} -\bar{A}_j \left(\frac{j\pi}{2\alpha}\right) \alpha \cos\phi \sin\left(\frac{j\pi\theta}{2\alpha}\right) - \bar{C}_j \frac{R}{r} \alpha \sin\left(\frac{j\pi\theta}{2\alpha}\right)$$

where $\bar{A}_j = \left(\frac{1}{R\gamma_o}\right)A_j$, $\bar{B}_j = \left(\frac{1}{R\gamma_o}\right)B_j$, $\bar{C}_j = \left(\frac{1}{R\gamma_o}\right)C_j$ . . *(4.9A)*

Distortion displacements

$$w_D = \sum_{m=1}^{MT} \sum_{n=2}^{NT+1} -2[\Psi_{on}\cos(n\phi) + \Psi_{en}\sin(n\phi)][\bar{A1}_{mn}\sin^2\left(\frac{m\pi\theta}{\alpha}\right) + \bar{A2}_{mn}\sin\left(\frac{(m+1)\pi\theta}{\alpha}\right)\sin\left(\frac{m\pi\theta}{\alpha}\right)]$$

$$v_D = \sum_{m=1}^{MT} \sum_{n=2}^{NT+1} [\Psi_{on}\sin(n\phi) + \Psi_{en}\cos(n\phi)]\bar{B}_{mn}\sin\left(\frac{m\pi\theta}{\alpha}\right)$$

$$u_D = \sum_{m=1}^{MT} \sum_{n=2}^{NT+1} [\Psi_{on}\cos(n\phi) + \Psi_{en}\sin(n\phi)]\bar{C}_{mn}\sin\left(\frac{m\pi\theta}{\alpha}\right)$$

where $\bar{A1}_{mn} = \left(\frac{\alpha}{r\gamma_o}\right)A1_{mn}$, $\bar{A2}_{mn} = \left(\frac{\alpha}{r\gamma_o}\right)A2_{mn}$

$\bar{B}_{mn} = \left(\frac{\alpha}{r\gamma_o}\right)B_{mn}$, $\bar{C}_{mn} = \left(\frac{\alpha}{r\gamma_o}\right)C_{mn}$ . . *(4.10A)*

Solution B1A

Rigid section displacements

$$w_R = \sum_{j=1}^{JT} 2\bar{A}_j \frac{R}{r} \alpha \cos\phi \sin^2\left(\frac{j\pi\theta}{4\alpha}\right)$$

$$v_R = \sum_{j=1}^{JT} -2\bar{A}_j \frac{R}{r} \alpha \sin\phi \sin^2\left(\frac{j\pi\theta}{4\alpha}\right) - \bar{B}_j \frac{R}{r} \alpha \sin\left(\frac{j\pi\theta}{\alpha}\right)$$

$$u_R = \sum_{j=1}^{JT} -\bar{A}_j \left(\frac{j\pi}{2\alpha}\right) \alpha \cos\phi \sin\left(\frac{j\pi\theta}{2\alpha}\right)$$

where $\bar{A}_j = \left(\frac{1}{R\gamma_o}\right)A_j$, $\bar{B}_j = \left(\frac{1}{R\gamma_o}\right)B_j$ . . *(4.11A)*

Distortion displacements

$$w_D = \sum_{m=1}^{MT} \sum_{n=2}^{NT+1} -2[\Psi_{on}\cos(n\phi) + \Psi_{en}\sin(n\phi)][\bar{A}1_{mn}\sin^2\left(\frac{m\pi\theta}{\alpha}\right) + \bar{A}2_{mn}\sin\left(\frac{(m+1)\pi\theta}{\alpha}\right)\sin\left(\frac{m\pi\theta}{\alpha}\right)]$$

$$v_D = \sum_{m=1}^{MT} \sum_{n=2}^{NT+1} -2[-\frac{1}{n}\Psi_{on}\sin(n\phi) + \frac{1}{n}\Psi_{en}\sin(n\phi)][\bar{A}1_{mn}\sin^2\left(\frac{m\pi\theta}{\alpha}\right) + \bar{A}2_{mn}\sin\left(\frac{(m+1)\pi\theta}{\alpha}\right)\sin\left(\frac{m\pi\theta}{\alpha}\right)]$$

$$u_D = \sum_{m=1}^{MT} \sum_{n=2}^{NT+1} [\Psi_{on}\cos(n\phi) + \Psi_{en}\sin(n\phi)]\bar{B}_{mn}\sin\left(\frac{m\pi\theta}{\alpha}\right)$$

where $\bar{A}1_{mn} = \left(\frac{\alpha}{r\gamma_o}\right)A1_{mn}$, $\bar{A}2_{mn} = \left(\frac{\alpha}{r\gamma_o}\right)A2_{mn}$,

$\bar{B}_{mn} = \left(\frac{\alpha}{r\gamma_o}\right)B_{mn}$ . . *(4.12A)*

This solution uses single precision throughout. The following displacement and strain were taken as zero:

$$U_c(\theta) = 0 \text{ and } \varepsilon_\phi = 0$$

Solution B2

Rigid section displacements

$$w_R = \sum_{j=1}^{JT} 2\bar{A}_j \frac{R}{r} \alpha \cos\phi \sin^2\left(\frac{j\pi\theta}{4\alpha}\right)$$

$$v_R = \sum_{j=1}^{JT} -2\bar{A}_j \frac{R}{r} \alpha \sin\phi \sin^2\left(\frac{j\pi\theta}{4\alpha}\right) - \bar{B}_j \frac{R}{r} \alpha \sin\left(\frac{j\pi\theta}{\alpha}\right)$$

$$u_R = \sum_{j=1}^{JT} -\bar{A}_j \left(\frac{j\pi}{2\alpha}\right) \alpha \cos\phi \sin\left(\frac{j\pi\theta}{2\alpha}\right) - \bar{C}_j \frac{R}{r} \alpha \sin\left(\frac{j\pi\theta}{2\alpha}\right)$$

where $\bar{A}_j = \left(\frac{1}{R\gamma_o}\right)A_j$, $\bar{B}_j = \left(\frac{1}{R\gamma_o}\right)B_j$, $\bar{C}_j = \left(\frac{1}{R\gamma_o}\right)C_j$ . . *(4.13A)*

Distortion displacements

$$w_D = \sum_{m=1}^{MT} \sum_{n=2}^{NT+1} [\Psi_{on}\cos(n\phi) + \Psi_{en}\sin(n\phi)][\bar{A}1_{mn}[\sin(\frac{2(m+1)\pi\theta}{\alpha}) - (m+1)\sin(\frac{2\pi\theta}{\alpha})] + \bar{A}2_{mn}[\sin(\frac{(2m+1)\pi\theta}{\alpha}) - (2m+1)\sin(\frac{\pi\theta}{\alpha})]]$$

$$v_D = \sum_{m=1}^{MT} \sum_{n=2}^{NT+1} [\Psi_{on}\sin(n\phi) + \Psi_{en}\cos(n\phi)]\bar{B}_{mn}\sin(\frac{m\pi\theta}{\alpha})$$

$$u_D = \sum_{m=1}^{MT} \sum_{n=2}^{NT+1} [\Psi_{on}\cos(n\phi) + \Psi_{en}\sin(n\phi)]\bar{C}_{mn}\sin(\frac{m\pi\theta}{\alpha})$$

where $\bar{A}1_{mn} = \left(\frac{\alpha}{r\gamma_o}\right)A1_{mn}$, $\bar{A}2_{mn} = \left(\frac{\alpha}{r\gamma_o}\right)A2_{mn}$

$\bar{B}_{mn} = \left(\frac{\alpha}{r\gamma_o}\right)B_{mn}$, $\bar{C}_{mn} = \left(\frac{\alpha}{r\gamma_o}\right)C_{mn}$ . . *(4.14A)*

Solution B3

Rigid section displacements

$$w_R = \sum_{j=1}^{JT} 2\bar{A}_j \cos\phi \sin^2\left(\frac{j\pi\theta}{4\alpha}\right)$$

$$v_R = \sum_{j=1}^{JT} -2\bar{A}_j \sin\phi \sin^2\left(\frac{j\pi\theta}{4\alpha}\right) - \bar{B}_j \sin\left(\frac{j\pi\theta}{\alpha}\right)$$

$$u_R = \sum_{j=1}^{JT} -\bar{A}_j \frac{r}{R}\left(\frac{j\pi}{2\alpha}\right)\cos\phi \sin\left(\frac{j\pi\theta}{2\alpha}\right) - \bar{C}_j \sin\left(\frac{j\pi\theta}{2\alpha}\right)$$

where $\bar{A}_j = \left(\frac{\alpha}{r\gamma_o}\right)A_j$, $\bar{B}_j = \left(\frac{\alpha}{r\gamma_o}\right)B_j$, $\bar{C}_j = \left(\frac{\alpha}{r\gamma_o}\right)C_j$ . . *(4.15A)*

Distortion displacements

$$w_D = \sum_{m=1}^{MT}\sum_{n=1}^{NT+1} -2[\Psi_{on}\cos(n\phi) + \Psi_{en}\sin(n\phi)][\bar{A}1_{mn}\sin^2\left(\frac{m\pi\theta}{\alpha}\right) + \bar{A}2_{mn}\sin\left(\frac{(m+1)\pi\theta}{\alpha}\right)\sin\left(\frac{m\pi\theta}{\alpha}\right)]$$

$$v_D = \sum_{m=1}^{MT}\sum_{n=1}^{NT+1} [\Psi_{on}\sin(n\phi) + \Psi_{en}\cos(n\phi)]\bar{B}_{mn}\sin\left(\frac{m\pi\theta}{\alpha}\right)$$

$$u_D = \sum_{m=1}^{MT}\sum_{n=1}^{NT+1} [\Psi_{on}\cos(n\phi) + \Psi_{en}\sin(n\phi)]\bar{C}_{mn}\sin\left(\frac{m\pi\theta}{\alpha}\right)$$

where $\bar{A1}_{mn} = \left(\frac{\alpha}{r\gamma_o}\right)A1_{mn}$, $\bar{A2}_{mn} = \left(\frac{\alpha}{r\gamma_o}\right)A2_{mn}$

$\bar{B}_{mn} = \left(\frac{\alpha}{r\gamma_o}\right)B_{mn}$, $\bar{C}_{mn} = \left(\frac{\alpha}{r\gamma_o}\right)C_{mn}$ . . *(4.16A)*

Solution B4

Rigid section displacements

$$w_R = \sum_{j=1}^{JT} 2\bar{A}_j \cos\phi \sin^2\left(\frac{j\pi\theta}{4\alpha}\right)$$

$$v_R = \sum_{j=1}^{JT} -2\bar{A}_j \sin\phi \sin^2\left(\frac{j\pi\theta}{4\alpha}\right) - \bar{B}_j \sin\left(\frac{j\pi\theta}{\alpha}\right)$$

$$u_R = \sum_{j=1}^{JT} -\bar{A}_j \frac{r}{R}\left(\frac{j\pi}{2\alpha}\right)\cos\phi \sin\left(\frac{j\pi\theta}{2\alpha}\right) - \bar{C}_j \sin\left(\frac{j\pi\theta}{2\alpha}\right)$$

where $\bar{A}_j = \left(\frac{\alpha}{r\gamma_o}\right)A_j$, $\bar{B}_j = \left(\frac{\alpha}{r\gamma_o}\right)B_j$, $\bar{C}_j = \left(\frac{\alpha}{r\gamma_o}\right)C_j$ . . *(4.17A)*

Distortion displacements

$$w_D = \sum_{m=1}^{MT}\sum_{n=1}^{NT+1} [\Psi_{on}\cos(n\phi) + \Psi_{en}\sin(n\phi)][\bar{A1}_{mn}[\sin(\tfrac{2(m+1)\pi\theta}{\alpha}) - (m+1)\sin(\tfrac{2\pi\theta}{\alpha})] + \bar{A2}_{mn}[\sin(\tfrac{(2m+1)\pi\theta}{\alpha}) - (2m+1)\sin(\tfrac{\pi\theta}{\alpha})]]$$

$$v_D = \sum_{m=1}^{MT}\sum_{n=1}^{NT+1} [\Psi_{on}\sin(n\phi) + \Psi_{en}\cos(n\phi)]\bar{B}_{mn}\sin\left(\frac{m\pi\theta}{\alpha}\right)$$

$$u_D = \sum_{m=1}^{MT}\sum_{n=1}^{NT+1} [\Psi_{on}\cos(n\phi) + \Psi_{en}\sin(n\phi)]\bar{C}_{mn}\sin\left(\frac{m\pi\theta}{\alpha}\right)$$

where $\bar{A1}_{mn} = \left(\frac{\alpha}{r\gamma_o}\right)A1_{mn}$, $\bar{A2}_{mn} = \left(\frac{\alpha}{r\gamma_o}\right)A2_{mn}$

$\bar{B}_{mn} = \left(\frac{\alpha}{r\gamma_o}\right)B_{mn}$, $\bar{C}_{mn} = \left(\frac{\alpha}{r\gamma_o}\right)C_{mn}$ . . *(4.18A)*

Solution B5

Rigid section displacements

$$w_R = \sum_{j=1}^{JT} -\bar{A}_j \cos\phi \sin\left(\frac{j\pi\theta}{2\alpha}\right)$$

$$v_R = \sum_{j=1}^{JT} \bar{A}_j \sin\phi \sin\left(\frac{j\pi\theta}{2\alpha}\right) - \bar{B}_j \sin\left(\frac{j\pi\theta}{\alpha}\right)$$

$$u_R = \sum_{j=1}^{JT} \bar{C}_j \frac{r}{R} \cos\phi \sin\left(\frac{j\pi\theta}{2\alpha}\right) - \bar{D}_j \sin\left(\frac{j\pi\theta}{2\alpha}\right)$$

where $\bar{A}_j = \left(\frac{\alpha}{r\gamma_o}\right)A_j$, $\bar{B}_j = \left(\frac{\alpha}{r\gamma_o}\right)B_j$

$\bar{C}_j = \left(\frac{\alpha}{r\gamma_o}\right)C_j$, $\bar{D}_j = \left(\frac{\alpha}{r\gamma_o}\right)D_j$ . . *(4.19A)*

Distortion displacements

$$w_D = \sum_{m=1}^{MT} \sum_{n=2}^{NT+1} -2[\Psi_{on}\cos(n\phi) + \Psi_{en}\sin(n\phi)][\bar{A}1_{mn}\sin^2\left(\frac{m\pi\theta}{\alpha}\right) + \bar{A}2_{mn}\sin\left(\frac{(m+1)\pi\theta}{\alpha}\right)\sin\left(\frac{m\pi\theta}{\alpha}\right)]$$

$$v_D = \sum_{m=1}^{MT} \sum_{n=2}^{NT+1} [\Psi_{on}\sin(n\phi) + \Psi_{en}\cos(n\phi)]\bar{B}_{mn}\sin\left(\frac{m\pi\theta}{\alpha}\right)$$

$$u_D = \sum_{m=1}^{MT} \sum_{n=2}^{NT+1} [\Psi_{on}\cos(n\phi) + \Psi_{en}\sin(n\phi)]\bar{C}_{mn}\sin\left(\frac{m\pi\theta}{\alpha}\right)$$

where $\bar{A1}_{mn} = \left(\frac{\alpha}{r\gamma_o}\right)A1_{mn}$, $\bar{A2}_{mn} = \left(\frac{\alpha}{r\gamma_o}\right)A2_{mn}$

$\bar{B}_{mn} = \left(\frac{\alpha}{r\gamma_o}\right)B_{mn}$, $\bar{C}_{mn} = \left(\frac{\alpha}{r\gamma_o}\right)C_{mn}$ . . *(4.20A)*

Solution B6

Rigid section displacements

$$w_R = \sum_{j=1}^{JT} -\bar{A}_j \cos\phi \sin\left(\frac{j\pi\theta}{2\alpha}\right)$$

$$v_R = \sum_{j=1}^{JT} \bar{A}_j \sin\phi \sin\left(\frac{j\pi\theta}{2\alpha}\right) - B_j \sin\left(\frac{j\pi\theta}{\alpha}\right)$$

$$u_R = \sum_{j=1}^{JT} \bar{C}_j \frac{r}{R} \cos\phi \sin\left(\frac{j\pi\theta}{2\alpha}\right) - \bar{D}_j \sin\left(\frac{j\pi\theta}{2\alpha}\right)$$

where $\bar{A}_j = \left(\frac{\alpha}{r\gamma_o}\right)A_j$, $\bar{B}_j = \left(\frac{\alpha}{r\gamma_o}\right)B_j$

$\bar{C}_j = \left(\frac{\alpha}{r\gamma_o}\right)C_j$, $\bar{D}_j = \left(\frac{\alpha}{r\gamma_o}\right)D_j$ . . (4.21A)

Distortion displacement

$$w_D = \sum_{m=1}^{MT} \sum_{n=2}^{NT+1} [\Psi_{on}\cos(n\phi) + \Psi_{en}\sin(n\phi)][\bar{A}1_{mn}[\sin(\tfrac{2(m+1)\pi\theta}{\alpha}) - (m+1)\sin(\tfrac{2\pi\theta}{\alpha})] + \bar{A}2_{mn}[\sin(\tfrac{(2m+1)\pi\theta}{\alpha}) - (2m+1)\sin(\tfrac{\pi\theta}{\alpha})]]$$

$$v_D = \sum_{m=1}^{MT} \sum_{n=2}^{NT+1} [\Psi_{on}\sin(n\phi) + \Psi_{en}\cos(n\phi)]\bar{B}_{mn}\sin\left(\frac{m\pi\theta}{\alpha}\right)$$

$$u_D = \sum_{m=1}^{MT} \sum_{n=2}^{NT+1} [\Psi_{on}\cos(n\phi) + \Psi_{en}\sin(n\phi)]\bar{C}_{mn}\sin\left(\frac{m\pi\theta}{\alpha}\right)$$

where $\bar{A1}_{mn} = \left(\frac{\alpha}{r\gamma_o}\right)A1_{mn}$, $\bar{A2}_{mn} = \left(\frac{\alpha}{r\gamma_o}\right)A2_{mn}$

$\bar{B}_{mn} = \left(\frac{\alpha}{r\gamma_o}\right)B_{mn}$, $\bar{C}_{mn} = \left(\frac{\alpha}{r\gamma_o}\right)C_{mn}$ . . (4.22A)

Solution B7

Rigid section displacements

$$w_R = \sum_{j=1}^{JT} -\bar{A}_j \frac{R}{r}\alpha \cos\phi \sin\left(\frac{j\pi\theta}{2\alpha}\right)$$

$$v_R = \sum_{j=1}^{JT} \bar{A}_j \frac{R}{r}\alpha \sin\phi \sin\left(\frac{j\pi\theta}{2\alpha}\right) - \bar{B}_j \frac{R}{r}\alpha \sin\left(\frac{j\pi\theta}{\alpha}\right)$$

$$u_R = \sum_{j=1}^{JT} \sin\left(\frac{j\pi\theta}{2\alpha}\right)\left[\bar{C}_j \alpha \cos\phi - \bar{D}_j \frac{R}{r}\alpha\right]$$

where $\bar{A}_j = \left(\frac{1}{R\gamma_o}\right)A_j$, $\bar{B}_j = \left(\frac{1}{R\gamma_o}\right)B_j$

$\bar{C}_j = \left(\frac{1}{R\gamma_o}\right)C_j$, $\bar{D}_j = \left(\frac{1}{R\gamma_o}\right)D_j$ . . (4.23A)

Distortion displacements

$$w_D = \sum_{m=1}^{MT}\sum_{n=2}^{NT+1} -2[\Psi_{on}\cos(n\phi) + \Psi_{en}\sin(n\phi)][\bar{A}1_{mn}\sin^2\left(\frac{m\pi\theta}{\alpha}\right) + \bar{A}2_{mn}\sin\left(\frac{(m+1)\pi\theta}{\alpha}\right)\sin\left(\frac{m\pi\theta}{\alpha}\right)]$$

$$v_D = \sum_{m=1}^{MT}\sum_{n=2}^{NT+1} [\Psi_{on}\sin(n\phi) + \Psi_{en}\cos(n\phi)]\bar{B}_{mn}\sin\left(\frac{m\pi\theta}{\alpha}\right)$$

$$u_D = \sum_{m=1}^{MT}\sum_{n=2}^{NT+1} [\Psi_{on}\cos(n\phi) + \Psi_{en}\sin(n\phi)]\bar{C}_{mn}\sin\left(\frac{m\pi\theta}{\alpha}\right)$$

where $\bar{A1}_{mn} = \left(\frac{\alpha}{r\gamma_o}\right)A1_{mn}$, $\bar{A2}_{mn} = \left(\frac{\alpha}{r\gamma_o}\right)A2_{mn}$

$\bar{B}_{mn} = \left(\frac{\alpha}{r\gamma_o}\right)B_{mn}$, $\bar{C}_{mn} = \left(\frac{\alpha}{r\gamma_o}\right)C_{mn}$ . . (4.24A)

Solution B8

Rigid section displacements

$$w_R = \sum_{j=1}^{JT} -\bar{A}_j \frac{R}{r}\alpha\cos\phi\sin(\frac{j\pi\theta}{2\alpha})$$

$$v_R = \sum_{j=1}^{JT} \bar{A}_j \frac{R}{r}\alpha\sin\phi\sin(\frac{j\pi\theta}{2\alpha}) - \bar{B}_j \frac{R}{r}\alpha\sin(\frac{j\pi\theta}{\alpha})$$

$$u_R = \sum_{j=1}^{JT} \sin(\frac{j\pi\theta}{2\alpha})[\bar{C}_j\alpha\cos\phi - \bar{D}_j\frac{R}{r}\alpha]$$

where $\bar{A}_j = (\frac{1}{R\gamma_o})A_j$, $\bar{B}_j = (\frac{1}{R\gamma_o})B_j$

$\bar{C}_j = (\frac{1}{R\gamma_o})C_j$, $\bar{D}_j = (\frac{1}{R\gamma_o})D_j$ . . *(4.25A)*

Distortion displacements

$$w_D = \sum_{m=1}^{MT}\sum_{n=2}^{NT+1} [\Psi_{on}\cos(n\phi) + \Psi_{en}\sin(n\phi)][\bar{A}1_{mn}[\sin(\frac{2(m+1)\pi\theta}{\alpha}) - (m+1)\sin(\frac{2\pi\theta}{\alpha})] + \bar{A}2_{mn}[\sin(\frac{(2m+1)\pi\theta}{\alpha}) - (2m+1)\sin(\frac{\pi\theta}{\alpha})]]$$

$$v_D = \sum_{m=1}^{MT}\sum_{n=2}^{NT+1} [\Psi_{on}\sin(n\phi) + \Psi_{en}\cos(n\phi)]\bar{B}_{mn}\sin(\frac{m\pi\theta}{\alpha})$$

$$u_D = \sum_{m=1}^{MT}\sum_{n=2}^{NT+1} [\Psi_{on}\cos(n\phi) + \Psi_{en}\sin(n\phi)]\bar{C}_{mn}\sin(\frac{m\pi\theta}{\alpha})$$

where $\bar{A}1_{mn} = (\frac{\alpha}{r\gamma_o})A1_{mn}$, $\bar{A}2_{mn} = (\frac{\alpha}{r\gamma_o})A2_{mn}$

$\bar{B}_{mn} = (\frac{\alpha}{r\gamma_o})B_{mn}$, $\bar{C}_{mn} = (\frac{\alpha}{r\gamma_o})C_{mn}$ . . *(4.26A)*

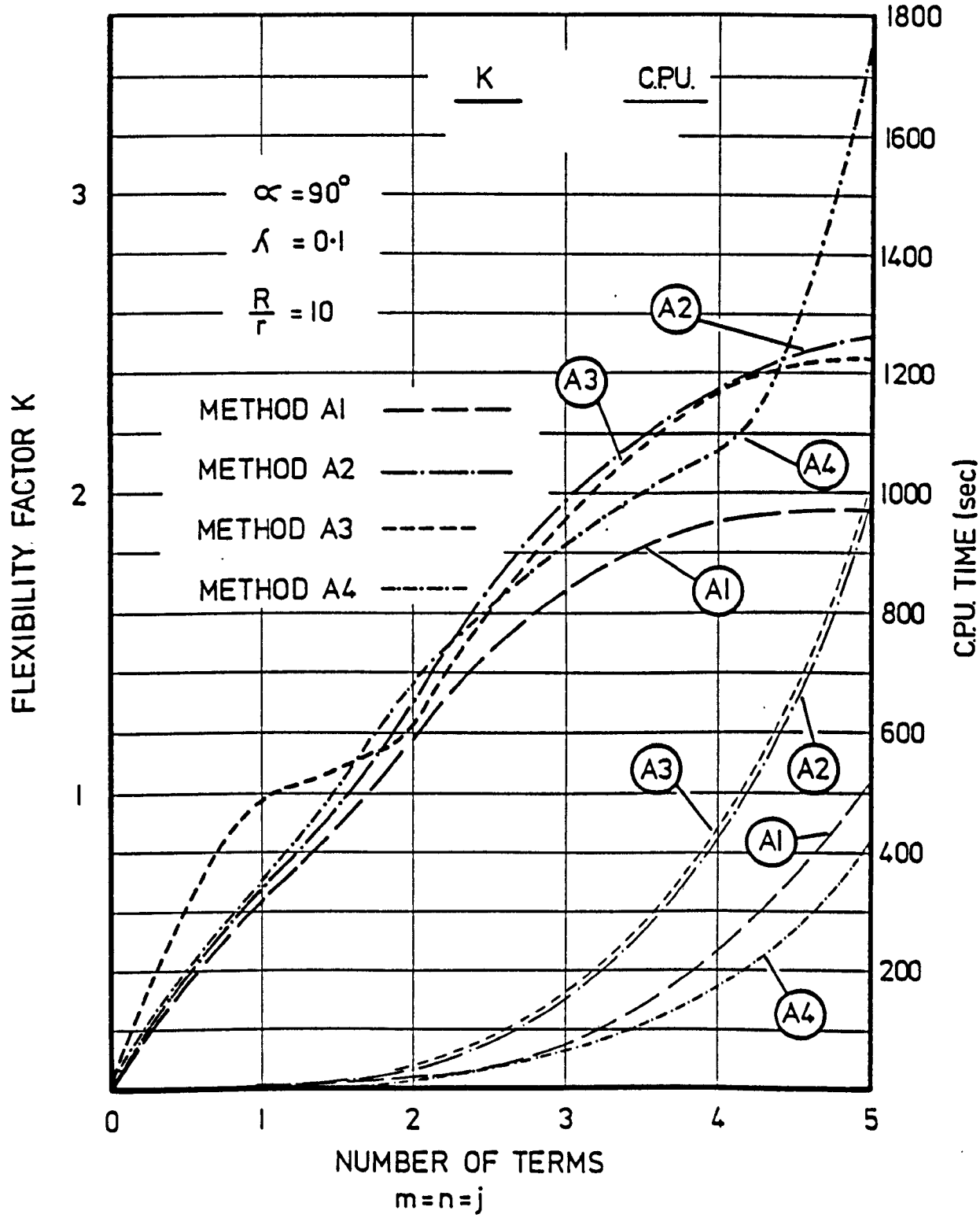

INTEGRATION: SIMPSONS RULE

where $\bar{N}_\theta = 9$ and $\bar{N}_\varphi = 31$

FIG. 4·1A

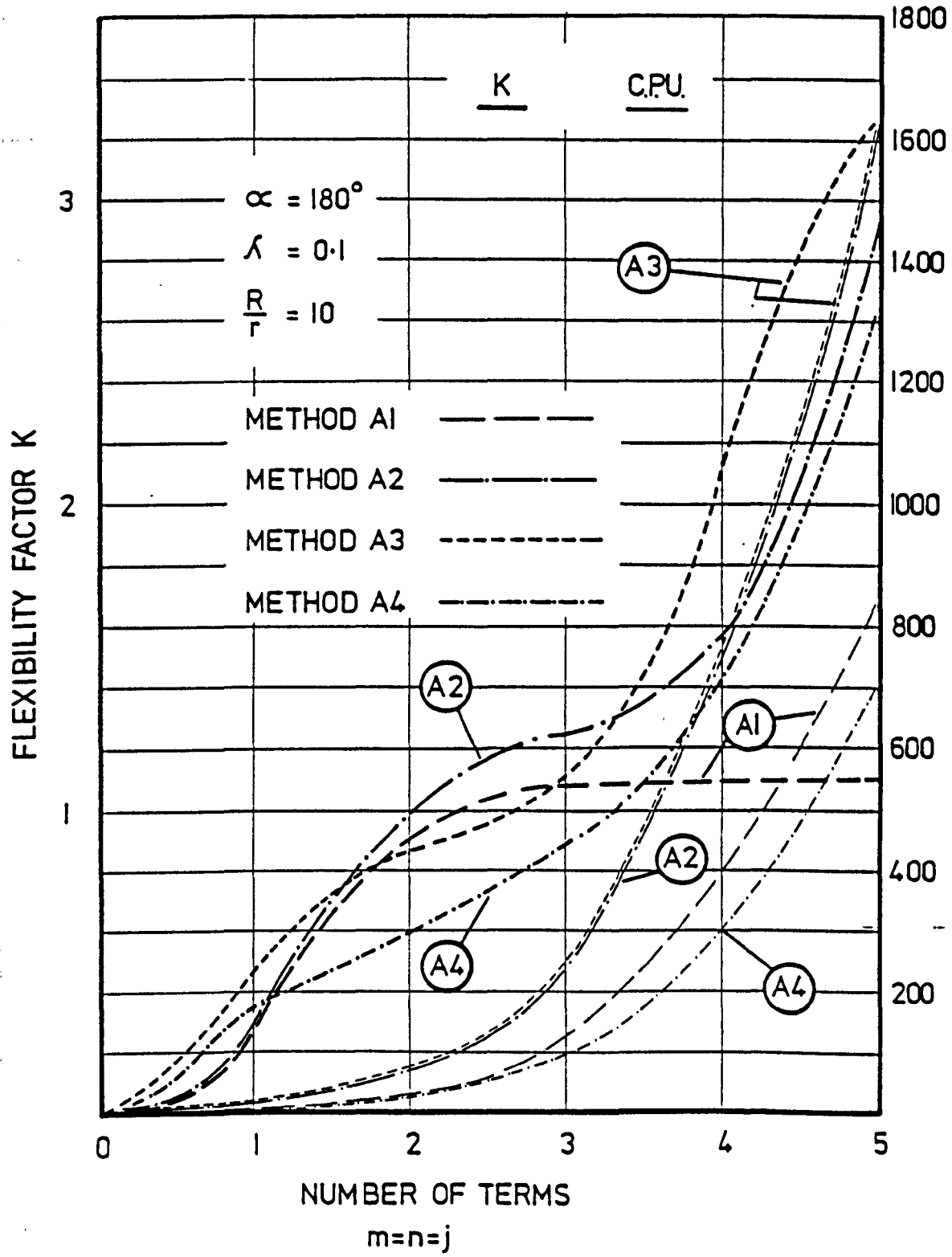

INTEGRATION: SIMPSONS RULE

where $\bar{N}_\theta = 15$ and $\bar{N}_\phi = 31$

FIG. 4·2A

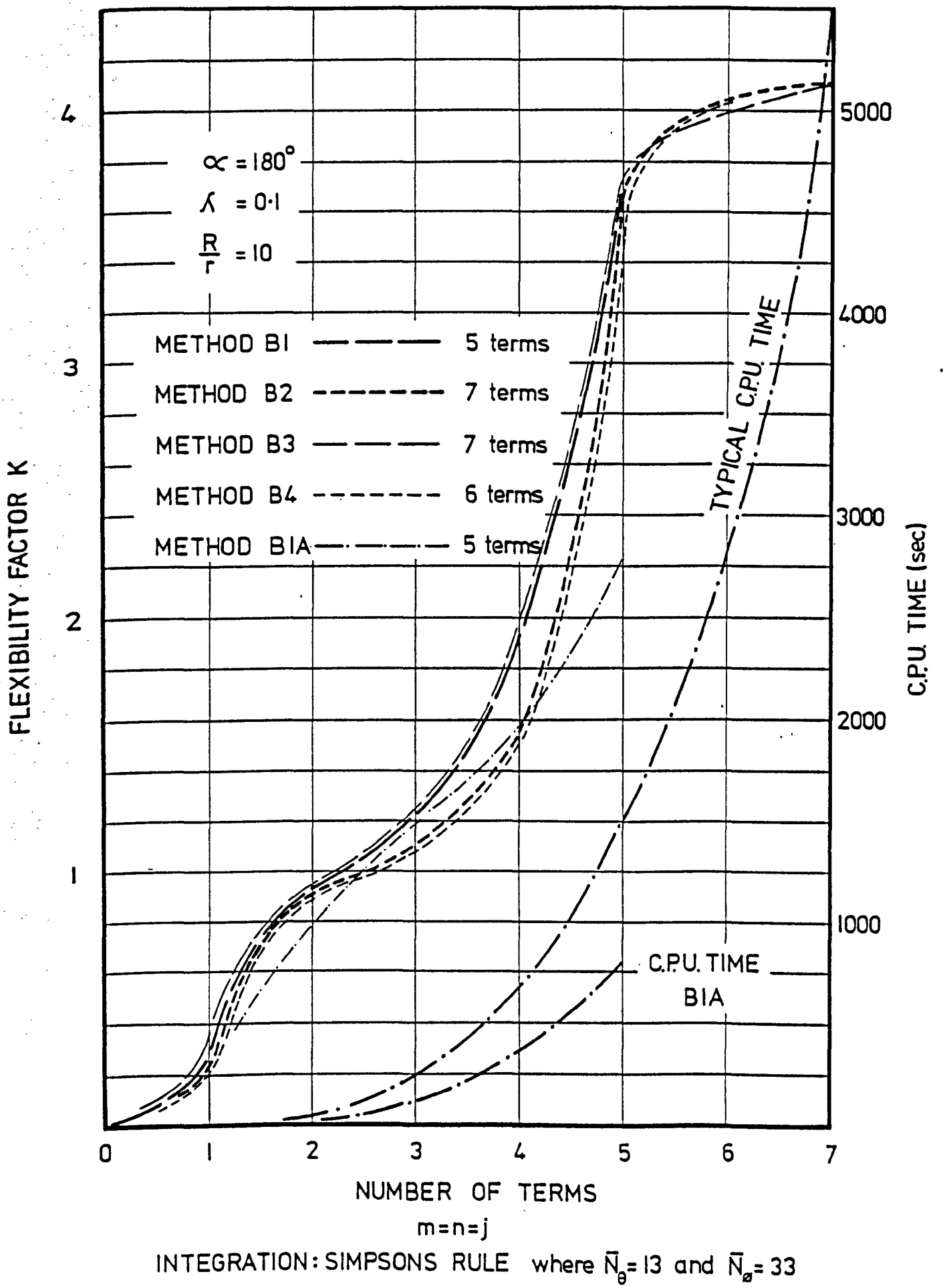

m=n=j

INTEGRATION: SIMPSONS RULE where $\bar{N}_\theta = 13$ and $\bar{N}_\phi = 33$

FIG. 4·3A

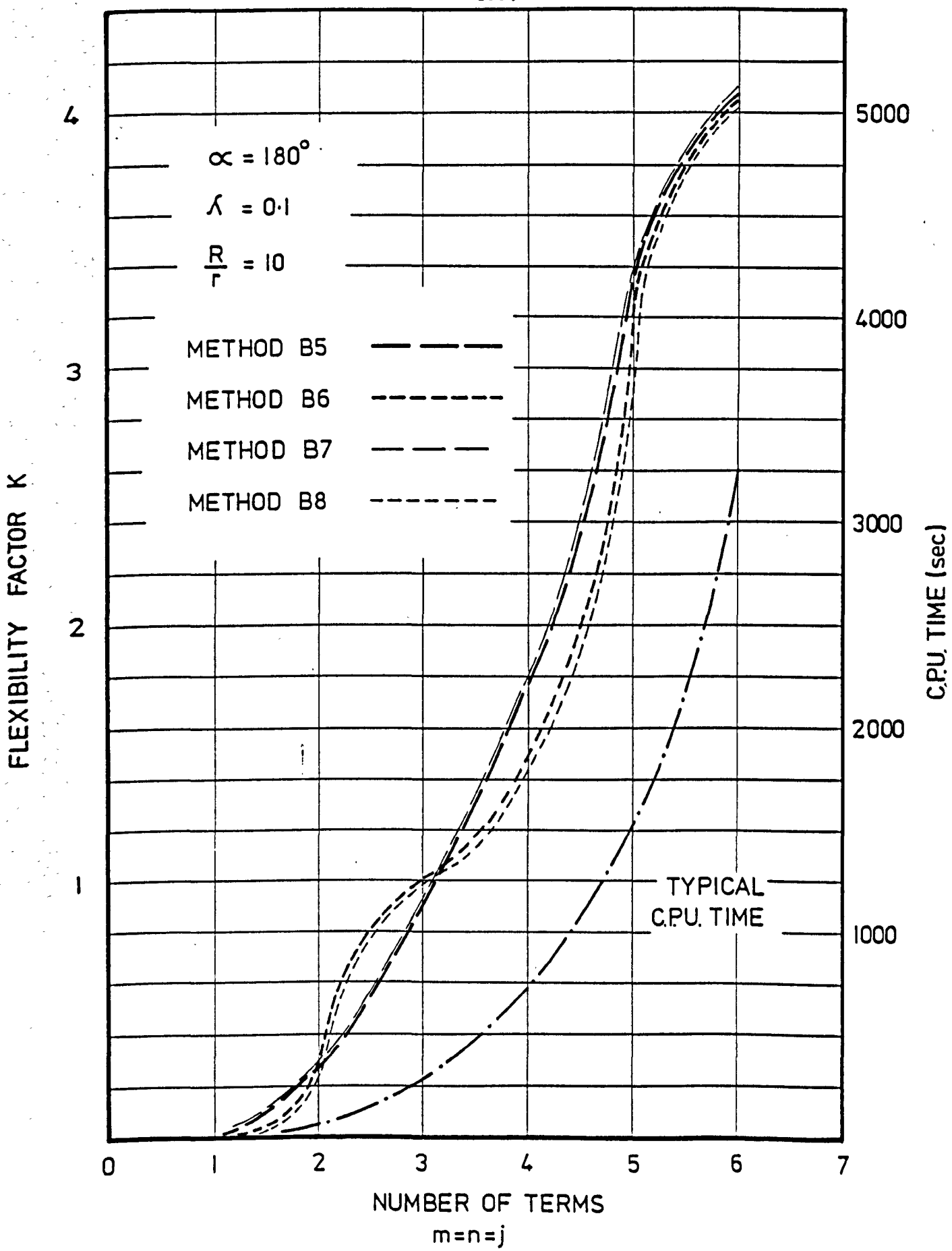

INTEGRATION: SIMPSONS RULE where $\bar{N}_\theta = 13$ and $\bar{N}_\varphi = 33$

FIG. 4·4A

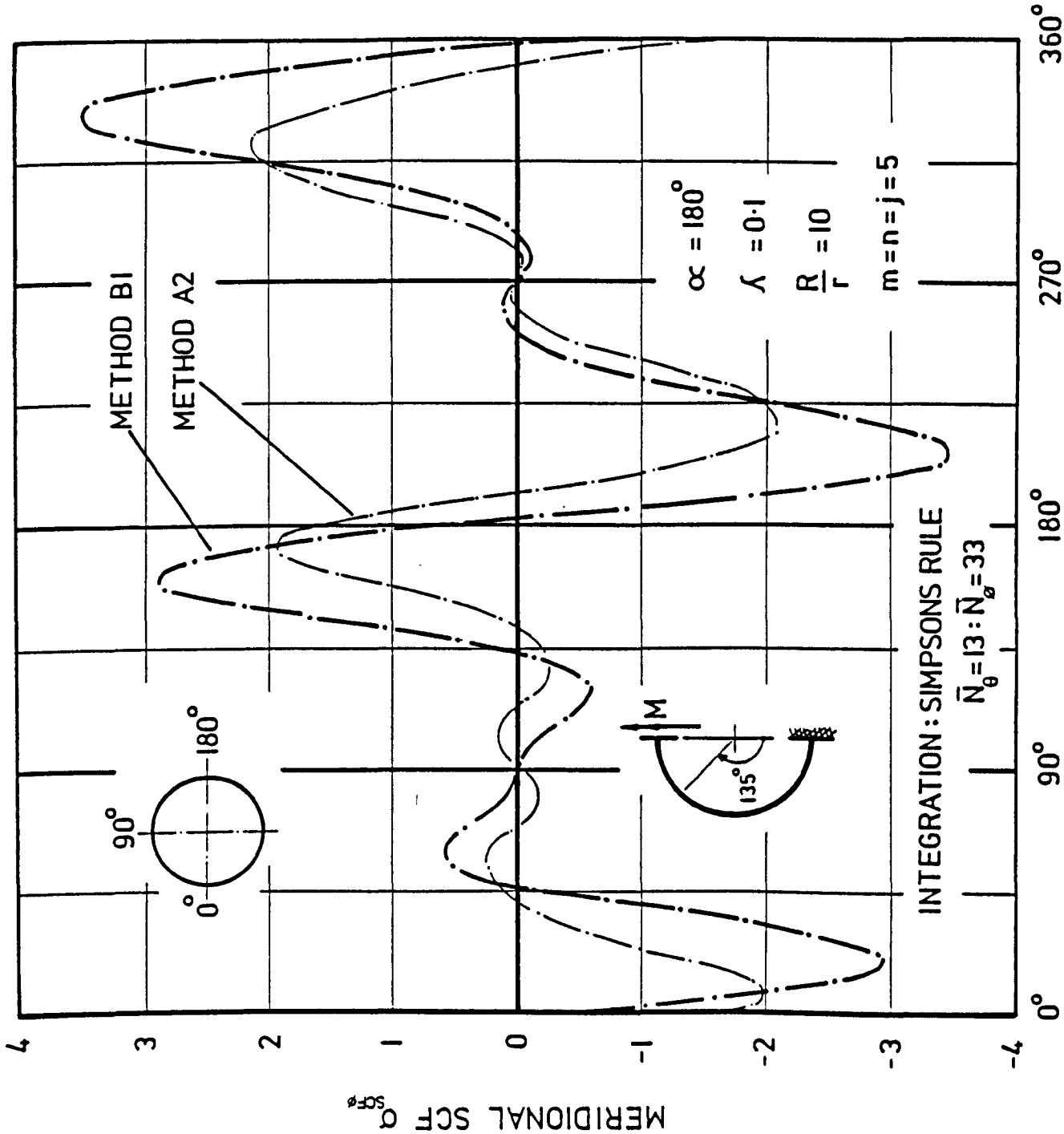

STRESS DISTRIBUTIONS

FIG. 4·5A

APPENDIX (5)

Solution of a 180° Bend Using Circumferential Symmetry Solution-C1

APPENDIX 5: Solution of a 180° Bend Using Circumferential Symmetry - Solution C1

The circumferential symmetry displayed by this bend arises from the equilibrium conditions peculiar to the geometry (Figure 5.1A). Using the rigid-section displacement form as in equation (3.10):

$$w_R = -H_c(\theta)\cos\phi$$

$$v_R = H_c(\theta)\sin\phi - T_c(\theta)$$

$$u_R = \gamma_c(\theta)r\cos\phi - U_c(\theta)$$

Taking a plane of symmetry through the bend centre at $\theta = 0$, the displacement series for w_R, v_R and u_R are as follows:

1. For $\gamma_c(\theta)$ the boundary conditions are:

   at $\theta = 0$, $\gamma_c(\theta) = 0$

   together with symmetry about the plane through $\theta = 0$.

   These conditions are satisfied using an even fourier series of the form:

$$\gamma_c(\theta) = \frac{1}{R}\sum_{j=1} B_j \sin^2\left(\frac{j\pi\theta}{\alpha}\right) \quad \ldots \quad (5.1A)$$

2. For $H_c(\theta)$ the boundary conditions are:

   at $\theta = 0$, $H_c(\theta) = 0$

   together with anti-symmetry about $\theta = 0$.

   These conditions are satisfied using an odd fourier series of the form:

$$H_c(\theta) = \sum_{j=1} A_j \sin\left(\frac{j\pi\theta}{\alpha}\right) \quad \ldots \quad (5.2A)$$

3. For $T_c(\theta)$ the boundary conditions are:

at $\theta = \mp\frac{\pi}{2}$, $T_c(\theta) = 0$

together with symmetry about $\theta = 0$.

These conditions are satisfied using an even fourier series of the form:

$$T_c(\theta) = 2 \sum_{j=1,3} C_j \cos^2\left(\frac{j\pi\theta}{\alpha}\right) - 2 \sum_{j=2,4} C_j \sin^2\left(\frac{j\pi\theta}{\alpha}\right) \quad . . \quad (5.3A)$$

4. For $U_c(\theta)$ the boundary conditions are:

at $\theta = 0$, $U_c(\theta) = 0$

together with anti-symmetry about $\theta = 0$.

These conditions are satisfied using the following odd fourier series:

$$U_c(\theta) = \sum_{j=1} D_j \sin\left(\frac{j\pi\theta}{\alpha}\right) \quad . . \quad (5.4A)$$

The meridional variation of the distortion displacements will use the form given by equations (3.20), (3.41) and (3.46). The variation of these displacements in the circumferential direction is as follows:

1. For $w(\theta)$ the boundary conditions are:

$$\text{at } \theta = 0 \ , \ w(\theta) = 0$$

$$\text{at } \theta = \mp\frac{\pi}{2} \ , \ w(\theta) = \frac{\partial w(\theta)}{\partial \theta} = 0$$

together with anti-symmetry about $\theta = 0$.

These conditions are satisfied using the following odd fourier series:

$$w(\theta) = \sum_{m=1} A1_m[\sin(\frac{4m\pi\theta}{\alpha}) + 2m\sin(\frac{2\pi\theta}{\alpha})] + A2_m[\sin(\frac{2(2m+1)\pi\theta}{\alpha}) - (2m+1)\sin(\frac{2\pi\theta}{\alpha})] \quad . . \quad (5.5A)$$

2. For $v(\theta)$ the boundary conditions are:

$$\text{at } \theta = 0 \text{ and } \theta = \mp\frac{\pi}{2} \ , \ v(\theta) = 0$$

together with anti-symmetry about $\theta = 0$

These conditions are satisfied using the following odd series:

$$v(\theta) = \sum_{m=1} B_m \sin(\frac{2m\pi\theta}{\alpha}) \quad . . \quad (5.6A)$$

3. For $u(\theta)$ the boundary conditions are identical to $v(\theta)$, hence:

$$u(\theta) = \sum_{m=1} C_m \sin(\frac{2m\pi\theta}{\alpha}) \quad . . \quad (5.7A)$$

A summary of the displacements is as follows:

Rigid section displacements

$$w_R = \sum_{j=1}^{JT} -\bar{A}_j \frac{R}{r} \alpha \cos\phi \sin\left(\frac{j\pi\theta}{\alpha}\right)$$

$$v_R = \sum_{j=1}^{JT} \bar{A}_j \frac{R}{r} \alpha \sin\phi \sin\left(\frac{j\pi\theta}{\alpha}\right) - 2\frac{R}{r}\alpha\bar{C}_j\left[\Psi_{oj}\cos^2\left(\frac{j\pi\theta}{\alpha}\right) - \Psi_{ej}\sin^2\left(\frac{j\pi\theta}{\alpha}\right)\right]$$

$$u_R = \sum_{j=1}^{JT} \bar{B}_j \alpha \cos\phi \sin^2\left(\frac{j\pi\theta}{\alpha}\right) - \bar{D}_j \frac{R}{r}\sin\left(\frac{j\pi\theta}{\alpha}\right)$$

where $\bar{A}_j = \frac{1}{R\gamma_o}A_j$, $\bar{B}_j = \frac{1}{R\gamma_o}B_j$

$\bar{C}_j = \frac{\quad}{R\gamma_o}C_j$, $\bar{D}_j = \frac{\quad}{R\gamma_o}D_j$ . . *(5.8A)*

Distortion displacements

$$w_D = \sum_{m=1}^{MT}\sum_{n=2}^{NT+1}\left[\Psi_{on}\cos(n\phi) + \Psi_{en}\sin(n\phi)\right]\left[\bar{A}1_{mn}\left[\sin\left(\frac{4m\pi\theta}{\alpha}\right) + 2m\sin\left(\frac{2\pi\theta}{\alpha}\right)\right] + \bar{A}2_{mn}\left[\sin\left(\frac{2(2m+1)\pi\theta}{\alpha}\right) - (2m+1)\sin\left(\frac{2\pi\theta}{\alpha}\right)\right]\right]$$

$$v_D = \sum_{m=1}^{MT}\sum_{n=2}^{NT+1}\left[\Psi_{on}\sin(n\phi) + \Psi_{en}\cos(n\phi)\right]\bar{B}_{mn}\sin\left(\frac{2m\pi\theta}{\alpha}\right)$$

$$u_D = \sum_{m=1}^{MT}\sum_{n=2}^{NT+1}\left[\Psi_{on}\cos(n\phi) + \Psi_{en}\sin(n\phi)\right]\bar{C}_{mn}\sin\left(\frac{2m\pi\theta}{\alpha}\right)$$

where $\bar{A1}_{mn} = \left(\frac{\alpha}{r\gamma_o}\right)A1_{mn}$, $\bar{A2}_{mn} = \left(\frac{\alpha}{r\gamma_o}\right)A2_{mn}$

$\bar{B}_{mn} = \left(\frac{\alpha}{r\gamma_o}\right)B_{mn}$, $\bar{C}_{mn} = \left(\frac{\alpha}{r\gamma_o}\right)C_{mn}$ . . *(5.9A)*

A comparison of this solution and the final form of solution given in the main text is shown in Figure (5.2A) and (5.3A).

In integration the limits used were:

in the circumferential direction $0 \leq \theta \leq \mp\frac{\pi}{2}$

in the meridional direction $0 \leq \phi \leq 2\pi$

This solution used double precision throughout and was computed on a VAX 750 computer.

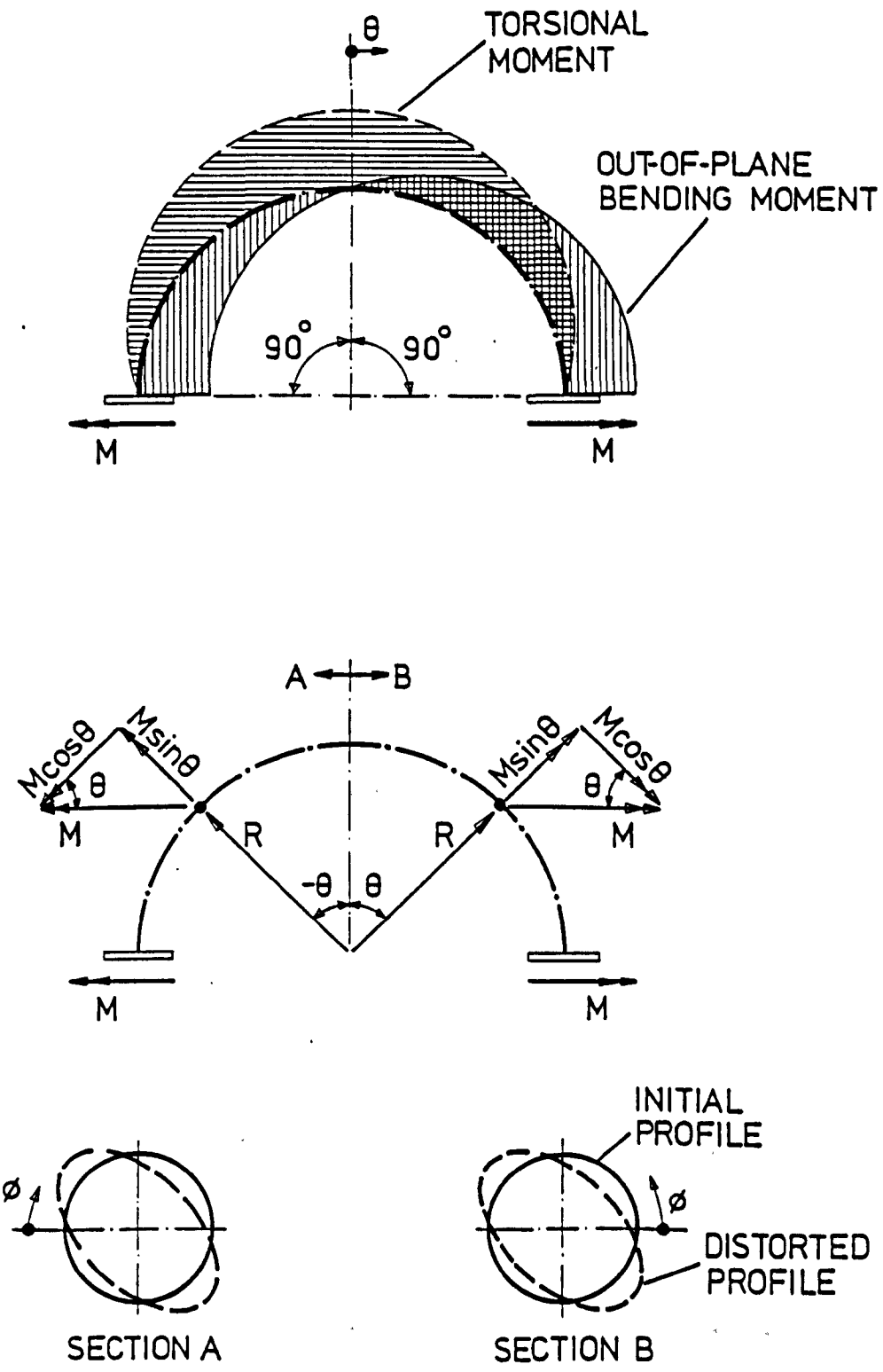

GENERAL LOADING AND DISTORTION
180° BEND

FIG. 5·1A

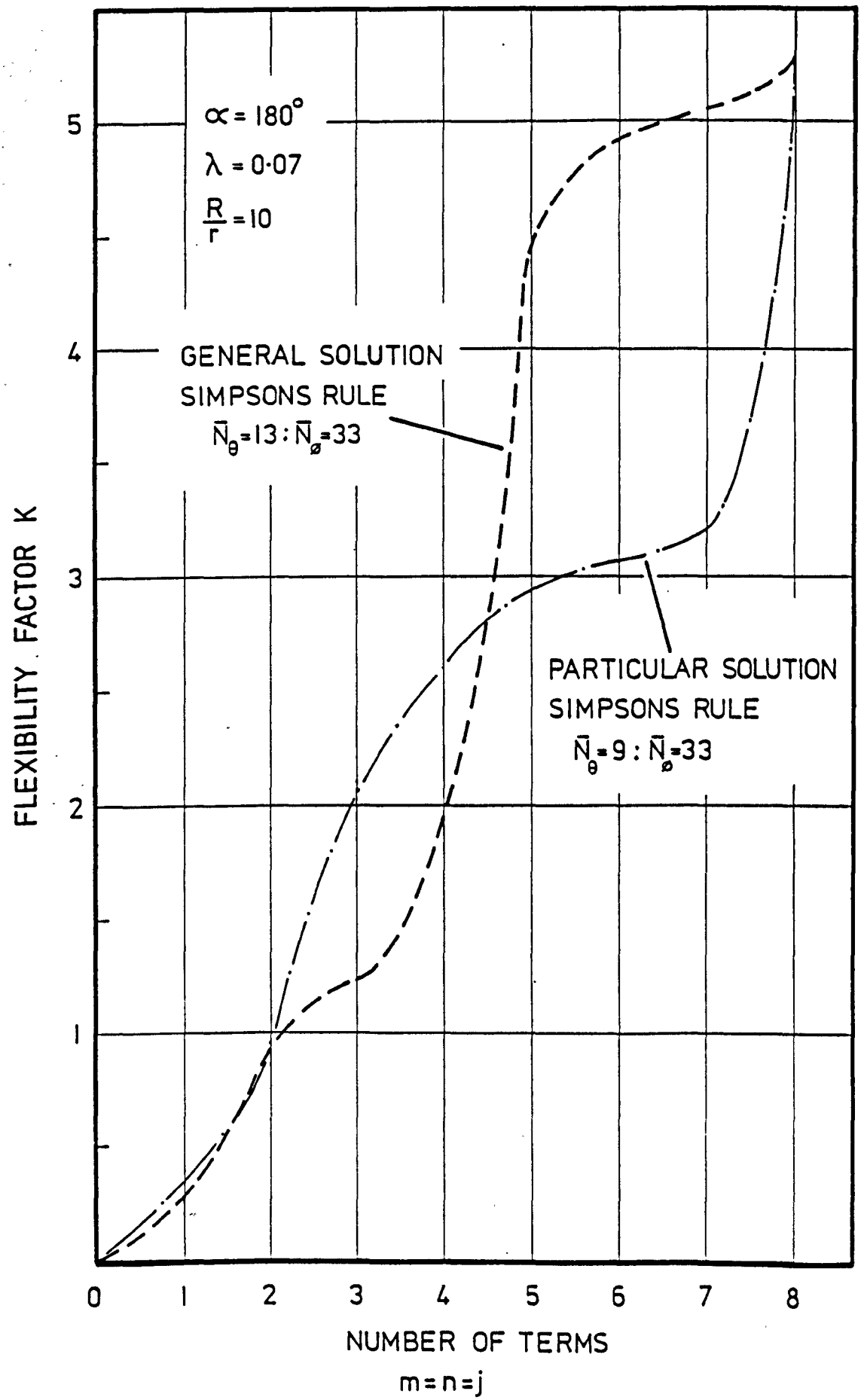

CONVERGENCE CHARACTERISTICS

FIG. 5·2A

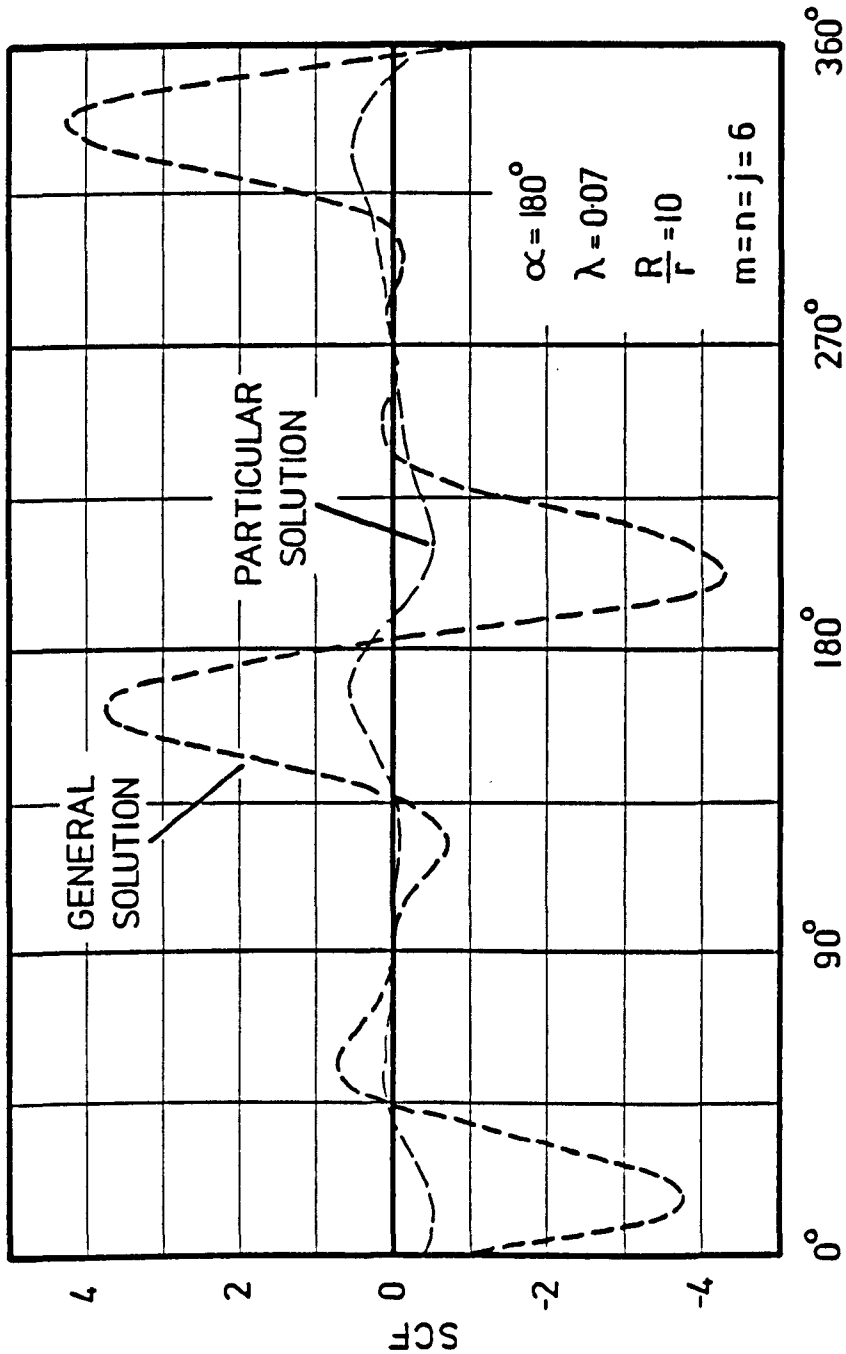

MERIDIONAL STRESS AT θ=135°

FIG. 5·3A

APPENDIX (6)

Results from Mensuration Exercise on a 180° Pipe Bend Assembly

APPENDIX 6: Results from Mensuration Exercise on a 180° Pipe Bend Assembly

The actual plots on cross-section were computed from the average of the outside diameters measured at ϕ = 0°/180° and ϕ = 90°/270° using the dial gauge readings given in Table No. 6.1A.

The tangent dimensions were measured as:

L_1 = 24.0 in

L_2 = 24.0 in

L_3 = 18.0 in

	SECTION NUMBER																
	2	4	5	6	7	8	9	10	11	12	13	14	15	16	17	18	20
0	243	243	243	243	243	243	243	243	243	243	243	243	243	243	243	243	243
10	243	245	246	247	233	239	243	245	235	252	238	231	241	251	238	243	240
20	236	247	260	247	233	236	245	247	225	257	237	227	237	251	225	247	238
30	234	248	269	240	230	229	246	243	230	252	234	214	231	244	230	246	232
40	233	248	277	237	224	220	244	237	248	250	225	202	220	233	240	247	229
50	231	248	296	233	220	210	240	236	263	247	216	188	212	224	256	247	223
60	231	246	306	232	217	205	236	239	284	245	200	181	205	220	260	248	223
70	230	243	309	232	213	197	235	244	301	232	183	175	196	217	268	253	224
80	230	239	317	230	204	194	228	249	314	222	167	167	186	210	278	256	226
90	229	235	323	225	198	196	226	252	315	220	163	161	174	200	286	261	230
100	228	230	322	217	197	187	230	254	319	250	172	158	168	192	277	271	237
110	228	225	317	208	200	180	234	250	320	261	184	156	168	180	267	279	245
120	226	220	301	200	198	177	238	246	299	261	190	159	165	167	251	289	251
130	220	225	281	195	197	178	240	243	283	258	189	159	164	157	231	296	257
140	214	210	264	195	199	183	246	247	258	255	189	163	163	152	216	302	259
150	208	203	240	198	203	190	253	253	243	253	188	170	164	150	203	306	258
160	203	195	227	201	204	198	258	256	240	241	185	174	165	149	191	307	255
170	198	188	215	198	203	201	260	252	238	229	180	173	164	143	189	305	250
180	193	184	217	195	204	209	270	254	243	226	174	172	168	142	176	298	245
190	190	181	226	195	189	199	256	252	255	230	157	145	146	144	183	292	240
200	193	183	243	204	192	196	251	255	269	236	155	141	145	144	201	286	236
210	197	187	273	206	194	197	243	254	285	239	152	141	149	148	219	280	231
220	202	195	299	219	195	197	237	253	305	236	156	142	146	158	221	275	227
230	207	203	320	217	195	198	232	249	312	232	157	144	146	158	245	272	225
240	215	215	321	215	195	200	226	250	316	230	152	149	149	161	259	271	226
250	220	230	335	213	200	194	229	254	322	229	152	150	158	168	269	270	227
260	225	237	341	218	198	196	230	254	317	232	158	153	165	180	272	266	228
270	227	238	322	225	198	197	226	254	312	229	165	161	175	199	283	260	232
280	228	239	324	230	201	201	225	253	306	232	176	162	182	202	280	252	235
290	228	240	318	231	202	206	223	250	316	234	183	176	192	214	292	245	238
300	228	239	314	237	203	211	225	250	316	240	183	189	199	223	296	238	239
310	229	239	307	245	208	217	232	256	312	247	190	200	211	236	294	235	241
320	229	238	296	250	214	221	230	256	306	248	199	206	215	249	292	235	244
330	232	239	284	245	220	222	227	250	297	250	202	214	221	258	283	237	246
340	237	240	267	242	225	222	227	240	276	246	213	225	227	253	267	240	249
350	238	241	246	242	228	223	225	235	257	242	221	231	227	249	256	243	248

TABLE No. 6.1A

DIAL GAUGE READINGS ON CROSS-SECTIONS ($in \times 10^{-3}$)

SPECIMEN No.2 - 180^{o} - Sch 40

	MERIDIONAL ANGLE (deg)							
	0	45	90	135	180	225	270	315
2	2868	2880	2864	2813	2764	2750	2789	2810
4	2864	2967	2874	2821	2754	2826	2791	2803
5	2935	2872	2906	2868	2795	2879	2834	2845
6	3124	3066	3172	3154	3135	3166	2838	3106
7	3127	2975	2878	2964	3105	3153	2800	3104
8	3090	2857	2837	2867	3091	3121	2812	3103
9	3137	2982	2808	2965	3076	3176	2923	3149
10	3156	3047	3053	3057	3145	3177	2957	3138
11	3258	3377	3383	3420	3296	2598	2829	3126
12	2945	2844	2884	2853	2947	2934	2718	2955
13	2877	2750	2623	2714	2898	2911	2777	2946
14	2782	2620	2602	2620	2853	2912	2735	2868
15	2910	2775	2619	2769	2916	2933	2840	2962
16	2945	2848	2877	2852	2943	2931	2755	2973
17	3186	3187	3051	3224	3050	2965	2655	2908
18	2744	2795	2853	2878	2870	2858	2804	2735
20	2750	2783	2833	2886	2892	2857	2808	2723

TABLE No. 6.2A

WALL THICKNESS MEASUREMENTS (in x 10^{-4})

SPECIMEN No.2 - 180^{o} - Sch 40

	0/180	90/270
2	6.611	6.632
4	6.602	6.642
5	6.465	6.651
6	6.674	6.683
7	6.711	6.66
8	6.721	6.663
9	6.718	6.653
10	6.681	6.692
11	6.518	6.655
12	6.669	6.664
13	6.721	6.635
14	6.732	6.643
15	6.718	6.656
16	6.671	6.679
17	6.52	6.667
18	6.632	6.617
20	6.639	6.613

TABLE No. 6.3A

PRINCIPAL OUTSIDE DIAMETERS (in)

SPECIMEN No.2 - 180° - Sch 40

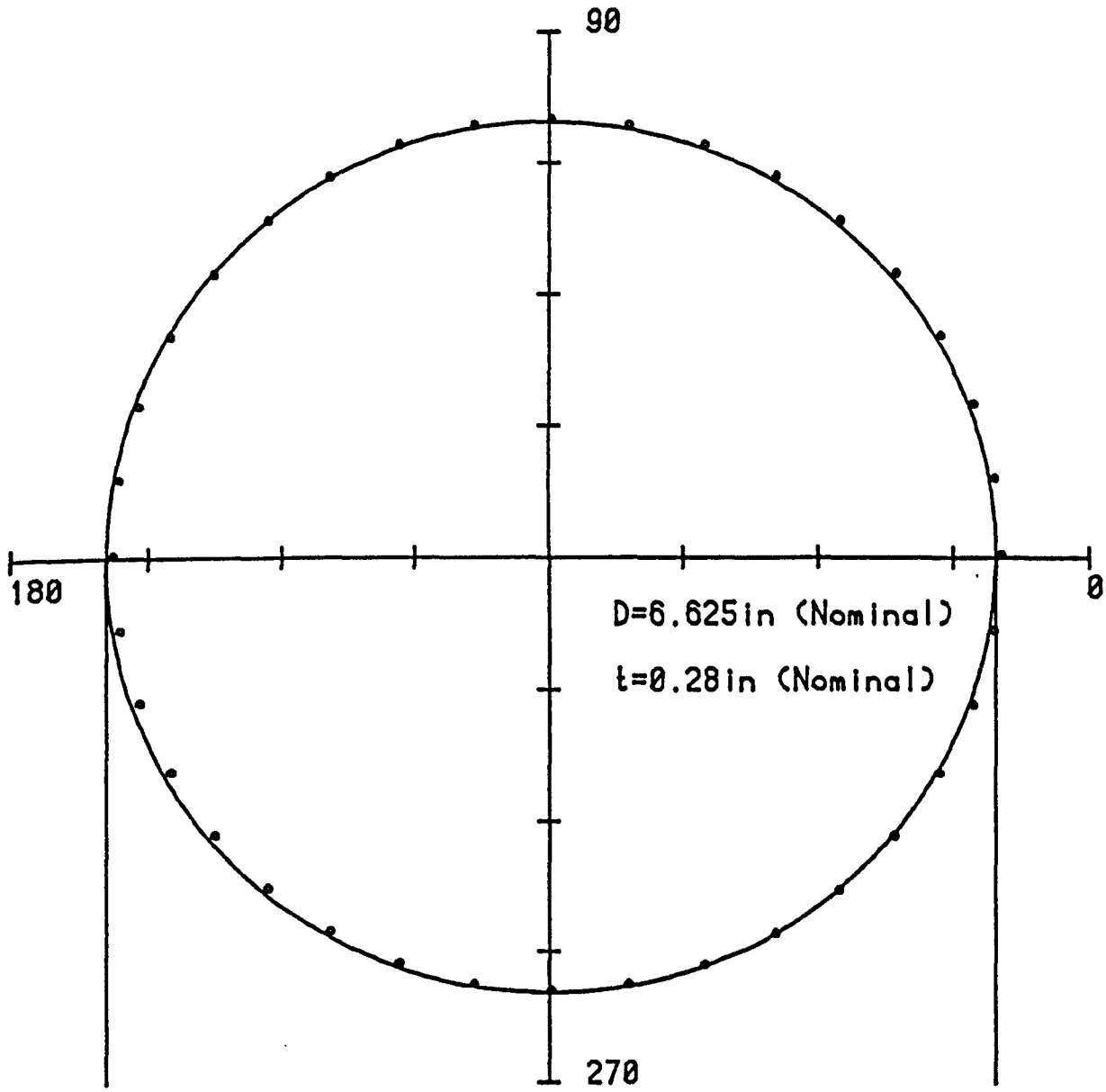

OVALITY

SPECIMEN No.2-180deg-Sch40

SECTION No.2

AVERAGE OUTSIDE DIAMETER (in) = 6.6190
Max=6.6315 Min=6.6045

AVERAGE WALL THICKNESS (in) = 0.2817
Max=0.288 Min=0.275

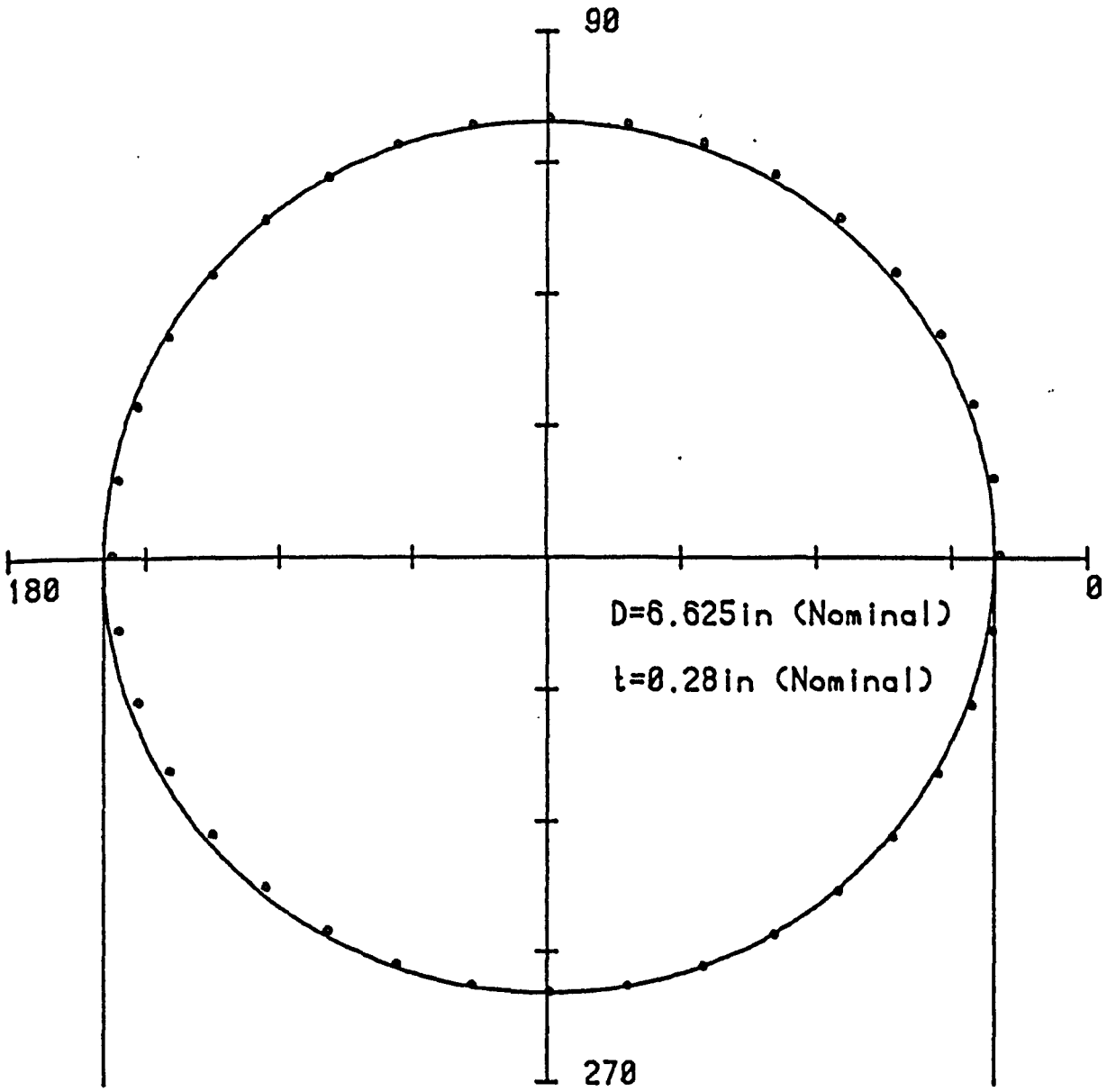

OVALITY

SPECIMEN No.2-180deg-Sch40

SECTION No.4

AVERAGE OUTSIDE DIAMETER (in) = 6.6223
Max=6.648 Min=6.598

AVERAGE WALL THICKNESS (in) = 0.2838
Max=0.2967 Min=0.2754

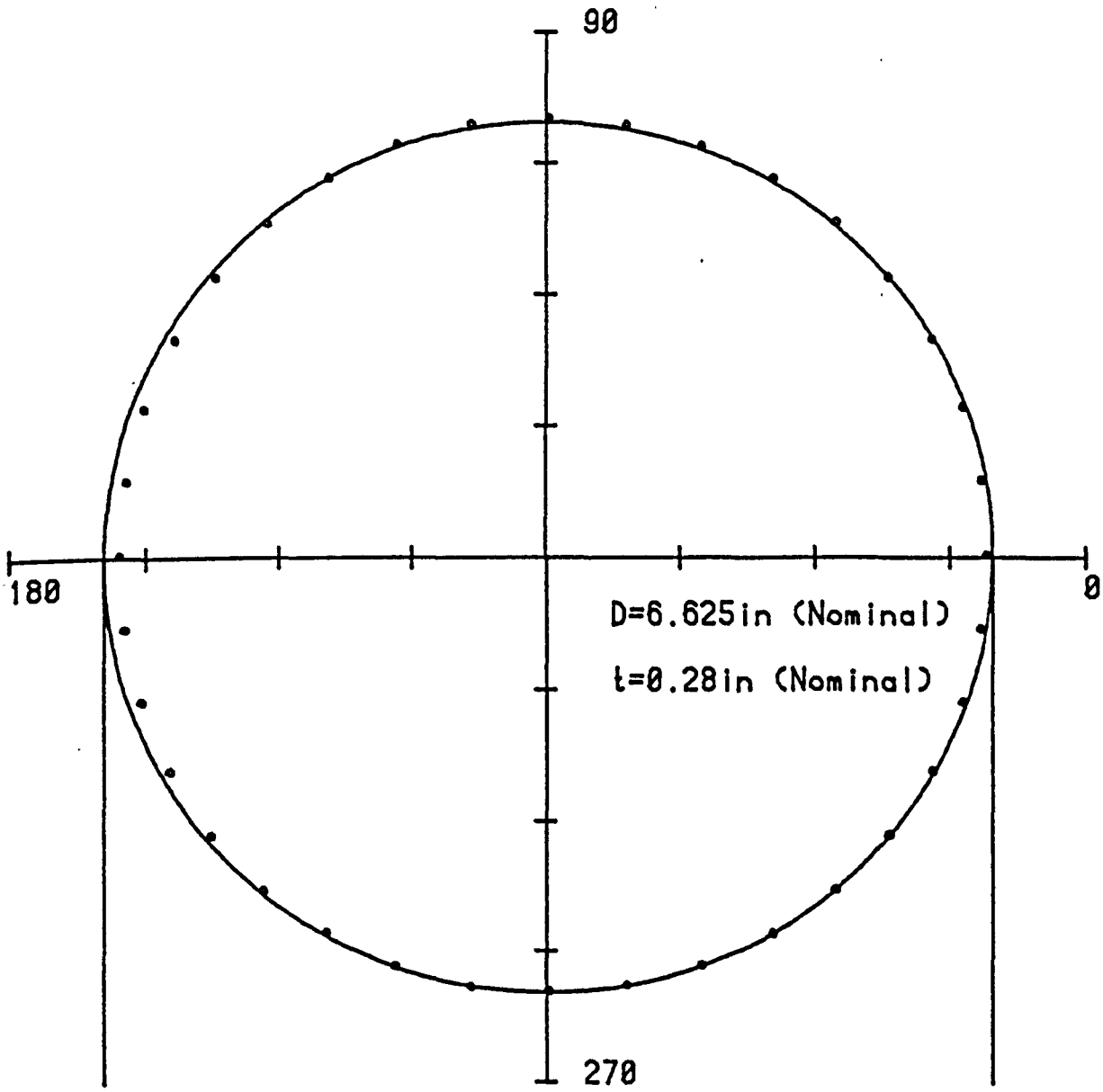

OVALITY

SPECIMEN No.2-180deg-Sch40

SECTION No.5

AVERAGE OUTSIDE DIAMETER (in) = 6.5758
Max=6.6635 Min=6.4655

AVERAGE WALL THICKNESS (in) = 0.2867
Max=0.2935 Min=0.2795

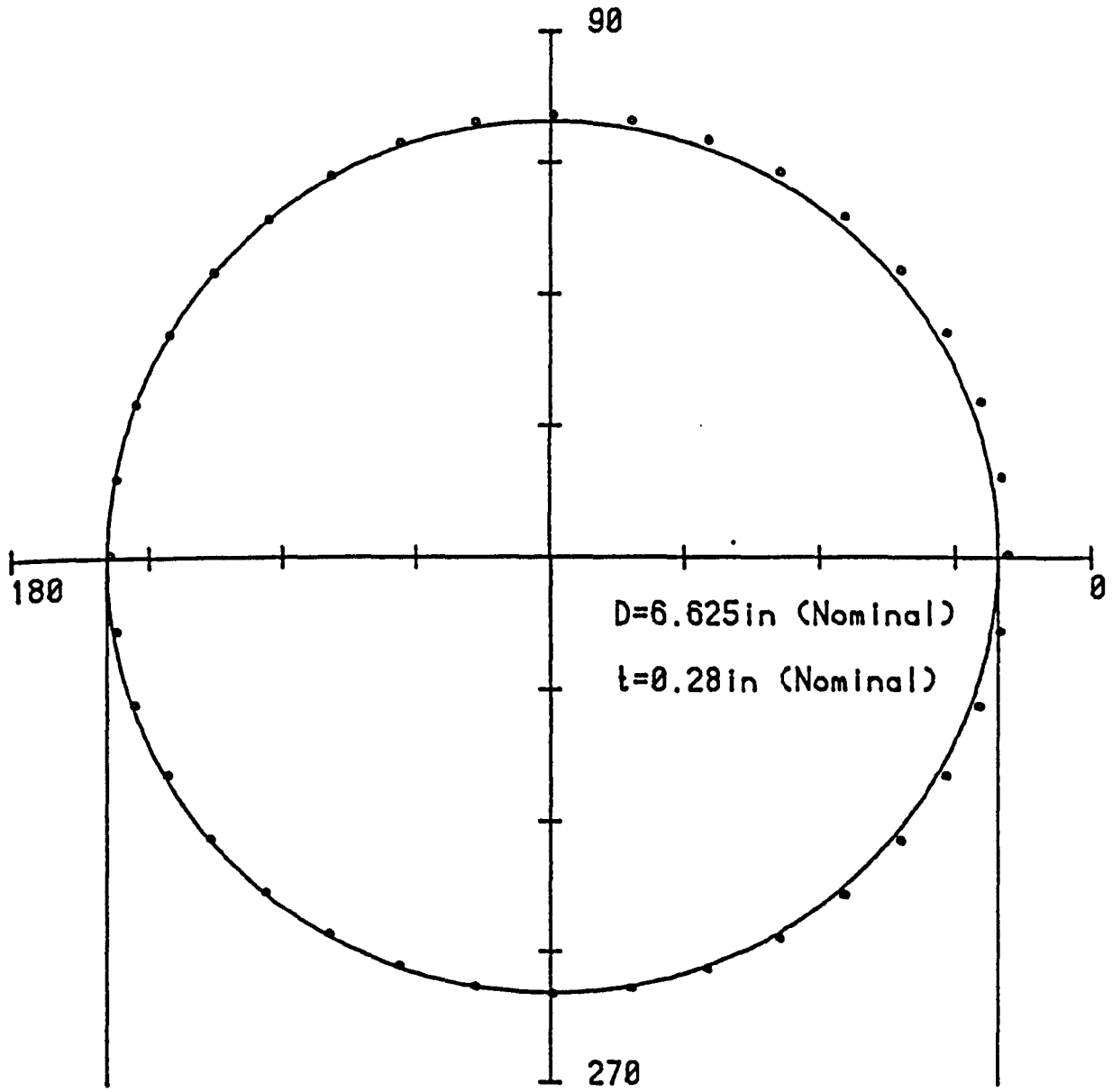

OVALITY

SPECIMEN No.2-180deg-Sch40

SECTION No.6

AVERAGE OUTSIDE DIAMETER (in) = 6.6793
Max=6.6905 Min=6.6715

AVERAGE WALL THICKNESS (in) = 0.3095
Max=0.3172 Min=0.2838

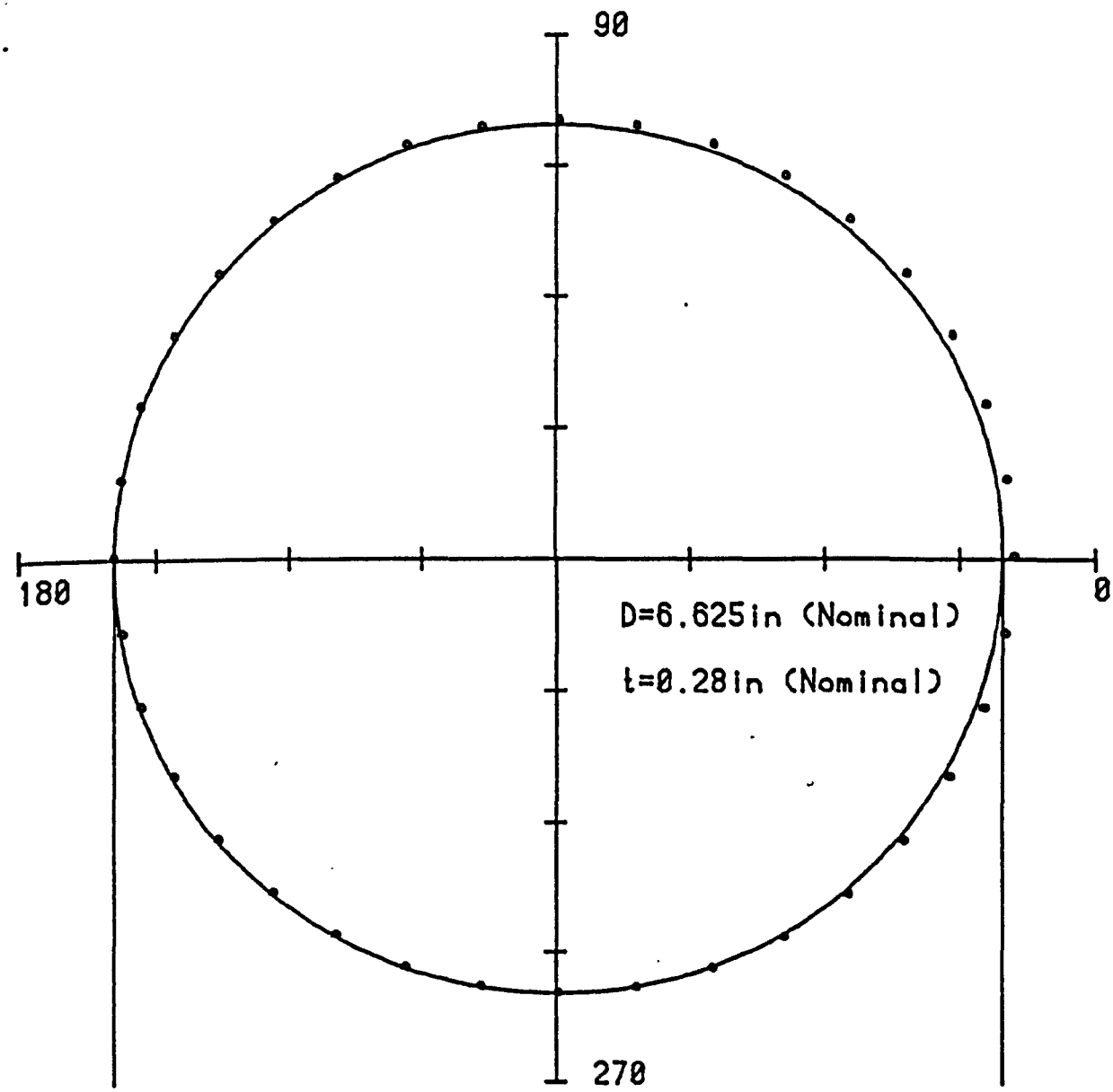

OVALITY

SPECIMEN No.2-180deg-Sch40

SECTION No.7

AVERAGE OUTSIDE DIAMETER (in) = 6.6794
Max=6.711 Min=6.66

AVERAGE WALL THICKNESS (in) = 0.3013
Max=0.3153 Min=0.28

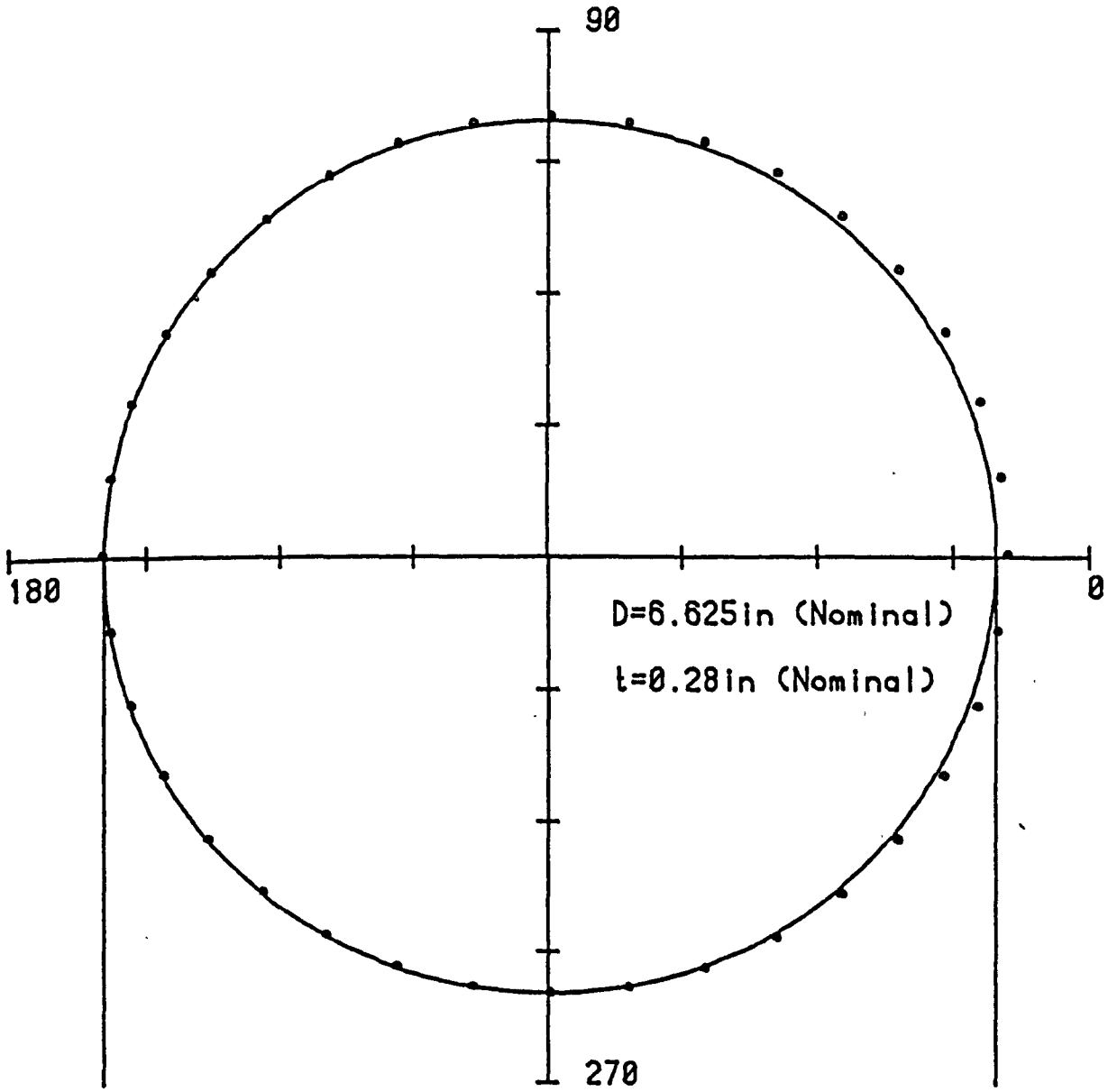

OVALITY

SPECIMEN No.2-180deg-Sch40

SECTION No.8

AVERAGE OUTSIDE DIAMETER (in) = 6.6789
Max=6.7215 Min=6.6555

AVERAGE WALL THICKNESS (in) = 0.2972
Max=0.3121 Min=0.2812

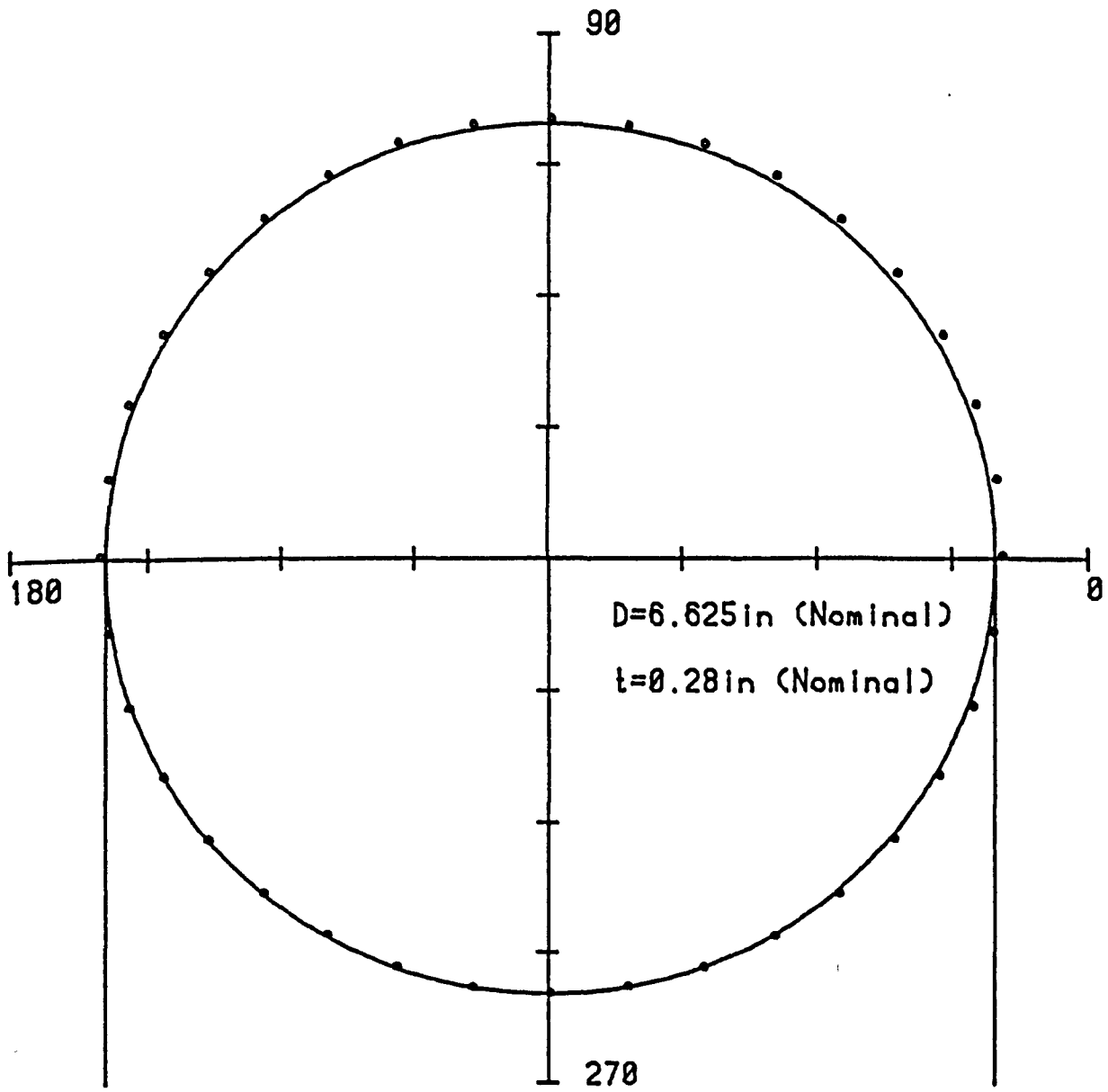

OVALITY

SPECIMEN No.2-180deg-Sch40

SECTION No.9

AVERAGE OUTSIDE DIAMETER (in) = 6.6785
Max=6.716 Min=6.655

AVERAGE WALL THICKNESS (in) = 0.3027
Max=0.3176 Min=0.2808

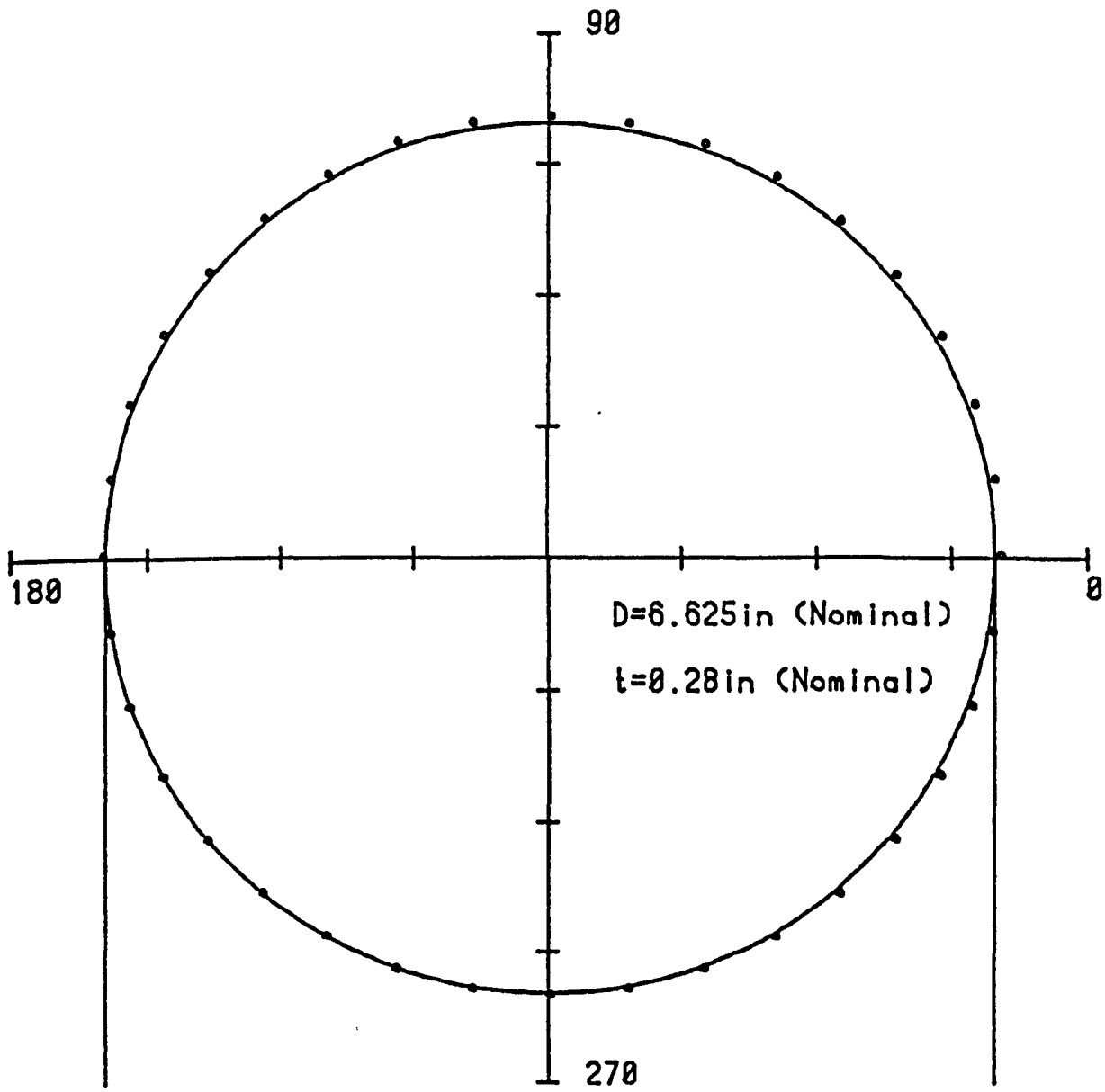

OVALITY

SPECIMEN No.2-180deg-Sch40

SECTION No.10

AVERAGE OUTSIDE DIAMETER (in) = 6.6825
Max=6.692 Min=6.67

AVERAGE WALL THICKNESS (in) = 0.3091
Max=0.3177 Min=0.2957

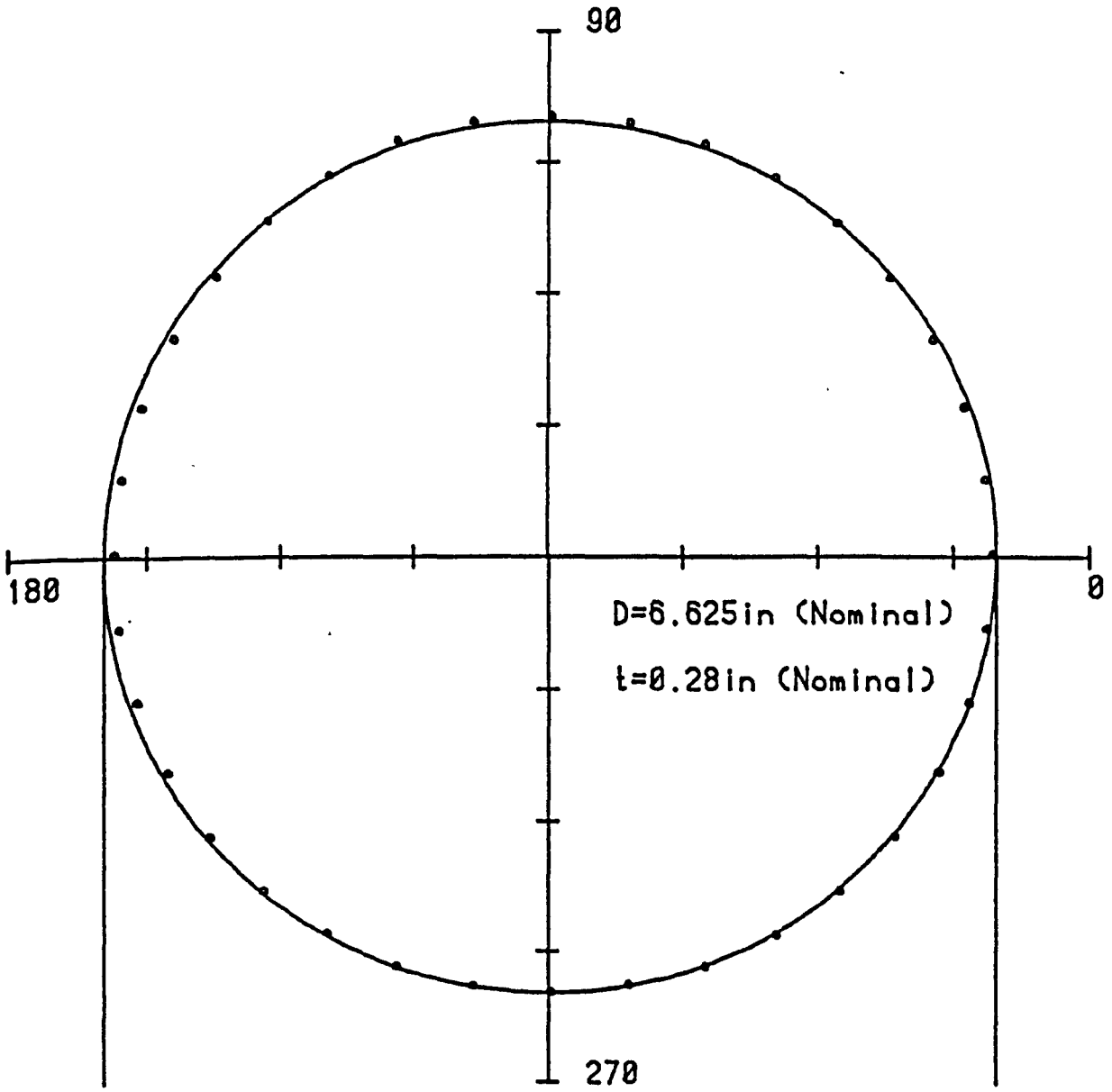

OVALITY

SPECIMEN No.2-180deg-Sch40

SECTION No.11

AVERAGE OUTSIDE DIAMETER (in) = 6.5956
Max=6.666 Min=6.516

AVERAGE WALL THICKNESS (in) = 0.3161
Max=0.342 Min=0.2598

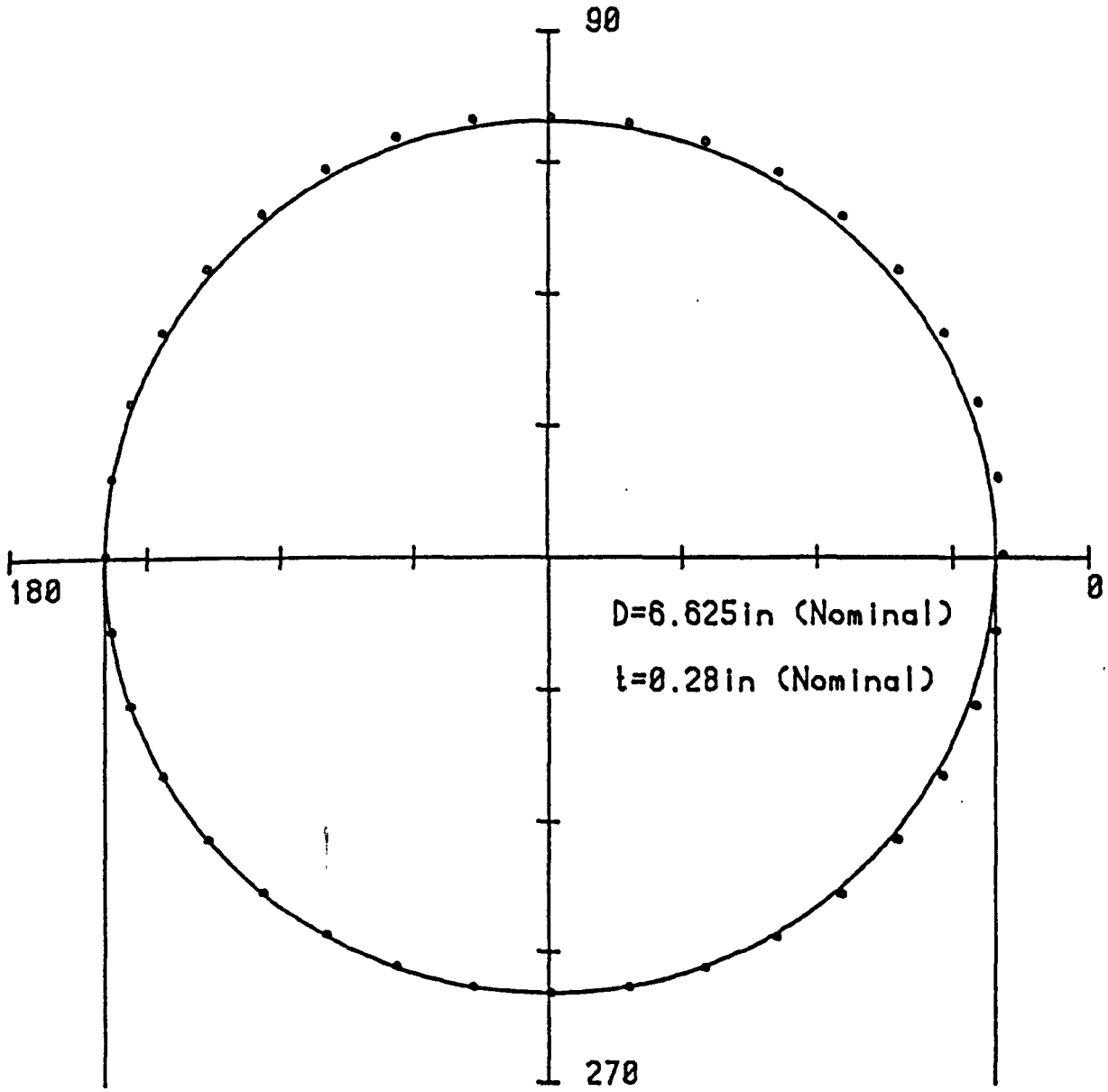

OVALITY

SPECIMEN No.2-180deg-Sch40

SECTION No.12

AVERAGE OUTSIDE DIAMETER (in) = 6.6901
Max=6.7125 Min=6.6565

AVERAGE WALL THICKNESS (in) = 0.2885
Max=0.2955 Min=0.2718

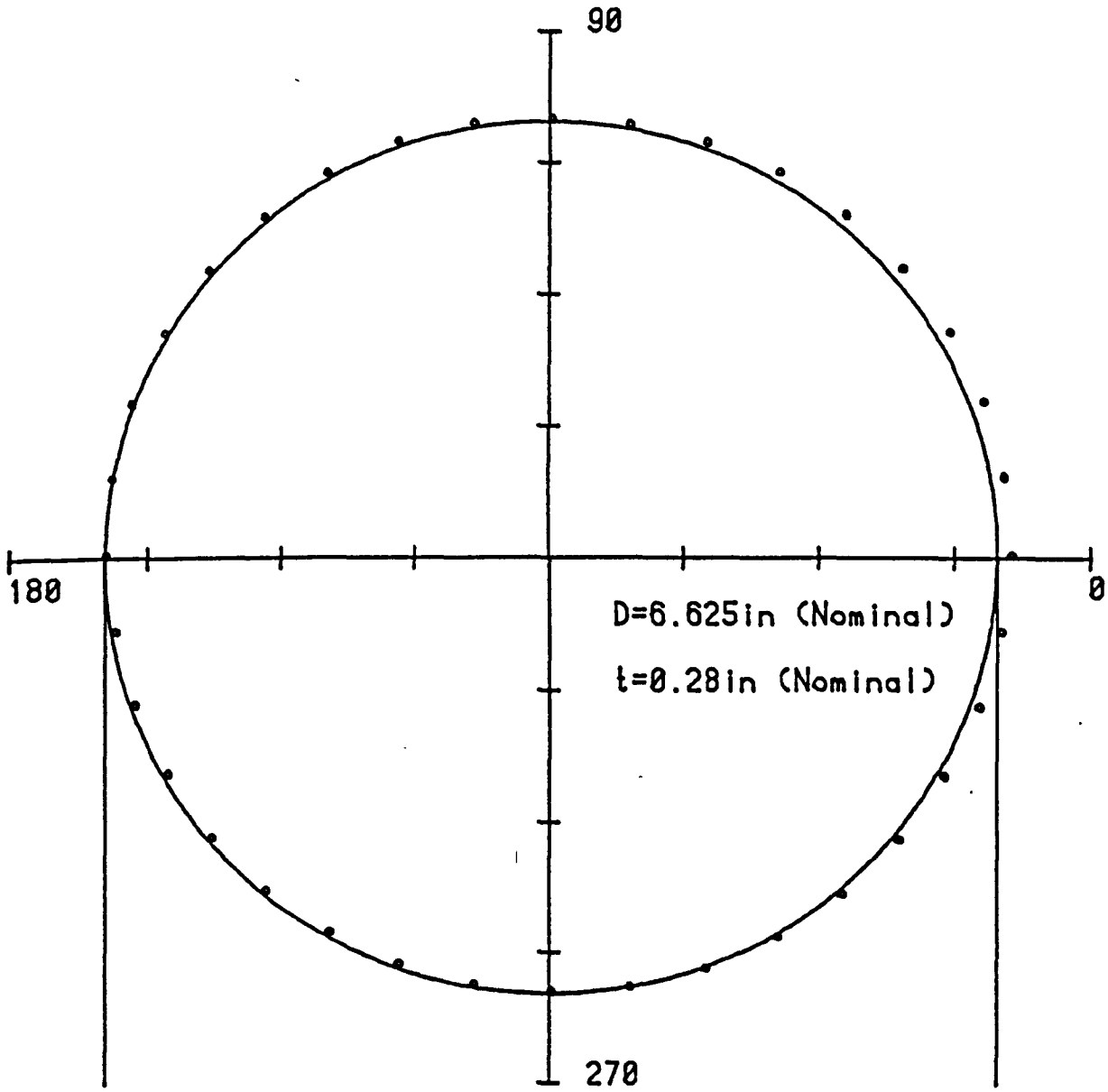

OVALITY

SPECIMEN No.2-180deg-Sch40

SECTION No.13

AVERAGE OUTSIDE DIAMETER (in) = 6.6793
Max=6.7225 Min=6.6305

AVERAGE WALL THICKNESS (in) = 0.2812
Max=0.2946 Min=0.2623

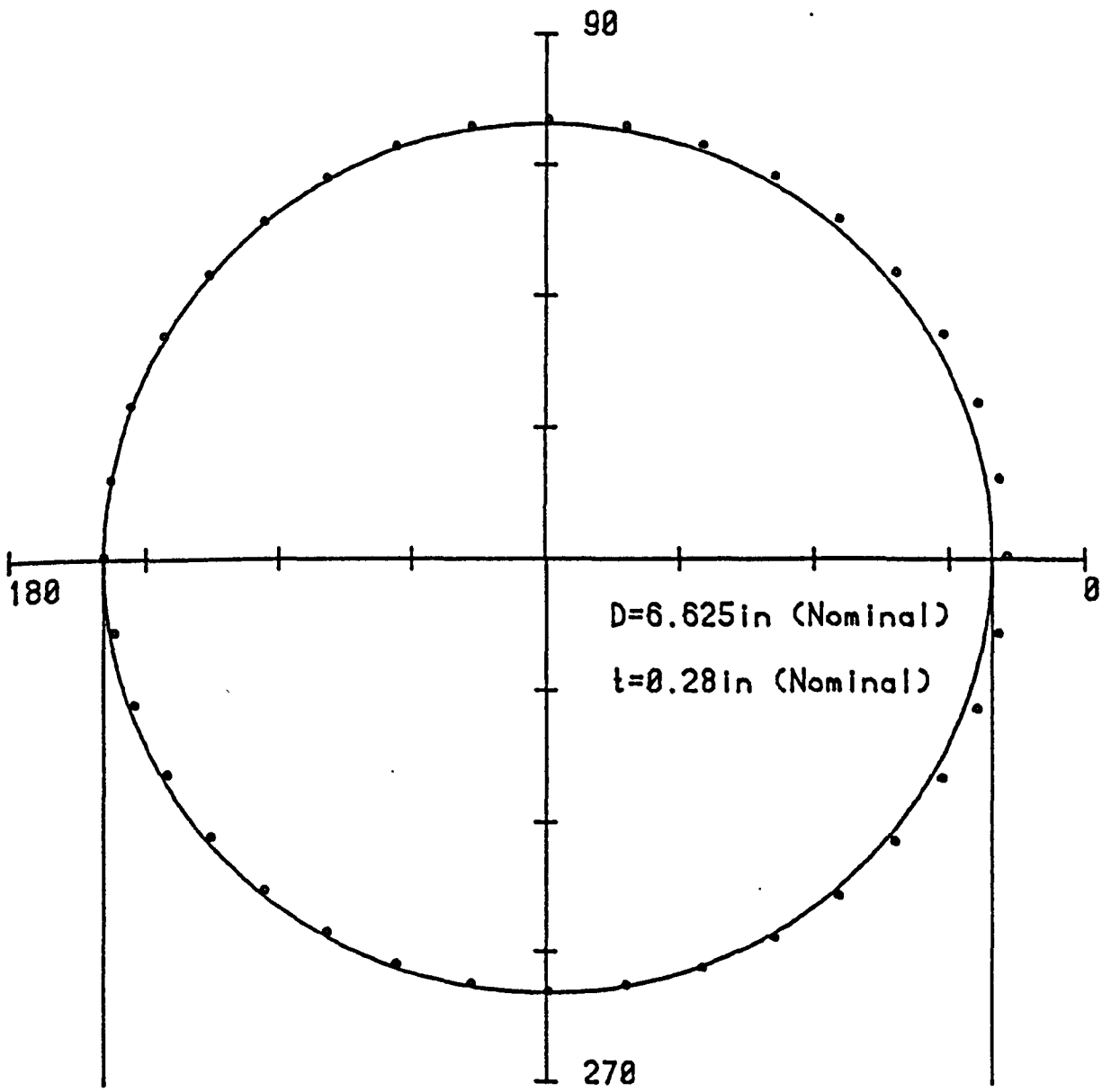

OVALITY

SPECIMEN No.2-180deg-Sch40

SECTION No.14

AVERAGE OUTSIDE DIAMETER (in) = 6.6747
Max=6.734 Min=6.639

AVERAGE WALL THICKNESS (in) = 0.2749
Max=0.2912 Min=0.2602

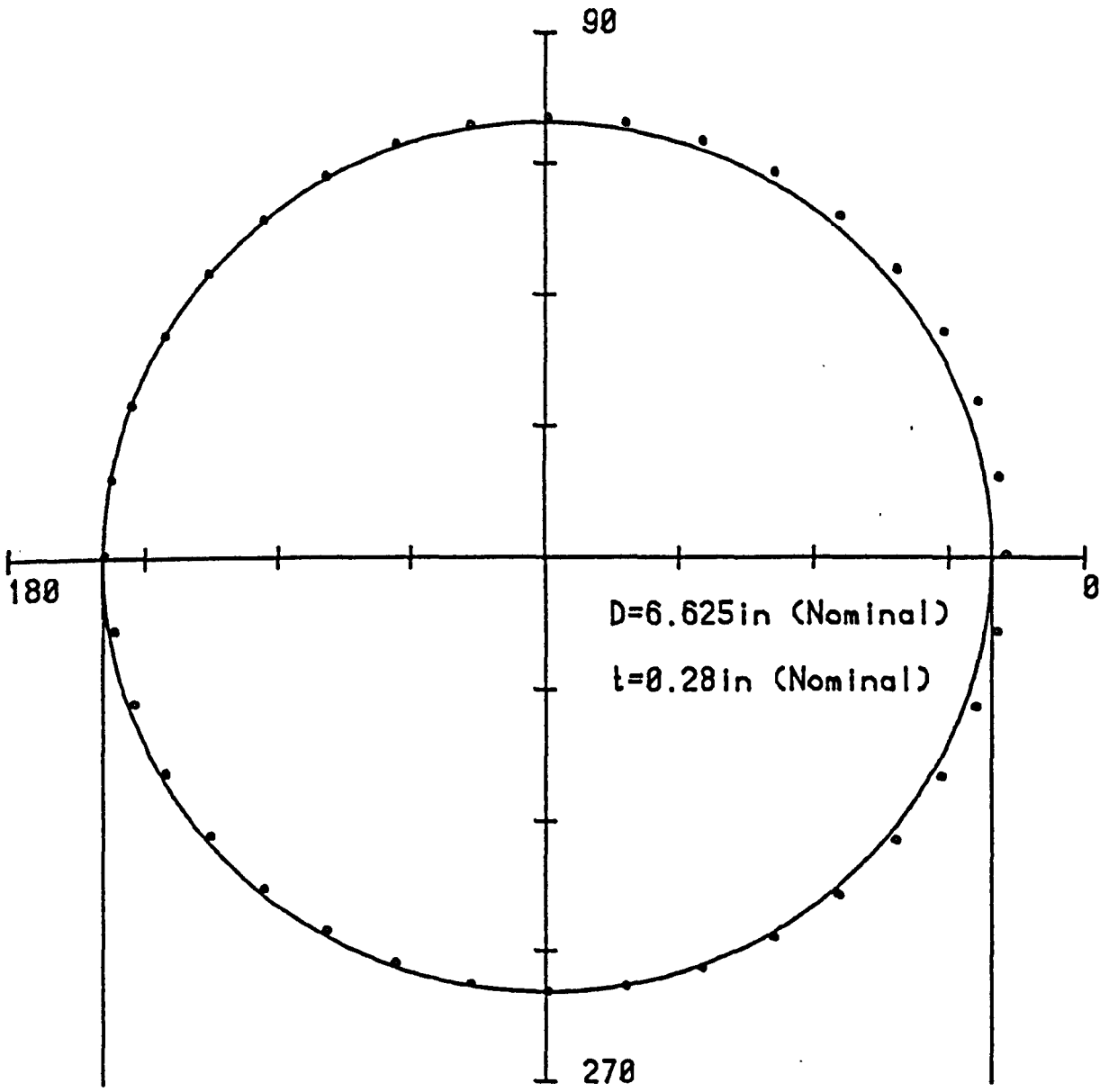

OVALITY

SPECIMEN No.2-180deg-Sch40

SECTION No.15

AVERAGE OUTSIDE DIAMETER (in) = 6.6785
Max=6.718 Min=6.656

AVERAGE WALL THICKNESS (in) = 0.2841
Max=0.2962 Min=0.2619

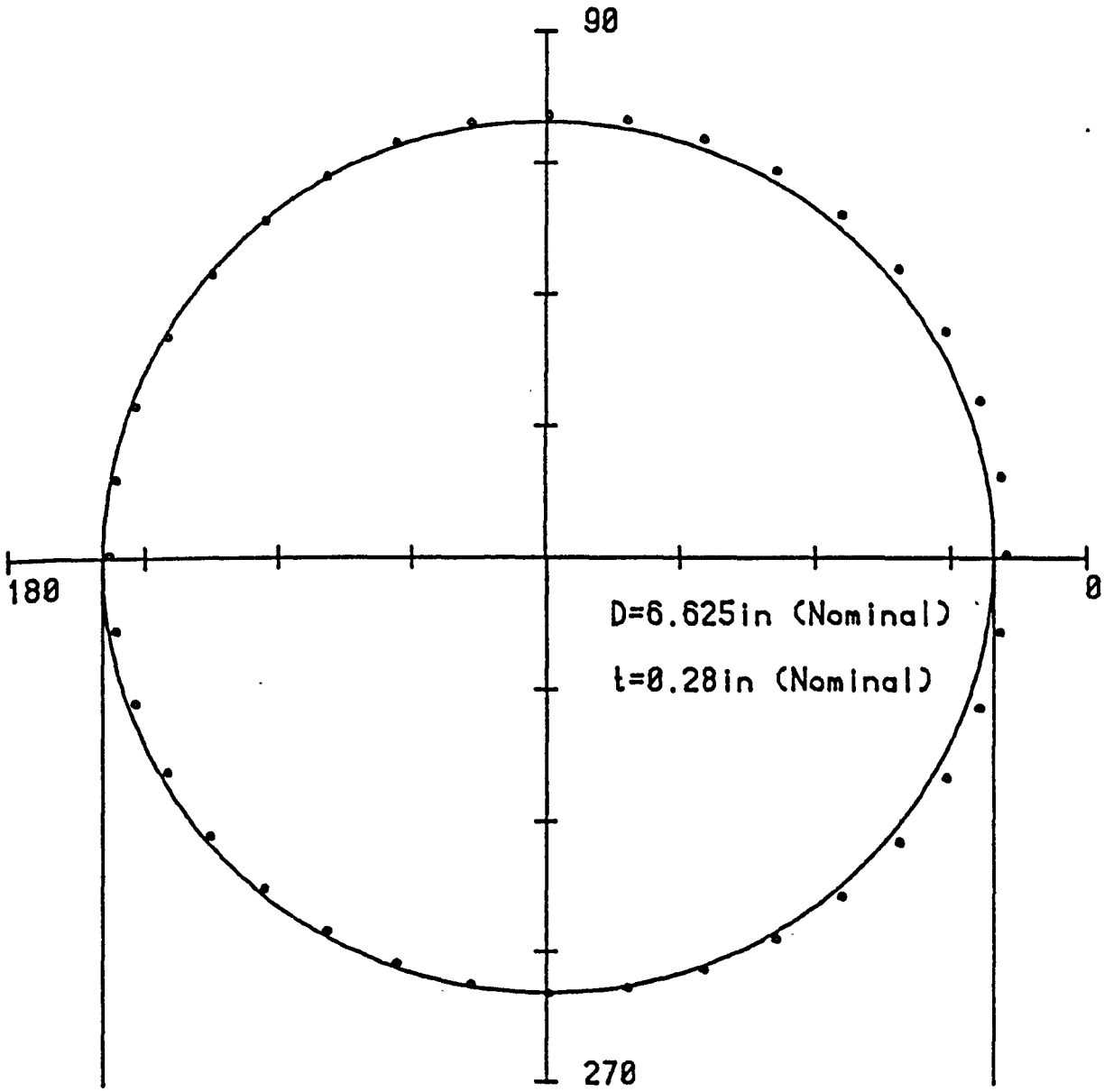

OVALITY

SPECIMEN No.2-180deg-Sch40

SECTION No.16

AVERAGE OUTSIDE DIAMETER (in) = 6.6757
Max=6.691 Min=6.664

AVERAGE WALL THICKNESS (in) = 0.2891
Max=0.2973 Min=0.2755

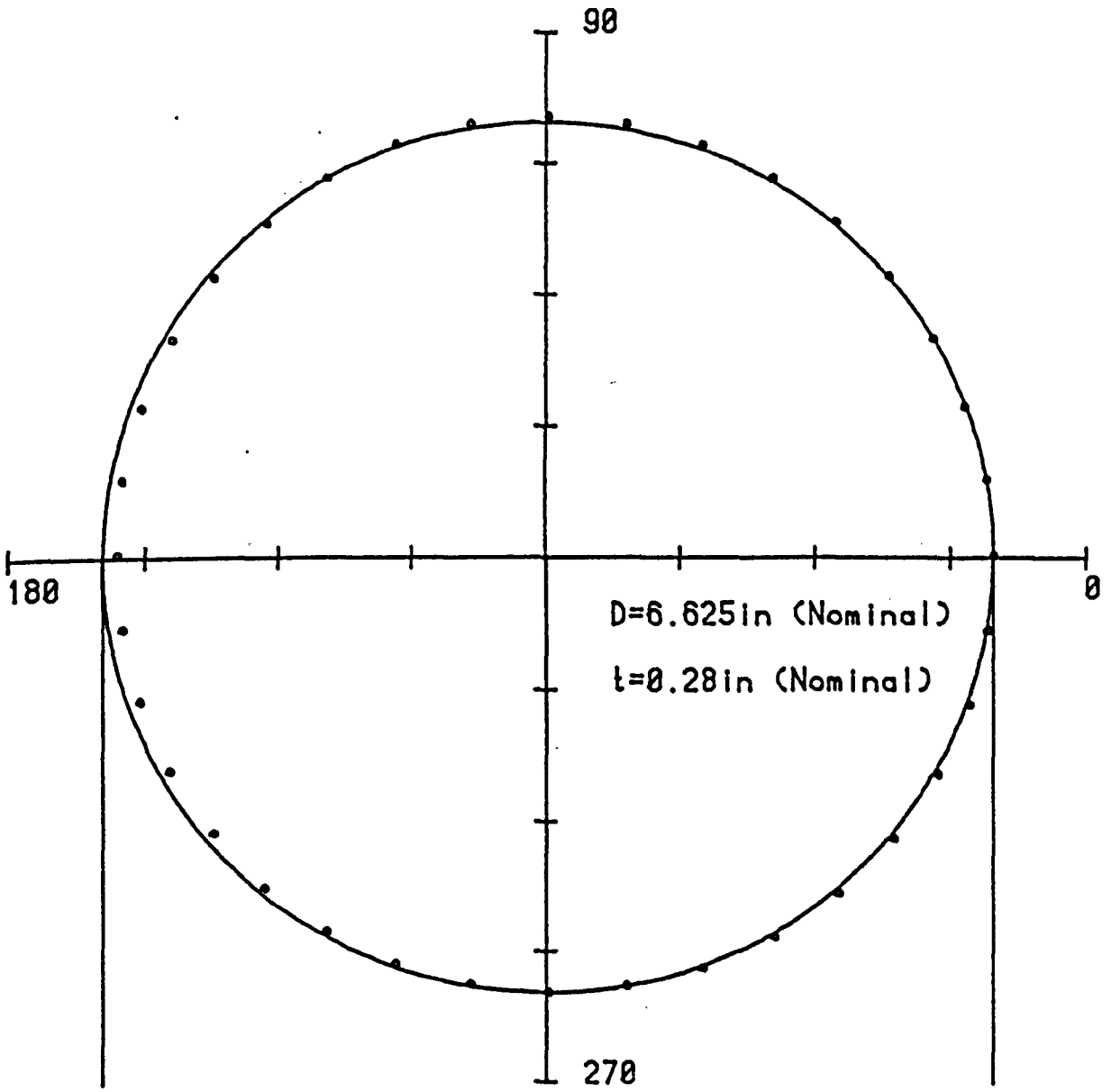

OVALITY

SPECIMEN No.2-180deg-Sch40

SECTION No.17

AVERAGE OUTSIDE DIAMETER (in) = 6.5960
Max=6.6685 Min=6.5185

AVERAGE WALL THICKNESS (in) = 0.3028
Max=0.3224 Min=0.2655

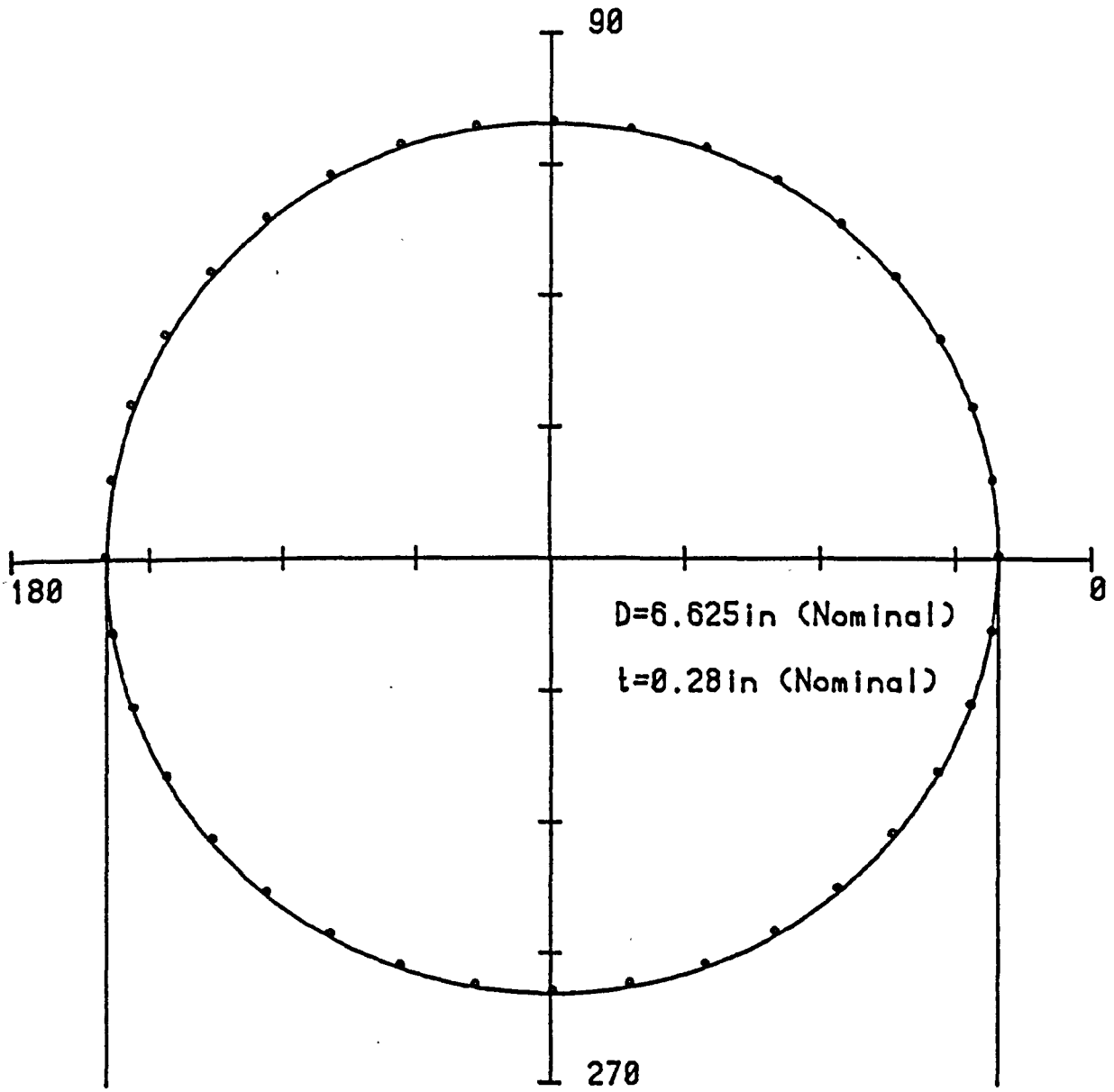

OVALITY

SPECIMEN No.2-180deg-Sch40

SECTION No.18

AVERAGE OUTSIDE DIAMETER (in) = 6.6236
Max=6.6415 Min=6.6125

AVERAGE WALL THICKNESS (in) = 0.2817
Max=0.2878 Min=0.2735

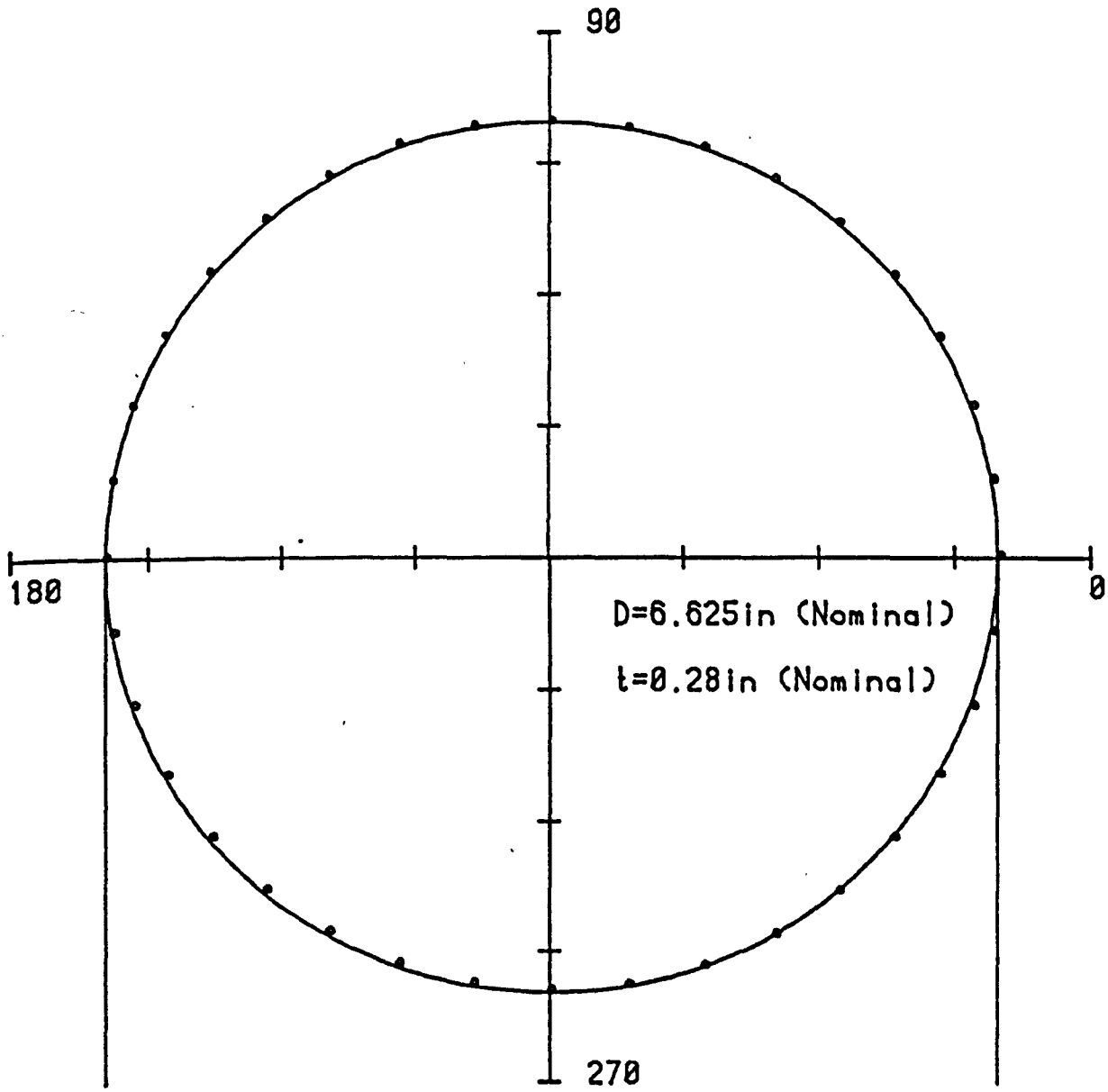

OVALITY

SPECIMEN No.2-180deg-Sch40

SECTION No.20

AVERAGE OUTSIDE DIAMETER (in) = 6.6275
Max=6.655 Min=6.599

AVERAGE WALL THICKNESS (in) = 0.2817
Max=0.2892 Min=0.2723

APPENDIX (7)

Evaluation of Flexibility Factors for Pipe Bends with Connected Tangents

APPENDIX 7: Evaluation of Flexibility Factors for Pipe Bends with Connected Tangents

This appendix presents the rotation terms involved in the determination of the flexibility factor for pipe bends with connected tangents.

The flexibility factor for both in and out-of-plane loading is defined generally as:

$$K = \frac{\gamma - \gamma_T}{\gamma_0}$$

where γ = the overall rotation of the bend assembly determined from experiment;

γ_T = the relevant rotation of both tangents;

γ_0 = the nominal rotation . . *(7.1)*

The terms evaluated here are the nominal rotation γ_0 and the tangent rotation γ_T. The tangent rotation is further defined as:

$$\gamma_T = \gamma_{TF} + \gamma_{TL}$$

where γ_{TF} = relevant rotation of the fixed tangent;

γ_{TL} = relevant rotation of the loaded tangent.

. . *(7.2)*

The nominal rotation is defined as:

$$\gamma_0 = \frac{MR\alpha}{EI} \qquad . . \quad (7.3)$$

The moment arm used in defining M for both loading cases is shown in Figure (7.1A).

The terms of γ_o, γ_{TF} and γ_{TL} for the loading cases of in-plane and out-of-plane are given in Tables 7.1A - 7.4A. These terms are evaluated for the bend angles of 180°, 90° and 45°.

The notation of dimensions and loading is that shown in Figure (7.1A).

TABLE 7.1A: In-plane loading - nominal rotations.

Bend angle	γ_o
180°	$\frac{WR\pi}{EI}[L_A + L_T + R]$
90°	$\frac{WR\pi}{2EI}[L_A + L_T + R\sin(\frac{\pi}{4})]$
45°	$\frac{WR\pi}{4EI}[L_A + L_T\cos(\frac{\pi}{4}) + R[\cos(\frac{\pi}{8}) - \cos(\frac{\pi}{4})]]$

where L_A = length of moment arm

L_T = length of tangent

TABLE 7.2A: In-plane loading - tangent rotations.

Bend angle	γ_{TF}	γ_{TL}
180°	$\frac{WL_T}{EI}[L_A + \frac{1}{2}L_T]$	$\frac{WL_T}{EI}[L_A + \frac{1}{2}L_T]$
90°	$\frac{WL_T}{EI}[L_A + L_T + R]$	$\frac{WL_T}{EI}[L_A + \frac{1}{2}L_T]$
45°	$\frac{WL_T}{EI}[L_A + L_T\cos(\frac{\pi}{4}) + R[1-\cos(\frac{\pi}{4})]]$	$\frac{WL_T}{EI}[L_A + \frac{1}{2}L_T\cos(\frac{\pi}{4})]$

where L_A = length of moment arm
L_T = length of tangent

TABLE 7.3A: Out-of-plane loading - nominal rotations.

Bend angle	γ_o
180°	$\frac{WR\pi}{EI}[L_A + L_T]$
90°	$\frac{WR\pi}{2EI}[L_A + L_T]$
45°	$\frac{WR\pi}{4EI}[L_A + L_T\cos(\frac{\pi}{4})]$

where L_A = length of moment arm
L_T = length of tangent

TABLE 7.4A: Out-of-plane loading - tangent rotations.

Bend angle	γ_{TF}	γ_{TL}
180°	$\frac{WL_T}{EI}[L_A + \frac{1}{2}L_T]$	$\frac{WL_T}{EI}[L_A + \frac{1}{2}L_T]$
90°	$\frac{WL_T}{GJ}[L_A + L_T + R]$	$\frac{WL_T}{EI}[L_A + \frac{1}{2}L_T]$
45°	$\frac{WL_T}{GJ}[L_A + L_T\cos(\frac{\pi}{4}) + R[1-\cos(\frac{\pi}{4})]]$	$\frac{WL_T}{EI}[L_A + \frac{1}{2}L_T\cos(\frac{\pi}{4})]$

where L_A = length of moment arm

L_T = length of tangent

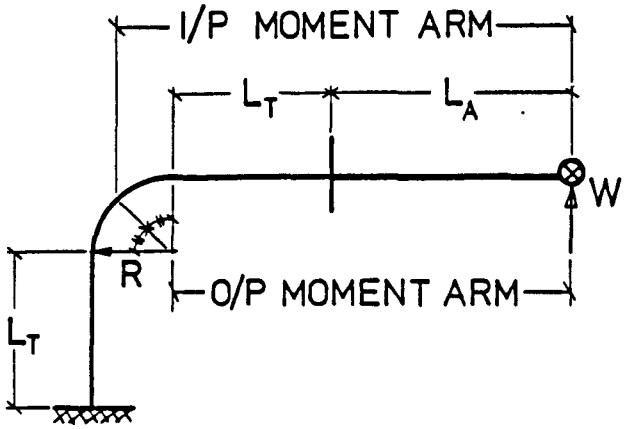

90° BEND

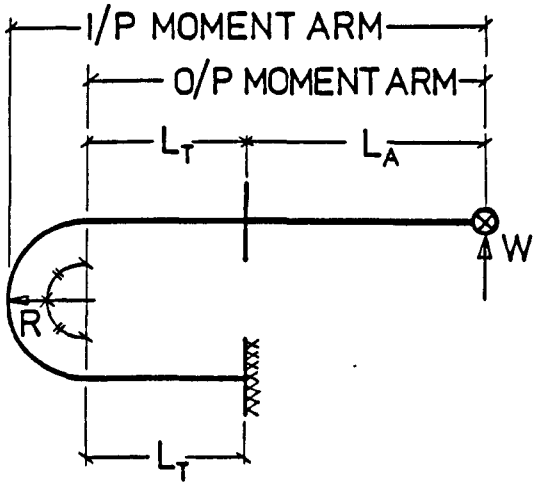

180° BEND

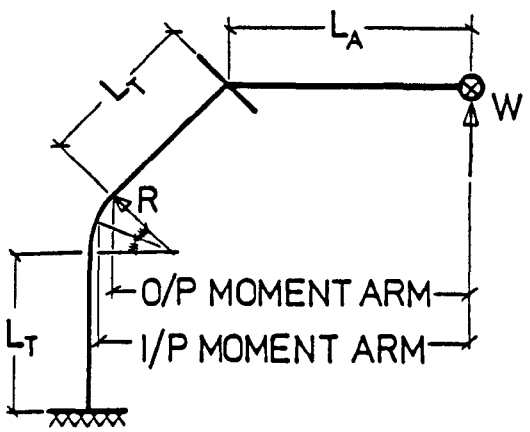

45° BEND

NOTATION

FIG. 7·1A

APPENDIX (8)

Room Temperature Elastic Behaviour of the CERL-Planer Capacitance Strain Gauge

Report No. CGI on

Measurement of Strain on Pipe Bends under Room Temperature Elastic Conditions using the CERL-Planer Capacitance Strain Gauge.

Part of

INELASTIC BEHAVIOUR OF PIPEWORK COMPONENTS

for

The Reactor Group, UKAEA

Agreement No. 4R53584B

by

Kenneth Rae

1. Summary

The CERL-PLANER capacitance strain gauge is used extensively on a variety of applications normally at elevated temperatures in the range of 500 to 600°C. Most of the published literature relates to the behaviour and long term stability at these temperatures.

This report deals primarily with the behaviour and performance of the type C5 capacitance gauge under room temperature elastic conditions with particular regard to their application to pipe bends of 6 inches nominal bore.

In mounting the gauge on the surface of the pipe methods using wedges and bending the feet are examined. It is shown that the latter method of bending the feet is to be preferred. When mounted on wedges the gauge can prove to be inaccurate on all but machined sections of known dimensions, being dependent on the relatively geometry of the wedges.

Gauge calibration compatible with the in-situ condition is shown to be essential for accurate results. In the measurement of bending strain, for example, the actual strain can be underestimated by between 20 to 30% when the standard calibration is used.

2. Contents

3. Introduction

This report presents the results of the first stage of a two part programme being carried out at the university on the CERL-PLANER capacitance strain gauge (type C5). The work forms a subsidiary part of a main research programme on the inelastic behaviour of pipework components [1] *1 where capacitance gauges will be used extensively in the measurement of strain at elevated temperature (570°C) on a variety of stainless steel type 316 pipe bend specimens.

For the first part of this work, which forms the basis of this report, attention is focused primarily on the measurement of bending strains under room temperature elastic conditions. This is a consequence of the various forms of loading on the bend specimens where bending strains predominate. The second part of the work concerning the experience at elevated temperature will be treated independently and presented in a separate document.

The need for this work arose from the results of a series of room temperature tests carried out on a 90° Sch.10 bend specimen where with the capacitance gauges mounted on wedges, differences of up to -80%*2 were recorded between the capacitance gauge and similarly located electrical resistance gauges. This particular bend specimen (No. 7 - 90° - Sch.10) was the first to be tested with wedges. Prior to this on the pilot scheme [2] the capacitance gauges were mounted with the feet bent to accommodate the curvature of the section (6 inches N.B.) giving comparisons of around - 20%.

---

*1 Reference number see section 7.

*2 For comparison with electrical resistance gauges the sign convention adopted is as follows:

$$\% \text{ diff} = \left[1 - \frac{\text{strain (resistance)}}{\text{strain (capacitance)}} \right] \times 100$$

In an attempt to improve upon this figure it was decided to adopt the method of wedge mounting following essentially along the same lines as HEATHER, BROWNE and DÉR [3]. It should be mentioned, however, that bending the feet of the gauge presents a delicate and precarious operation and further is totally against the manufacturers recommendations. The method of wedge mounting naturally introduced further problems such as the actual manufacture of the wedges and the development of new techniques in mounting the gauge. Following satisfactory tests on a proving ring, the method was applied to the pipe bend specimen. Here, however, the poor comparison cast some doubt on the method and accordingly a series of tests were initiated to examine the problem. Primarily, these consisted of further tests on the proving ring followed by a series of tests using a four point loading beam. A theoretical analysis of the gauge displacement behaviour was also carried out.

The high cost of the capacitance gauge together with damage due to repeated use has naturally limited the scope of the work. However, the results from the test programme, due in part to the choice of tests, appear to have been sufficient to substantiate the findings. Other aspects concerning the behaviour and use of the gauge which arose during the course of the tests are also discussed.

4. Development of Wedge Mounting

4.1 General

The capacitance strain gauge has been designed specifically for application to flat surfaces or those with large radii of curvature. The application here to pipe bends of 6 inches NB necessitates either bending the feet of the gauge to accommodate the increase in curvature or alternatively reducing the curvature artificially by means of wedges mounted on the surface (Fig. 1).

Mounting of the gauge using wedges is a fairly straight forward operation although as we shall see it does require the development of additional techniques. The principle employed requires two wedge-shaped blocks of the parent material contoured to meet the surface curvature. These are attached (spot welded) to the surface at virtually the same height as the surface along thin edges normal to the gauge axis (Fig. 2). The gauge is then mounted in the usual way on the flat surfaces provided by the wedges. This permits surface movements to be transferred directly to the gauge via the wedges. Change in the gauge length is then accounted for by a simple factor K defined as:

$$K = \frac{\text{capacitance gauge length (unstrained)}}{\text{distance between wedge attachments.}}$$

The use of wedges has been reported by HEATHER, BROWNE and DÉR [3] with apparent success using the type C4 gauge. Employing much larger wedges on pressurised machined tube sections of 34 mm (1.34 inches) outside diameter comparisons of capacitance and resistance gauge strains are given as 305. με and 281. με respectively (ie + 8%). This incidentally appears to be the only reported in situ calibration with

resistance gauges. Further comparison was made with a capacitance gauge mounted directly on a tube section of 140.4 mm (5.53 inches) outside diameter. The comparison here, however, was made with the wedge mounted counterpart. Experience here shows that direct mounting made on a 6 inch NB bend (outside diameter = 6.625 inches ⌜=⌝ 168 mm) causes the capacitance plates to come in contact as a result of rotation of the feet and require a substantial preset tensile strain to separate the capacitance plates. As we shall see, application of the gauge in this manner can introduce substantial errors, particularly so when the standard displacement calibration is used.

4.2 Manufacture of Wedges

In applying this method to the pipe bend specimen the first problem encountered was the actual manufacture of the wedges. Based on the nominal outside diameter of 6.625 inches (168 mm) the wedge geometry necessary to provide a flat surface for gauge mounting requires a virtually flat wedge with the curvature on the inside hardly visible (Fig. 3). Naturally the overall dimensions of the wedge require an object which is not too small in terms of ease of handling but at the same time not too large, bearing in mind the space restrictions on the bend layout. With the help of Fig. 4 an overall size of 7 x 4 x 0.97 mm thick (0.27 x 0.16 x 0.04 inches) with a wedge angle of at most 8° was chosen as the optimum (Fig. 5). These dimensions correspond to a 16 mm (0.63 inches) gap between the wedges.

The method of manufacture adopted (Fig. 6) used a strip cut from a specimen length of Sch 40 SS pipe clamped via a backing strip to an angle piece, the latter allowing rotation of the whole assembly to

achieve the correct wedge angle. This machined strip was then cut up into the required widths using an AGIE CUT spark eroder giving around a dozen wedges per strip. Later versions dispensed with the fine edge on the wedge by increasing the thickness here to around 0.002 inches (0.05 mm). Wedges with the inside surface machined flat were also manufactured and although they appeared virtually indistinguishable from the others they did not appear to fit as neatly on the proving ring.

4.3 Initial Tests on Proving Ring

4.3.1 General

In order to grasp the necessary techniques and further establish the performance of the method it was decided prudent to conduct a series of tests on a proving ring before embarking on application to the bend. Here the technique of spot welding the leading edge of the wedges was established with the wedges sufficiently far apart to ensure complete support for the feet of the gauge. Measurement of the gap was accomplished using small calipers measuring from the centre line of the spot welds.

The proving ring employed (Fig. 7) was cut from a specimen length of Sch 40 SS pipe machined to ensure circularity of section. In tension loading the ring was hung from one of the main test frames and dead weights applied to a cradle attached to the ring, in compression the dead weights were simply sat on the ring support. For comparison with capacitance strain the ring was equipped with two 20 mm (0.79 inches) resistance gauges (SHOWA F - 20). These were read through

a "BUDD" strain recorder. The capacitance gauge was read through the 1050 ASL unit via an APPLE computer.

Values of strain in these tests and all subsequent tests was computed from the slope of a best fit straight line evaluated via in-house computing. In all a total of eight tests. No 1R to No 8R were conducted on three capacitance gauges on the proving ring. The manufacturer's calibration (which is based on a flat bed linear displacement) for these gauges is shown in Fig. 8. This calibration was applied using a best fit 5 - degree polynomial for both these tests and all subsequent tests using 21 data points.

4.3.2 Results

The results of each test are shown in Fig. 9 to Fig. 11. A summary of these results is given in Table No. 1. In Fig. 9 and 10, "corrected" strain includes the factor K for gauge length. In test No. 1R and 2R small toolmakers clamps bearing on $\frac{1}{8}$" diameter ball bearings were used to clamp the gauge, on all other tests the gauge was spot welded. In test No. 4R and onwards compression of the ring necessitated removal of the assembly from the main loading frame resulting in a possibly poor earth connection. This was rectified in Test No. 6R using an additional earth from the gauge leads to the ring (Fig. 12).

Use of the partition between the leads along the gauge axis (Fig. 13) and a top cover did little but change the zero capacitance without any significant change to the absolute value of strain.

TABLE No. 1: Initial tests on proving ring.

Test No.	Gauge No.	Strain direction	Capacitance unstrained (pf)	Comparison with ERSG*	Condition
1R	C5-3750	neg	0.7560	- 4%	No partition, No cover Gauge clamped to wedges.
2R	C5-3750	neg	0.7427	- 4%	Same as test No. 1R.
3R	C5-3751	neg	1.0079	-10.5%	No partition, No cover Gauge welded to wedges.
4R	C5-3751	pos	1.0071	-15%	Same as test No. 3R.
5R	C5-3752	pos	1.1966	-13%	No partition, No cover Gauge welded to wedges
6R	C5-3752	pos	1.1996	- 7%	Additional Earth.
7R	C5-3752	pos	1.1946	- 8%	Partition along gauge axis.
8R	C5-3752	pos	1.1880	- 7%	Partition and cover.

$$* \% \text{ Diff} = \left[1 - \frac{\text{Strain ERSG}}{\text{K x strain C.G}}\right] \text{x } 100$$

4.4 Application to Bend Specimen

4.4.1 General

As a result of the reasonably satisfactory performance on the proving ring it was decided to proceed with the method for mounting on the bend specimen. This particular specimen (No. 7 - 90° - Sch 10) was designated for an elevated temperature (570°C) forward creep test in an in-plane bending closing mode. Details of the temperature part of this test will be omitted here, the attention being focused on the preliminary room temperature work. This part of the test can be sub-divided into two parts. Firstly, there was a detailed elastic strain distribution test to determine the points of maximum strain (meridional direction) around the bend mid-section followed by an elastic calibration of the capacitance gauges using resistance gauges of comparable length.

The bend was equipped for the elevated temperature test with three active capacitance gauges and one dummy gauge to measure the drift characteristics at temperature. Our interest here shall be concerned with the two meridional gauges No. 1 and No. 3. The general set up of the gauges is shown in Fig. 14 showing clearly the limitations in space arising from the copper heating sheath [4]. Here we can also see the small ceramic posts used to isolate the gauges from gauge lead movement. This latter problem would appear to be peculiar to pipe bends where with the mineral insulated gauge leads attached to the bend surface the inherent flexibility of the bend can cause the gauge leads to move relative to the gauge with the movement being transmitted to the gauge via the nichrome coils. It has been difficult to completely assess the extent of this on active gauges as it was first observed on dummy gauges which of course should not respond to loading outwith temperature

effects. Clearly visible in Fig. 14 are partitions, employed along the gauge axis and between adjacent gauges. This was recommended to the writer as good practice at an earlier stage when an attempt was being made to improve on the 20% difference between bent feet capacitance gauges and the resistance gauges. However, from tests on the proving ring the partitions appear to have little effect.

4.4.2 Results

4.4.2.1 Strain Distribution

The strain distribution test using a series of resistance gauges (Fig. 15) gave symmetrical values and position of maximum meridional strain as shown in Fig. 16. In passing, it is noted that they compared well with THOMSON's theory [5] which accounts for the restraining effect of tangent pipes.

4.4.2.2 Capacitance Gauge Calibration

Calibration of the capacitance gauges located at the points of maximum meridional strain was attempted using 20 mm resistance gauges (SHOWA F - 20). In the first test the capacitance gauges give raw comparisons of -60% and -80% for gauges No 1 and No 3 respectively (Fig. 17). Introducing the correction (see footnote to Table 1, page 488) for gauge length of (about) 1.2 reduced these values to -32% and -50%. These comparisons were in complete contrast to those obtained earlier on the proving ring where results of around -10% were achieved.

The stress-strain system on the proving ring although not exactly identical with that of the bend was considered sufficiently similar for comparison purposes, bending strains predominating in both cases.

Also the techniques employed in mounting the wedges and the gauges were identical on both systems. To ensure that this was so the bend was removed from the test rig to the bench to facilitate the wedge and gauge attachment. Thereafter, routine checks on instrumentation, ASL-APPLE interface and software were carried out. All such checks showed the equipment was operating satisfactorily. That all these aspects were satisfied left no clear explanation as to the poor comparison with the results of the proving ring. Being faced with this apparently unexplained behaviour was frustrating and in an attempt to improve the comparisons it was decided to "experiment" with the gauge layout on the bend. The alternative option of complete dismantling the set up and reassembling with new wedges and gauges was not considered. In fact these experiments led to an extensive number of tests extending to a period of over 6 months during which numerous modifications were made to the layout. Some of the main changes made were as follows:

removal of top covers and partitions between gauges and along the gauge axis;

replacement of gauges and gauge leads;

spot welding gauge directly to the bend through the wedges;

varying the gap between the wedges;

removal of the ceramic posts.

These main changes and other numerous secondary modifications appeared to have little effect on the absolute value of strain. Accordingly when it was realised that no further improvement could be achieved the bend was heated up for the elevated temperature (570°C) stage of the test. It was then found that when the temperature exceeded around 400°C

the gauges refused to balance on the A.S.L. equipment. This was eventually discovered to be due to a breakdown in resistance of the ceramic terminal posts at temperature and was the reason for their removal on the final test. The symptoms were not present at room temperature which made diagnosis difficult and it took three heating up periods before this fault was discovered. No particular pattern emerged from all the tests conducted and it is felt that the cycling in temperature did little more than introduce a further complication. The final test adopted for calibration showed some improvement however, the comparison being reduced to between -30% and -50%. In this test (Fig. 18) all partitions had been removed together with the ceramic posts. Gauge No 3 had been replaced twice and was now mounted with the feet bent, also gauge No 1 was spot welded through the wedge to the bend. Thus gauge length corrections were not required in these cases.

5. Further Tests on Gauges

5.1 General

As a result of the extremely poor comparison obtained on the bend specimen using wedges, a more detailed series of tests were begun.

These comprised the following:

(a) Further tests on the proving ring

(b) Tests on a four point loading beam

(c) Tensile tests.

This work was further supplemented by some analytical work into the deformation of the gauge.

5.2 Further Tests on Proving Ring

5.2.1 General

To confirm the initial tests on the proving ring, a further three tests (No. 9R to 11R) were carried out using two capacitance gauges.

Test No. 9R and 10R were essentially a repeat of the earlier tests on the same wedges as before. In test No. 11R the wedges were removed, gauge feet bent and the gauge mounted directly on the ring. Here, as opposed to bending the feet by hand, a small jig was used to prevent gross deformation of the arches.

5.2.2 Results

The results of a typical test (No. 11R) are given in Fig. 19. A comparison of the results is given below in Table No. 2 which shows favourable agreement with the initial tests.

TABLE 2: Further tests on proving ring.

Test No.	Gauge No.	Strain direction	Capacitance unstrained (pf)	Comparison with ERSG	Condition
9R	C5-3752	neg	1.1941	-10%*	No partition along gauge axis, no cover, additional earth. Gauge spot welded.
10R	C5-3752	neg	1.1958	-11%*	Repeat of Test No. 9R.
11R	C5-3731	pos	1.2415	- 6%	No partition, no cover, additional earth, feet of gauge bent and clamped to ring.

*Corrected for Gauge Length

5.3 Tests on Four Point Loading Beam

5.3.1 General

Here a series of fifteen tests (No. 1B to 15B) were conducted on a total of seven capacitance gauges. The experimental set up employed the normal four point loading beam (Fig. 20) giving pure bending along the centre section. Comparison with capacitance strain was made using a 20 mm resistance gauge (SHOWA F - 20) mounted on the beam adjacent to the capacitance gauge. The capacitance gauge was clamped to the beam using small clamps bearing on 1/16" diameter ball bearings (Fig. 21).

5.3.2 Results

The results of a typical test (No. 1B) are shown in Fig. 22. A summary of the results is given in Table 3.

In most cases the comparison varied betweeen -20 to -30%. However, the elevation of one foot had a marked effect indicating a sensitive response to relative wedge geometry. Throughout all these tests top covers and partitions were not used. Consequently, care was required when moving in the vicinity of the rig to minimise the change in dielectric.

Initially, tests were conducted on the beam by displacing the beam at both ends and at one end to check the beam characteristics. As expected this did not alter the test results and one end displacement was used thereafter.

TABLE 3: Results of four point loading beam.

Test No.	Gauge No.	Strain direction	Capacitance unstrained (pf)	Comparison with ERSG	Condition
1B	C5-3746	pos	0.7795	-22%	Displacement at both ends.
2B	C5-3746	pos	0.7785	-23%	Displacement at R/H end.
3B	C5-3746	pos	0.7785	-22%	Repeat of Test No. 2B.
4B	C5-3746	neg	0.7900	-25%	Displacement at both ends.
5B	C5-3746	neg	0.7899	-24%	Displacement at R/H end.
6B	C5-3746	pos	0.6873	-10.5%	Displacement at R/H end 0.01 in (0.25 mm) shim under R/H foot.
7B	C5-3746	neg	0.7243	-11%	Displacement at R/H end 0.01 in (0.25 mm) shim under R/H foot.
8B	C5-3747	pos	0.8496	-12%	Displacement at R/H end.
9B	C5-3747	pos	0.6924	+ 3%	Displacement at R/H end 0.015 in (0.4 mm) shim under R/H foot.
10B	C5-3747	pos	0.9876	- 1%	Displacement at R/H end 0.015 in (0.4 mm) shim under L/H foot.
11B	C5-3730	pos	0.8867	-11%	Displacement at R/H end.
12B	C5-3737	pos	0.6819	-17.5%	Displacement at R/H end.
13B	C5-3749	pos	0.8498	-24%	Displacement at R/H end.
14B	C5-3735	pos	0.7121	-28%	Displacement at R/H.
15B	C5-3731	pos	0.7396	-29%	Displacement at R/H.

5.4 Tensile Tests

5.4.1 General

Two forms of tensile test were carried out. In the first group the capacitance gauge was mounted on the beam section employed previously in the four point loading beam set up. In the second, a manufacturers calibration rig borrowed from BNL* was used (Type TR100/9082/1/75). A total of six tests (No. 1T to 6T) were carried out using five capacitance gauges. Prior to mounting on the calibration rig three of the gauges were dimensioned using a shadow graph.

5.4.2 Results

The results of the tensile tests (No. 1T to 3T) are shown in Fig. 23 to 25. A comparison of these results is shown below in Table 4. The initial non-linearity followed by both the capacitance and resistance gauge was due mainly to initial curvature of the beam and means that the tests are not entirely satisfactory. Also the small number of tests conducted does not justify any firm conclusion to be drawn.

Use of the calibration rig required some skill in operation and this is perhaps reflected in the results (Fig. 26 to 28). It is interesting to note here that of the gauges examined the nominal value of 0.7pF did not always correspond to zero strain. It will also be apparent that the experimental points do not coincide with the manufacturers. This results from the use of the actual unstrained gauge length as opposed to the nominal. However, it would appear to have little significance on the calibration.

In measurement, the gauge lengths differed little from the nominal value (Fig. 29). However, arch spans and heights were lower than

* Berkeley Nuclear Laboratories - C.E.G.B.

TABLE 4: Tensile tests.

Test No.	Gauge No.	Strain direction	Capacitance unstrained (pf)	Comparison with ERSG	Condition
T1	C5-3746	pos	0.7691	-13%	No partition, no cover. Additional Earth, Gauge clamped.
T2	C5-3746	pos	0.7691	- 5%	Repeat of Test No. T1.
T3	C5-3730	pos	0.8933	+10%	Same conditions as Test No. T1

nominal values together with variations in capacitance gap. Measurement of the capacitance gap was an average value, as in all the three gauges examined the plates were not quite parallel.

5.5 Analytical Work

5.5.1 General

The analytical work presented here was intended initially to serve as an explanation to the behaviour observed during the experiments. As we shall see it was possible to confirm only particular trends to a limited degree.

The work began with a purely geometrical analysis of the gauge similar to that employed by NOLTINGK [6]. This was followed by a flexibility analysis [7] considering bending effects only. Both these approaches, although able to model the symmetric linear displacements reasonably well, were difficult to use in the case of unsymmetrical deformation. For this type of displacement pattern a method proposed by CHENG and HOFF [8] using the differential equations derived from shell theory was adopted. This solution in matrix form is given in the appendix.

5.5.2 Results

The CHENG and HOFF type of analysis gave reasonable comparison with a typical gauge calibration (Fig. 30). Here the theoretical curve was based on the nominal dimensions of the gauge as given by the manufacturer. Using this analysis a variety of permutations in prescribed displacement were examined. Firstly, presetting of the gauge in horizontal displacement, as expected appeared to make little difference

to the calibration (Fig. 31). Preset of the gauge in vertical displacement altered the capacitance range but has no effect on the resulting strain, although the actual experiments did show a difference. However, when an arbitary incremental rotation of the feet together with a horizontal displacement, simulating a bending strain, was applied, there was a rotation of the calibration curve (Fig. 32). In effect this means the original calibration is incorrect for this case.

The effect was further magnified by introducing an initial rotation to one foot of the gauge.

The analysis of course, is based on small displacements. At around $\mp 2000\ \mu\varepsilon$ in horizontal displacement movement of the bottom arch exceeds the thickness of the arch (0.1 mm $\widehat{=}$ 0.004 in). The analysis further assumes an initially symmetrical gauge formed of arcs of a circle with the capacitance plates parallel and horizontal. Only a slight deviation from these requirements in the actual gauge would make it difficult to predict the behaviour. This was evident on the three capacitance gauges measured, where in each case the plates were not parallel.

5.5.3 Miscellaneous

In this section a theoretical comparison is made on the results from the proving ring and the four point loading beam. The comparison is intended simply as a check on the resistance gauges and is by no means exhaustive.

Four Point Loading Beam

Using MACAULAY'S method [7] gives a longitudinal strain along the central section of the bend as:

$$\varepsilon_b = \frac{\mp 6ty}{2\left[a^2 - \frac{k}{b}\right]}$$

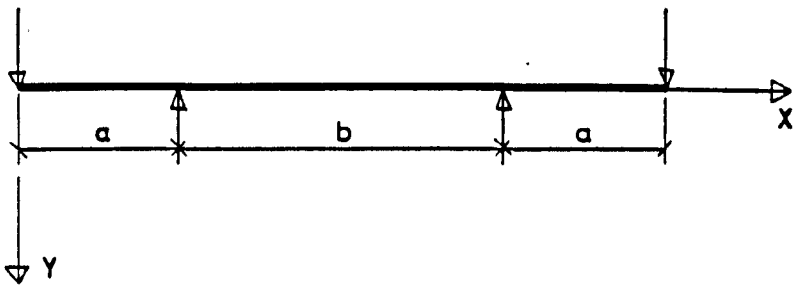

where t = beam thickness (in)

y = end displacement (in)

$k = (a^3 - (a+b)^3 + b^3)$

Using the dimensions given in Fig. 20 and a symmetrical end displacement of 10 mm $\widehat{=}$ 0.394 in results in a longitudinal strain of +646 $\mu\varepsilon$. Comparing this with the result of Test No. 1B where the slope B = +61.876, gives a longitudinal strain of +618.76 $\mu\varepsilon$, i.e. a difference of 4%.

Proving Ring

From TIMOSHENKO [9] the meridional strain ε_ϕ can be approximated by:

$$\varepsilon_\phi = \frac{1}{E}\left[\frac{P}{2A} \mp \frac{M_o t}{2I}\right]$$

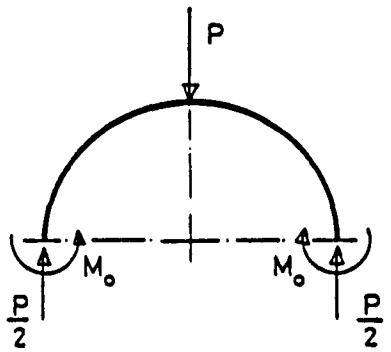

where M_o = bending moment (lbf.in)

$$= \frac{PR}{2}\left[1 - \frac{2}{\pi}\right]$$

P = applied load (lbf)

R = nominal radius (in)

t = wall thickness (in)

I = second moment of area (in^4)

A = cross-sectional area (in^2)

E = Young Modulus (lbf/in^2) = 28.2×10^6

Using the dimensions given in Fig. 7 and a load P = 500N ≙ 112.4 lbf results in a meridional strain of -159 $\mu\varepsilon$. Comparing this with Test No. IR (Fig. 9) where the slope = -0.302 gives a strain of -163 $\mu\varepsilon$, i.e. a difference of 3%.

6. Conclusions

The main conclusion to be drawn from this work is that the additional work involved in the use of wedges does not merit their use. On all but machined sections the method of wedges would appear to be unsatisfactory (at best comparisons of around -10%). However, on commercial pipe bends the tolerances on dimension affect the gauge mounting. No attempt was made to determine the actual geometry of the gauge layout on the bend, although mensuration of the bend specimens [10] indicated "good" circularity of section. Poor comparison on the pipe bend would appear to be the result of a relative difference in wedge geometry in either elevation, rotation, or both resulting from the fact that the wedges rest on an imperfect surface over the area of contact. Although this has not been firmly established, the experimental and analytical work does show varying degrees of sensitivity to small variations. Bending of the feet of the gauge, however, presents a much simpler and more straightforward operation giving improved and, perhaps more importantly, reasonably predictable results. There will of course be practical limits to this method but they have not been explored.

Above all, however, it is considered essential that in the use of the capacitance gauge comparison be made with resistance gauges in situ. This practice has always been used although it has not been common place to date in other establishments. This was confirmed during a recent tour of laboratories using the gauge. Unfortunately, the in situ type calibration can usually only cover a limited strain range. Thus the manufacturers calibration or some similar full range calibration has to be used in conjunction with the in situ work. On the general

matter of gauge calibration there would appear to be widespread use in this country and abroad of calibrations which are not strictly compatible with the in situ state. The manufacturers linear displacement rig, for example, is suitable for horizontal linear displacement only and was not designed to cope with other forms of displacement. It is worth pointing out, however, that the manufacturer's handbook on gauge installation does suggest other forms of calibration. The advantages of a ready-made and compact rig are perhaps its main source of attraction. The sensitivity to bending strains using such a calibration is discussed by NOTLINGK [6]. To account for bending he suggested that the gauge be considered as 0.05 mm (0.002 in) above the surface. Essentially this is an attempt to increase the strain and is the result of two tests carried out on different beam sections. It has been shown, however, that the capacitance gauge when mounted symmetrically will always underestimate the bending strain. This has been confirmed by the work carried out here giving values of between -20 to -30%. Introducing the unsymmetrical displacement as on the four point loading beam can further alter this comparison by more than 50%. That this sensitivity was not evident from the analytical work is some indication of the initial unsymmetrical form of the gauge.

It should perhaps have been obvious that the use of wedges would introduce inponderables in the strain magnitude. If the spot weld location for the gauge is on top of the wedge it means that the effective strain seen by the gauge is amplified in some way by the distance above the surface. This will have least effect for membrane type strain (such as the tests by HEATHER, BROWNE and DÉR where wedges were first used on machined surfaces). It will be most severe for bending type

strain. Unfortunately, the bending situation is not easily assessed because the movement transmitted to the gauge feet is transferred via the edge weld attachment on the wedge and could depend on the rotational stiffness of that weld as well as the surface topography under the wedge, etc. Welding the wedge completely down as has been practised seems undesirable too, since the gauge length has become indeterminate. Even if these effects could be quantified it would be necessary to be able to separate membrane and bending effects before a satisfactory assessment could be made.

7. References

1. K. Rae — First Progress Report on Inelastic Behaviour of Pipework Components for The Reactor Group, UKAEA Agreement No. 4R53584B September 1979

2. J. Spence, J.T. Boyle, B.W. Leitch — First Progress Report on Experimental Creep Programme on Pipe Bend Specimens for The Reactor Group, UKAEA Agreement No. 4R52952B

3. C.W. Heather, R.J. Browne, T.J. Dér — Application of Cerl-Planer High Temperature Strain Gauges for The Measurement of Hoop Strains in Tubular Components CEGB Report No. SE/SSD/RN/80/066 November 1980

4. K. Rae — Report No. T1 Elevated Temperature Distribution Test - Specimen No. 4 - 90° - Sch 40 Part of Experimental Creep Programme on Pipe Bend Specimens for The Reactor Group, UKAEA Agreement No. 4R52952B May 1981

5. G. Thomson — The Influence of End Constraints on Pipe Bends Doctoral Thesis, Strathclyde University 1980

6. B.E. Noltingk, D.F.A. McLachlan, C.K.V. Owen, P.C. O'Neill — High-Stability Capacitance Strain Gauge for Use at Extreme Temperatures Proc. Inst. Elect. Eng. Vol. 119 July 1972

7. Coull, Dykes — Fundamentals of Structural Theory McGraw Hill, 1972

8. S. Cheng, N.J. Hoff — Bending of Thin Circular Rings Inst. J. Solids Structures Vol. II 1975

9. S. Timoshenko — Strength of Materials
Part II Advanced Theory and Problems
Second Edition
Van Nostrand, 1941

10. K. Rae — Report No. D1 on Mensuration of Bend Assemblies
Part of Inelastic Behaviour of Pipework Components for
The Reactor Group, UKAEA
Agreement No. 4R53584B
February 1981

8. Appendix

Matrix formulation of CHENG and HOFF analysis.

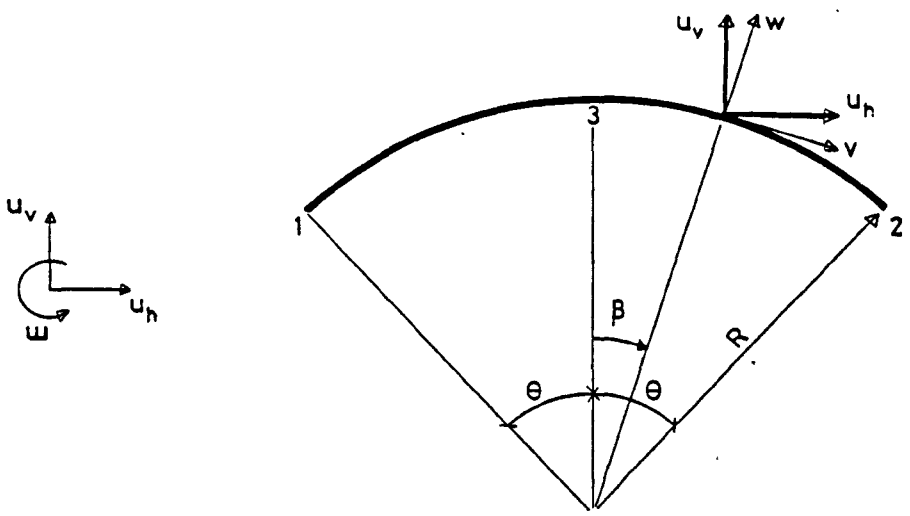

$$
\begin{bmatrix} u_{v1} \\ u_{h1} \\ \omega_1 R \\ u_{v2} \\ u_{h2} \\ \omega_2 R \end{bmatrix} = \left[\begin{array}{cccc|cc} \cos\theta+\theta\sin\theta & \sin\theta & 1 & 0 & -\theta\cos^2\theta-\sin\theta(\cos\theta+\theta\sin\theta) & \theta\sin\theta\cos\theta-\sin\theta(-\sin\theta+\theta\cos\theta) \\ -\sin\theta+\theta\cos\theta & \cos\theta & 0 & 1 & \theta\sin\theta\cos\theta-\cos\theta(\cos\theta+\theta\sin\theta) & \theta\sin^2\theta-\cos\theta(-\sin\theta+\theta\cos\theta) \\ \theta & -1 & 0 & 0 & 2\cos\theta & -2\sin\theta \\ \cos\theta+\theta\sin\theta & -\sin\theta & 1 & 0 & \theta\cos^2\theta+\sin\theta(\cos\theta+\theta\sin\theta) & \theta\sin\theta\cos\theta+\sin\theta(\sin\theta-\theta\cos\theta) \\ \sin\theta-\theta\cos\theta & \cos\theta & 0 & 1 & \theta\sin\theta\cos\theta-\cos\theta(\cos\theta+\theta\sin\theta) & \theta\sin^2\theta-\cos\theta(\sin\theta-\theta\cos\theta) \\ 0 & 1 & 0 & 0 & 2\cos\theta & 2\sin\theta \end{array}\right] \begin{bmatrix} w_o \\ v_o \\ A \\ B \\ C_1 \\ C_2 \end{bmatrix}
$$

$$
w_3 = w_o + A
$$

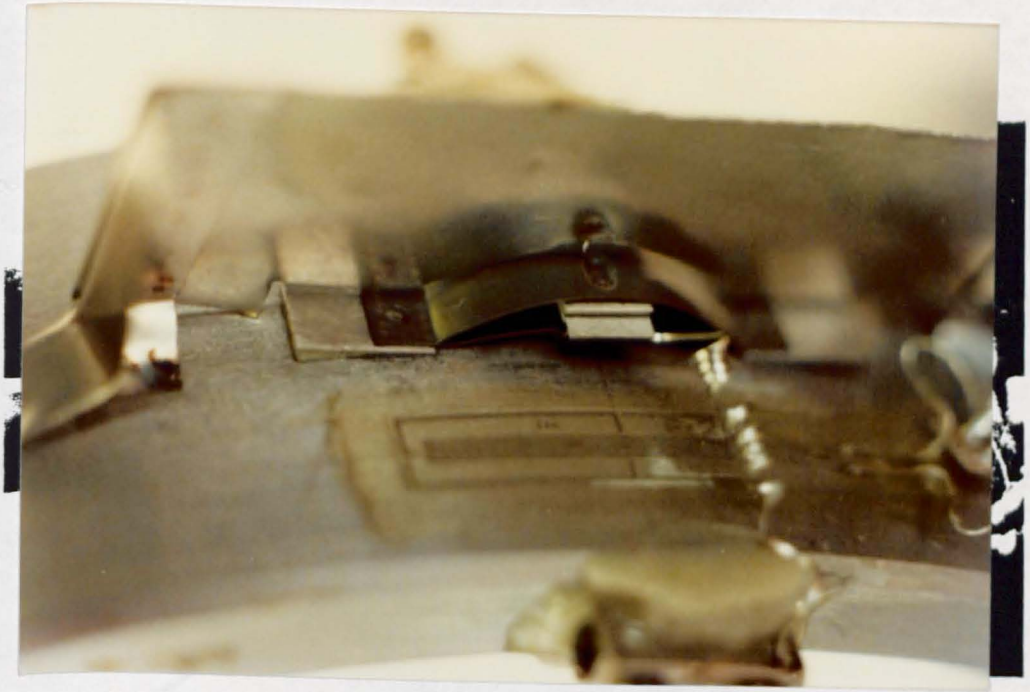

CAPACITANCE GAUGE
MOUNTED ON WEDGES

FIG. 1

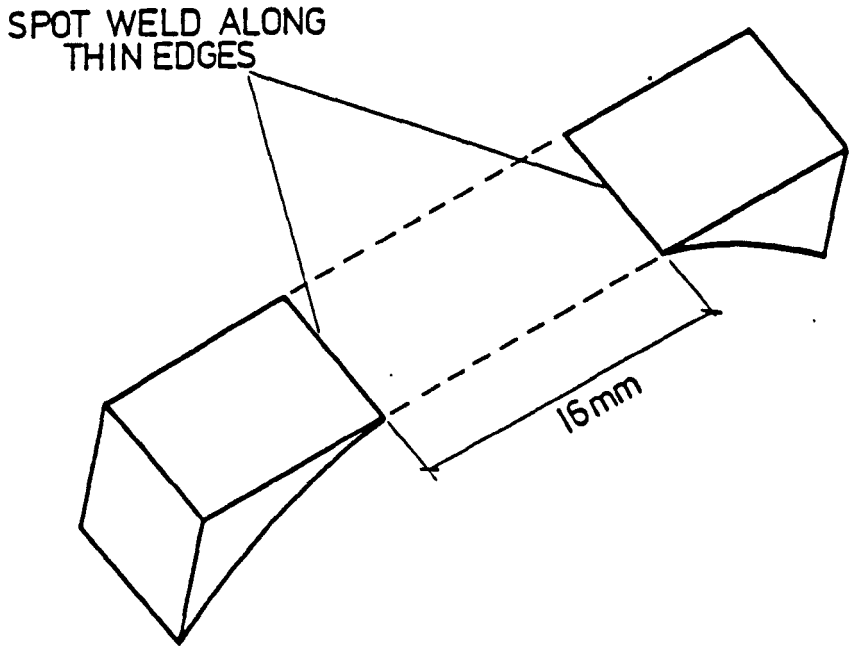

ATTACHMENT OF WEDGES

FIG. 2

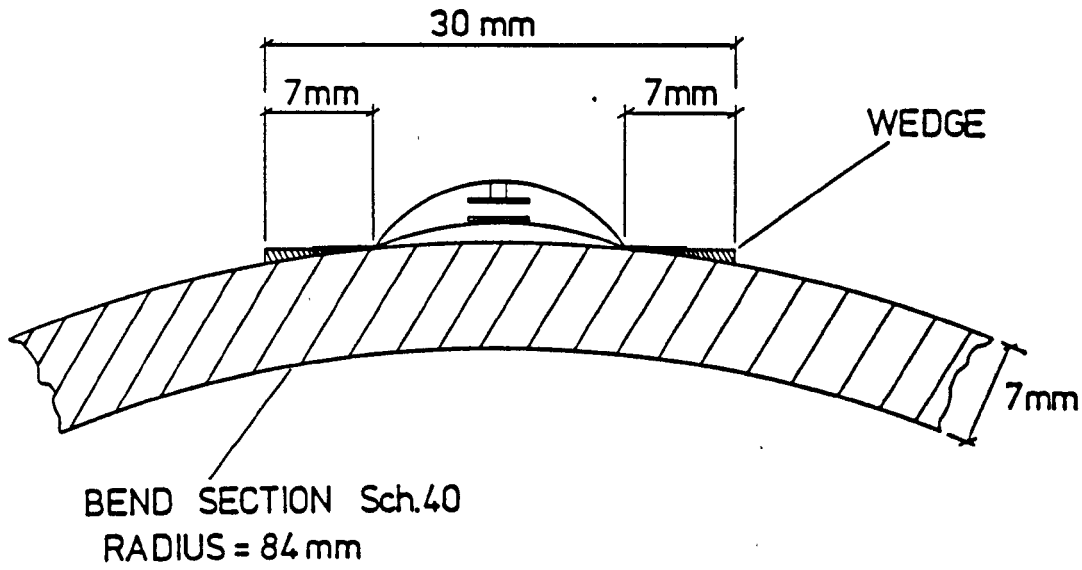

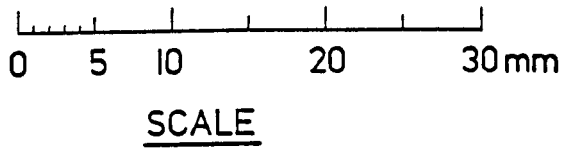

RELATIVE DIMENSIONS
OF WEDGES

FIG. 3

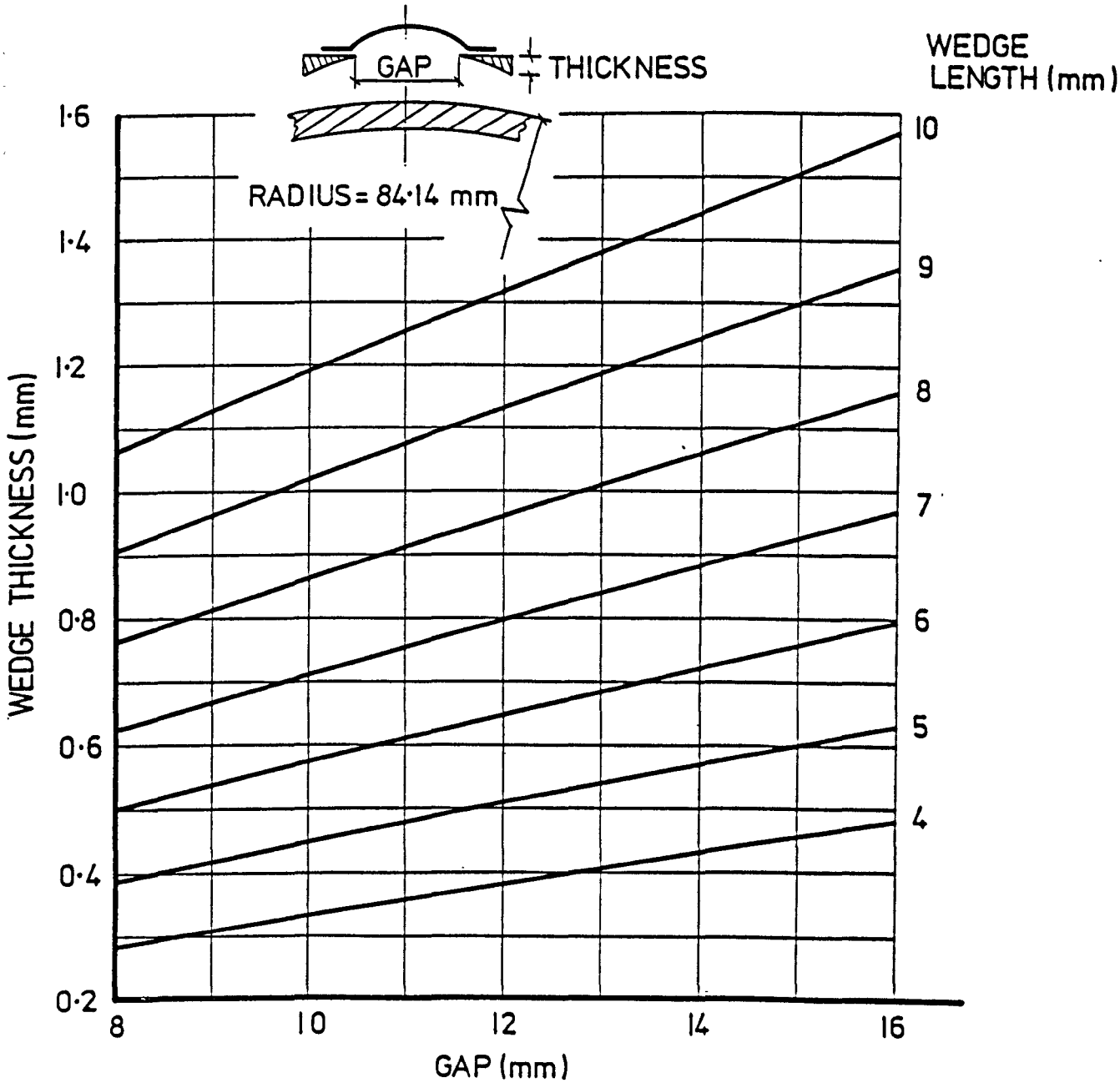

WEDGE THICKNESS VARIATION

$$\text{thickness} = \sqrt{R^2 - \left[\frac{x}{2}\right]^2} - \sqrt{R^2 - \left[\frac{x}{2} + l\right]^2}$$

where R = outside radius

x = gap

l = length of wedge

FIG. 4

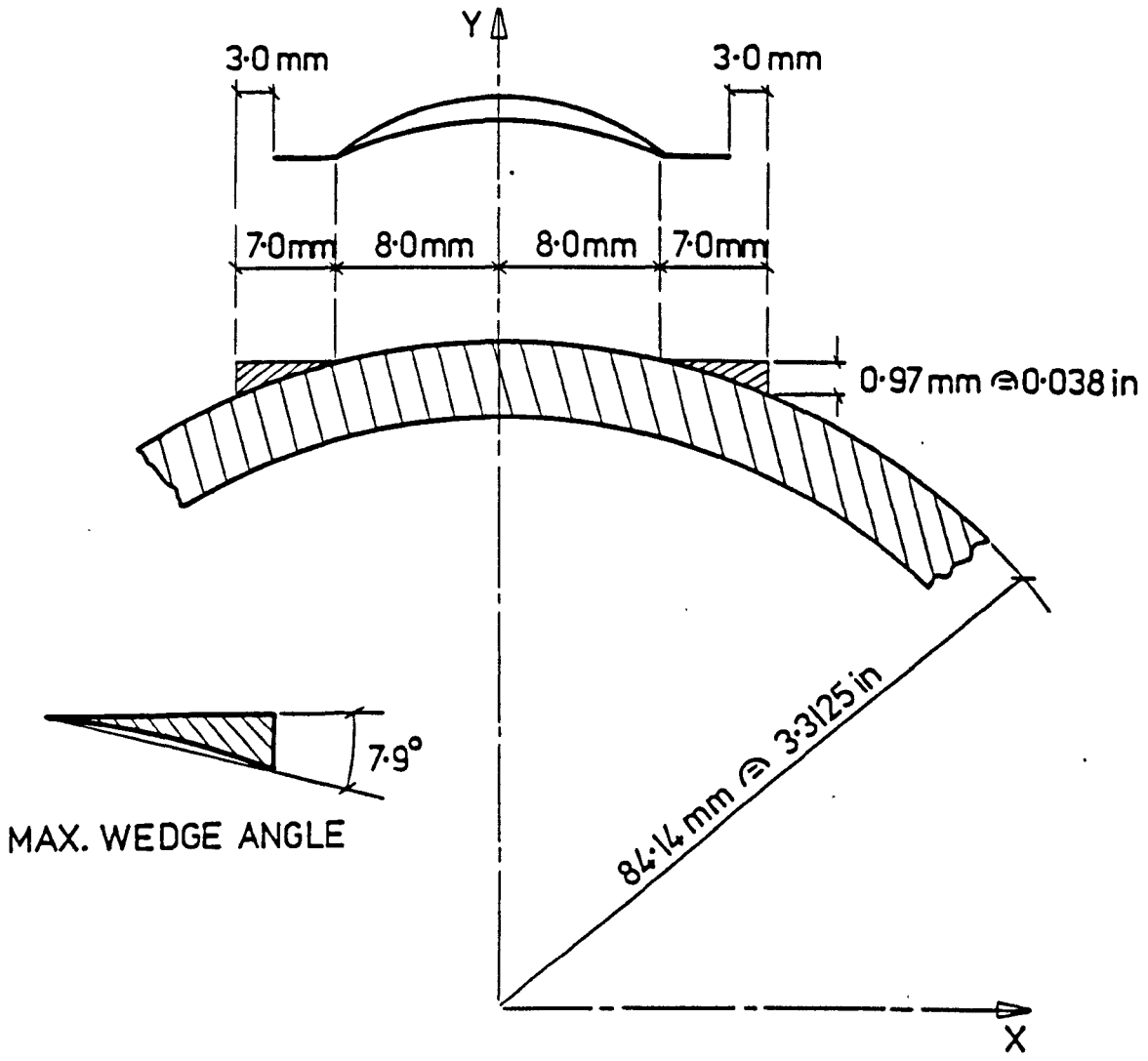

WEDGE DIMENSIONS

FIG. 5

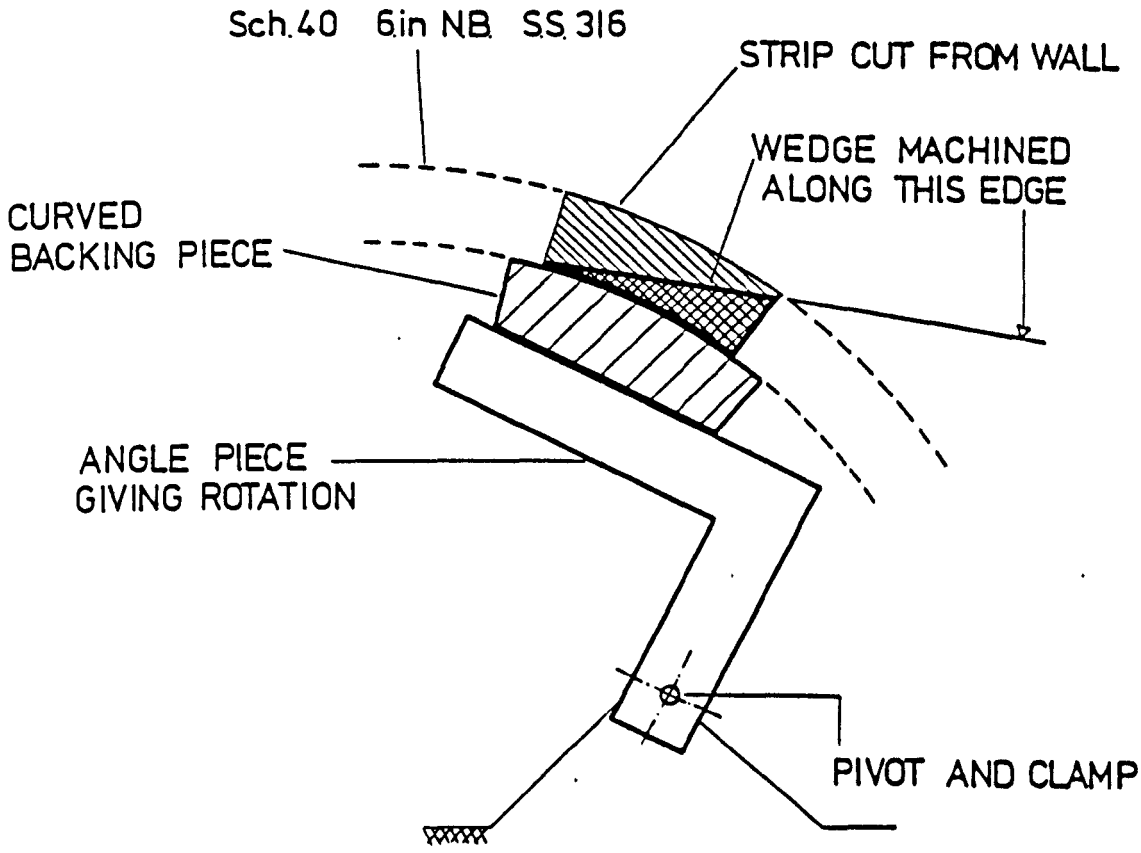

MANUFACTURE OF WEDGES

FIG. 6

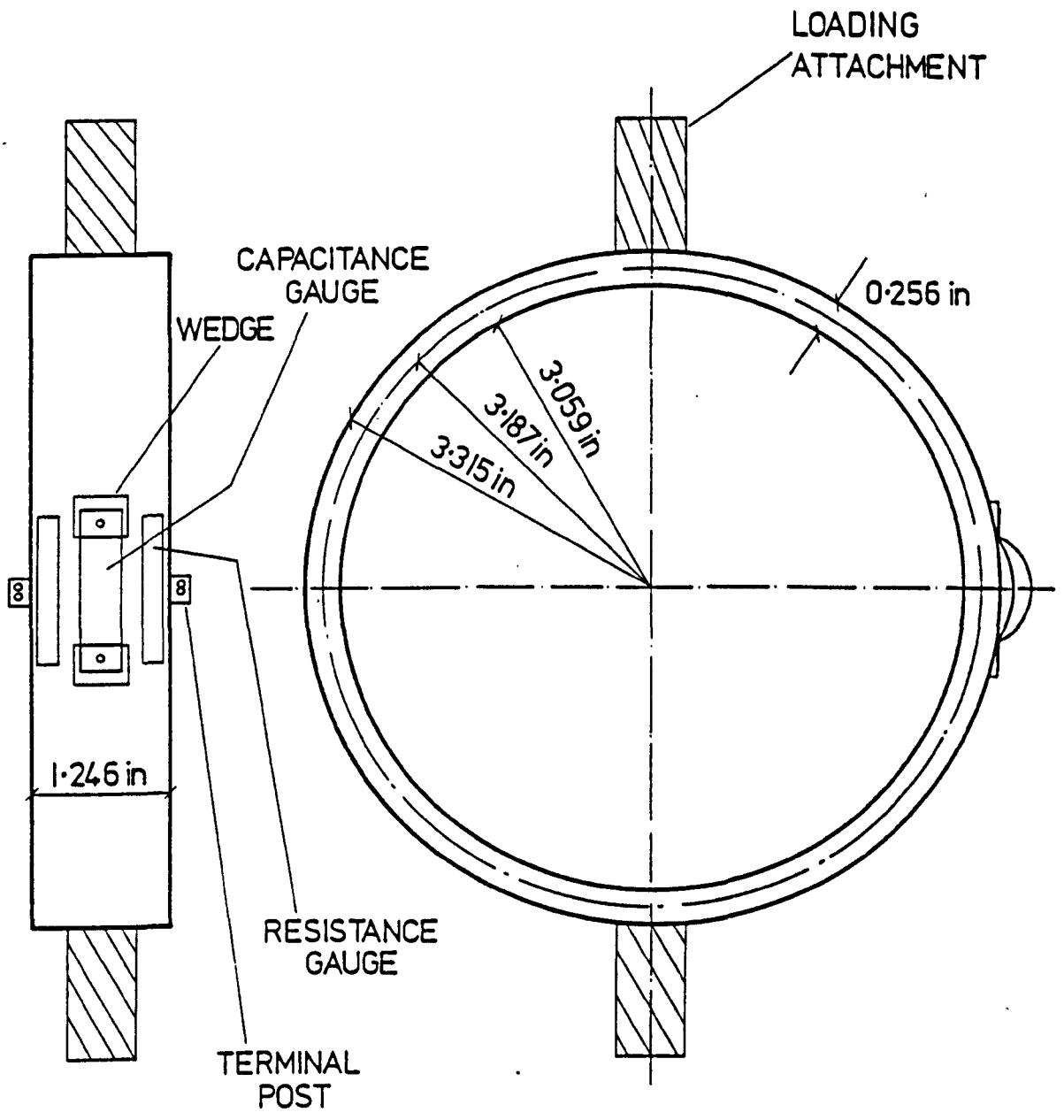

PROVING RING

FIG. 7

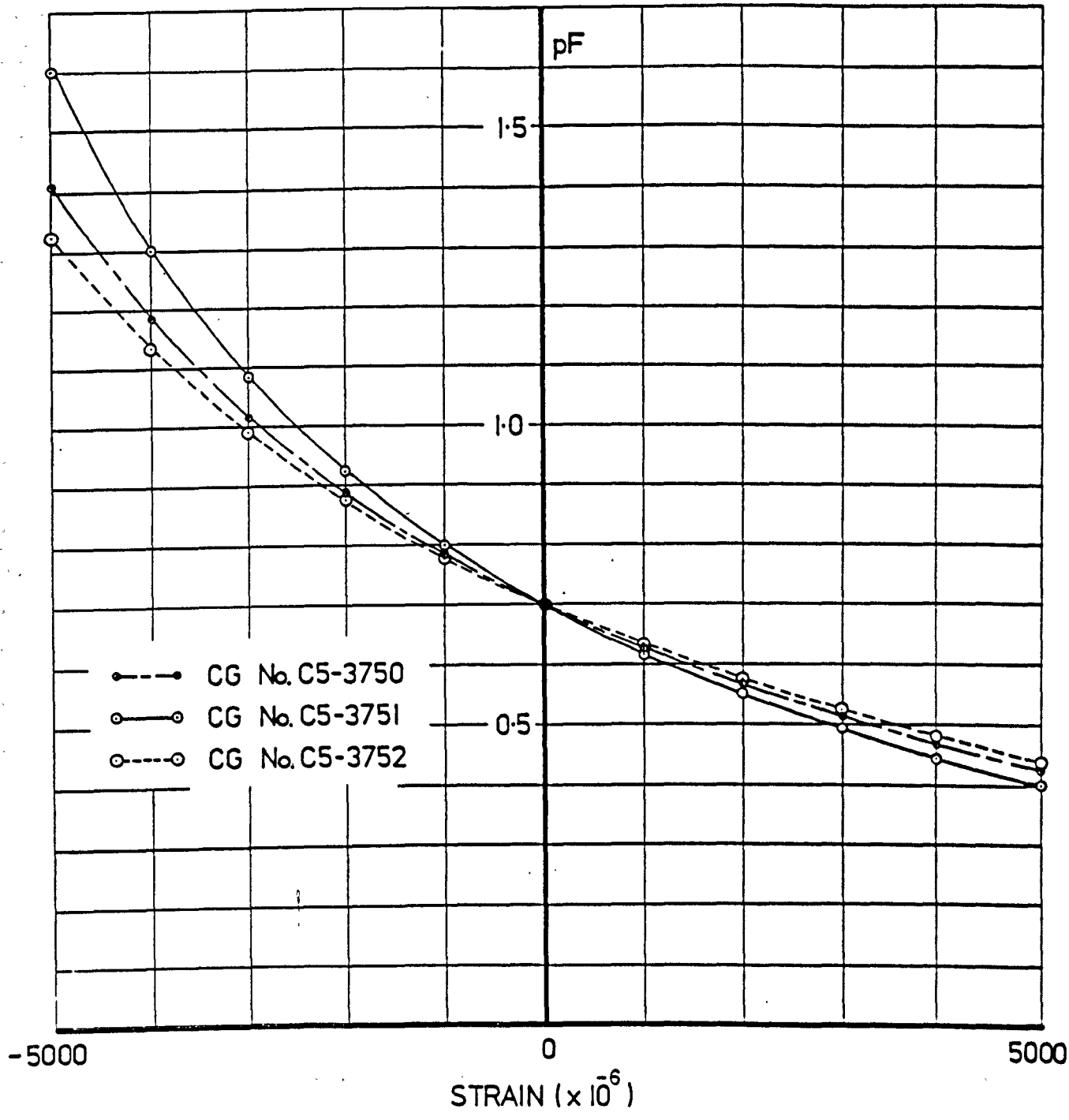

CAPACITANCE GAUGE CALIBRATION

FIG. 8

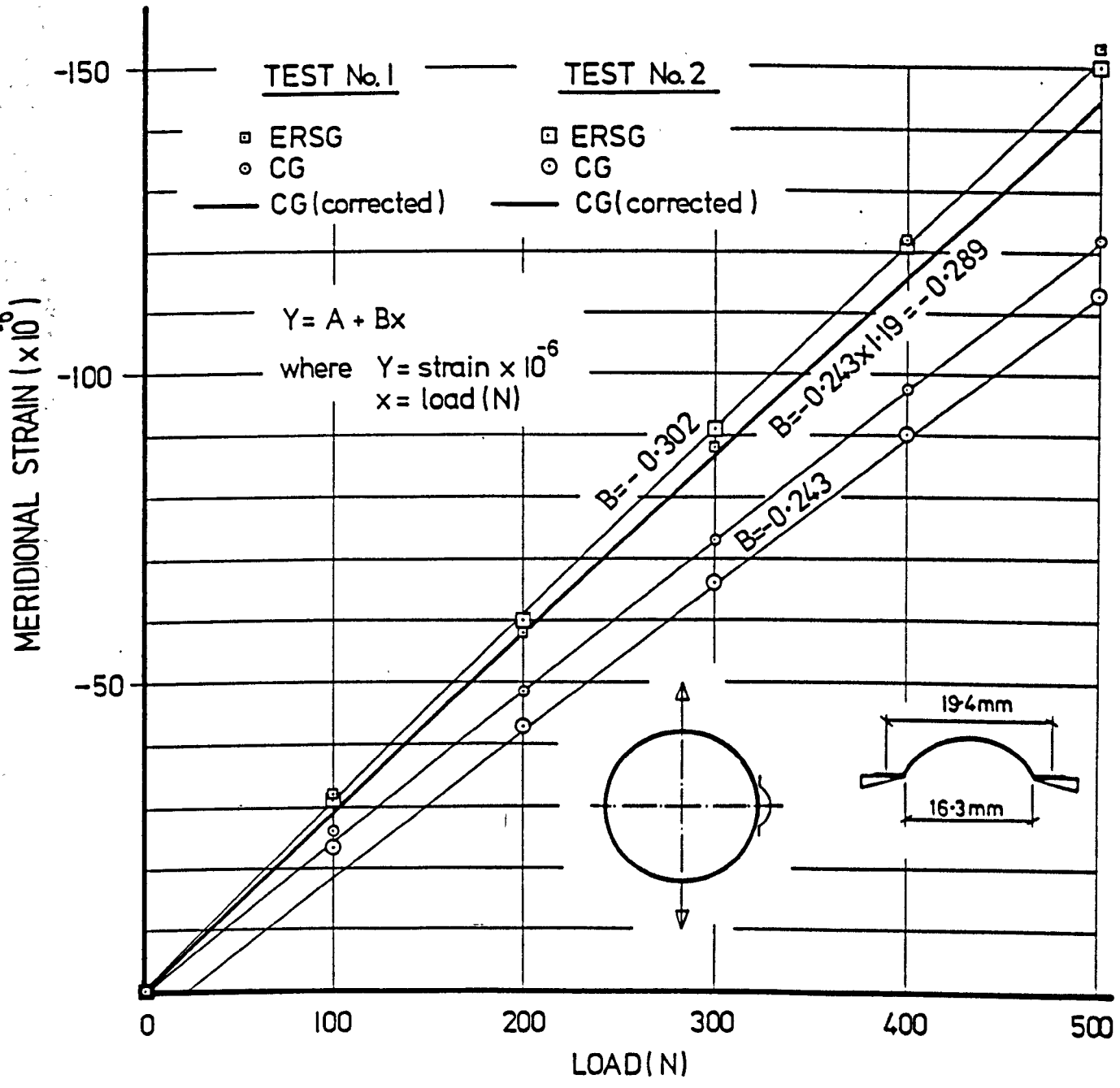

PROVING RING TEST No.1 & No.2R

CG No. C5-3750

FIG. 9

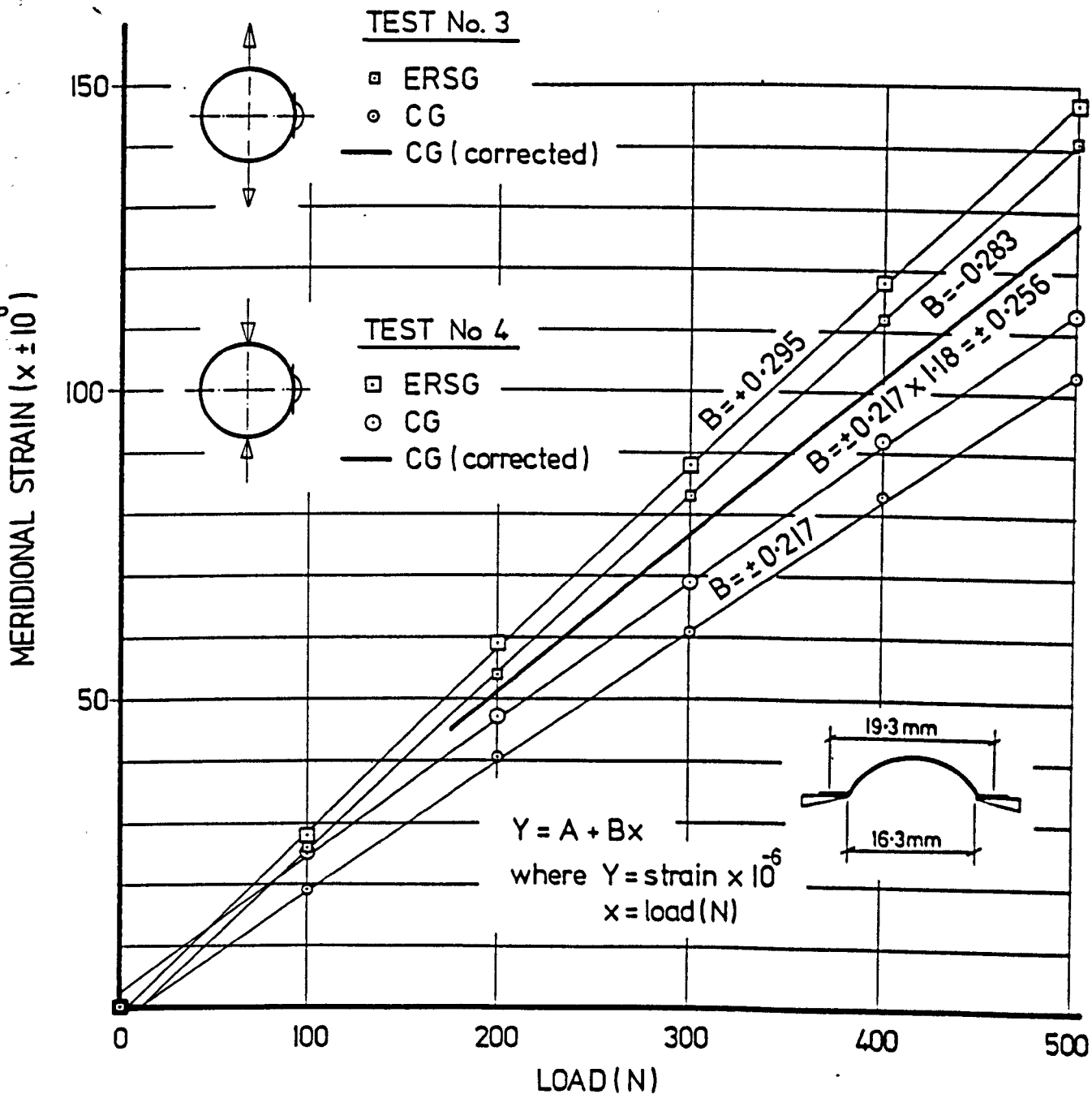

PROVING RING TEST No.3 & No.4R
CG No.C5-3751

FIG. 10

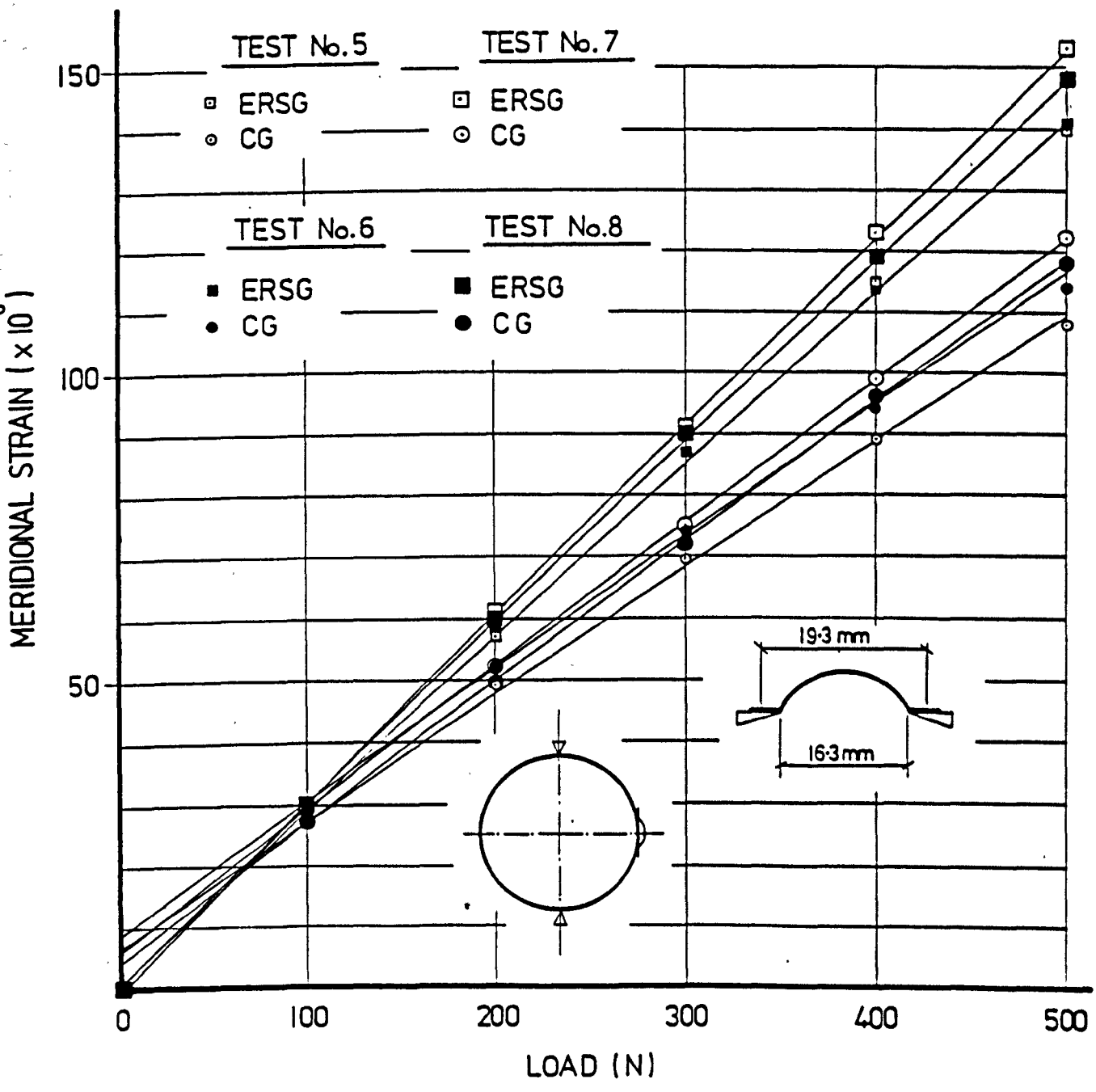

PROVING RING TEST No.5 - No.8R
CG No. C5-3752

FIG. 11

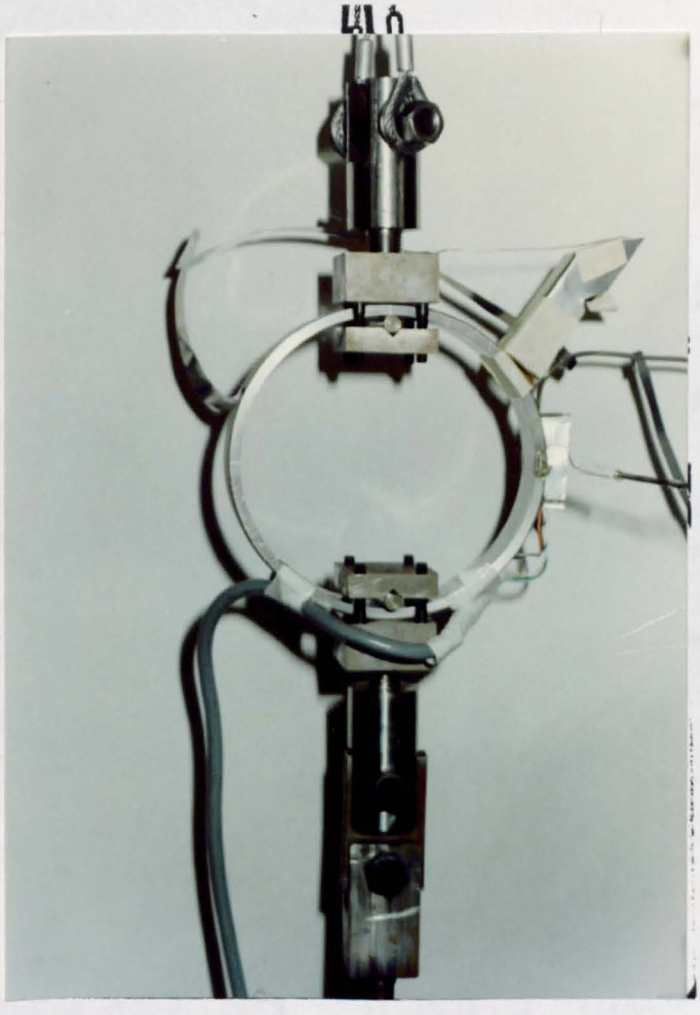

PROVING RING

FIG. 12

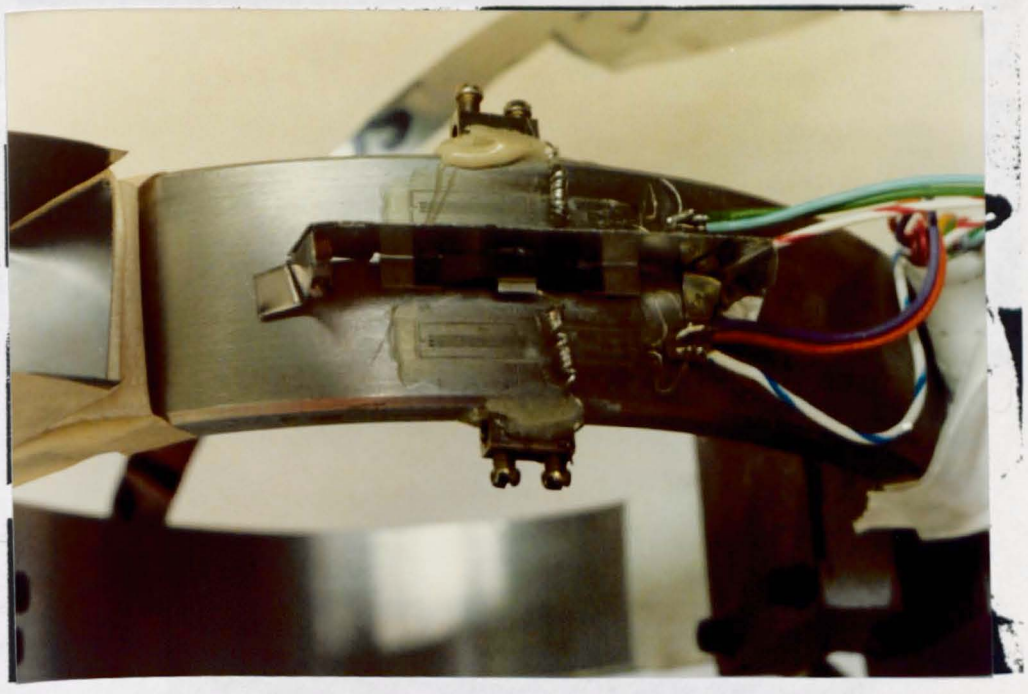

PARTITION ON PROVING RING

FIG. 13

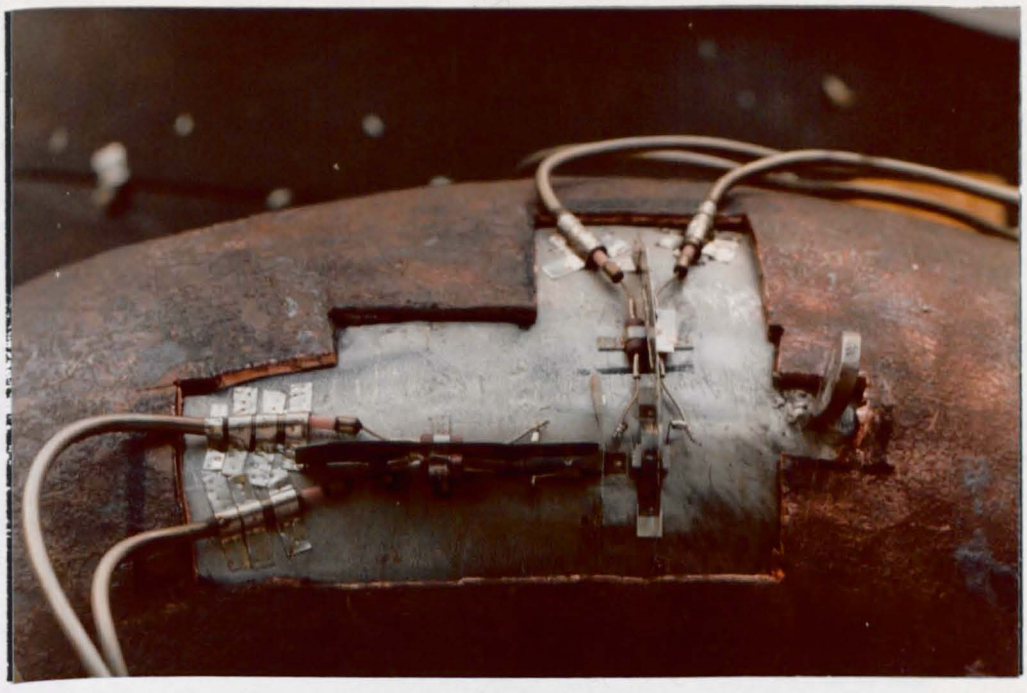

GAUGE No.3 MERIDIONAL

GAUGE No.2 CIRCUMFERENTIAL

GAUGE No.1
MERIDIONAL

GAUGE LAYOUT

FIG. 14

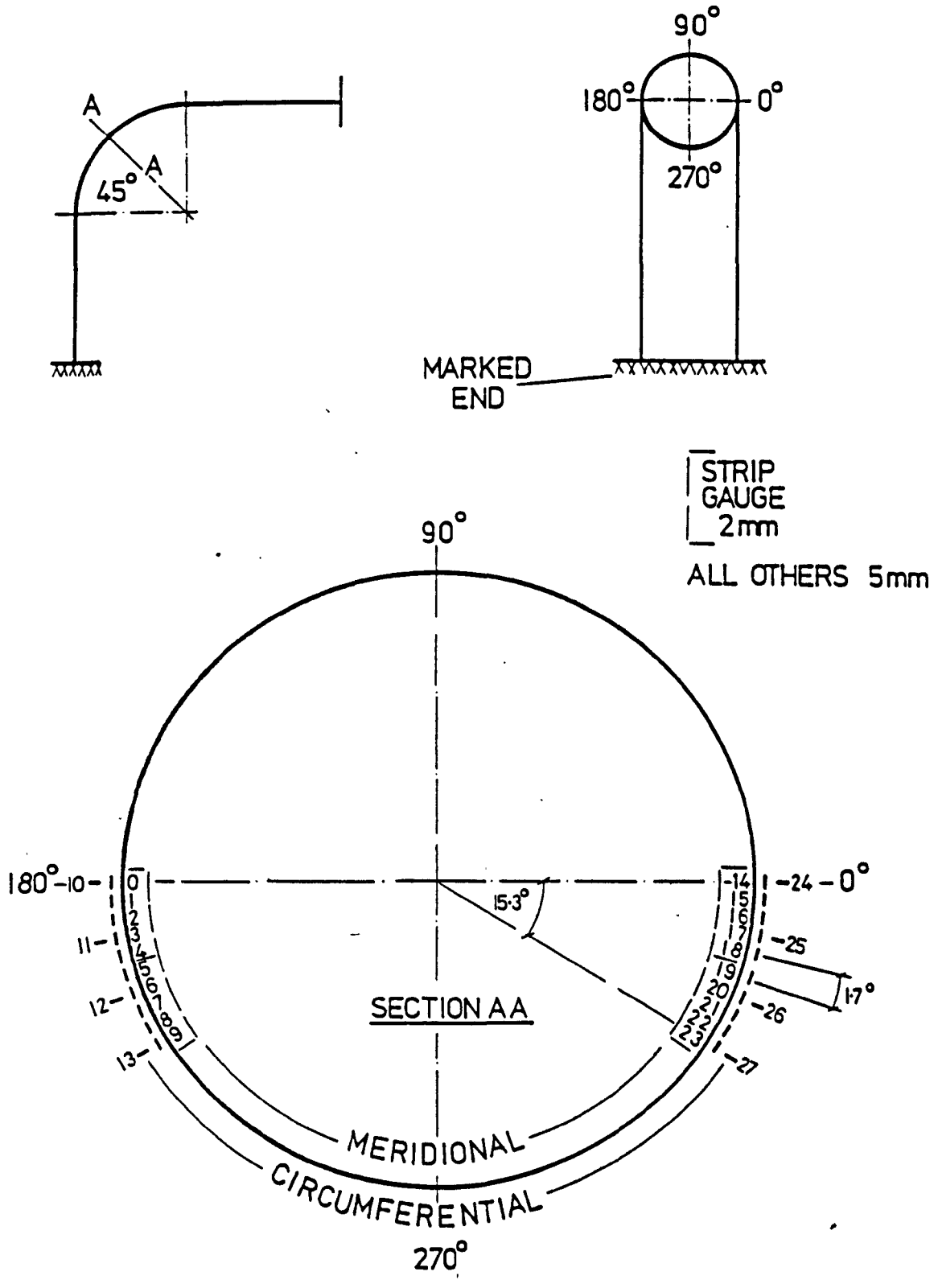

STRAIN GAUGE LAYOUT

R.T. ELASTIC – STRAIN DISTRIBUTION

FIG. 15

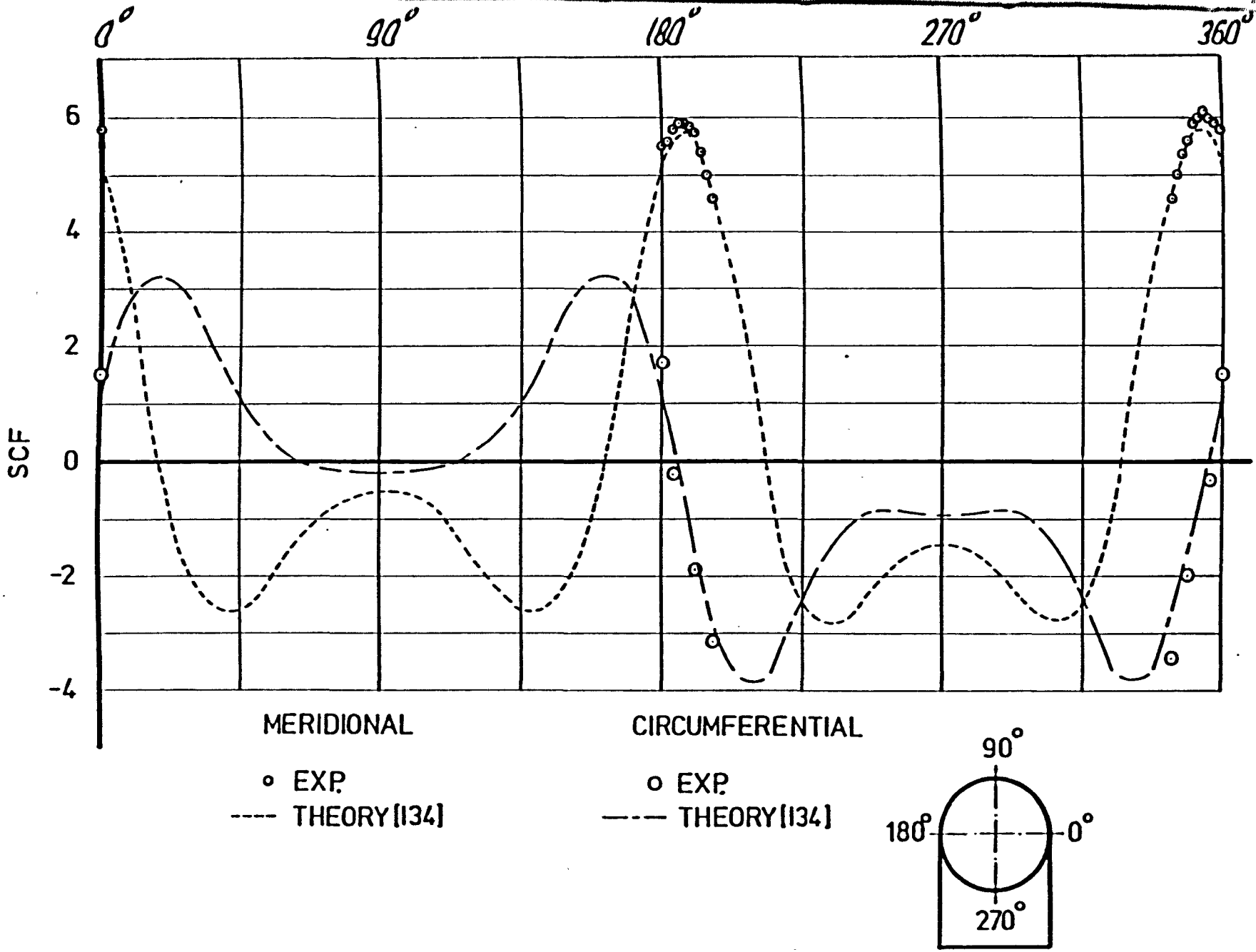

R. T. ELASTIC - STRAIN

FIG. 16

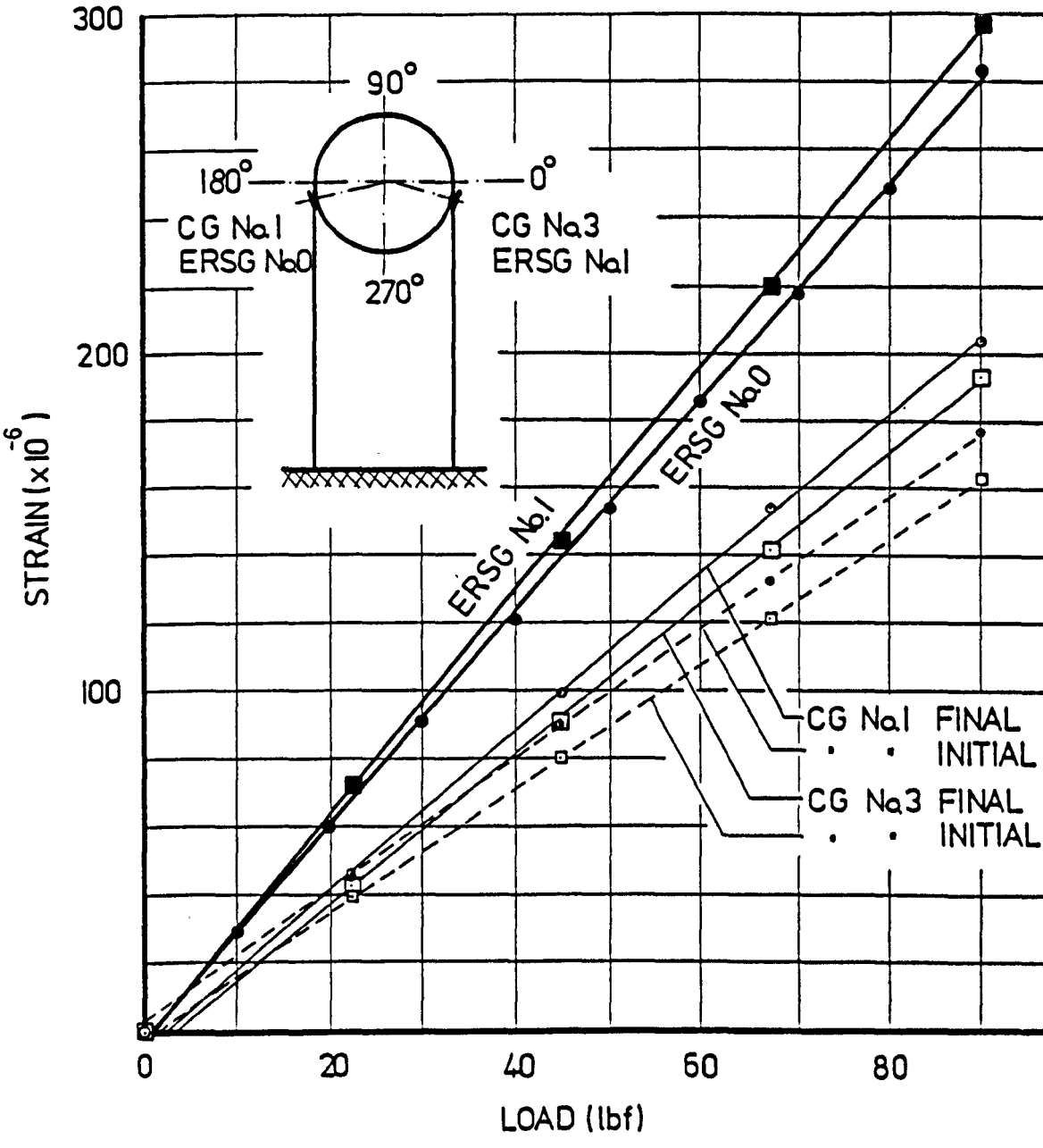

R.T. ELASTIC
IN-PLANE BENDING CLOSING

FIG. 17

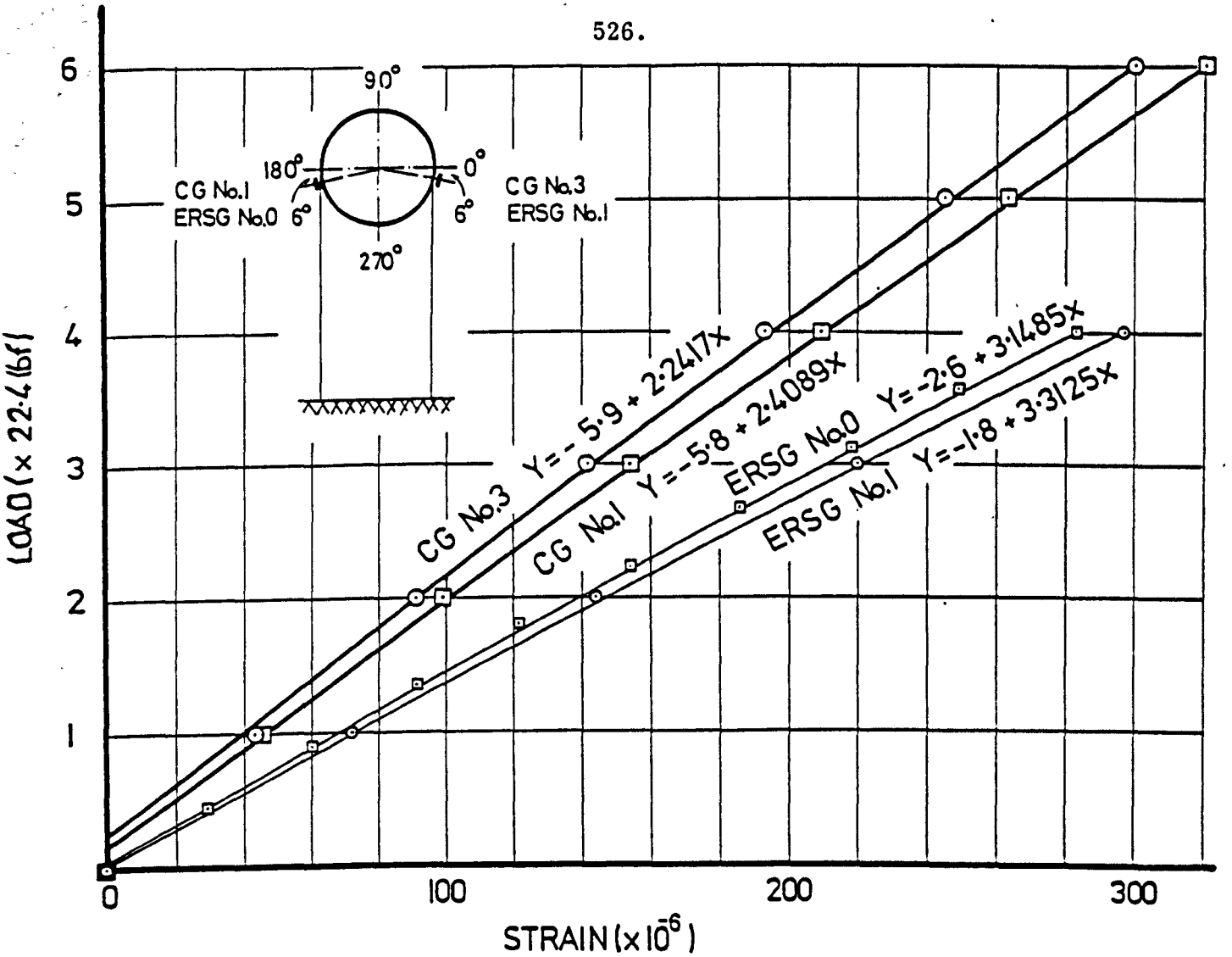

best line fit $Y = A + Bx$ where Y = strain $\times 10^{-6}$
x = load - lbf

ERSG:- GL=20mm, GF= 2·14

R.T. ELASTIC CALIBRATION
IN-PLANE BENDING CLOSING MODE

FIG. 18

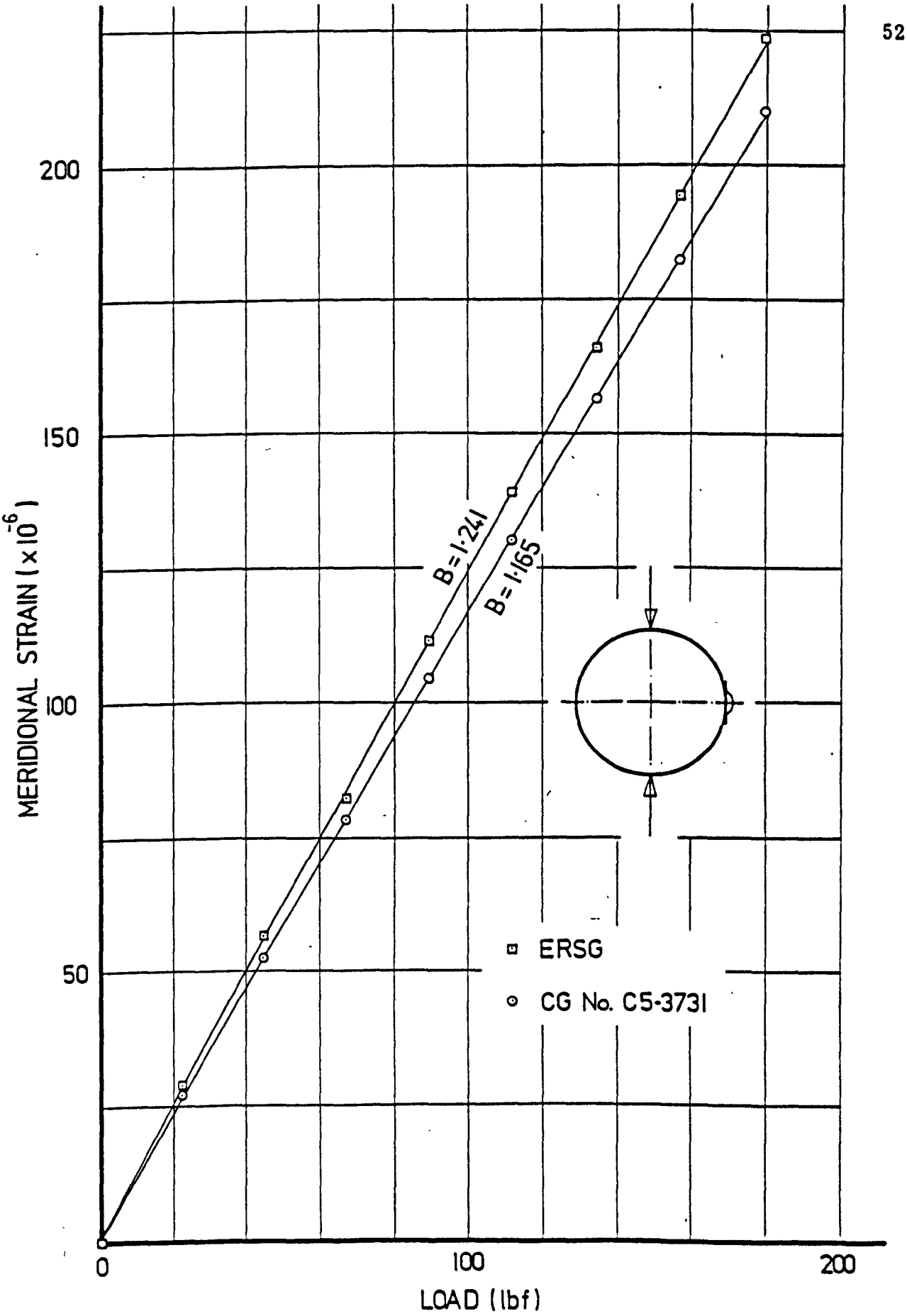

PROVING RING
TEST No.11R
FIG.19

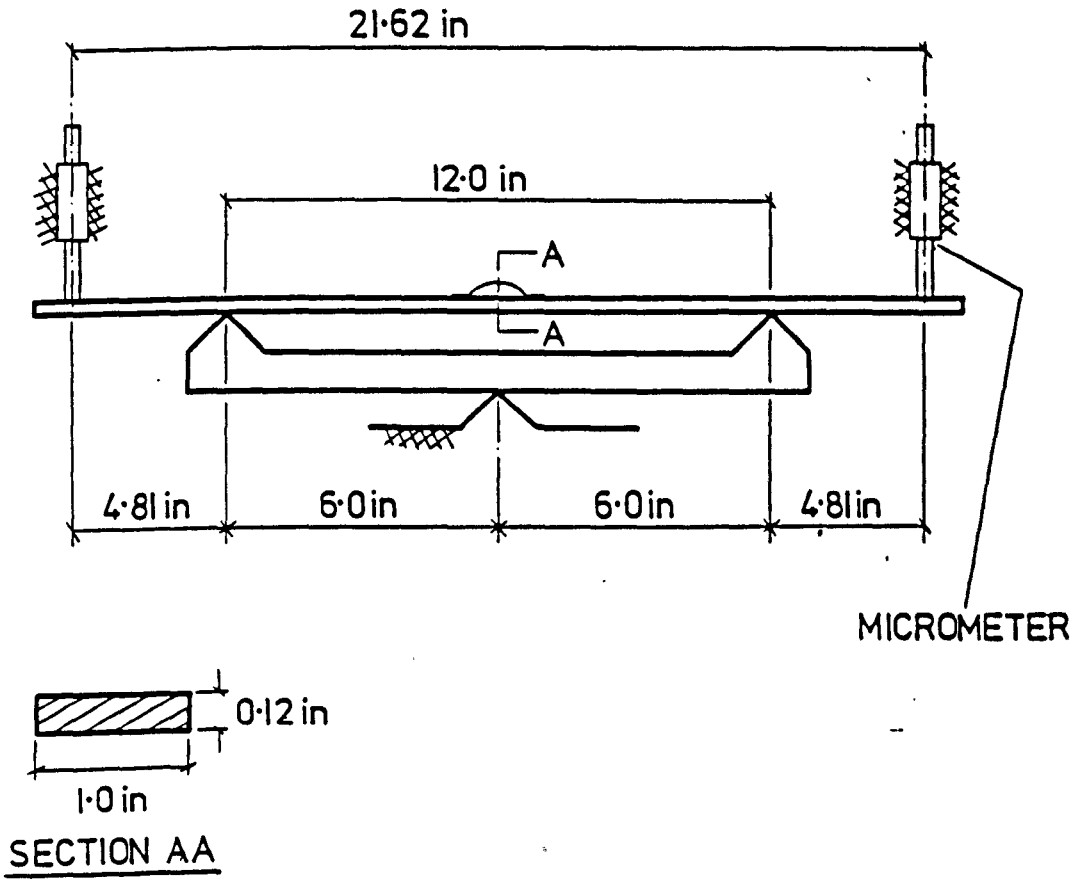

FOUR POINT LOADING BEAM

FIG. 20

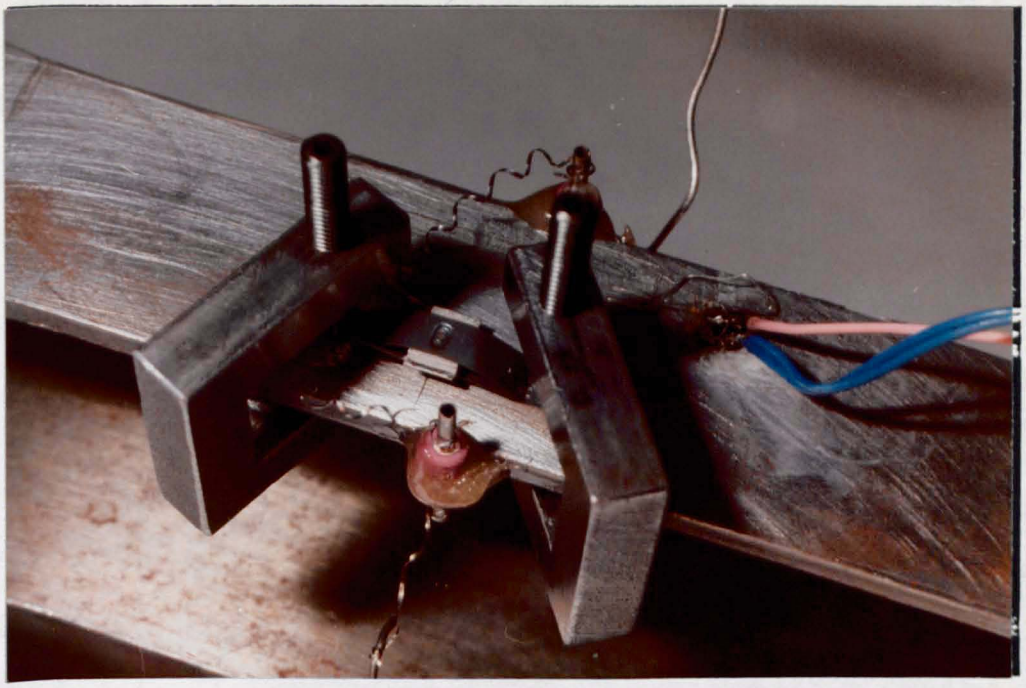

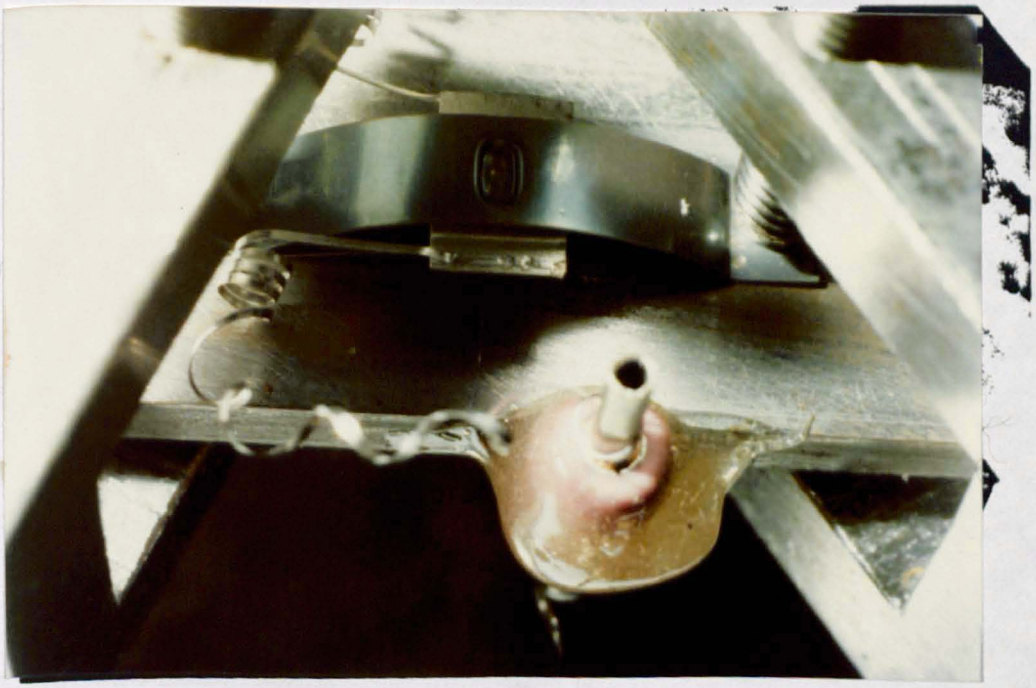

FOUR POINT LOADING BEAM

FIG. 21

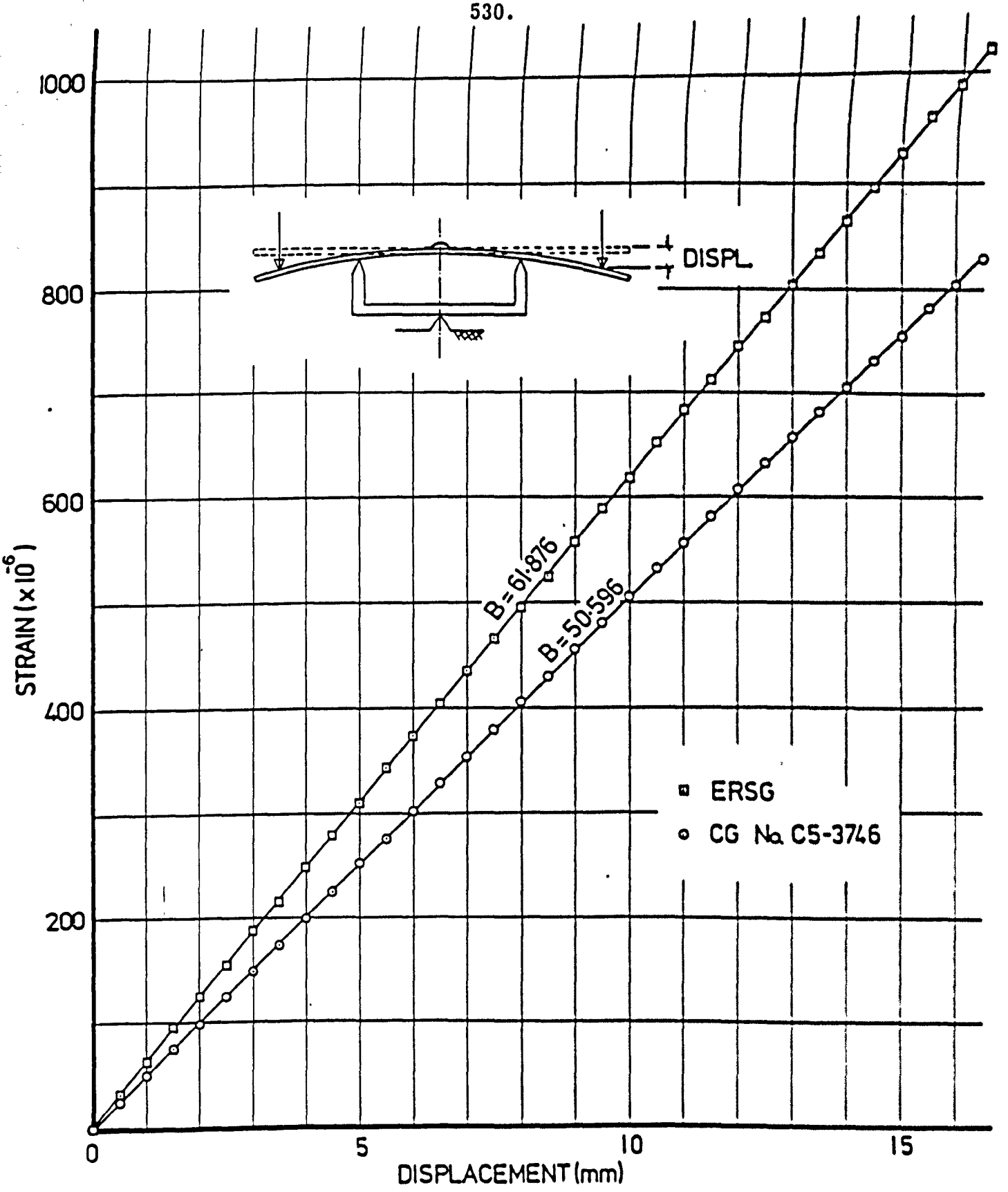

FOUR POINT LOADING BEAM

TEST No. 1B

FIG. 22

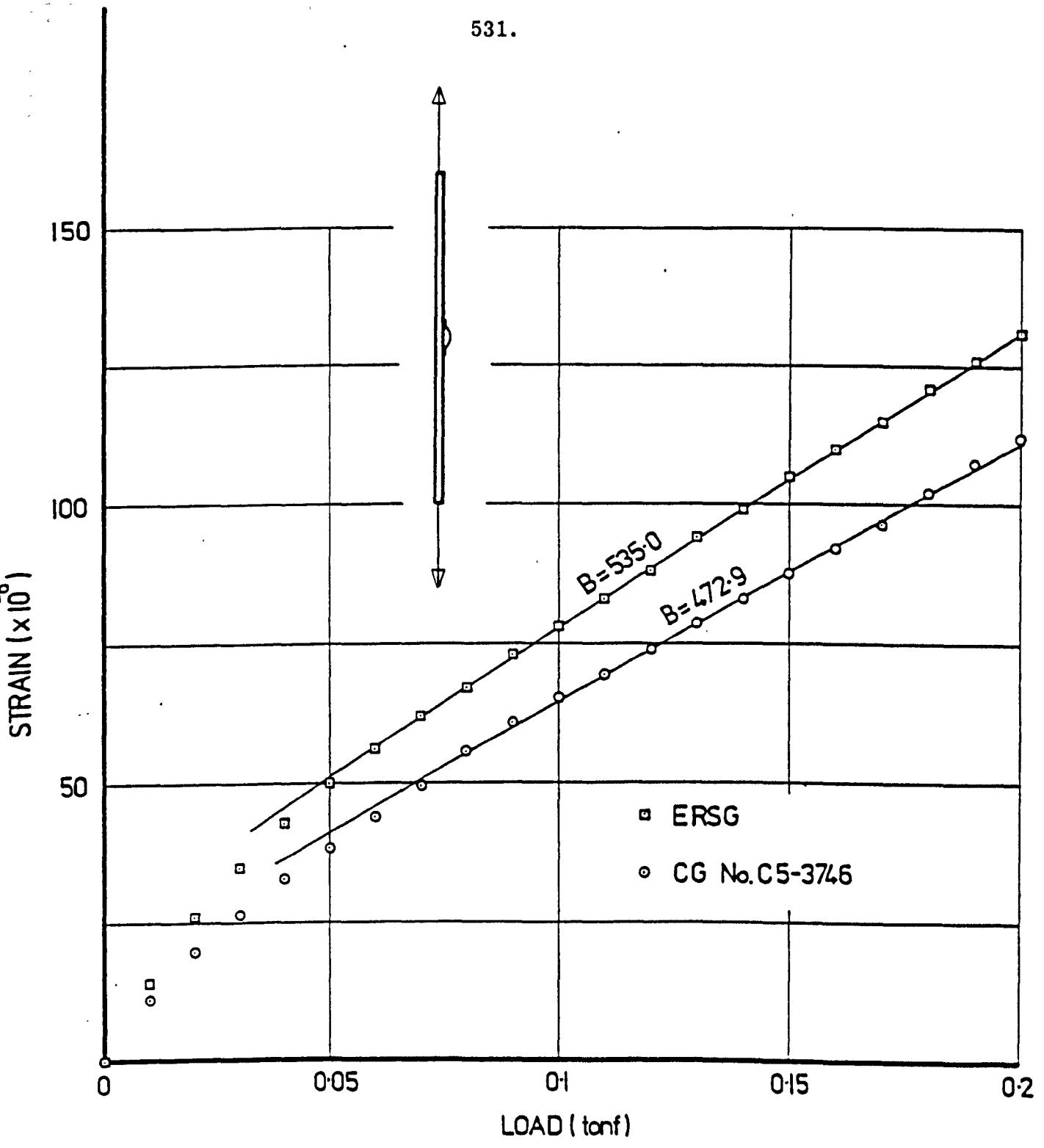

TENSILE TEST

No. IT

FIG. 23

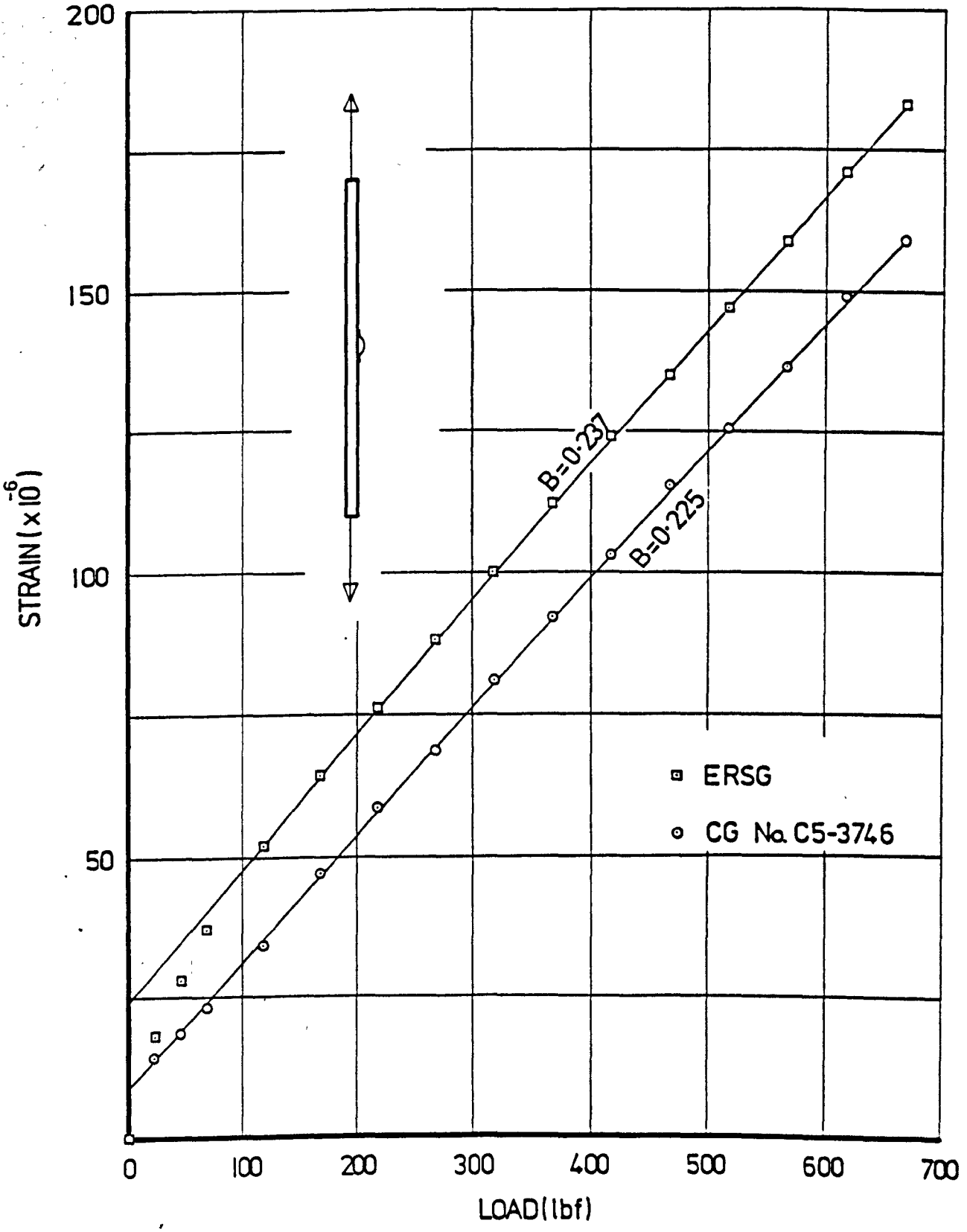

TENSILE TEST

No. 2T

FIG. 24

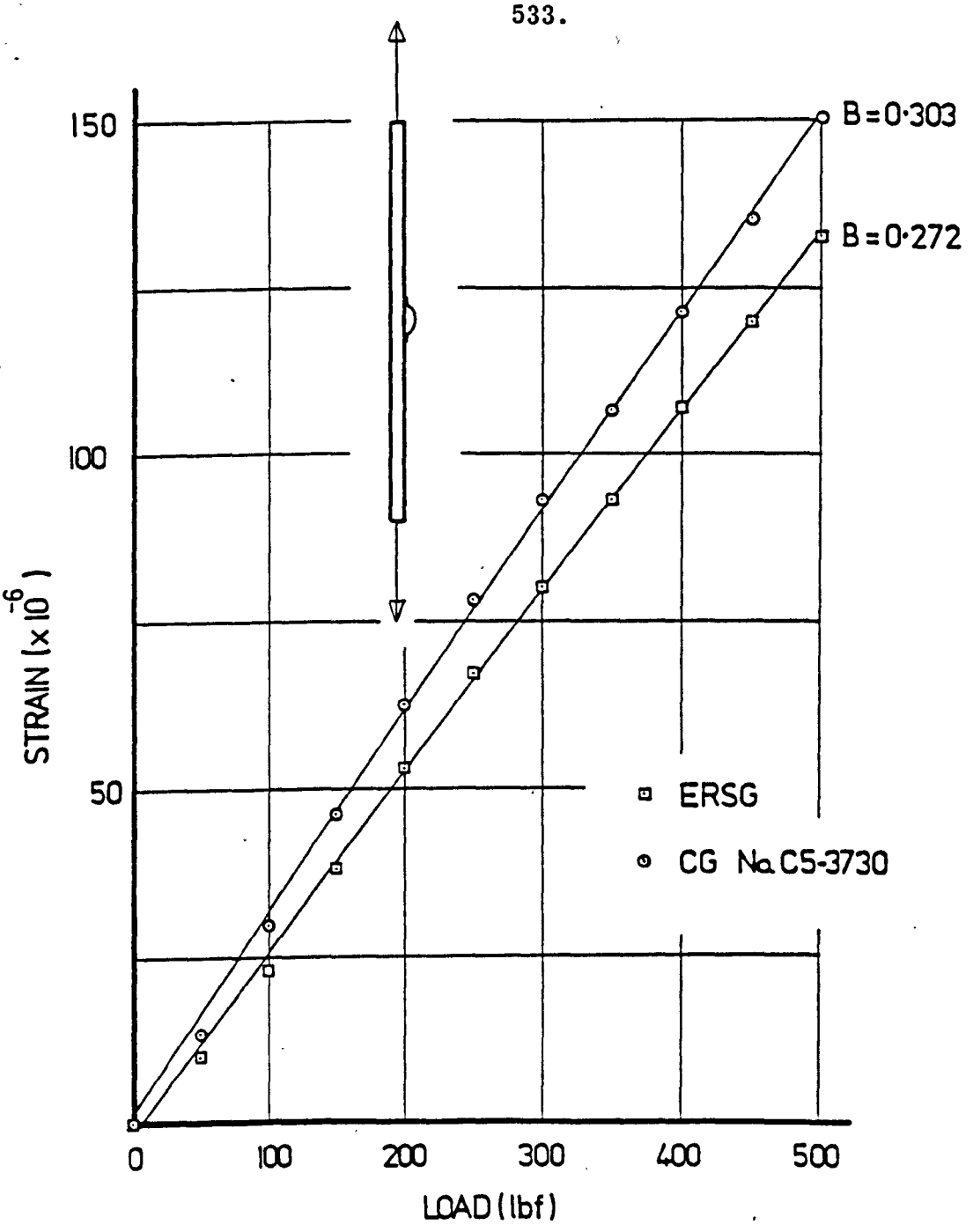

TENSILE TEST

No. 3T

FIG. 25

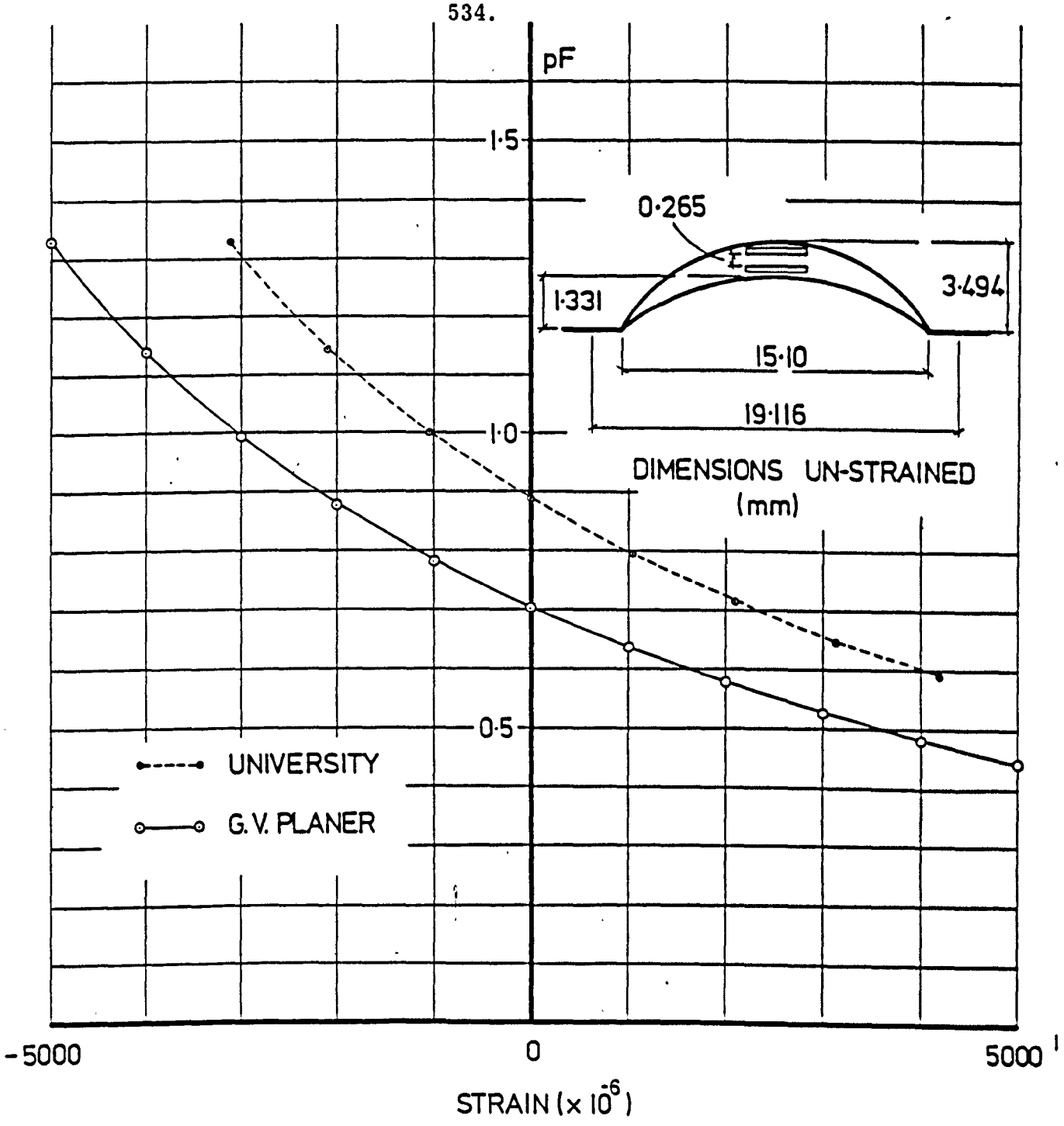

CAPACITANCE GAUGE CALIBRATION

No. C5-3731

TEST No. 4T

FIG. 26

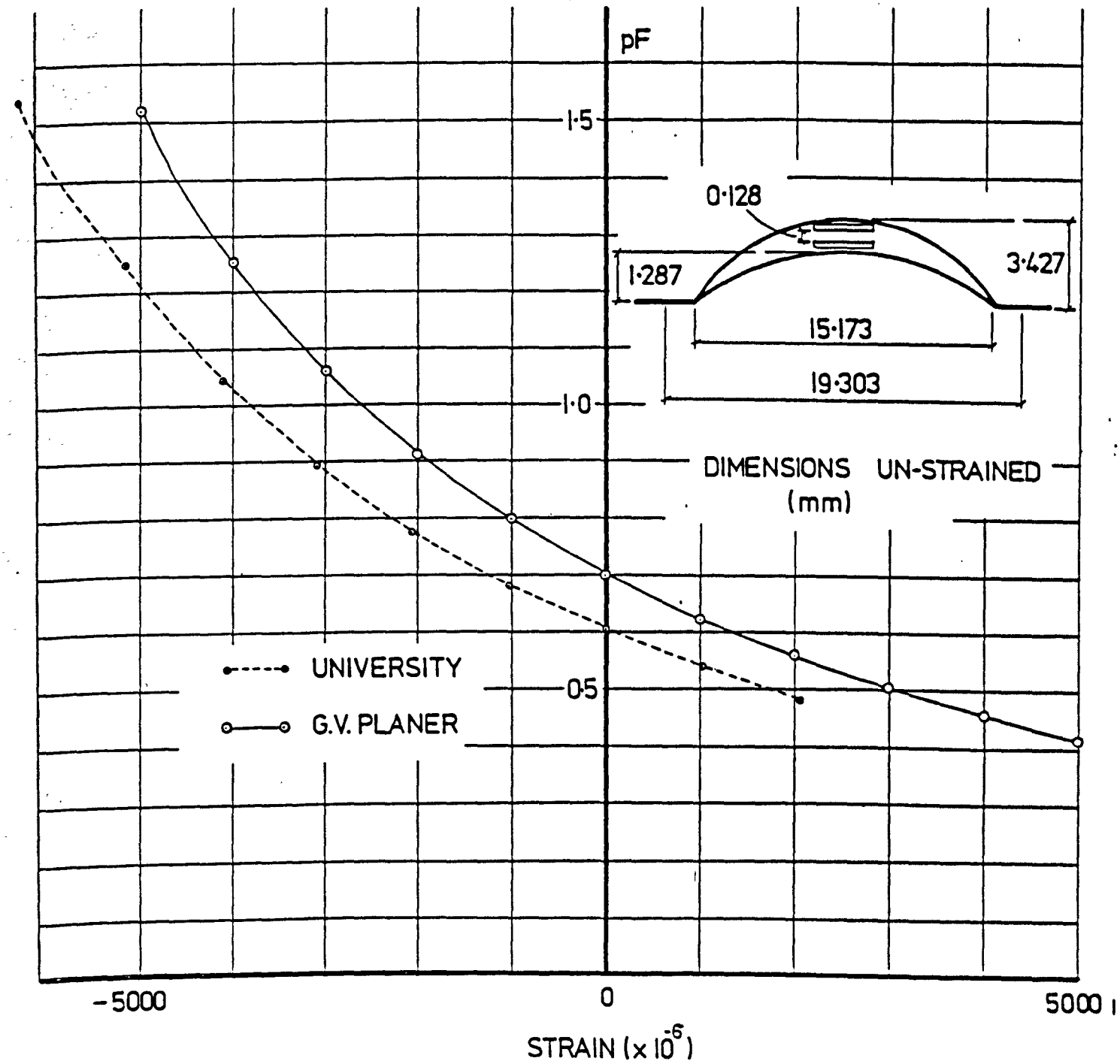

CAPACITANCE GAUGE CALIBRATION

No. C5-3735

TEST No. 5T

FIG. 27

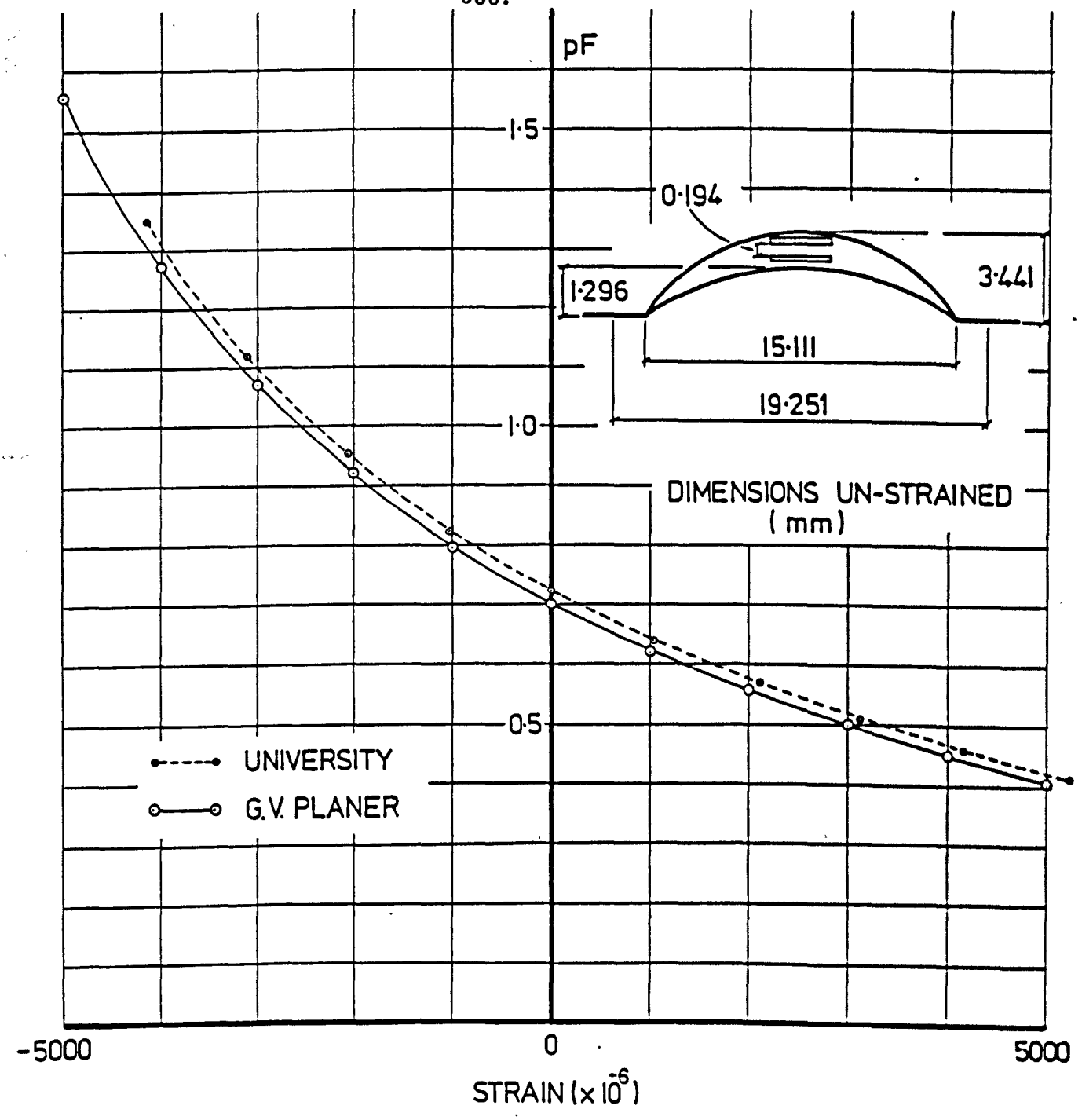

CAPACITANCE GAUGE CALIBRATION

No. C5-3749

TEST No. 6T

FIG. 28

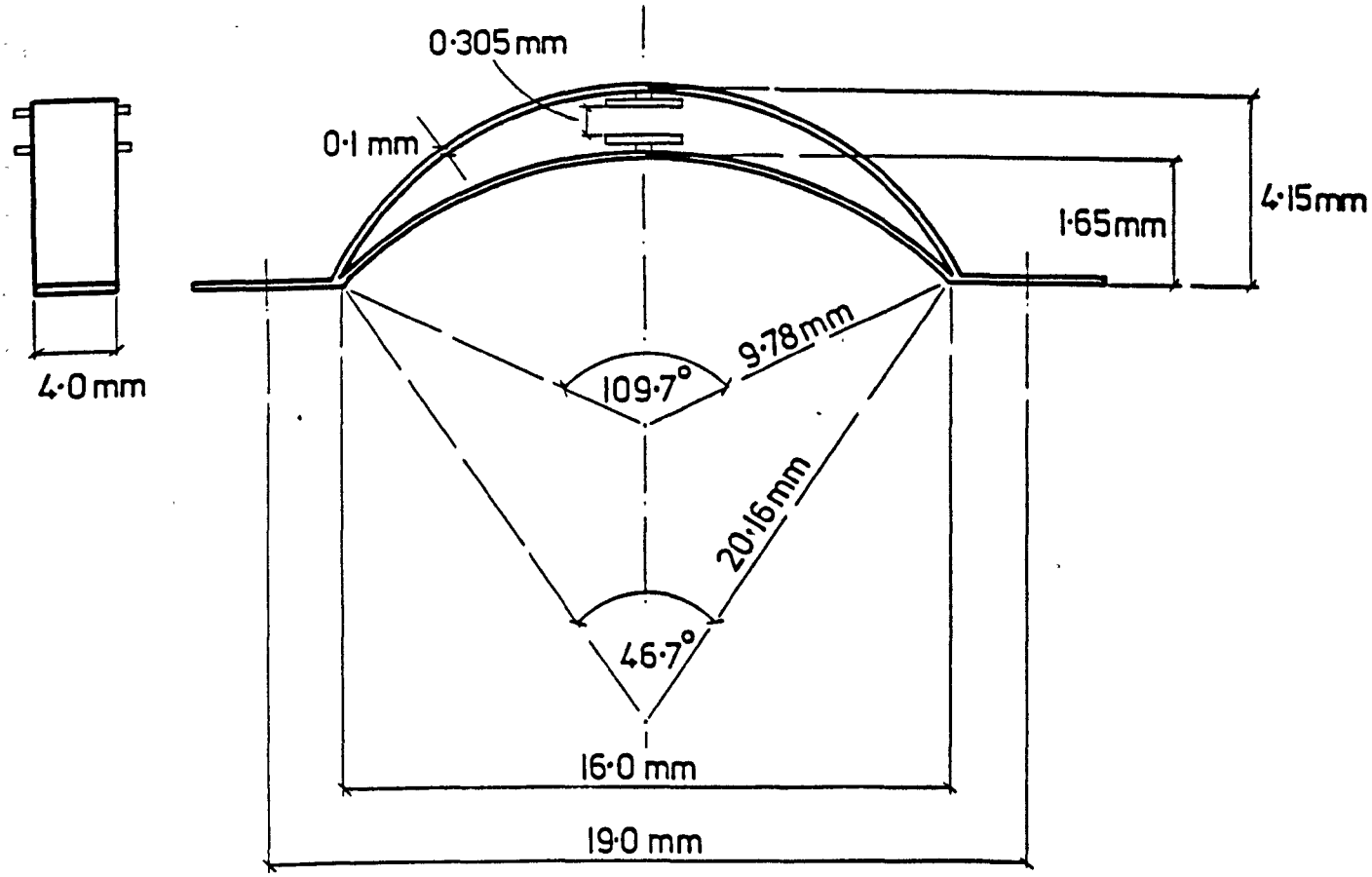

NOMINAL DIMENSIONS

FIG. 29

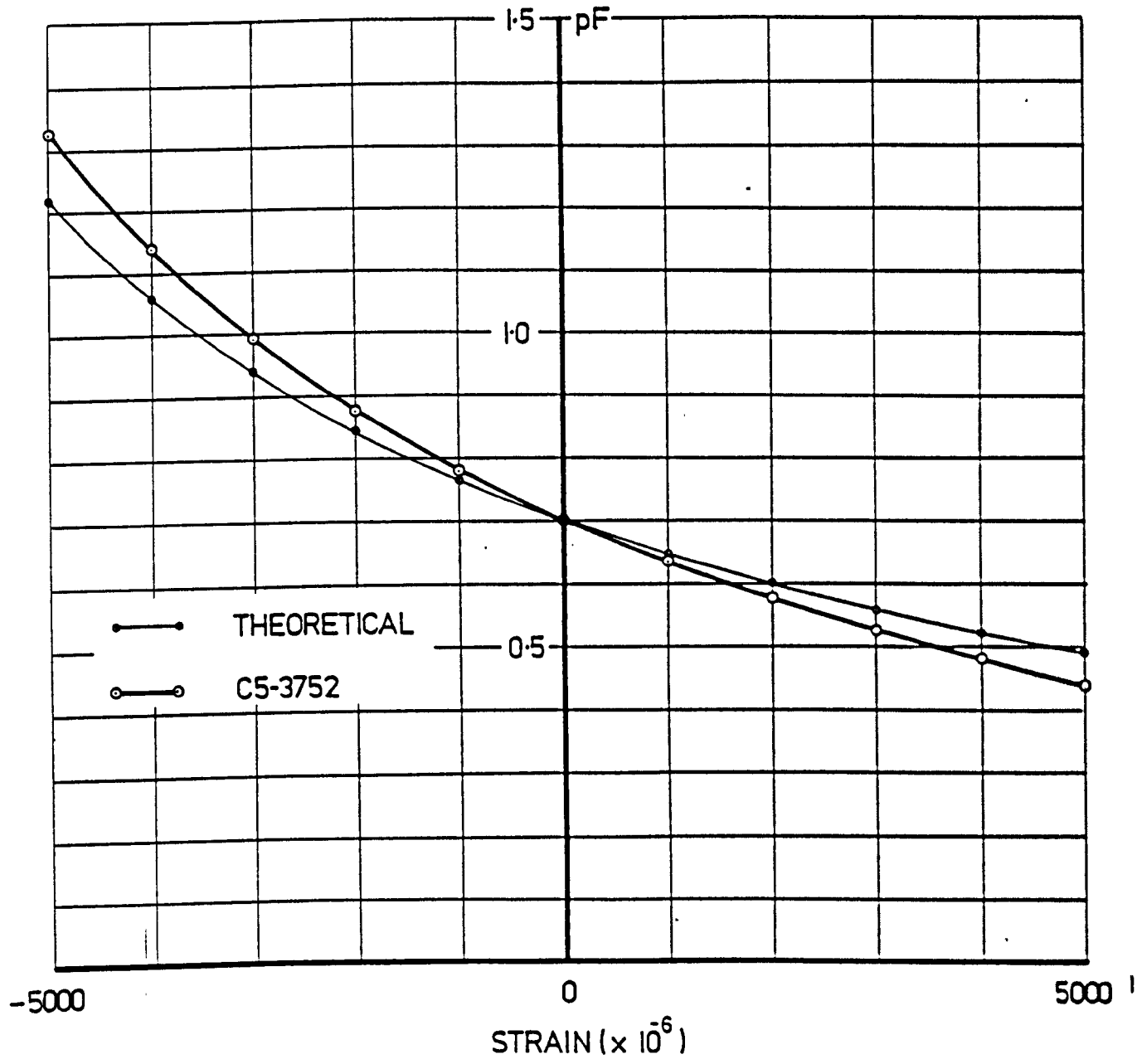

GAUGE CALIBRATION

ACTUAL- THEORETICAL

FIG. 30

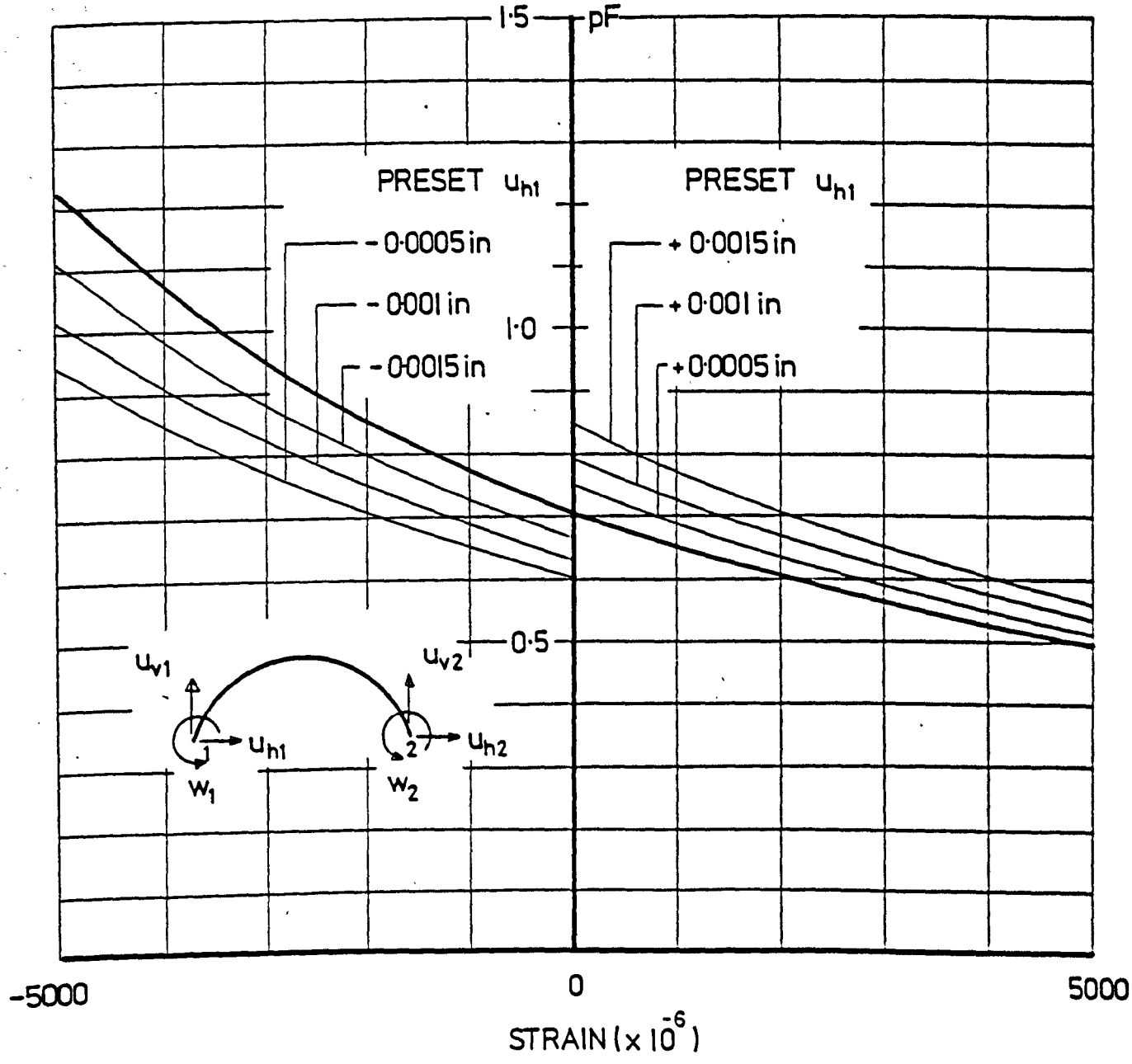

HORIZONTAL PRESET

FIG. 31

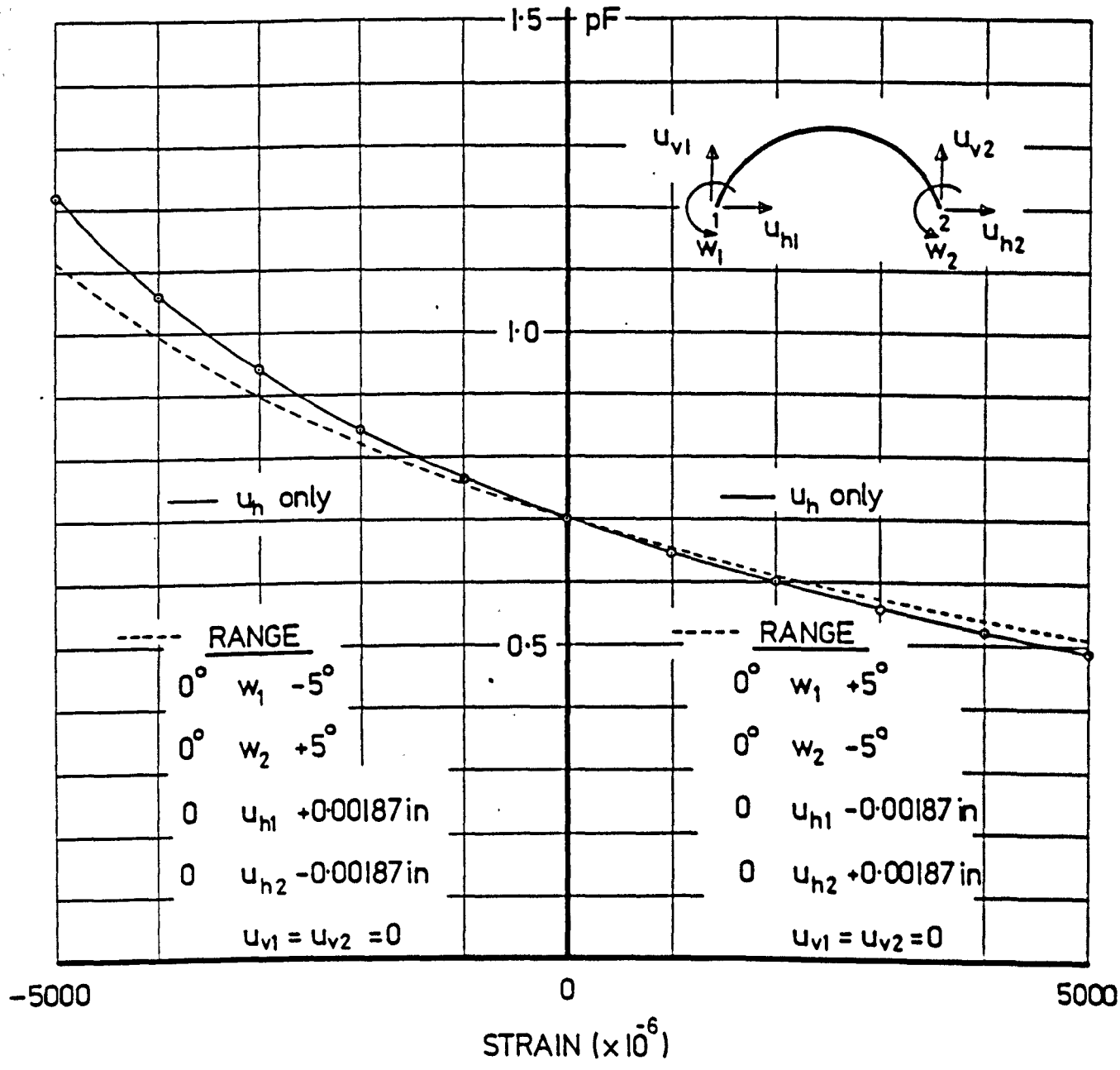

LINEAR AND ROTATIONAL DISPLACEMENT

FIG. 32

APPENDIX (9)

Development Work in Temperature Distribution

Report No. T1 on

Elevated Temperature Distribution Test

Specimen No. 4 - 90° - Sch 40

Part of

EXPERIMENTAL CREEP PROGRAMME ON PIPE BEND SPECIMENS

for

The Reactor Group, UKAEA

Agreement No. 4R52952B

by

Kenneth Rae

May 1981

1. Summary

This report presents the results of a series of elevated temperature distribution tests carried out on Specimen No. 4 - 90° - Sch 40.

Previous work at elevated temperature [1]* has shown that around the bend there can exist a differential of approximately 30°C between the extrados and the intrados of the bend. In an attempt at reducing this differential, development work has led to supplementing the low conductivity of the stainless steel by the use of a 1/8 in thick layer of copper. Here the bend is totally enclosed in a fabricated copper sheath resulting in a stable differential of ±3°C at 570°C around the bend mid-section.

With the prospect of increasing the test temperature to 600°C, tests carried out in excess of 600°C indicate the system should be satisfactory.

---

*Reference number, see Section 6.

2. Contents

3.1 Introduction

The need for this work arose following the completion of an elevated temperature forward creep test on Specimen No. 3 - 90° - Sch 40 [2]. As a check essentially on the performance of the heating system, the number of thermocouples employed on this test was increased to 12. This highlighted quite clearly that a differential of around 30°C existed between the extrados and the intrados of the bend, the latter being the source. The problem is inherent in the shape of the bend and to a lesser degree the method of heating which in turn relies on the conductivity of the stainless steel. Earlier elevated temperature tests on Specimen No. 1 - 180° - Sch 40 [3] and No. 2 - 180° - Sch 40 [4] employed only 4 thermocouples positioned on the neutral axis so that although the large differential still existed it was not recorded.

A commercially available heating system was identified [5] requiring little modification to the test rigs. However, the cost was prohibitive at around £5000 per bend. Further, the installation of a completely new system, heating the bend internally as opposed to externally would be expected to have some teething problems, although such a system would not be expected to hamper conditions in regard to capacitance strain gauges. However, it was decided more expedient to examine firstly methods of improving the existing system (Fig. 1).

The main objective was to remove the discrete form of heating produced by the heating tapes, and secondly, improve the conductivity of the stainless steel to give a more uniform temperature distribution across the section. Attaching a more conductive layer of metal to the bend surface satisfies both needs. For this purpose copper was chosen, having a thermal conductivity of approximately 20 times [6] that of

stainless steel and being relatively easy to form. In order to minimise any stiffening effect induced by this copper sheath and at the same time enhance the conductivity, a thickness of 1/8 in was chosen. This reduced the conductivity comparison to approximately 9 and as we shall see in Section 4 was a fortuitous choice.

3.2 General Description

The development work comprised essentially two tests, i.e. one without and one with the copper sheath, using the 45°/90° test rig as shown in Fig. 1. Both tests were conducted at 570°C extending to 500 hr and 1000 hr respectively. To determine the validity and range of the system the temperature was increased to 600°C and greater during the latter test.

The first test carried out on Specimen No. 4 was essentially a repeat of the elevated temperature test on Specimen No. 3 with the internal packing of insulation removed. The position of the 24 thermocouples employed on this test is shown in Fig. 2.

The second test incorporated a 1/8 in thick copper layer enclosing the bend. This copper layer or sheath was fabricated by hand in six parts, being split in the circumferential (longitudinal) direction for ease of fitting and removal (Fig. 3). Stainless steel bands around the copper ensured a tight fit to the bend. The number of thermocouples used on this test was increased to 27. Prior to commencing the test a check was made to determine the stiffening effect, if any, induced by the copper sheath. With the copper at room temperature this was considered a "worse case" for comparison. The effect was examined using an in-plane bending closing mode test.

On both tests a loading arm was attached to the free end of the specimen to simulate actual test conditions.

The thermocouples used throughout were chromel-alumen-D10K 21 S.W.G. (0.8 mm dia) with an insulation of vitreous silica fibre braid. In the first test the thermocouples were mounted using beads and held on to the bend surface using stainless steel tabs. In the second test,

for convenience, the ends were flattened and spot welded to the bend surface. Although this practice would appear to be frowned upon (for obscure reasons), tests carried out on this type and those formed with a bead showed no significant difference.

3.3 Heating System

Heating of the bend on both tests was accomplished using three I.T.Q. - 250 Isopad heating tapes wound around the bend*. For the purpose of distribution, this allowed the specimen to be subdivided into three zones with each zone powered and controlled independently. Temperature control was by a thermocouple actuated zero crossing switch box (Isopad C.S.W./1000) using a thermocouple from the central section of the bend. Insulation of the bend was provided by two layers of 8 lbf/cuft blanket on the exterior.

---

*In the case where copper was used the tapes were wound around the outside surface of the copper.

4. Results

The results of the first test are shown in Fig. 4. The average temperatures taken between 191 hr and 287 hr are given in Table 1. These values give an average temperature around the bend section of 577.5°C with a maximum differential of 32.4°C.

The dramatic drop in temperature as recorded by thermocouples No. 23 and No. 24 was due to failure of the bottom heating tape. Following this discovery the test was discontinued.

The results of the second test using the copper are shown in Fig. 5. As a result of the high temperature and consequently high heat loss being experienced at the free flange the test was shut down at around 300 hr. Gaskets formed of hard packed insulation (1 in thk) were inserted at both the free and fixed ends. Further modifications included at this time were the addition of thermocouple No. 27 at the base plate and replacement of a faulty thermocouple No. 10 with No.10A. As a result of the flange insulation the loading beam temperature was reduced by approximately 65%. The average temperatures measured between 492 hr and 709 hr are given in Table 2. These average values result in an average temperature around the bend of 569.4°C with a maximum differential of 5.8°C.

A comparison of the two tests is given in Fig. 6, illustrating clearly the vast improvement using the copper sheath. This trend is reflected on thermocouples positioned on the neutral axis and along the tangent pipes.

Stiffening of the bend due to the copper sheath was examined under an in-plane bending closing mode test. Rotation of the loading beam was measured using dial gauges (Fig. 7). The decrease in rotation was negligible (0.005°).

Results from the latter part of the second test are given in Table 2. Here the maximum differential around the bend section increased slightly to 7.4°C from an overall average of 625.2°C. The system, however, was working at full capacity to maintain this temperature. A reduction to 600°C would give some margin for adjustment and possible reduction in differential.

5. Discussion

This development work has led to a fairly simple and effective heating system retaining the original set up.

The maximum differential of 5.8°C compares well with other more sophisticated methods. For example, work by GRIFFITH and RODABAUGH [7] and IMAZU [8] quote temperature differentials of 5°C and 15°C respectively, although full details are not available. Further, the additional cost of about £400 per bend for purchase and fabrication compares excellently with £5000 for the commercial system.

However, on removal of the copper sheaths significant scaling on both the inside and outside surface was observed. This may limit their useful life but is unlikely to be important compared with the duration of the test programme. A specimen is presently being prepared for an elevated temperature forward creep test using this system.

At present, the fabrication of further copper sheaths is under way.

TABLE 1: Average temperatures 191 hr - 287 hr.

Thermocouple No.	Temperature (°C)
1	508.6
2	559.2
3	561.8
4	577.6
5	573.2
6	581.0
7	570.8
8	564.4
9	576.8
10	587.0
11	594.2
12	573.8
13	551.4
14	567.6
15	582.6
16	578.4
17	571.0
18	553.0
19	561.2
20	580.4
21	579.8
22	574.0
23	526.0
24	535.8

TABLE 2: Average temperatures 492 hr - 709 hr, 805 hr - 974 hr.

Thermocouple No.	Temperature (°C) 492 hr - 709 hr	805 hr - 974 hr
1	525.5	574.0
2	566.37	619.4
3	558.12	612.0
4	565.62	618.2
5	569.0	621.8
6	567.12	621.6
7	568.0	622.4
8	571.12	626.8
9	569.62	624.8
10A	568.12	622.8
*10	560.0	616.0
11	573.0	630.2
12	567.75	624.4
13	569.87	627.0
14	570.0	626.8
15	569.25	625.4
16	572.87	630.6
17	565.5	620.4
18	570.25	626.0
19	570.12	626.0
20	568.0	623.2
21	558.25	609.4
22	561.62	612.2
23	557.62	609.0
24	558.12	609.4
25	505.12	549.8
26	219.87	239.8
27	134.25	144.4

*Faulty thermocouple replaced by No. 10A

6. References

1. K. Rae — Seventh Progress Report on Experimental Creep Programme on Pipe Bend Specimens for The Reactor Group, UKAEA Agreement No. 4R52952B Sept 1980

2. K. Rae — Report No. H.T.1. on Elevated Temperature Forward Creep Test on Specimen No. 3 - 90° - Sch 40, part of the Experimental Creep Programme on Pipe Bend Specimens for The Reactor Group, UKAEA Agreement No. 4R52952B Report in preparation

3. K. Rae — Sixth Progress Report on Experimental Creep Programme on Pipe Bend Specimens for The Reactor Group, UKAEA Agreement No. 4R52952B Feb 1980

4. K. Rae — Fifth Progress Report on Experimental Creep Programme on Pipe Bend Specimens for The Reactor Group, UKAEA Agreement No. 4R52952B Sept 1979

5. Ref. No. E9.8.10780/DAT/HS/SALES 10 Oct 1981 Proposal on Heating System Carbolite Furnaces Ltd, Bamford, Sheffield

6. R.E. Boltz G.L. Tuve — Handbook of Tables for Applied Engineering Science 2nd Edition C.R.C.

7. Griffith Rodabaugh — Report on Tests of Two 4 in Sch 10 Elbow Assemblies Applied Mechanics Section, Reactor Division, Oak Ridge National Laboratory Dec 1974

8. Imazu
Miura
Nagata
Okaboyashi

Elevated Temperature Elastic-Plastic-Creep Test of an Elbow subjected to In-Plane Moment Loading
Press. Ves. and Piping Conf., A.S.M.E., Mexico, 1976

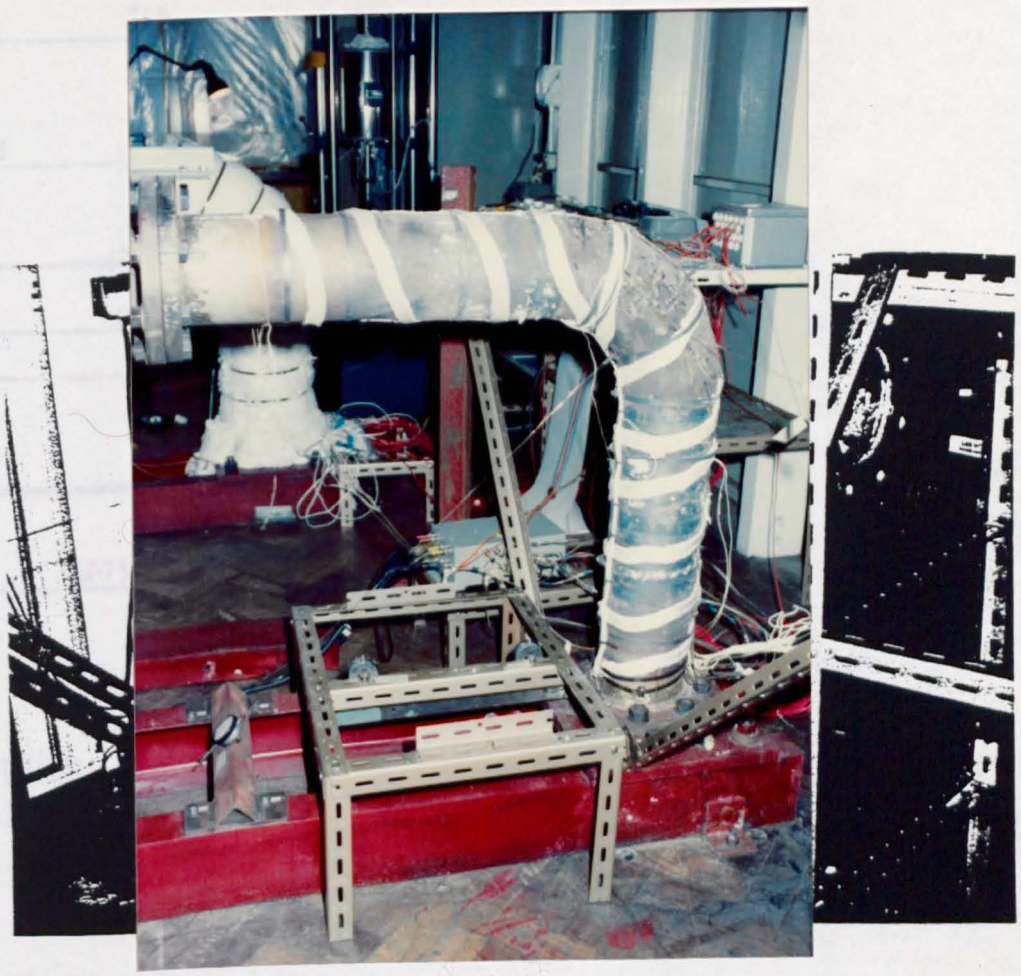

HEATING SYSTEM

FIG. 1

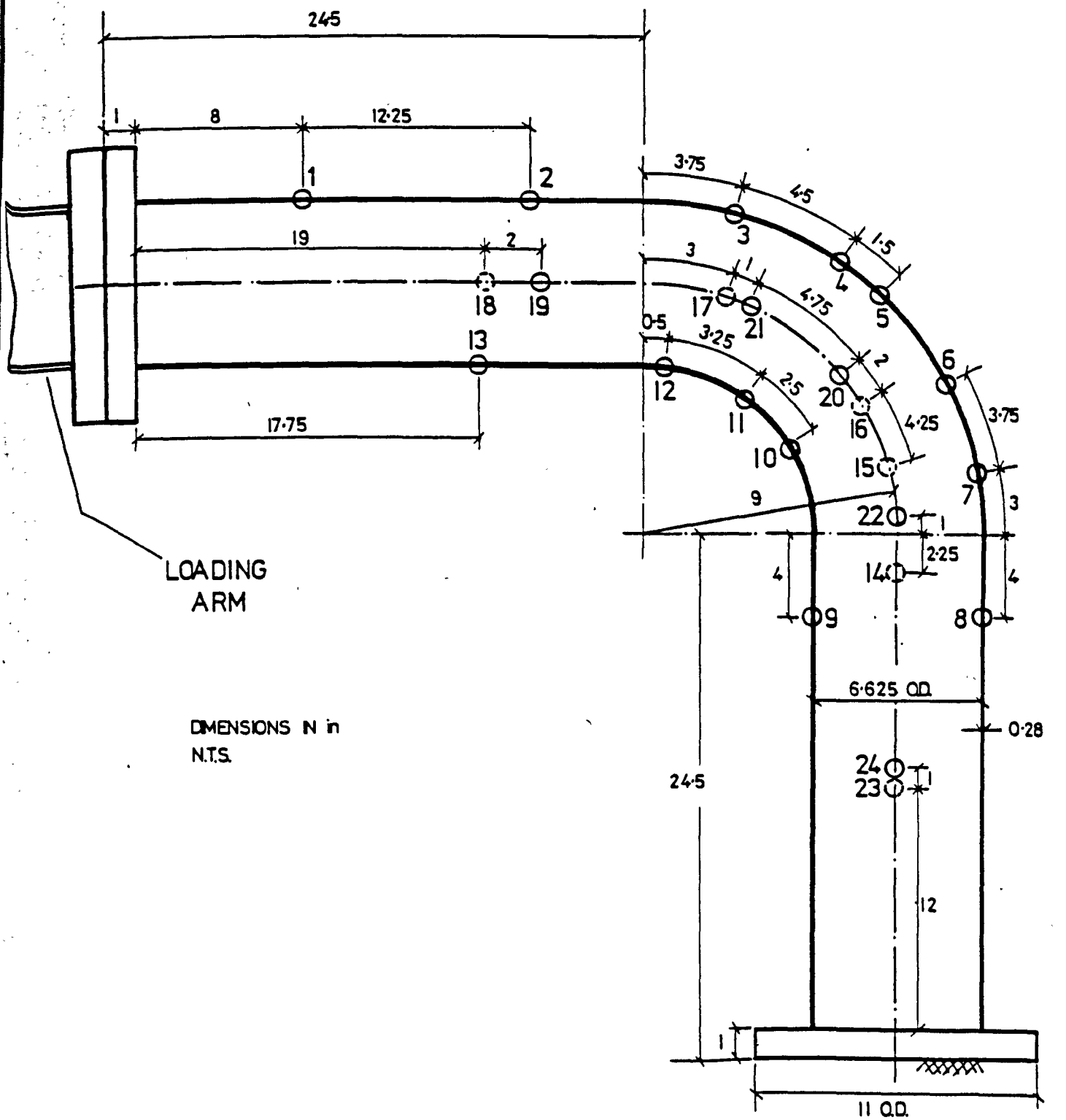

LAYOUT OF THERMOCOUPLES
WITHOUT COPPER
FIG. 2

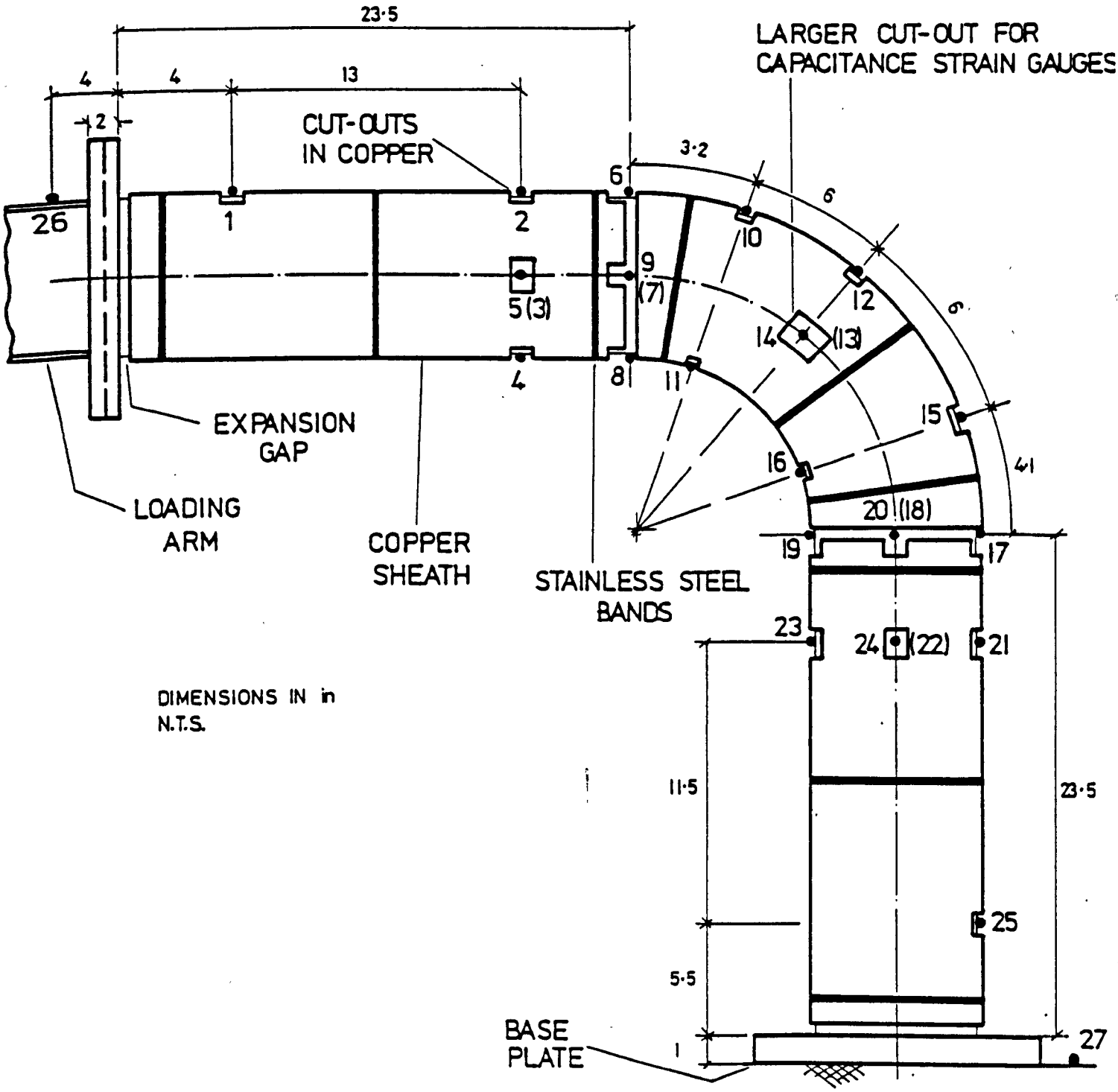

LAYOUT OF THERMOCOUPLES
WITH COPPER

FIG.3

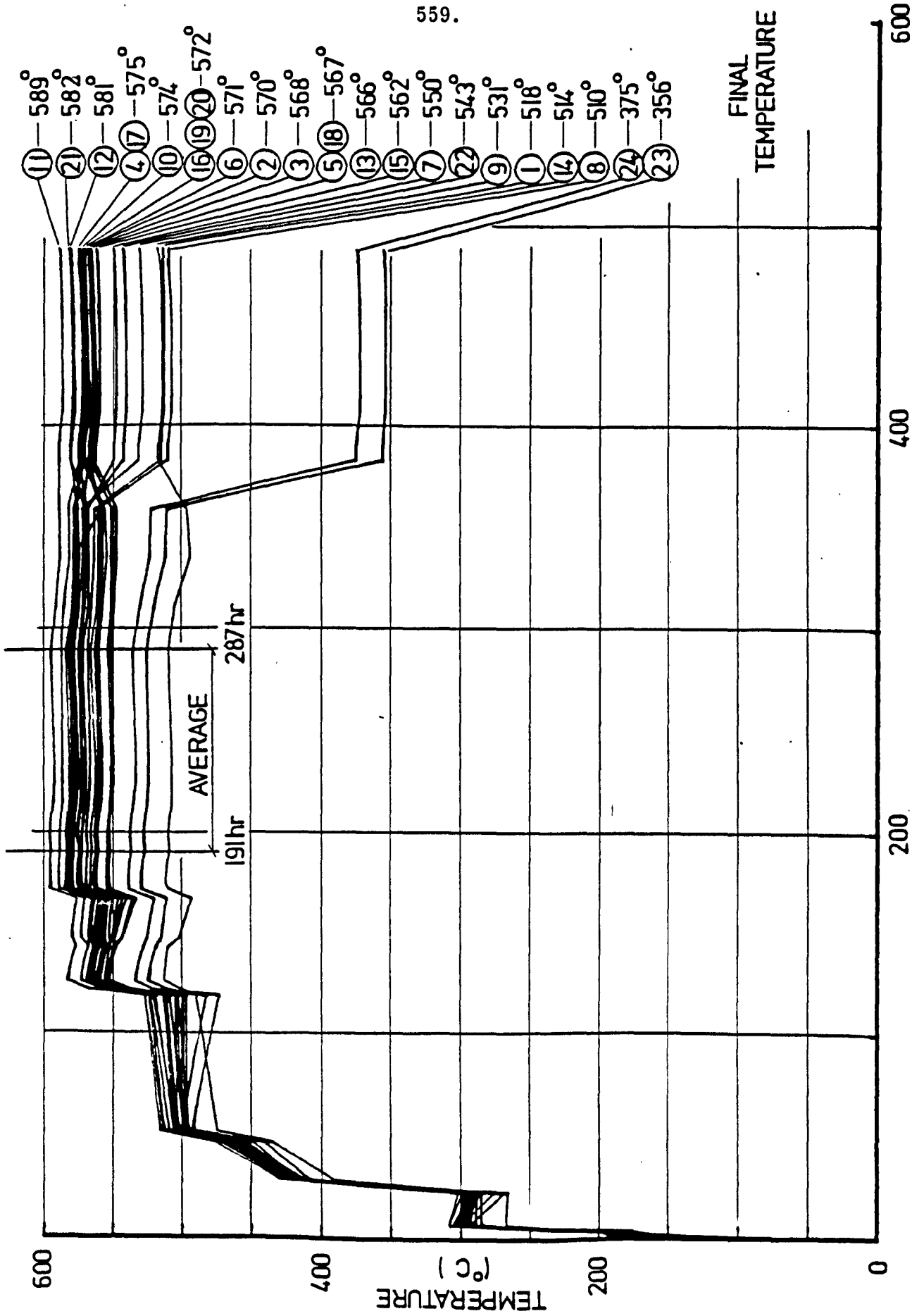

TEMPERATURE VARIATION
WITHOUT COPPER

FIG. 4

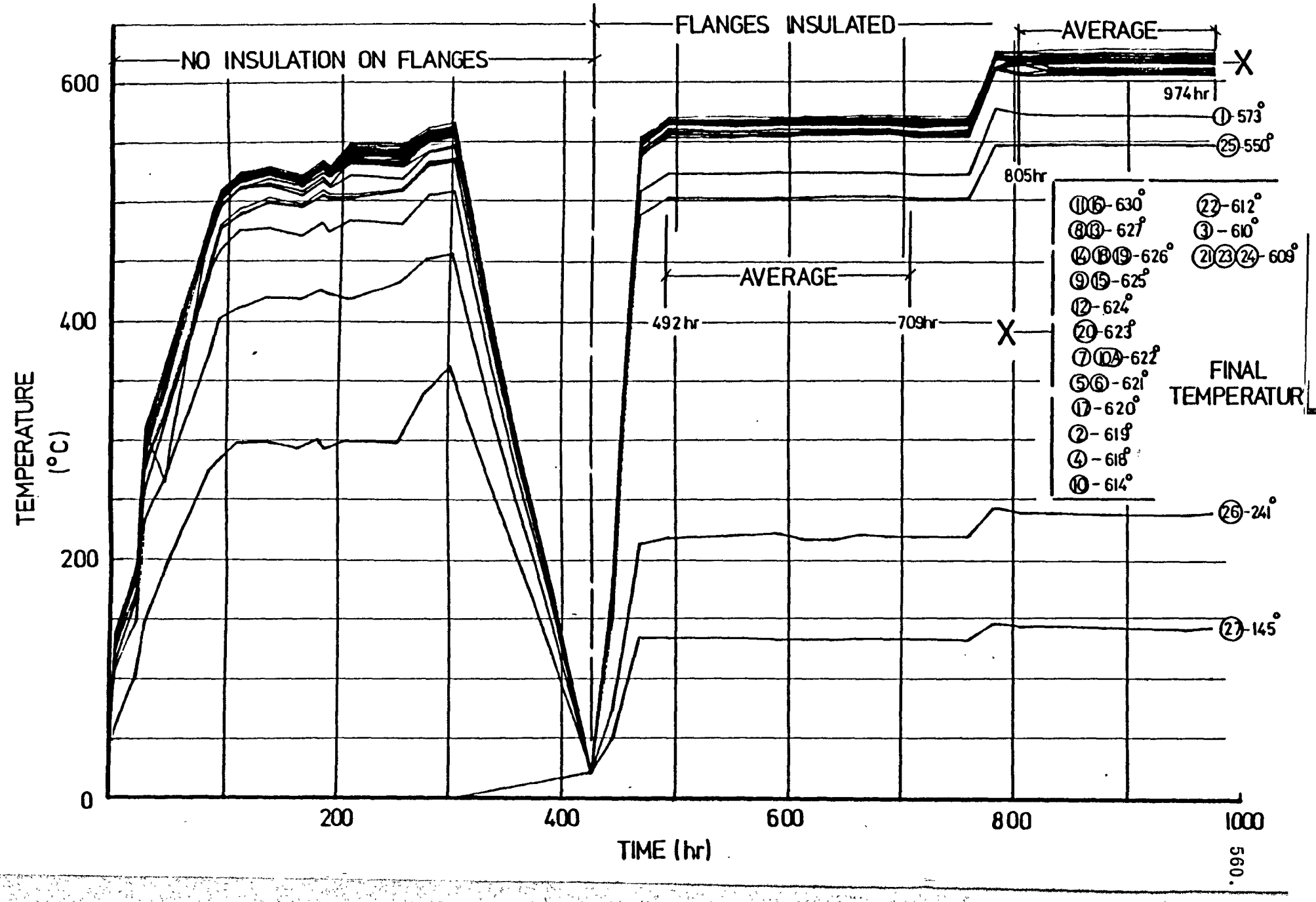

TEMPERATURE VARIATION WITH COPPER

FIG. 5

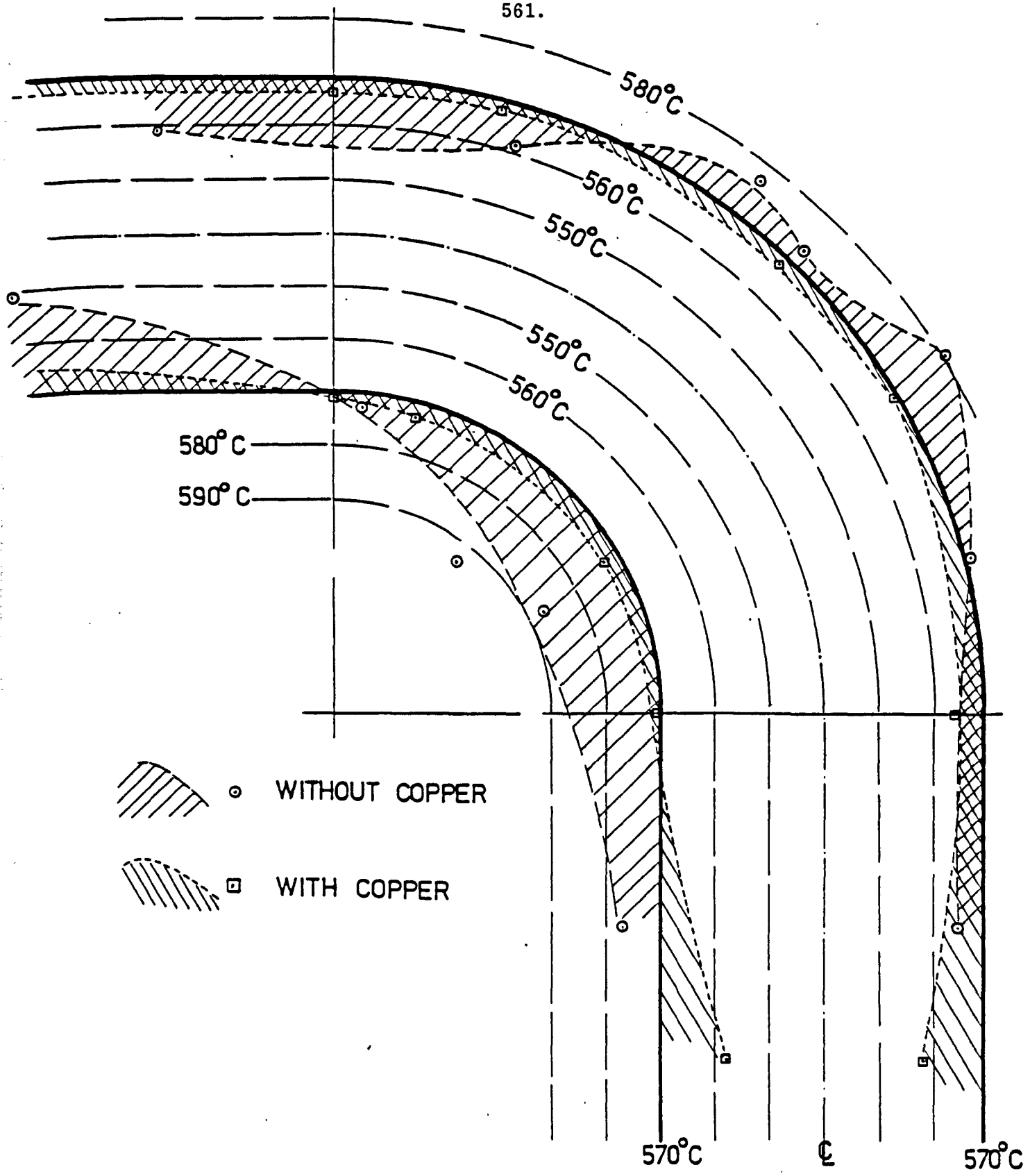

TEMPERATURE VARIATION
ALONG INTRADOS AND EXTRADOS
FIG. 6

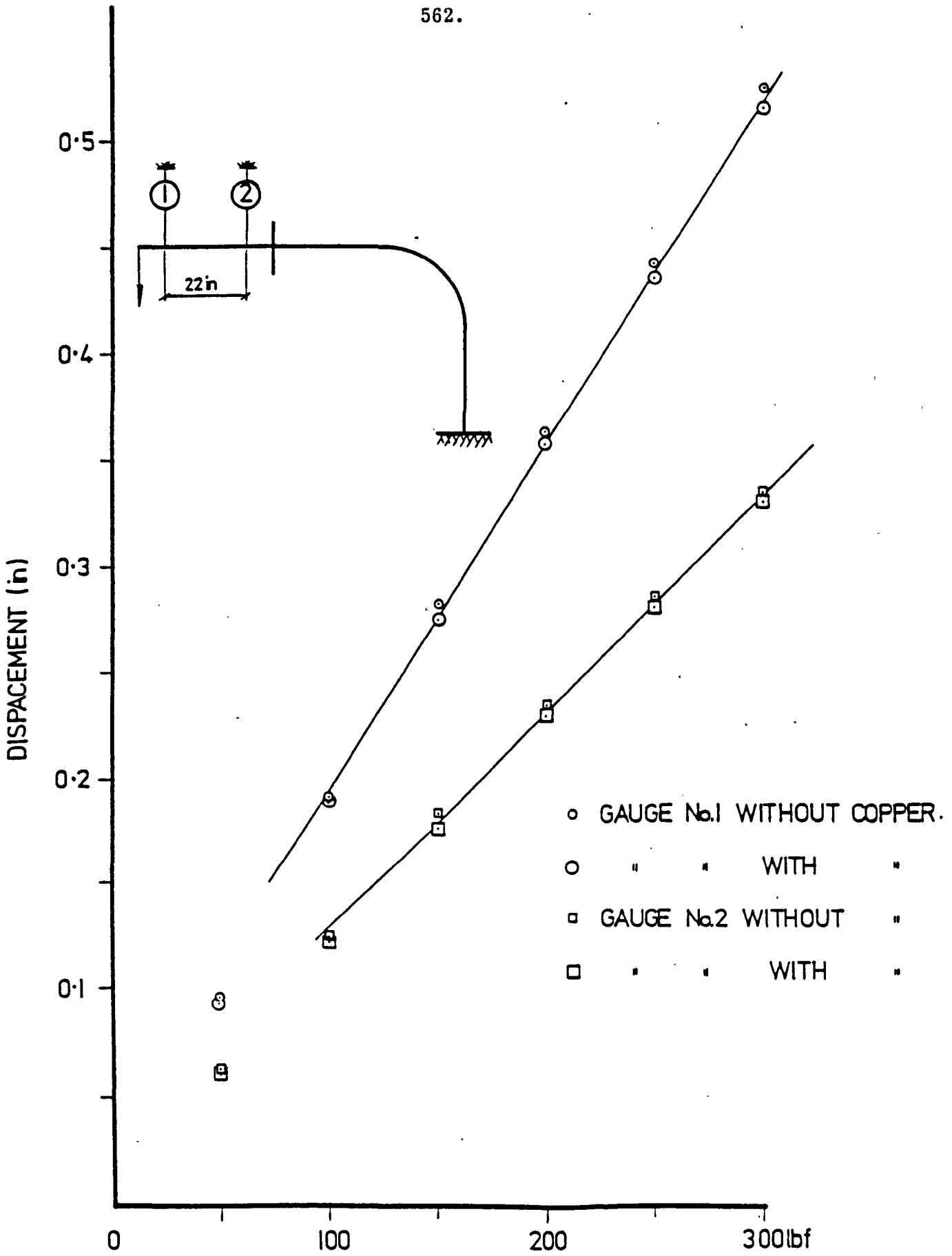

BEND ROTATION

FIG. 7

ACKNOWLEDGEMENTS

All of the work presented excluding the final computer solutions was carried out in the Department of Mechanics of Materials of the University of Strathclyde. The author wishes to record his thanks to:

Professor J. Spence, ARCST, BSc, MSc, PhD, DSc, CEng, MI MechE, head of the department, who supervised the project, for his advice and assistance and the use of the department's facilities;

United Kingdom Atomic Energy Authority, who provided financial support for the experimental programme;

Dr. J.T. Boyle, BSc, PhD, AFIMA and Dr. G. Thomson, BSc, PhD, CEng, MI MechE, for their help and advice on various aspects of the theory;

Mr. J. Fraser, BSc, Mr. A. Smith, Chief Technician, Mr. A. Lambie and many others of the technician staff who provided invaluable assistance during various parts of the experimental programme;

University of Strathclyde Computing Department and Ferranti PLC for the use of their facilities;

Mrs. F. Anderson for her care and expertise in typing the thesis.